AGARD-CP-526

AGARD-CP-526

AGARD

ADVISORY GROUP FOR AEROSPACE RESEARCH & DEVELOPMENT
7 RUE ANCELLE 92200 NEUILLY SUR SEINE FRANCE

AGARD CONFERENCE PROCEEDINGS 526

Airbreathing Propulsion for Missiles and Projectiles

(Propulsion Aérobie des Missiles et Projectiles)

Papers presented at the Propulsion and Energetics Panel 79th Symposium held in Villepreux, Nr Bordeaux, France, 11th—15th May 1992.

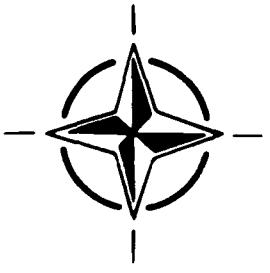

NORTH ATLANTIC TREATY ORGANIZATION

AGARD-CP-526

AGARD

ADVISORY GROUP FOR AEROSPACE RESEARCH & DEVELOPMENT
7 RUE ANCELLE 92200 NEUILLY SUR SEINE FRANCE

AGARD CONFERENCE PROCEEDINGS 526

Airbreathing Propulsion for Missiles and Projectiles

(Propulsion Aérobie des Missiles et Projectiles)

Papers presented at the Propulsion and Energetics Panel 79th Symposium held in Villepreux, Nr Bordeaux, France, 11th—15th May 1992.

North Atlantic Treaty Organization
Organisation du Traité de l'Atlantique Nord

The Mission of AGARD

According to its Charter, the mission of AGARD is to bring together the leading personalities of the NATO nations in the fields of science and technology relating to aerospace for the following purposes:

- Recommending effective ways for the member nations to use their research and development capabilities for the common benefit of the NATO community;
- Providing scientific and technical advice and assistance to the Military Committee in the field of aerospace research and development (with particular regard to its military application);
- Continuously stimulating advances in the aerospace sciences relevant to strengthening the common defence posture;
- Improving the co-operation among member nations in aerospace research and development;
- Exchange of scientific and technical information;
- Providing assistance to member nations for the purpose of increasing their scientific and technical potential;
- Rendering scientific and technical assistance, as requested, to other NATO bodies and to member nations in connection with research and development problems in the aerospace field.

The highest authority within AGARD is the National Delegates Board consisting of officially appointed senior representatives from each member nation. The mission of AGARD is carried out through the Panels which are composed of experts appointed by the National Delegates, the Consultant and Exchange Programme and the Aerospace Applications Studies Programme. The results of AGARD work are reported to the member nations and the NATO Authorities through the AGARD series of publications of which this is one.

Participation in AGARD activities is by invitation only and is normally limited to citizens of the NATO nations.

Published September 1992

ISBN 92-835-0685-5

Printed by Specialised Printing Services Limited
40 Chigwell Lane, Loughton, Essex IG10 3TZ

AGARD

ADVISORY GROUP FOR AEROSPACE RESEARCH AND DEVELOPMENT
7 RUE ANCELLE — 92200 NEUILLY-SUR-SEINE — FRANCE
TELEPHONE: (1)47 38 57___ TELEX: 610176 AGARD
TELEFAX: (1)47 38 57 99

ST/26/8 September 1992

AGARD's TECHNICAL EVALUATION REPORTS (TERs)

To Recipients of CP 526

AGARD is assessing the usefulness of its Technical Evaluation Reports (TER) such as the one included in this Conference Proceedings. In the past, AGARD has often published them separately from the Conference Proceedings and you may also have seen examples of these.

We should be very grateful if you would spend a few minutes answering these few questions.

Thank you very much

A J Wennerstrom
Director

First we should like to ask you about TERs you may have seen previously.

1. Have you seen AGARD TERs in the past:

   a. separately from a Conference Proceedings?

      Often ☐ Sometimes ☐ Never ☐

   b. bound as part of one?

      Often ☐ Sometimes ☐ Never ☐

2. Have you read a TER even when you have not attended the corresponding meeting?

   Yes ☐ No ☐

3. Have you found TERs useful for giving a review of the state-of-the-art in a specific field?

   Often ☐ Sometimes ☐ Rarely ☐ Never ☐

Please turn over

4. Have you found TERs useful for identifying new lines of research or development that might be followed in a specific field?

Often ☐ Sometimes ☐ Rarely ☐ Never ☐

5. Have you found TERs useful for giving an overview or executive summary of the papers in an AGARD conference proceedings?

Often ☐ Sometimes ☐ Rarely ☐ Never ☐

Now we should like to ask you about the TER in this conference proceedings.

6. Was it useful for giving you a review of the state-of-the-art?

Yes ☐ No ☐

7. Was it useful for identifying new lines of research or development?

Yes ☐ No ☐

8. Was it useful for giving you an overview or executive summary of the papers in the conference proceedings?

Yes ☐ No ☐

9. Please add any other comments.

10. Did you attend the meeting? Yes ☐ No ☐

Are you an AGARD Panel Member? Yes ☐ No ☐

11. Name (optional): .....

Organisation: .....

Address: .....

.....

.....

Thank you for taking the trouble to complete this. Please return it to

(from Europe):

AGARD/SPE
7 rue Ancelle
92200 Neuilly-sur-Seine
France

(from North America only):

AGARD/SPE
Unit 21551
APO AE 09777

Recent Publications of the Propulsion and Energetics Panel

CONFERENCE PROCEEDINGS (CP)

Engine Cyclic Durability by Analysis and Testing
AGARD CP 368, September 1984

Gears and Power Transmission Systems for Helicopters and Turboprops
AGARD CP 369, January 1985

Heat Transfer and Cooling in Gas Turbines
AGARD CP 390, September 1985

Smokeless Propellants
AGARD CP 391, January 1986

Interior Ballistics of Guns
AGARD CP 392, January 1986

Advanced Instrumentation for Aero Engine Components
AGARD CP 399, November 1986

Engine Response to Distorted Inflow Conditions
AGARD CP 400, March 1987

Transonic and Supersonic Phenomena in Turbomachines
AGARD CP 401, March 1987

Advanced Technology for Aero Engine Components
AGARD CP 421, September 1987

Combustion and Fuels in Gas Turbine Engines
AGARD CP 422, June 1988

Engine Condition Monitoring -- Technology and Experience
AGARD CP 448, October 1988

Application of Advanced Material for Turbomachinery and Rocket Propulsion
AGARD CP 449, March 1989

Combustion Instabilities in Liquid-Fuelled Propulsion Systems
AGARD CP 450, April 1989

Aircraft Fire Safety
AGARD CP 467, October 1989

Unsteady Aerodynamic Phenomena in Turbomachines
AGARD CP 468, February 1990

Secondary Flows in Turbomachines
AGARD CP 469, February 1990

Hypersonic Combined Cycle Propulsion
AGARD CP 479, December 1990

Low Temperature Environment Operations of Turboengines (Design and User's Problems)
AGARD CP 480, May 1991

CFD Techniques for Propulsion Applications
AGARD CP 510, February 1992

Insensitive Munitions
AGARD CP 511, July 1992

Combat Aircraft Noise
AGARD CP 512, April 1992

ADVISORY REPORTS (AR)

Alternative Jet Engine Fuels *(Results of Working Group 13)*
AGARD AR 181, Vol.1 and Vol.2, July 1982

Suitable Averaging Techniques in Non-Uniform Internal Flows *(Results of Working Group 14)*
AGARD AR 182 (in English and French), June/August 1983

Producibility and Cost Studies of Aviation Kerosines *(Results of Working Group 16)*
AGARD AR 227, June 1985

Performance of Rocket Motors with Metallized Propellants *(Results of Working Group 17)*
AGARD AR 230, September 1986

Recommended Practices for Measurement of Gas Path Pressures and Temperatures for Performance Assessment of Aircraft Turbine Engines and Components *(Results of Working Group 19)*
AGARD AR 245, June 1990

The Uniform Engine Test Programme *(Results of Working Group 15)*
AGARD AR 248, February 1990

Test Cases for Computation of Internal Flows in Aero Engine Components *(Results of Working Group 18)*
AGARD AR 275, July 1990

Test Cases for Engine Life Assessment Technology *(Results of Working Group 20)*
AGARD AR 308, September 1992

LECTURE SERIES (LS)

Ramjet and Ramrocket Propulsion Systems for Missiles
AGARD LS 136, September 1984

3-D Computation Techniques Applied to Internal Flows in Propulsion Systems
AGARD LS 140, June 1985

Engine Airframe Integration for Rotorcraft
AGARD LS 148, June 1986

Design Methods Used in Solid Rocket Motors
AGARD LS 150, April 1987
AGARD LS 150 (Revised), April 1988

Blading Design for Axial Turbomachines
AGARD LS 167, June 1989

Comparative Engine Performance Measurements
AGARD LS 169, May 1990

Combustion of Solid Propellants
AGARD LS 180, July 1991

Steady and Transient Performance Prediction of Gas Turbine Engines
AGARD LS 183, May 1992

AGARDOGRAPHS (AG)

Manual for Aeroelasticity in Turbomachines
AGARD AG 298/1, March 1987
AGARD AG 298/2, June 1988

Measurement Uncertainty within the Uniform Engine Test Programme
AGARD AG 307, May 1989

Hazard Studies for Solid Propellant Rocket Motors
AGARD AG 316, September 1990

REPORTS (R)

Application of Modified Loss and Deviation Correlations to Transonic Axial Compressors
AGARD R 745, November 1987

Rotorcraft Drivetrain Life Safety and Reliability
AGARD R 775, June 1990

Theme

In future NATO will be faced with more advanced detection and interception systems, so it will be increasingly necessary to develop missiles able to penetrate these defences by flying at low altitude, with diversified trajectories.

In addition, to reduce the vulnerability of air, ground or sea launching platforms, it will be necessary to increase the range of weapons launched from these platforms. Accordingly, because of economic and flexibility considerations an increased utilisation of *air-breathing propulsion for missiles and projectiles* is highly probable.

This Symposium examined the evolution of techniques and technologies related to the following systems:
- liquid fuel ramjets and ramrockets
- turbojets and turborockets.

Particular emphasis was put on the associated components or disciplines, such as inlets, combustion, liquid or solid fuels, test facilities, engine integration etc.

Thème

Face à la progression prévisible des moyens de détection et d'interception, il sera de plus en plus nécessaire pour l'OTAN, de développer des missiles capables de pénétrer ces défenses en volant à basse altitude, et en suivant des trajectoires diversifiées.

De plus, pour réduire la vulnérabilité des plates-formes de lancement, qu'elles soient aériennes, terrestres ou maritimes, on recherchera une allonge plus grande de leurs armes.

Par conséquent, une utilisation accrue de la *propulsion aérobie des missiles et projectiles* est prévisible, car elle est économique et permet une grande flexibilité d'emploi.

Ce Symposium a examiné l'évolution des techniques et technologies relatives aux systèmes suivants:
- statoréacteurs et statofusées
- turboréacteurs et turbofusées.

Un accent particulier a été mis sur les composants ou disciplines associés, tels que: entrées d'air, combustion, propergols liquides ou solides, matériaux, moyens d'essais, intégration du moteur, etc...

Propulsion and Energetics Panel

ACKNOWLEDGEMENT

The Propulsion and Energetics Panel wishes to express its thanks to the National Authorities from France for the invitation to hold this meeting in Villepreux, Nr Bordeaux, France, and for the facilities and personnel which made this meeting possible.

Contents

* Published in classified volume CP-526 (Supplement).

* Published in classified volume CP-526 (Supplement).

* Published in classified volume CP-526 (Supplement).

Technical Evaluation Report

by

Ing. en Chef M. Petre
Direction Générale de l'Armement
France

1 INTRODUCTION

IGA Estournet from France and Dr D.M. Dix from the United States introduced this 79th Symposium of the Propulsion and Energetics Panel. In different terms they both put great emphasis on the link that has to be made between airbreathing propulsion and military requirements.

There is certainly a need for weapons with larger range, more precision, low signature and greater speed. This requirement leads to airbreathing propulsion which brings range and speed.

A number of missiles using turbojets or ramjets already fielded or under development have been named: ALCM, OTOMAT, ASMP, ANS, ASLP, C22, APACHE, MILAS.

New technologies in the field of airbreathing propulsion could also be considered to fulfil future requirements, for instance RUSTIQUE and VFDR. In the actual trend of decreasing spending for defence, emphasis has to be given to cost-efficiency. Simulations can help if they are reliable.

2 ORGANISATION OF THE TECHNICAL EVALUATION REPORT

The technical evaluation will be divided in two parts. The first one will follow the order of the different Sessions of the Symposium; that is to say:

Session I	Ramjets and ramrockets: survey papers
Session II	Ramjets and ramrockets: propulsion systems
Session III	Ramjets and ramrockets: combustion, fuels, materials
Session IV	Projectile airbreathing propulsion
Session V	Aerodynamics and engine integration
Session VI	Turbojets and turborockets
Session VII	Common techniques.

The second part (paragraph 10) will try to relate the technologies that have been presented to possible future requirements in order to present a global outlook of the potential of airbreathing propulsion for the future.

3 SESSION I – RAMJETS AND RAMROCKETS: SURVEY PAPERS

Five papers were presented at this Session chaired by Ph. Cazin. The objective was to give a general overview of the most promising ramjet and ramrocket technologies in the perspective of operational use:

Ramjet propulsion for Mach 3—4.5 missiles was presented by J.-M. Laurent (Paper 1) in a very well structured Paper dealing with operational needs, air-intakes, fuel injection, internal thermal protection, prediction methods and test methods. The ongoing work leads to a super scramjet with liquid fuel.

F. Zarlingo (Paper 2) reviewed the status of the Supersonic Low Altitude Target Program using liquid ramjet propulsion and an integrated booster. Eight flight tests were performed that validated the propulsion system even if the flights were not a total success.

French experience on the Rustique Ducted Rocket (Paper 3) was presented by B. Petit and A. Ravier. The Rustique Concept has already been tested in flight five times and will have two more flight tests in 1993 (20 km altitude at Mach 3—3.8). The design of the Rustique ducted rocket aims at compactness, simplicity and reduction of cost using a nozzleless booster and an unchoked gas generator for autoadjustment of combustion. The optimum use for Rustique is a 200—250mm calibre tactical medium range missile of high average velocity (Mach 2.5).

Advances in Ducted Rocket Technology (Paper 4) was presented by W. Donaldson. The evaluation of the Variable Flow Ducted Rocket (VFDR) started in 1986 and will go on up to 1994 with ground tests. VFDR has a nozzleless booster for air-launched application and can be used with a solid gas generator or liquid fuel, for instance, high energy boron fuel. It is a candidate for an air-to-air application.

Potential missile flight performance gains from improvements to the propulsion system (Paper 5) presented by M.S. Ivey and R.K. Oldham was studied with a 3D flight simulation and a 1D propulsion simulation. This Paper intended to look at a stand-off missile application, but was not apparently supported by research work. It could have been considered for Session VII.

Conclusions of Session I

(1) Ramjet technology is ready for new applications, in particular for tactical missiles as demonstrated by the very interesting presentations of Session I.

(2) Applications will be decided according to different criteria, among them cost. It should be useful to have more knowledge of the costs versus performances of the different concepts presented.

(3) Signature and manoeuvrability potential of ramjets that could have importance for some applications should have been taken into greater consideration.

4 SESSION II – RAMJETS AND RAMROCKETS: PROPULSION SYSTEMS

Four papers were presented at this Session, chaired by B. Crispin, oriented towards testing of propulsion systems (but different from those of Session I):

Development Testing of Throttleable Ducted Rockets (Paper 6) presented by H.-L. Besser related to up to scale 1 testing of different types of Solid Propellant Ducted Rocket (SDR) at different stages: basic development, advanced development including HWIL (hardware in the loop) test with flight trajectory simulation.

Liquid Fuelled, Hypersonic Airbreathing Engines for Tactical Missile Applications (Paper 7) presented by

P.J. Waltrup related to the Dual Combustor Ramjet (DCR) compared to scramjets (supersonic combustion ramjets) and ramjets (subsonic combustion ramjets).

Air film cooled combustors by J. Valazza and V. Protat (Paper 9) related to testing at scale 1 of film cooling by perspiration and by air through perforated materials.

Extending Missile Range with Boron Solid Fuel Ramjet Engines (Paper 10) by B. Dunn and S. Leisch related to up to half scale testing of an engine for an air-to-air application. This Paper could have been presented in Session III.

Conclusions of Session II

(1) Logic and means of testing of ramjet propulsion systems up to scale 1 exist. HWIL tests with flight trajectory simulation are necessary to find the best compromises and to conduct flight tests in good conditions.

(2) Efficiency of air film cooled combustors has been demonstrated in HWIL simulation for flights up to 2000 s. Film cooling improves engine performances because combustion instabilities have been mainly eliminated.

(3) Dual Combustor ramjets have scientific interest, but seem far from application.

5 SESSION III – RAMJETS AND RAMROCKETS: COMBUSTION, FUELS, MATERIALS

The first part of Session III was chaired by B. Zeller, the second part by D.W. Netzer. Eight papers were presented on three topics:

Solid fuel for ramjet engines,
Combustion instabilities and oscillations,
Thermal protection and structure.

5.1 Solid Fuel for Ramjet Engines

Three presentations on this topic:

Paper 11 by B. Mahé, C. Perut, C. Masson, and C. Vigot gave a general overview of the different types of compositions that could be used for solid fuel ramjet engines. Compositions with low metal content, that is to say, with low signature, have been tested in a combustion chamber of 200 mm diameter for choked and unchoked ramjets. Compositions with magnesium, carbon and boron have been tested in various combustion chambers.

Paper 12 by G.E. Jensen and F. Zarlingo presented results of ground tests of a hydrocarbon fuelled solid-fuel ramjet engine adapted to meet air-to-ground requirements at low altitude for flight of about 40 n. miles.

Paper 13 by G.E. Jensen presented results of direct-connect tests of a high energy hydrocarbon solid fuel ramjet for an air-to-air application. The foreseen missile had two bypass inlets and one forward inlet. Variable by-pass ratios and different fuel grain geometry adapted to the missions were tested. Difficulties appeared concerning environment, especially storage of the solid fuel with cycling ($-65°$ F + 165° F).

5.2 Combustion Instabilities and Oscillations

Paper 14 by J.M. Samaniego, B. Yip, T. Poinsot and S. Candel was about flow instabilities, in a two-dimensional two-inlet side-dump combustor fed with an air/propane mixture. Visualisation of instabilities with a CCD camera provided an insight into the flame structure and its interaction with the entering jets. Fuel-rich and fuel-lean modes were studied but main results concerned the fuel-rich mode.

Paper 15 by M.N.R. Nina and G.P.A. Pita presented an experimental analysis of combustion oscillations with reference to ramjet propulsion. The influences of flow rate, fuel air ratio and bluff body geometry on the predominant frequencies of combustion driven oscillations were measured.

5.3 Thermal Protection and Structure

Three very interesting Papers were presented on thermal protection and structure:

D. Abbé and G. Gonthier (Paper 16) described work performed on thermal protection systems for different types of ramjet combustion chambers. Logic of selection of materials including scale 1 tests was presented for different missions from a few seconds to 3000 seconds at various speeds and altitudes. In each case, specific constraints must be taken care of such as thermal endurance, structural capacity, cost and manufacturing aspects.

A. Chevalier (Paper 17) presented an example of composite structural material applied to a ramjet engine that could be used for a surface-to-surface mission of 30 km, that is to say about 45 s of flight. The objective was to obtain a reduction in production cost of 50% and be sure the composite structure using phenolic resin met the specifications concerning static pressure, dynamic pressure, stiffness and thermal strength. Cutting of air intake port covers by a pyrotechnic chain was another innovative aspect of the engine.

D. Crapiz (Paper 18) described work performed on thermostructural materials that could be used for ramjets with high performance, that is, long range and high speed. SIC-SIC and C-SIC materials have low density and lead to a mass reduction (over 10%) on a missile. They hold high temperature without ablation and can be used for combustors and throats.

Conclusions of Session III

(1) Different types of solid fuel for ramjet engines have been tested according to the needs of the mission. Solid fuel ramjets seem to be ready for application at least for low altitude missions. However, it has been demonstrated that environmental conditions play an important role regarding the choice of the solid fuel. Thus, we recommend studying these environmental aspects as soon as possible at the research level.

(2) Scientific work on combustion instabilities and oscillations has led to some interesting results. It appears also that the mechanisms involved are complex and dependent on many parameters. This illustrates the difficulty in achieving reliable predictive models.

(3) Thermal protection plays a very important part in the realisation of a ramjet combustor. Whilst it is always possible to adapt a thermal protection system to a combustor, we recommend that the design concept of the combustor includes thermal protection and that the whole system be tested and qualified.

(4) Composite materials applied to ramjet engines look very promising – work should be pursued on this topic.

6 SESSION IV – PROJECTILE AIRBREATHING PROPULSION

This Session was chaired by A. Whitehouse and presented three Papers:

Paper 19 by P.J. Elands, E. Dijkstra, R.G. Veraar, P.A.O.G. Korting and R.G. Tieskens concerned a 120mm gun launched

solid fuel ramjet propelled kinetic energy penetrator. Theoretical work was performed with a performance prediction model. Tests were realised with a connected pipe facility. Spinning was not studied.

Paper 20 by P. Petit and B. Boissiere concerned an artillery projectile of 155mm with ramrocket propulsion. A projectile of 43.5kg using an unchoked ducted rocket was designed, tested on the ground and then in flight. Design work was performed for an anti-aircraft 40mm projectile and an anti-tank 120mm projectile.

Paper 21 by R. Mönig and M. Moll was about a 160mm projectile equipped with ramjet or ramrocket engine. Performance simulations were performed for a 50kg projectile. An air-defence kinetic energy projectile (142—160mm, 15—20kg) and an anti-tank ram accelerated kinetic energy projectile (140mm, 20kg) were also considered.

Conclusion of Session IV

(1) Ramjet or ramrocket propulsion should increase velocity, range and accuracy of projectiles and reduce their time of flight. However, use in guns brings constraints on integration (fins), length, withstanding of pressure, acceleration and spin. Ejection at the muzzle is also to be considered carefully. It has yet to be proven that the advantages of ramjet or ramrocket propulsion for projectiles are high enough to warrant advanced research.

7 SESSION V – AERODYNAMICS AND ENGINE INTEGRATION

Five papers were presented in this Session chaired by C. Hirsh.

Paper 22 by P. Champigny and C. Sans described different types of inlet configurations used for projectiles or missiles and digital methods used to calculate the influence on drag and lift. For instance, the drag of a four inlet missile will come from the body (45%), the inlets (40%) and tail (15%). Calculations were also made about the influence of inlet geometry on drag.

Paper 23 by H.L. Weinreich and K. Triesch compared performances of different circular intakes used on an anti-radiation missile of 220mm diameter. Tests were made to evaluate critical pressure, sensitivity to incidence, air mass flow characteristics, external drag and range.

Paper 24 by W.-D. Pohl and E.-O. Krohn presented multiple-inlet configurations for missiles with skid to turn control mode such as an anti-ship missile. Wind tunnel tests were used to compare configurations with four inlets. Experience was up to Mach 2.3.

Paper 25 by C. Richards examined the aerodynamics of side-mounted air intakes for supersonic missiles. Particular emphasis was made of twin intake configurations and four cruciform intakes. Incorporation of forebody vortex control by addition of small strakes was judged favourable to efficiency.

Conclusions of Session V

(1) Aerodynamics of ramjet missiles is complex due to different inlet configurations and integration possibilities. However, prediction models and tests allow good knowledge of in-flight behaviour.

(2) Ramjet and ramrocket propulsion contributes heavily to the design and performance of missiles. Because of this, very close integration, aerodynamics, control and signature should be studied together. So we recommend creating inside research centres and company teams in charge of these three disciplines for which a new name has to be found.

8 SESSION VI – TURBOJETS AND TURBOROCKETS

The first part of the Session was chaired by W. Wagner, the second part by M. Mulero. The seven papers presented had two different objectives:
Turbines for cruise application
Turbojets and turborockets for small missiles.

8.1 Turbines for Cruise Application

Four papers relate to this objective:

Paper 27 by W.H. Reardon and A.J. Cifone described development and qualification of the United States Cruise missile propulsion system.

The program started in 1970 — 5471 engines have been produced under two definitions: F107 and F112. 25,000 hours of tests have been conducted for qualification and development. Missile service interval has been extended from three years to five years; seven and 10 years are considered. Each engine is required to function for 25 hours.

Paper 28 by D.A. Jay and M.R. Dale presented the joint expendable turbine concept demonstrator program for subsonic and supersonic applications. Objectives on the program are −60% on cost, −40% on consumption and +100% on thrust (compared to 1985 level). Four companies have realised engines using new materials (Allison, Garret, Teledyne, Williams) in phase I. Phase II started in 1990 and will foster non-metallic component producibility. Design life is 25 hours.

Paper 30 by J.P. Lopez and C. Mischel described work on an axial quadri-stage compressor for a TRI 60.30 engine. Performance of the new engine has been calculated and confirmed by tests.

Paper 36 by J.M. Stricker and R.E. Quigley III presented a propulsion comparison for future long range supersonic cruise missiles used for different applications: air-to-ground, reconnaissance vehicle, target drone and air-to-air. Different mission profiles were considered, some of them needing subsonic and supersonic flights in sequence which may raise difficulties in the missile geometry.

8.2 Turbojets and Turborockets for Small Missiles

Three papers were presented on this topic:

Paper 32 by J. Lilley described development of a low cost expendable turbojet engine for Non-Line-of-Sight (NLOS) applications which need minimum signature, on-demand thrust variation and competitiveness with solid rockets. Nineteen engines were produced by six contractors and compared under different criteria. Models of seven types of missiles have been developed to assess performance. It has been noted that NLOS has started again at MICOM with a rocket motor, in spite of the interesting work performed on turbojets.

Paper 33 by C. Le Tallec was about development of an air turborocket for a small missile. A prototype engine is to be developed after a modelling phase currently in progress. The air-turbo-rocket should have a low signature, be compact,

flexible and have a reduced cost compared to a turbojet for ranges from 20 to 40km.

Paper 35 by C. Rodgers et al. focused on small expendable turbojets in the 50—150lbf thrust range and predictions of their aerothermodynamic performance. The objective was to identify design variables that could lead to cost saving. Design simplification and use of low cost ceramic materials were some of the avenues suggested.

Conclusions of Session VI

(1) Subsonic turbojets are in service for cruise missile applications and bring full satisfaction.

(2) Supersonic turbojets are considered but should be compared to ramjets for similar applications. More work has to be done to consider development.

(3) Use of expendable turbojets and turborockets for small missile applications will heavily depend on cost reduction in production. Comparison with rocket motors should be pursued.

9 SESSION VII – COMMON TECHNIQUES

Two papers were presented at this Session chaired by M.N.R. Nina:

Paper 37 by P. Hebrard, G. Lavergne, A. Torgue, F. Bismes and G. Heid was about prediction of ramjet and ramrocket combustion performance by isothermal experiments and computation codes. Flow visualisation techniques in combustion chambers are used to feed hydraulic and aerodynamic simulations. The influence of injection conditions was also studied, which led to information on combustion instabilities.

Paper 38 by B. Burdette presented work performed on high energy fuels for airbreathing missiles. Liquid, gel and solid fuels were considered and tested.

Conclusions of Session VII

(1) Realistic prediction of performances is of high importance because it reduces the need for ground experiments and flight tests.

(2) High energy airbreathing missile fuels are well known.

10 RELATION BETWEEN TECHNOLOGIES AND POSSIBLE FUTURE REQUIREMENTS

The Introduction and Keynote Address put emphasis on the possibility of using airbreathing propulsion for future requirements. The chart that follows tries to make a correlation between a type of application, the engine considered and the status of the engine. This work has been done with the information given at the Symposium, which may be incomplete.

The observation that could be made when reading this chart is that the ramjet is very often considered, but scarcely chosen for development. Concentration of research and advanced research on a few of the most promising applications are perhaps to be considered for the future.

11 GENERAL CONCLUSION

This 79th Symposium of the Propulsion and Energetics Panel has demonstrated the very good scientific understanding of airbreathing propulsion technology. This is not so surprising for turbojets which have been in service for some years in quite a number of applications; it is very promising for ramjets that have yet to take the place they should have due to new trends in military requirements.

In this spirit it would have been useful to have had a session on systems with papers comparing different types of ramjet and turbojet for various missions.

Two recommendations could be considered for airbreathing propulsion:

(1) Consider at research level aerodynamics, control and signature reduction as an integrated discipline.

(2) Concentrate research on ramjet propulsion towards the most promising application.

The implementation of these recommendations as well as others included in the report could help airbreathing propulsion to develop in the future.

Application	Engine	status
strategic	**turbojet** supersonic turbojet **liquid fuel ramjet**	fielded (ALCM) simulations ASLP
prestrategic	**liquid fuel ramjet**	fielded (ASMP)
air to air (interception)	rustique VFDR hydrocarbon SFRJ	flight tests (1993) ground tests (1994) ground tests
anti-AWACS	Boron SFRJ	ground tests
air to ground	**turbojet** hydrocarbon SFRJ supersonic turbojet	fielded (Tomahawk,Apache) ground tests simulations
ground to air	rustique	flight tests (1993)
anti-radiation	rustique	flight tests (1993)
anti-ship	turbojet liquid fuel ramjet rustique throttleable ducted rocket	fielded (Otomat, Milas...) ANS (2 flight tests) 5 flight tests ground tests
ground to ground (FOGM)	**turbojet** air-turborocket	development (but no program) simulation
projectile	SFRJ	1 flight test
subsonic target	turbojet	fielded
supersonic target	liquid fuel ramjet supersonic turbojet	8 flight tests (but no program) simulations
UAV (reconnaissance)	turbojet supersonic turbojet	simulations simulations
decoys	?	?

Keynote Address

AIRBREATHING PROPULSION FOR MISSILES AND PROJECTILES: A LOOK AT THE PAST AND THE FUTURE

by

Dr Donald M. Dix
Office of the Secretary of Defense
United States

Airbreathing propulsion for missiles has come a long way. But it still has a long way to go. I thought perhaps it might be fitting to review where airbreathing missiles have been, and project where they might go.

In order to engage in such a review and projection, some framework is desirable. The framework I shall use is to consider advanced technology systems in three generic categories. Category One is composed of those systems for which technical feasibility has not been demonstrated — a hypersonic airbreathing missile is a good case in point. Category Two is composed of those systems for which technical feasibility has been demonstrated, but for which usefulness has not been demonstrated. In military parlance, usefulness is of course synonymous with having a viable mission to perform. With this definition — and speaking only for the United States — an integral-rocket-ramjet-powered missile currently falls in this category. Category Three is obviously composed of systems for which both feasibility and usefulness has been demonstrated — the strategic cruise missile (ALCM) is a good current example. The goal of those of us in the technology business is to advance to Category Three, and once there, improve upon it.

The nature of technology efforts tends to be different in each of these three categories. And it tends to be helpful to recognize in which category you are working. In Category One — technical feasibility not demonstrated — the efforts are purely technological in nature. We try to prove that something will work. This is straightforward. In Category Three — both feasibility and usefulness demonstrated — the efforts are again almost purely technological in nature. We try to make something work "better", where "better" is fairy well defined. These efforts are also reasonably straightforward. The major potential pitfall is that "usefulness" may be only temporary in nature — the buggy whip was useful in its time, but there is no current demand for better buggy whips. However, in Category Two — technical feasibility has been demonstrated, but usefulness has not — the nature of the effort tends to be more diffuse. We try to make something work "well enough," where the definition of "well enough" tends to be elusive. This presents a continual conflict between working to advance the state of technology, on the one hand, and working to convince someone that what is already available is suitable for some military missions, on the other hand. Being in Category Two can be similar to being in never-never land.

With this framework in mind, let's briefly review the history of airbreathing propulsion for missiles. I am told that the first known example of an airbreathing cruise missile was concocted in 1917 by Lawrence Sperry. It was called the aerial torpedo, and was funded by the United States' Navy at a total cost of $50,000. It is reported that this device actually did become airborne, but there seems to be no record of any successful flights. Given the state-of-the-art at the time, it is probably fortunate that airbreathing missiles remained in Category One.

Airbreathing missiles appear to have first emerged from Category One in World War II, with the advent of the V-1 Buzz bomb. There is no doubt that the pulse jet engine, although crude and inefficient, demonstrated the technical feasibility of airbreathing propulsion for missiles. Whether the V-1 also demonstrated usefulness — to a sufficient degree to place this form of airbreathing missiles in Category Three — might be arguable. Although the V-1 had the range, its guidance system, in reality a simple autopilot, provided a rather large circular error probable. On the other hand, the target — London and its suburbs — was rather large indeed.

Not too much more was heard from airbreathing missiles until the 1950s, when the widespread development of nuclear weapons did two things. First, these weapons appeared to solve the accuracy problem associated with land-attack versions of these kinds of missiles. Second, these weapons placed a high premium on long-range air defense. In the United States, a host of airbreathing missiles appeared in this time period: Quail, Mace, Hound Dog, Bomarc, Regulus, and Talos. They were used either as decoys or to expand the "footprint" of manned vehicles. There is no doubt that these systems clearly demonstrated the technical feasibility of both turbine-powered and ramjet-powered missiles, placing them firmly in Category Two. Again, whether these missiles demonstrated sufficient usefulness for a Category Three designation is problematical. In any case, their existence did not spawn much effort to make them better. And they were shortly superseded by longer range ballistic missiles on the one hand, and faster, shorter range rocket-powered missiles on the other hand. If airbreathing missiles ever achieved the status of Category Three in this time period, it was distinctly temporary.

In the United States, airbreathing propulsion for missiles came of age in the 1970s. Small, expendable turbine engines were shown to be feasible. Combined with advances in guidance, and also smaller nuclear warheads in the strategic case, these developments made the air-launched cruise missile, the Tomahawk land attack missile, and the Harpoon anti-ship missile very useful. Of course, the usefulness of the strategic cruise missile has — thankfully — never been

demonstrated in warfare, but the usefulness of the tactical missiles has been so demonstrated. So there is no doubt that subsonic, turbine-engine powered missiles are currently in Category Three. The usefulnes of the increased range has been firmly established, and further enhanced by the increased survivability offered by low signature configurations.

The recent history of supersonic airbreathing missiles, be they ramjet-powered, ducted-rocket powered, or turbine-engine powered, is not quite so dramatic — certainly not in the United States, at any rate. The advanced low volume ramjet (ALVRJ) demonstrated the integral rocket/ramjet concept for a liquid fueled ramjet, and a relative — the advanced strategic air launched missile (ASALM) — was also successfully tested. But the United States never found a need for the increased range at supersonic speeds (as compared to a rocket-powered missile). Since the 1960s, we have worked at various times on integral rocket ramjets for a variety of supposed missions: liquid-fueled ramjets both for anti-air and for targets; solid-fueled, variable flow ducted rockets for anti-air, scramjets for anti-air, solid-fueled ramjets for long range attack and projectile propulsion; and some fledgling efforts on supersonic expendable turbojets. All of these efforts have remained squarely in Category Two. At the moment, the supersonic airbreathing missile that we have that is closest to Category Three is the variable flow ducted rocket being pursued by the Air Force for an upgrade to the advanced medium range air-to-air missile (AMRAAM). But it hasn't made it yet.

Meanwhile of course, in the world outside the United States, at least some supersonic airbreathing missiles would appear to be in Category Three. Our host nation has demonstrated that with the ASMP, and we hear plans for both the ANS and the ARE Our British friends have the Sea Dart and Bloodhound. And of course the CIS has the venerable pair, the SA-4 and SA-6.

So in the 75 years since the first $50,000 investment in Lawrence Sperry's aerial torpedo, it's clear that airbreathing propulsion for missiles has come a long way. It has progressed from an idea far ahead of its time to an idea whose time has come — at least in some areas. However, it must be noted that the only unanimous agreement on the systems that are firmly in Category Three are the turbine-powered subsonic missiles. As you look over the program for this symposium, you will note that the majority of papers concern applications that would be judged — either unanimously or by a substantial body of opinion — to be in Category Two. And of course, the hypersonic airbreathing missile remains in Category One.

What can be said about the future? Projecting the future depends not only on forecasting the state of technology, but also on forecasting the military need and forecasting the opportunities for demonstrating the usefulness of the technology. These forecasts are particularly important to systems in Category Two. With this in mind, I'm going to pass over lightly the turbine-powered subsonic cruise missiles, even though some of you know that I am a strong supporter of the genre. Nevertheless, their usefulness has been demonstrated, the need will continue to exist, and you will hear during this symposium rather specific, quantitative plans to improve their capability.

With regard to military need, there is no doubt that the outlook has changed dramatically since this symposium was initially planned. There is no longer in the foreseeable future a potential for large-scale struggles for national survival. Rather, regional conflicts of uncertain origins pose the greatest threat to world security. And it is likely that these uncertain adversaries will be well equipped. From the United States' view, this means less forward deployment; sharply constrained defense budgets; continued emphasis on deterrence; increased emphasis on power projection; reduced tolerance for both military and civilian casualties, and for protracted conflict; and increased dependence on coalition warfare. Many of these factors apply to all NATO nations, as well.

This new environment has many implications, and I have neither the time nor the qualifications to discuss all of them. To oversimplify a bit, the implications of most relevance here are that future military needs will include weapons with greater accuracy, higher speed, longer standoff ranges, and lower observables, in various mixtures. We can expect the relative emphasis on weapons, as opposed to platforms, to increase as a direct consequence of constrained budgets. The need for greater accuracy, higher speed, and greater stealth arises directly from the need for greater power projection and the desire to terminate hostilities quickly. The need for longer standoff ranges arises directly from the need for greater power projection and the reduced tolerance for casualties. What I've just described is a prescription for those airbreathing missiles and projectiles that are currently in Category Two.

Just in case this philosophical argument is not persuasive, I must point out that in the science and technology arena, the Department of Defense has embarked on seven specific thrusts. Five of these thrusts are of particular relevance here: global surveillance and communications; precision strike; air superiority and defense; sea control and undersea superiority, and advanced land combat. Again, time does not permit a detailed description. But the first thrust is aimed at exploiting the "information explosion" to locate targets quickly and accurately. The other four thrusts are aimed at specific areas of warfighting, and all of them include emphasis on greater weapon stand-off range — for both missiles and projectiles — and quicker response. There seems to be little doubt that opportunities exist for airbreathing missiles and projectiles to satisfy future military needs — and this is good news for those systems in Categories One and Two.

The opportunities for demonstrating technology capabilities appear to be increasing, and this is also good news for systems in Category Two. As many of you know, the United States is instituting a new defense acquisition strategy. Selected features of this new strategy are of particular interest here. To quote from the Secretary of Defense "The end of the Soviet threat . . . enables us to cancel some modernization efforts and to emphasize longer periods for research and development and for testing and proving the value of systems before buying . . . Under the new United States' acquisition strategy, there will be heavy emphasis on government-supported R&D to maintain the technology base. More work will be done with prototypes to demonstrate capabilities and prove out concepts." *(end of quote)* Although there are of course details to be worked out, it is reasonable to infer that there will be opportunities to demonstrate the capabilities of airbreathing missiles and projectiles without first having to demonstrate there is no technical risk.

I suggest that the existence of potential military needs and the opportunity to demonstrate capabilities means we do not need to be distracted in our efforts to advance the state of technology — the peril of being in Categories One and Two.

We need to set aggressive technological goals in order to focus better our efforts in those technology areas which are familiar to everyone in this audience — materials and structures; aerodynamics of inlets; turbine engine componentry; combustion, both subsonic and supersonic; higher energy fuels; and signature control. We should always be able to answer the three basic questions of (1) What are we trying to accomplish; (2) By when; and (3) What difference will it make? This is the quickest way to achieve Category Three status, and I challenge each of you to answer these questions.

Of course, in our quest for Category Three status, we certainly have to maintain frequent and intense contact with the potential user. The persistent issues of the tradeoffs between cost and performance, speed and stealth, and others, need to be clearly understood by all concerned. For example, current lore dictates "low cost" propulsion systems; but a "low-cost" propulsion system that increases the size and cost of a missile required to perform a given mission is not a laudable goal. Fortunately, simulation tools are becoming available that will allow both user and technologist to understand these generic tradeoffs with very little effort. It is up to us to use them, so that the "well-enough" criterion for Category Three is sufficiently well defined.

By the way of summary, I think the prospects for moving the totality of airbreathing propulsion for missiles and projectiles into Category Three are encouraging: the new military missions will exist; there will be opportunities to demonstrate the undeniable capabilities offered; and we have it in our power to move technology forward.

Of course, constrained defense budgets make it even more imperative that we make the best possible use of our collective resources. This symposium is an excellent opportunity to move in this direction. In today's environment, it is only prudent that we, the members of the NATO community, share the lessons learned and the technology to increase the state-of-the-art of airbreathing missile propulsion. The ultimate results are greater deterrence to regional conflicts, and quicker decisive outcomes and far fewer casualties in the event of conflict. Nothing could be more important.

Propulsion par statoréacteur pour missiles dans le domaine Mach 3 à 4,5

Jean-Marie LAURENT
Pascal GARNERO
AEROSPATIALE MISSILES
BP 84 92322 Châtillon Cédex
France

RESUME

L'augmentation de portée et les exigences de pénétrabilité imposent aux missiles de nouvelle génération à voler plus vite et souvent plus haut. La propulsion par statoréacteur se prête bien à ces exigences, mais par rapport aux premières générations de missiles, les spécifications techniques deviennent très contraignantes.

L'exposé ci--après présente les différents aspects concernés : entrée d'air, combustibles, protection thermique de chambre de combustion, moyens de prévision et moyens d'essais.

Les technologies nécessaires aux missiles de la classe Mach 3-4,5 existent, leur industrialisation doit permettre d'optimiser au moindre coût la mise au point de tels missiles.

1. EVOLUTION DU BESOIN ET DES SPECIFICATIONS

Les progrès réalisés dans le domaine des systèmes de détection et de défense conduisent à imposer aux missiles de nouvelles spécifications très contraignantes pour lesquelles les technologies actuellement disponibles sont insuffisantes ou inadaptées.

Parmi tous les paramètres des spécifications de base des missiles actuellement en service, deux ont pris une importance particulière dans le cas des applications longue portée, ce sont :

- l'augmentation de la probabilité de pénétration des défenses adverses et parallèlement la diminution de la détectabilité, ce qui entraîne les spécificités suivantes :

* trajectoires variées avec en particulier des pénétrations finales adaptées : piqué à grande vitesse avec manoeuvres, palier basse altitude grande vitesse avec manoeuvres ...

* possibilité d'éviter des intercepteurs pendant la phase croisière à grand nombre de Mach et haute altitude par la réalisation de manoeuvres à fort facteur de charge

* signature du missile la plus faible possible

- la diminution de la vulnérabilité des plates-formes de lancement, spécialement des avions lanceurs qui demande un allongement conséquent de la portée.

Les principales caractéristiques d'un missile répondant à ces critères sont les suivantes :

* *Mach de vol en croisière entre 3 et 4,5 à des altitudes comprises entre 20 et 30 km*

* *Phase de pénétration finale à grande vitesse et forts facteurs de charge*

* *Grande capacité de manoeuvres à basse et haute altitude*

* *Portée comprise entre quelques centaines et plusieurs milliers de kilomètres*

* *Signature minimale*

La prise en compte de ces exigences a conduit **AEROSPATIALE MISSILES** en étroite coopération avec **l'ONERA** et sous la coordination des **Services Officiels Français**, à définir une nouvelle génération de missiles supersoniques à propulsion par statoréacteur pour lesquels de nombreuses études technologiques sont en cours.

Cet exposé donne les perspectives concernant les travaux sur les statoréacteurs pour missiles longues portées :

- technologies des principaux sous-ensembles concernés, entrées d'air, combustibles, protections thermiques pour chambre de combustion

- moyens de prévision

- moyens d'essais.

Ne figurent pas ici les études relatives à la motorisation des missiles courtes portées qui relèvent essentiellement du mode de propulsion par statofusée.

2. TECHNOLOGIES DES SOUS-ENSEMBLES

Les évolutions des spécifications de besoin ont des conséquences très importantes, quelquefois contradictoires sur des sous-ensembles majeurs du système propulsif . Parmi ces sous-ensembles, trois font l'objet de nombreux travaux de recherche, ce sont :

- les entrées d'air

- les combustibles et les systèmes d'injection associés

- les protections thermiques de chambre de combustion

2. 1. Les entrées d'air

Les entrées d'air sont l'élément capital qui détermine les performances du système propulsif.

En fait, c'est l'association entrée d'air col statoréacteur qui fixe la poussée maximale (manoeuvrabilité) et la consommation minimale (portée).

La figure 1 montre que les domaines qui répondent à ces deux spécifications principales n'ont pas forcément de secteurs en commun et que pour répondre de manière idéale au besoin, une variation de la géométrie des entrées d'air et de la tuyère est nécessaire.

De plus, une tuyère variable permettrait :

- d'orienter la poussée par exemple avec une tuyère bidimensionnelle.

- de servir éventuellement de tuyère pour l'accélérateur intégré, ce qui éviterait toute éjection de pièce lors de la phase de transition.

Contrebalançant tous ces avantages, la complexité introduite par une tuyère variable, surtout du fait de la présence de l'accélérateur intégré, fait que ce principe n'est actuellement pas retenu comme prioritaire.

Les entrées d'air à géométrie variable ont donc été étudiées ; les difficultés techniques proviennent essentiellement de l'ambiance thermique élevée due à l'échauffement cinétique. La complication qu'elles introduisent et surtout le surcoût de prix déciderait suivant les applications de retenir ou non cette technologie.

Quant à la spécification de signature minimale, les entrées d'air pouvant être une des sources d'augmentation de signature, de nombreux travaux portant sur les matériaux, les formes et la position sont en cours.

2.2. Les combustibles et les systèmes d'injection associés

Pour le type de missile considéré, les variétés de trajectoires envisagées et en particulier les différences d'altitude, imposent l'utilisation d'un combustible liquide pour atteindre un rapport de débit suffisant.

Trois types de carburant peuvent être envisagés, leurs principales caractéristiques sont résumées ci-après :

	Kérosène	Carburant synthèse	Boue au bore
d : densité	0,78	1,04	1,25
Is : Impulsion spécifique (Mach 2) (s)	1670	1560	1700
d * Is	1300	1620	2125

Le produit densité x impulsion spécifique est représentatif de la compacité énergétique du carburant et à encombrement constant, l'augmentation de dxIs permet d'accroître la portée dans les rapports suivants :

	Kérosène	Carburant synthèse	Boue au bore
d * Is / Réf.	Réf.	+ 24,6%	+ 63,5%
Portée / Réf.	Réf.	+ 12,7%	+ 49,3%

L'emploi des boues au bore semble être très prometteur pour allonger de manière significative la portée, mais son utilisation opérationnelle nécessite le développement de techniques spécifiques de mise en oeuvre et d'injection.

En effet, pour éviter dans le temps les phénomènes de décantation, au carburant composé d'un mélange de kérosène ou de carburant de synthèse avec des particules de bore, on ajoute un additif donnant au produit des propriétés thixotropiques.

Ces propriétés très intéressantes pour le stockage et même la vulnérabilité amènent à développer des technologies relatives au pompage du carburant pour lui donner une fluidité suffisante pour son transfert.

De plus, les particules de bore hautement énergétiques sont difficiles à initier en combustion et demandent l'emploi d'injecteurs spécifiques permettant une répartition optimum dans la chambre de combustion.

En parallèle de ces difficultés technologiques, les trajectoires de très longue durée à des vitesses élevées augmentent par échauffement cinétique de manière significative la température des réservoir et circuit carburant.

Pour se prémunir de tout effet de vaporisation ou d'ébullition nucléaire le long des parois, la circulation du carburant se fait à forte pression, nécessitant d'adapter les injecteurs pour conserver des courbes de débit compatibles avec la régulation de la combustion.

2. 3. Protections thermiques pour chambre de combustion

Dans leur grande majorité, les protections thermiques internes (PTI) des chambres de combustion de statoréacteurs modernes sont à base de matériau élastomère moulé directement dans les structures de la chambre.

Le principe de l'isolation repose sur une dégradation (pyrolyse puis carbonisation) progressive qui pour les temps de fonctionnement actuellement requis, permet de maintenir les structures à des températures acceptables (< 600 C) avec des épaisseurs raisonnables (< 10 mm).

Du fait de l'augmentation conséquente des temps de fonctionnement, la PTI doit permettre un équilibre thermique supportable par les structures et ceci en régime permanent.

Les principales difficultés liées à ces nouvelles applications sont de concilier les deux impératifs suivants :

- compatibilité avec l'accélérateur intégré générant des pressions pouvant atteindre 150 bar

- fortes sollicitations thermomécaniques lors de la phase finale de pénétration

Pour répondre à ces exigences, **AEROSPATIALE MISSILES** travaille sur deux axes :

- les protections thermiques à renforts structurés tridimensionnels

- le refroidissement pariétal

2. 3. 1. *Les protections thermiques structurées*

Le choix des matériaux et de l'architecture correspondante dépend en premier lieu de la compatibilité avec l'accélérateur. Outre la nécessité de bonnes caractéristiques de collage propergol/PTI, les propriétés mécaniques de la protection conduisent à des solutions qui peuvent être classées en deux grandes catégories :

* la PTI possède pendant la phase initiale de l'accélérateur un allongement suffisant (> 1%), dans ce cas, les efforts de pression internes peuvent être repris en totalité ou partiellement par la structure externe.

Des solutions à matrice élastomère ou rigidimère peuvent être utilisées avec une structure interne tridimensionnelle permettant d'obtenir, après dégradation éventuelle de la matrice, une coque rigide suffisamment résistante pour soutenir à elle seule les contraintes de la phase finale

* la PTI ne possède pas l'allongement nécessaire ni les propriétés mécaniques suffisantes, dans ce cas l'architecture doit permettre de limiter les efforts sur la protection, par exemple en pressurisant l'interstice entre la PTI et la structure. L'utilisation de céramiques armées est alors possible en couche pare-flammes

L'architecture de ce type de protection doit prendre en compte tous les problèmes de dilatations différentielles qui évoluent au cours de la trajectoire, quelque fois de manière contradictoire.

Les principaux avantages de ces solutions sont :

- le collage relativement aisé du propergol

- la complexité d'ensemble faible ou limitée

2. 3. 2. *Le refroidissement pariétal*

Bien connu pour son application dans les chambres de combustion de turboréacteurs, le refroidissement pariétal consiste à injecter le long de la paroi de la chambre un film d'air qui bloque les échanges thermiques entre la flamme et la structure.

Séduisant dans son principe, plus complexe à mettre en oeuvre que les protections thermiques, les recherches sur ce concept font l'objet d'une étroite collaboration entre l'**ONERA** et **AEROSPATIALE MISSILES**.

Deux types de matériau peuvent être utilisés :

- tôles multiperforées, la répartition des perçages est issue d'études de cartographies thermiques en tenant compte des évolutions de cette cartographie suivant les phases de trajectoire.

Ce concept permet d'obtenir un très bon compromis entre la résistance structurale de la chambre et l'efficacité de refroidissement

- tôles poreuses obtenues par frittage ; solution optimale du point de vue du refroidissement avec un rendement très proche de 1, la tenue à la pression interne du fait de la faible résistance mécanique du matériau en traction et en compression impose la mise en place d'une coque métallique de soutien. De plus la différence de pression nécessaire à l'injection d'air est plus importante que dans le cas des tôles multiperforées.

Les principaux avantages de ces solutions sont :

- aucune limitation de temps de fonctionnement

- température de paroi externe sensiblement égale à la température athermane de vol

Cependant la présence de l'accélérateur intégré complique l'architecture et demande l'interposition d'un liner entre la surface interne de la structure et le propergol.

3. MOYENS DE PREVISION

Les phénomènes physiques complexes apparaissant dans le système propulsif des missiles à statoréacteur et l'absence de moyens de calculs efficaces nécessitaient, dans le passé, l'adoption d'une méthodologie basée principalement sur une approche empirique incluant des phases expérimentales longues et coûteuses.

L'utilisation exclusive de moyens expérimentaux ne suffit plus aujourd'hui, en terme de temps et de coût, pour définir et optimiser les nouvelles configurations.

Aussi, grâce aux progrès récents des technologies informatiques et des méthodes de calcul numérique, un changement de méthode de travail est apparu. Il est maintenant possible de simuler numériquement les écoulements tridimensionnels sur l'avant-corps, dans la prise d'air, dans la chambre de combustion et dans la tuyère de ces missiles.

AEROSPATIALE MISSILES a donc beaucoup investi dans la mise au point de codes de calcul, en coopération avec des laboratoires de recherche (**ONERA**, Laboratoire de combustion **EM2C** de l'Ecole Centrale de Paris ...), ainsi que dans l'acquisition de moyens informatiques puissants de façon à compléter sa méthodologie de travail.

Les outils de calcul composés de codes tridimensionnels Euler et Navier-Stokes moyennées ainsi que de logiciels de maillage sont des aides à la conception complémentaires aux essais en soufflerie.

3.1. Outils opérationnels

L'analyse numérique de l'évolution du tube de courant traversant le système propulsif d'un missile à statoréacteur débute par le calcul de l'écoulement autour de l'avant-corps. Les valeurs locales de la pression totale, du nombre de Mach, de l'incidence et du dérapage au droit de la prise d'air ainsi que le débit capté et la hauteur de la couche limite sont à déterminer afin d'optimiser la position et la géométrie du piège à couche limite externe ainsi que de la prise d'air avec sa carène et ses flancs.

Les outils numériques utilisés se composent d'un code de calcul Euler couplé éventuellement avec un code de couche limite, tridimensionnels, et d'un code P.N.S (Navier-Stokes Parabolisées) comportant un modèle de turbulence de type Balwin-Lomax. Le code PNS est principalement utilisé pour affiner, dans le cas des configurations supersoniques, la détermination des effets visqueux, en particulier les tourbillons d'extrados et les décollements de couche limite sur l'avant-corps.

La figure 2 présente la répartition du coefficient de pression sur un missile à statoréacteur obtenue à l'aide d'un code Euler ainsi que la trace du maillage sur le corps du missile.

La figure 3 présente schématiquement le phénomène d'interaction des tourbillons d'extrados d'un missile en incidence avec ses prises d'air ainsi qu'une comparaison calcul PNS / essais pour l'étude de cette interaction.

L'évolution du tube de courant jusqu'à l'entrée de la chambre de combustion est ensuite étudiée à l'aide d'un code Euler tridimensionnel multidomaine capable de calculer des géométries complexes avec piège à couche limite interne et obstructeur en fin de diffuseur simulant l'obstruction de la chambre de combustion. Ce type de simulation permet de déterminer avec une bonne précision la courbe caractéristique des prises d'air pour l'ensemble des fonctionnements possibles, du supercritique au subcritique, dans le cas où les interactions choc/couche limite ne sont pas prépondérantes [cf. figure 4]. La prise en compte du piège à couche limite dans ce type de calcul permet de simuler correctement la perte de débit due au piège et le déplacement correspondant du choc droit terminal mais ne permet pas une analyse précise de l'écoulement dans le piège lui-même qui est le siège d'importants effets visqueux.

Dans le cas où les effets visqueux deviennent prépondérants dans le diffuseur, l'analyse s'effectue à l'aide d'un code Navier-Stokes bidimensionnel muni d'un modèle de turbulence algébrique. Ce code permet de prendre en compte les interactions choc/couche limite et de simuler correctement la structure de l'écoulement capté par le piège à couche limite interne (cf. figure 5).

L'étude numérique du fonctionnement des chambres de combustion s'effectue actuellement suivant deux phases :

- Une première phase pour le calcul de l'écoulement *réactif supposé prémélangé* à l'aide d'un code tridimensionnel Navier-Stokes développé par l'**ONERA** utilisant un modèle de combustion de type Flamme-Cohérente développé par le Laboratoire de combustion **EM2C** de l'Ecole Centrale de Paris. Cependant du fait du temps de calcul élevé en tridimensionnel, un balayage en richesse n'est pas encore possible, ce qui nécessite le passage à la deuxième phase. A titre d'exemple, la figure 6 présente une comparaison calcul/essai au niveau de la visualisation, du champ du terme source dans la chambre d'étude bidimensionnelle avec deux entrées d'air latérales du laboratoire **EM2C.**

- Une deuxième phase permet de prendre en compte la cinétique du kérosène à l'aide d'un code de calcul de chimie complexe avec 19 espèces et 360 équations ainsi que l'injection du carburant liquide. Cet outil de calcul du rendement de la chambre de combustion, permet un balayage complet en richesse à partir d'une décomposition de la chambre de combustion en réacteurs bien mélangés dont la description est définie par l'utilisateur à partir des résultats issus de la première phase.

Enfin, l'écoulement dans la tuyère est étudié avec un code Euler tridimensionnel, mono ou bi-espèce, qui permet d'étudier éventuellement la confluence avec l'écoulement extérieur, pour les tuyères à déflexion notamment.

3.2. Outils en cours de développement

Dans la stratégie de mise au point de codes de calcul aptes à l'étude des missiles à statoréacteur, l'activité est principalement consacrée à l'amélioration de nos outils pour une meilleure prise en compte de la physique ainsi que pour des études spécifiques.

Pour le calcul du fonctionnement des entrées d'air, on compte poursuivre l'adaptation du code Navier-Stokes bidimensionnel, en particulier pour le calcul des configurations subcritiques afin d'étudier le déclenchement du pompage aérodynamique. Des travaux Navier-Stokes tridimensionnels sont également prévus pour traiter des géométries fortement tridimensionnelles.

Pour l'étude des chambres de combustion, les efforts portent sur les écoulements diphasiques, sur l'adaptation du modèle de combustion à la combustion du kérosène et sur la réduction du temps de calcul. Ainsi le calcul complet permettant d'obtenir le rendement de combustion et la perte de charge pourra être réalisé avec ce code pour différentes richesses injectées. La prédiction des limites de fonctionnement du moteur est un des buts à atteindre.

Le même outil de calcul pourra également traiter l'écoulement dans les tuyères ce qui permettra de prendre en compte la cinétique chimique.

En mettant en oeuvre des outils numériques adaptés à l'étude de ses statoréacteurs, **AEROSPATIALE MISSILES** se donne des moyens d'aide à la conception complémentaires aux expérimentations en soufflerie.

Cette méthodologie doit permettre d'analyser et d'optimiser plus rapidement et à moindre coût les configurations nouvelles de missiles aérobies.

4. MOYENS D'ESSAIS

La mise au point des chambres de combustion pour des domaines de vol très étendus nécessite encore un nombre d'essais important de façon à couvrir de manière systématique l'ensemble du domaine et de pouvoir évaluer les marges disponibles.

Les essais au banc permettent également de tester et de développer tous les sous-ensembles associés : entrée d'air, régulation, protections thermiques, séquence de transition ...

De plus avant les essais en vol, la cohérence de tous ces sous-ensembles doit être vérifiée par des essais de synthèse mettant en jeu tous les éléments du système propulsif.

Le moyen d'essais spécifique statoréacteur doit donc permettre de réaliser aussi bien des essais "simples" de combustion, que des essais mettant en oeuvre quasiment le missile complet.

C'est pourquoi **AEROSPATIALE MISSILES** s'est doté depuis 1978 au Subdray d'une soufflerie à rafale répondant à toutes ces exigences y compris celles correspondant aux nouveaux besoins, en particulier :

- domaine de simulation Mach > 4,5

- stockage d'air compatible avec la simulation de trajectoires très longue portée

Les principales caractéristiques de ce moyen sont :

- trois lignes de test permettant des essais en

* conduite forcée

* jet semi libre

* jet libre pour des diamètres inférieurs à 200 mm

- possibilité d'enchaîner toutes les phases de fonctionnement : accélérateur intégré, séquence de transition, statoréacteur

- réalisation de simulations de trajectoires avec une précision inférieure à 1 %

- caractéristiques de la génération d'air :

* débit maximal : 300 kg/s

* pression maximale : 80 bar

* température maximale : 1100 K

- limites actuelles du domaine simulé :

* Mach : 4,7

* altitude : 33 km

De nombreuses extensions sont en cours avec en particulier une adaptation du superstatoréacteur pour les applications hypersoniques.

5. CONCLUSIONS

A partir de l'expérience acquise en particulier lors du développement du missile ASMP, et avec la collaboration de l'**ONERA, AEROSPATIALE MISSILES** dispose pour la propulsion par statoréacteur de technologies éprouvées qui permettent de répondre aux exigences d'un missile de croisière supersonique longue portée.

Pour les applications à très longue portée et très grande vitesse, les études technologiques sur les principaux sous-ensembles du statoréacteur montrent la faisabilité de missiles ayant un nombre de Mach de croisière pouvant atteindre 4,5.

Ces nouvelles technologies, maintenant disponibles, seront à la base d'une nouvelle génération de moteur ; elles sont à industrialiser pour obtenir un système propulsif opérationnel.

Au delà de ces vitesses de croisière, dans le domaine de l'hypersonique, des études amont sont déjà engagées en particulier sur les technologies du superstatoréacteur, les moyens de prévision et d'essais associés.

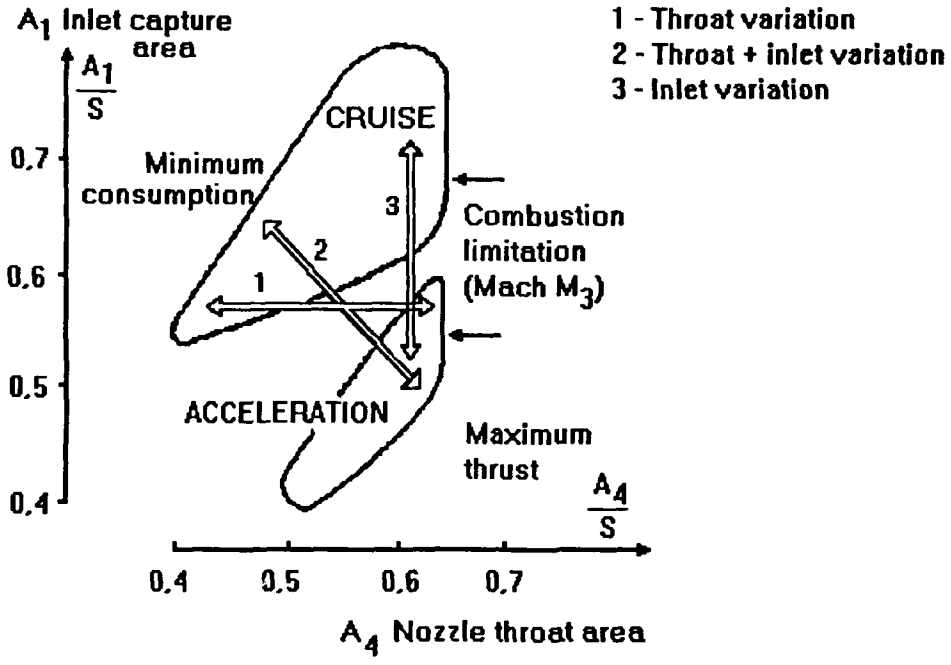

Planche 1

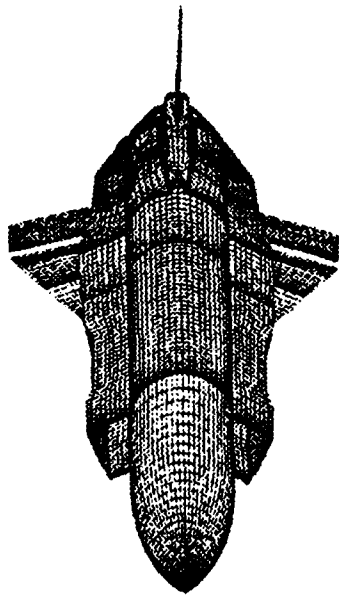

MAILLAGE SURFACIQUE

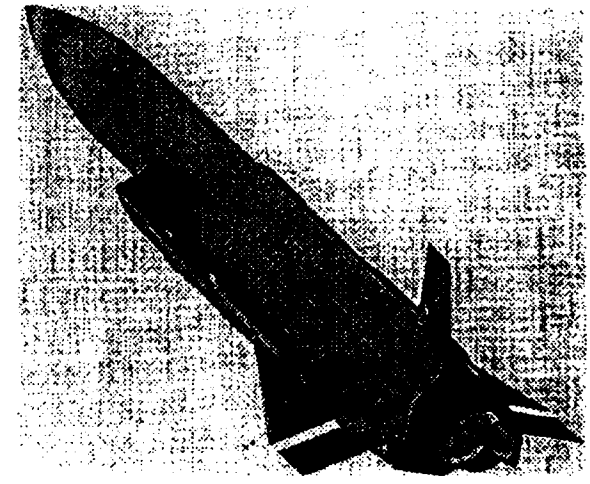

REPARTITION DU COEFFICIENT DE PRESSION

CALCUL EULER 3D D'UN MISSILE A STATOREACTEUR
M = 3,5 α = 5°

Planche 2

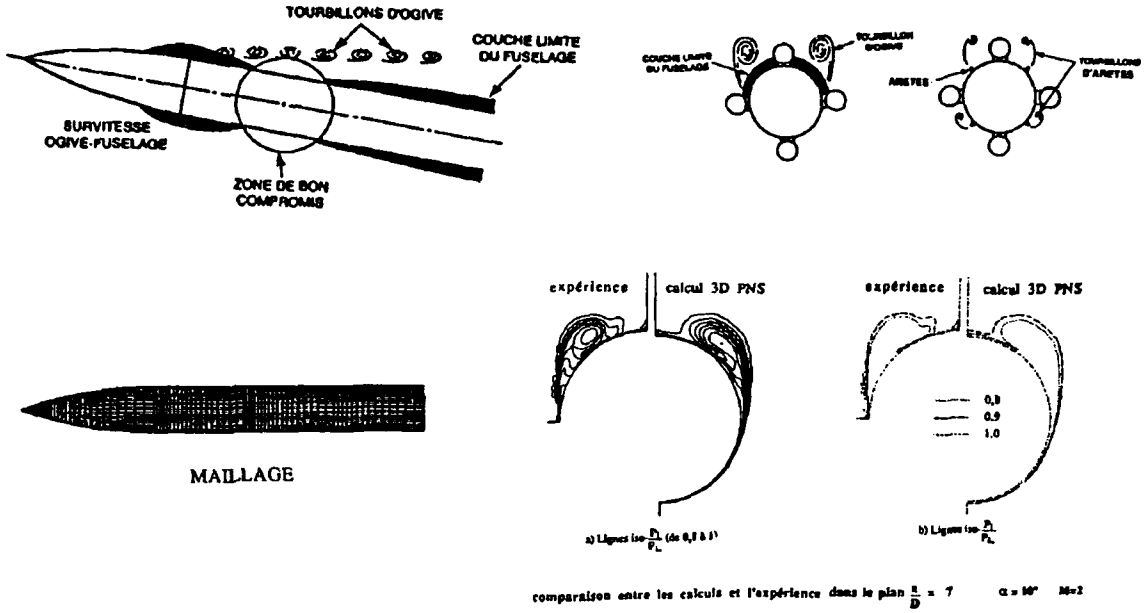

comparaison entre les calculs et l'expérience dans le plan $\frac{x}{D} = 7$ $\alpha = 16°$ $M=2$

INTERACTION ECOULEMENT EXTERNE / ENTREES D'AIR
SUR UN MISSILE EN INCIDENCE

Planche 3

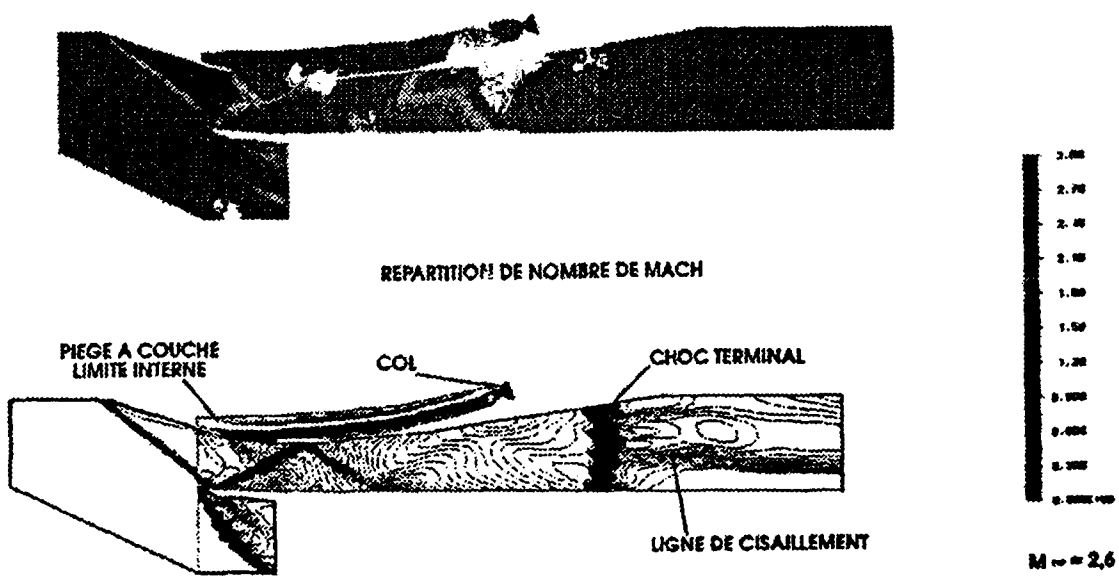

LIGNES ISO - NOMBRE DE MACH
$\Delta = 0,02$

CALCUL EULER 2D D'UNE PRISE D'AIR SUPERSONIQUE DE STATOREACTEUR

Planche 4

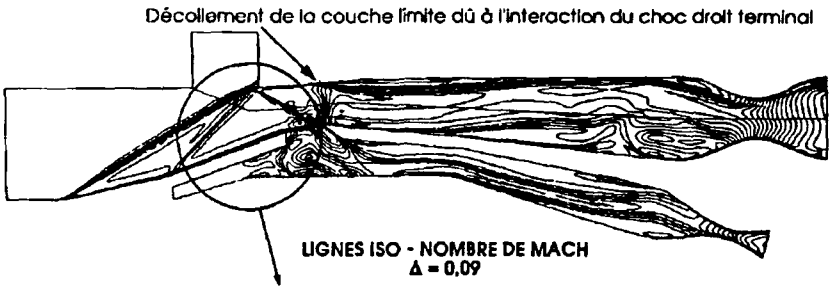

PROFILS DE VITESSE AU NIVEAU DE L'ENTREE DU PIEGE A COUCHE LIMITE INTERNE

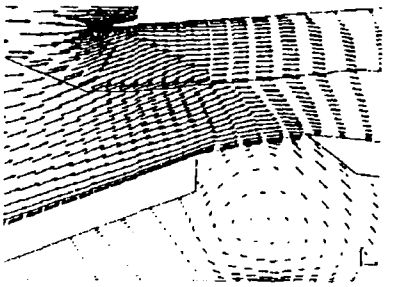

CALCUL NAVIER-STOKES MOYENNE BIDIMENSIONNEL
PRISE D'AIR SUPERSONIQUE M3 AVEC COLS EN FIN DE DIFFUSEUR ET EN FIN DE PIEGE A COUCHE LIMITE

Planche 5

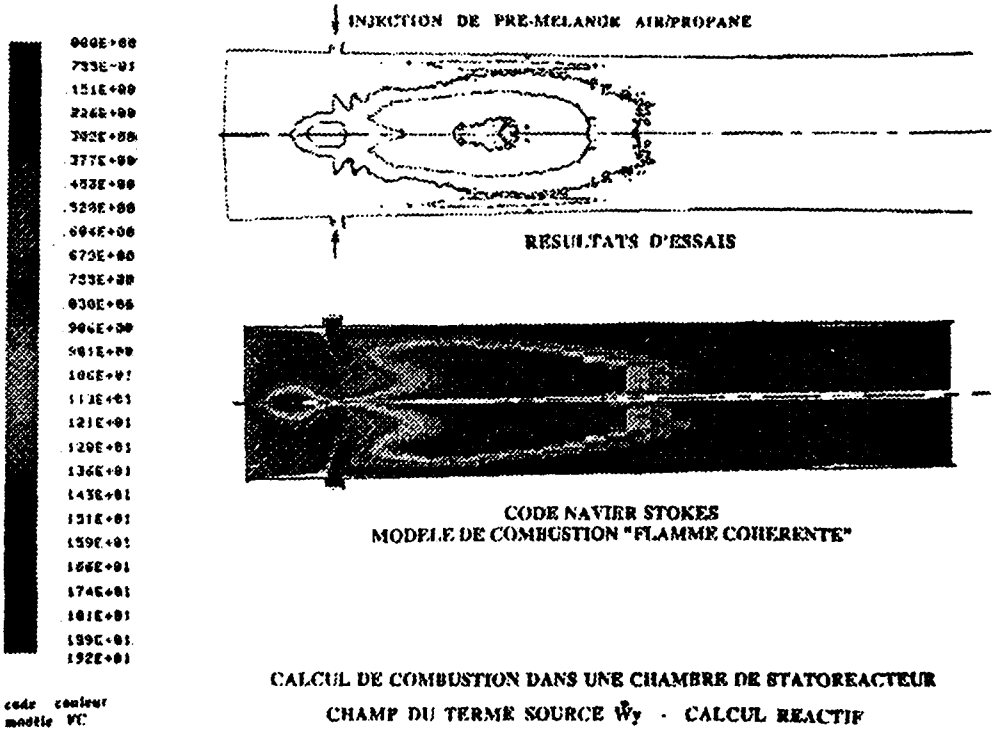

CALCUL DE COMBUSTION DANS UNE CHAMBRE DE STATOREACTEUR
CHAMP DU TERME SOURCE $\dot{W}_y$ - CALCUL REACTIF

Planche 6

Discussion

Question from Dr M.G. PHILPOT, DRA Farnborough UK

I was interested in the use of film cooling in the ramcombustor. Does this approach require new liner materials or can existing alloys be used ?

Author's reply

No, the selected materials have already been developped for other applications. The problems that have been solved concerned mainly the architecture of the porous materials along the combuster in order to maintain their efficiency during the whole flight.

POTENTIAL MISSILE FLIGHT PERFORMANCE GAINS FROM IMPROVEMENTS TO THE PROPULSION SYSTEM

M S Ivey and R K Oldham

Air Vehicle Performance Department
Defence Research Agency
Pyestock, Farnborough,
Hampshire, GU14 OLS, UK

SUMMARY

Future developments in the propulsion of ramjet powered missiles will aim to widen the launch envelope, extend the operating range and lengthen the period of powered flight to give a more potent terminal manoeuvre phase. In this paper, some of the possible methods of achieving these aims have been critically assessed for typical stand-off and air-to-air missiles. For both types of missile, the use of a high density fuel for the main propellant would produce quite significant performance gains but storage and plume visibility problems have to be overcome. Gains can also be made for both missiles by optimising the relative amounts of boost and main propellant to match the required launch envelope. The benefits of inlet and exhaust variability have been explored for the stand-off missile. The latter option is the more favourable prospect for range enhancement but the design of a low pressure loss variable mechanism will be difficult. The range of the air-to-air missile depends primarily on its launch Mach number and the range can be further increased by using a highly lofted trajectory with an unpowered terminal phase. The maximum and minimum fuel flow rates needed for this missile are related to the altitude limits of its flight envelope.

1. INTRODUCTION

Guided missiles which fly at high supersonic speeds have the choice of either a pure rocket or a ramjet propulsion system. The principal advantages of a pure rocket are simplicity, small size and lack of any requirement for an air inlet duct. By comparison, the advantages of a ramjet engine are related to its high specific impulse and thrust control. Hence ramjet propulsion is most suitable for stand-off missiles where long range coupled with a high cruise Mach number are prime requirements. Another important potential application for ramjets is in air-to-air missiles intended for beyond visual range (BVR) combat. The low fuel consumption considerably increases fly-out range, with power sustained all the way to the target. Furthermore, the controllability of the ramjet engine, provides a wide flight envelope and enables the missile to manoeuvre without loss of energy. As a result the ramjet powered missile will be much more able to follow and successfully attack a manoeuvring enemy aircraft. Ramjets can also be used for other types of weapon (such as long range surface-to-air missiles) but this paper concentrates on their application to air launched vehicles.

In the Defence Research Agency (DRA) at Farnborough, we are seeking to quantify the possible future performance gains that might be obtained from ramjet powered stand-off and air-to-air missiles. Two datum vehicles have been conceived which are representative of the likely geometry and performance of each type. Complete missions and important phases of the flight of these datum vehicles have been explored using a trajectory simulation program which includes a one-dimensional model of the propulsion system.

The potential improvement features considered so far in this study have focussed on launch conditions, boost motor sizing and the use of high energy fuels. Optimisation of the flight trajectory of air-to-air missiles has been examined and some consideration has been given to the possible use of variable geometry in the larger stand-off missile.

2. THE TRAJECTORY SIMULATION PROGRAM

The computer code used in this study was originally developed at the Wright Laboratory of the USAF and calculates the complete missile trajectory, given its launch conditions, guidance laws and control logic. The prediction is done with a three-dimensional, point mass, flight and mission simulation routine using vehicle aerodynamic data from flight condition dependent look-up tables. The total flight profile is defined by a series of events, each of which represents a discrete phase of the missile flight. Both guidance and propulsion events are specified for the missile and each event is terminated when the input value of a prescribed variable is reached (eg altitude for a guidance event or missile weight for a propulsion event). Information is also specified for the motion of the launch and target aircraft.

The code represents the missile propulsion system in the form of a one-dimensional performance model which is capable of handling both liquid fuelled ramjets and solid fuelled, air breathing ramrockets. In addition, the propulsion model can also simulate the performance of pure rocket motors (in this case only used for the boost phase at the start of the missile flight). During each propulsion event, limits can be set on the fuel flow rate, fuel/air ratio and the proximity of the intake to its critical operating condition. Intake performance, based on the flight Mach number and vehicle incidence, is obtained from input data files. These files give the critical pressure recovery and capture area ratio of the intake derived either from flow predictions or wind tunnel tests. Fluid properties and the combustion temperature rise are determined from another set of look-up tables for the particular ramjet fuel being used.

3. STAND-OFF MISSILE PERFORMANCE

A schematic diagram of the datum vehicle showing some of its major components is presented on Figure 1. The missile is optimised for low level launch at 0.85 Mach number, climb to high altitude, cruise supersonically and then to make a powered dive onto the target. The datum missile is assumed to be of cylindrical cross-section with four variable fins at the rear to give

extra lift and provide motion control. In order to make a stealthy approach to the target, the missile has a single air intake wrapped around its upper surface. A low critical pressure recovery is assumed for the intake in order to allow for the compromised shape needed to produce its stealthy characteristics.

A solid rocket boost motor is cast into the ramjet combustion chamber and this motor is assumed to operate for about six seconds after the missile is fired from the launch aircraft. When the rocket burns out, there is a rapid pressure drop in the ramjet combustion chamber which triggers the release of the booster nozzle and the air inlet port covers. Sustain fuel is then injected and combustion with the intake air supply commences. Different sets of aerodynamic characteristics are used for the two vehicle flight modes, ie boost and air breathing phases.

Developments of such a stand-off missile can have several aims, eg a higher altitude trajectory, longer range or the ability to make more avoidance manoeuvres during target approach. This paper concentrates on possible approaches to increasing the operating range whilst retaining the same datum flight trajectory. For most of the improvement techniques considered, the overall external geometry of the datum missile is held constant and so its aerodynamic characteristics remain the same.

3.1 Effect of amount of boost

After being launched at low altitude, the booster motor accelerates the vehicle in level flight up to a transition Mach number of 2.37. About half of the available liquid fuel is then burnt during the climb up to high altitude and the remainder is consumed during the cruise and final dive. One possible method of extending the missile range whilst retaining its external dimensions is to have less boost fuel and make use of the volume saved to increase the size of the liquid fuel tank. In the datum missile the liquid fuel tank and the combustion chamber containing the boost fuel have almost identical volumes. Any volume transfer implies a reduced ramjet chamber length which might affect the efficiency and stability of the combustion process. However, the size of the chamber will in general be determined by the need to have a sufficient storage space for the boost propellant rather than a minimum length for efficient combustion in the air breathing mode. It is the trade-off between booster fuel and sustain fuel masses that it is of interest here.

The effects of this fuel transfer on missile range are presented on Figure 2 for a range of launch Mach numbers and the resulting end of boost Mach numbers for each case are plotted on Figure 3. At the datum launch Mach number of 0.85, a maximum range increase of 9% can be obtained by a 15% reduction in the volume of the boost fuel which allows a corresponding increase in the volume of sustain fuel. The lower density of the liquid fuel means that the mass transfer is not even but there is a slight benefit from the reduced missile launch weight. With a 20% volume transfer, the end of boost Mach number is reduced to 2.13 and a considerable amount of liquid fuel (about 15% of the total mass) is used in further accelerating the missile before it can start the climb. The ramjet is operating very inefficiently under these conditions and further transfer between solid and liquid fuels leads to the situation where the end of boost Mach number is so low that the missile cannot produce sufficient thrust to accelerate away.

Figures 2 and 3 also show the effect of a 5% fuel volume transfer in the opposite direction. The transition Mach number increases to 2.41 but this only produces a small saving in the fuel needed to complete the climb. The volume transfer reduces the total mass of liquid fuel by nearly 5% which results in a 7% loss of range.

The effect of launching at Mach numbers of 0.60 and 0.75 is also shown on Figure 2. For the datum missile there is a 12% range deterioration if the launch is at 0.6 Mach number. As previously, the explanation concerns the extra amount of liquid fuel needed to accelerate away from the lower transition Mach number of 2.23. If fuel volume is transferred at the lower launch Mach numbers, there is initially a small improvement of range but the benefit rapidly disappears beyond about 5% boost reduction. Hence it seems that a boost to liquid fuel exchange would only be attractive if the missile will always be launched at the higher Mach number, when a shift of around 15% in the volume balance would give the optimum result.

3.2 Effect of using high density fuel

Much work has already been done on the development of high density fuels for ramjets because of the obvious performance benefits which they offer. The sustain fuel in the datum missile has been assumed to be RJ6 which is one of the highest density liquid fuels currently available. In order to make further gains from increasing the fuel density, one possibility is to use a slurry made up from a metal powder dissolved in a liquid hydrocarbon. Of the possible metals that could be chosen, boron has the highest volumetric heating value (about four times that of a jet engine fuel like JP4). In order to illustrate the potential improvements, trajectory calculations were done for the datum missile using boron slurries of various strengths as the sustain fuel. As shown in the following table, results were obtained for two conditions, ie assuming a constant volume fuel tank or allowing the tank size to vary to keep the same datum range.

Effect of using boron slurry for sustain fuel			
Boron loading (by weight)	50%	60%	70%
Constant volume fuel tank			
% Range increase	7	23	44
% Missile weight increase (at launch)	2	5	7
Fixed range			
% Missile length reduction	1	4	7

These results show that a large range improvement can be achieved if it is possible to use fairly high concentrations of boron. Also the significant range benefit from using a 70% boron slurry is little affected by the 7% increase in overall missile launch weight. As seen in the table, the alternative approach of keeping range fixed and using the fuel change to reduce missile length has only a small effect and the corresponding weight reduction is not shown but turns out to be minimal (less than 2%).

The potential range increase for a fixed size could be very attractive if this was an important goal. However, the difficulties of using a slurry type of fuel are considerable and get worse with a higher metal fraction. There are three major problem areas which have to be overcome:-

i The fuel system (valves, pump and injectors) have to be able to cope with the metal particles and thixotropic nature of the slurry.

ii The exhaust plume from a ramjet engine burning a slurry fuel is highly visible, both optically and using Infra-red detection.

iii The suspended metal particles tend to settle out and solidify with time, so it will be difficult to meet the long term storage requirements of most missiles.

While research could probably overcome the handling and storage difficulties of slurry fuels, the observability aspect is more intractable. However this may be less important in some applications, in which case high density fuels offer quite a promising route for further missile development.

3.3 Effect of variable geometry intake

If the intake capture area is increased and no other constraints are applied, the ramjet fuel consumption reduces, which improves the missile range. This result occurs because flow within the ramjet is controlled by the choking conditions in the exhaust nozzle (throat area A_5).

$$Q\sqrt{T_4}/A_5P_4 = \text{a constant (depending only on the gas properties)}$$

The mass flow Q increases with the larger capture area causing the combustion chamber pressure P_4 to increase so that the intake operates with a higher pressure recovery. The combustion temperature T_4 can then be lower to give the required thrust, due to the increases in the mass flow and nozzle exit Mach number, and less fuel is therefore burnt.

The top limit to this method of range improvement comes from the need to prevent the terminal shock from being expelled from the front of the intake. In this sub-critical mode of operation, some of the air compressed by the shock system spills over the intake cowl causing an increase in vehicle drag and possibly leading to flow instability (buzz). As the capture area is increased, the intake operating point moves closer to the critical condition until eventually the pressure margin (difference between the operating intake pressure recovery and its critical value) reaches a set limit. When this occurs, P_4 cannot increase any further, so the mass flow reaches a fixed value given by the throat choking condition. With the nozzle mass flow and upstream pressure both being fixed, the available thrust also reaches a limiting value.

During high altitude cruise the intake is operating with a pressure margin of about 26%, ie well clear of the critical condition. There is plenty of margin for increasing the capture area during this phase of the flight with some gain from the lower fuel consumption. Figure 4 shows the effect of using a variable geometry intake where the capture area is increased at the start of the cruise leg (capture area held at the datum value for launch and climb). A capture area increase of about 35% is possible before the intake pressure limit is reached and there is insufficient cruise thrust. The increase of range only rises to about 7% for a significant increase of capture area.

The datum missile is designed such that the thrust limit is first met at the start of the climb. The combination of the low altitude air conditions and the missile event command to accelerate up to its cruise Mach number creates a high thrust requirement and the intake is on its pressure margin limit for the first 2000 m of the ascent. If the intake capture area were to be increased 10%, the intake would hit its pressure margin limit a few seconds earlier, so the fuel supply would have to be reduced, creating less thrust and a less rapid acceleration. The lack of thrust would be further accentuated by the lower inlet compression and the missile would have to climb to 7000 m before the pressure margin limit was overcome. If the capture area were to be opened any further, the pressure limit would force the fuel flow to turn down even more and there would not be enough thrust to make the climb. If the intake capture area of the datum missile is increased by 10% for all of its flight, an 11% range enhancement is obtained following a launch at 0.85 Mach number (as shown by the dashed line on Figure 4). However this benefit almost disappears if a wide launch envelope is required. At a launch Mach number of 0.6, more thrust is needed to accelerate away from the post-boost conditions. This increased thrust can just be produced with the capture area opened 5% but the missile slows down if further variability is attempted.

If both the climb and cruise phases of the flight are optimised and launch conditions are ignored, then a maximum range improvement of about 14% is achievable as seen on Figure 4. The intake capture area would need to be opened 10% for the climb and 30% for cruise, each geometry change contributing about half of the total range enhancement.

In order to reduce drag and give a stable air flow, the intake will be covered during aircraft carriage and also possibly during the boost phase. If an intake cover could be designed which is not completely removed at the end of boost but is released at the top of climb it would provide a method of increasing the capture area. There are likely to be penalties on the intake pressure recovery with this arrangement but, whatever variable geometry method is used, there will inevitably be an increase in the missile drag and possibly some loss of lift. Figure 4 shows the effect on range of increases in the vehicle drag coefficient (the same percentage increase has been assumed for all phases of the flight). Virtually all the range improvement from a 30% increase of capture area would be lost if there was an attendant 4% rise in drag.

It will be very difficult to avoid some drag increase with a variable geometry arrangement and there may also be a detrimental effect on the vehicle lift characteristics. Moreover the possible need to incorporate stealth features into the shape of the intake will make variability a more difficult design problem. While these adverse effects cannot readily be quantified, it is clear that the small potential benefit make the variable geometry intake rather an unattractive development target unless a narrow launch envelope can be tolerated.

3.4 Effect of variable geometry nozzle

If the throat area of the ramjet nozzle is reduced, fuel consumption drops and hence a range increase obtained. The explanation and limitations of this trade-off are very similar to the reasons for the performance gains from intake variability. Choking conditions in the nozzle throat fix the value of the flow function and, since the air flow is determined by the intake capture area, any reduction in throat area must be accompanied by an increase in chamber pressure P_4. The higher upstream total pressure gives an increase in the nozzle

exit Mach number so that T_4 can be a lower value and still give the same exit gas velocity. This means that less fuel is needed to produce the same amount of thrust.

If the throat area of the datum vehicle is reduced 5% at all operating conditions, a range increase of 6% is obtained. About three-quarters of the fuel saving occurs during the early part of the climb and the intake is on its pressure margin limit up to an altitude of about 4000 m. If the throat area is further reduced, the pressure limit extends to a higher altitude and insufficient thrust can be generated to sustain the climb. The reasons for this performance shortfall are exactly the same as those which occur when the intake capture area is increased. If the missile has to be capable of a low Mach number launch very little change in the nozzle throat area is possible, again because of the need to have sufficient thrust to accelerate after the boost phase.

When the nozzle throat area is closed 5% the pressure margin during cruise is still quite large (about 22%). Hence a variable throat offers the possibility of reducing the cruise fuel flow with a consequent increase of range. Figure 5 shows the results obtained from trajectory calculations where the datum throat area is maintained up to the top of the climb and then closed by varying amounts for the rest of the flight. With a 20% throat area reduction the cruise pressure margin is down to about 8% and a 10% increase in range is obtained. If the throat is further closed, the intake reaches its pressure margin limit and the cruise Mach number cannot be sustained.

The computer code for the trajectory calculations allows for performance losses in the ramjet nozzle by applying a vacuum thrust efficiency. For the datum vehicle, a typical nozzle efficiency of 0.97 has been applied and at cruise conditions this corresponds to a thrust coefficient of 0.96. A variable nozzle may well be less efficient, and Figure 5 accordingly shows the effects of reducing nozzle efficiency by 2% and 4%. It is seen that the latter loss would more than wipe out the benefit to be gained from throat area reduction.

The design of a variable area nozzle throat is a very difficult problem due to the limited space available, the high local temperatures and the need to minimize flow passage irregularities. One possible arrangement using four circular inserts is illustrated on Figure 6. The inserts would be located between the rear control fins and could be spring loaded to drive them into their cruise location. As indicated, there could be a portion on the upstream side of each insert which burns away when it enters the gas stream, the aim being to smooth the contracting passage area variation. Unfortunately it is not possible to do any similar blending on the downstream side and the flow pattern in the whole throat region will be very complex. There is likely to be local over expansion around the inserts and shockwave terminations will produce pressure losses which will add to the basic turbulence and flow mixing penalties. It is unlikely that any computational methods will be able to model such a very mixed flow and experimental work would be needed to quantify the resulting efficiency loss. It should be pointed out that the inserts as sketched on Figure 6 give a geometric throat area reduction of 20%. With the non-axial nature of the flow as it contracts to the throat, it is likely that significantly smaller inserts would give the required 20% reduction in effective passage area. Such a size change would obviously lessen the efficiency penalty but again this conclusion can only be quantified by an experimental investigation.

Nevertheless it is not unreasonable to assume that the loss could be kept to less than 2%, so that a 5% to 10% improvement in missile range would be achievable. Further gains are possible if a narrow high Mach number launch envelope is acceptable.

4. AIR-TO-AIR MISSILE PERFORMANCE

The ducted rocket air-to-air missile considered in this paper is assumed to have a length and diameter similar to existing advanced BVR missiles. The basic missile arrangement is shown in figure 7. Following launch, the missile is accelerated to a Mach number at which the ramjet can operate, by means of a nozzleless boost motor which is cast into the main ramjet combustion chamber. The boost motor burns out after 2.2 seconds and transition to ramjet sustain motor power then occurs. The main combustor is supplied with air via a pair of two dimensional intakes offset at 90 degrees relative to one another. The primary gas generator produces fuel rich exhaust gas combustion products from a hydrocarbon based solid fuel and the rate at which these gases are supplied to the main combustor is controlled by a valve with a variable flow area. The boost propellent and sustain propellant charges represent 22% and 11% of the missile launch mass respectively.

The missile is guided towards a target using a lofted form of proportional navigation. The trajectory followed by the missile depends upon the degree of lofting that is commanded and the relative positions of the launch and target aircraft. The impact of variations in both are examined in this paper, but most of the calculations are based on a datum case where the target and launch aircraft are both flying at an altitude of 6000 m.

4.1 Launch characteristics

As with the stand-off missile, to determine the performance required of the boost motor it is necessary to establish the minimum operating Mach number of the ramjet and the most arduous launch condition that is envisaged for the missile. The preferred boost motor size will generally be the smallest that is capable of meeting both these requirements, thereby providing the maximum amount of sustain motor fuel possible for a given propulsion system weight.

The launch envelope that is specified for a missile will depend upon the relative importance to the operator of operational flexibility in the launch phase and missile capability against targets flying at extreme ranges or altitudes. For the purposes of this study it has been assumed that the missile should be capable of being launched at a minimum Mach number of 0.5 at sea level, thereby placing the greater emphasis on the former requirement. This fixes the lower boundary of the launch envelope, but given the choice, the missile would normally be launched at a higher altitude and Mach number for optimum range performance.

With a fixed booster motor burn duration, the Mach number at which transition to ramjet power occurs will vary according to the launch condition. The transition Mach number must always be high enough to ensure positive acceleration of the missile in the airbreathing mode. The lower boundary is defined as that providing an initial minimum acceleration of 0.5 g.

After the transition from boost motor power to ramjet propulsion the fuel flow rate stabilises at its maximum value until the commanded cruise Mach number is approached. The resultant axial acceleration forces applied to the missile 0.5 seconds after transition are plotted in Figure 8 against transition Mach number for

fuel flow rates of 2.9%, 4.3% and 5.7% of sustain propellant launch mass per second. The performance of the propulsion system is dependent not only on the fuel flow rate but also on the characteristics of the fuel rich solid propellant used in the gas generator. A fuel with a calorific value of 34500 MJ/m^3 is assumed for this missile giving a sea level specific impulse of 650 s for the installed propulsion system. At a launch altitude of 6000 m the required acceleration rate of 0.5 g in level flight is achieved at a transition Mach number of between 1.85 and 1.9 for all three fuel flow rates examined. However, at sea level there is a much stronger dependence on fuel flow rate. Sustained ramjet powered flight is impossible at this altitude with the lower fuel flow rate, but the required acceleration is possible with the higher fuel flow rates and is achieved at slightly lower transition Mach numbers than at altitude. At high transition Mach numbers the acceleration rate falls off as the ultimate cruise Mach number for the given fuel flow rate is approached. Some deterioration in performance is to be expected if the missile is required to climb during the transition phase, but the minimum acceleration margin specified for level flight adequately caters for this effect.

From the data presented in the figure it is apparent that the higher airframe drag at sea level makes this condition critical for the selection of the maximum required fuel flow rate. Since there is little advantage in selecting a value that is higher than necessary, a maximum rate of 4.3% of sustain propellant launch mass per second appears to be close to optimum for the datum missile. The minimum transition Mach numbers that must be achieved by the boost motor are therefore 1.8 and 1.85 at sea level and 6000m respectively.

Figure 9 shows how transition Mach number varies with booster propellant mass for various different launch Mach numbers at sea level and at 6000 m. Boost motor thrust is held constant and therefore the burn duration is allowed to vary. The sea level condition again represents the more difficult design target due to the higher airframe drag levels. At this altitude the required launch and end of boost Mach numbers of 0.5 and 1.8 respectively can be achieved with a boost propellent charge sized at 22% of the missile launch weight. If the minimum launch requirement is relaxed to a Mach number of 0.7 at sea level then this datum boost charge can be decreased by 12%, whilst an increase in the propellent of a similar magnitude would be required if a launch capability at a Mach number of 0.3 were required. At 6000 m altitude and using the datum boost charge the minimum launch Mach number is 0.3. This boost motor therefore gives a generous launch envelope at altitude, and a 10-15% reduction in the size of the component would be feasible if the low level launch requirements were relaxed (eg by raising the minimum launch Mach No to 0.7).

Although the missile may be capable of being launched from low Mach number conditions it is desirable to achieve the highest launch Mach number possible since this increases the range of the missile and decreases its time of flight to a target. Figure 10 gives an example of the variation in range that can be achieved by a missile following a typical lofted trajectory for different launch conditions. For comparison the range of a non-lofted missile is also shown and it is evident that the lofting leads to a greater sensitivity to the launch Mach number.

4.2 Steady state ramjet performance

Since the ducted rocket missile would normally be programmed to follow a lofted trajectory towards its target, for range and seeker performance reasons, level steady state flight would rarely be achieved. But examining the performance of the ramjet under these conditions is helpful in providing a guide to the Mach number and altitude combinations that can be achieved. Figure 11 shows the fuel flow rates and turndown ratios required to sustain the datum missile in steady, level flight, plotted against Mach number for different altitudes. Contours of constant fuel-air ratio are also shown. The figure indicates the need to reduce the fuel flow rate as altitude is increased, in order to control the missile to an acceptable Mach number. Although the propulsion system may be capable of being designed for operation at a Mach number approaching a value of 4.0, in practice the missile must be limited to lower speeds in order to provide a radome stagnation temperature that is no greater than about 800K. Beyond this temperature the structural integrity of conventional radar seekers may be jeopardised due to the ablation of the radome, and thermal background noise can affect the seeker performance.

With a constant fuel flow rate of 4.3% of total fuel mass per second, the maximum Mach number in level flight at sea level is 2.5, increasing to 3.5 at an altitude of 5000 m, at which point aerodynamic heating effects would have a detrimental impact on the seeker. Sustained flight at significantly higher altitudes would not be possible. Variable control over the fuel flow rates permits operation over a wider range of altitudes and Mach numbers. For instance a turn down ratio of 5 (max/min fuel flow = 5) would enable the missile to fly at 15000 m altitude at a Mach number of 3.3, but sustained flight at altitudes of 20000 m or greater would not be possible. Increasing the turn down ratio to a value of 10 would permit flight at 20000 m at a Mach number of 3.4. Brief excursions to higher altitudes might also be feasible since the limited acceleration rate and effect of missile manoeuvring would tend to reduce the Mach numbers achieved in an actual flight from the steady state values presented here. These turn down ratios are based on a maximum fuel flow rate sized for operation at sea level. If a minimum launch altitude of 5000 m was accepted then the maximum fuel flow rate could be reduced by about 30% and a turn down ratio of 7.5 would still allow flight beyond 20000 m.

Figure 11 also shows how the combustor fuel-air ratio - (and hence cycle temperature) is influenced by the flight altitude and Mach number. The values presented are well below the stoichiometric fuel air ratio of 0.14, which would be encountered during a maximum fuel flow rate acceleration from a low transition Mach number. The minimum cruise fuel-air ratio of just below 0.06 would occur at a Mach number of 2.5 at the tropopause (Alt = 11500 m). Below this Mach number, the ramjet cycle becomes very inefficient because of the low ram pressure rise and low intake flow. Above Mach 2.5, while the cycle efficiency continues to improve, the thrust requirement due to the greater drag, increases faster and a higher fuel-air ratio is needed to compensate. If the missile was taken to the radome temperature limit, which corresponds to Mach 3.7 at this altitude, a fuel-air ratio of 0.075 would be required. The fuel-air ratio also rises rapidly as the missile approaches the altitude ceiling which lies just beyond 25000 m due to the low air density. At these high altitudes operation at the lower Mach number may be impossible due to combustion stability problems associated with low combustion pressures.

In selecting the optimum altitude and Mach number at which the ramjet should operate, the relative importance of a low time of flight for the missile versus fuel conservation needs to be considered. Figure 12 shows the impact of the flight condition on the fuel consumption per kilometer of missile flight. It is evident that whilst there is some benefit in the ultimate range that can be obtained by optimising the cruise Mach number, by far the greatest advantage is achieved by flying as high as possible.

4.3 Missile flight performance

In an air-to-air combat the propulsion system design and the chosen flight trajectory will have an impact on the achievable missile range, the time of flight and the terminal flight dynamics. These criteria, in conjunction with the missile guidance system and warhead performance will determine the kill probability of the missile for any particular engagement.

In simple flyout and intercept simulations with both launch and target aircraft flying at 6000 m and 0.9 Mach number it has been found that whilst a commanded cruise Mach number of 3.5 gives a good performance from a head on launch aspect, tail chase performance at longer ranges is enhanced by the adoption of a commanded Mach number of 3.0 thereby reducing the rate of fuel consumption for greater endurance. In order to maximise the range of the missile a lofted trajectory is desirable, but the degree of lofting used may have a bearing on the kill probability of the missile at intercept. At the longest launch ranges the missile can attain dive angles of 60° when the missile is lofted to a high altitude. However, the preferred terminal elevation angle maybe strongly influenced by the radar cross section characteristics of the target aircraft. Many current aircraft designs present strong signatures at low angles, particularly if the engine intakes or nozzles are visible, whilst newer stealth aircraft may have a low frontal signature, but be more visible when viewed from above. Other considerations influencing the terminal elevation include the target doppler response, the effectiveness of aircraft jamming countermeasures, and the engagement terminal dynamics.

The optimum missile trajectory is therefore not clear and may change according to the nature of the engagement or the target. The effects on range of three alternative lofting assumptions will be considered here. These consist of a high loft and a low loft both with a commanded altitude of 25000 m and a climb pitch up g of 5.0 and 3.0 respectively. The third trajectory has zero lift (level flight) at 6000 m altitude. An example of the flight trajectory and fuel flow for an intermediate range is plotted on Figure 13.

The maximum launch ranges of the missile for flights with target impact occurring firstly under ramjet power at a Mach number of 3.0 and secondly unpowered with a coast phase to a terminal Mach number of 2.0 are presented in the following table. Note that these are not the fly-out ranges, but the distance to the target at the moment of missile launch.

Maximum Launch Ranges (km)								
Turn down ratio	10.0		7.5		5.0		1.0	
Powered/ Unpowered Intercept	P	U	P	U	P	U	P	U
Head on Launch range								
High loft	100	220	95	200	80	180	31	71
Low loft	50	80	50	80	50	80	32	56
No loft	41	51	41	51	41	51	32	48
Tail chase Launch range								
High loft	31	82	31	73	31	63	17	32
Low loft	23	30	23	30	23	30	17	28
No loft	21	26	21	26	21	26	17	25
Note: P = Powered intercept, terminal Mach No = 3.0 U = Unpowered intercept, terminal Mach No = 2.0								

A high degree of lofting is shown to produce great benefits in the potential launch range of the missile, particularly in conjunction with a higher turn down ratio capability and a head on launch aspect. The high loft guidance command enables the missile to climb more rapidly to efficient cruise altitudes and generally increases the maximum altitude attained since the commanded altitude of 25000 m is only reached by the longest range flights.

The fuel flow rate of the missile is initially set to the maximum but it is progressively cut back, firstly as the required cruise Mach number is approached and then as the missile climbs to higher altitudes where the lower airframe drag permits reduced thrust levels. If a powered approach to the target is required then the fuel flow rate increases again as the operating altitude of the missile falls as shown in Figure 13. At longer launch ranges than that shown in the figure, the terminal phase may be unpowered and therefore the missile is able to consume much of the remaining fuel at relatively high altitudes, thereby gaining a significant range advantage. The missile then dives towards the target, taking advantage of a steep flight path to maintain its high kinetic energy level to counter any target evasive manoeuvring.

The influence of the assumed level of turn down ratio on the missile flight is shown in Figure 14 for a head on high loft engagement with a launch range of 100 km. The first missile with a turn down ratio of one has a fixed flow rate gas generator with a choked nozzle (ie the burn rate is independent of the main combustion chamber pressure). This missile achieves a very high thrust level in an early stage of flight, giving it a peak Mach number of 4.1. This is beyond both the commanded value of 3.0 and the radome limit. However, the missile runs out of fuel well before the target is reached and it therefore has a low terminal velocity. Introducing a variable area gas generator nozzle to give a turn down ratio of 5 enables the missile to achieve a much longer powered flight phase although some overspeed does occur at high altitudes and the missile runs out of fuel during the dive. The highest turn down ratio of 10 results in a trajectory that is powered almost to missile impact, thereby increasing the terminal Mach number as indicated in Figure 14. During these long range high loft engagements the missile attains an altitude of 20000 m or more, but for other shorter range trajectories the peak altitude may not exceed 15000 m and the minimum demanded fuel flow rate for a Mach number of 3.0 can be met with a reduced turn down ratio of 5 or less. The importance of achieving higher turn down ratios is therefore dependent on the trajectory that is to be flown. A turn down ratio approaching 10 maybe an important design requirement in order to prevent overspeed if the missile must be capable of sea level launch and also be able to fly at altitudes above 25000 m (eg against high altitude or long range targets) or if dives at very steep angles under power are required. A relatively small relaxation in these requirements could reduce the turn down ratio to nearer 5.

If flights of 100 km or more are of secondary importance because of long range targeting limitations, the ramjet may still provide a significant advantage over a rocket powered missile for engagements with a launch range of 50 km or less. At such ranges the latter missile is likely to be unpowered in the terminal flight phase and any high g manoeuvring that is required to track an evading target aircraft will result in a rapid loss of velocity. On the other hand at these ranges the ramjet will still be under power and will be able to increase the thrust from its sustain motor in order to compensate for high manoeuvre drag levels. However, for these shorter range engagements against targets flying at medium altitudes highly lofted trajectories are not necessary and the high turn down ratio capability will not be fully utilised.

Another advantage of the ramjet is that its variable thrust level would give some scope for an 'intelligent' guidance system to be used to vary the flight guidance commands dependent on the target launch range, by adopting a throttled back very high altitude approach to a target at extreme ranges, whilst a very high Mach number, low loft trajectory could be employed against shorter range adversaries that are well within the launch success zone.

4.4 Effect of variations on boost/sustain fuel ratio

The datum missile discussed in this paper has boost motor and gas generator fuel masses in the proportion of 2:1. The following table shows the effects on missile range and time of flight of changing the ratio to provide boost motors 10% bigger and smaller than the datum, within the same power plant volume (ie gas generator changes are 20% smaller and bigger, respectively).

	-10%	Datum	+10%
Boost/sustain mass	1.50	2.00	2.75
Boost propellant (% launch wt)	19.8	22.0	24.2
Sustain propellant (% launch wt)	13.2	11.0	8.8
10 km launch range			
Time of flight (s)	9.9	9.6	9.4
Terminal Mach number	2.78	2.85	2.89
Fuel remaining (%)‡	88.6	72.6	56.0
25 km launch range			
Time of flight (s)	22.4	22.0	21.8
Terminal Mach number	2.97	2.97	2.97
Fuel remaining (%)‡	53.1	39.4	23.4
75 km launch range			
Time of flight (s)	66.1	66.4	70.0
Terminal Mach number	2.76	2.10	1.43
Fuel remaining (%)‡	0.0	0.0	0.0
‡ Relative to datum sustain fuel mass at launch			

The boost motor provides a much greater thrust than the sustain motor but at lower specific impulse. Therefore, the missile with the 10% bigger boost motor has an average velocity that is 2.5% greater for a 10 km launch range, reducing to a 1.5% advantage at 25 km, whilst at the longest launch range it has the lowest average velocity because sustain fuel exhaustion occurs relatively early in the flight and the missile coasts to the target with a terminal Mach number of only 1.43. Increasing the size of the boost motor would therefore seem to be unattractive since it produces only a very marginal time of flight benefit at the shortest launch ranges and its long range performance is significantly worse.

As discussed in section 4.1, reducing booster motor size by 10% has a detrimental impact on the launch envelope, increasing the minimum Mach number to 0.65 at sea level. However the previous table shows there is little or no loss in intercept performance at altitude. The missile average velocity is reduced by 4% at 10 km launch range and 2.5% at 25 km due to the lower initial acceleration rates. At longer ranges the performance is actually enhanced. Thus at 75 km range the terminal Mach number is as high as 2.76 as the missile has only just exhausted its sustain motor fuel supply. These results show that reducing the size of the boost motor in order to increase gas generator size has considerable attraction when "long reach" is required, although some relaxation in minimum launch requirements must be accepted.

4.5 Propellant performance improvements

The datum missile has been assumed to have current state-of-art propellants for both booster and gas generator. Propellant research may be able to achieve improvements in propellant performance which may be exploited either for further increases in range or for reductions in missile size. As with the stand off missile, the impact of potential improvements to the ramjet fuel have been examined.

Enhanced performance of the ducted rocket gas generator may be achievable through the introduction of advanced high performance fuels such as boron based propellants similar to the slurries mentioned in section 3.2. Figure 15 shows the effects of using an advanced gas generator fuel of this type, assumed to offer an increase in volumetric heat release of 30% (comprising of a 10% gain in lower calorific value and a 20% increase in density). The reduction in the fuel-air ratio that can be achieved with the advanced fuel is evident when a comparison is made with the datum performance shown in Figure 11. The maximum fuel flow rate is determined by the requirement to provide the same 0.5 g acceleration at a transition Mach number of 1.80 as the datum missile. A reduction in the maximum fuel flow rate of 13% provides the same transition performance as the datum missile. The lower fuel flow rates and increased density of this advanced fuel give large increases in range since, following the initial climb phase, a greater proportion of the fuel is available for high altitude flight. A sample of the ranges that may be achieved by a missile using this high energy sustain fuel is indicated in the following table.

Maximum Launch Ranges (km)				
	Advanced Fuel		Datum Fuel	
Powered/ Unpowered Intercept	P	U	P	U
Head on Launch range				
Low loft	146	190	50	80
No loft	54	64	41	51
Tail chase Launch range				
Low loft	34	44	23	30
No loft	28	33	21	26
Note: P = Powered intercept, terminal Mach No = 3.0 U = Unpowered intercept, terminal Mach No = 2.0 Turn Down Ratio = 10				

The ultimate range potential of this missile is probably well beyond the capabilities of near term targeting and seeker developments, but the missile is able to reach targets at much longer ranges than the datum missile with ramjet power on, with resultant benefits against aircraft adopting evasive manoeuvres.

5. CONCLUSIONS

The possible future development route for ramjet powered missiles has been investigated using a trajectory simulation program which includes a one-dimensional engine model. Typical stand-off and air-to-air missiles have been conceived for the study and areas for potential performance improvements have been explored.

The conclusions for the stand-off missile are as follows:-

i A range improvement of up to 9% could be obtained by reducing the size of the boost motor but the missile would then be limited to high Mach number launch conditions.

ii High density fuels offer the possibility of a significant increase in range or duration of powered flight. For the datum vehicle considered in this study, a 44% range enhancement could be gained if a 70% boron slurry was used for the sustain fuel. However, the missile will then be easier to detect and problems with the fuel system and long term storage have to be overcome.

iii Performance improvements from intake variability do not seem very attractive because the potential gains are small and it will be difficult to engineer, particularly if stealth requirements have also to be considered.

iv If the nozzle throat area is closed 20% at the top of climb, a range enhancement of 10% is obtained and this improvement is even higher if only high Mach number launches are specified. A method of varying the nozzle throat area by using four inserts is presented but it was not possible to predict the efficiency loss incurred. All the range enhancement would be lost if the variable geometry produced about a 4% worsening of the nozzle efficiency.

The conclusions for the air-to-air missile are:-

i The datum missile has a boost motor sized to permit sea level launch at a Mach number of 0.5. A 10% reduction in the size of this component would significantly improve the long range performance of the missile but the minimum launch Mach number would be raised to 0.65, or the minimum launch altitude would rise to 6000 m.

ii The achievable range is very dependent on the launch Mach number. Increasing the actual launch Mach number from 0.5 to 0.9 gives 30% range improvement with a medium loft trajectory.

iii The maximum Mach number of the missile is governed by the temperature limitations of the seeker whilst the minimum Mach number is determined by the need to ensure an adequate ramjet cycle pressure ratio. A commanded Mach No of 3.0 provides a good overall level of performance for both head-on and tail-chase engagements.

iv The range of the missile may be optimised by adopting a lofted flight trajectory with a cruise altitude of 20000 m or greater. Significant further increases in range are possible if the missile is able to descend to its target unpowered. However, long range highly lofted trajectories lead to high terminal dive angles, which could introduce greater homing difficulties against some targets.

v A turn down ratio of 10 is required for extended duration flight at altitudes from sea level to beyond 20000 m to prevent overspeed. If the minimum altitude is raised to 5000 m a turn down ratio of 7.5 is adequate, whilst a value of only 5.0 will suffice if the flight envelope lies between sea level and 15000 m.

vi The use of a high density, high performance gas generator propellant could enable head on launch ranges to be increased by 30% with level flight, rising to a range extension of over 100% for some lofted trajectories.

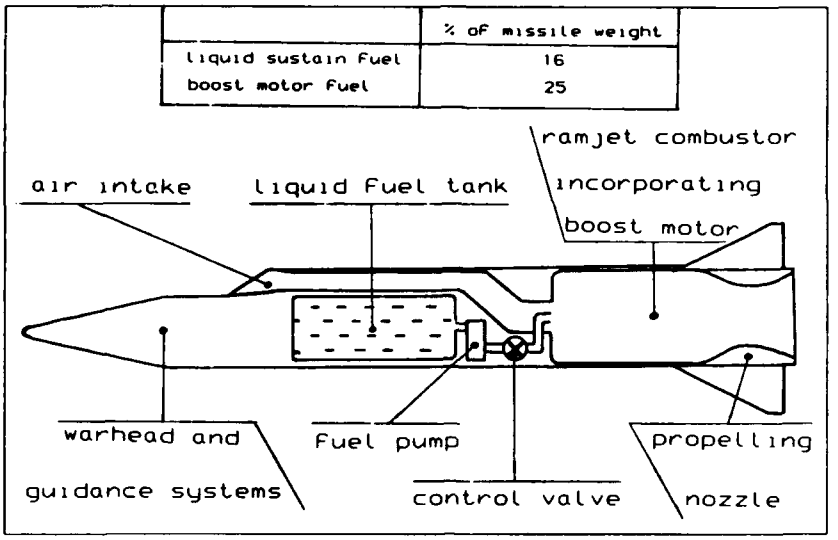

Figure 1 Stand Off Missile

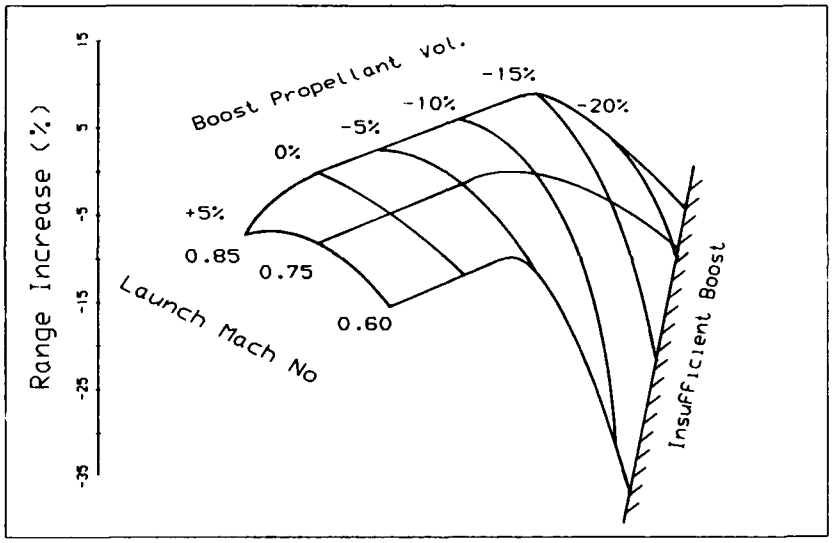

Figure 2 Effect Of Amount Of Boost On Missile Range

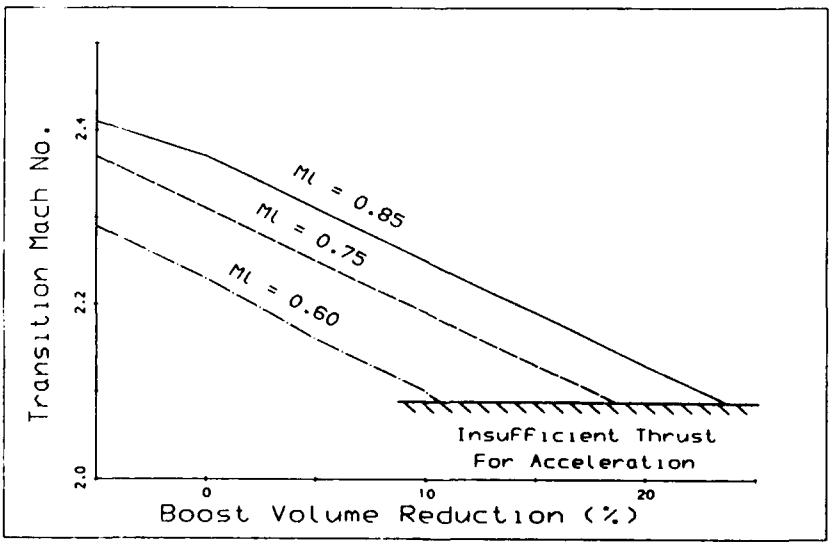

Figure 3 Boost Motor Volume vs. Transition Mach No.

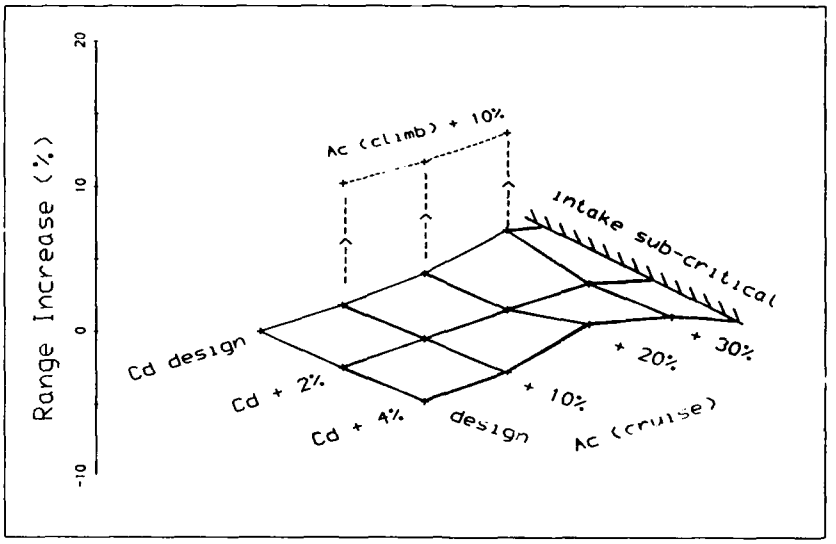

Figure 4 Capture Area Increased For Cruise

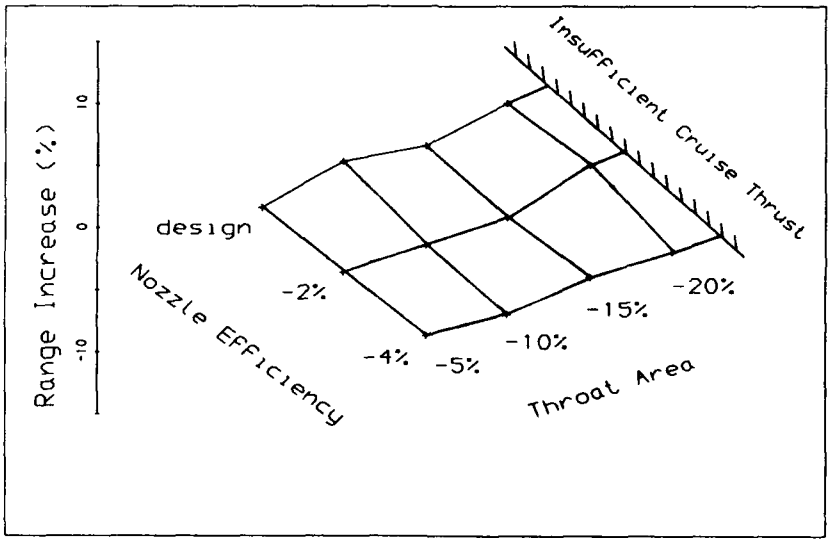

Figure 5 Nozzle Area Reduced For Cruise

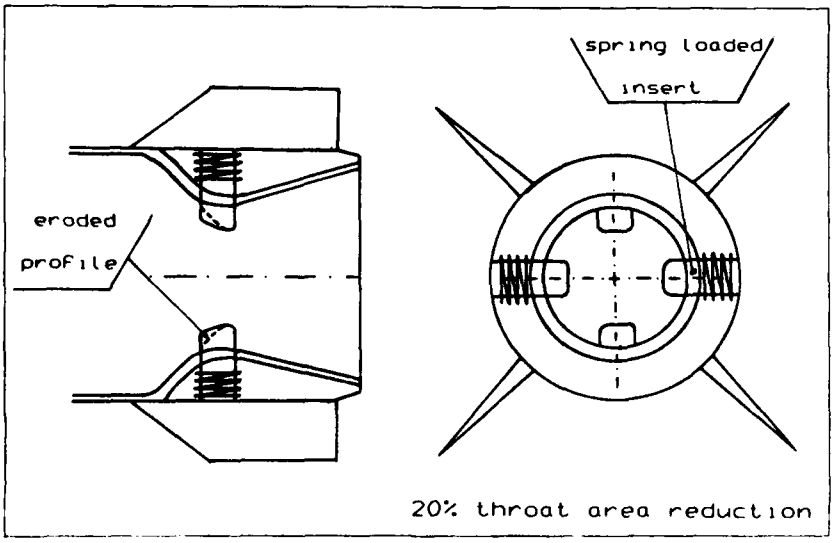

Figure 6 Variable Geometry Nozzle

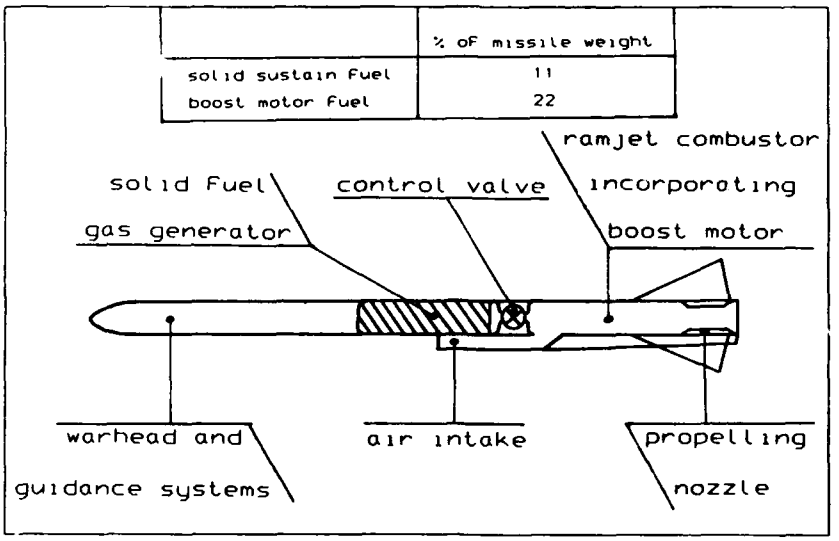

Figure 7 Air-to-Air Missile

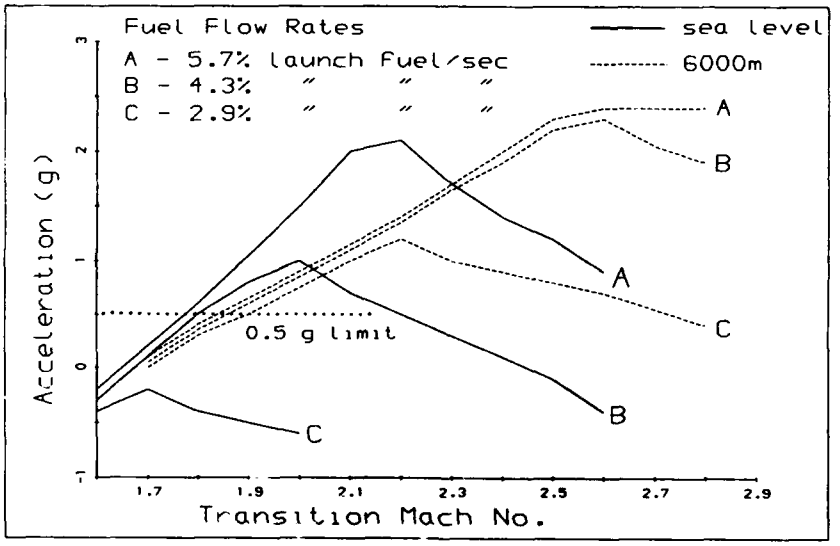

Figure 8 Transition Performance

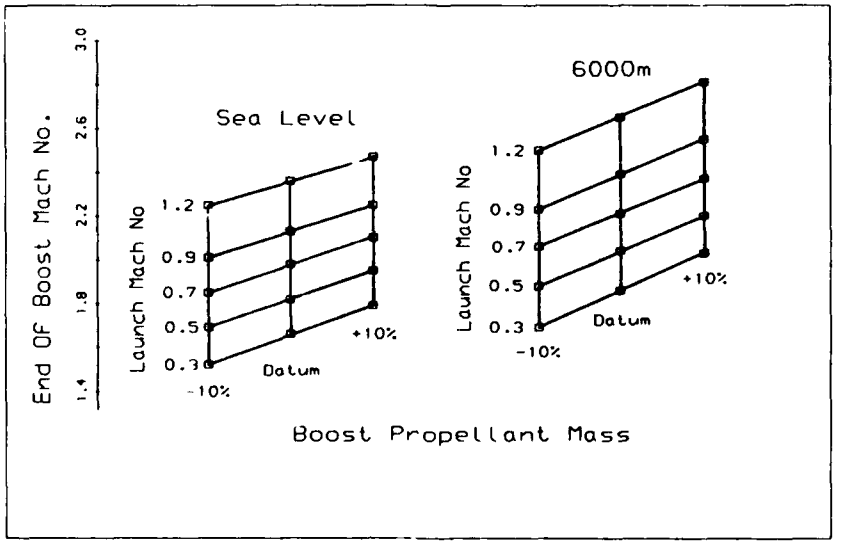

Figure 9 Boost Motor Performance

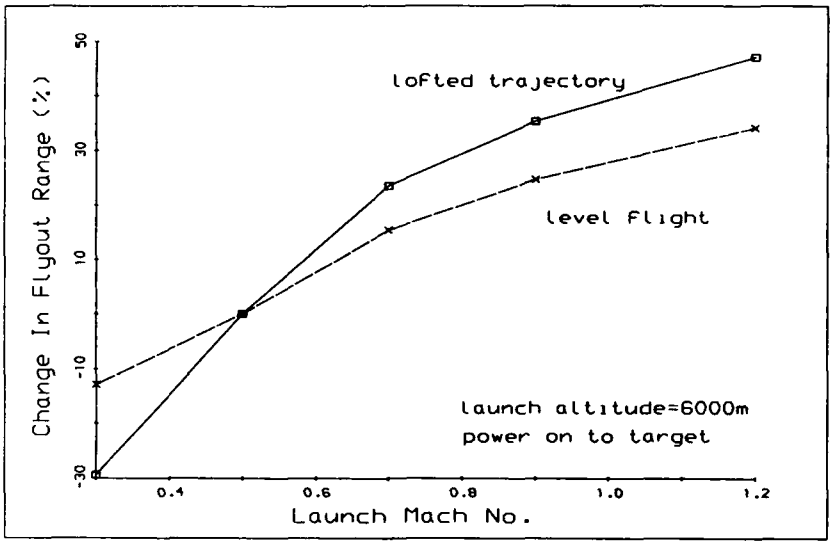

Figure 10 Range vs. Launch Mach No.

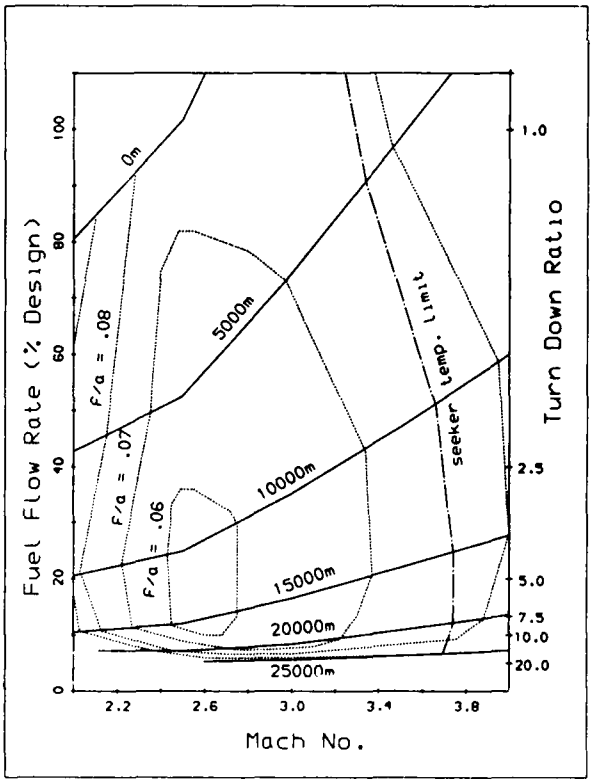

Figure 11 Steady State Performance – Datum Fuel

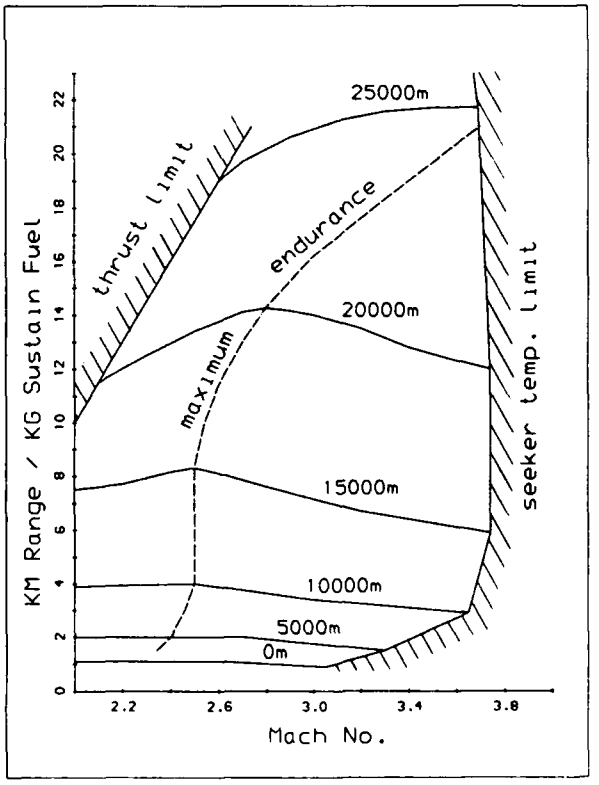

Figure 12 Steady State Maximum Endurance

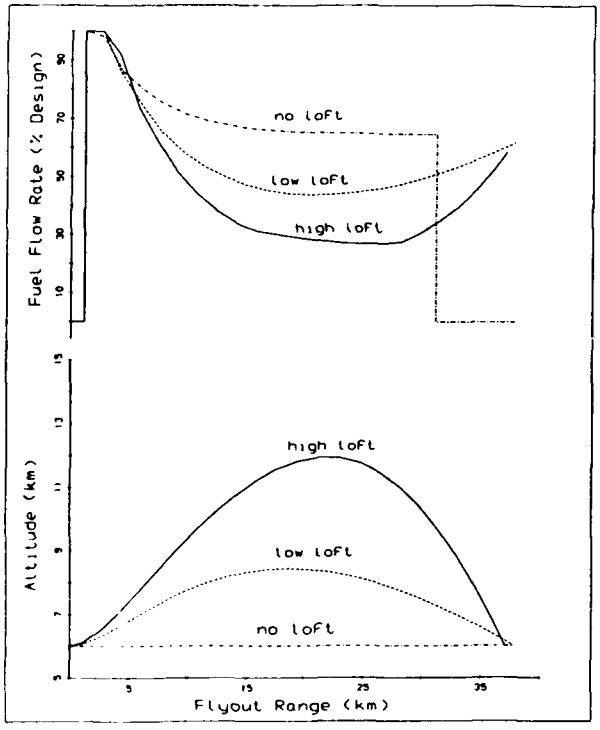

Figure 13 Effect Of Lofting

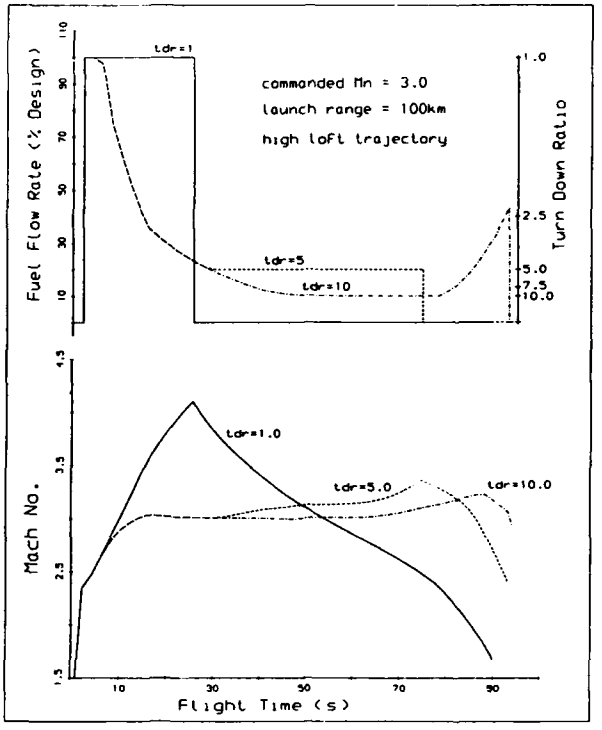

Figure 14 Effect Of Turn Down Ratio

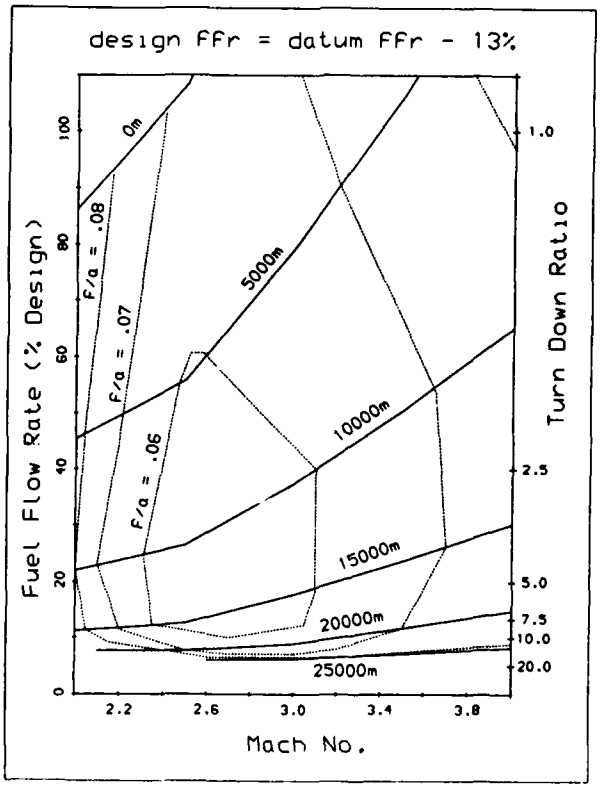

Fig.15 Steady State Performance – Advanced Fuel

Discussion

Question from A. CHEVALIER, AEROSPATIALE

What is the value of the combustion efficiency of a boron loading of 70 % ?

Author's reply

During the high altitude cruise phase of the stand-off missiles flight, the combustion efficiency when operating with a 70 % boron slurry was assumed to be 87 %. This value can be compared with the 93 % efficiency wich was applied for the flight of the datum missile using RJ6 as its sustain fuel.

Question from M. KAUFMANN

Is the temperature limit of 800°K based on test results ?

Author's reply

The temperature limit of 800K was based on flight simulations for this type of air-to-air missile. A stagnation temperature of up to 1200K might be acceptable when there is only a short period of very high speed flight and the radome area is relatively small.

DEVELOPMENT TESTING OF THROTTLEABLE DUCTED ROCKETS

by
Hans-Ludwig Besser
Messerschmitt-Bölkow-Blohm GmbH
Postfach 80 11 69, 8000 München 80

SUMMARY

Throttleability, being a current requirement for modern air-breathing missile propulsion systems, adds considerable complexity to the development of ducted rockets. Problems are especially inherent in the development of

- pressure sensitive propellants
- hot gas valves (especially for particle laden flow)
- ramcombustors featuring high performance over widely varying operating conditions.

The use of propellant ingredients with high heating value but unfavourable combustion characteristics, like boron, is an additional challenge in the development of high energy ducted rocket systems.

Extensive testing and a well conceived test philosophy are needed to achieve satisfactory development results.

MBB, together with its subsidiary Bayern-Chemie, has been engaged in the field of throttleable ducted rockets for more than a decade. This paper summarizes test procedures which have been established to address the strongly interrelated development problems and presents examples of test results derived from the development of a ducted rocket engine for a supersonic antiship missile.

LIST OF SYMBOLS

A	area
d	diameter
F	thrust
η	efficiency
λ	1/equivalence ratio, $\lambda = (\dot{m}_{air}/\dot{m}_{fuel})/(\dot{m}_{air}/\dot{m}_{fuel})_{stoich.}$
$\dot{m}$	mass flow
M	mach number
p	pressure
t	time
T	temperature
v	velocity
$\dot{v}$	acceleration

Subcripts

s	set value
o	free stream

Abbreviations

d/c	direct connect
fj	freejet

1. INTRODUCTION

Solid Propellant Ducted Rockets (SDR) have been under investigation since the 1950's. Several SDR engines were flight tested, while only one system reached operational status in the SAM 6 "Gainful" antiaircraft missile deployed by the USSR in the late 1960's. All of these SDR-systems had no active fuel flow control, which means that they either had a fixed fuel flow or a predetermined fuel flow profile by using staged propellant grains with different burn rates. A system, which couples gasgenerator and ramcombustor pressure by subcritical gasgenerator flow (like the French "Statoreactor Rustique") has a limited autothrottling capability depending on the pressure exponent of the propellant and the ramcombustor pressure range. This allows a limited adaptation of the engine thrust to flight altitude and velocity, but does not provide active thrust control to allow acceleration or manoeuvring at constant speed from drag/thrust balanced flight conditions.

Active control is a feature of the throttleable SDR that makes it a promising candidate for tactical missile propulsion. Throttleable ducted rocket technology has been under development in Europe and the US since the 1970's. MBB together with its subsidiary Bayern Chemie (both are currently part of the Deutsche Aerospace) have performed a predevelopment of a throttleable SDR using a high energy boron propellant. The engine having a diameter of 350 mm was a candidate for application in the French-German supersonic antiship missile ANS. The predevelopment was concluded in 1987 by a direct connect performance demonstration and semi-freejet boost/sustain transition tests, both done with flightweight engine hardware. Work on this technology is continuing, and currently concentrates on throttleable SDR systems of small diameter ($\leq$ 200 mm), mainly for air/air or air/ground applications.

An overview of the experience gained in approximately 20 years of work in the field of fixed flow and throttleable ducted rockets using boron propellants was given in [1]. A test philosophy, established to address adequately the complex and interrelated development problems of a throttleable SDR, is an important part of this experience.

In the following text, test procedures for the different phases of the development of a throttleable SDR will be outlined and illustrated by examples from MBB's technology and development work in this field.

2. TESTING PHILOSOPHY FOR THE THROTTLEABLE DUCTED ROCKET

Testing is a major cost driver in development. Testing expenses depend on numerous factors. Among the most important are:

- test setup being on component-, subsystem- or system-level
- scale and type of the hardware involved (e.g. experimental or flightweight hardware)
- propellant mass used for the test.

It appears desirable to perform a great portion of development testing on component level, with subscale or simplified hardware and with short burn-times. On the other hand, function, interaction and compatibility of all components have to be proven in a test setup of adequate similarity to the authentic engine as early as possible. A sound tradeoff has to be made between reduced testing expense and the risk of discovering serious technical problems in a late development phase, where any need for a substantial redesign endangers a program in terms of time schedule and funding. An adequate test philosophy has to anticipate where testing on a subsystem level, or with hardware of greater refinement, is inevitable already in an early development phase.

All important components of a throttleable ducted rocket are indicated in the schematic drawing of Fig. 1. The air delivery system consists of the air-intakes, the subsonic air ducts and the bends at the ramcombustor dump station. The air ducts are closed by port covers during operation of the integrated booster. The sketch shows a four inlet side dump configuration, which is frequently used in modern missile systems. The fuel feeding system consists of the gasgenerator case, the propellant grain and the control-valve. The oxygen deficient propellant produces fuel rich primary combustion products. In modern systems, the propellant is frequently metallized to obtain a high volumetric heating value. The grain frequently has an end burning configuration as shown in the sketch. The control valve incorporates the adjustable gasgenerator throat and the fuel injectors. The ramcombustor forms the case for the integrated booster, and therefore does not contain internal

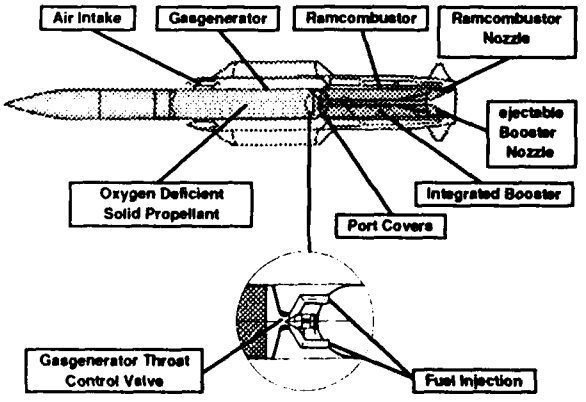

Fig. 1 Solid Propellant Ducted Rocket (SDR)

installations (like flameholders). The ramjet nozzle may house an ejectable or consumable coaxial nozzle for the integrated booster, unless the system uses a nozzleless booster. Both gasgenerator-and ramcombustor-cases need a thermal protection system which usually is based on ablative materials. More details on SDR systems are given in [2].

Fig. 2, 3 and 4 give a general impression of a development testing logic for a throttleable ducted rocket. Of course, modifications will occur for each program, depending on the detailed engine configuration and the technological status of the components to be integrated. The illustration of the testing scheme is subdivided into three parts, where

Fig. 2 illustrates the general ground testing procedures for the integrated SDR-propulsion system

Fig. 3 and 4 present a more detailed testing logic for the development of the throttleable ducted rocket being the key subsystem

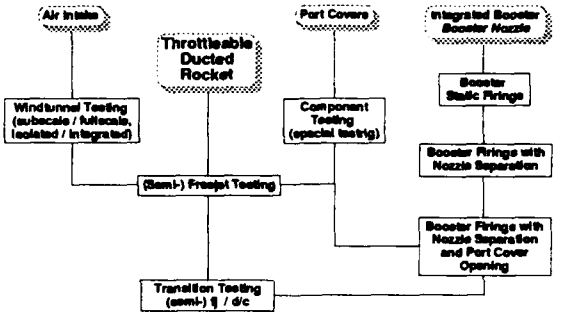

Fig. 2 Development Testing Logic - Integrated SDR Propulsion System

All components and subsystems, as indicated by the shaded boxes in Fig. 2, can be developed in parallel for a long period, provided that interfaces can be clearly specified at the beginning of the hardware development. The main development testing steps are indicated for the air intakes, the port covers and the integrated booster. The box 'Throttleable Ducted Rocket' refers to Fig. 3 and 4. The air intakes and the combustor system of the throttleable ducted rocket are combined for freejet or semi-freejet testing. Also, integrated testing of the port covers should be performed at this development stage to prepare for the transition tests. Transition testing, including integrated booster operation, booster nozzle separation (if applicable), port cover opening, gasgenerator and afterburner ignition followed by a full or part time cruise operation, may be performed in direct connect- or (semi) freejet-testing. Freejet testing and transition testing are most frequently performed with flightweight hardware. These steps then lead over to flight testing.

The testing logic shown in Fig. 3 corresponds to a phase which may be called 'Basic Development'. This is the phase where technology for the propulsion system is to be established. This technology is usually directed to a specific application. Most programs, however, which were funded in the past, were restricted to this basic development phase and did

not proceed to advanced development, flight testing or an operational system. Nevertheless, sound and comprehensive work in the basic development phase is the key to success in subsequent development phases. The biggest portion of testing during the development of a throttleable SDR is accumulated in this phase. Test expenses, however, are kept within limits due to the fact that testing in this phase is done in subscale (although not recommendable for systems with a fullsize diameter below 200 mm) and/or experimental (heavyweight) hardware, and mostly with reduced burn times.

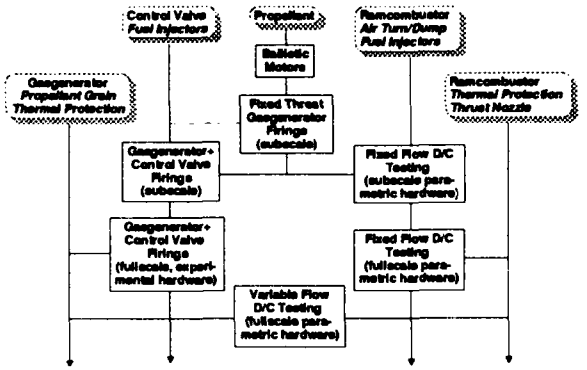

Fig. 3 Development Testing Logic - Throttleable Solid Propellant Ducted Rocket, Phase I - Basic Development

Obtaining a propellant, which has reached a certain level of technical maturity is a prerequisite for the development of the control valve and the ramcombustor. Basic screening of a propellant formulation is usually done by testing in ballistic motors (e. g. 2 x 4 inch tube/end burners). This has to be followed by fixed throat gasgenerator firings, which give more reliable information about the burning behaviour of a propellant within the operational pressure range. These static gasgenerator firings, usually done in subscale, may also be used to investigate the compatibility of the propellant and gasgenerator throat configurations corresponding to an anticipated control valve design.

The subsequent testing phase covers the optimization of a control valve concept (hardware design as well as controller software) and a ramcombustor geometry. Testing may remain in subscale hardware, but there is a need for increased burning times for the investigation of the control valve. Geometrical variability is the main requirement for the design of the test hardware, which consequently is not inexpensive.

Control valve development with variable flow gasgenerator firings, and ramcombustor optimization with fixed flow direct connect tests, can be done independently, thus facilitating the testing procedures. During this parallel development, the fuel injector interface between the two subsystems has to be carefully considered. It does not appear reasonable to combine the control valve and the ramcombustor in subscale testing, because the control valve hardware usually is a segment or a simplified version of the fullscale design rather than a subscale duplicate.

The last testing phase of basic development is done with fullscale hardware. The hardware, however, is still the experimental type of design to allow sufficient variability. The optimization process for the control valve and the ramcombustor is verified and refined during this testing phase. As soon as function and satisfactory performance of both subsystems have been demonstrated in separate testing, they can be combined in variable flow direct connect tests. These tests feature significantly increased complexity and cost, especially for the so called 'hardware in the loop flight simulation' which will be explained in detail in section 3.3.

Furthermore, during this testing phase, a special gasgenerator or grain design (determined by a preliminary missile design), the thermal protection of the gasgenerator and ramcombustor, and the ramcombustor thrust nozzle may be introduced into the test program. The problems inherent in those components can be adressed adequately only with fullscale hardware and sufficiently extended burn times.

The development problems associated with function and performance of the propellant, the control valve and the ramcombustor are strongly interrelated. Fig. 5 illustrates this interrelationship. As a consequence, basic development of these components or subsystems turns out to be an iterative process. It is desirable but not always attainable to perform most of these iterations during the subscale testing phase.

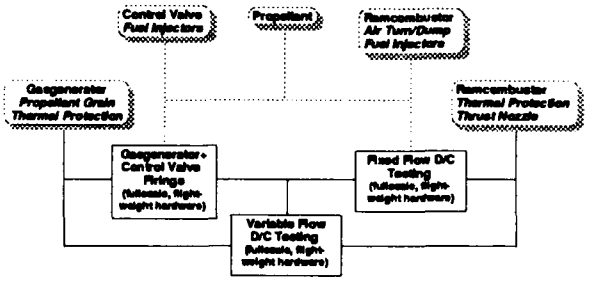

Fig. 4 Development Testing Logic - Throttleable Solid Propellant Ducted Rocket, Phase II - Advanced Development

Fig. 4 refers to an advanced development phase which occurs when a program proceeds from technology accumulation towards the realization of an operational propulsion system. Now, the criteria for optimized design of subsystems and components, having been established in basic development, need to be applied to flightweight hardware. Usually, a lot of compromises have to be made between optimum geometries and hardware weight, producibility and cost. Consequently, the fullscale testing of the basic development phase has to be repeated with the flightweight hardware to investigate the resulting effects on function and performance. Except for the verification of ramcombustor performance in fixed flow direct connect tests, major portions of testing in this phase need to be done with full burn time (i. e. full propellant mass) of the system. If the test facility allows a close simulation of the

flight trajectories required by a mission, the variable flow direct connect testing in this phase can be considered a sound proof of the feasibility and performance of a subsequent flying system.

Expenses for testing, and possibly required hardware modifications, are significantly increased during this phase. Unfortunately, problems inherent in large propellant grains and the endurance of lightweight components and thermal protection systems are not fully explored until this late stage in development. In the worst case, iterative development steps induced by these problems may lead back to the technological development of phase I.

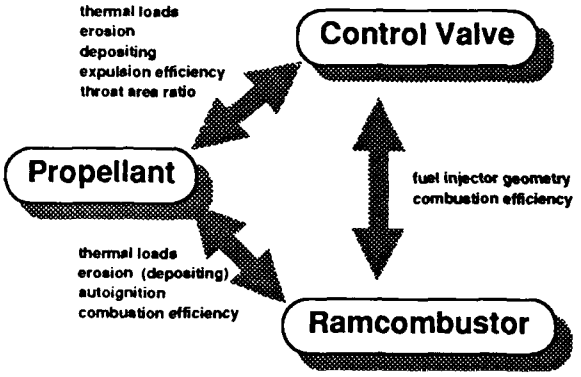

Fig. 5 Interrelated Development Problems

3. SELECTED TESTING MILESTONES

This section will illustrate several steps of the development testing logic explained above. Within the scope of this paper, of course, only some highlights can be presented of a process which usually lasts close to a decade and includes hundreds of tests. The examples of hardware and test results given in the following are mostly taken from the development work for the engine of an antiship missile (i. e. ANS and its predecessors). This means that we are dealing with a development characterized by the following requirements :

- volumetric heating value of the propellant ≈ 60 MJ/dm^3 (AP/PB formulation with about 40 % boron content)
- turn down ratio ≈ 1 : 4

3.1 Basic Development - Subscale Testing

One of the earliest steps in the development of a throttleable ducted rocket is the investigation of propellants by Fixed Throat Gasgenerator Firings.

These tests can be used to characterize

- burning behaviour of the propellant at different pressures
- pressure exponent
- expulsion efficiency (i. e. residues in the gasgenerator after burnout)
- depositing behaviour (referring to an undesirable variation of the gasgenerator throat)

Fig. 6 Fixed Throat Gasgenerator Firing

The photograph of Fig. 6 shows a fixed throat firing with half the diameter of the real engine (i. e. 25 percent of the cigaret burner cross section). The gasgenerator exhausts into a simple tube, where fuel rich afterburning occurs with entrained air, if the primary combustion products are of sufficiently high temperature. This may provide preliminary indications about autoignition and afterburning characteristics. Mainly, however, this is done to reduce air pollution.

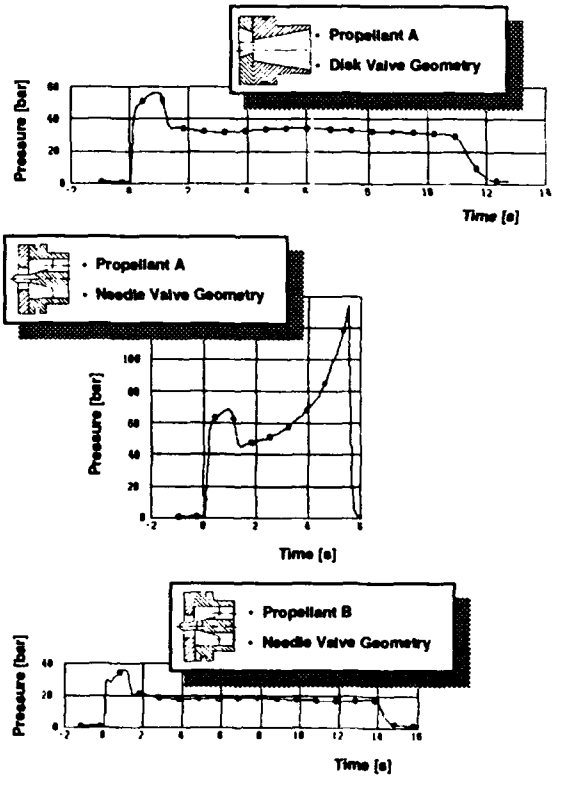

Fig. 7 Depositing Characteristics Determined By Propellant Formulation And Gasgenerator Throat Configuration [1]

Expulsion efficiency data obtained from these tests allow a grading of different propellant formulations. However, they cannot be used reliably to infer the expulsion efficiency full size grain, where the characteristic length of the gasgenerator and the operational pressure profile are additional important parameters.

Results concerning depositing are more reliable, if instead of a simple nozzle, a gasgenerator throat geometry is used which simulates a possible control valve configuration. Fig. 7 shows pressure traces of fixed throat gasgenerator firings obtained with propellant formulations having different depositing characteristics. Formulation A, having unfavourable depositing characteristics produces a smooth pressure trace when tested with a throat geometry simulating a disk-valve.

Testing with a needle valve geometry led to the blow off of the safety valve after a rapid progression of the internal pressure. A second formulation B, having only moderate depositing tendencies, appears to be compatible with the needle valve geometry at least for limited burn times.

After the screening of feasible throat configurations, and having obtained some feedback on ramcombustor performance with a suitable fuel injection geometry, conceptual control valve designs can be made. Resulting hardware has to undergo functional testing by performing cold gas flowchecks (air) and Gasgenerator/Control Valve Firings. The same tests may be used to develop or prove controller software.

Subscale hardware allows testing with propellant grains of reduced size. On the other hand, a scaled down control-valve design poses problems concerning

- producibility of the hardware
- increased susceptibility to depositing
- adverse influence on the formation of gasgenerator residues.

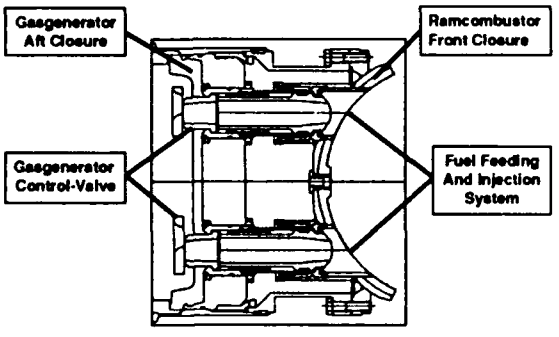

Fig. 8 Fullscale Interstage Design With Control Valve And Fuel Injection

These problems may be overcome, if it is possible to test a representative segment of a fullscale design. This was done in the ANS-development, where the valve design featured two rotary sliders controlling four gasgenerator exit ports at the upstream end of straight blast tubes. Preliminary testing of this design, illustrated by fig. 8, used hardware with one fullscale slider controlling two throats. The photograph of fig. 9 shows the gasgenerator aft closure with the control element (A safety valve is also shown on the bottom of the closure).

Fig. 9 Gasgenerator Aft Closure With Control Valve For Subscale Testing

Fig. 10 presents the test setup with

- the subscale gasgenerator (50 % of fullscale grain burning surface)
- the hydraulic actuator below the blast tubes
- the blast tubes exhausting into two downstream vessels.

The downstream vessels exhaust through choked nozzles and allow an evaluation of the massflow. Massflow evaluation provides important diagnostics of the control valve function and should be considered essential. If there are several blast tubes, evaluation of individual massflows is highly desirable.

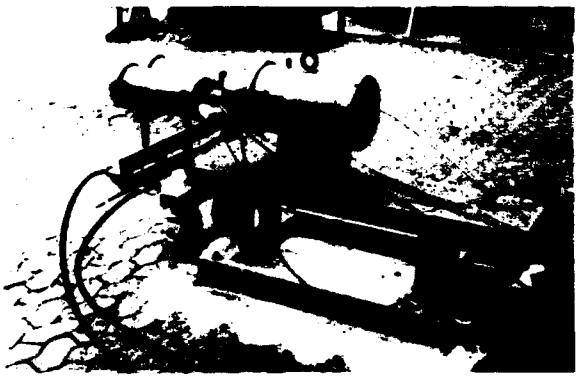

Fig. 10 Test Setup For Subscale Gasgenerator/Control Valve Firing

Parallel to the control valve investigation, the basic optimization of the ramcombustor is carried on by Fixed Flow Direct Connect Tests.

These tests should use a 'parametric hardware', which allows a variety of geometrical modifications. Fig. 11 presents a sketch of parametric ramcombustor hardware used in the SDR-predevelopment for ANS. The chamber diameter is 240 mm (50 % of the cross section of the fullscale system).

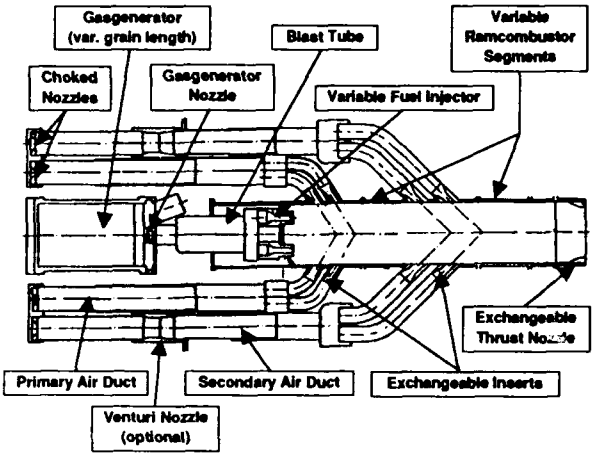

Fig. 11 Subscale Parametric Hardware For Direct Connect Tests

The gasgenerator, featuring a variable length grain, exhausts through a single choked nozzle. Primary combustion products are led through a blast tube to a distributor chamber. The aft closure of this chamber is exchangeable to incorporate different injector configurations. A staged air injection is required to burn boron efficiently at fuel lean conditions. To optimize the important parameters, the hardware allowed

- an independent adjustment of primary and secondary air flow by choked nozzles at the upstream end of the air ducts
- an independent adjustment of the primary and secondary air injection velocities by exchangeable inserts for the inlet ports
- a variation of chamber length upstream of the primary air injection, between the air injection stations, and of total chamber length
- a variation of the ramcombustor Mach number by exchangeable thrust nozzles.

Fig. 12 shows a photograph of the parametric engine on the test stand.

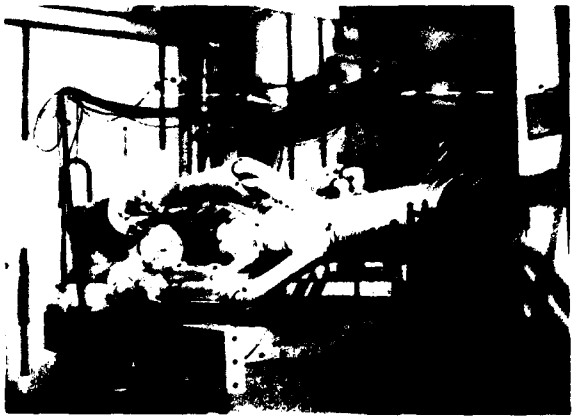

Fig. 12 Direct Connect Test Setup - Subscale Engine

Here, the gasgenerator is installed in a vertical position, which facilitates handling. This setup was used only in an early part of the test activities.

This type of engine allows a precise differentiation of the parameters influencing combustion efficiency. However, when optimum configurations are developed from testing with this type of hardware, several reservations have to be made:

- In an operational engine, airflow partitioning and air injection velocities are not independent parameters and both have a major influence on total pressure loss.
- Air injection conditions are less 'well defined' in an operational engine, since the air ducts sit close to the ramcombustor and induce narrow bends at the inlet ports.
- The realization of optimized fuel injector configurations is restricted by the control valve interface.
- A fuel injector configuration showing promising results in a parametric engine as shown above, may act substantially different when coupled with a variable gasgenerator throat.

Nevertheless, testing with parametric hardware provides a sound understanding of the relative importance of parameters determining ramcombustors performance. This technological basis is a precondition for finding adequate solutions in the subsequent development steps.

3.2 Basic Development - Fullscale Testing

As soon as propellant, control valve, controller software, and ramcombustor configuration have reached a sufficient maturity, testing can progress to fullscale hardware.

The setup for fullscale Gasgenerator/Control Valve Tests resembles that of the subscale development phase. The trials, however get more severe, especially with increased burning times and give more reliable information about the formation of deposits and residues and the endurance of the components. Furthermore, fullscale control valve hardware may uncover problems concerning for example

- increased actuation loads/torque needed to adjust the control element(s)
- clearances of a gear actuating several control elements
- tolerances in the assembly of several control elements affecting the min./max. throat area.

These can lead to impaired adjustment accuracy and dynamic behaviour of the valve, and to marginal control loop stability. The torque requirement has to be adapted to be compatible with the performance of an actuator which can be integrated into a subsequent flightweight design.

Many such problems had to be solved on the way to an optimized control valve for ANS. Fig. 13 shows the resulting design with two rotary sliders throttling four gasgenerator outlet ports. The circular control edges of the sliders have a smooth

nozzle contour and exhibit a low susceptibility to deposits.

Fig. 13 Optimized Control Valve Configuration [3]

Typical tasks for the fullscale Direct Connect Testing are

- to define the ramcombustor configuration for a subsequent flightweight design
- to evaluate a preliminary performance envelope of the propulsion system under consideration
- to investigate ramcombustor - control valve interaction
- to investigate ramcombustor thermal protection.

The first two items are usually performed in a fixed flow configuration with burn times below 30 seconds. The last item as well as the third need more extended burn times and are frequently combined in variable flow tests.

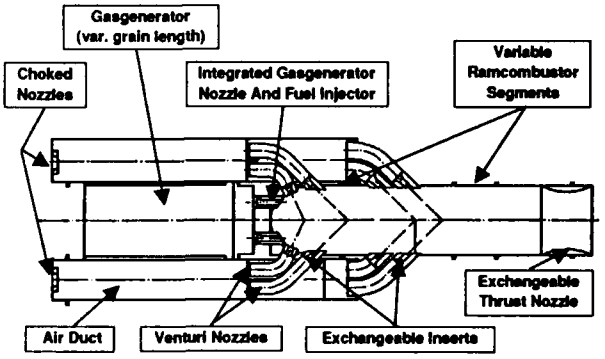

Fig. 14 Fullscale Parametric Hardware For Direct Connect Tests

Fig. 14 presents a sketch of the test hardware used in the ANS program for this development step. The design is closer to an operational engine than the subscale predecessor, but still offers some variability. Main features of the design are:

- The gasgenerator aft closure incorporates four blast tubes with fixed throats at the upstream end which can be replaced by the control valve.
- The ramcombustor dome has a fixed configuration.
- Total chamber length and distance between the air injection stations can be varied by exchanging tube segments.
- Air inlet ports can be varied by exchangeable inserts affecting both air flow partition and air injection velocities.
- Primary airflow can be measured by venturi-nozzles installed in the upstream part of the primary air ducts.
- Choked nozzles can be installed at the upstream end of the four air ducts to simulate the acoustical properties of an operational design.
- The thrust nozzle is exchangeable, mainly to apply different materials for different burn times and to test divergent nozzles.

Fig. 15 shows the fullscale parametric engine integrated on the test stand.

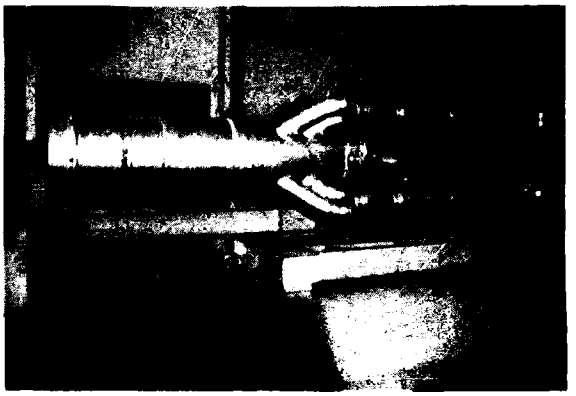

Fig. 15 Direct Connect Test Setup - Fullscale Engine

Since subscale hardware does not scale length (combustion processes depend on residence time), the fullscale hardware has a reduced l/d ratio (about 70% for the ANS hardware).Starting from subscale optimization results, this requires refinement of the air/fuel injection geometry.

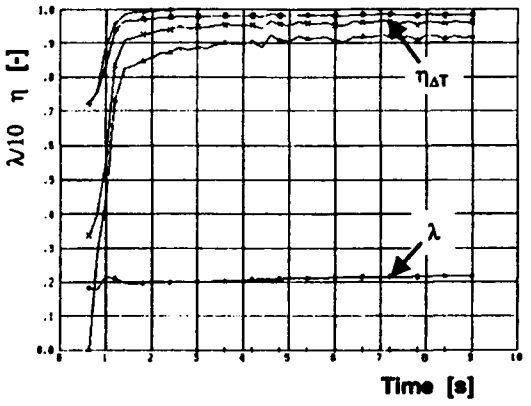

Fig. 16 Fixed Flow D/C Test Results - Fullscale Engine

Test results gained during this phase allow a more realistic extrapolation to an operational system with one reservation left:
The air turn/dump geometry of a flightweight design may produce a less optimum flow pattern and induce

- reduced performance (combustion efficiency, pressure loss)
- locally increased thermal stress and erosion on the thermal protection system.

To give an example of fixed flow d/c test results, fig. 16 presents a plot of performance data gained with the optimized engine for max. thrust - max. fuel flow conditions. Fig. 17 shows plotted data from a variable flow d/c test using a closed loop flight trajectory simulation technique, discussed in the next section. The simulated trajectory was a dive from altitude flight (6 km) to sea level. The plot on top of fig. 17 gives the simulated values of altitude and range, the lower plots show the traces of thrust and commanded and adjusted gasgenerator pressure. The peak in gasgenerator pressure and thrust between 30 and 40 sec is induced by the pullup manoeuvre ending the dive.

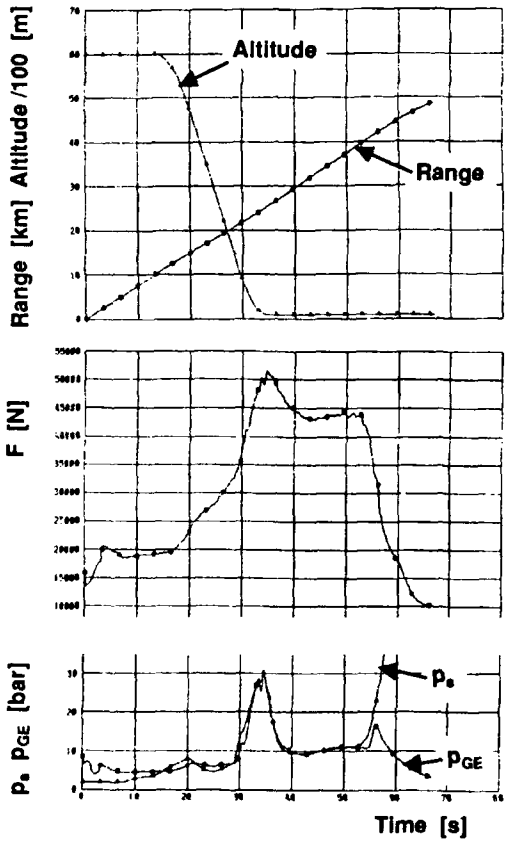

Fig. 17 Results Of A Variable Flow D/C Test With Flight Trajectory Simulation- Fullscale Engine

3.3 Advanced Development - Fullscale Testing

In the advanced development phase, a flightweight engine design has to be derived from the configurations optimized previously. The resulting hardware usually features no geometrical variability and is modified only at considerable expense. The need for modifications however is inevitable and therefore it should be considered whether hardware simplification without compromising the authenticity of test results is possible. For example, high quality material (eg. high strength steel) and sophisticated manufacturing procedures (e.g. flow forming) need not be applied, if a ramcombustor case will be used only for afterburning tests at moderate pressure.

Design and testing of flightweight hardware affect each other strongly. The design must provide features not inherent in a real flight engine, like

- attachments to the test bench, to support the engine and to react engine thrust, or
- a safety valve for the gasgenerator, etc.

Test procedures in turn have to accommodate special provisions for multiple reuse of flightweight components, like

- comprehensive hardware inspections
- posttest cooling of components which have undergone an aging heat treatment as last manufacturing step. For example, pyrolyzing propellant and liner residues in the gasgenerator generate heat over a considerable time and can well overheat a structure made of high strength (e.g. maraging) steel.

The setup for Gasgenerator/Control Valve Firings corresponds to the previous testing efforts. Flightweight gasgenerator hardware has to be made of high strength material. The control valve may use a flight-type actuator or remain with an experimental actuation unit, depending on the aims and fundings of a program.

Debugging of the control valve can partly be made with reduced burning times. Here, a combination of the flighttype control valve with experimental (heavywall) gasgenerator hardware is recommendable.

Tests with a full burn time, simulating an operational pressure profile, are finally used to prove the correct function and endurance of the control valve, gasgenerator structure and thermal protection. Fig. 18 illustrates this type of testing. The simulated flight trajectory includes a climb from sea-level to high altitude, high altitude cruising, a dive back to sea level and a final manoeuvring phase with maximum thrust. Fig. 18 shows traces of the pressure commanded by the gasgenerator controller, the pressure adjusted by the valve and the relative position of the valve. Nearly the entire area ratio of the valve is used to cover the required pressure range. The spikes in the pressure and valve position traces occurring between 60 and 120 sec correspond to a commanded 'wiping' motion of the valve to strip off deposits and preserve the maximum throat area.

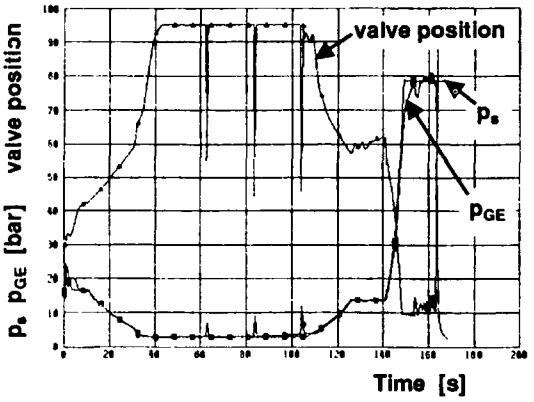

Fig. 18 Results Of A Gasgenerator/Control Valve Firing - Fullscale Flightweight Hardware, Full BurnTime

Direct Connect Testing of flightweight hardware is the most authentic trial for cruise phase operation which can be performed in ground testing.

Fixed flow d/c tests with reduced burn times form only a minor part of this activity. They are done to verify performance figures, and to prove that the flightweight design has succeeded in keeping close to optimized configurations determined in the preceding development steps. If successful, the results will resemble those of fig. 19, which were gained with the ANS flighttype engine. Combustion efficiency data are given along with the equivalence ratio for simulated cruise flight conditions at low altitude.

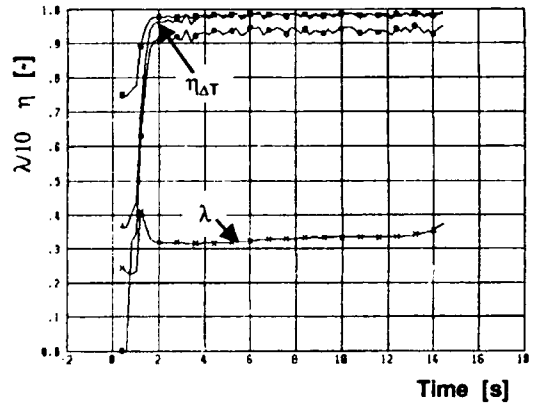

Fig. 19 Fixed Flow D/C Test Results - Fullscale Flightweight Engine

Variable flow d/c tests combine all components of the cruise engine. Conducted with full burn time, they demonstrate function, endurance, and integrated performance of the system. Fig. 20 shows the ANS flightweight engine installed on the test bench for a variable flow d/c test. The gasgenerator is located in a vessel for posttest watercooling to prevent the structure (flow formed case, maraging steel) from damage. The vertical device on the upper side of the gasgenerator is the safety valve. The control valve incorporated in the interstage section uses an experimental hydraulic actuator. The ramcombustor and the air ducts feature a flightweight design, but are made of conventional steel. The convergent/divergent thrust nozzle is a C/C structure with SiC antioxidizing-impregnation. All engine sections are connected by key locks.

Fig. 20 Fullscale Flighweight Hardware For Variable Flow Direct Connect Tests

In order to test as close to reality as possible, MBB has developed a procedure, to 'fly' an engine on the test bench. The so called Hardware In The Loop Flight Simulation [3] needs some explanation, which shall be done referring to fig. 21.

The upper half of fig. 21 represents the flight parameters, while the lower half illustrates the flight simulation during ground testing.

During flight, engine thrust acts against inertia, gravitation and aerodynamic forces of the missile. A Machmeter and the Inertial Navigation System (INS) provide measured values of Mach number and acceleration as input data to the speed control system implemented in the control computer. In the example shown, the speed controller consists of a Mach number controller and a cascade controller for the gasgenerator pressure. The Mach number controller adjusts the set value of gasgenerator pressure to increase or reduce thrust, until the Mach number required by the specified trajectory is reached. The pressure controller adjusts the gasgenerator pressure by providing set values for the throat area of the gasgenerator control valve. This output closes the loop for the speed control.

For ground testing, the algorithms of the speed control code can be implemented on a test facility computer.

Usually, this computer also controls massflow and stagnation temperature of the air fed into the engine corresponding to simulated flight conditions. According to fig. 21, this features a closed loop control of air massflow and air temperature. Air heating is done by a vitiator using gaseous hydrogen as fuel. Make up oxygen is added to the air corresponding to the vitiator massflow (not shown in fig. 21). Consequently, the temperature controller includes cascade controllers for hydrogen and oxygen massflow.

An additional code for the simulation of missile dynamics provides the missing link between the test bench and the

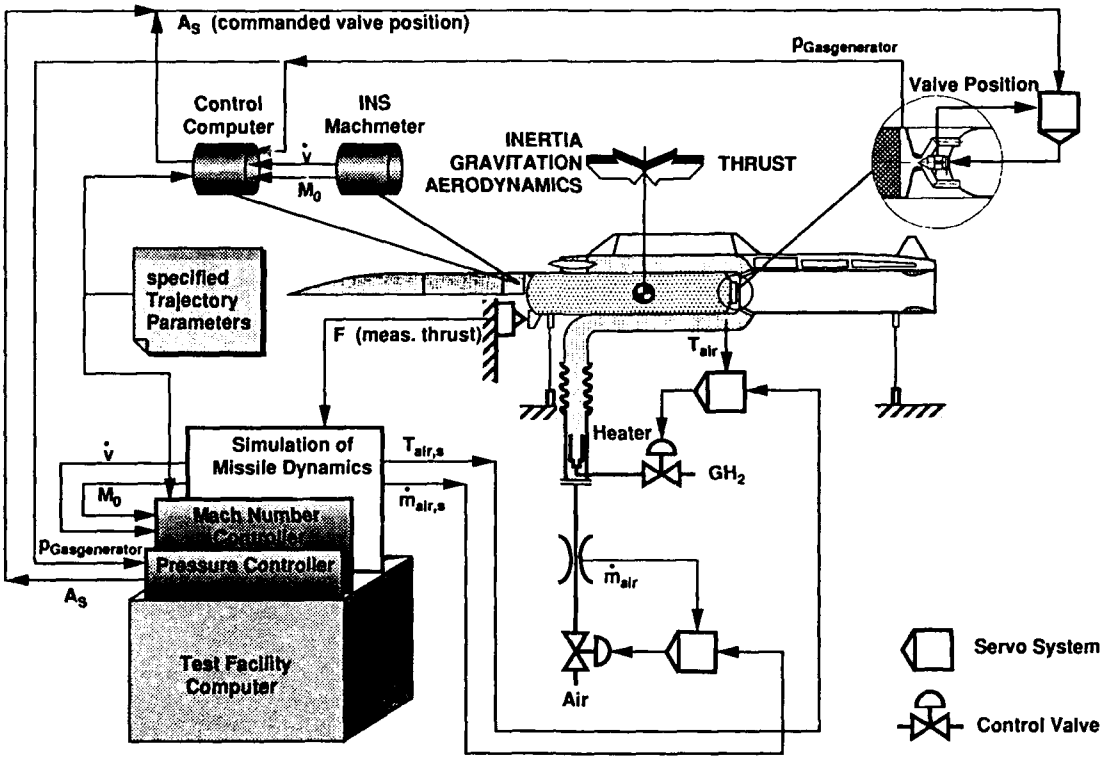

Fig. 21 Hardware In The Loop Flight Simulation

speed control system. By determining

- measured thrust
- currently 'simulated ' missile mass (calculated from a set initial mass and the integrated propellant massflow)
- currently 'simulated' flight conditions (altitude, Mach number, angle of incidence)

the coefficients of thrust and drag and a 'simulated' acceleration can be calculated. A first integration provides velocity and Mach number for the next control cycle. A second integration provides the flight path, the new altitude and the covered range over ground.

Acceleration and Mach number are fed into the speed controller code as input values and provide the basis for the determination of set values for the test facility controllers for air massflow and air temperature.

Fig. 22 (as well as fig. 16 of section 3.2) gives another example of test results gained with this technique. Here, a sea level trajectory was simulated. A cruise phase at some initial Mach number was followed by an acceleration phase to a higher Mach number after a specified range. The mission ends with a max. thrust phase for terminal manoeuvring. From top to bottom, fig. 22 presents traces of

- the range over ground at the specified constant altitude
- the Mach number
- the acceleration determined by the simulation of missile dynamics
- set value p_s and measured value p_{GE} of the gasgenerator pressure.

After a short initial disturbance caused by the starting sequence of the pressure controller at gasgenerator ignition, the Mach number is adjusted correctly to the set initial value. The reduction of the gasgenerator pressure at 30 sec is due to an increased burning surface of the bottle shaped grain. This also causes only very moderate disturbances in the traces of acceleration and Mach number. At the end of the acceleration phase, the Mach number control is deactivated and replaced by a set value adjuster, which produces input data for the pressure controller according to the specified manoeuvring. In this phase, engine thrust did not completely compensate for the drag induced by the simulated manoeuvres, which resulted in a moderate decrease in Mach number. Set and measured values of the gasgenerator pressure correspond very well for the complete test. The oscillations occuring at the beginning of the max. pressure phase are induced by problems inherent in adjusting a very small throat area of the control valve at the given cycle time of the control loop. The pressure controller damps the oscillations by reducing the gain of the control loop.

3.4 Testing Of The Integrated SDR Propulsion System

Freejet testing and transition testing are the main milestones in ground testing of the integrated SDR propulsion system.

Usually, windtunnel facilities of sufficient size and capability (pressure, blow time) are not available nor affordable to per

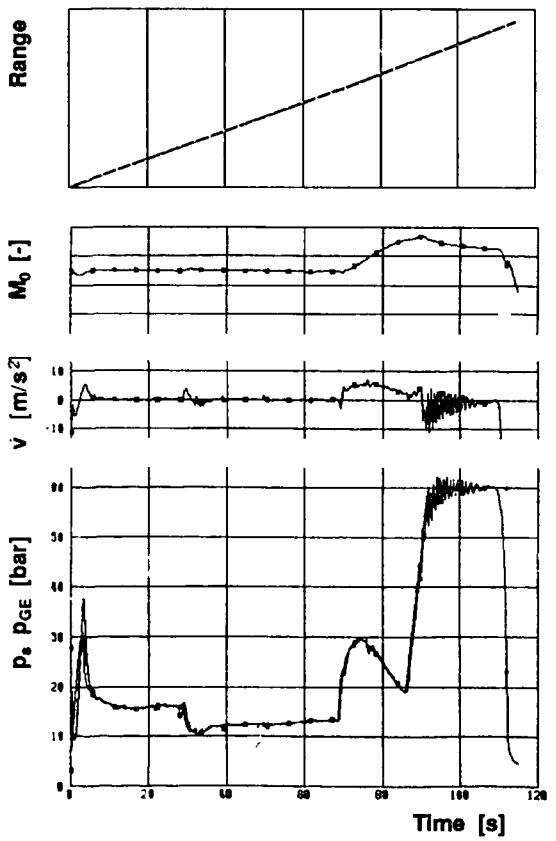

Fig. 22 Results Of A Variable Flow D/C Test With Flight Trajectory Simulation - Fullscale Flightweight Engine

form freejet testing with the integrated missile. Consequently, semi-freejet testing is applied, which can be done on the development test bench, if the facility features sufficient airflow capacity. For semi-freejet testing, each air intake of the propulsion module is fed by an individual small windtunnel nozzle, designed to simulate the required Mach number. This setup is shown by the photograph of fig. 23.

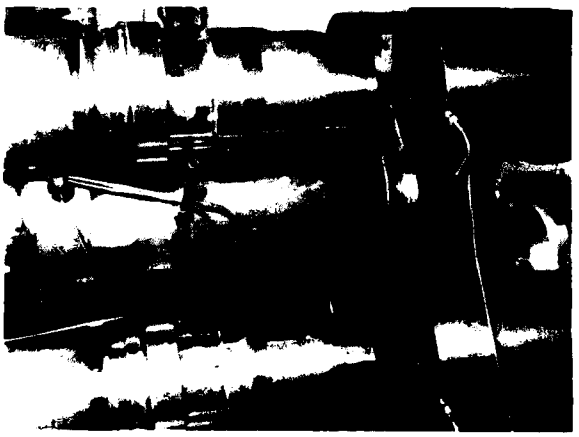

Fig. 23 Setup For Semi-Freejet Testing - Circular Laval Nozzles, Axisymmetric Air Intakes

Semi-freejet testing does not allow the simulation of

- the influences of incidence and forebody
- varying Mach numbers (which would require variable geometries for the windtunnel nozzles)
- flight conditions at higher altitude (which would require an ejector device enclosing the test setup).

Thrust cannot be measured accurately from semi-freejet testing. Therefore it must be determined using the ramcombustor total pressure.

Semi-freejet testing of the integrated sustainer propulsion system with reduced burn times is an appropriate tool to investigate interactions of ramcombustor and air intakes and the engine startup at takeover from the boost phase.

Testing of the transition phase from boost to sustain operation may be done either in a semi-freejet or d/c setup. Both options offer advantages and disadvantages :

- Semi-freejet transition testing provides a simulation which is very near to flight conditions. Interactions of air intake start, booster tailoff, booster propellant slivers and ramcombustor ignition are closely reproduced. On the other hand, a subsequent cruise operation with full burn time is not feasible, if the mission includes variable flight conditions.
- For d/c transition testing, the ram air must be bypassed during the operation of the integrated booster. At booster burnout and portcover opening this air must be switched over to the engine by a big and fast valve. This process may affect the transition time. Furthermore, this test procedure is insensitive to pressure transient phenomena which may lead to a failure of the flight system. Here, however, the opportunity exists to add a simulated cruise operation after the boost and transition phase. Thus, the full mission of the propulsion system can be simulated on the test bench.

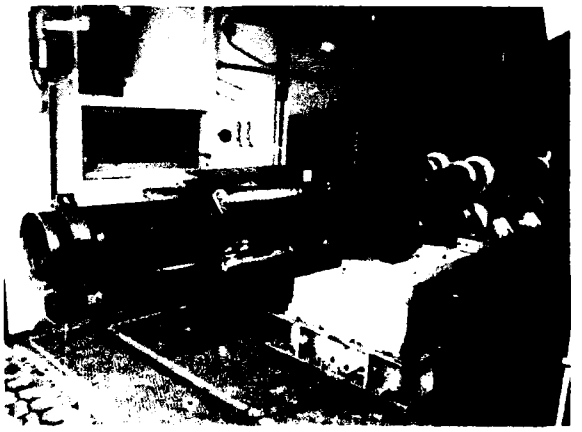

Fig. 24 Setup For Semi-Freejet Transition Testing - Fullscale Flightweight Engine

It is recommendable to conduct both types of transition testing, if sufficient funding is available. The main issue of semi-

freejet transition testing is to prove the proper function of the propulsion system. D/C transition testing with subsequent full time sustainer operation provides a demonstration of system endurance, especially regarding the ramcombustor thermal insulation which is stressed by the preceding booster firing.

Fig. 24 shows the fullscale flightweight engine (cf. section 3.3) with the integrated booster installed on the test bench for a semi-freejet transition test. In this case, the ramcombustor is a flow formed structure made of maraging steel. The coaxial (ejectable) booster nozzle can be seen inside the ramjet nozzle. The setup features a gasgenerator of reduced length for a short sustainer operation after the transition phase.

Fig. 25 illustrates typical results derived from a transition test. The diagrams show the time span between booster tail-off and thrust buildup of the sustainer engine. The upper diagram gives the trace of the longitudinal acceleration evaluated from chamber pressure. The transition time is defined by the period where the longitudinal acceleration is negative. The resulting decrease of Mach number, shown by the lower diagram, is a determining factor for the ability of the ramjet to reaccelerate.

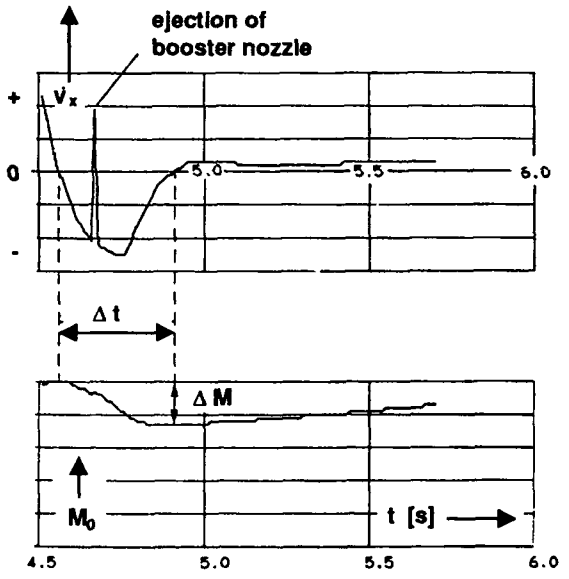

Fig. 25 Results Of Transition Testing

4. CONCLUDING REMARKS

This paper reviewed the philosophy of ground testing for the throttleable ducted rocket as applied in the development activities of MBB and Bayern Chemie. To date more than 2000 tests have been performed with ducted rocket systems and components in basic and advanced development phases of several programs. The examples given in the paper demonstrate the advanced technical standard that has been achieved in this field. The hardware in the loop flight simulation technique has proven to be an especially valuable tool to prepare a sound basis for the final and most costly trial - flight test.

REFERENCES

[1] Besser, H.-L.; Strecker, R.
Overview of boron ducted rocket development during the last two decades.
Second international symposium on special topics in chemical propulsion : Combustion of boron-based solid propellants and solid fuels.
Lampoldshausen, Germany 1991

[2] Besser, H.-L.
Solid propellant ramrockets. AGARD-LS-136, 1984

[3] Thomaier, D.
Speed control of a missile with throttleable ducted rocket propulsion. AGARD-CP-431, 1987

Discussion

Question from R. MONING

Is there agreement between the air temperature in the connected pipe and freestream investigations with the flight conditions ?

Did you observe a significant influence of the air temperature ?

Author's reply

Air temperature is adjusted according to the simulated flight conditions both in connected pipe and semi-freejet tests.

The influence of air temperature on combustion efficiency depends on the type of fuel used.

If the geometry of the air ducts and the air injection into the ramcombustor is fixed, an air temperature different from the real flight conditions will lead to air injection velocities and pressure not representative of the real system.

THE DUAL COMBUSTOR RAMJET: A VERSATILE PROPULSION SYSTEM FOR HYPERSONIC TACTICAL MISSILE APPLICATIONS[1]

by

Paul J. Waltrup
The Johns Hopkins University
Applied Physics Laboratory
Laurel, Maryland 20723
U.S.A.

SUMMARY

Procedures for designing and maximizing the performance of Dual Combustor Ramjet (DCR) engines and vehicles powered by this engine are presented. Comparisons of DCR powered vehicles with scramjet powered vehicles for Mach 4 to 8 flight show that the DCR provides better performance at the Mach 4 flight condition, while the scramjet is better at Mach 8. Comparisons of the DCR with a ramjet for Mach 3 to 6 flight, with both having the same, but low, thrust level at Mach 3, show that the DCR exhibits better performance at and near the cruise condition at Mach 6, and similar performance during acceleration. Suggested additional comparisons to broaden the scope of the conclusions are also given.

NOMENCLATURE

A	- area
C_{t_g}	- gross engine thrust coefficient
C_{t_n}	- net vehicle force coefficient
DCR	- dual combustor ramjet
ER	- fuel-air equivalence ratio = fuel-air ratio/stoichiometry
HHC	- heavyhydrocarbon
M	- Mach number
p	- pressure
T	- thrust, temperature
w	- mass flow rate
Z	- altitude
α	- angle-of-attack in degrees
η_{KE}	- supersonic inlet kinetic energy efficiency
η_n	- exit nozzle stream thrust efficiency
η_{pt}	- inlet total pressure recovery

Subscripts

a	- air stream
b	- gas generator base
cr	- critical
des	- design
gg	- gas generator
i	- maximum inlet area
max	- maximum
o	- overall; free stream
ss	- supersonic inlet
t	- stagnation conditions
0	- free stream station
1	- inlet cowl plane
2	- inlet throat
3	- prior to normal shock in gas generator and ramjet inlet
4	- diffuser exit
s	- after scramjet precombustion shock
5	- combustor exit
6	- nozzle exit

Superscripts

*	- gas generator or ramjet combustor throat

INTRODUCTION

The design of tactical missiles involves the integration of many complex parts including, but not limited to, boost and sustain propulsion, airframe, aerodynamics and control, materials, guidance, ordnance and fuze, fuel supply and control, and power. Additionally, mission requirements and launcher constraints, when combined, define the flight envelope and range, and weight, volume and external missile geometry, respectively.

In this paper, we will concentrate on the sustainer propulsion system and its integration with the aerodynamics and airframe, insofar as they influence and/or affect net vehicle thrust performance. In particular, this paper addresses the use of the Dual Combustor Ramjet (DCR) as the sustainer engine for hypersonic (up to Mach 8) flight of tactical, liquid fueled missiles, and compares net vehicle performance with that achieved with supersonic combustion ramjet (scramjet) and conventional subsonic combustion ramjet engines. It also presents the methodology necessary to guide the design the DCR engine.

To present this methodology requires that a particular mission and launcher constraint be selected, but the general approach is not dependent on the particular selection, only the exemplary results presented herein. The constraints chosen here are the same as those presented in Ref. 1, i.e.,

(1) The missile is to fit in a circular or square launcher;

(2) The missile is to be rocket boosted to either Mach 3 or 4 after which the airbreathing sustainer will accelerate the vehicle to its cruise Mach number of either 6 or 8;

[1] This work was supported by the Johns Hopkins University Applied Physics Laboratory with a Stuart S. Janney Fellowship.

(3) The sustainer engine will be either a fixed geometry DCR, scramjet or ramjet; and

(4) The sustainer engine will use Shelldyne-H (RJ-5) fuel burning at 100% efficiency and fly within the tropopause at 50K ft. (15.24 km) altitude.

Within these constraints, the objective is to present the methodology necessary to select the DCR's inlet design Mach number, air flow split and area contraction ratio, subsonic combustor size, and supersonic combustor area ratio to maximize net vehicle performance. Additionally, the merits of using the DCR over either a scramjet or ramjet sustainer are discussed using exemplary comparisons between the three candidate engines shown in Figure 1.

THE DUAL COMBUSTOR RAMJET ENGINE

Prior to presenting the design methodology or performance comparisons, a brief description of the DCR engine [Fig. 1(b)] and its cycle is appropriate to orient the reader in its operation and to point out similarities and differences between it and either the ramjet or scramjet engines depicted in Fig's. 1(a) and 1(c), respectively. As shown in Fig. 1(b), the dual combustor ramjet is an engine that combines the best features of both the scramjet and dump combustor ramjet in a single cycle. As will be seen latter, this results in an engine that operates much like a conventional ramjet at the lower flight speeds (Mach 3 to 5) but also like a scramjet at the higher flight speeds (Mach 6 and above).

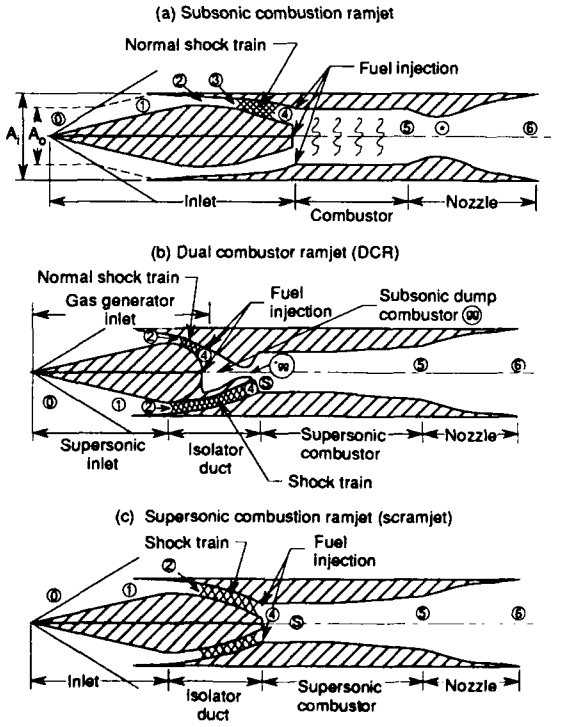

Fig. 1 Engine schematics of (a) subsonic combustion ramjet, (b) dual combustor ramjet, and (c) supersonic combustion ramjet

The DCR[2] evolved from the desire to use pure heavyhydrocarbon (HHC) fuels at hypersonic speeds rather than blends of HHC fuels with "logistically unsuitable" but very reactive liquid fuels (e.g., boranes) or oxidizer pilots (e.g., chlorine trifloride), which had traditionally been required for efficient HHC combustion in scramjets, even at speeds greater than Mach 7[3]. In practice, efficient supersonic combustion requires that the combination of air static enthalpy, HHC enthaply and enthalpy (including heat release) of the very reactive fuel (or oxidizer pilot reacting stoichiometrically with a portion of the HHC fuel) has to be approximately 15,000 BTU/lbm (34.89 MJ/kg) of HHC fuel or greater. For example, using pentaborane (as the reactive fuel additive) mixed with RJ-5, Fig. 2 shows the weight percent of B_5H_5 needed as a function of fuel-air equivalence ratio, ER, to achieve greater than an 80% fuel combustion efficiency for Mach 4 and 7 flight at the inlet exit static enthalpies shown. For stoichiometric combustion at Mach 4, the fuel mixture carried on the missile has to exceed 29% by weight pentaborane.

To eliminate any dependence on these pyrophoric, caustic and/or toxic additives, it was recognized that pure HHC fuels would have to be preprepared to exceed this minimum enthalpy requirement prior to injection into the supersonic combustor. Essentially, this meant heating and cracking the HHC fuel to high temperature and light gaseous or angstrom size particulate (carbon) species prior to injection. To achieve this meant using either an energy source external to the propulsion system, at the expense of a loss in weight and volume for other vehicle stores as well as unusable (propulsive) energy, or an energy source that was an integral part of the engine cycle and used all of the energy directly for propulsion. The latter was deemed simpler and more efficient and evolved into what is now called the dual combustor ramjet.

In the DCR, the inlet diffusion process is the same as that in the scramjet, only a small portion of the air captured by the inlet (typically 1/3rd or less) is split off and further diffused to provide a subsonic air stream to a small subsonic dump combustor imbedded within the main scramjet engine. The ingested air is then mixed and reacted stoichiometrically in the dump combustor with some of the HHC fuel to produce a hot [> 4500°R (2500°K)], mainly gaseous stream. Initially, it was not known whether the remainder of the HHC fuel could be injected, heated and cracked within this hot gas stream without quenching the initial combustion process because of the large amount of unreacted fuel (ER >= 4 in the dump combustor) present. Mestre and Ducourneau, however,

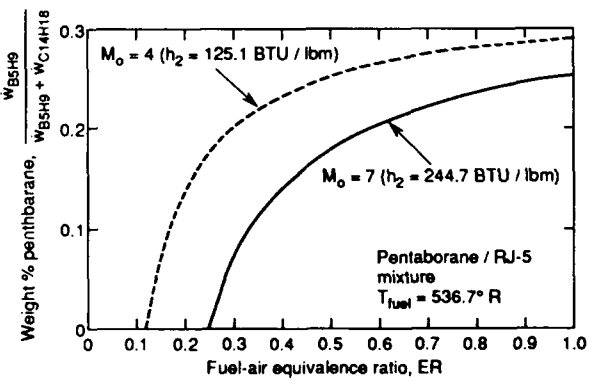

Fig. 2 Percent pentaborane necessary to burn RJ-5 in a typical scramjet combustor

demonstrated that a flame could be maintained with liquid heavyhydrocarbon fuels up to an ER of 7.7[4] at conditions simulating Mach 3 to 4 flight. Consequently, all of the HHC fuel used in the DCR can be, and is, injected (non-uniformly) into the dump combustor, generating a hot, cracked, partially reacted, fuel-rich stream. Because of its fuel-rich operation, the dump combustor is quite often referred to as the gas generator.

The gas generator exhaust products are then injected axially through a geometric throat into the supersonic combustor; the exit speed may be either sonic or supersonic, depending on the gas generator exit design. In either case, the energy and composition of these exhaust products are such that they permit efficient combustion to take place in the 1 to 2 ms residence time available in the supersonic combustor, even at flight speeds as low as Mach 3. Here, the air entering the supersonic combustor, which comprises 2/3rd's or more of the air captured by the inlet, bypasses the gas generator supersonically as shown in Fig. 1(b). The nearly constant area duct between the supersonic inlet and supersonic combustor provides more than sufficient length to isolate the precombustion compression field (or shock train) generated by the supersonic combustion process from the supersonic diffusion process in the inlet[5].

The hot, fuel-rich exhaust from the gas generator then mixes and reacts with the supersonic air stream in the supersonic combustor, and the combustion process is just as it would be in any scramjet with axial injection[5-7]. The only real difference is that the axial injector is rather large in this case, the fuel is quite hot and contains some combustion products, and the length of supersonic combustor required to achieve high fuel combustion efficiencies for the Mach 3 to 8 speeds discussed herein is approximately twice that required in a borane fueled scramjet. This latter difference is partially (if not completely) due to the use of axial fuel injection in the DCR versus normal fuel injection in the scramjet. Finally, like in the pure scramjet, there is no combustor exit geometric throat in the DCR, requiring the combustor exit Mach number, M_5, to be unity or greater. This, in turn, can limit the total amount of heat added to less than stoichiometry at the lower flight speeds (just like in a scramjet), and the exit nozzle expansion process does not always begin with a Mach number of unity; the initial conditions will vary with flight speed and the amount of heat addition.

DCR DESIGN METHODOLOGY

As alluded to previously, the intent of this section is to present the methodology necessary to select the inlet design Mach number, M_{des}, inlet air flow split, w_{ass}/w_{ass}, inlet area contraction ratio, A_i/A_2, gas generator throat size, $(A^*/A_i)_{ss}$, and supersonic combustor area ratio, $A_5/(A_{2ss} + A_b + A^*_{ss})$ when designing a DCR. Here, it assumed that the isolator duct carrying the supersonic air from the inlet to the supersonic combustor is constant area, i.e., $A_{2ss} = A_{4ss}$. This, however, is not the case for the ramjet or DCR gas generator inlets where $A_4 >> A_2$. Here, modulation of the normal shock total pressure by varying the initial Mach number, M_3, between stations 2 and 4 is necessary to keep the fixed geometry combustor exit throat choked for ER's of unity or less. As will be seen shortly, however, very little total pressure modulation is required to keep the throat choked once the ER of the gas generator or ramjet is above unity.

Supersonic and Gas Generator Inlets: In order to start this procedure requires some knowledge of, or assumption about the, inlet's compressive performance. The point of departure used in this study is the empirically derived correlation of supersonic inlet kinetic energy efficiency, η_{KE}, as a function of diffuser throat (or) exit-to-free stream Mach number ratio, M_2/M_0, presented in Ref. 1 based on data from two dimensional, annular and modular scramjet inlets in the Mach 3 to 8 range. This correlation is shown in Fig. 3 and is expressed by:

$$\eta_{KE} = 1 - 0.4(1 - M_2/M_0)^4 \qquad (1)$$

This correlation, in turn, can be rearranged to express the total pressure recovery of the supersonic inlet, p_{t2}/p_{t0}, as a function of effective inlet contraction area ratio, A_0/A_2, as shown in Fig. 4 (from Ref. 1) for flight at 50K ft. (15.24 km) altitude. Both also tacitly assume that η_{KE} is not a function of angle-of-attack since insufficient data were available to deduce any such dependency. However, dependency is implicit in that A_0/A_2 and M_2 are both dependent on α.

The results show that for each flight Mach number, p_{t2}/p_{t0} decreases with increasing contraction ratio until a maximum value of A_0/A_2 is reached, and that further increases in A_0/A_2 are not possible. Consequently, there are definite upper limits on inlet area contraction (at least for the data correlated), with the maximum being 8.5 at $M_0 = 7$. This has important ramification in two areas. First, a number of parametric studies (including some of the author's) have overlooked these upper limits, perhaps resulting in some erroneous conclusions for fixed geometry inlet scramjets. Secondly, not only does the upper limit have to be considered, but also the air capture characteristics, A_0/A_i, of the inlet and flight envelope. For instance, as will be seen latter, an inlet designed for Mach 4 to 8 flight will have much different inlet area contraction limits than one designed for Mach 3 to 6 flight, mainly because the area contraction limits shown in Fig. 4 cannot be exceeded at any flight Mach number, not just at the highest.

The data and correlations shown in Fig's. 3 and 4 can be used to define the critical pressure recovery of the DCR's gas generator inlet as well as that of the conventional subsonic combustion ramjet's inlet. If we permit a normal shock to occur at station 2 for each point along each curve shown in Fig. 4 (each will have a different Mach

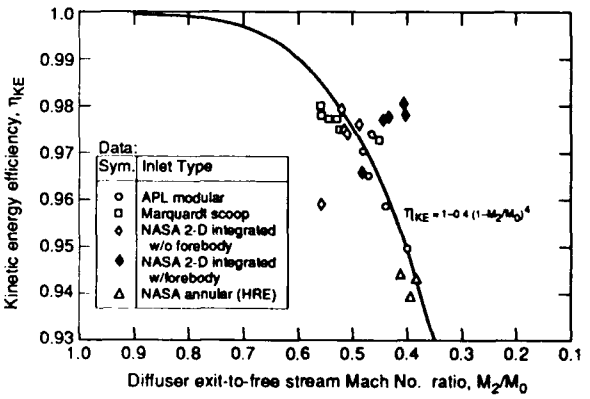

Fig. 3 Supersonic inlet kenetic energy efficiency as a function of diffuse exit-to-free stream Mach Number ratio (from Ref. 1).

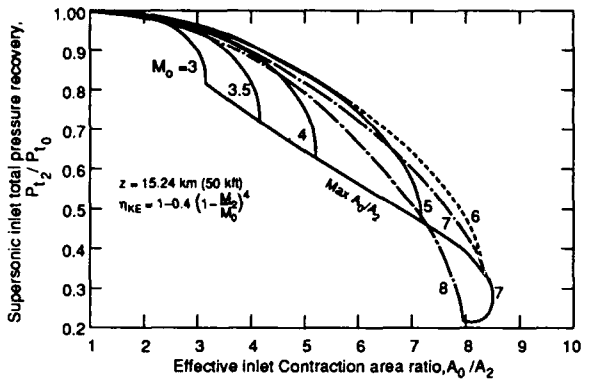

Fig. 4 Supersonic inlet total pressure recovery as a function of effective area contraction ratio

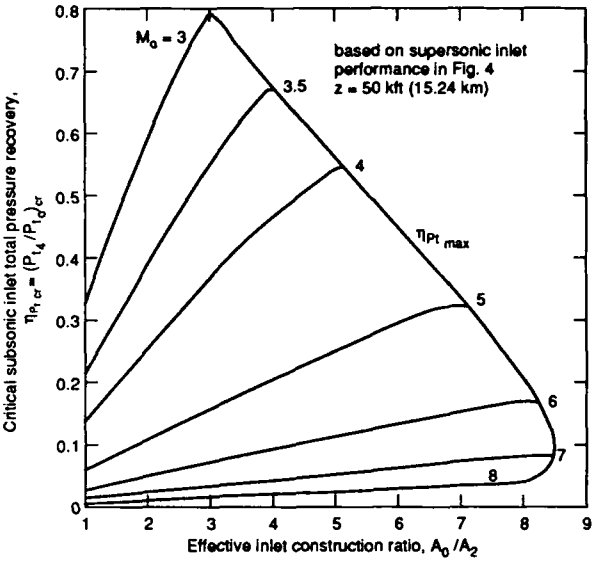

Fig. 5 Critical gas generator inlet total pressure recovery as a function of inlet area contraction ratio and flight Mach number

number, M_2), then a curve of critical total pressure recovery, $\eta_{pt\ cr} = (p_{t4}/p_{t0})_{cr}$, as function of A_0/A_2 can be generated as shown in Fig. 5. Here, the values of A_0/A_2 have the same limits as those in Fig. 4. As expected, the maximum critical pressure recoveries at each M_0 correspond to the maximum area contraction ratios of the supersonic inlet (Fig. 4). For example, the maximum critical total pressure recovery for $M_0 = 3$ occurs at $A_0/A_2 = 3.13$ with a value of 0.795.

Up to this point in the discussion, no consideration has been given to the specific inlet design, i.e., its design Mach number, geometry and the amount of external (A_0/A_1) and internal (A_2/A_1) contraction. However, the maximum contraction ratios shown in Fig's. 4 and 5 are based on the captured stream tube (A_0) of the inlet, not its maximum air capture (A_1). Consequently, a specific inlet geometry must be introduced at this point to determine the maximum geometric area contraction (A_1/A_2) for a given inlet design. The inlet chosen is the same as that presented in Ref. 1, i.e., a 12.5° half angle cone. At this point, it is not necessary to specify its design Mach number since subsequent results can be presented as a function of M_{des}, M_0 and the range of Mach numbers (e.g., $M_0 = 4$ to 8) over which the vehicle will fly. However, a 12.5° half angle cone inlet cannot externally compress the flow to the maximum value shown in Fig. 4, It is therefore assumed that there is a 20% internal area contraction ($A_1/A_2 = 1.2$), with any remaining contraction achieved by an external isentropic compression surface whose wave structure always falls within the cowl.

With the inlet geometry thus defined, it is now possible to directly relate the maximum values of A_0/A_2 given in Fig's. 4 and 5 to the specific inlet geometry. This requires that the maximum air capture of the inlet be known as a function of M_{des}, M_0 and angle-of attack. Note that the air capture for an axisymmetric conical design is a maximum at $\alpha = 0°$. This is not the case for assymetric inlet geometries where $(A_0/A_2)_{\alpha>0}$ can exceed $(A_0/A_1)_{\alpha=0}$ (see, e.g., Ref. 1). In either case, multiplying $(A_0/A_2)_{max}$ in Fig. 4 by (A_1/A_0) as a function of M_0 and M_{des} (the values of A_0/A_1 for all of these cases are given in Ref. 1) will yield a set of curves of $(A_1/A_2)_{max}$ for each case. Since the maximum values of A_0/A_2 shown in Fig. 4 cannot be exceeded, the value of A_1/A_2 for a given M_{des} and flight Mach number range will then be the minimum of these maximums.

If we take the flight Mach number ranges to be Mach 4 to 8, Mach 3.5 to 7 and Mach 3 to 6, then the minimum of the maximum values of A_1/A_2 can be plotted as a function of M_{des} as shown in Fig. 6. The results show that as both the Mach number range and inlet design Mach number increase, the maximum value of A_1/A_2 increases, with this increase being almost linear with M_{des}. This is to be expected since A_0/A_1 increases almost linearly with M_0 and M_{des}. Here, for example, $(A_1/A_2)_{max}$ is 7.92 for an M_{des} of 7 and above for a flight Mach number range of 4 to 8. However, when $M_{des} = 4$, $(A_1/A_2)_{max}$ decreases by 34% to 5.24 for this same flight Mach number range. Note that these maximums apply to both the inlet for the scramjet combustor and the inlet for the ramjet and DCR subsonic combustors in this paper.

Gas Generator: With the inlet performance defined as above, it is now possible to present the design philosophy and methodology used for the gas generator along with specific exemplary cases. Since the intent of the gas generator is to prepare all of the HHC fuel for efficient combustion within the tandem supersonic combustor, it must efficiently ingest the small fraction of air (1/3rd or less of the total engine air flow) diffused subsonically to it, maintain a stable flame with fuel flows of 4 to 8 (or more) times stoichiometry with a minimum of total pressure loss, heat and crack the unreacted fuel to light gaseous or angstrom size carbon species, and accelerate the hot, fuel-rich mixture to sonic or supersonic speeds through a geometric throat prior to axial injection in the supersonic combustor. All of this is accomplished using a small, subsonic dump combustor with multiple (two or more) air inlets.

Two or more air ducts entering the dump plane of the gas generator are required to induce a recirculation zone in the center of the dump plane. This can be accomplished by partitioning the annular flow at the cowl plane of the symmetric inlet discussed above into symmetric quadrants, with two or more quadrants feeding the gas generator and the remainder supplying supersonic air to the supersonic combustor[7,8]. Alternatively, a single air supply duct could be bifurcated prior to reaching the gas generator . In either case,

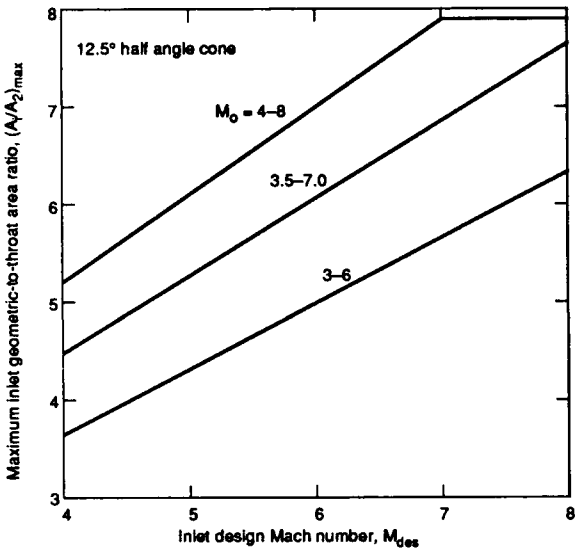

Fig. 6 Maximum inlet geometric contraction as function of inlet design Mach number and flight Mach number range.

the recirculation zone between ducts at the head end of the dump combustor provides a region where a near stoichiometric HHC flame can be established and maintained to provide the heat source needed to heat and decompose the remainder of the HHC fuel. The remainder of the HHC fuel is then injected such that it does not migrate to the center of the dump plane dome, rather it mixes and interacts with the heated combustion products further downstream, preventing quenching of the initial flame.

The mixture of hot, fuel rich products is then accelerated through a fixed geometry, geometric throat, A^*_{ss}, the size of which is a function of the inlet performance and air capture, dump combustor total pressure losses, gas generator fuel-air equivalence ratio, ER_{ss}, and thermodynamic properties of the exhaust products. Since all of the gas generator air plus fuel mass must pass through this throat without it unchoking for a given flight Mach number and altitude, then its minimum size relative to the air capture streamtube, $(A^*/A_0)_{ss}$, can be initially determined from conservation of mass using the maximum critical total pressure recoveries in Fig. 5, and assuming a 20% dump combustor total pressure loss, irrespective of the inlet's design Mach number. For reference, the fuel used in these studies is room temperature Shelldyne-H (RJ-5) with a chemical composition of $C_{14}H_{18}$, a heat of formation of +20 kcal/gm-mole, a lower heating value of 9.97 kcal/gm, a specific gravity of 1.07, a stoichiometric fuel-air ratio of 0.0728356, and a molecular weight of 186.298 gm/gm-mole.

The results from just such a sizing are shown in Fig. 7, where values of $(A^*/A_0)_{ss\ min}$ are presented as a function of ER_{ss}, M_0 and flight altitude. For the gas generator inlet total pressure recoveries shown in Fig. 5, these curves represent the minimum throat areas needed to maintain $M^*_{ss} = 1$. Larger throat sizes are permitted but not smaller. As expected, the lower the altitude, the more air that is captured and the larger the required size of the gas generator throat. At a given altitude (ie. 15.24 km), it is apparent that the gas generator must be sized for the lowest flight Mach number provided the ratio of air capture from one flight Mach number to the next is less than the ratio of the minimum gas generator throat sizes. For the

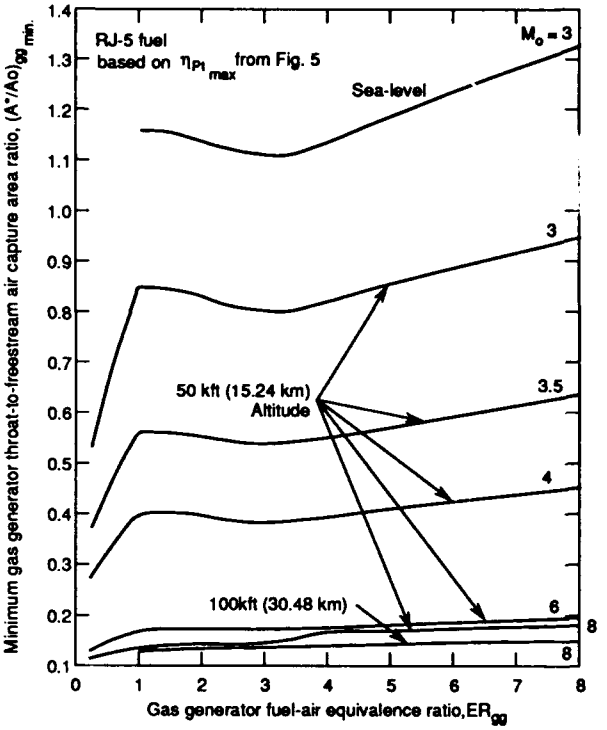

Fig. 7 Minimum gas generator throat size as a function of flight Mach number, fuel-air equivalence ratio and altitude for $\eta_{Pt_{gg_{max}}}$

12.5° conical inlet used in this paper, this is indeed what happens, i.e., the gas generator throat is sized by the mass flow and gas generator exit thermodynamic properties at the lowest flight Mach number.

Perhaps the most important feature illustrated in Fig. 7, however, is that the change in the required gas generator throat size above stoichiometry compared to that below stoichiometry is small. Since throat area is directly proportional to the total pressure required to maintain a choked throat, and the overall DCR engine almost always operates with $ER_{ss} > 1$ regardless of M_0, M_{des}, flight Mach number range and w_{ass}/w_{ass}, then these results show that the DCR gas generator inlet will operate at or near its critical total pressure recovery over most of its flight regime, especially at the lower flight speeds. For example, for $w_{ass}/w_{ass} = 7$ ($ER_{ss\ max} = 8$ for an overall engine equivalence ratio, ER_o, of unity) and $M_0 = 3$, which exhibits the largest variation in the gas generator total pressure required to maintain a choked throat, the total pressure required at $ER_{ss} = 3$ ($ER_o = 0.375$), where the total pressure requirement is a minimum, is only 16% less than the maximum critical total pressure recovery at $ER_{ss} = 8$ ($ER_o = 1$). At Mach 6 this difference is approximately 18% but grows to over 72% at Mach 8. This is why, as will be seen in subsequent comparisons, the DCR is as efficient or more efficient than the ramjet at the lower flight speeds.

Returning now to the example being developed previously, if the air capture characteristics of the 12.5° conical inlet are incorporated into Fig. 7 as a function of M_{des} and flight Mach number range, then the results in Fig. 7 can be replotted as shown in Fig. 8. Here the minimum gas generator throat-to-inlet area ratio, $(A^*/A_i)_{ss\ min}$, is plotted versus supersonic combustor-to-gas generator air flow split, w_{ass}/w_{ass}, for inlet design Mach numbers between 4 and 8 and the three flight Mach number

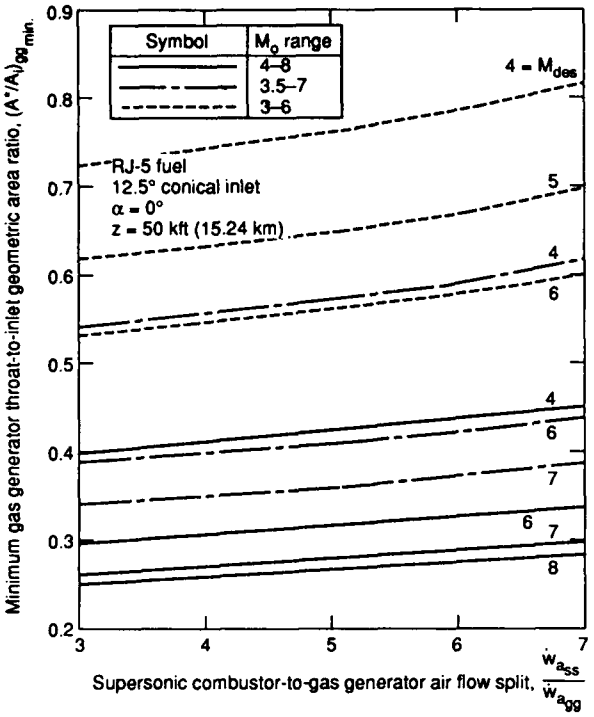

Fig. 8 Gas generator throat size as a function of inlet design Mach number, flight Mach number range and air flow split.

ranges discussed in Fig. 6. These results show that the largest gas generator throat corresponds to the lowest inlet design Mach number for a given flight Mach number range, and that the throat size increases as the flight Mach number range is lowered. Both are to be expected since the lower the inlet design Mach number, the more air that is captured at a given Mach number below M_{des}, and the minimum flight Mach number, which sizes the gas generator throat, is progressively lower.

One final parameter that can influence the performance of the DCR's gas generator (and supersonic combustor as well) is the potential mismatch between the gas generator exit static pressure and the precombustion shock static pressure when the two streams meet at the entrance to the supersonic combustor [station s in Fig. 1(b)]. Here, there is no problem if the air duct exit static pressure is less than or equal to the static pressure required to keep the gas generator's throat choked. However, if it exceeds this minimum, then the gas generator throat could unstart, requiring the gas generator inlet to unstart (ingest less mass). While this could be troublesome to the overall engine performance, most, if not all of the loss in performance could be made up for by adding additional fuel in the gas generator (which would react in the supersonic combustor) provided the overall engine ER is less than unity. Since this is only an issue during acceleration at the lower flight Mach numbers (when the maximum overall ER is usually less than unity due to thermal choking limitations in the supersonic combustor), it has not been considered in the examples given in this study.

Supersonic Combustor: The DCR's supersonic combustor operates just like any other scramjet combustor with axial fuel injection[1,5-7]. As stated previously, the only differences are that the size of the fuel injector (gas generator throat) is large compared other designs, the fuel now contains some products of combustion, and the fuel is quite hot[1] and contains some particulate matter (carbon) when $ER_{ss} > 1$. Additionally, there is always a base area between the gas generator throat and the air ducts supplying the supersonic combustor (see Fig. 1). In this study, it has been assumed that the ratio of the base area-to-supersonic inlet duct area, A_b/A_{2ss}, is a constant 0.35 based on previous engine designs. Furthermore, the supersonic combustor exit-to-inlet area ratio, rather than being the traditional ratio of A_5/A_4, is define as $A_5/(A^*_{ss} + A_b + A_{2ss})$. Finally, because wall skin friction losses play such an important role in the performance of the supersonic combustor, it is assumed that the ratio of supersonic combustor wetted wall area-to-supersonic inlet duct area, A_w/A_{2ss}, is a constant 70 based on a minimum combustor length of 50 in. (1.27 m) and body diameter of 19.7 in. (50 cm) regardless of the combustor area ratio.

The reader is referred to the references for further details of the supersonic combustion process.

DCR ENGINE AND VEHICLE PERFORMANCE

Up to this point, no details of the selection process for inlet design Mach number (M_{des}), inlet (or combustor) air flow split (w_{ass}/w_{asg}) or supersonic combustor area ratio have been addressed. It is the intent of this section to present the methodology used to select all three. Furthermore, while the nozzle exit-to-inlet geometric area ratio, A_6/A_1, will influence vehicle performance (increasing or decreasing fuel specific impulse at a given ER_o, decreasing the engine gross thrust coefficient and increasing body wave drag for a fixed A_1 as A_6/A_1 increases), varying it will not influence the general conclusions of the comparisons of the DCR with the ramjet and scramjet in the next section and, as such, A_6/A_1 has not been varied in this study. It is taken to be unity in all cases. Finally, an exit nozzle stream thrust efficiency of 0.98 was assumed for of the DCR engine performance numbers given below.

To begin this process, gross engine thrust coefficients (C_{t_g}'s) were computed as a function of ER_o and M_o, using the analyses presented in Refs. 2 and 5-7, as a function of M_{des}, w_{ass}/w_{asg} and $A_5/(A_{2ss} + A_b + A^*_{ss})$ at the boundaries of the flight Mach number regimes used, i.e., at Mach 3 and 6 for the M_o = 3 to 6 flight regime and at Mach 4 and 8 for the Mach 4 to 8 flight regime. Here, M_{des} was varied between Mach 4 and 8 for the Mach 4 to 8 flight regime, and Mach 4 and 6 for the Mach 3 to 6 flight regime. Two inlet air flow splits (3:1 and 7:1) were used in the Mach 4 to 8 flight regime to illustrate its influence on performance at the higher flight speeds, whereas only one (3:1) was considered for the Mach 3 to 6 flight regime. The supersonic combustor area ratio was varied between unity and two in one quarter increments for each inlet design Mach number, flight Mach number and inlet air flow split. Finally, the computations at Mach 3 and 4 were made for zero degrees angle-of-attack only, where acceleration is important and maneuvering is secondary. On the other hand, those at Mach 6 and 8 were done at α = 0° and +-5°, since this portion of the flight includes cruise as well as the initiation of any final maneuvers.

The chemistry throughout the inlet(s) and combustor(s) of all three engine types is assumed to be in thermochemical equilibrium at each of the flight conditions. In the exit nozzle, however,

the thermochemistry in the expansion process is taken to be 2/3rd's frozen (at the combustor exit conditions) and 1/3rd in equilibrium.

The computed values of C_{t_g} as a function of ER_o for Mach 4 flight with $\alpha = 0°$ and $w_{a_{ss}}/w_{a_{gg}} = 3$ are shown in Figure 9 to illustrate the operation of the DCR at the lower flight speeds and its sensitivity to M_{des}. Three important effects are shown. First, increasing the combustor area ratio at a given ER_o decreases engine efficiency or thrust, but not significantly, although more so at the higher values of ER_o. For example, increasing the combustor area ratio from 1.25 to 2.00 at an $ER_o = 0.5$ with $M_{des} = 6$ will decrease C_{t_g} by approximately 6%.

Secondly, and far more importantly, increasing the supersonic combustor area ratio markedly increases the maximum C_{t_g} permitted before thermal choking ($M_5 = 1$) takes place whenever ER_o is less than unity. For example, for $M_{des} = 6$, increasing $A_5/(A_{2_{ss}} + A_b + A^*_{gg})$ from unity to 1.5 increases $C_{t_{g\ max}}$ from 0.315 to 0.848, a 270% increase, due entirely to the higher maximum ER_o permitted at the larger combustor area ratio ($ER_{o\ max} = 0.654$ vs 0.215). Finally, increasing M_{des} decreases C_{t_g} at a given ER_o and combustor area ratio. For example, at an $ER_o = 0.5$, increasing M_{des} by one Mach number decreases C_{t_g} by 9 to 12%.

Since acceleration and therefore thrust, is a primary consideration at the lower flight speeds, the results in Fig. 9 have been replotted in Fig. 10 to provide a direct comparison of inlet design Mach number and combustor area ratio on the maximum gross engine thrust coefficient. Also included are the corresponding values of $C_{t_{g\ max}}$ for an inlet air flow split of 7:1. The effect of increasing the air flow split from 3:1 to 7:1 on $C_{t_{g\ max}}$ is seen to be negligible at a given $ER_{o\ max}$. Increasing the air flow split does, however, decrease $ER_{o\ max}$ and the corresponding $C_{t_{g\ max}}$, for a given combustor area ratio except when $ER_{o\ max}$ is unity, in which case there is no change, and when $A_5/(A_{2_{ss}} + A_b + A^*_{gg})$ = unity, in which case both increase except for the $M_{des} = 8$ case.

Furthermore, if the selection of M_{des} and combustor area ratio were to be based on these results alone, one would chose the lowest M_{des} and largest combustor area ratio since maximum thrust is the major figure of merit at the sustainer takeover Mach number. This, however, is not the case at the cruise Mach number, as will be seen in subsequent

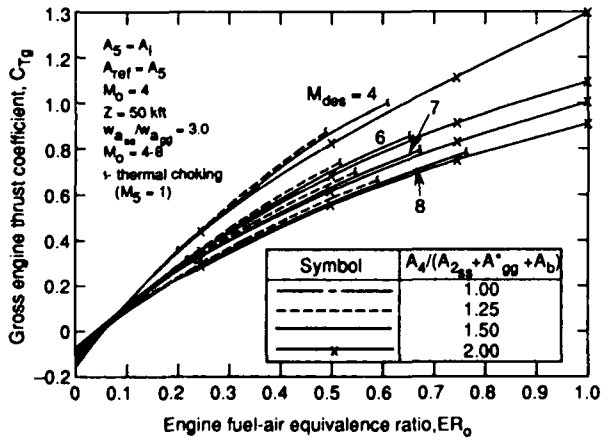

Fig. 9 Mach 4 DCR engine gross thrust coefficient as a function of overall equivalence ratio, inlet design Mach number and combustor area ratio; M_o = 4-8, 3:1 air flow split.

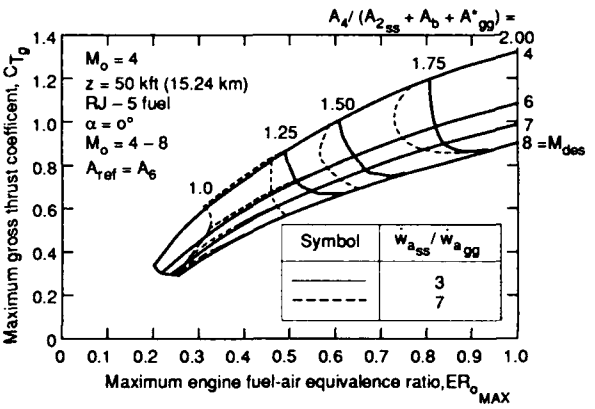

Fig. 10 Maximum DCR engine gross thrust coefficient at Mach 4, M_o = 4-8.

discussions. Consequently, the choice of M_{des} and combustor area ratio are deferred until latter.

Similar conclusions can be shown for the Mach 3 to 6 flight regime engine design when flying at Mach 3 as shown in Fig. 11. Here, however, the maximum ER_o's are less than those shown in Fig. 10 (which are for $M_o = 4$) for a given combustor area ratio but the values of $C_{t_{g\ max}}$ at a given ER_o and M_{des} are higher. These differences are due to the lower flight Mach number and concomitant inlet performance changes, nothing else.

To make the actual judgement on M_{des} and $A_5/(A_{2_{ss}} + A_b + A^*_{gg})$, it is necessary to consider the net force on the vehicle. The procedures as well as computed values of additive, leading edge, cowl and control surface wave, body and control surface friction, and lift drag are given in Ref. 1 assuming a 19.7 in. (50 cm) diameter body with a length-to-diameter ratio of 8 and $A_6/A_i = 1.0$. The corresponding plots are shown in Fig's. 12 through 16, where either maximum ($ER_o = 1$ or $ER_{o\ max}$) or near cruise ($ER_o = 0.5$) net vehicle force coefficients (C_{t_n}) are presented as a function of inlet design Mach number and combustor area ratio for the upper and lower Mach number limits of the Mach 4 to 8 and Mach 3 to 6 flight regimes. Note, also, that for a given fuel combustion efficiency, the net vehicle force coefficients shown are indicative of net vehicle specific impulse ($I_{sp\ net}$) since there is a one-to-one correspondence between force and $I_{sp\ net}$, i.e., $I_{sp\ net}$ = net force/fuel flow rate. Here, for a given M_o and ER_o, there is no change in the fuel flow from one combustor area ratio to the next for a given M_{des}.

Figures 12-14 present the results for the Mach 4 to 8 flight regime. At Mach 4 (Fig. 12), the conclusions presented for Fig. 10 are still valid, just the absolute values of force are lower in Fig. 12 due to the inclusion of the inlet and external vehicle drags, i.e., the maximum net vehicle force occurs at a combustor area ratio of 2 (where $ER_{o\ max}$ reaches unity) and an inlet design Mach number of 4, and increasing the inlet air flow split from 3:1 to 7:1 decreases performance except when $A_5/(A_{2_{ss}} + A_b + A^*_{gg}) = 1$ or 2. Furthermore, the dependence of $C_{tn\ max}$ on M_{des} decreases with increasing M_{des}.

At Mach 8, on the other hand, these conclusions are no longer valid. Both Fig's. 13 (3:1 air flow split) and 14 (7:1 air flow split) shown that the optimum inlet design Mach number is approximately 7 for all combustor area ratios, angles-of-attack and ER_o's. One could argue that $M_{des} = 6$ could be considered the optimum when $\alpha = 0°$ and $ER_o = 0.5$,

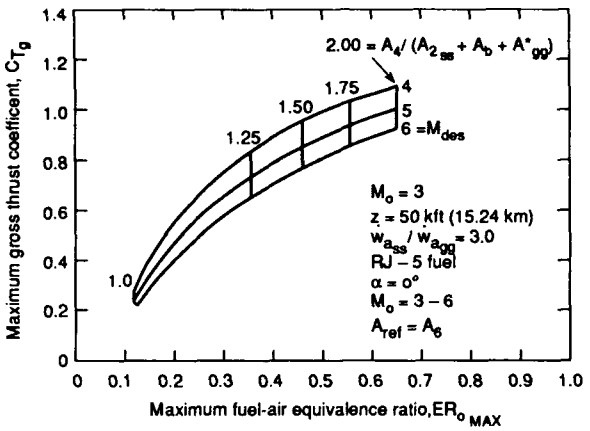

Fig. 11 Maximum DCR engine gross thrust coefficient at Mach 3.

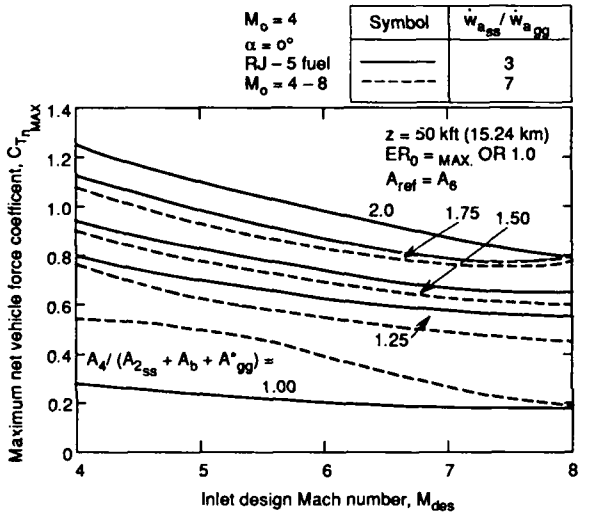

Fig. 12 Net DCR vehicle force coefficient at Mach 4.

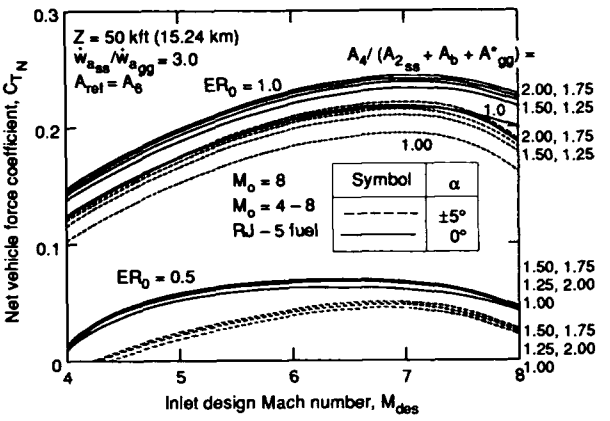

Fig. 13 Net DCR vehicle force coefficient at Mach 8, 3:1 inlet air flow split.

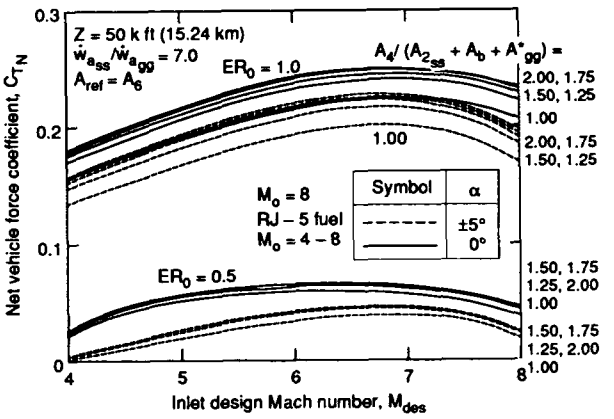

Fig. 14 Net DCR vehicle force coefficient at Mach 8, 7:1 inlet air flow split.

and it would provide somewhat better performance than a Mach 7 design at Mach 4 (Fig. 12). However, very little of the flight is spent at Mach 4; most is at the cruise condition. Additionally, since cruise will likely occur at $\alpha > 5°$, and any acceleration at or near the cruise condition will take place when $ER_o = 1$, then $M_{des} = 7$ is taken as the optimum for the rest of this study for both air flow splits.

The choice of the optimum supersonic combustor area ratio for an engine operating in the Mach 4 to 8 flight regime is not quite as obvious. At Mach 4 (Fig. 12), it is clear that the choice should be a combustor area ratio of 2.0. At Mach 8 with $ER_o = 1$, the choice is, again, a combustor area ratio of 2.0 for both air flow splits (Fig's. 13 and 14, respectively) and angles-of-attack, although the net vehicle performance at an area ratio of 1.75 for the 3:1 air flow split is comparable to that at an area ratio of 2.0 when $\alpha = 0°$ (<3% difference). When $ER_o = 0.5$, however, the optimum supersonic combustor area ratio is not the same as that for $ER_o = 1.0$. It is either 1.50 or 1.75. In this case, the net vehicle performance is the same for both combustor area ratios irrespective of the angle-of-attack. Note, however, that the decrement in performance when the combustor area ratio is changed from either 1.50 or 1.75 to either 1.25 or 2.00 at these Mach 8 flight conditions is also small (<3%).

The choice, then, is between the optimum supersonic combustor area ratio for an accelerating vehicle (when ER_o = unity or its maximum) and that at or near cruise (when $ER_o = 0.5$). Since a significant portion of a tactical missile's fuel can be consumed during acceleration and terminal maneuvers unless it has a significant cruise requirement, and since the difference in performance at the Mach 8, near cruise condition between a combustor area ratio of 1.75 (or 1.50) and 2.00 (or 1.) is small, then the choice made herein for o imum vehicle performance for an accelerating vehicle is a combustor area ratio of 2.00 and an inlet design Mach number of 7.0. Alternatively, for a cruise type vehicle, while $M_{des} = 7.0$ is still preferred, a supersonic combustor area ratio of 1.75 would be chosen because of its better performance near the cruise condition. While a supersonic combustor area ratio of 1.50 would achieve the same cruise performance at Mach 8, it would have 12 to 13% lower performance than the 1.75 area ratio at Mach 4. For a combination acceleration and cruise vehicle, the choices would be the same as those for an accelerating vehicle, i.e., $M_{des} = 7.0$ and $A_5/(A_{2_{ss}} + A_b + A^*_{ss}) = 2.0$, with the attendant small (< 3%) sacrifice in cruise performance. The latter will be used in subsequent comparisons of DCR powered vehicles with scramjet powered vehicles.

The choices of optimum inlet design Mach number and supersonic combustor area ratio for a vehicle intended for Mach 3 to 6 flight are not quite as obvious. Figure 15, which presents net vehicle performance for Mach 3 flight, shows that the

optimum M_{des} is the lowest investigated (M_{des} = 4) and the optimum supersonic combustor area ratio is the largest investigated, viz., 2.0. While these conclusions are similar to those drawn for the Mach 4 to 8 flight vehicle (Fig. 12), one major difference is that the maximum ER achievable at Mach 3 is 0.65 (see Fig. 11) compared to unity at Mach 4 for the Mach 4 to 8 flight vehicle with $A_5/(A^*_{ss} + A_b + A_{2ss})$ = 2.0.

At Mach 6, on the other hand, the choice of M_{des} and combustor area ratio are a strong function of angle-of-attack. Figure 16 shows that a significantly higher vehicle performance can be achieved at α = 0° with ER_o = 0.5 or 1.0 when M_{des} = 6.0 than at any of the lower inlet design Mach numbers. For example, for a combustor area ratio of 1.25 and ER_o = 1.0, the net vehicle performance with M_{des} = 6.0 is 12% higher than that when M_{des} = 5.0. For α = 5°, however, the preferred inlet design Mach number is 5 when ER_o = 0.5 or 1.0, with the M_{des} = 6.0 performance being somewhat lower (2 to 3%). Additionally, the preferred supersonic combustor area ratio for acceleration at Mach 6 is 1.25 at either angle-of-attack while that for near cruise (ER_o = 0.5) is unity, followed closely by an area ratio of 1.25, where net vehicle performance decreases by 1.5 to 2%. It is apparent, therefore, that the preferred supersonic combustor area ratio and inlet design Mach number for Mach 6 flight are at or near the opposite end of the parametric spectrum from those preferred at Mach 3.

The final selection of both M_{des} and $A_5/(A_{2ss} + A_b + A^*_{ss})$ must, therefore, be based on the intended use of the vehicle and heuristic arguments thereof. If we follow the arguments used in the selection process for the Mach 4 to 8 flight vehicle, then accelerative performance dominates leading to the selection of M_{des} = 6.0, assuming that very little time is spent at Mach 3 and there is sufficient thrust. Furthermore, a supersonic combustor area ratio of 1.25 would be chosen provided sufficient net thrust at Mach 3 is possible with M_{des} = 6.0 and $A_5/(A_{2ss} + A_b + A^*_{ss})$ = 1.25. On the other hand, for a cruise type vehicle, the same combustor area ratio would be chosen (1.25), but with M_{des} = 5.0. If the vehicle required a combination of acceleration and cruise, then the latter would still hold, i.e., M_{des} = 5.0 and $A_5/(A_{2ss} + A_b + A^*_{ss})$ = 1.25. In fact, with M_{des} = 5.0, the acceleration at Mach 3 would be enhanced compared to the Mach 6.0 design. The latter will be used in subsequent comparisons of a ramjet powered vehicle with the DCR powered vehicle.

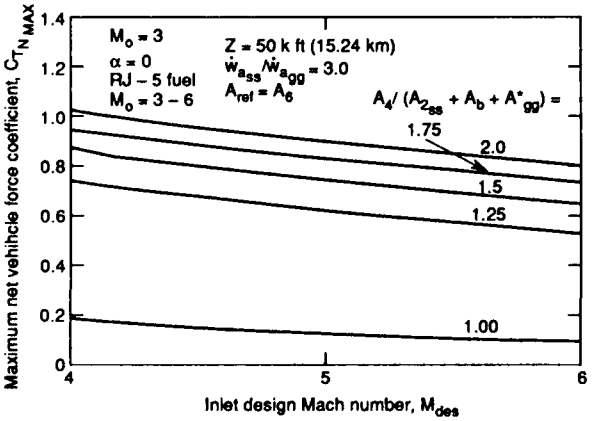

Fig. 15 Net DCR vehicle force coefficient at Mach 3, 3:1 inlet air flow split.

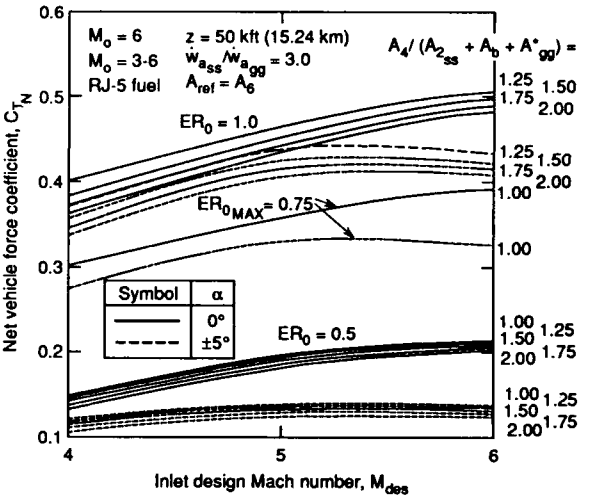

Fig. 16 Net DCR force coefficient at Mach 6, 3:1 air flow split

DCR, SCRAMJET AND RAMJET VEHICLE PERFORMANCE COMPARISONS

With the DCR engine design methodology and designs of DCR engines for two different flight regimes set, comparisons of DCR powered sustainer vehicles with either a scramjet or conventional ramjet can now be made. In each comparison, identical vehicle and external engine sizes are maintained so that one-to-one comparisons between engine types can be made.

DCR and Scramjet Powered Vehicle Comparisons: First we will compare the DCR powered vehicle performance of the previous sections with the scramjet net vehicle performance presented in Ref. 1 for Mach 4 to 8 flight within the tropopause. For the scramjet, the optimum supersonic combustor area ratio given in Ref. 1 is 4.0 with an optimum inlet design Mach number between 6 and 7. The comparisons are presented in Fig. 17, where, for completeness, C_{tn} is plotted as a function of M_{des} for Mach 4 flight with α = 0° and $ER_o = ER_{o\ max}$, and for Mach 8 flight with α = 0° and 5° and ER_o = 0.5 and 1.0. Included are both the 3:1 and 7:1 DCR inlet air flow split vehicles along with the scramjet vehicle.

For Mach 4 flight with α = 0° [Fig. 17 (a)], the comparisons show that the net performance of both the 3:1 and 7:1 inlet air flow split DCR powered vehicles is superior to that of the scramjet, with the performance difference being 10% to 15%, depending on M_{des}. It is also apparent that the performance of the 3:1 and 7:1 inlet air flow split DCR designs are nearly identical.

At Mach 8 with α = 0°, the opposite is true, i.e., the net vehicle performance using a scramjet is superior to that of either of the DCR powered vehicle designs. For ER_o = 1 and M_{des} = 7, the net performance of the scramjet vehicle is approximately 19% higher than that of the 7:1 inlet are flow split DCR powered vehicle and 25% higher than that for the 3:1 design. When ER_o decreases to 0.5, these same conclusions hold, i.e., the net performance of the scramjet powered vehicle is superior to the DCR powered vehicles. However, the net vehicle performance of the 7:1 and 3:1 DCR powered vehicles is now approximately the same.

For Mach 8 flight with α = 5° and ER_o = 0.5 or 1.0 [Fig. 17 (b)], the results and conclusion are the

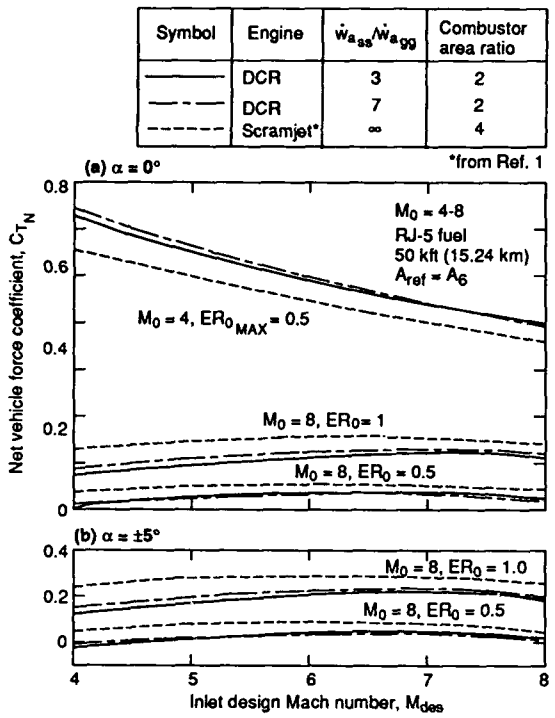

FIG. 17 Comparison of DCR and Scramjet net vehicle force coefficients for Mach 4 to 8 flight.

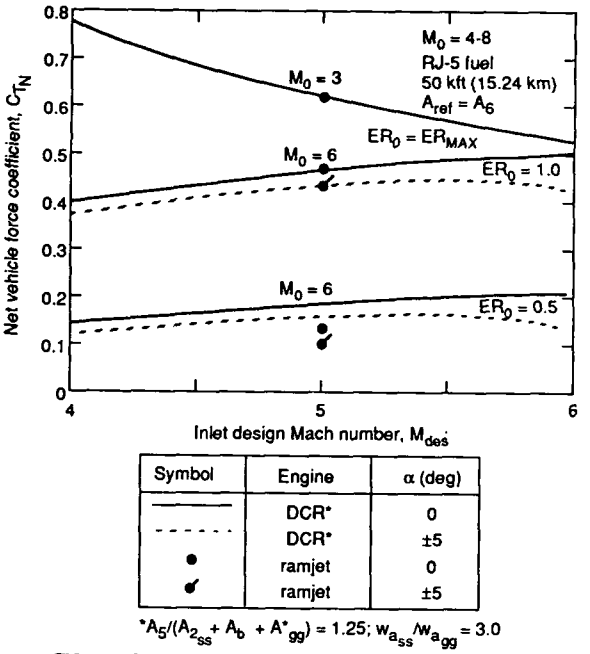

FIG. 18 Comparison of DCR and Ramjet net vehicle force coefficients for Mach 3 and 6 flight for $M_{des} = 5$

same, only the absolute values of engine performance are slightly lower.

To summarize the results for Mach 4 to 8 flight, the DCR powered vehicles have better performance than the scramjet powered vehicle during acceleration at Mach 4. For Mach 8 flight, however, the performance of the scramjet powered vehicle is higher than either DCR powered vehicle design irrespective of the ER_o and angle-of-attack. Finally, the DCR engine with a 7:1 inlet air flow split exhibits better accelerative performance than the 3:1 inlet air flow split design for Mach 8 flight and approximately the same performance for acceleration at Mach 4 and cruise at Mach 8.

Comparisons of net vehicle performance for the Mach 3 to 6 flight conditions have not been made in this study. It is, however, expected that the difference in performance between the DCR and scramjet powered vehicles at Mach 3 will be even greater than those presented in the previous comparisons at Mach 4, and that the DCR performance at Mach 6 will be comparable (or perhaps better) than that of the scramjet. This will be the subject of a future study.

DCR and Ramjet Powered Vehicle Comparisons:
Comparisons of the DCR powered vehicle designed for the Mach 3 to 6 flight regime have been made with a conventional subsonic combustion ramjet powered vehicle of identical size. Here, the inlet performance of the ramjet up to its throat is taken to be the same as that for the DCR's gas generator inlet (Fig. 5). Similarly, a 20% combustor total pressure loss has been assumed. The exit nozzle stream thrust efficiency, however, is taken as 0.985 (vs 0.980 in the DCR) since the nozzle expansion process will be more efficient than that in the DCR due to the presence of a geometric throat (Mach 1 initial conditions for all flight conditions).

In order to make a one for one comparison between the ramjet and DCR, a consistent figure of merit from one engine to the other is required. In this example, the ramjet has been designed to produce the same gross thrust as the DCR at Mach 3 with $M_{des} = 5$ and $A_5/(A_{2_{ss}} + A_b + A^*_{gg}) = 1.25$. Thus, both the ramjet and DCR will have identical maximum gross thrust coefficients at $M_0 = 3$ of 0.736 (See Fig. 11). To achieve this in the ramjet requires that the exit nozzle throat size, A^*, and overall ER be iterated until a $C_{t_{g\ max}}$ of 0.736 is achieved using the maximum critical total pressure recovery given in Fig. 5. The resulting values are $A^*/A_o = 0.5846$ and ER = 0.32.

The comparisons are presented in Fig. 18 for both the Mach 3 and 6 flight conditions. Again, net vehicle force coefficient is presented as a function of M_{des} for the DCR with the ramjet performance numbers shown only at its design Mach number of 5 (dark circles). At Mach 3, the performance of the DCR and ramjet are identical, this point being the figure of merit for this comparison. At Mach 6, however, the DCR has better performance than the ramjet for $ER_o = 0.5$, and similar performance for $ER_o = 1.0$. For Mach 6 with = 5° and $ER_o = 0.5$, the DCR's performance is approximately 32% higher than that for the ramjet. Here, the better performance of the at $ER_o = 0.5$ is attributed to the fact that the DCR's gas generator inlet is operating near its maximum critical total pressure recovery while the ramjet inlet is not. As ER_o increases, however, the pressure recovery of the ramjet inlet increases rapidly towards the critical operating value while that for the DCR changes only slightly. Consequently, at $ER_o = 1.0$, the overall performance of the ramjet and DCR powered vehicles are comparable, at least for the example used.

Were another design contraint requiring more thrust at Mach 3 to be imposed, then the throat size and $ER_{o\ max}$ of the ramjet would both increase and it is expected that the performance of the DCR powered vehicle would be better than that for the ramjet powered vehicle at both the $ER_o = 0.5$ and 1.0, Mach

6 flight conditions. This statement (or observation) will be the subject of a follow-on study.

CONCLUDING REMARKS

The methodology needed to design and maximize the performance of dual combustor ramjet engines has been presented. The results of these design studies and subsequent comparisons of the ramjet, scramjet and DCR powered vehicles lead to the following conclusions and recommendations:

1. The optimum inlet design Mach number for DCR powered vehicles flying between Mach 3 and 6 and Mach 4 and 8 is approximately one Mach number less than the maximum flight Mach number;

2. The optimum DCR supersonic combustor area ratio decreases as the flight Mach number regime decreases unless thrust becomes a problem at the minimum flight Mach number for the lower Mach number flight regime;

3. DCR powered vehicles perform better than scramjet powered vehicles at the lower flight Mach numbers and vice versa at the higher flight Mach numbers, at least in the Mach 4 to 8 flight regime investigated;

4. The larger the amount of air ingested by the DCR's supersonic combustor, the better its performance at the higher flight Mach numbers, i.e., it operates more and more like a scramjet. At the lower flight Mach numbers, no definitive conclusion could be reached within the limited parametrics investigated in this study;

5. When DCR and ramjet powered vehicles are designed to have the same maximum net thrust at Mach 3 for Mach 3 to 6 flight, the DCR exhibits better performance at and near cruise at the highest flight Mach number and similar performance at stoichiometry; and

6. It is recommended that comparisons of the DCR and scramjet be made for the Mach 3 to 6 flight regime. It is also recommended that the DCR and ramjet be compared using a higher required thrust level at Mach 3 than that used in this study to broaden the scope of the conclusions.

REFERENCES

1. Waltrup, P.J., Billig, F.S. and Stockbridge, R.D.,"Engine Sizing and Integration Requirements for Hypersonic Airbreathing Missile Applications", AGARD-CP-307, No. 8, March 1982,

2. Billig, F.S., Waltrup, P.J. and Stockbridge, R.D.,"The Integral Rocket Dual Combustion Ramjet: A New Propulsion Concept", J. of Spacecraft and Rockets, Vol. 17, No. 5, September-October, 1980, pp 416-424.

3. Waltrup, P.J.,"Hypersonic Airbreathing Propulsion: Evolution and Opportunities", AGARD-CP-428, No. 12, April, 1987.

4. Mestre, A. and Ducourneau, F.,"Recent Studies on the Spontaneous Ignition of Rich Air-Kerosene Mixtures", Office National d'Etudes et de Recherches Aerospatiales (ONERA) TP-1209, Chatillon, France, 1973.

5. Billig, F.S., Corda, S. and Pandolfini, P.P.,"Design Techniques for Dual Mode Ram-Scramjet Combustors", AGARD-CP-479, June, 1990.

6. Waltrup, P.J., Billig, F.S. and Stockbridge, R.D.,"A Procedure for Optimizing the Design of Scramjet Engines", J. of Spacecraft and Rockets, Vol. 16, No. 3, May-June, 1979, pp 163-172.

7. Billig, F.S.,"Ramjets with Supersonic Combustion", AGARD-LS-136, August, 1989.

8. White, M.E., Stevens, J.R., Keirsey, J.L., Van Wie, D.M. and Mattes, L.A., "Investigation of Cowl Vent Slots for Stability Enhancement in MITS Scramjet Inlets", AIAA-88-2956, July, 1988.

Semi-propergols pour Statofusée

B. Mahé, C. Perut

SNPE, Défense/Espace
Centre de Recherches du Bouchet
91710 Vert-Le-Petit
France

et

C. Vigot, C. Masson

Office National d'Etudes et de Recherches Aérospatiales (ONERA)
Direction de l'Energétique
91120 Palaiseau
France

SOMMAIRE

Cet article décrit les différentes familles de semi-propergols étudiés et développés par la SNPE et l'ONERA en vue d'une application en générateur de gaz pour statofusée.

Ces semi-propergols sont adaptés à un fonctionnement soit en générateur de gaz séparé, soit en générateur de gaz intégré (configuration "rustique"). Ils peuvent être classés en trois grandes familles selon leur niveau de discrétion et leur performance énergétique:

a. les compositions discrètes sans particule métallique,
b. les compositions automodulables pour statofusée rustique à faible taux de particules métalliques,
c. les compositions à fort taux de particules:
   . magnésium,
   . carbone,
   . bore.

Pour chaque famille, les principales caractéristiques des compositions les plus représentatives sont décrites.

SUMMARY

The purpose of this paper is to describe the different families of fuel-rich solid propellants studied and developped at SNPE and ONERA for ducted rocket applications.

These propellants are adjusted wether for choked gas generator or for unchoked gas generator configurations. They are ordered in three classes depending on their optical signature characteristic and their energetic performance:

a. smokeless propellants without metal,
b. reduced smoke compositions with a low rate of metals for "rustique" ducted rocket.
c. high energy propellants with a high rate of particles:
   . magnesium,
   . carbon,
   . boron.

Major properties of various fuel-rich solid propellants of each families are described.

NOMENCLATURE.

Liste de symboles.

CSF	Coefficient de sensibilité au frottement Julius Peters
C_F	Coefficient de poussée
C*	Vitesse caractéristique
e_b	Epaisseur à brûler
em	Allongement maximal à la rupture
f	Rapport de mélange combustible/air
fs	Rapport de mélange stoechiométrique
F	Poussée
IAD	Indice d'aptitude à la détonation derrière barrière
Is	Impulsion spécifique
K	Vie de pot
M	Nombre de Mach
$\dot{m}$	Débit
n_{a-b}	Exposant de pression sur la plage de pression [a, b]
P	Pression statique
Sm	Contrainte maximale à la rupture
T	Température
t	Temps
V	Vitesse
Vc_{a-b}	Vitesse de combustion sur la plage de pression [a, b]
Z	Altitude
α_{a-b}	Coefficient de sensibilité à la température initiale à pression constante, sur la plage de température [a, b]
η	Viscosité à la coulée
η_c	Rendement de combustion
$\pi_{K\ a-b}$	Coefficient de sensibilité à la température initiale à serrage constant, sur la plage de température [a, b]
ρ	Masse volumique du semi-propergol
φ	Richesse
Ø	Diamètre

Indices:

0: Infini amont
2: Fin de la prise d'air
3: Chambre de combustion
4: Col
c: Combustion
g: Générateur de gaz
i: Conditions d'arrêt isentropique

1. INTRODUCTION.

Le statofusée à combustible solide offre un système propulsif attractif du fait de sa simplicité de conception et de sa compacité, comparées à celles d'un statoréacteur à combustible liquide [1]. Le stockage et la maintenance s'apparentent à ceux d'une munition ou d'un missile classique à propulseur fusée.

Son intérêt résulte de l'évolution et du développement des semi-propergols solides, aussi appelés propergols aérobies (fuel-rich solid propellants), alimentant le générateur de gaz qui peut être intégré dans la chambre de combustion aérobie ou séparé de celle-ci (figure 1).

Depuis les années 1970, l'ONERA et SNPE en collaboration étroite, ont cherché à développer ces semi-propergols. L'ONERA a porté son effort sur l'étude et la modélisation des mécanismes de combustion ainsi que sur la recherche de nouvelles formulations. SNPE a développé sa compétence dans les domaines de la recherche et de la mise au point des formulations, de la caractérisation et de l'adaptation des propriétés physico-chimiques, mécaniques et de sécurité de ces produits. SNPE développe ces combustibles solides en vue de leur industrialisation.

Dès 1976, un missile expérimental de calibre 400 mm et de portée voisine de 100 km, démontrait une impulsion spécifique très élevée. Plus récemment (1983/1985), pour des applications sol-air courte et moyenne portée, un statofusée de faible coût et d'architecture simplifiée dite "rustique", le MPSR [3], était testé avec succès dans un large domaine de vol (altitude, Mach et manoeuvrabilité).

Cet article est destiné à faire un bilan des connaissances acquises à ce jour, tant par l'ONERA que par SNPE, dans le domaine de ces semi-propergols. Il décrit les caractéristiques de faisabilité, de sécurité, les propriétés mécaniques, balistiques et énergétiques des principales familles de matériaux étudiées. Les produits présentés ont subi une caractérisation à une échelle significative.

La plupart des semi-propergols développés ont été évalués en combustion avec l'air, à échelle grandeur, sur les installations d'essais au sol de l'ONERA (calibre 100 à 400 mm) dans les conditions de simulation de vol des missions envisagées.

Les matériaux encore au stade de la recherche laboratoire, ou n'ayant pas débouché sur une caractérisation suffisante, ne sont pas pris en compte.

2. GENERALITES SUR LES SEMI-PROPERGOLS.

2.1 Applications à la propulsion par statofusée.

Le choix du semi-propergol solide alimentant le générateur de gaz du statofusée et par la même des ingrédients le constituant dépend:
- des caractéristiques de la mission (domaine de vol, vitesse, manoeuvrabilité),
- de la diversité des trajectoires ((auto)-régulation du débit),
- de la discrétion du jet (visible, électromagnétique ou infrarouge),
- de la place et/ou de la masse disponible(s) pour le chargement,
- du mode de combustion (frontal ou radial),
- des conditions thermiques de stockage et d'emploi,
- des coûts d'étude et de développement (industrialisation, unités produites, mission).

Deux configurations du générateur de gaz, généralement placé en amont de la chambre du statofusée (Fig. 1), sont utilisées:

- la première à générateur de gaz séparé: la pression de combustion du chargement est réglée par une ou plusieurs tuyère(s) amorcée(s),
- la seconde à générateur de gaz intégré encore appelée version "rustique": le fonctionnement du générateur n'est pas découplé de celui de la chambre de combustion.

Si la modulation du débit est nécessaire, elle est effectuée dans le premier cas par l'intermédiaire d'une vanne de régulation, dans le second elle est assurée uniquement par les propriétés balistiques du semi-propergol [2,3].

Les semi-propergols étudiés en France sont généralement développés pour un domaine de fonctionnement du générateur compris entre 2 et 8 MPa dans la configuration générateur de gaz séparé, et entre 0,2 et 1 MPa dans la version rustique. Toutefois, des pressions de fonctionnement différentes peuvent être requises pour certaines applications.

Le débit gazeux apporté par le générateur est entre autre fonction de la surface de combustion du bloc. Le mode de combustion (frontal ou radial) détermine ainsi le domaine de vitesse de combustion nécessaire.

La nécessité de pouvoir moduler le débit gazeux du générateur en fonction du débit d'air entrant dans la chambre du statofusée imposera la recherche d'exposants de pression élevés.

D'une manière générale, pour permettre un fonctionnement nominal dans un large domaine de température d'emploi, une faible sensibilité de la vitesse de combustion à la température initiale du chargement sera requise.
Ceci permet par ailleurs de disposer d'une plus forte capacité de modulation.

2.2 Constituants des compositions développées.

Ces semi-propergols [2,4] comportent généralement:

- un **liant combustible** réticulable dont la dégradation génère des gaz réducteurs.
  Les plus couramment employés sont les liants polybutadiènes en raison de leur caractère fortement réducteur.

L'utilisation d'un liant à caractère oxydant (polyester plastifié par une huile nitrée, ...) ou encore azidé (PAG), peut présenter un intérêt pour la recherche de propriétés spécifiques.

- un **oxydant solide** pulvérulent, en faible proportion allant de 25 à 50% suivant les caractéristiques recherchées.
  Le perchlorate d'ammonium et les oxydants organiques sont généralement les plus utilisés.
- des **combustibles additionnels** qui sont généralement des particules hydrocarbonées, métalliques ou de carbone, dont l'emploi dépend des spécifications d'utilisation recherchées (caractéristiques cinétiques, énergétiques ou de discrétion).
- des **additifs** éventuels tels que des accélérateurs de combustion, des catalyseurs de réticulation, des agents anti-oxydants ou des additifs stabilisant la combustion, peuvent être introduits en faible proportion pour optimiser les caractéristiques du matériau (faisabilité, tenue au vieillissement, propriétés mécaniques, cinétiques et balistiques).

La capacité du semi-propergol à fournir des gaz réducteurs est d'autant plus élevée que le taux d'oxydant est faible.

2.3 Combustion des semi-propergols.
La combustion des semi-propergols est différente de celle d'un propergol classique [4,5].

L'oxydant est introduit en quantité réduite afin de pyrolyser le liant hydrocarboné et dans le but de fournir ainsi les gaz combustibles. L'analyse des produits issus de la dégradation montre une très forte proportion d'hydrocarbures lourds et une très grande complexité du mélange. Aux faibles taux de perchlorate d'ammonium, l'existence d'un résidu carboné solide témoigne du processus de dégradation de la phase condensée du semi-propergol. Des phénomènes de combustion instationnaires intrinsèques peuvent alors apparaître lorsque le résidu se détache périodiquement de la surface sous forme de strates [6].

A titre d'exemple, la figure 3 [5] présente, pour chaque domaine de pression, une description schématique de la combustion d'un semi-propergol à faible taux de perchlorate d'ammonium. Les vitesses de combustion mesurées expérimentalement sont comparées aux résultats d'un modèle de calcul mis au point à l'ONERA [5].

2.4 Formulation des compositions.
Les critères qui orientent les études de formulation sont la faisabilité, les caractéristiques de sécurité, les propriétés mécaniques, les performances énergétiques ainsi que les propriétés cinétiques et balistiques [2,4,7].

Le procédé mis en oeuvre pour réaliser ces semi-propergols est identique à celui qui est utilisé classiquement en propergol solide: homogénéisation du matériau par malaxage, puis mise en forme des chargements par coulée sous vide ou injection. L'utilisation de liants thermodurcissables, impose une viscosité à la coulée de la pâte faible (< 20 000 poises) ainsi qu'une vie de pot compatible avec la réalisation des chargements (> 5 heures).

Les matériaux obtenus doivent posséder des propriétés mécaniques dont le niveau est fonction du type de chargement, libre ou moulé-collé, du taux de remplissage et des sollicitations mécaniques engendrées par les contraintes thermiques subies au cours du stockage et des périodes opérationnelles.

D'une manière générale, le taux de liant dans les semi-propergols est important, ce qui a pour conséquence un coefficient de dilatation linéaire supérieur à celui des propergols classiques. Cette caractéristique conduit à rechercher des propriétés mécaniques d'un niveau plus élevé.

La recherche de performances énergétiques conduit à envisager l'incorporation d'un taux maximal d'éléments réducteurs; dans le cas de charges solides, celui-ci est en général limité par le critère de faisabilité. Le taux minimum d'éléments oxydants nécessaire pour assurer la dégradation du liant est limité par les propriétés balistiques requises: délai d'allumage, absence de résidus, stabilité de la combustion, vitesse de combustion, ...

Les propriétés cinétiques doivent être réglées en fonction de la configuration du générateur de gaz envisagée, de la géométrie du chargement, de la durée de fonctionnement et de la nécessité ou non de pouvoir moduler le débit.

L'obtention de rendements de combustion optimums nécessite dans bien des cas, et en particulier dans celui des générateurs contenant des particules solides (bore, ...), la mise au point de moteurs spécifiques, ayant une architecture adaptée (dispositif d'injection, manches à air, chambre de combustion).

Un bon comportement des semi-propergols aux épreuves de sécurité est également recherché.

L'optimisation des compositions en fonction des propriétés décrites a permis la mise au point d'une large gamme de semi-propergols qui peuvent être classés dans les grandes familles suivantes:

a. les compositions discrètes sans particule métallique,
b. les compositions automodulables pour statofusée rustique à faible taux de particules métalliques,
c. les compositions à fort taux de particules:
   . magnésium,
   . carbone,
   . bore.

3. PERFORMANCES ENERGETIQUES DES SEMI-PROPERGOLS DEVELOPPES.
Selon l'application envisagée, on peut être amené à privilégier:

- l'impulsion spécifique (Is) dans le cas où la masse du générateur de gaz (chargement de semi-propergol) est figée,
- l'impulsion spécifique volumique (ρ.Is) dans le cas où le volume du générateur de gaz est imposé.

Ces performances énergétiques sont à considérer dans un domaine de poussée spécifique (f.Is) requis par la mission à effectuer.

Elles dépendent de nombreux facteurs tels que:

- le taux et la nature des comburants et des combustibles utilisés, notamment des métaux tels que le bore,
- les conditions de fonctionnement du statofusée (domaine de vol en altitude et vitesse, rapport de mélange combustible/air, géométrie et rapport de détente de la tuyère, ...), c'est à dire, de manière plus pratique, de la richesse injectée du mélange combustible/air, de la température génératrice de l'air, de la pression de fonctionnement et du rapport de détente de la tuyère.

Les performances énergétiques des différentes familles de semi-propergols développés sont comparées sur les diagrammes des figures 4 et 5, en terme d'impulsion spécifique volumique en fonction de la poussée spécifique.
Leurs formulations sont précisées par la suite.
Les calculs thermodynamiques sont réalisés en employant le code de calcul NASA SP-273, [8].
Ces résultats sont présentés pour deux cas de calculs de référence: le premier dans les conditions d'un vol à basse altitude (Z= 0) à Mach 2 et le second pour un vol à haute altitude (Z= 30 000 m) et Mach 5.

Les valeurs d'impulsion spécifique volumique obtenues en fonction d'une valeur de référence de poussée spécifique par rapport à l'air, sont précisées dans le tableau 1.
En considérant seulement l'aspect énergétique, l'intérêt du bore est évident et bien connu. En conséquence, les semi-propergols au bore (35 et 40%) développés présentent des niveaux de performances élevés.

L'intérêt des compositions à fort taux de magnésium réside essentiellement dans le gain d'impulsion obtenue aux fortes poussées comparées aux semi-propergols classiques.
Ce type de composition conduit à une valeur élevée du rapport stoechiométrique.

Le classement par famille de produits, en terme d'impulsion spécifique volumique à poussée spécifique donnée, s'établit comme suit:

"bore"> "carbone"> "magnésium"> "automodulable"> "discrète".

Ceci dépend bien évidemment du taux de charges réductrices introduites mais dans l'ensemble cet ordre est respecté.

4. CARACTERISTIQUES PAR FAMILLE.

4.1 Compositions discrètes sans particule métallique.

L'intérêt principal de ces compositions repose sur l'absence totale de particule métallique, ce qui leur confère des qualités de discrétion.

Ces compositions possèdent généralement un fort taux de liant polybutadiène et contiennent éventuellement une charge hydrocarbonée.

Les performances énergétiques sont directement liées au taux d'oxydant, les valeurs maximales correspondent au liant pur. A titre d'exemple, la figure 6 donne, pour une composition à liant PBHT, l'évolution

				Conditions basse altitude M_0= 2	Conditions haute altitude M_0= 5
Famille de Semi-propergols	**Réf.**	**fs**	**ρ (kg/m^3)**	**ρ.Is (g/cm^3) à f.Is=50 s**	**ρ.Is (g/cm^3) à f.Is=70 s**
"discrète"	D1	0,1107	1060	1236	969
	D2	0,1428	1295	1262	1016
	D3	0,1744	1266	1048	875
	D4	0,1793	1307	1056	883
"automodulable"	R1	0,1773	1334	1140	935
	R2	0,1559	1252	1178	953
"carbone"	C1	0,1357	1440	1430	1118
	C2	0,1489	1637	1488	1182
"magnésium"	M1	0,2940	1557	1257	1023
"bore"	B1	0,1611	1626	1862	1254
	B2	0,1361	1546	1992	1331
	B3	0,1608	1621	1862	1247

Rapport de détente de la tuyère: Basse altitude 5,7/1
Haute altitude 1/0,0117

TABLEAU 1: Performances énergétiques des semi-propergols développés.

de l'impulsion spécifique et de l'impulsion spécifique volumique en fonction du taux de perchlorate d'ammonium.

Ces performances théoriques ne peuvent être atteintes que si la dégradation totale du liant est obtenue; pour cela un taux minimum d'oxydant est nécessaire. Dans le cas contraire, la présence après tir de résidus de combustion compacts est observée dans le générateur de gaz. Dans le cas des compositions contenant entre 25 et 30% de perchlorate d'ammonium, la masse de ces résidus de combustion peut atteindre jusqu'à 15% de la masse initiale du bloc.

Au delà du problème des résidus, les formulations de ces semi-propergols sont adaptées de manière à prendre en compte le type de mission considérée. En particulier la capacité de modulation peut être réglée par la nature de l'oxydant utilisé (oxydant minéral ou organique) et la présence ou non d'un combustible auxiliaire [5].

Dans le tableau 2 sont regroupées les principales caractéristiques des compositions représentatives de cette famille de produits.

Deux des compositions présentent un exposant de pression élevé (> 0,5) qui permet d'envisager un taux de modulation élevé.

Les rendements de combustion ont été évalués en chambres de statofusées de diamètre 180 ou 200 mm.
Ces évaluations ont été effectuées en conduite forcée sur des foyers à quatre entrées d'air latérales pour différentes conditions de simulation de vol.
Dans le tableau 3, des exemples de valeurs expérimentales obtenues sont précisées dans deux conditions de vol de référence:

- un vol à basse altitude et à Mach 2,
- un vol à moyenne altitude à Mach plus élevé (≈ 3),

Le rendement de combustion est exprimé ici comme le rapport de la richesse brûlée théorique (correspondant à une combustion complète) à la richesse injectée:

$$\eta_c = \varphi_b/\varphi_i$$

Les compositions ont été évaluées dans les configurations à générateurs de gaz séparé

Semi-propergol	D1	D2	D3	D4
. Formulation				
liant + additifs	70	40	52,4	31,7
oxydant organique	30	60	-	-
oxydant minéral	-	-	47,6	48,3
additif hydrocarboné	-	-	-	20,0
. Faisabilité				
η (poises)	2 000	6 000	5 000	14 000
K (heures)	7	4	12	5
. Propriétés mécaniques				
Sm (MPa)	0,8	1,2	1,2	0,9
em (%)	150	80	60	30
. Masse volumique				
ρ (kg/m^3)	1060	1295	1266	1307
. Sécurité				
CSF (N)	100	0% à 353 N	0% à 353 N	0% à 353 N
Mouton 30 kg (m)	-	2	2,5	2,5
IAD (cartes)	150	110	< 1	< 1
. Propriétés cinétiques				
$V_{c\ à\ 5,0\ MPa}$ (mm/s)	0,9	2,5 à 5	-	-
$V_{c\ à\ 0,6\ MPa}$ (mm/s)	-	-	1,75	2,4
n	0,35	0,5 à 0,6	0,1	0,8
$\alpha_{233\ à\ 333\ K}$ (%/K)	-	-	≈ 0,4	0,50
$\pi_{K,\ 233\ à\ 333\ K}$ (%/K)	0,55	-	-	-

TABLEAU 2: Caractéristiques des semi-propergols discrets sans particule métallique.

Ces compositions ayant un taux élevé de liant, présentent une faisabilité excellente. Les viscosités à la coulée sont faibles avec une vie de pot de plusieurs heures. Ceci permet d'envisager la réalisation aisée de chargements, même de géométrie complexe, suivant des procédés de mise en oeuvre classique. Dans la plupart des cas, la simple coulée par gravité est suffisante.

De même, la présence d'un fort taux de liant leur confère d'excellentes caractéristiques mécaniques, compatibles avec la réalisation de chargements moulés-collés à fort taux de remplissage.

(D1) et intégré (D3 et D4) pour des durées de fonctionnement pouvant atteindre 50 secondes.
Ces semi-propergols ne présentent pas de difficultés d'allumage. Ils conduisent à l'absence de résidus dans le générateur de gaz à l'exception de la composition D1 qui possède un taux de résidus de l'ordre de 10% [9].

Les évolutions de pressions dans le générateur de gaz et dans la chambre de combustion sont régulières, le fonctionnement est stable. Dans tous les cas, la pyrophoricité des gaz issus du semi-propergol avec l'air est obtenue.

Semi-propergol	D1	D3		D4	
Configuration	"séparée"	"intégrée"		"intégrée"	
Simulation de vol altitude (km) Mach de vol	 1,5 2,0	 0 2,0	 10 2,9	 0 2,0	 10 2,9
Générateur de gaz: $T_{initiale}$ (K) Pg (MPa) Vc (mm/s)	 - 3,2 0,8	 293 0,62 -	 293 0,35 -	 293 0,66 2,63	 293 0,34 1,55
Combustion statofusée φ_i P_{3i} (MPa) η_c	 0,38 0,35 0,91	 0,50 0,50 0,95	 0,90 0,25 0,80	 0,66 0,53 0,94	 0,80 0,25 0,87

TABLEAU 3: Résultats d'essais de combustion avec des semi-propergols discrets.

4.2 Compositions automodulables pour statofusée rustique à faible taux de particules métalliques.

La spécification principale imposée aux semi-propergols automodulables pour "rustique" est une adaptation permanente du débit gazeux du générateur au débit d'air entrant dans la chambre du statoréacteur, celui-ci étant fonction des conditions de vol du missile (vitesse-altitude) [3].

Le générateur fonctionnant à une pression voisine de celle régnant dans la chambre du statofusée, elle même réglée par les conditions de vol, la modulation ne peut être obtenue que si le semi-propergol possède un exposant de pression élevé (supérieur à 0,5) et ceci jusqu'à des pressions de fonctionnement d'autant plus faibles que l'altitude maximale est élevée.

L'utilisation de chargements à combustion radiale conduit à rechercher des vitesses de combustion faibles (environ de 1,5 à 2,5 mm/s à 0,8 MPa) dans le domaine de pression de fonctionnement envisagé.

De plus, les applications visées "tous temps", imposent un faible coefficient de sensibilité de la vitesse de combustion à la température initiale du chargement.
Par nature, ce type de semi-propergol à très faible vitesse de combustion présente un coefficient α généralement élevé [10].

L'obtention simultanée de ces caractéristiques est particulièrement difficile à réaliser et peut nécessiter l'utilisation de charges organiques et/ou métalliques.
Pour des raisons de discrétion, le taux d'additif métallique n'excède pas 10%.

Le réglage des vitesses de combustion se fait par adaptation du taux de catalyseur de combustion, en intégrant l'influence des divers additifs entrant dans la formulation (additif métallique, charge hydrocarbonée, granulométrie du perchlorate d'ammonium).

Les caractéristiques de ces produits sont indiquées dans le tableau 4.

Semi-propergol	R1	R2	R3
. Formulation			
liant + additifs	33	50	40
oxydant minéral	42	40	15
additifs hydrocarbonés	15	-	35
additifs métalliques	10	10	10
. Faisabilité			
η (poises)	5	1	10
K (heures)	5	> 10	5
. Propriétés mécaniques			
Sm (MPa)	0,75	2,0	0,8
em (%)	15	200	24
. Masse volumique			
ρ (kg/m^3)	1330	1267	1363
. Sécurité			
CSF (N)	250	0% 353 N	0% à 353 N
Mouton 30 kg (m)	2	≥ 4	1
. Propriétés cinétiques			
$V_{c\ à\ 0,85\ MPa}$ (mm/s)	1,8	2,1	2,0
$n_{0,2\ à\ 0,7\ Mpa}$	0,6	0,63	1,0
$\alpha_{233\ à\ 333\ K}$ (%/K)	0,3	0,15	0,25

TABLEAU 4: Caractéristiques des semi-propergols automodulables pour statofusée "rustique".

Ces compositions ne présentent pas de problème de faisabilité. Le niveau mécanique obtenu sur la composition R2 permet d'envisager des densités de chargement élevées.
Pour ces niveaux de vitesse de combustion faibles, les capacités de modulation sont élevées (exposant de pression fort et coefficient de sensibilité α faible).

La loi de vitesse de combustion et par suite la capacité de modulation peut être adaptée aux besoins de l'application visée, ceci en ajustant la formulation du combustible.

Par exemple, une plus faible valeur d'exposant peut être souhaitée à forte pression pour limiter la consommation du chargement durant la phase d'accélération du booster. De même une forte capacité de modulation peut être requise à faible pression lors d'un vol à haute altitude, afin de limiter l'évolution de la richesse injectée du générateur de gaz et garder ainsi un fonctionnement optimum du statofusée.
Un exemple de l'évolution de la vitesse de combustion en fonction de la pression dans le domaine 0,1 à 10 MPa est présenté sur la figure 7 pour un semi-propergol automodulable de ce type.
Les mesures de vitesse de combustion ont été réalisées sur échantillons par la technique ultrasonore appliquée au semi-propergol [5,6,11] dans ce large domaine de pression.

Un très important programme d'évaluation balistique de ces semi-propergols sur statofusée à l'échelle 100 et 180 mm, a été mené ces dernières années dans le cadre du développement exploratoire du missile à statofusée rustique MPSR [3].

De manière générale, le statofusée rustique, par sa conception à générateur intégré et son unique plan d'injection, se prête assez mal à la combustion des semi-propergols à fortes teneurs en particules, dans le cas où celles-ci sont injectées en phase solide ou liquide dans la chambre aérobie.

A titre d'exemple, les résultats d'essais de combustion en chambre de statofusée (diamètre 180 mm) concernant les deux compositions R1 et R2, sont présentés dans le tableau 5. Les conditions d'essais en conduite forcée sont comparables à celles précédemment décrites.

Les optimisations de la formulation du semi-propergol, de la chambre de combustion et des dispositifs d'injection afin d'obtenir une bonne efficacité de combustion, peuvent être dans ce cas plus délicates que pour les configurations classiques de statofusée.

La pyrophoricité des gaz de combustion avec l'air a toujours été obtenue même dans les conditions de fonctionnement difficiles à basse pression (P_g < 0,2 MPa) et faible température initiale ($T_{init.} \approx 233$ K) du chargement. La combustion est régulière et stable.
Cependant, pour certains semi-propergols, à faible vitesse de combustion, et ce malgré la présence favorable de particules métalliques, la combustion peut devenir instable dans ces conditions de fonctionnement. Les très faibles vitesses de combustion sont en effet défavorables à une bonne éjection des résidus carbonés de la matrice polymérique.

L'optimisation de la chambre de combustion du statofusée rustique et l'amélioration des caractéristiques balistiques de ces semi-propergols, ont conduit à des valeurs de rendement de combustion élevées en dépit de la rusticité des dispositifs d'injection et de l'architecture de la chambre de combustion, ainsi que de la présence de particules solides (organiques ou métalliques).

4.3 Compositions à fort taux de particules.

4.3.1 Semi-propergols au magnésium.

La recherche de semi-propergols destinés à alimenter en combustible des statofusées devant assurer une forte accélération au missile a conduit à retenir des compositions fortement chargées en magnésium.

Par rapport aux autres métaux envisageables pour ce type d'applications (Al, Zr, ...) [2], le magnésium présente l'avantage d'être introduit généralement à l'état gazeux dans la chambre du statofusée.

Semi-propergol	R1		R2	
Configuration	"intégrée"		"intégrée"	
Simulation de vol altitude (km) Mach de vol	 0,8 1,9	 2,3 2,1	 0 2,2	 12 3,1
Générateur de gaz $T_{initiale}$ (K) Pg (MPa) Vc (mm/s)	 293 0,58 1,98	 333 0,59 2,24	 293 0,68 1,88	 293 0,33 1,25
Combustion statofusée φ_i P_{3i} (MPa) η_c	 0,57 0,50 0,90	 0,74 0,40 0,86	 0,53 0,57 0,95	 1,0 0,24 0,89

TABLEAU 5: Résultats d'essais de combustion avec des semi-propergols pour applications "rustiques".

Les travaux menés sur cette famille de semi-propergols ont porté sur la recherche du taux minimum de perchlorate d'ammonium conduisant à l'absence de résidu de combustion, et sur la recherche du taux maximum de magnésium compatible avec une faisabilité correcte.

A titre d'exemple, les caractéristiques d'une formulation à liant PBHT contenant respectivement 55 % et 60% de magnésium sont données dans le tableau 6.

Il convient de noter la sensibilité de ces compositions à l'électricité statique. Cette propriété impose de prendre des précautions particulières lors de l'ensemble des phases de fabrication et d'utilisation du matériau. Ces précautions sont destinées à éviter toute décharge électrique entre le semi-propergol et son environnement (manipulateur, moules, ... etc).

En principe, le magnésium ne présente pas de difficultés d'allumage et conduit à une combustion efficace dans le statofusée du fait de sa faible température de vaporisation (1376 K) très inférieure à celles des points de fusion et de vaporisation de l'oxyde (3073 et 3373 K respectivement).

A titre d'exemple, des travaux suédois [12] ont conduit à la combustion efficace du magnésium dans les conditions de fonctionnement à basse altitude et Mach 2, dans un large domaine de richesse injectée.

Par ailleurs, l'addition de magnésium dans les semi-propergols est couramment utilisée afin de favoriser l'allumage et la combustion d'autres métaux présents dans le semi-propergol.

4.3.2 Semi-propergols au carbone.
L'intérêt du carbone réside dans le fait qu'il permet d'accéder à un niveau énergétique élevé (> 1400 g.s/cm^3) tout en conservant de bonnes qualités de discrétion.

Cependant, il est bien connu que cet intérêt n'est réel que dans la mesure ou la combustion des particules de carbone est effective dans la chambre du statofusée. De ce fait, les travaux ont porté essentiellement sur l'étude expérimentale de la combustion des particules de carbone dans une chambre de statofusée.

Ces travaux ont été réalisés en utilisant une composition à 29% en masse de particules de carbone. Parallèlement, la gamme des formulations disponibles a été étendue; en particulier, des compositions disposant d'un exposant de pression élevé, donc modulables, ont été mises au point.

Les caractéristiques de ces semi-propergols sont indiquées dans le tableau 7.

La faisabilité de ces compositions est satisfaisante malgré l'utilisation de très fines particules de carbone. Les pâtes sont fortement pseudo-plastiques, ce qui conduit à utiliser préférentiellement le procédé d'injection pour la mise en forme des blocs.

Les propriétés mécaniques sont d'un excellent niveau, les fines particules de carbone ayant un fort pouvoir renforçant.

La difficulté de brûler efficacement les particules de carbone dans une chambre aérobie est essentiellement liée au faible temps de séjour de la particule dans les

Semi-propergol	M1	M2
. Formulation		
liant + additifs	17	17
oxydant minéral	23	28
magnésium	60	55
. Faisabilité		
η (poises)	25	8
K (heures)	2	3
. Propriétés mécaniques		
Sm (MPa)	0,90	0,97
em (%)	21	47
. Masse volumique		
ρ (kg/m^3)	1557	1564
. Sécurité		
CSF (N)	-	210
Mouton 30 kg (m)	-	2,75
Sensibilité à l'électricité statique	sensible	sensible
. Propriétés cinétiques		
$V_{c\ à\ 5,0\ MPa}$ (mm/s)	13	22
n	0,35	0,35
$\alpha_{233,\ 333\ K}$ (%/K)	-	0,55

TABLEAU 6: Caractéristiques des semi-propergols au magnésium.

Semi-propergol	C1	C2
. **Formulation**		
liant + additifs	33	42
oxydant minéral	30	10
carbone	29	40
additif métallique	8	8
. **Faisabilité**		
η (poises)	5 000	20 000
K (heures)	10	3
. **Propriétés mécaniques**		
Sm (MPa)	0,7	2,2
em (%)	60	34
. **Masse volumique**		
ρ (kg/m^3)	1442	1637
. **Propriétés cinétiques**		
$V_{c\ à\ 5,0\ MPa}$ (mm/s)	14	5
n	0,2	0,69

TABLEAU 7: Caractéristiques des semi-propergols contenant des particules de carbone.

zones de recirculation, à température élevée.

Le rendement de combustion est très sensible à la nature et la qualité (teneur en produits volatils) du carbone ainsi qu'à la granulométrie des particules.

La composition C1 a été évaluée dans une chambre de statofusée de diamètre 100 mm à entrées d'air latérales et pour différentes conditions de fonctionnement en altitude (0 à 10 km) et de nombre de Mach (2 à 3,5).

L'allumage du générateur de gaz ne présente pas de difficulté particulière (figure 8) quelle que soit la configuration (générateur de gaz séparé ou intégré). La pyrophoricité avec l'air est acquise. Le taux de résidus faible (< 0,5%) est comparable à celui d'un semi-propergol classique.

L'étude des principaux paramètres de fonctionnement montre que la combustion des particules de carbone utilisées est particulièrement sensible à la vitesse de l'écoulement dans la chambre et à la pression (temps de séjour), mais aussi à la température génératrice de l'air.

A titre d'exemple, les résultats suivants ont été obtenus dans le cas du fonctionnement d'un moteur simulant, en conduite forcée, des conditions de vol à moyenne altitude (≈ 10 km) et nombre de Mach de 3,5. Les valeurs de rendements de combustion enregistrées sont comprises entre 0,85 et 0,95 suivant la configuration du générateur de gaz, le mode d'injection, la richesse injectée du combustible (≈ 0,4 à 0,6) et le nombre de Mach interne dans la chambre (de 0,3 à 0,2).

L'intérêt d'une configuration en générateur de gaz intégré ou séparé n'est pas clairement démontré, néanmoins la version séparé permet d'utiliser des dispositifs d'injection plus spécifiques qui permettent d'obtenir un léger gain sur les rendements de combustion. La maîtrise de la pression et du débit dans le générateur de gaz ne pose pas de problème particulier (Fig. 8) et l'absence de dépôt sur les injecteurs ainsi que dans la chambre de combustion restent un atout majeur, en plus de la discrétion, comparé à des compositions contenant du bore.

4.3.3 Semi-propergols au bore.
Du point de vue énergétique, les compositions au bore sont potentiellement intéressantes lorsque des critères de discrétion ne sont pas imposés. Leur utilisation se heurte cependant à deux problèmes spécifiques: d'une part des problèmes de faisabilité aux taux de charge élevés, d'autre part des difficultés à faire brûler les particules de bore dans la chambre de combustion aérobie.

Les compositions au bore sont constituées d'un liant, de perchlorate d'ammonium, de bore et éventuellement d'additifs destinés à faciliter la combustion [13].

Le liant est généralement à base de polybutadiène à terminaisons carboxyles (PBCT). Bien qu'ayant une viscosité supérieure à celle du polybutadiène hydroxytéléchélique (PBHT), il présente par rapport à celui-ci l'avantage de ne pas réagir au contact des impuretés présentes à la surface des particules de bore. Il est en effet couramment observé que l'incorporation de bore dans du PBHT conduit à des pâtes ayant une viscosité très élevée, incompatibles avec une mise en oeuvre correcte.

Il a été démontré [14] que ceci est dû à l'apparition dans le milieu d'espèces de très fortes masses moléculaires lorsque le mélange bore/PBHT est soumis à de fortes contraintes de cisaillement, ce qui est le cas au cours du malaxage (figure 9).

Le perchlorate d'ammonium est introduit à un taux compris entre 25 et 35%. Les granulométries utilisées tiennent compte de la faisabilité et des propriétés cinétiques requises.

Les particules de bore sont fines (de l'ordre du micron) afin d'assurer une combustion correcte. Un traitement chimique spé-

cifique permet éventuellement d'améliorer la faisabilité.

Enfin l'incorporation en faible quantité (quelques %) d'un autre métal peut être favorable à l'augmentation de la température dans le générateur de gaz ou dans la chambre de combustion. Ceci conduit à l'amélioration des rendements de combustion.

Le mode de combustion frontal impose de disposer de vitesses de combustion élevées (entre 10 et 15 mm/s), pour assurer les débits nécessaires à la pression de fonctionnement.

Le réglage de cette vitesse de combustion est en général obtenu en adaptant la formulation (granulométrie du perchlorate d'ammonium, taux et nature du catalyseur de combustion).

L'utilisation de blocs pleins permet également d'envisager un réglage de la vitesse de combustion par la technique des blocs à fils: la combustion du semi-propergol est accélérée en noyant dans la matrice un ou plusieurs fils métalliques.

Le tableau 8 regroupe les principales caractéristiques de formulations représentatives de la famille de semi-propergols au bore développés.

Les viscosités à la coulée, comprises entre 10 000 et 20 000 poises, conduisent à des taux limites de bore de l'ordre de 40%, un taux minimum de perchlorate d'ammonium étant nécessaire pour assurer la décomposition du liant (de 25 à 30 %).

Les températures critiques à l'épreuve du cook-off sont faibles (≈ 120°C), comparées à celles des propergols composites classiques à liant inerte. Cependant la réaction observée n'est pas violente: le matériau brûle. Ce comportement particulier (combustion à faible température) est général pour l'ensemble des semi-propergols étudiés. Il est très favorable du point de vue de la vulnérabilité.

La vitesse de combustion de ces matériaux peut aisément être réglée en adaptant la formulation, et ceci quelle que soit la configuration envisagée.

Dans le cas de ces semi-propergols, la combustion des particules de bore dans une chambre aérobie pose des problèmes spécifiques liés à la présence d'oxyde de bore enrobant les particules et à la nécessité d'obtenir des températures élevées du mélange "air/produits de combustion" afin d'initier et d'entretenir la combustion du bore.

L'emploi de métaux peut contribuer à l'augmentation de la température de combustion primaire des gaz du générateur et faciliter ainsi l'allumage des particules de bore. Des architectures de chambre spécifiques et des dispositifs d'injection adaptés sont aussi requis, dans certains cas, afin d'améliorer la combustion du bore [15,16].
Le surplus de masse de la chambre de combustion dû à ces aménagements, peut pénaliser les performances du système propulsif.

De plus, dans le cas de la configuration à générateur séparé, les dépôts d'oxyde de bore sur les organes de transfert et d'in-

Semi-propergol	B1	B2	B3	B4
. Configuration envisagée générateur de gaz	séparée		"rustique"	
combustion du bloc	frontale			frontale accélérée par fils
. Formulation				
liant PBCT + additifs	30	30	30	32
oxydant	30	25	30	30
bore	35	40	35	33
additifs métalliques	5	5	5	5
. Faisabilité				
η (poises)	12 000	20 000	15 000	10 000
K (heures)	6	5	5	7
. Propriétés mécaniques				
Sm (MPa)	2,1	1,6	2	2,0
em (%)	37	50	43	75
. Masse volumique				
ρ (kg/m^3) *	1616	1642	1631	1595
. Sécurité				
CSF (N)	345	-	221	-
Mouton 30 kg (m)	2,5	-	2,75	-
. Vulnérabilité				
Cook-off	116	-	121	-
. Propriétés cinétiques				
$V_{c\ à\ 5.0\ MPa}$ (mm/s)	14	10	-	-
$V_{c\ à\ 0.6\ MPa}$ (mm/s)	-	-	12	15
n	0,1	0,1	0,3	0,16

TABLEAU 8: Caractéristiques des semi-propergols au bore.

Semi-propergols	B1	B2
Configuration du générateur de gaz	"séparée"	"intégrée"
Débit d'air (kg/s) Température Tio (K)	6,7 520	6,7 520
Pression générateur (MPa) Vitesse de combustion (mm/s) Richesse injectée	1,4 10,3 0,34	0,7 13,0 0,42
Rendement de combustion **Perte de charge** **C_***	**0,95** **0,84** **0,49**	**0,91** **0,84** **0,587**

TABLEAU 9: Résultats d'essais de combustion avec des semi-propergols au bore.

jection (injecteurs/vannes) peuvent être la cause de bouchage entraînant une augmentation importante de la pression dans le générateur de gaz.

La combustion des particules de bore est à ce jour assez bien maîtrisée en chambre statofusée [17]. Son efficacité est sensible, entre autres, aux paramètres de fonctionnement du statofusée tels que le Mach et la pression dans la chambre de combustion, la température génératrice de l'air, ...

Les résultats d'essais au sol de deux semi-propergols au bore (35%) dans des conditions simulant en conduite forcée un vol à Mach 2 et basse altitude sont comparés sur la figure 10 et dans le tableau 9, l'une en configuration séparée, l'autre en version intégrée.

Pour certaines missions, en particulier à basse altitude, la configuration générateur intégré peut concurrencer la version générateur séparé habituellement plus favorable pour la combustion du bore. La version intégrée conduit à une architecture simplifiée donc plus facile à mettre en oeuvre.

Les rendements de combustion sont comparables à ceux obtenus avec des semi-propergols moins chargés en bore. Malgré l'augmentation de masse due à l'architecture particulière de la chambre dans le cas des semi-propergols au bore, la comparaison en terme de masse ou/et de portée peut s'avérer plus favorable que pour un engin à semi-propergol classique [17].

5. CONCLUSION.

Les semi-propergols présentés dans cet article sont représentatifs des principales familles de matériau développées en France pour une application statofusée. Ils ont subi une caractérisation à une échelle significative, permettant de déterminer leur domaine d'application.

Les développements exploratoires (Probatoire 400 mm, SIMS, MPSR1, ...) réalisés dans le cadre des compositions discrètes ou des semi-propergols automodulables pour missile rustique ont conduit à un nombre élevé de fabrications (plus d'une tonne de produit dans certains cas) et de caractérisations.

La démonstration de la maîtrise de la fabrication ainsi que des caractéristiques mécaniques et balistiques d'une large gamme de semi-propergols a été faite.

Les efforts de recherche et de mise au point se poursuivent en particulier sur les compositions au bore qui posent des problèmes de faisabilité et celles au carbone qui peuvent présenter des difficultés de combustion dans certaines conditions.

Les semi-propergols développés sont tout à fait adaptables à différentes applications dans le domaine de la propulsion.

REMERCIEMENTS.
Les auteurs expriment leurs remerciements aux Services Officiels Français DME (STPE et STSMT) et DRET (Groupe 07) pour leur soutien constant dans le domaine des recherches concernant les semi-propergols.

REFERENCES BIBLIOGRAPHIQUES.

1 Cazin, P. , "Les Statoréacteurs à Combustible Liquide", AGARD Lecture Series n°136 on Ramjet and Ramrocket Propulsion Systems for Missiles, 1984.

2 Davenas, A. et Collaborateurs, "Technologie des Propergols Solides", Editions Masson, 1989.

3 Petit, B., Ravier, A., "Expérience Française sur le Statofusée "Rustique" et Perspectives d'Application", 79th Symposium AGARD on Airbreathing Propulsion for Missiles and Projectiles, 1992, Paper 1.3.

4 Nadaud, L., Reynaud, F., Moutet, A., "Combustibles Solides pour Statoréacteurs: Combustibles Solides Autopyrolysables", La Recherche Aérospatiale, n° 1, 1977, pp 31-38.

5 Fourest, B., Masson, C., "Recherche et Développement de Propergols à Fort Exposant de Pression", 21th International Annual Conference of ICT, Karlsrhue, 1990.

6 Fourest, B., Cauty, F., "Etude de la Combustion Instable d'un Semi-propergol par Mesure Directe Ultrasonore", 17th International Annual Conference of ICT, Karlsrhue, 1986.

7 Besser, H.L., "Solid Propellant Ramrocket", AGARD Lecture Series n°136, 1984, pp 7.1-7.30.

8 Gordon, C., Mc Bride, B.J., "Computer Program for Calculation of Complex Chemical Equilibrium Compositions, Rocket Performance, Incident and Reflected Schocks, and Chapman-Jouguet Detonations", NASA SP-273, 1971.

9 Berard, J.D., Doriath, G., Perut C., "Recherche et Mise au Point d'un Propergol Solide pour Statofusée", 58th Symposium AGARD on Ramjets and Ramrockets for Military Applications, 1985, p. 24.1-24.10.

10 Fourest, B., "Sensibilité à la Température Initiale de la Vitesse de Combustion des Propergols et Semi-propergols Solides Composites à Base de Perchlorate d'Ammonium", La Recherche Aérospatiale, n° 6, 1989, pp 67-76.

11 Kuentzmann, P., Demarais, J.C., Cauty, F., "Mesure de la Vitesse de Combustion des Propergols Solides par Ultrasons", La Recherche Aérospatiale, n° 1, 1979, pp 55-72.

12 Gunners, N.E., Liljegren, T., "Studies of Fuel-Rich Magnesium-HTPB-Propellants for Solid Ducted Rocket", 1977, pp 9.1-9.14.

13 Mahé, B., Perut, C., "Boron Propellants for Ducted Rocket Application", 2nd Int. Symposium on Special Topics in Chemical Propulsion: Combustion of Boron-Based Propellants and Solid Fuels, Lampoldshausen, 1991.

14 Mayen M., "Mixing of Hydroxyl-Terminated Polybutadiene and Boron", 2nd Int. Symposium on Special Topics in Chemical Propulsion: Combustion of Boron-Based Propellants and Solid Fuels, Lampoldshausen, 1990.

15 Messerchmitt-Bolkow-Blohm, Patent n°78 033 15, 1978.

16 Vigot, C., Bardelle, L., Nadaud, L., "Improvement of Boron Combustion in a Solid-Fuel Ramrocket", AIAA, 1986, Paper 86-1590.

17 Vigot, C., Cochet, A., Guin, G., "Combustion Behavior of Boron-based Solid Propellants in a Ducted Rocket", 2nd Int. Symposium on Special Topics in Chemical Propulsion: Combustion of Boron-Based Propellants and Solid Fuels, Lampoldshausen, 1991.

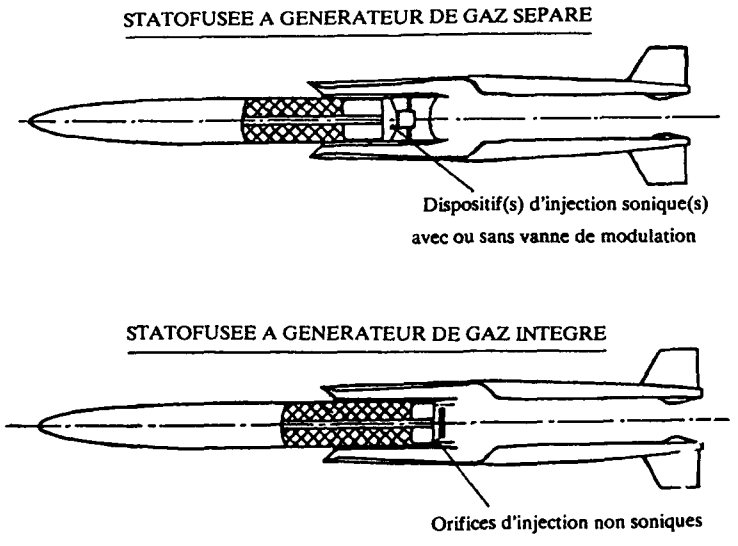

Figure 1: Configurations de générateurs de gaz du statofusée.

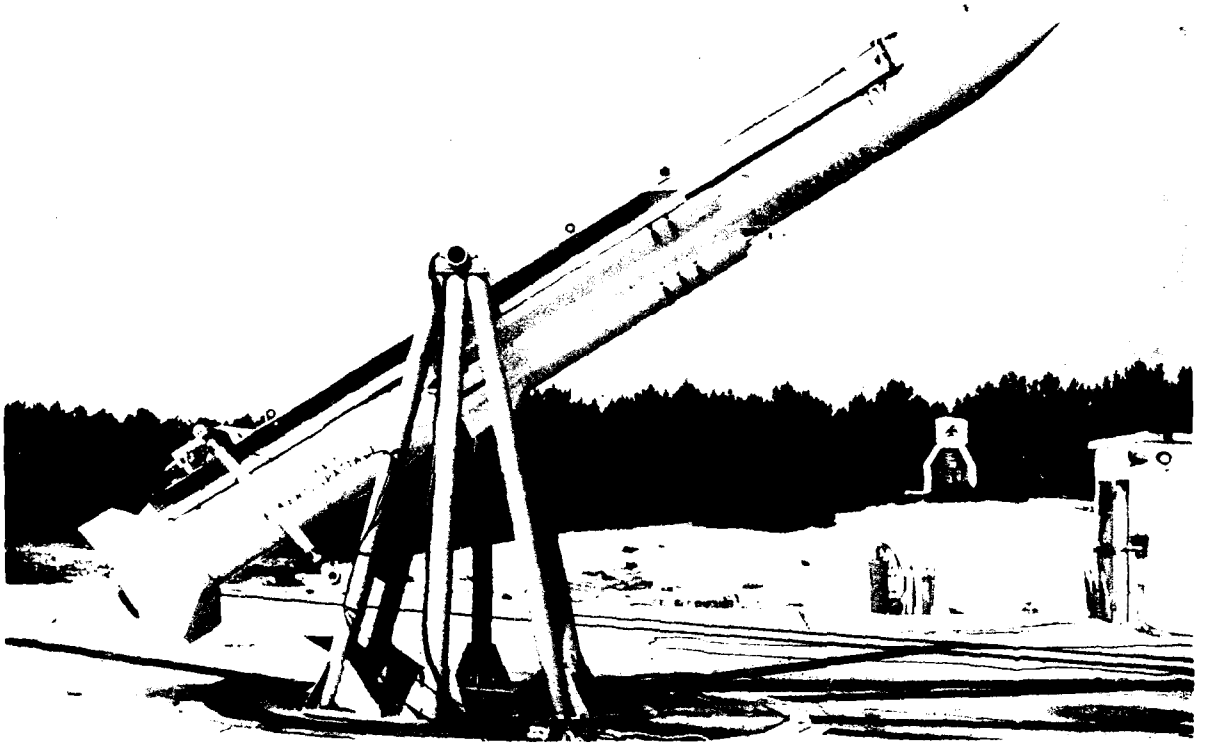

"Probatoire 400"

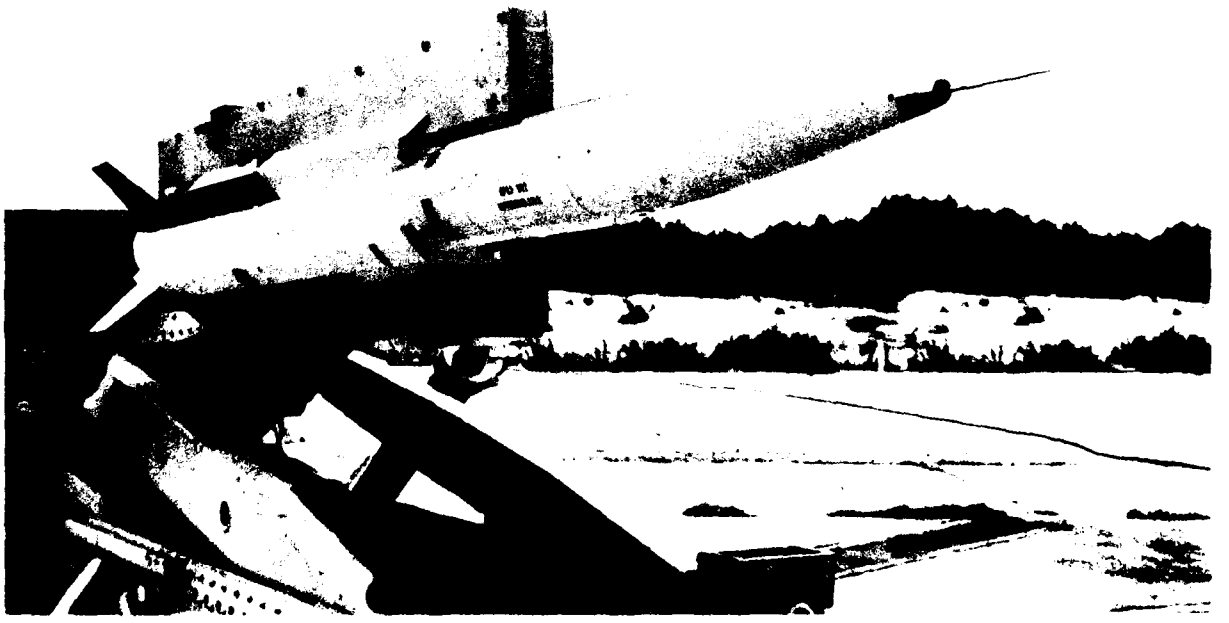

"Petit Missile rustique (MPSR)"

Figure 2: Exemples d'application du statofusée [1]

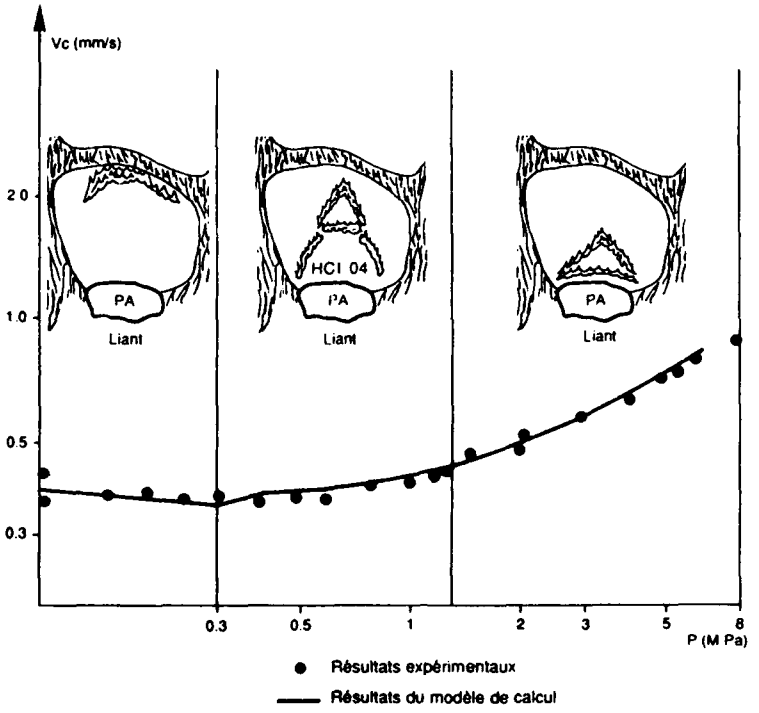

Figure 3: Modélisation de la combustion d'un semi-propergol à faible taux d'oxydant (ONERA [5]).

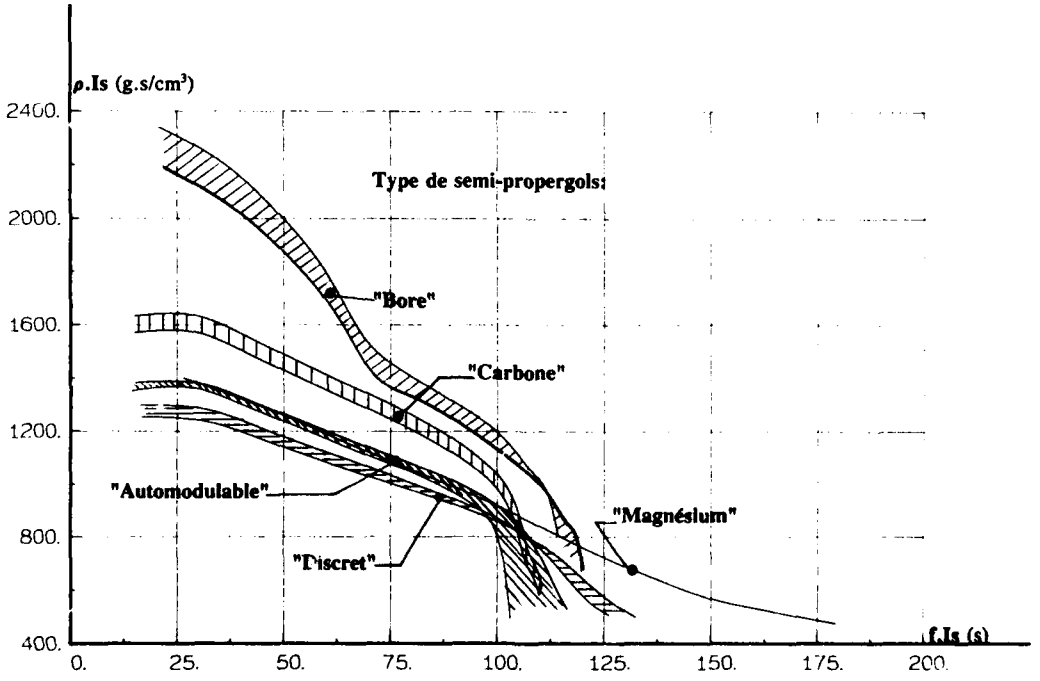

Figure 4: Performances énergétiques des semi-propergols développés. (Conditions: Basse altitude, Mach 2)

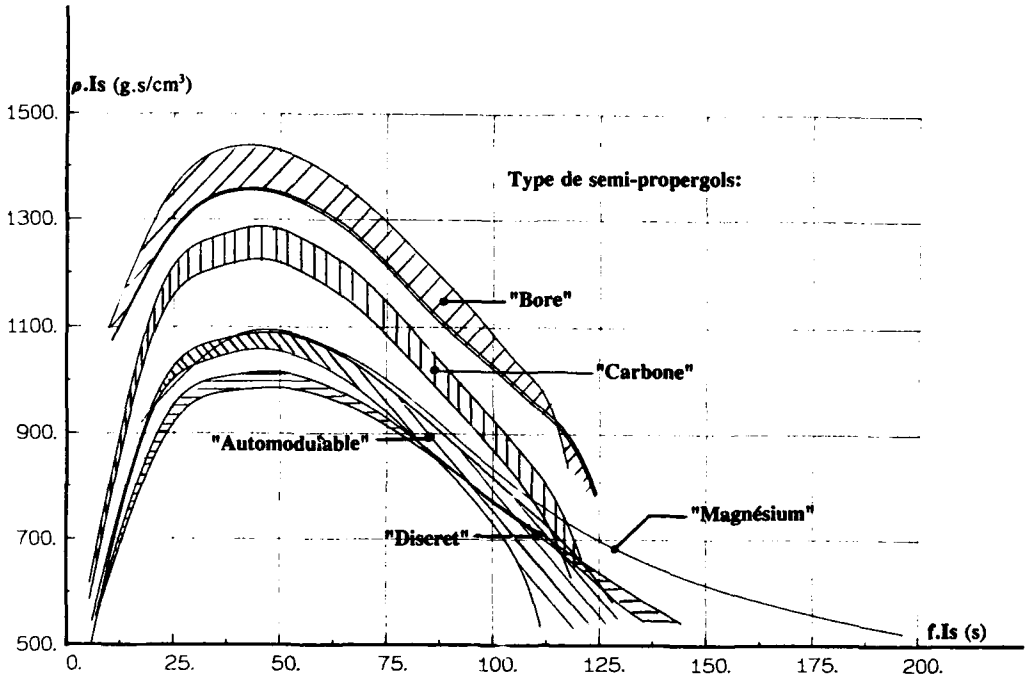

Figure 5: Performances énergétiques des semi-propergols développés.
(Conditions: Haute altitude, Mach 5)

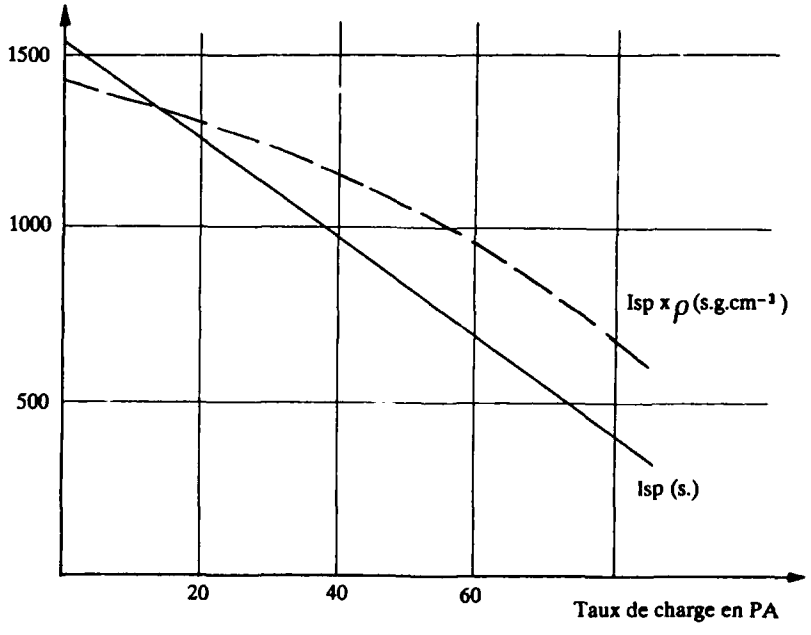

Figure 6: Influence du taux d'oxydant sur les performances théoriques de semi-propergols discrets sans particule métallique.
(Conditions: Basse altitude, Mach 2)

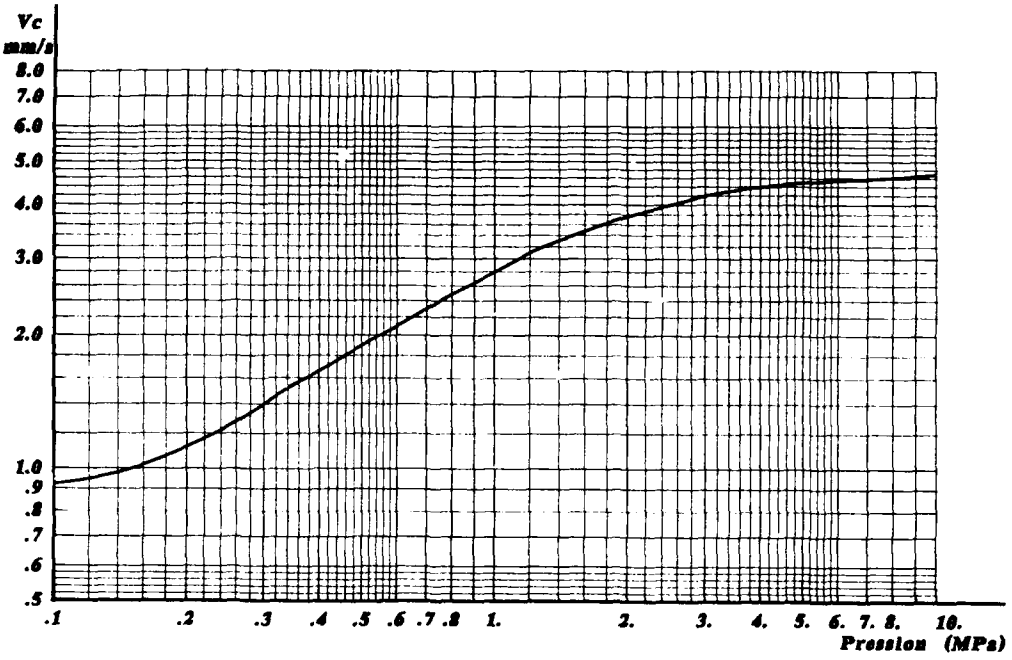

Figure 7: Evolution de la vitesse de combustion d'un semi-propergol pour application "rustique" en fonction de la pression. Détermination faite par la technique ultrasonore.

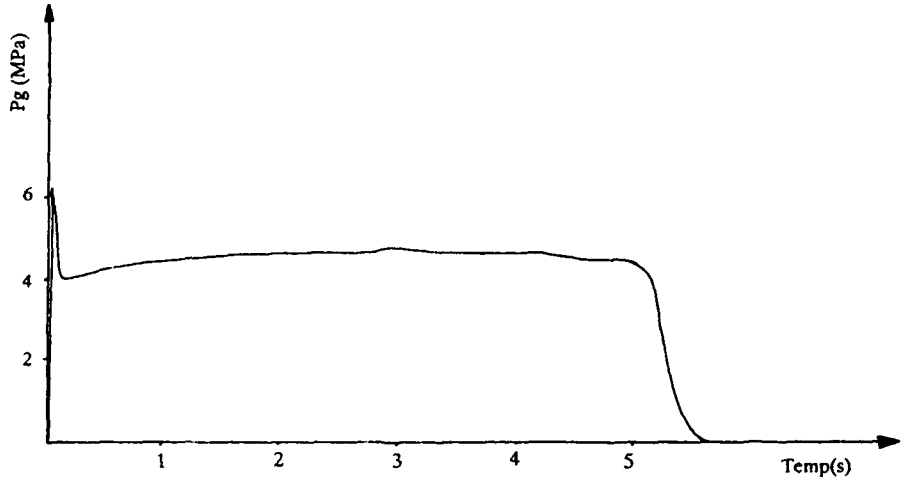

Figure 8: Enregistrement de la pression dans le générateur de gaz séparé au cours d'un essai de semi-propergol au carbone.

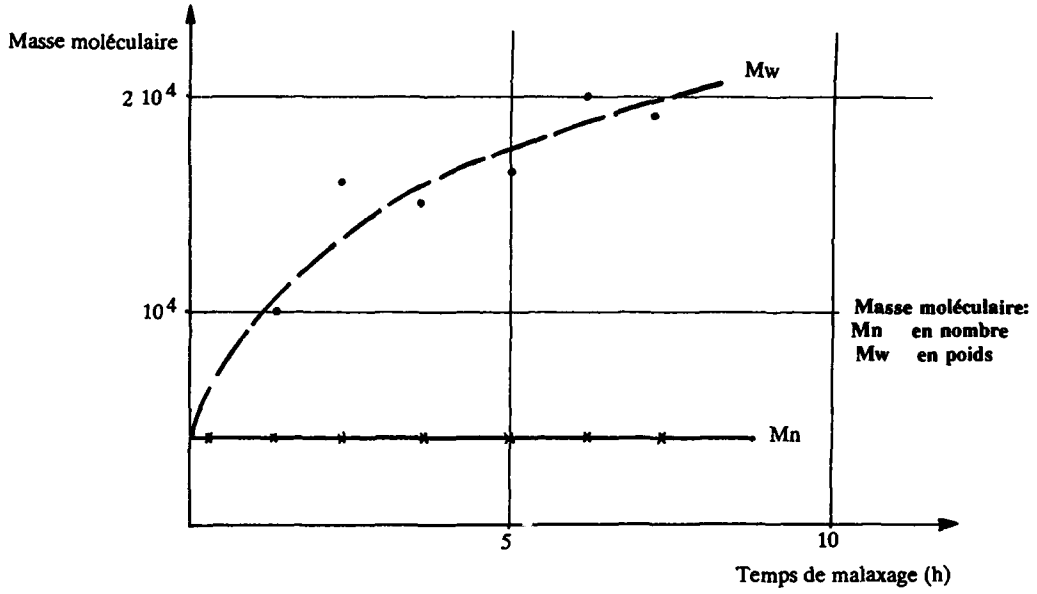

Figure 9: Evolution de la masse moléculaire du PBHT en fonction du temps de malaxage d'un mélange PBHT/Bore (50/50)

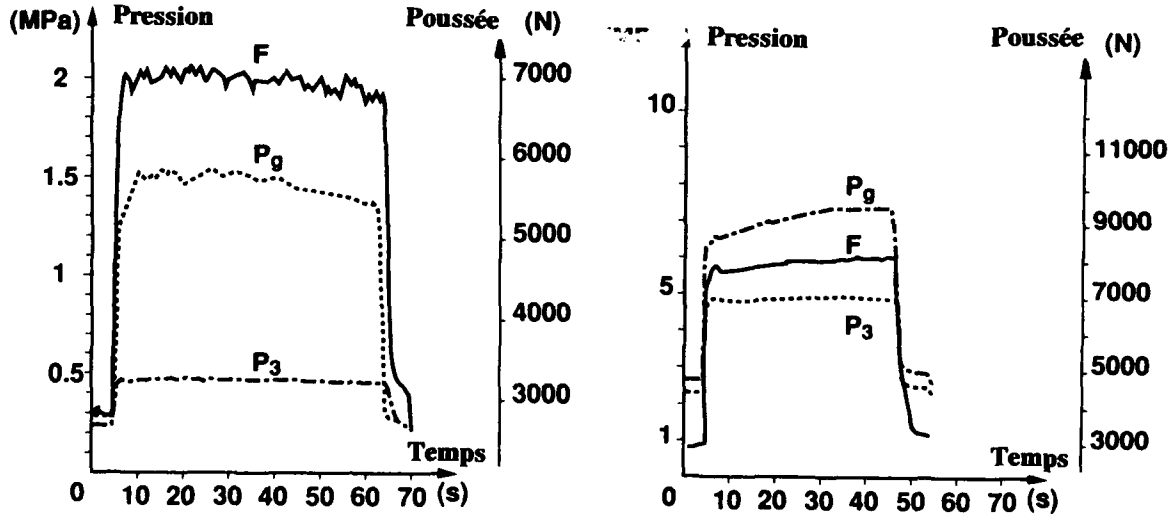

Générateur de séparé

Générateur de gaz intégré

Figure 10: Enregistrement des pressions et de la poussée au cours d'essais de semi-propergols au bore [16].

Combustion Instabilities in a Side-Dump Model Ramjet Combustor

J.M. Samaniego
B. Yip
T. Poinsot
S. Candel
E.M2.C Laboratory, CNRS, Ecole Centrale Paris
92295 Châtenay-Malabry CEDEX, FRANCE

ABSTRACT

Combustion instabilities are often observed in coaxial and side-dump combustors, and can be detrimental to their performance. This study is aimed at identifying the physical mechanisms underlying combustion instabilities in these geometries. Recent studies performed on side-dump geometries have focused on hydrodynamic instabilities under non-reacting conditions. The present work has been conducted on a two-dimensional two-inlet side-dump combustor, fed with a premixture of air and propane in order to examine reacting flow instabilities. Results from a stable combustion regime are presented in order to provide a basis for comparison with a low-frequency instability mode (520 Hz) which occurs at other combustor operating conditions. The flowfield structure is investigated using high speed Schlieren visualization and conditional C_2 imaging. Simultaneous pressure, inlet velocity and global C_2 emission measurements are used to investigate the nature of the instability. Different processes involved in the instability mode are identified such as the acoustics of the combustor, the oscillatory motion of the jets underlying periodic jet-on-jet impingement and a complex behavior of the reaction zones. Furthermore, by obtaining an experimental local Rayleigh index distribution, it has been possible to identify the driving mechanisms of this instability.

1 INTRODUCTION

Many flight vehicles are propelled by ramjets including certain missiles and aircraft prototypes. Side-dump combustors are being investigated as an alternative to coaxial-dump combustors for a light and compact propulsion system. Combustion instabilities often appear in such devices and can be detrimental to their performance (Ref 1,2). These instabilities can cause large amplitude mechanical vibrations which may result in structural damage to the vehicle. Flame oscillations associated with combustion instabilities can cause hot spots in the combustion chamber which also may be damaging. Furthermore, these instabilities can create strong acoustic pressure oscillations causing a destabilization of the inlet shock-wave system.

Several studies have been conducted to investigate the causes of combustion instabilities in ramjet combustors. Mode shape measurements in coaxial and side-dump devices have shown that combustion instabilities are frequently associated with natural acoustic eigenmodes of the system, involving the combustor and the inlet or inlets (Ref 3,4). The coupling between the acoustic resonant modes and the combustion processes is responsible for sustaining the instability: Oscillations are amplified when pressure and heat release fluctuations are positively correlated in time (Ref 5,6,7). Furthermore, images from Schlieren visualization have shown that vortex shedding is a common feature in dump combustors and may play a major role in combustion instabilities (Ref 8,9,10). In addition, convective waves (entropy or vorticity waves) may occur under certain conditions and take a part in the process (Ref 10,11,12). In this case, the resonant modes differ in frequency and in shape from the acoustic eigenmodes of the system and are interpreted as coupled convective-acoustic oscillations.

While coaxial-dump combustors have been already extensively studied, less work has concerned side-dump arrangements. In side-dump geometries, the impingement of two or more jets is an important feature of the combustor flowfield. Recent studies have shown that jet impingement on a plate or jet-on-jet impingement can sustain flow instabilities (Ref 13,14). Clark (Ref 4) investigated low-frequency combustion instabilities in two-inlet, side-dump ramjet combustors with different inlet and combustor lengths. The results of these studies indicated that the dominant instability mode was approximately the same in all cases (300 Hz) and could be associated with different longitudinal acoustic modes, depending on the inlet and combustor lengths. Clark (Ref 4) speculated that the fluid dynamics associated with the dump station create a mechanism for unsteady heat release. Water-channel experiments have been conducted with two-dimensional side-dump devices and have demonstrated that the side-dump inlet configuration creates certain unsteady hydrodynamic features (Ref 15,16). First, the impingement of the two inlet flows led to an antisymmetric flapping motion of the two jets. Secondly, unsteady streamwise vorticity was generated in the stagnation region and was phase-locked with the flapping motion of the jets. This vorticity generation was viewed as an important mixing process in chemically reacting flows. Nosseir and Behar (Ref 15) concluded that this phenomenon would produce periodic heat release due to the enhanced mixing associated with these vortices. Although non-reacting flow experiments reveal many important features of the unsteady flow in side-dump ramjet combustors, they may not reproduce certain mechanisms found in reacting flows which result from heat addition.

To investigate instability mechanisms associated with the reacting flowfield, a two-dimensional premixed air/propane side-dump combustor has been designed. In the present study, results concerning a low-frequency com-

bustion instability are reported. Images from Schlieren visualization along with those from C_2 radical light emission reveal a complex evolution of the reacting flowfield inside the combustor during the instability cycle. We begin with a brief presentation of the experimental set-up (Section 2). The combustor behavior and dynamics are described in Section 3. A detailed analysis of an unstable regime is given in Section 4 and the results obtained are discussed in Section 5.

2 EXPERIMENTAL CONFIGURATION

The combustion chamber has a rectangular cross-section of 70×60 mm^2 and is 340 mm in length (Fig. 1). It is equipped with quartz side-walls to allow optical access and is closed at one end (this end will be called the dome wall). A mixture of air and propane is injected through two inlets with rectangular cross-sections of 5×60 mm^2 which are located on the top and bottom walls of the combustion chamber. The injection sections are positionned at 40 mm from the dome wall. The upper and lower combustor walls are ceramic and are surrounded with a layer of insulating material. Ignition is achieved using a spark ignitor located in the dome wall.

The air is supplied by a compressor through a storage pressure vessel into the two inlets and the two air flows are metered by sonic nozzles. Propane is metered by sonic nozzles and injected into each duct downstream of the air flow metering section. The inlet geometry is presented in Fig. 2. The average inlet velocities and equivalence ratios were the same for each inlet and could be varied from 15 to 100 m/s and from 0 to 2.00, respectively. The Reynolds number, based on the inlet width, ranges from 4×10^3 to 2.5×10^4.

Pressure oscillations in the inlets were measured using flush-mounted microphones (Brüel and Kjaer type 4136). Pressure fluctuations in the combustion chamber were measured with a "semi-infinite" waveguide microphone arrangement fitted in the dome wall (Fig.3) (Ref 17,18). The waveguide is formed of a tube of 6 mm inner diameter and 30 meters long. A microphone is mounted perpendicular to the waveguide, at 22.6 cm from the inner part of the dome wall. In this system, pressure fluctuations on the dome wall propagate in the waveguide at the local speed of sound and are dissipated by viscous effects in the waveguide termination (Ref 19). The measured pressure fluctuation is equivalent to the pressure fluctuation on the dome wall, phase-shifted due to the travel time between the combustor and the microphone and attenuated by viscous effects. The waveguide is water-cooled and fed with nitrogen in order to maintain a constant temperature inside the tube and to control the travel time of the pressure waves between the combustor and the microphone. These precautions are necessary in order to obtain accurate pressure phase angle measurements. Calibrations performed during the experiments indicated that the average error in the pressure phase angle is less than 10 degrees (Ref 20). Inlet velocity fluctuations were measured using a constant temperature hot-film anemometer (DISA C17).

The light emission from free radicals like C_2 or CH existing in the entire volume of the combustion chamber was isolated by an interferential filter and focused onto a EMI 9871B photomultiplier. This signal monitored the global heat release fluctuations. Imaging of radical species from the flame was performed using two different imaging systems. The resulting images provide the time-averaged or phase-averaged spatial distribution of the C_2 or CH light emission integrated over a line of sight. Time-averaged images were obtained with a CCD video camera (PULNIX TM 440) and were recorded on a McIntosh II equipped with an ORKIS frame-digitizer. Phase-averaged images representing one complete instability cycle were obtained using an intensified CCD camera (Photometrics system 200). The image intensifier (PCO Computer Optics) was used as a fast shutter with time exposures of 50 μs. This imaging system permitted the integration of multiple image exposures. An inlet pressure signal, bandpass filtered and time-delayed, was taken as a reference and was used to control the multiple-triggering of the intensifier. The resulting image was the sum of approximately 160 exposures, conditionnally sampled at a selected phase relative to the pressure signal. Phase-averaged images corresponding to different phase angles were obtained by varying the time delay (Ref 21).

A high speed movie camera (NAC model E-10 EE) operating at 5000 $frames/s$ was used to record Schlieren images. Signal traces from pressure measurements and global C_2 light emission measurements, taken simultaneously with the Schlieren film, were used to sort out the Schlieren images corresponding to the phase angles selected for the C_2 emission conditional images.

3 STABLE AND UNSTABLE COMBUSTION

The difference between stable and unstable combustion in a turbulent combustor is often subjective and these terms need to be defined. In the present study, stable combustion is defined as those operating regimes where the pressure and radical light emission spectra do not exhibit discrete peaks. Unstable combustion corresponds to operating regimes for which strong peaks exist in the power spectra and indicate that a combustion instability is triggered.

First, we present visualizations of a typical stable regime in order to describe the structure of the reacting flow (section 3.1) and, secondly, we identify two regimes of low-frequency combustion instability (f = 500 Hz) (section 3.2).

3.1 Stable combustion

A typical regime of stable combustion, for operating conditions of V_{inlet}=20 m/s and ϕ=0.85, is now characterized with Schlieren visualization and time-averaged CH imaging.

Schlieren photographs show that the two side jets are bent towards the exhaust and interact near the combustor centerline (Fig. 4a). The jet counterflow geometry defines two separate regions inside the test section: a small volume bounded by the dome wall and the jets (this will be called the "dome zone") and the remaining volume extending from the jets to the exhaust section (this will be called the "main zone"). Near the injection sections, the interface between the cold jets and the hot recirculating gases is well defined and slightly corrugated. In the region where the jets interact, a large zone of small-scale structures can be seen, spreading mainly towards

the exhaust section. This shows that the flowfield is two-dimensional near the injection section and becomes three-dimensional when impingement of the jets on the combustor centerline occurs. Furthermore, the mixing layers of both jets feature high frequency vortices (as demonstrated by Schlieren films).

A comparison of the Schlieren photographs and the CH emission images shows the location of the reaction zones relative to the jets. Time-averaged CH emission image indicates the presence of two distinct zones of high CH emission intensity separated by the two impinging jets (Fig. 4b). These zones are distributed near the centerline of the combustion chamber and will be referred to as: the "dome combustion zone" and the "main combustion zone". On both sides of the two jets, elongated regions of significant CH emission intensity are observed. These zones may be associated with combustion within the mixing layers. The dome combustion zone is located close to the impingement region. In this region, the flow is decelerated due to the counterflow geometry and combustion may easily be sustained. The main combustion zone is located at about 5 cm downstream of the impingement region. Small-scale turbulence is generated by the jet-on-jet impingement and is convected towards the exhaust. In this case, the mixing processes between the entering cold reactants and the recirculating products are greatly enhanced. It is possible that the distance between the jet impingement region and the main combustion zone is correlated to the mean axial convection speed in this zone and a characteristic ignition delay time.

3.2 Unstable combustion

Two low-frequency unstable modes have been identified : a fuel-rich mode for V_{inlet} around 20 m/s and ϕ around 1.20 and a fuel-lean mode for V_{inlet} around 17 m/s and ϕ around 0.85. Both modes are characterized by a frequency close to 500 Hz corresponding to the quarter-wave mode of the combustion chamber (Ref 20). This frequency appears on all signals as evidenced by the power spectrum estimates (Fig. 5).

In the following, we focus on the fuel-rich unstable mode which is characterized by higher pressure and heat release fluctuations.

4 DESCRIPTION OF THE FUEL-RICH UNSTABLE REGIME

In this section we examine in more detail a fuel-rich unstable mode for an inlet velocity of 20 m/s and an equivalence ratio of 1.2. This unstable mode is characterized by an oscillation frequency of 520 Hz and combustor pressure fluctuation amplitudes of 1000 Pa. Furthermore, the global C_2 emission fluctuations are in phase with the pressure oscillations in the chamber and exhibit amplitudes near to 15 % of the mean value. A first harmonic at 1040 Hz is also present in the power spectral densities (Fig. 5a). During the instability, the amplitude of the inlet velocity fluctuations is about 50 cm/s, which represents 2.5 % of the mean inlet velocity.

To better understand the mechanisms involved in this combustion instability, the analysis of one instability cycle has been performed by comparing phase-averaged C_2 images with Schlieren photographs taken from a 16 mm high speed film (section 4.1). Some aspects of the unsteady combustion are then identified : pulsating combustion in the dome region and convection of reaction zones donwstream of the jet impingement region (section 4.2). In addition, the local Rayleigh index is plotted to determine the locations where driving and damping occur (section 4.3).

4.1 Flowfield visualisation

Figure 6 shows a sequence of conditionally averaged C_2 images taken at equally-spaced intervals during the same instability(38° or 0.2 ms). Accompanying the phase-averaged C_2 images are corresponding Schlieren images representing the same phase angles during the cycle. These images show the first 14 cm of the combustion chamber. The inlet jets undergo a "clapping" type motion which is symmetric about the combustor centerline. The jets impinge upon one another near the centerline at the moment of greatest total heat release (phase angle 0°), as determined by the photomultiplier signal. After this interaction, the jets separate and bend out towards the exhaust plane. Later in the cycle, the jets straighten out and eventually meet again at the center of the chamber.

Comparison of the Schlieren and phase-averaged C_2 images shows that combustion in the dome region is strongly affected by the instability. At phase angle 0°, two separate burning regions are seen as in the case of stable combustion (Fig. 4b): a lower intensity region in the dome (which has just been formed) and a large region of high combustion intensity corresponding to the main combustion zone. Separating these two zones is the region where the jets of fresh gases interact and combustion is particularly weak. The high reaction rate appears in the Schlieren image as a region of intense three-dimensional turbulence.

Between the phase angles 38° and 191°, the overall intensity in the main combustion zone decreases while the dome combustion zone increases in both size and intensity. During this period the jets bend toward the exhaust plane. This movement of the jets may be attributed to the volumetric expansion of gases produced by the dome combustion. Between the phase angles 229° and 305°, the dome combustion zone accelerates forward and merges with the main combustion zone, creating a single large combustion region. However, between the phase angle 267° and 305°, two small reacting pockets can be seen to burn outward from the single combustion zone toward the entering gases. At phase angle 343°, convection due to the inlet gas streams has forced the two pockets to move back toward the chamber centerline, where they coalesce to reform the first combustion zone in the dome region.

4.2 Unsteady combustion phenomena

Unsteady combustion phenomena are analyzed by subtracting the background to the series of C_2 phase-averaged images. The new images represent the fluctuating part of the heat release rate field. The background image only shows one combustion zone spreading downstream from the jet-impingement region, which can be associated with the main combustion zone. The dome combustion zone, where partial extinction is observed during the instability, does not appear in this image (Fig. 7).

The sequence of images of fluctuating heat release show a complex pattern with several reaction zones (Fig. 8). The displacement of the dome reaction zone towards the exhaust is again visible. The images at phase angles 267° and 305° show the creation of two pockets, aligned with the inlet axis and symmetric about the combustor centerline, while the previous dome combustion zone has already moved toward the exhaust. These pockets were already identified in Fig. 6 and are located near the head of the jets just before they interact. At a phase angle of 343°, the jets interact and the pockets, which are moving with the jets, recreate a dome combustion zone.

The evolution of the reaction zones can be reproduced by plotting their axial and transverse position over three instability cycles. Figure 9a shows the transverse positions of the reacting pockets along the inlet axis as well as the positions of the elbows of the jets. These pockets are created at each cycle. They are located near the elbows of the jets and are moving together towards the centerplane of the combustor at the mean inlet velocity. Figure 9b shows the axial position of the reaction zones along the centerplane of the combustor. It can be seen that the dome combustion zone is created when the reacting pockets merge in the dome region. This reacting zone stays approximately at the same position for about one half cycle. Then it moves towards the exhaust at an average velocity of about 20 m/s which is close to the bulk velocity in the hot gases. These results show that convective processes are present along the inlet axis as well as along the combustor centerplane.

Furthermore, Fig. 9b shows that the life-time of the reaction zones is about three instability cycles. Convection of a burning region present in the flow during three cycles explains the complex pattern of the fluctuating heat release sequence (Fig. 8). The image of phase angle 114° shows the presence of three zones along the centerline of the combustor that we shall call first, second and third zones. As we have just seen, the first zone comes from the interaction of reacting pockets convected by the jets. The sequence from phase angle 191° to 305° shows that the second zone corresponds to the first zone of the previous cycle that has been convected downstream. In a similar way, the third zone corresponds to the second zone of the previous cycle, and to the first zone two cycles before.

If we now look at the phase velocity of the reaction zones along the combustor central axis we observe that unsteady combustion occurs in two different ways : 1) in the dome combustion zone, this velocity is close to zero; 2) downstream of the jet impingement region, this velocity is close to the mean axial velocity in the hot gases (see Fig. 9b). We can deduce that, in the dome region, unsteady combustion occurs in a pulsating way whereas donwstream it occurs in a convective way. This is also characteristic of the fuel-lean combustion instability (Ref 20). Unsteady combustion phenomena are different on both parts of the jet impingement region.

4.3 Rayleigh criterion

The coupling between pressure and heat release fluctuations is generally viewed as the main mechanism of combustion instabilities in practical combustors (Ref 7). As a result, the correlation between fluctuations in pressure and heat release may be used to express a condition for which the driving of combustion instabilities may occur. This condition, known as Rayleigh's criterion, is expressed by :

$$R = \frac{1}{V}\frac{1}{T}\int_V \int_T p(\mathbf{x},t)\, q(\mathbf{x},t)\, dt\, d\mathbf{x} > 0$$

where T is the instability period, V is the volume of the combustion chamber, t is time and $\mathbf{x}$ is the location of a point in the combustor. A local form of this expression is given by the local Rayleigh index which is defined as :

$$R(\mathbf{x}) = \frac{1}{T}\int_T p(\mathbf{x},t)\, q(\mathbf{x},t)\, dt$$

In the present experiment, most of the heat release occurs within the first 14 cm of the combustion chamber (as evidenced by the phase-averaged images). The combustion zone is compact in comparison with the acoustic wavelength. Hence, the pressure may be assumed constant in phase and amplitude within the combustion zone and the Rayleigh criterion may be expressed by the correlation between the pressure oscillations on the dome wall and the global heat release fluctuations $Q(t)$, where $Q(t) = \int_V q(\mathbf{x},t)\, d\mathbf{x}$. As mentioned above, the pressure oscillations on the dome wall are in phase with the global C_2 emission fluctuations, and as a consequence, the Rayleigh index R is positive: driving occurs and the instability is sustained.

Although the global heat release $Q(t)$ is in phase with pressure ($R > 0$), there are regions in the flow which damp the oscillation ($R(\mathbf{x}) < 0$) as well as regions which enhance it ($R(\mathbf{x}) > 0$). In order to determine the regions where driving or damping occurs, the two-dimensional distribution of the local Rayleigh index is computed from the C_2 phase-averaged images. This result reveals the complexity of this unstable regime (Fig. 10). Several zones of damping and driving are observed. Acoustic energy appears to be dissipated in the dome combustion zone, and amplified in the main combustion zone. In addition, two pockets representing positive Rayleigh index are located on both sides of the dome combustion zone, relative to the centerline of the combustion chamber. The overall effect may be determined by integrating the local Rayleigh index over the whole image. This calculation results in a positive value indicating that energy is added to the acoustic field and this result is consistent with the global Rayleigh index previously computed.

5 DISCUSSION

5.1 Comparison to cold flow experiments

Stable and unstable combustion are characterized by a symmetric behavior of the combustor flow relative to the centerline and by the existence of two reaction zones. Antisymmetric flapping of the jets, evidenced by cold flow experiments in side-dump geometries, was not observed in most reacting cases probably because of dilatation and acceleration. For unstable combustion, symmetric acoustic modes are preferentially excited because the flame position is symmetric relative to the two inlets.

5.2 Driving mechanism

Different processes are involved in this combustion instability: the quarter-wave mode of the combustion chamber, the jet dynamics and the combustion zone fluctuations. The Rayleigh index distribution shows that the instability is driven by the coupling between the pressure oscillations in the combustion chamber and the convection of reaction zones downstream of the jet impingement region.

This can be modelled in the following way. Let us consider a one dimensional flowfield experiencing pressure oscillations with a constant phase and amplitude distribution at a frequency f. Because of the low oscillation frequency, the spatial distribution of the pressure field over the reacting zone may be neglected and we can write :

$$p(x,t) = P\cos(2\pi ft)$$

Now, if we examine a spatial perturbation of heat release convected at a constant speed V, the local heat release may be written as :

$$q(x,t) = Q\cos[2\pi(x - Vt)/\lambda]$$

The local Rayleigh index would be expressed by :

$$R(x) = PQcos(2\pi fx/V)$$

For this idealized model the Rayleigh index distribution would have a sinusoidal pattern with wavelength $\lambda = V/f$, and would show a succession of damping and driving zones. The average wavelength associated with the pattern of phase angle 114° in Fig. 8 is approximately $H/2$ where H is the height of the combustor. It is also the wavelength associated with the pattern of the Rayleigh index distribution, both in the dome region along the inlet axis and in the main region along the combustor centerline (Fig. 10). The average convection speed, deduced from the wavelength and the frequency, is close to the jet inlet velocity. It appears that the distribution of the local Rayleigh index may be explained by the convection of reaction zones in a sinusoidally time-varying pressure field.

6 CONCLUSION

This paper describes a study of a two-dimensional two-inlet side-dump combustor fed with a mixture of air and propane. The present results concern symmetric operating conditions with respect to the two inlets. Stable and unstable regimes have been identified which depend on the inlet velocity and the equivalence ratio. Schlieren visualization, radical imaging with an intensified CCD camera and simultaneous pressure, inlet velocity and C_2 emission light measurements, have been used to characterize the combustor behavior.

Imaging of the flowfield has provided an insight on the flame structure and its interaction with the entering jets. The geometry of the flowfield inside the combustion chamber with or without instability is symmetric with respect to the combustor centerline. For stable combustion, the flowfield was characterized by the presence of two zones of intense heat release located on both sides of the jet impingement region and were distributed along the combustor centerline.

An unstable fuel-rich regime ($V_{inlet} = 20\ m/s$, $\phi = 1.2$, $f = 520\ Hz$) was studied using a conditional imaging technique. The quarter-wave mode of the combustor is excited during the instability and was associated with a complex evolution of the jets and the flame. Pressure fluctuations in the test section were in phase with the global C_2 emission, indicating that the instability was sustained by energy addition to the acoustic field. Detailed analysis of Schlieren photographs along with C_2 phase-averaged images showed that oscillatory motion of the jets is accompanied by severe oscillations of the flame zones. A two-dimensional distribution of the Rayleigh index as well as images of the unsteady reaction rate in the combustor suggested that the instability was due to convection of reaction zones along the combustor axis. These zones were initially generated by the periodic impingement of the jets on the symmetry axis.

Added information concerning the fuel-lean instability will be presented in a future publication. It appears that instabilities may also be driven by the pulsating combustion in the dome region. This shows that even in our idealized geometry the coupling mechanisms leading to low-frequency combustion instabilities are not unique and illustrates the difficulty of devising predictive models.

References

1. Harrje, D. J. and Reardon, F. H. (1972), "Liquid propellant rocket instability", Report No. NASA SP-194.

2. Webster, F. F. (1989),"Ramjet Development Testing: Which Way is Rigth?",*J. Propulsion* **5**(5), pp. 565-576.

3. Crump, J. E., Schadow, K. C., Yang., V. and Culick, F. E. C. (1986),"Longitudinal Combustion Instabilities in Ramjet Engines: Identification of Acoustic Modes",*J. of Propulsion and Power* **2**(2), pp. 105.

4. Clark, W. H. (1982),"Experimental Investigations of Pressure Oscillations in a Side Dump Ramjet Combustor",*J. of Spacecraft and Rockets* **19**(1), pp. 47-53.

5. Lord Rayleigh (1945), "Theory of Sound". Dover, New York.

6. Culick, F. E. C. (1987),"A Note on Rayleigh's Criterion",*AIAA J.* **21**(10), pp. 1382-1390.

7. Sterling, J. D. and Zukoski, E. E. (1991),"Nonlinear Dynamics of Laboratory Combustor Pressure Oscillations",*to appear in Comb. Sci. and Tech.*

8. Smith, D. A. and Zukoski, E. E. (1985), "Combustion Instability Sustained by Unsteady Vortex Combustion", *AIAA/SAE/ASME/ASEE 21st Joint Propulsion Conference*, AIAA Paper 85-1248, Monterey, California.

9. Poinsot, T., Trouvé, A. C., Veynante, D. P., Candel, S. M. and Esposito, E. J. (1987),"Vortex Driven Acoustically Coupled Combustion Instabilities",*J. Fluid Mech.* **177**, pp. 265-292.

10. Yu, K., Trouvé, A. and Daily, J. W. (1991),"Low Frequency Pressure Oscillations in a Model Ramjet Combustor",*In press in J. of Fluid Mech.*

11. Jou, W.-H. and Menon, S. (1986), "Numerical Simulation of the Vortex Acoustic Wave Interaction in a Dump Combustor", *AIAA 24th Aerospace Sciences Meeting*, AIAA Paper 86-0002, Reno, Nevada.

12. Humphrey, J. W. and Culick, F. E. C. (1987), "Acoustic-Energy Interactions in Ramjet Combustion Chambers", *AIAA/SAE/ASME/ASEE 23rd Joint Propulsion Meeting*, AIAA Paper 87-1872.

13. Ho, C. M. and Nosseir, N. S. (1981),"Dynamics of an Impinging Jet. Part 1. The Feedback Phenomenon",*J. Fluid Mech.* **105**, pp. 119-142.

14. Nosseir, N., Peled, U. and Hildebrand, G. (1987),"Pressure Field Generated by Jet-on-Jet Impingement",*AIAA Journal* **25**(10), pp. 1312-1317.

15. Nosseir, N. S. and Behar, S. (1986),"Characteristics of Jet Impingement in a Side-Dump Combustor",*AIAA Journal* **24**(11), pp. 1752-1757.

16. Miau, J. J., Mong, S. M., Sun, D. J. and Hong, Z. C. (1987), "Visualization of Flow in a Side-Inlet Square-Duct Using a Dye Injection Method", *AIAA 25th Aerospace Sciences Meeting*, AIAA Paper 87-0122, Reno, Nevada.

17. Chun, P. A., Lougadin, J. A., Nabity, J. A. and Ayler, S. E. (1988), "Recent Developments in Ramjet Pressure Oscillation Technology", *Combustion Instabilities in Liquid-Fuelled Propulsion Systems*, AGARD-CPP-449/450, Bath, U.K.

18. Guédel, A. and Farrando, A. (1986),"Experimental Study of Turboshaft Engine Core Noise",*Journal of Aicraft* **23**(10), pp. 763.

19. Pierce, A. D. (1981), "Acoustics: An Introduction to its Physical Principles and Applications". McGraw-Hill, New York.

20. Samaniego, ,J.M. (1992), "Etude des instabilités de combustion dans les statoréacteurs", Doctoral Thesis, Ecole Centrale Paris.

21. Yip, B. and Samaniego, J. M. (1991),"Conditionnaly Phase-averaged Radical Imaging for Combustion Instability",*to appear in Comb. Sci. and Tech.*

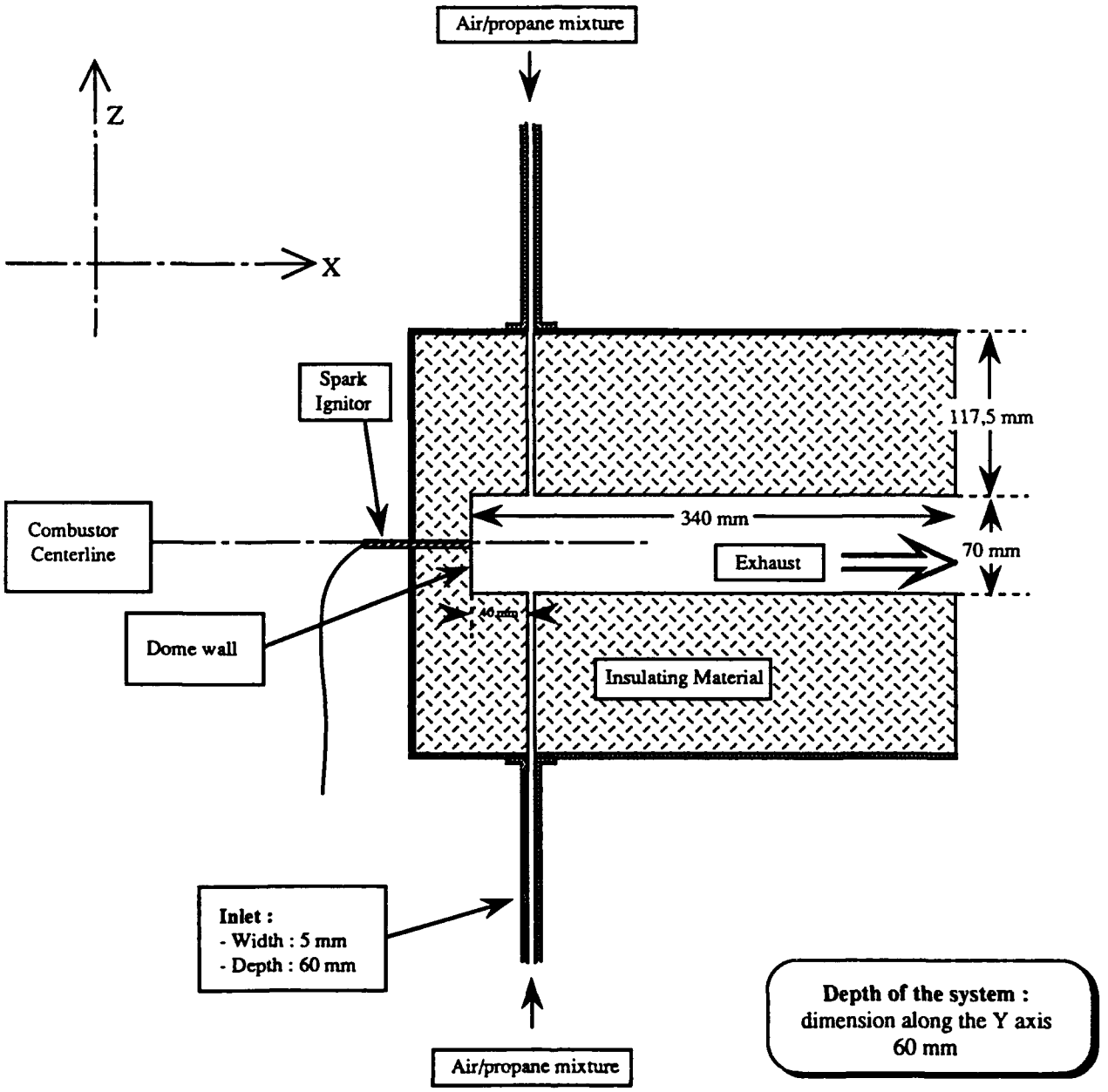

Figure 1: Schematic view of the combustion chamber.

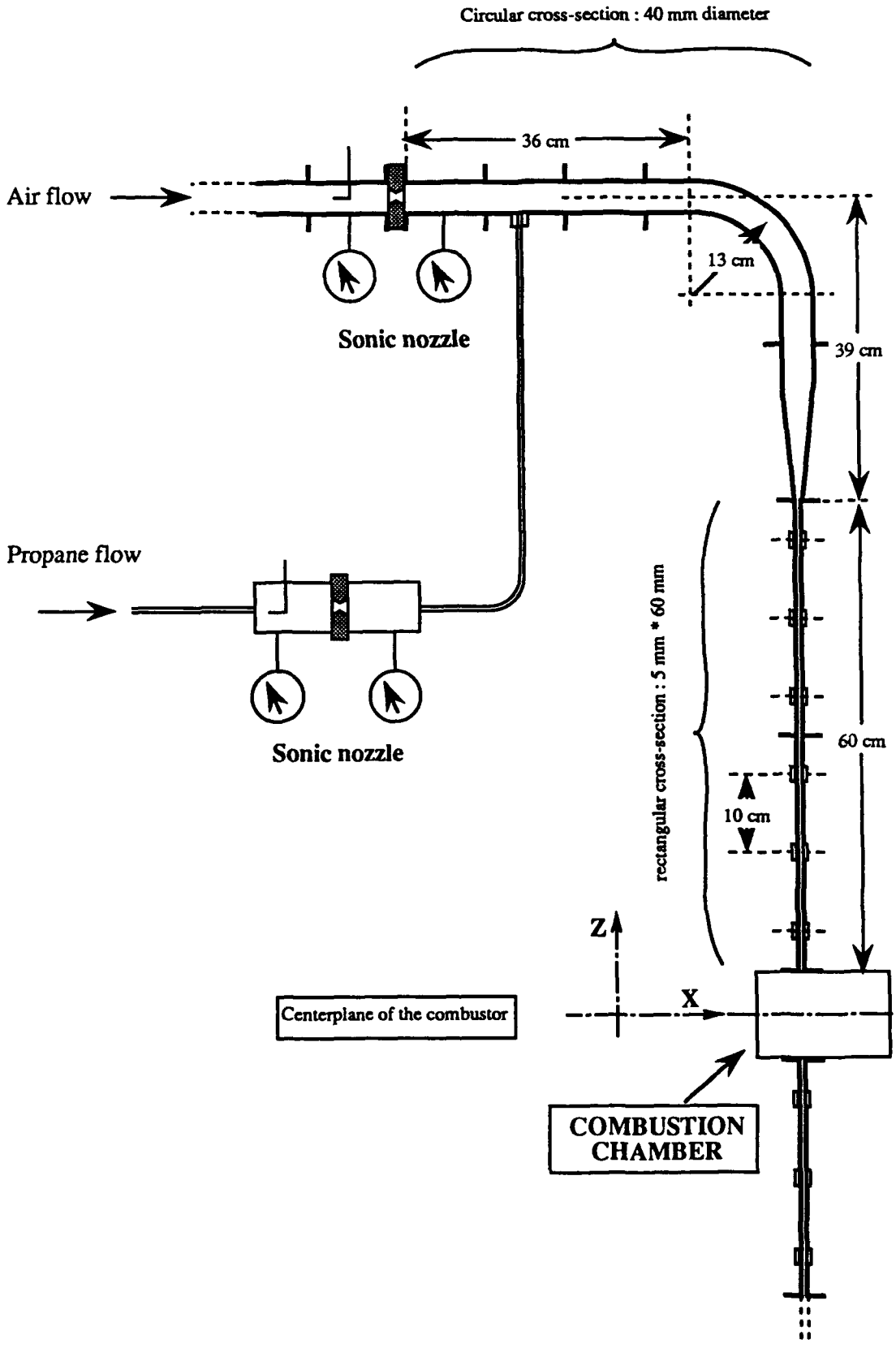

Figure 2: Schematic view of the upper inlet. the lower inlet is symmetric to the upper inlet relative to the centerline of the combustion chamber.

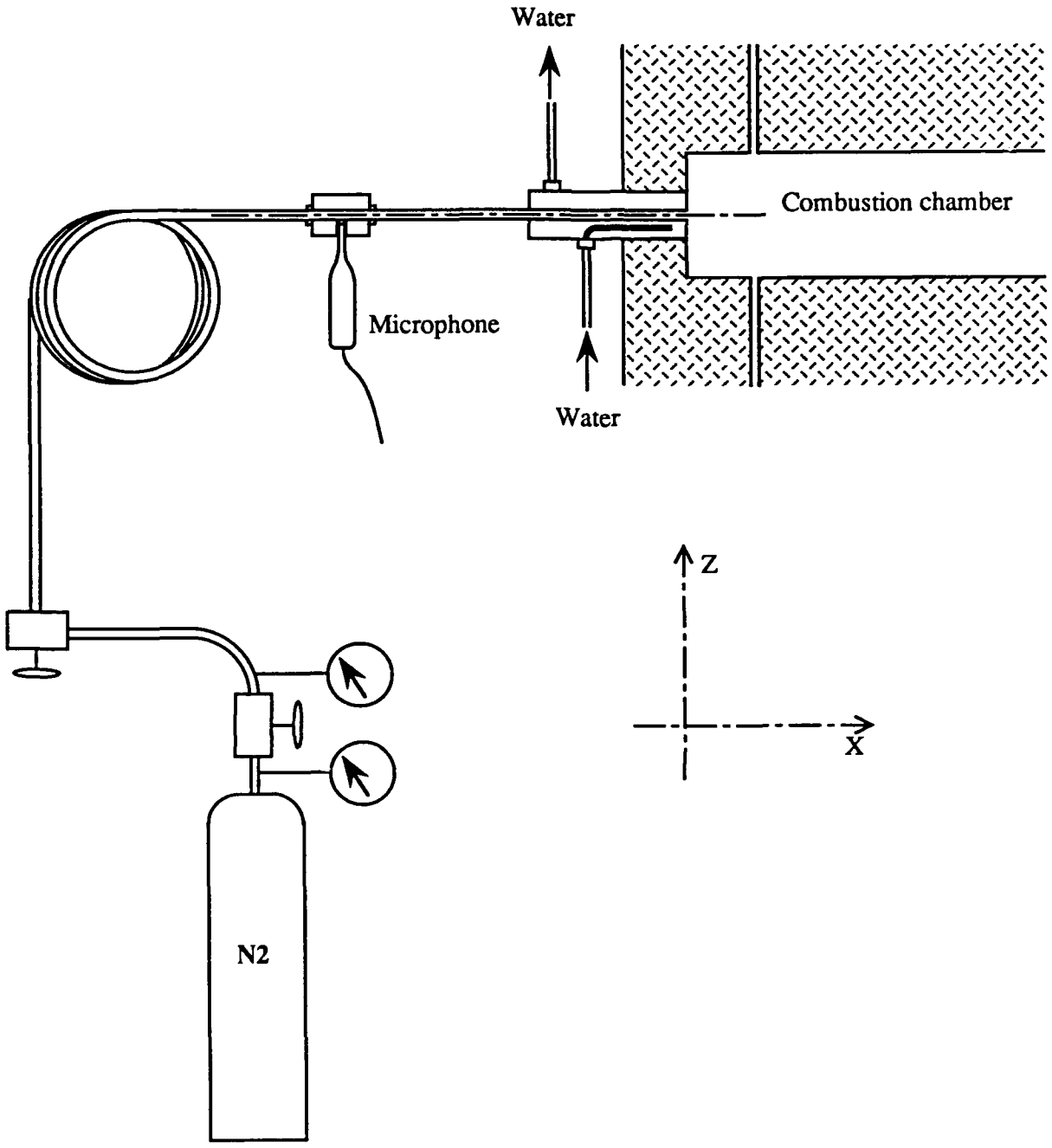

Figure 3: Detail of the waveguide used for pressure oscillations measurements on the dome wall of the combustion chamber.

a)

b)

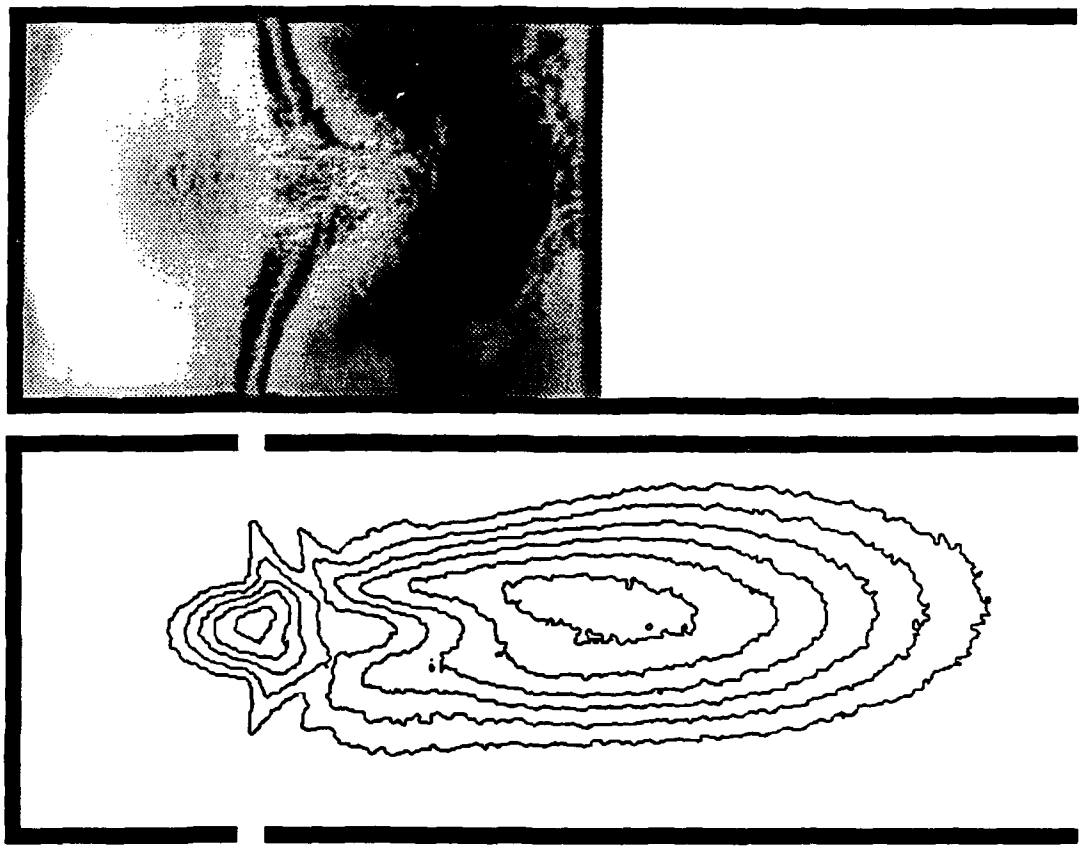

Figure 4: Stable combustion. a) Schlieren photograph, b) CH time-averaged image.

a)

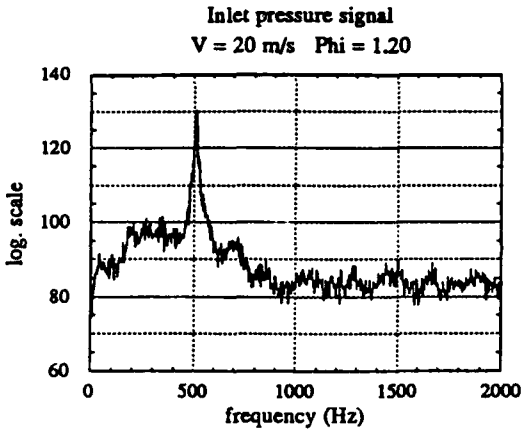

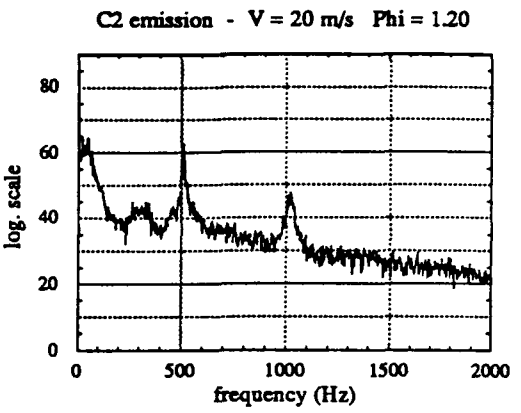

b)

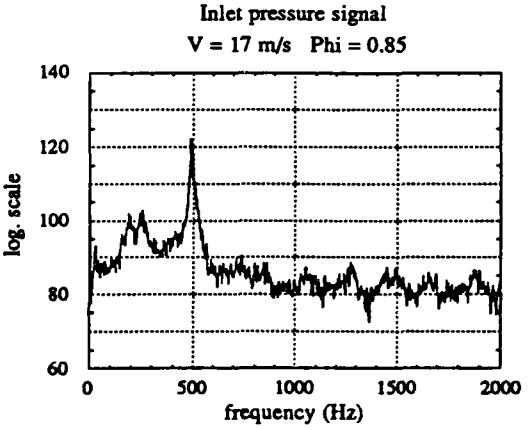

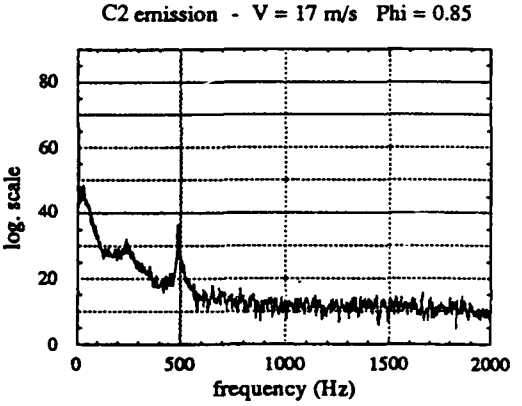

c)

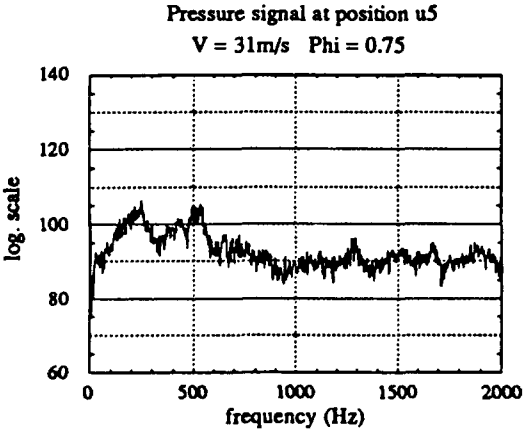

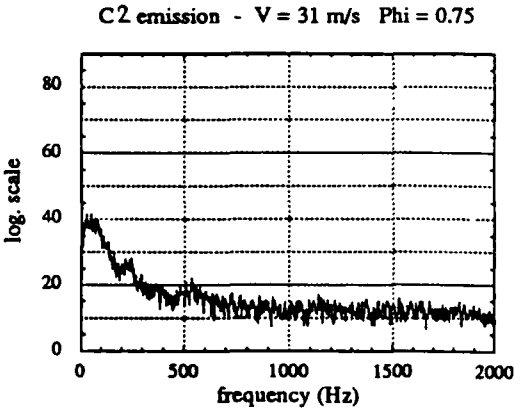

Figure 5: Power spectrum estimates of a microphone signal and the photomultiplier signal for three different operating conditions. a) $V = 20\ m/s$ and $\phi = 1.20$, b) $V = 17\ m/s$ and $\phi = 0.85$, c) $V = 31 m/s$ and ϕ=0.75. The microphone was located on the upper inlet at 56 cm from the dump plane.

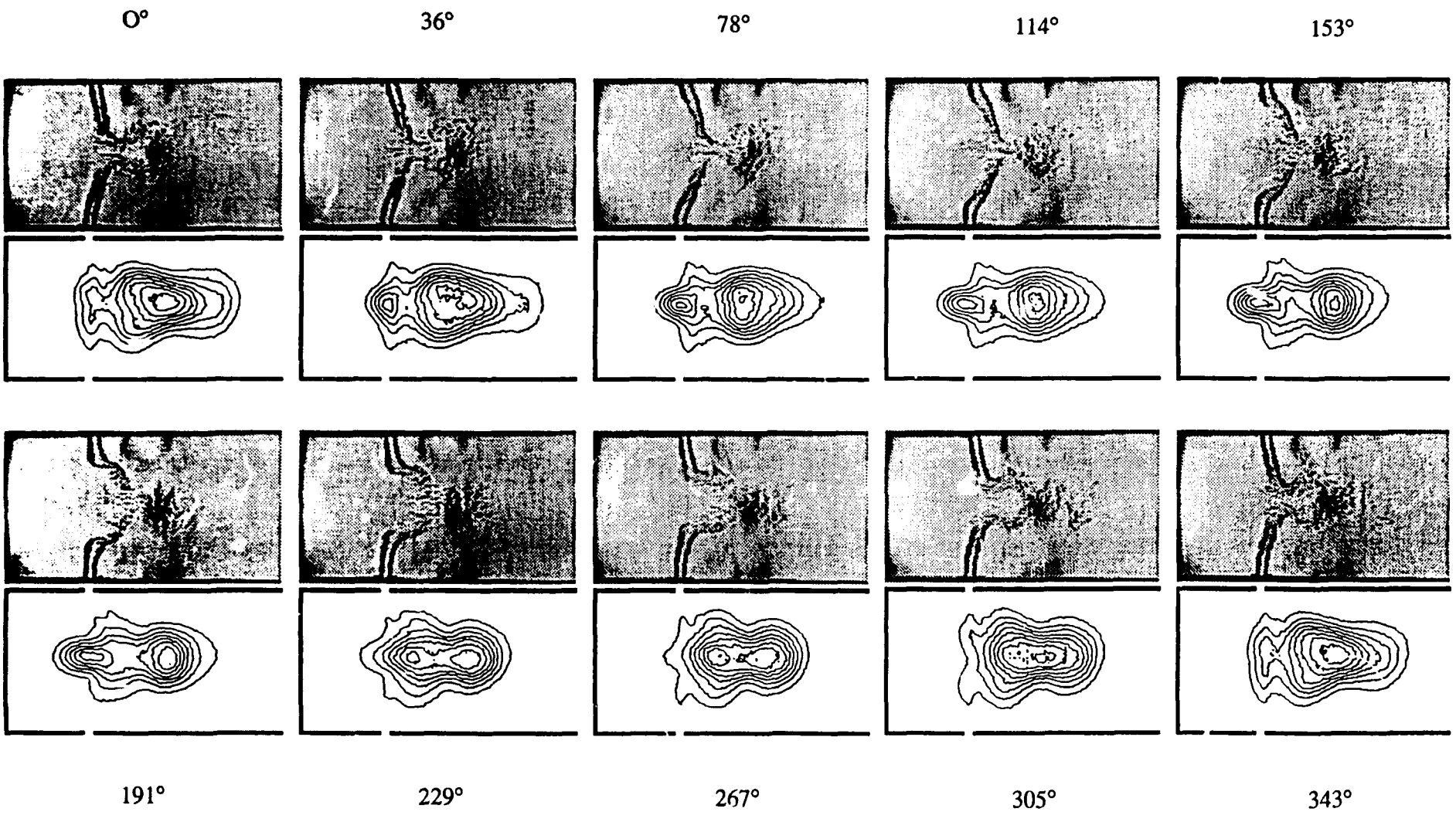

Figure 6: Sequence of Schlieren pictures taken from a high-speed film, with corresponding C_2 phase-averaged images. The phase angles are relative to the maximum pressure and heat release fluctuations. Pressure in the combustion chamber and heat release fluctuations are in phase.

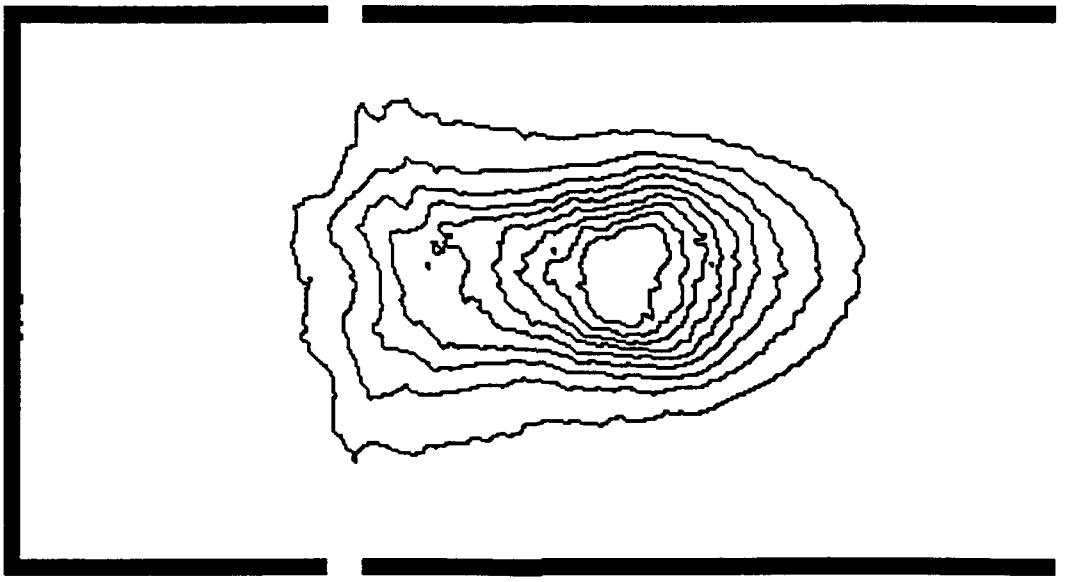

Figure 7: Spatial distribution of the local minimum heat release (or background of C_2 images of Fig. 6).

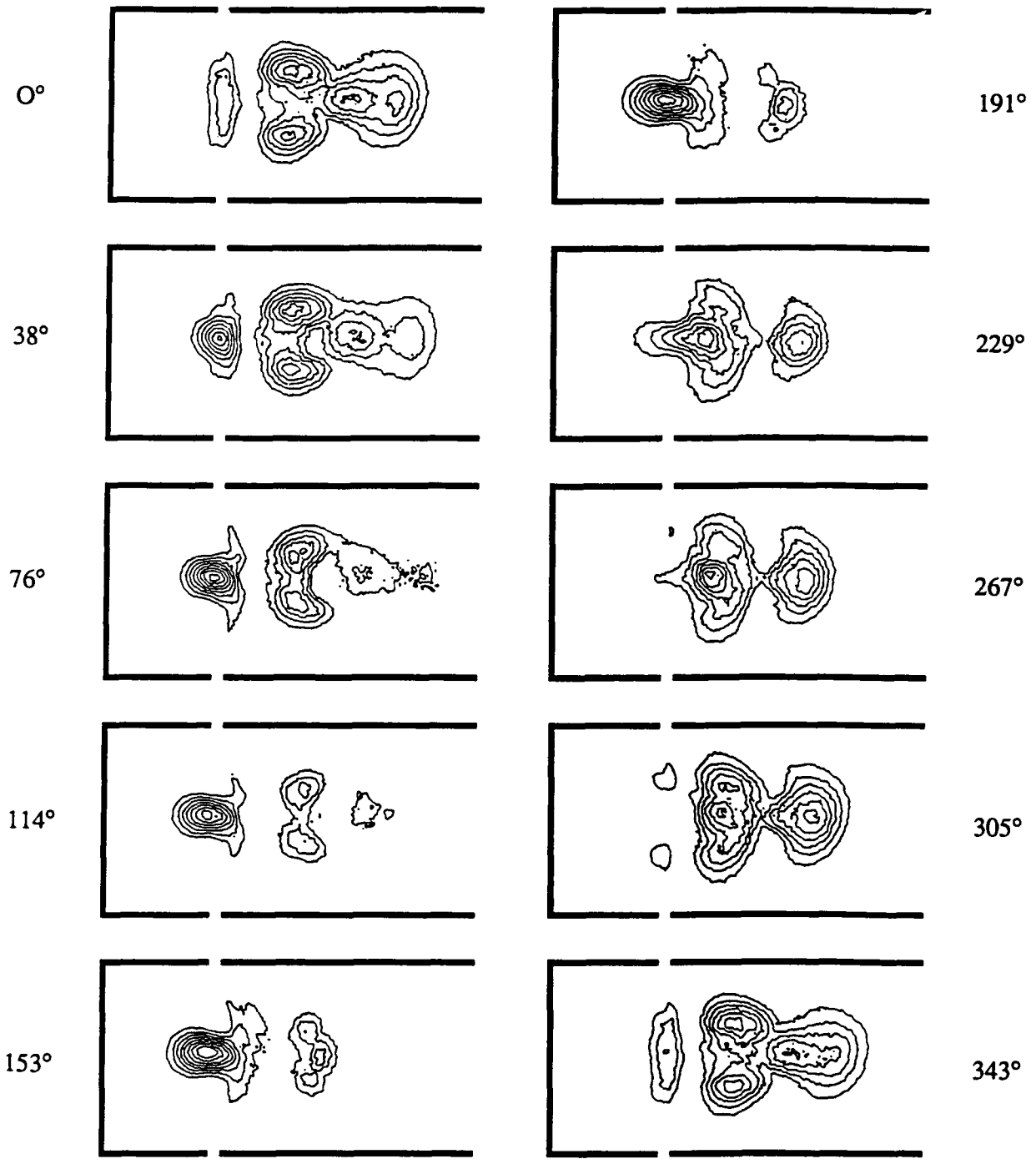

Figure 8: Sequence of images representing the excess of heat release, defined as the difference between the phase-averaged images with the spatial distribution of the local minimum heat release.

a)

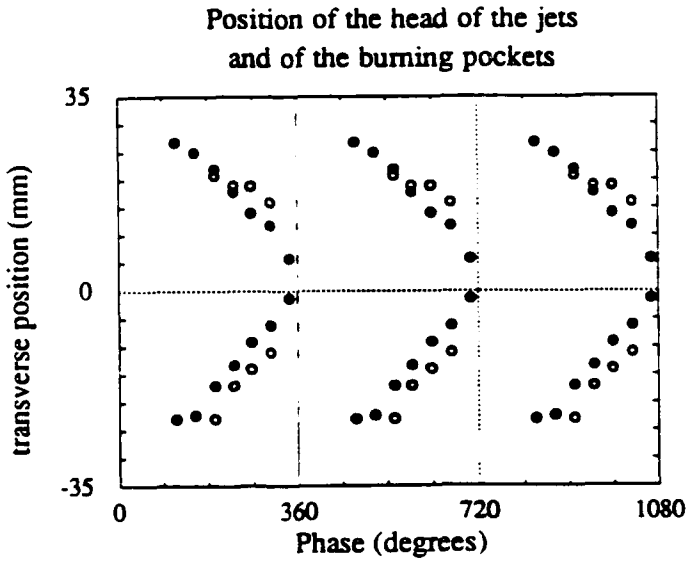

b)

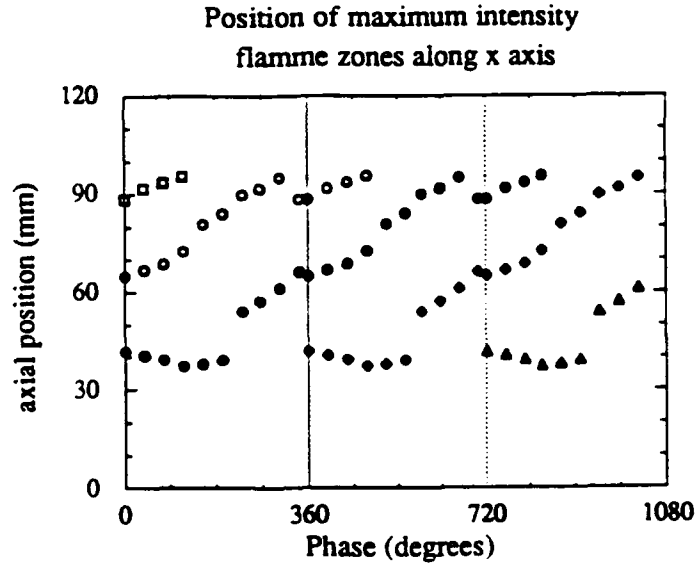

Figure 9: Axial and transverse positions of the reactions zones over three instability cycles. a) Transverse position of the reacting pockets (circles) and of the elbows of the jets (dots) along the inlet axis (vertical axis), as deduced from Fig. 8 and Fig.6. b) Axial positions of the reaction zones along the central axis of the combustor (horizontal axis), as deduced from Fig. 8.

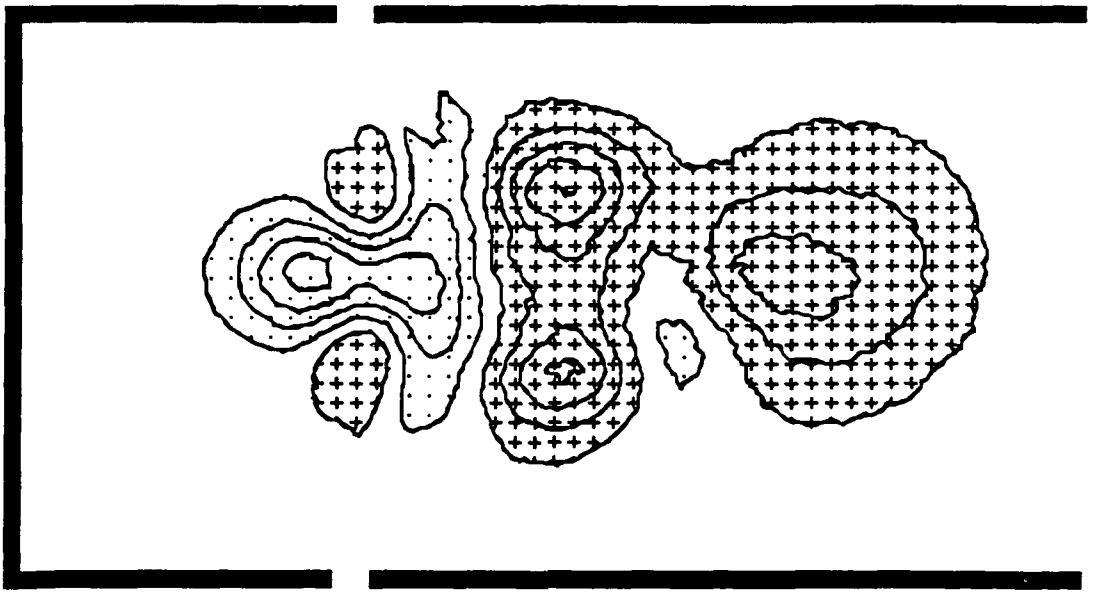

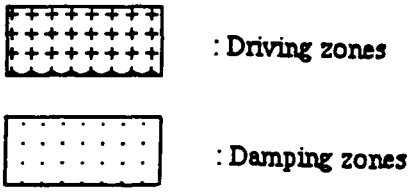

Figure 10: Spatial distribution of the local Rayleigh index.

Discussion

Question from M. PHILPOT, DRA, UK

Is the combustion instability problem sensitive to axial position of air inlets ports ?

Flow visualisations suggested an impedance mismatch at the air injection plane, so that the lean burn instability appeared to be forming its own local oscillation in the dome. If the air entered at the dome would this part of the phenomenom not be present ?

Author's reply

The instability is sensitive to the axial position of the inlet ports. In fact, geometrical parameters such as the lenght of the chamber, the width of the channel and the jet orientation also influence the mode selection process. Preliminary experiments carried on smaller scale combustors (one experiment was even conducted on a side dump burner having the size of a matchbox) indicated that the pattern of energy release strongly depends on the geometry. When the size of the dome is reducted to a certain point, it becomes difficult to reach a stabilized regime of combustion. At least, this is what we have observed when the model is fed with a mixture of air and propane at room temperature. However, combustion is more aesily stabilized even with a small dome if the reactant stream temperature is much higher as is the case in real devices. Experiments with a warm stream of reactants have not been carried-out in our laboratory.

Concerning the impedance behaviour invoked in the question, it is not easy to give a definite answer because we have no measurments of the velocity. It is true however that in the lean instability mode the fluctuations in the dome seem to be isolated from those taking place in the main combustion region located downstrem of the jet impingement point.

Question from M. VALAZZA

You showed combustion instabilities at medium frequency related with air inlets. Live tests show that in every case, there are combustion instabilities at high frequency. How do you explain this phenomenom ?

Author's reply

It very difficult to transpose tests at small scale to live tests besause of differences in functionning parameters, geometry and usable energy. Interaction with lateral flows is also different. However mechanisms of combustion instabilities that appear in our tests can also appear at higher frequencies when coupled with tangent modes. Other tests have to be performed in cylindrical geometry to see how flow and combustion combine to generate combustion instabilities. Numerical simulations can also be used.

EXPERIMENTAL ANALYSIS OF COMBUSTION OSCILLATIONS WITH REFERENCE TO RAMJET PROPULSION

by

M.N.R. Nina and **G.P.A. Pita**
Department of Mechanical Engineering
Instituto Superior Técnico
Avenida Rouisco Pais
1096 Lisbon, Portugal

1. ABSTRACT

The influences of flow rate, fuel air ratio and bluff body geometry on the predominant frequencies of combustion-driven oscillations were measured in a tube and disc combustor.

Small shifts in major frequencies were observed for different stabilizer geometries. By changing mass flow rate and at high velocities by changing the F/A ratio, discrete jumps in the frequency of large amplitude oscillations were produced in some of the configurations.

Measurements of the wall pressure oscillations amplitude along the cold duct, upstream from the flameholder confirm the presence of an acoustic three quarter wave. Changes in the cold duct length implies a difference in the main frequency of the pressure oscillations spectrum that was found to agree with the difference between two acoustic 3/4 waves corresponding to the two tube lengths.

2. NOMENCLATURE

ϕ - Equivalence Ratio
u - Mean Axial Velocity in the Flame Holder Inlet Plane
f - Frequency
l - Cold Duct Length
F/A - Fuel to Air Ratio
d - Flame Holder Diameter

3. INTRODUCTION

Combustion instabilities are present in every combustion chamber but the ramjet engine and the gas turbine engine afterburner are the two most well known examples: low frequency oscillations induce structural vibrations in the engine and the feeding lines leading to material and operational problems.

The unstable mode affects the blow off limits, the combustion efficiency and greatly enhances heat transfer rates on the combustion chamber surfaces. These problems have been extensively addressed in the past both from experimental and theoretical approaches.

The complex phenomena that are present in oscillating combustion have so far prevented the attainment of complete physical understanding.

The purpose of this paper is to examine some aspects of the interaction between fluid dynamics and acoustic instabilities and in particular to quantify the effects on amplitude and identify certain conditions of the onset of combustion oscillations in a tube and disc burner.

4. EXPERIMENTAL APPARATUS

Fig.1 shows the combustion rig located at IST, Lisbon, Portugal. It is constructed of stainless steel tube of 72 mm I.D. with a variable length. The fixed portion in the present test section is 695 mm long attached to a 600 mm or 1000 mm long combustor exhaust. At the inlet to the cold tube screens and honeycomb are installed to straighten the flow coming from the air supply through a tube 1805 mm long. The fuel, propane, is injected normal to the flow at a distance of 200 mm from the inlet through a 7 mm diameter tube, through 5 holes, into the upstream direction to ensure good mixing. The working section has to two sets of access ports, with a pitch of 50 mm. The ports can be used for pressure measurements, ionization probes, and thermocouples. It is also equipped with three quartz windows which give optical access to the flame downstream of the flame stabilizer. A fourth window is used to support the ignition spark plug and the radial traversing mechanism.

Fig.2 depicts the general scheme of the rig. Air is supplied by high pressure centrifugal fan through two Rottameters (R1,R2) with maximum flow rate of 80 gram/sec and one

Rottameter (R3) with a maximum capacity of 4 gram/sec. The fuel is supplied from eight propane bottles, 45 Kg each. The fuel Rottameters (R4,R5) have a maximum capacity of 4 gram/sec and 0.6 gram/sec, respectively. The maximum power output in the combustion chamber is in the range 40 to 100 kW. Ignition is obtained by a spark plug operated manually by switch (I2).

The flame stabilizers were supported in the center of the duct by four 2 mm diameter rods which extended from an external ring support , Fig.3. The ring had an outer diameter slightly less than 72mm to fit inside the combustor tube. It had a tapered cross-section with a maximum thickness of 3mm to minimized disturbance to the flow. All the flame holders had a diameter of 40 mm with a blockage ratio of 39% including the support, except flame holder H, a disc with 32mm diameter.

The stabilizer can be located in any position along the combustor. In the present tests, the stabilizer was mounted at 360 mm or 760 mm from the combustor exit, with the upstream length constant (l= 2740 mm).

Table 1 describes the flame holder configurations tested. The different geometries are shown in Fig.4. The disc flame holder (A) was 5mm thick. Configuration B had a circular cross-section in the upstream side and a corrugated star-shaped base in the downstream side, with eight fold symmetry. The inner diameter was 20 mm and the stabilizer length 20 mm. Configuration C had an equal geometry but the circular cross-section was in the downstream side and the star-shaped base in the upstream side. Configurations D and E were identical to configurations B an C respectively except for the length that was double (40 mm). Configuration F was a "cone" with the base facing upstream, the cone had steps in the external and in the internal surface. Configuration G was geometrically identical to configuration F but the "cone" base was pointing downstream. Configuration H was a disc with a 32mm diameter.

Configuration code	Flame holder geometry	Center ventilation Open	Closed
A	Disc	--	A2
B	Short Star facing Downstream	B1	B2
C	Short Star facing Upstream	C1	C2
D	Long Star facing Downstream	D1	D2
E	Long Star facing Upstream	E1	E2
F	Stepped Cone, base facing Upstream	F1	F2
G	Stepped Cone, base facing Downstream	G1	G2
H	Disc (diameter =32mm)	--	H2

To measure static pressure fluctuations a Kistler pressure transducer Model 211B5 was used, with an amplifier Model 5108. The maximum frequency response was 5 kHz. The measurements were performed upstream of the stabilizer in the cold pipe.

A data acquisition system was used, Data Translation Model 2824-PGL analog to digital converter with a maximum sampling rate of 50 000 sample per second, DMA and 12 bit resolution. A sampling rate of 5000 sample per second was used in most of the pressure measurements.

The data was processed in an IBM-PC, AT microcomputer.

5. RESULTS AND DISCUSSION

5.1 Measurements along the cold tube, upstream from the flame holder.

In order to detect the presence of a standing longitudinal wave in the cold duct, upstream from the flame holder, axial measurements of the wall static pressure oscillations along the duct were made with two different flame holders, B2 and H. With flame holder H two values of the equivalence ratio were tested: $\phi = 1$ and $\phi = 1.2$.

Fig.5 shows the variation of the wall pressure oscillations amplitude at the spectrum main frequency along the cold duct. The presence of the second harmonic of an acoustic quarter wave frequency (three-quarter wave) in the duct is detected in all tested cases. The spectrum main frequency measured was around 104 Hz. This value agrees with the

wave length of the measured standing wave.

The wave amplitude changes with the flame holder geometry and with the F/A ratio as it has been shown in Gutmark et all (1990). At each wall pressure trap the amplitude of the pressure oscillations depends from the flame holder, the axial velocity and the equivalence ratio.

5.2 Influence of the upstream duct length

In order to study the influence of the cold duct length in the frequency spectrum of the wall static pressure oscillations, a 430mm tube was attached upstream from the flame holder to the existing 2740mm tube, making the new cold duct 3170mm long.

Measurements with both tube lengths were made at a pressure tap located 360mm upstream from the flame holder with two different axial velocities, u=5m/s and u=15m/s. The velocities referred along this paper are mean velocities in the inlet plane of the flame holder. The flame holder used in this set of experiments was the smaller disc (flame holder H, D=32mm).

It was noted that, in order to compare these two cases, and as it will be shown later, for each duct length the main frequency changes with axial velocity, with fuel/air ratio and with the presence or the absence of noise (rough combustion).

Fig.6 plots the main frequency of the wall pressure oscillations spectrum and its respective amplitude measured with the two cold duct lengths. There was a decrease in the main frequency value with the increase in velocity in both cases and also a decrease in the frequency when the cold duct increases, as it was expected. The amplitude decreases with the increase in velocity, but there was an increase in amplitude with the cold duct length.

Fig.6 also shows that the main frequency detected in the pressure oscillations, at u=5m/s, was f=106Hz for a cold tube length of 2740mm, and f=89Hz for a tube length of 3170m, equivalence ratio $\phi=1.22$ and $\phi=1.32$. This difference in frequency corresponds to the difference between two 3/4 standing waves existing in the two tubes.

The pressure oscillations amplitude in both cases was high, corresponding to the production of intense noise (rough combustion).

For this velocity (u=5m/s), the two cases had low pressure oscillations amplitude (25-29 Pascal) and the main frequency was respectively 96Hz and 84 Hz, difference that also agrees with the difference between two acoustic waves corresponding to the two tube lengths.

For an axial velocity of u=15m/s the only two cases that are comparable are for $\phi=1.02$ where the amplitude is of the same order of magnitude. The corresponding frequencies are 89Hz and 80Hz, difference that also agrees with the difference between the two tube lengths.

For $\phi=1.15$ and $\phi=1.29$, u=15m/s, and the shorter cold tube, the pressure oscillations amplitudes are much smaller than with the longer cold tube, the difference between the two main frequencies in this situation does not agree with the difference between the two tube lengths. This corresponds to different interactions of the periodic heat release with the acoustic wave, along with Rayleigh criterion.

5.3 Influence of the combustion chamber length.

To study the influence of the combustion chamber hot length in the predominant frequency of the pressure oscillations, a 400mm tube was attached to the end of the previous combustion chamber, the total hot length becoming 760mm.

Tests were performed with the different flame holders, but the pressure oscillations in some conditions were so intense that it was not feasible to carry on with the experiments.

Only with flame holder C2 (short star facing upstream) we were able to get a full set of measurements. Fig. 7 shows for a constant equivalence ratio $\phi=1$, the change of the predominant frequency with the axial velocity. An increase in the predominant frequency with the increase of axial velocity is observed.

With the increase in the velocity the amplitude of the main frequency (around 108HZ) decreases and new frequencies arise in the spectrum at f=145Hz and for the higher velocity(u=16.45m/s) at f=233 Hz.

The same behavior can be observed in Fig.8 where for a constant velocity u=16.45m/s, the equivalence ratio changes. For lean or rich mixtures the predominant frequency is around 109Hz, increasing slightly this value as we approached stoichiometry. Near the stoichiometric mixtures the amplitude at this frequency decreases and a new frequency becomes predominant (f=240 Hz). In Fig.9 it can bee observed that for a lower velocity (u=8.22m/s) the pressure oscillations spectrum changes also with the equivalence ratio, but at this velocity the jump in frequency for $\phi=1$ did not occur as for the higher velocity. A decrease in the amplitude at 109Hz was noted, and new frequencies appeared in the spectrum but the 109Hz was still predominant.

Therefore it could be concluded that an increase in the main frequency was related to the increase in power release in the combustion chamber.

With a smaller combustion chamber, and with the same flame holder, Fig.10 shows the spectrum changes with the

axial velocity at a constant equivalence ratio $\phi = 1$.

At low velocities the predominant frequency was still between 103-107Hz, but increasing the velocity the amplitude of the main frequency decreases and at very high velocities (u = 13.16m/s) the spectrum does not present any predominant frequency.

Fig. 11 shows the main frequencies and its respective amplitudes measured with flame holder A2 (disc d=40mm) at a constant equivalence ratio $\phi = 1$, and different axial velocities.

At low velocities there was a jump in the main frequency of the pressure oscillations between 108 and 103 Hz corresponding to a high or low value of the amplitude (presence or absence of noise(rough combustion)).

Increasing the velocity the main frequency detected was around 103Hz and did not depend on the pressure oscillations amplitude.

The frequency jumps measured with changes in the axial velocity , using flame holder C2, have been observed for the other flame holders with the shorter combustion chamber.

5.4 Influence of combustion chamber wall temperature. It was noted that for a short time after start up, i.e., in the first minutes of the tests when the flame holder and the combustion chamber wall were still cold, no rough combustion was observed. Only after several minutes, when wall temperature was higher, rough combustion was detected. No measurements of wall temperatures were performed.

Fig.12 shows the wall pressure oscillation spectrum measured with flamehoder H (disc d=32mm), just after ignition (case a) and after 10 minutes of operation (case b): A shift in the predominant frequency from 98Hz to 107Hz and a 4 time increase in amplitude were observed. The difference in amplitude is such that in the cold condition the sound intensity is low and no rough combustion is detected.

6. CONCLUSIONS

The presence of a standing wave has been detected in the cold tube corresponding to a 3/4 acoustic wave with a pressure node near the flame holder.

A change in the cold tube length origins a shift in the main frequency of the pressure oscillations that agrees with a change in the identified 3/4 standing wave inside the tube. This agreement happens only for conditions when the pressure oscillations amplitude are of the same order of magnitude.

The main frequencies of the pressure oscillations detected in the spectrum can change due to:

- for lower velocities, with fuel/air ratio near stoichiometry, the main frequency had a slight shift (103Hz to 109Hz) but the amplitude increased drastically (corresponding to a large increase in noise production).

- for higher velocities, the same behavior of the frequency and its amplitude was observed, but near stoichiometry, a jump in the main frequency to a higher harmonic was observed, accompanied by a decrease in amplitude.

It has also been detected that the influence of the combustion chamber hot length was important, because in this situation if the combustion chamber is short, part of the flame outcomes from the combustion chamber with an important part of the heat release happening outside the combustion chamber. This induced a diminishing of the amplitude of the pressure oscillations and in some cases to the total absence of a predominant frequency in the pressure oscillations spectrum was observed.

This set of results showed an interaction between the heat release rate inside the combustion chamber and the amplitude and frequency of the pressure oscillations in the cold tube.

7. ACKNOWLEDGEMENTS

The authors would like to acknowledge the assistance of Mr. Amandio Ginga in performing part of the measurements.

The support of AGARD through Project P-55 is gratefully acknowledged.

8. REFERENCES

1. P.A. Libby, S. Sivasegaram and J.H. Whitelaw. "*Premixed Combustion*," Prog. Energy Combustion Science, Vol.12, pp.393-405, 1986.

2. M.V. Heitor, A.M.K.P. Taylor and J.H. Whitelaw. "*The Interaction of Turbulence and Pressure Gradients in a Baffle-Stabilized Premixed Flame*," Journal of Fluid Mechanics, Vol.181, pp.387-413, 1987.

3. G.P.A. Pita. "*Técnicas Experimentais em Escoamentos com e sem Combustão*," Ph.D. Thesis, Instituto Superior Técnico, Lisbon, Portugal, 1987.

4. K.C. Schadow, E. Gutmark and K.J. Wilson. "*Characterization of Large-Scale Structures in a Forced*

Ducted Flow with Dump," AIAA Journal, Vol.25, N·9, pp.1164-1170, September 1987.

5. K.C. Schadow, E. Gutmark, D.M.Parr, and V.A. Mahan. "*Effect of Shear Flow Dynamics in Combustion Processes,*" Journal of Combustion Science and Technology, Vol.54, pp.103-116, 1987.

6. K.C. Schadow, E. Gutmark, T.P. Parr, D.M. Parr, K.J. Wilson and J.E. Crump. "*Large Scale Coherent Structures As Drivers of Combustion Instability,*" Combustion Science and Technology, Vol.64, 4-6, pp.167, 1989.

7. E. Gutmark and K.C. Schadow. "*Flow Characteristics of Orifice and Tapered Jets,*"Physics of Fluids, Vol.30, pp.3448-3454, November 1987.

8. K.C. Schadow, E. Gutmark, T.P. Parr, D.M. Parr and K.J. Wilson. "*Combustion Enhancement by Axial Vortices,*" Accepted for Publication in Journal of Propulsion and Power, 1988.

9. M.N.R. Nina and G.P. Pita. "*Measurements of Fluctuating Gas Temperatures Using Compensated Fine Wire Thermocouples,*" AGARD Conf., Heat Transfer and Cooling in Gas Turbines, Conf. Proc.N·390, May 1985, Norway.

10. E.Gutmark, K.C.Schadow, M.N.R.Nina and G.P.A.Pita. "*Suppression of "Buzz" Instability by Geometrical design of the Flame holder*", 26th Joint Propulsion Conference, Orlando, 16-18 July 1990, AIAA paper N. 90-1966 (submited for publication in the J.Propulsion and Power).

11. E. Gutmark, K.C.Schadow, S.Sivasegaram and J.H.Whitelaw "*Interaction Between Fluid-Dynamic and Acoustic Instabilities in Combusing Flows within Ducts*" Combust. Sci. and Techn., 1991, Vol.79, pp.161-166

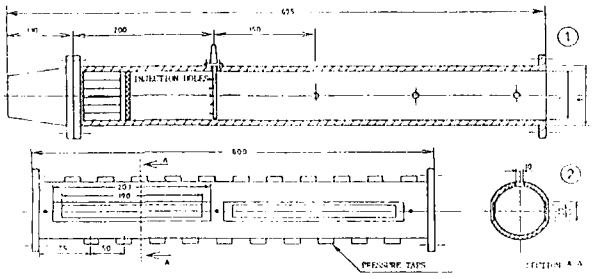

Fig. 1 - Combustion Rig

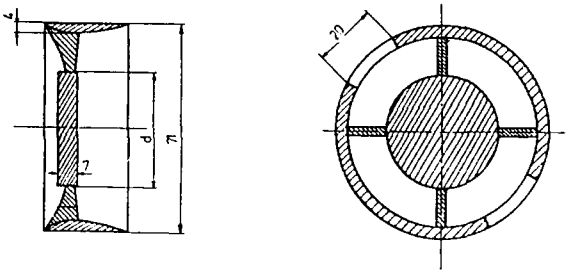

Fig. 3 - Flame Stabilizers Support

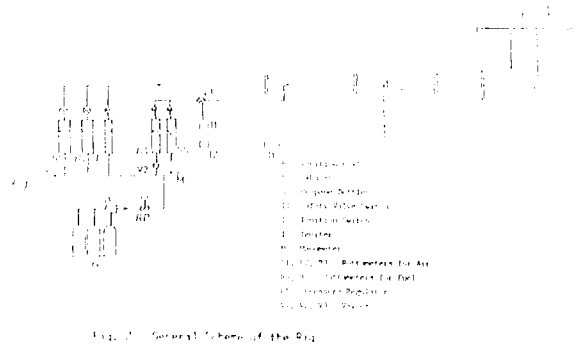

Fig. 2 - General Scheme of the Rig

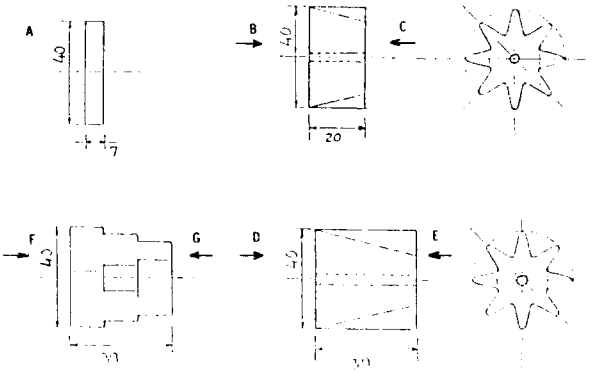

Fig. 4 - Flameholder configurations

→ Flow direction

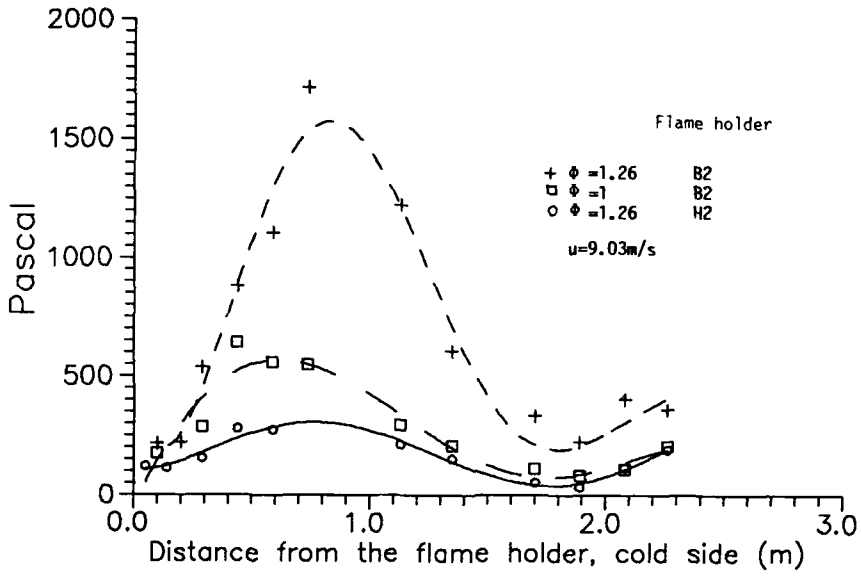

Fig.5 Pressure oscillations amplitude at the spectrum main frequency along the cold duct, upstream from the flame holder.

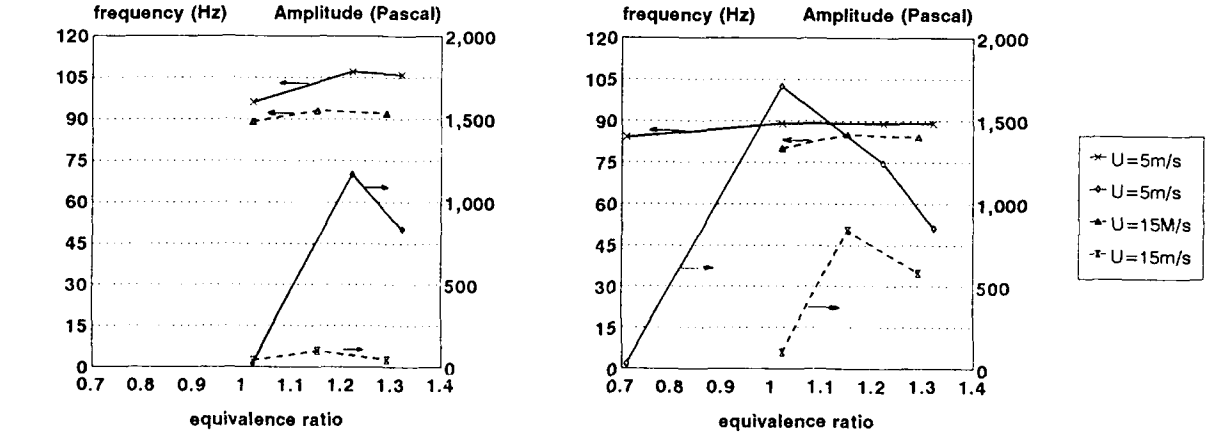

Fig. 6 Variation of the pressure oscillations main frequency and its amplitude with the F/A ratio for two cold duct lengths and two different axial velocities. Flame holder H.

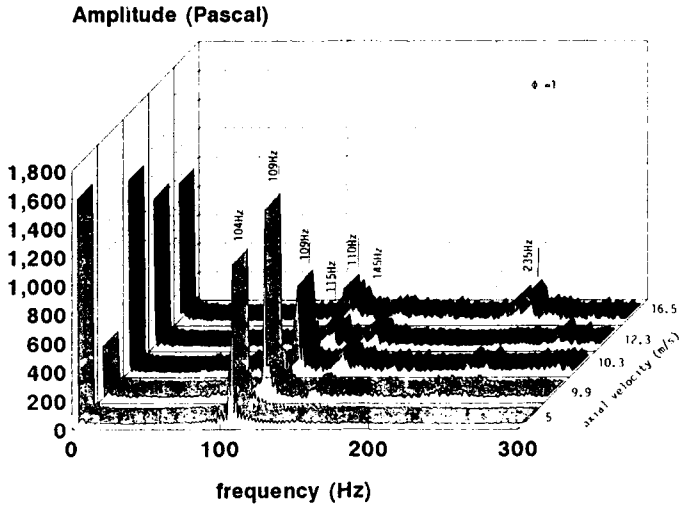

Fig.7 Variation of the wall pressure oscillations spectrum with the axial velocity, for a long combustion chamber (l=760mm) and constant F/A ratio.

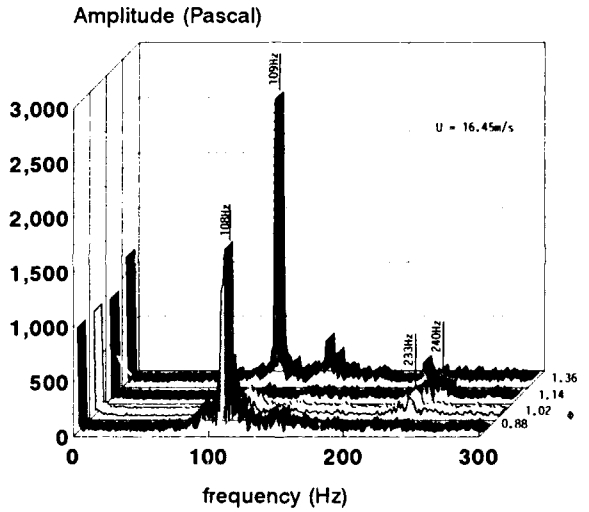

Fig.8 Variation of the wall pressure oscillations spectrum with the F/A ratio at constant axial velocity. Long combustion chamber (l=760mm) and constant axial velocity (u=16.45m/s)

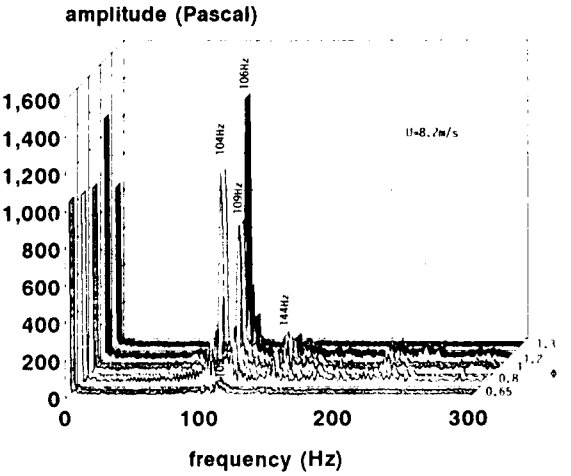

Fig.9 Variation of the wall pressure oscillations spectrum with the F/A ratio at constant axial velocity. Long combustion chamber (l=760mm) and constant axial velocity (u=8.22m/s)

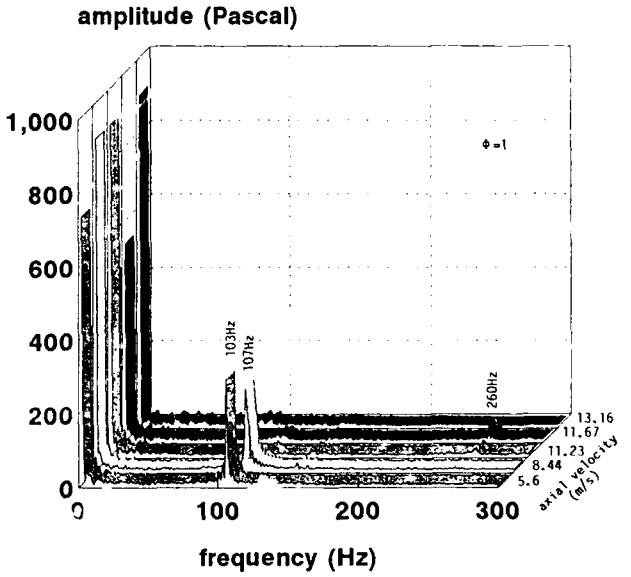

Fig.10 Variation of the wall pressure oscillations spectrum with the axial velocity, for a short combustion chamber (l=360mm) and constant F/A ratio.

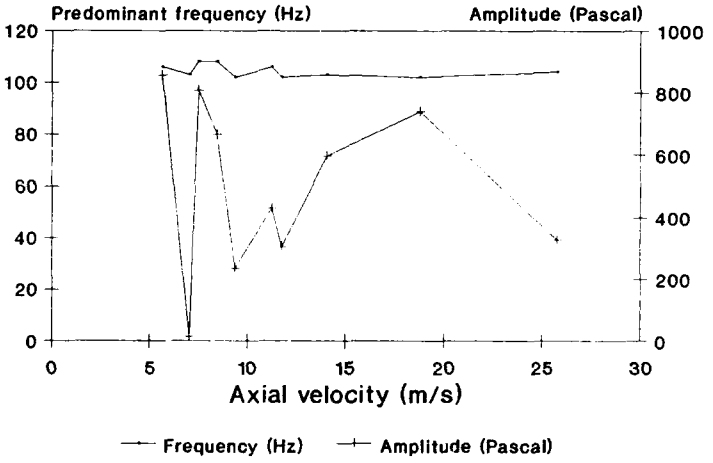

Fig.11 Predominant frequency and its respective amplitude for different axial velocities, at a constant equivalence ratio =1. Flame holder H and short combustion chamber (l=360mm).

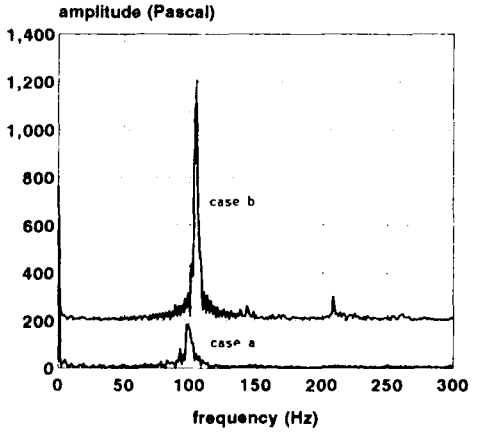

Fig.12 Pressure oscillations spectra just after ignition (case a) and after several minutes of operation (case b). (Amplitude scale of case b was offset by 200 Pa)

Ramjet Propulsion for Advanced Projectiles

R. Mönig, M. Moll
Rheinmetall GmbH
Ulmenstr. 125
D-4000 Düsseldorf
Germany

1. SUMMARY

The increasing effectiveness of future defense systems will lead to projectiles with extremely high impact energy, reduced flight times, and extended ranges.

With regard to these requirements gun launched projectiles using ramjet propulsion, show promising capabilities in weight, cost, and hit accuracy. If high maximum range and low crosswind sensitivity of projectiles is of primary interest, a compensation of drag can be obtained by ramjet propulsion at low fuel-to-air ratio. Moreover, with respect to applications against armored vehicles ramjet engines operating at nearly stochiometric conditions, can be even used to increase the kinetic energy of KE-rods.

The first part of the paper gives a survey on the main design objectives of ram-propulsion for projectile applications. A detailed theoretical analysis of advantages and limitations is presented for high performance ramjets. The second part deals with ramjet applications for artillery, air defense, and anti-armor weapons. Due to the high initial velocity provided by guns, ram-propulsion proves to be a very promising and efficient tool in order to meet the demands of future defense systems.

LIST OF SYMBOLS

c	velocity
h	enthalpy
M_0	freestream Mach number
κ	ratio of specific heats
η_{KI}	kinetic inlet efficiency
π_{tI}	inlet total pressure ratio

Subscripts

s	isentropic
t	total
0	freestream value
2	behind inlet

2. INTRODUCTION

Ramjet propulsion is limited to supersonic flight conditons in general. For ground-based missiles, this is a severe disadvantage in general. As a result, an additional accelerator engine (turbojet, turborocket, or rocket) is always required in order to pass the subsonic flight regime and to be able to use ram-propulsion at all. This does not hold for projectiles, however: supersonic velocities can be provided easily by the use of guns.

In general, projectiles show advantages in case where high hit accuracy combined with high impact energy is required at the target (KE-rods). Moreover, projectiles prove to be much more cost efficient than rockets.

The aerodynamic drag is always a problem for ballistically flying projectiles. This holds especially for artillery applications. In order to increase the effective ranges, base bleed units can be used generally. In this case, the base region is ventilated by a small amount of hot gas. This diminishment of drag results in an increase of range up to 25 per cent. This benefit, however, has to be payed for with a reduced payload.

The situation becomes even worse if the decrease in flight velocity shall be compensated by an additional rocket propulsion. This basically offers a post-acceleration capability (RAP projectile): however, the reduction of payload is not acceptable in most cases. The reason for this unsuitable behaviour is the poor specific impulse of rockets. Thus, from the very beginning, many investigations concentrated on the question how to increase the specific impulse of propulsion systems for gun fired projectiles.

An early answer was given by Trommsdorff (1936, published in /1/). He found that the performance of projectiles could be improved significantly, if a ramjet engine would replace the rocket motor. In this case the oxidizer has not to be carried within the propellant grain. Instead of this the oxidizer is simply taken from the ambient air. Subsequently, detailed theoretical and experimental investigations led to considerable improvements in the field of ramjet and ramrocket engines. (cf. f.ex. /2/, /3/).

At RHEINMETALL ramjet and ramrocket engines are being developed for already more than 20 years. A first operational ramjet projectile was designed for a freestream Mach number of 2. Investigation and development was continued for more than 10 years, starting in the early 1970's. Subsequent studies and investigations especially focused on the func-

tion and design of inlet and combustor components for a ramrocket projectile operating at Mach 5.0.

In the first part of the paper some basic considerations on ram-projectiles are given. Afterwards, three possible applications are discussed and compared to other possible solutions.

3. DESIGN CONSIDERATIONS ON RAM-PROJECTILES

Ramjet engines can be designed to meet the requirements of a wide range of operation tasks. Thus, the main engine components such as air intake, combustor and exit nozzle have to be designed with respect to these constraints and to the special problem of airframe - engine integration.

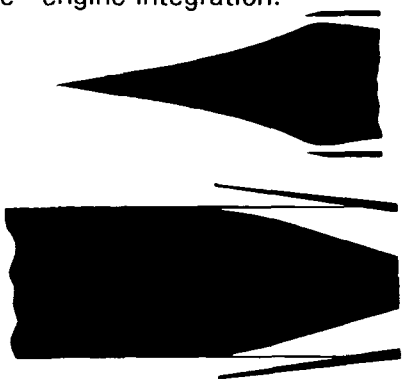

Fig. 1: Comparison of central and lateral air intake

With respect to the air intake it has to be decided whether a central or a lateral intake configuration is more convenient in a particular case (fig. 1). A lateral intake design allows seeker or warhead integration within the nose section. The total drag, however, is quite significant particularly at high supersonic velocities. Thus, a lateral intake is more advantageous for the lower supersonic Mach regime. For higher supersonic or even hypersonic operation a central inlet design offers the opportunity of a remarkable decrease in total drag.

Concerning the ramjet combustor, the solid propellant can be placed within the combustion chamber (ramjet, fig. 2a) or within a separate gas generator (ramrocket, fig. 2b). A combination of both concepts also is feasible (fig. 2c) and offers considerable advantages for certain applications.

The conventional ramjet burner yields the highest specific impulse due to the absence of any oxidizer within the propellant grain. Furthermore, it reveals certain advantages in operating behaviour if a variation of combustion pressure is expected to occur during the mission. In those cases the fuel massflow can be adapted to some degree to these varying conditions by means of a pressure dependent propellant burning rate. In any case, intake

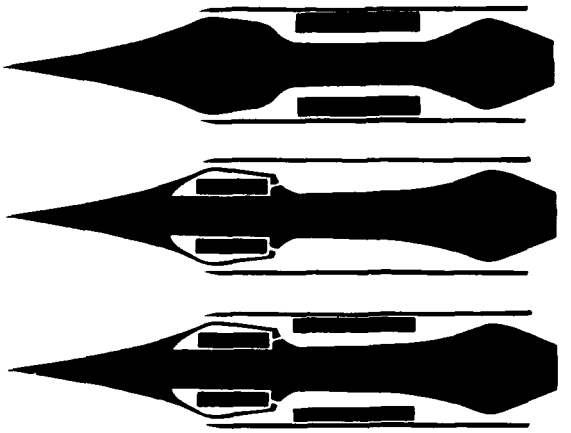

Fig. 2: Comparison of ramjet, ramrocket, and hybrid engine

operation has to be restricted to moderate angles of attack in order to avoid extinguishing of the combustor.

A separate high pressure gas generator, however, basically ensures a burner operation which is independent of flight conditions. Furthermore, the massflow of the gas generator can be adapted even to particular requirements by a particular geometry of the propellant. The available specific impulse, however, is lower than the values obtained for ramjets. Nevertheless, there are still remarkable improvements compared to solid propellant rockets.

For applications with both boost and sustainer operation, a combination of ramjet and ramrocket turns out to be most appropriate. During the boost phase gas generator and ramburner yield a high propellant massflow which leads to nearly stochiometric combustion and high total thrust. At cruise operation only the highly efficient ram-burner is in use. Thus both propellant massflow and thrust level are diminished in order to only compensate the total drag.

In order to determine the performance data of ram-engines, thermodynamical cycle computations have been carried out for the Mach number regime 2 to 7. With respect to a superior reliability, the calculations were primarily focused on ramrockets, utilizing a separate high pressure gas generator. A solid propellant with rather conventional fuel components was specified for the computations (heat of combustion = 17.49 kJ/g).

The calculations were performed with the efficiencies of air intake, combustion chamber and exhaust nozzle being estimated according to prior determined experimental data. The intake efficiency, in particular, strongly depends on flight velocity and flow deceleration. Consequently, this value has to be considered

as a function of freestream Mach number. For the deceleration to subsonic velocity it was assumed that the kinetic inlet efficiency is constant for the discussed Mach number range:

$$\eta_{KI}=\frac{h_{t2}-h_{s2}}{h_{t0}-h_0}=\frac{c_{s2}^2}{c_0^2}$$

In the above equation the subscript "s2" belongs to a fictitious station behind the inlet. The captured air flow is assumed to be again expanded to ambient pressure after passing the inlet.

The corresponding reccvery of total pressure can be derived as:

$$\pi_{tI}=[1-(\eta_{KI}-1)\frac{\kappa-1}{2}M_0^2]^{-\frac{\kappa}{\kappa-1}}$$

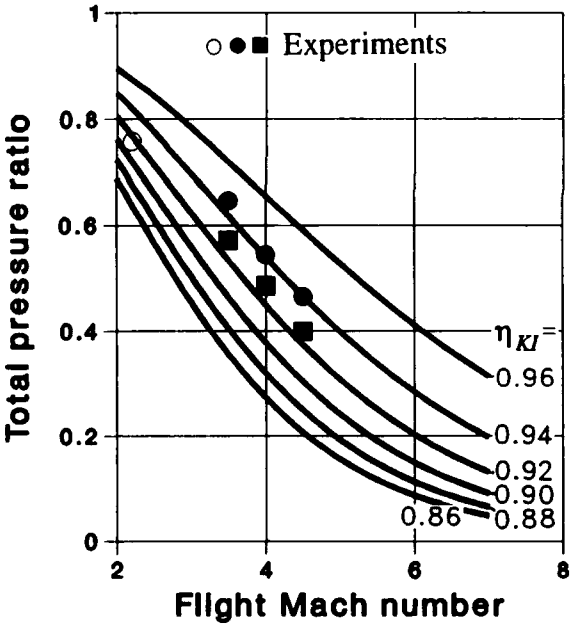

Fig. 3: Intake efficiency and total pressure recovery

The pressure recovery depending on flight Mach number and kinetic efficiency is shown in fig.3. Additionally, experimental data of different central air intakes developed in cooperation with DLR (/4/) are plotted within the same figure. The inlet efficiency of the different inlet designs showed values between 0.92 and 0.94. So for the performed cycle computations a kinetic intake efficiency of 0.92 was assumed for the entire Mach regime. Furthermore, the combustion was assumed to be 85 per cent efficient. In agreement with prior investigations the nozzle efficiency was specified to be 95 per cent.

The equivalence ratio was varied between 0.4 and 1.2. The subsequent calculations were carried out with the following assumptions:

- o flight at sea level
- o caliber 160 mm
- o central air intake
- o captured flow area equal to frontal area
- o burner exit area equal to projectile cross section
- o burner exit Mach number lower than 0.5
- o consideration of real gas and dissociation effects
- o meanline flow analysis

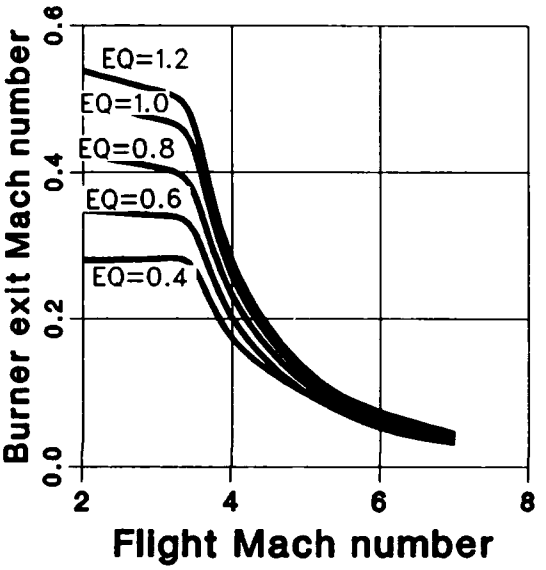

Fig. 4: Burner exit Mach number of ramrocket-projectiles

The performance prediction code is based on the fundamental works of several authors (/5/, /6/, /7/). Further extensions, particularly concerning internal iteration improvement and engine off-design performance have been included at RHEINMETALL.

The simulations show that the airflow has to be reduced below Mach 3.5 due to the Mach number limitation at the burner exit (fig. 4). At Mach 3 the area of captured airflow has to be reduced to approximately 70 percent of the burner area. At Mach 2 only 30 percent of the burner area are still permitted for the freestream area of captured flow. Thus, a lateral intake with low airflow capability is generally sufficient at low Mach operation if emphasis is put on cycle performance only.

Increasing the flight Mach number beyond 3.5 leads to distinctly decreasing burner exit Mach numbers. Thus, the burner area may be reduced for projectiles operating at high Mach numbers. With respect to the lower velocity

level within the combustion chamber the overall burner length may be reduced alternatively.

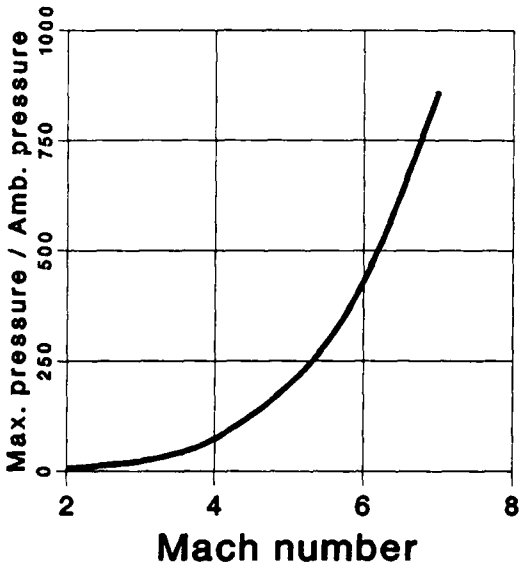

Fig. 5: Static pressure rise of ramrockets

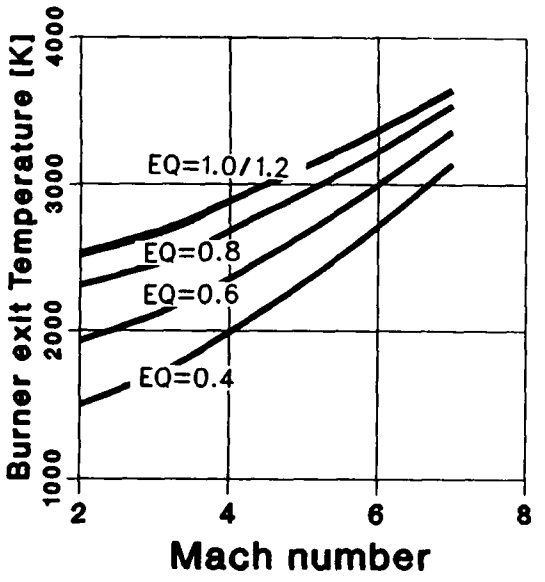

Fig. 6: Thermal loading of ramrockets

The development of pressure within the combustion chamber is shown in fig. 5. Due to the high dynamic pressure developing for hypersonic flight at sea level, comparatively high pressure values have to be taken into account for the interior flow. The static pressure of the burner increases to 200 bar at Mach 5. At Mach 6 the static pressure is doubled to more than 400 bar. For Mach 6.5 ram-operation nearly 650 bar of static pressure will develop within the combustion chamber. These values appear to be extremely high compared to missiles operating at hypersonic velocity and high altitude. However, the structural design of ram-projectiles is not at all affected by these pressure values. The reason is that for every projectile the structural integrity has to be ensured for gun firing. Pressure peaks in excess of 6000 bar lead to an initial acceleration of about 60000 g. Thus, the ram projectile has to be designed to withstand these extreme conditions without damage anyway.

A more serious problem is the thermal loading occuring at high Mach numbers and nearly stochiometric combustion (fig. 6). Burner exit temperatures exceed the 3000 K margin already at Mach 4.5 (equivalence ratio = 1). At Mach 6.5, the limit of 3500 K is reached. In spite of materials being resistant to extreme heat, operation at these conditions has to be restricted to much less than one second.

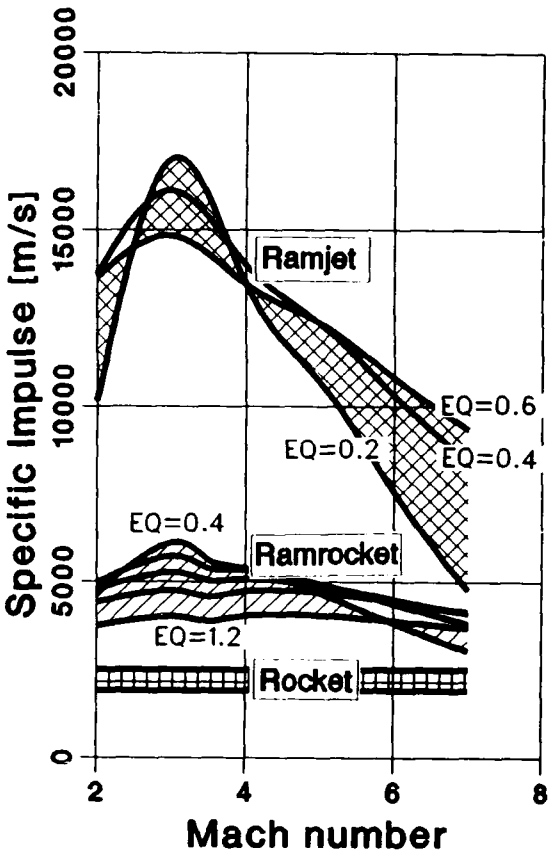

Fig. 7: Specific impulse of ramrockets

Combustion at lower fuel-to-air ratios appears to be uncritical up to Mach 5.5. For cruise at higher flight Mach numbers ram-operation must be restricted to equivalence ratios lower than 0.4 in order to avoid thermal overload. In any case, highly temperature resistant materials have to be used and ram operation is additionally limited to a few seconds only.

The development of specific impulse versus

Mach number is shown in Fig. 7 for ramjets, ramrockets and rockets, resp. The specific impulse of rockets is known to be always independent of flight velocity. The particular value depends on the performance of the propellant grain and nozzle design and is generally placed between 1900 m/s and 2500 m/s for state-of-the-art rocket motors.

The specific impulse of ramrockets is approximately twice as high for flight Mach numbers below 6. The most favorable operating range is found to occur for low fuel-to-air ratios in the vicinity of Mach 3. Beyond Mach 6 a decreasing value is observed, particularly for low fuel-to-air ratios. Generally, the specific impulse can be improved significantly if ramjet conceptions are used instead of ramrockets.

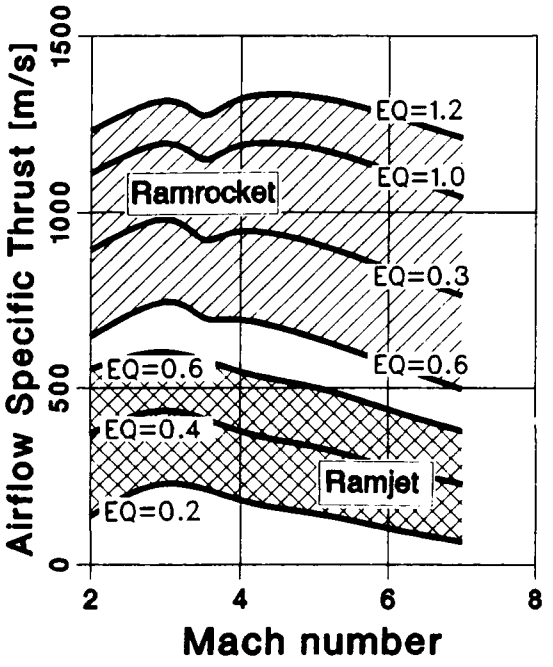

Fig. 8: Airflow specific thrust of ramrockets

The airflow specific thrust of ramjets, however, is fairly low for the entire operating range under discussion (fig. 8). The advantage of ramrockets becomes obvious in this context: high fuel-to-air ratios are basically possible in contrast to solid propellant ramjets, being generally limited to lower fuel-to-air ratios. Evidently, the available thrust of ramrockets is distinctly higher compared with ramjets.

4. APPLICATIONS

4.1 Extended range artillery shell

The design of a 155 mm artillery shell with ramjet propulsion is presented in fig. 9 (/8/). The projectile mainly consists of seeker, warhead, gas generator, lateral air intake, combustion chamber, nozzle and spreadable cone stabilizer.

Corresponding cycle computations were carried out in /9/ for several ramrocket/ramjet combinations, using a composite gas-generator propellant and a polyethylene (PE) ramjet propellant. The initial velocity was predicted to be 850 m/s at a total mass of 50 kg.

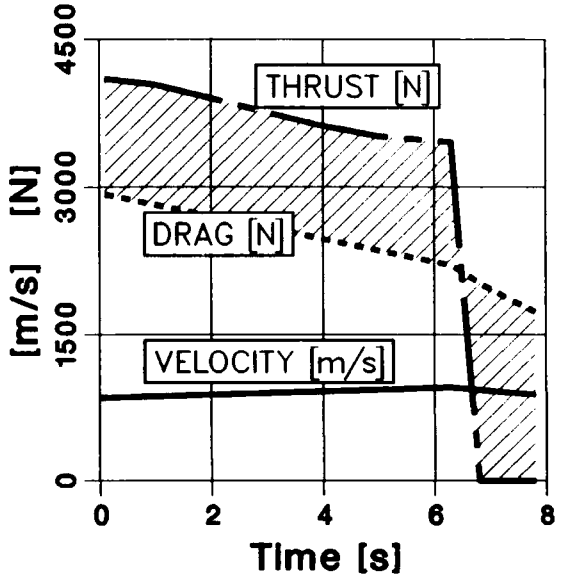

Fig. 10: Performance of medium-range artillery shell

It is evident from the above considerations that the most favorable engine for the discussed application is the ramjet engine. The high specific impulse of more than 12000 m/s is not reached by any of the other concepts. The thrust level, however, is fairly low due to the low burning rate of the PE-propellant. Furthermore, stable combustion is hard to achieve if high velocities and low inlet temperature have to be managed at the same time (/10/). Unfortunately, these conditions are very likely to occur at low flight Mach numbers.

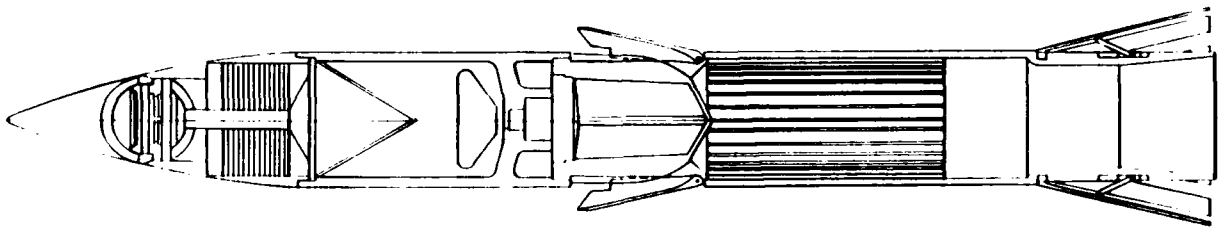

Fig. 9: RAM-propulsion artillery shell

The best results with regard to reliability and efficiency were obtained for a hybrid engine with 2/3 of the total fuel massflow delivered by a gas-generator. Thus, further investigations are focused on this concept.

The thrust-, drag-, and velocity-development for a medium range artillery projectile (x_{max} = 40 km) with ram propulsion is given in fig. 10. During the first phase of flight the installed thrust exceeds the total drag. Thus, an acceleration up to 950 m/s is achieved at burnout. The observed drop in thrust and drag is caused by the decreasing pressure and density of the atmosphere with increasing flight altitude.

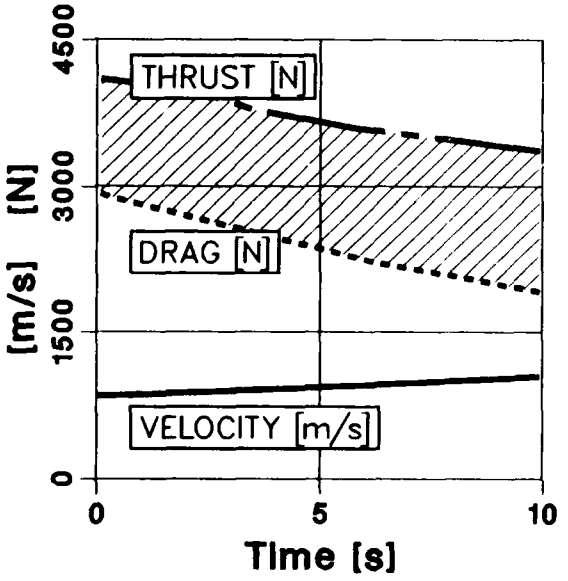

Fig. 11: Performance of long-range artillery shell

A further increase of maximum range can be achieved by enlarging the total propellant mass to 5.0 kg. As a result, the operation time of the engine is increased to nearly 10 seconds, allowing a range up to 65 km (fig. 11). If the initial projectile mass is kept constant, the payload has to be reduced consequently. Nevertheless, payloads consisting of hollow charges or anti radar warheads in combination with seeker and thrust vector control, appear to be highly efficient, expecially for long range applications.

4.2 Hypervelocity air defense projectile

Recent political developments impressively revealed the need of adequate air defense systems which are capable to destroy tactical and strategical missiles during flight. For long ranges, these needs are basically met by rokket systems. If economical aspects are considered additionally, gun fired projectiles show a suitable efficiency especially for short ranges up to 12 km ("last ditch defence"). In particular, drag compensated projectiles with ram propulsion, are highly efficient against TBMs, anti-tank helicopters, and aircrafts.

An appropriate design of an 160 mm air defense projectile operating at Mach 5 is presented in fig. 12 (/11/). The total initial mass is about 20 kg. The maximum effective operating range is 10 km.

The propulsion system consists of central air intake, gas-generator, ram-burner and nozzle. A total propellant mass of 3.7 kg is required for typical flight trajectories (5 km range at low altitude operation, 10 km altitude at 75 degrees firing angle).

The payload consists of small KE-flechets, which are activated by a special powder discharge unit. The beamrider projectile is guided by means of thrust vector control.

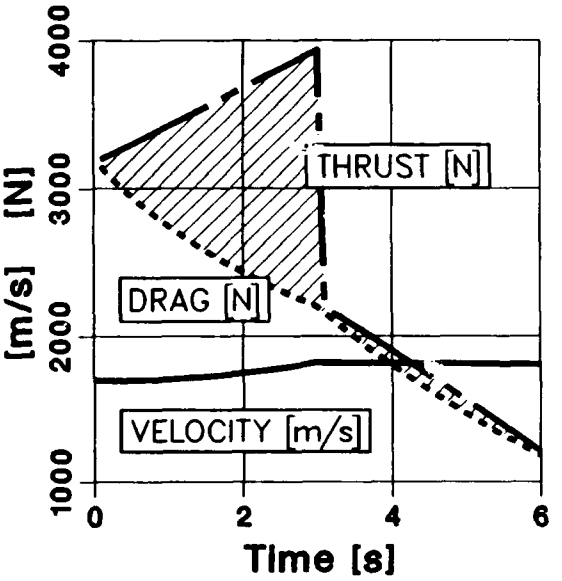

Fig. 13: Performance of air-defense ram-projectile

Thrust, drag and velocity development for a 75 degree mission is shown in fig. 13. During the first 3 seconds the engine thrust is comparatively high due to the additionally considered sea level missions. These flat trajectories are characterized by high static pressure and high drag as well. Regarding a mission to high altitude, the surplus of thrust leads to a final velocity of 1800 m/s. Subsequently, the thrust level is diminished to the drag value at medium and high altitudes by a corresponding propellant geometry.

For the considered trajectory temperature and pressure development within the combustion chamber are given in fig. 14. The static pressure decreases continuously with time of operation due to the lower air density at high altitude. The peak temperature of 1880 K, however, is achieved after 3 seconds of engine operation. This effect is caused by the constant fuel massflow in combination with the

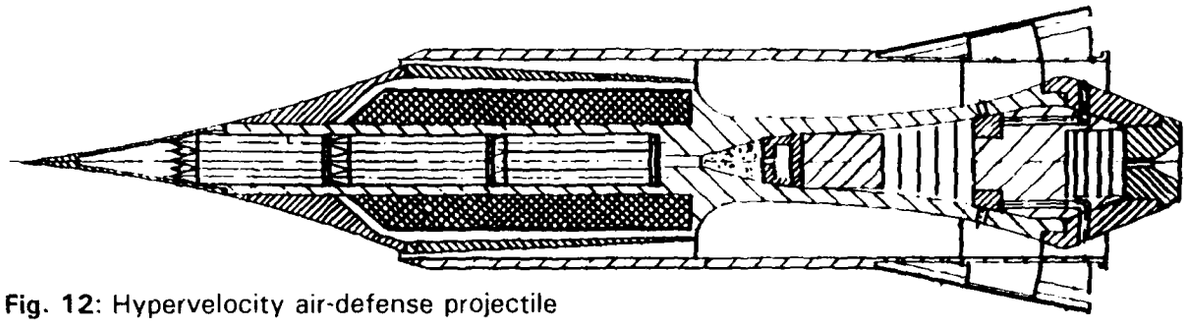

Fig. 12: Hypervelocity air-defense projectile

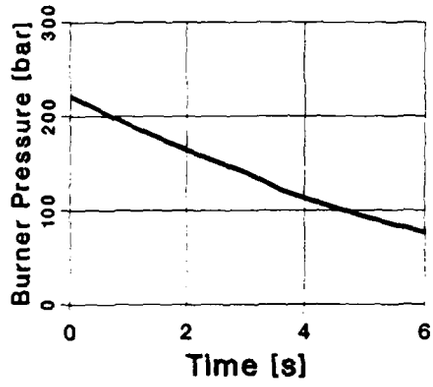

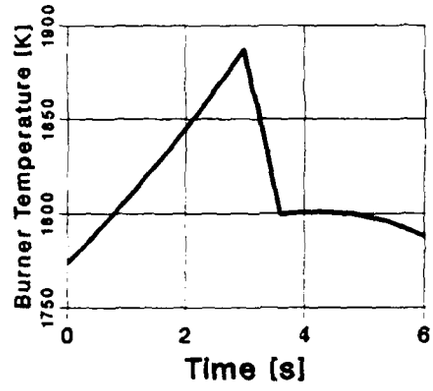

Fig. 14: Engine performance of air-defense projectile

decreasing airflow. Thus, the fuel-to-air ratio approaches its stochiometric value. This leads to an increased temperature at the burner exit. It is expected, however, that the high temperature can be managed for the required short period of time without major problems.

4.3 High performance KE-ammunition

With respect to the development of sophisticated armors (/12/), new standards of KE-ammunition have to be established in addition to conventional KE-projectiles. The use of hypervelocity missiles with rocket propulsion is a promising possibility in general. As a matter of fact, powerful KE-rockets are currently being developed at several locations.

KE-projectiles utilizing post-acceleration by ram-propulsion, offer similar effectiveness. However, these projectiles show some remarkable advantages in comparison with rocket systems, especially:

- o high hit accuracy
- o short range defeat capability
- o considerable cost reduction
- o firing capability by tank guns

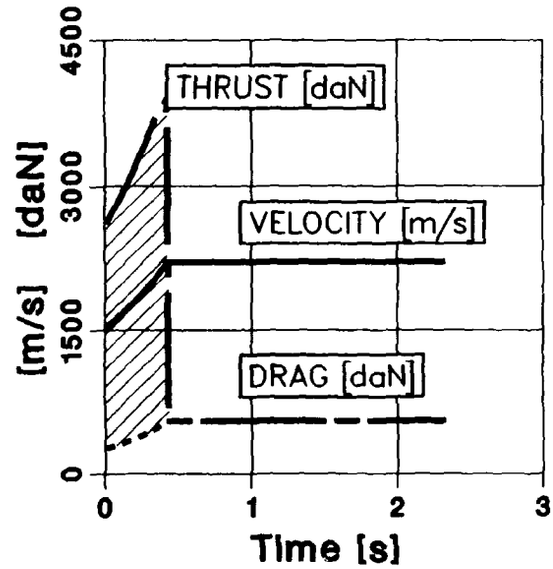

Fig. 16: Performance of KE-RAM-projectile

The sketch of a 140 mm ram-accelerated KE-projectile for ranges up to 5000 m is presented in fig. 15. The engine consists of a gas generator which operates during acceleration only. A composite propellant with oxidizer deficiency is used for this first phase of flight. The fuel massflow is approximately 9.3 kg/s.

The additional ramjet-burner is designed for compensation of drag at cruise. A hydrocarbon propellant (PE/HTPB) with specially shaped surface is used in this case (/13/). The

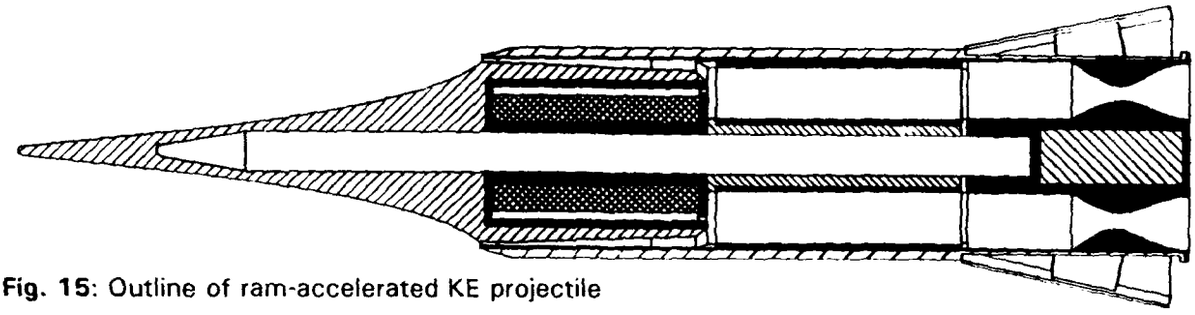

Fig. 15: Outline of ram-accelerated KE projectile

fuel massflow is diminished to 1.08 kg/s.

The initial total mass was determined to be about 20 kg. The initial velocity predicted by interior ballistical computations, is 1530 m/s. The main trajectory data are given in fig. 16. During the first 0.42 seconds of operation, the projectile is accelerated up to 2200 m/s (Mach 6.5). At burnout of the gas generator, a distance of roughly 780 m is reached by the projectile.

Due to constructional simplicity and maximum cost effectiveness the engine design was based on a fixed geometry throat and nozzle. Thus the throat cross-section was designed for Mach 6.5 flow conditions. The nozzle cross-section, however, was designed for Mach 5 engine performance in order to avoid thermal choking at lower flight velocities.

Due to these effects the area of captured flow is considerably reduced during the phase of acceleration (fig. 17a). The design value is obtained at Mach 6.5 only. The pressure development of the engine is presented in fig. 17b. During acceleration the pressure within the combustion chamber increases to nearly 350 bar. At cruise, the non-adapted nozzle causes the inlet normal shock to move downstream. Thus, the shock and diffuser-losses are distinctly increased. The pressure within the combustion chamber is consequently reduced to 260 bar.

The corresponding development of burner exit temperature is shown in fig. 17c. A peak temperature of more than 3400 K is achieved at the end of acceleration. In spite of the very short period of time, materials with extreme heat resistance are required for burner and nozzle. Even at cruise, a peak temperature of nearly 2900 K is reached at burner exit. With respect to these data, supersonic combustion would be highly desirable for the discussed application. The overall length limitations of combustion chamber and projectile, however, are in clear contrast to the requirements of supersonic combustion.

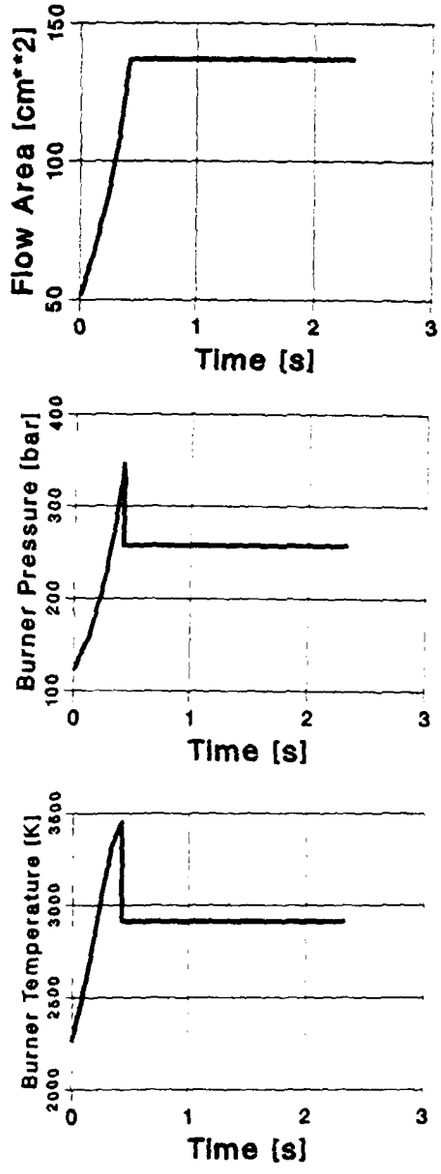

Fig. 17: Engine performance of KE-projectile

5. CONCLUSIONS

The present paper gives a survey on the performance and capabilities of projectiles using the concept of ram-propulsion. Very satisfying solutions for reliability and effectiveness are obtained for ramrocket propulsion and hybrid concepts as well. A superior specific thrust is obtained for ramjet-engines, but the absolute thrust level is fairly low in general.

The ram-engine applications presented in this paper show the benefits and efficiency of such concepts. For artillery applications the covered Mach number regime is low in general. Thus, ram-propulsion appears to be no severe problem from the technological point of view. Drastically higher requirements for air-intake and engine design are expected for a hypervelocity air-defense projectile. The extreme conditions, however, occuring to a ram-accelerated hypervelocity projectile, represent the technological limitation of ram-engines with subsonic interior flow.

Extremely high temperature and pressure levels occur at high velocity / low altitude operation. As a consequence, considerable progress in the field of materials with extreme heat resistance, hypervelocity aero-thermodynamics, and advanced computational fluid dynamics is absolutely necessary if hypervelocity ram-engines are to be developed. Nevertheless, the expected performance is very promising.

ACKNOWLEDGEMENT

The presented investigations were sponsored by the German Ministry of Defense under different contracts. The authors greatly acknowledge this promotion and the kind permission to publish this paper.

6. REFERENCES

1. Trommsdorff, W.: "High-Velocity Free-Flying Ram-Jet Units (TR-Missiles), AGARD, 1956

2. Waltrup, P.J., Billig, F.S., Stockbridge, R.D.: "Engine Sizing and Integration Requirements for Hypersonic Airbreathing Missile Applications", AGARD-CP-307, 1981

3. Fletcher, C.F., Lane, D.R.: "Service Experience with three Generations of Ramjets", AGARD-CP-307, 1981

4. Krohn, E.O., Triesch, K.: "Hochgeschwindigkeitseinläufe vom Typ RH", DLR, 1989

5. Svehla, R.A., McBride, B.J.: "FORTRAN IV Computer Program for Calculation of Thermodynamic and Transport Properties of Complex Chemical Systems", NASA report TN D-7056, 1973

6. Gordon, S., McBride, B.J.: "Computer Program for Calculation of Complex Chemical Equilibrium Compositions, Rocket Performance, Incident and Reflected Shocks, and Chapman-Jouguet Detonations", NASA report N 78 - 17724, 1976

7. Jäger, K., Kretschmer, J.: "Berechnung von Staustrahltriebwerken für Hochgeschwindigkeitsflugkörper", Institut für Raumfahrtantriebe, Stuttgart, IRA-84-IB-9, 1984

8. Moll, M.: "Artilleriegeschoß mit Staustrahlantrieb", internal report, 1983

9. Kramer, P.A., Kretschmer, J.: "Simulation des luftatmenden Antriebes für ein nachbeschleunigtes Geschoß", Institut für Raumfahrtantriebe, Stuttgart, 1983

10. Krohn, E.O., Triesch, K., Lips, H.R.: "Windkanaluntersuchungen an einem Staustrahltriebwerk mit Festbrennstoffen", DLR, 1978

11. Moll, M.: "KE-Staustrahlgeschoß - Flugkörperabwehrgeschoß", internal report, 1990

12. Schwartz, W.: "Explosive Reactive Armour", Military Technology, 8/1991

13. Meinköhn, D., Bergmann, J.W.: "Experimental Investigation of a Hydrocarbon Solid Fuel Ramjet", AGARD-CP-307, 1981

COMPARISON OF PERFORMANCES OF DIFFERENT CIRCULAR INTAKES

by
Hermann-L. Weinreich
Messerschmitt-Bölkow-Blohm GmbH
Postfach 80 11 69, 8000 München 80
and
Klaus Triesch
Deutsche Forschungsanstalt für Luft- und Raumfahrt
Linder Höhe, 5000 Köln 90

SUMMARY

Different circular front intakes with shock on lip Mach numbers ranging from 4.5 up to 5.57 have been investigated at DLR-Cologne and MBB under funding of the German MOD.

The closeable front intake concept (born in1985) offers high performance at Mach 3.6 transition in combination with exceptional low drag during boost and cruise.
Starting of the essential internal supersonic compression process could be achieved during initial centerbody translation at limited internal contraction and small capture area. A variety of corresponding Hy X intake models having different shock on lip Mach numbers, cowl angles, internal contractions, internal area distributions and cowl lip bluntness data were tested between Mach 3.5 and 4.5 and gave experience on starting phenomena and performance.

Fixed geometry intakes with external compression and quite different cowl angles (RH3A with cylindrical cowl, RH3C with large cowl angle) exhibited comparable or even better total pressure recoveries. The supercritical pre-entry drag characteristics below shock on lip Mach numbers however look most unfavourable.
Without consideration of incidence characteristics and the problems associated with closure of intake entrance area during boost, the RH3A - intake could be used instead of the Hy X - type intake for medium range air to ground missiles.

The RH3C - intake offers the highest value of total pressure recovery due to maximum external compression and proper cowl alignment. The corresponding high wave drag however prohibits any useful application of this type of intake.

LIST OF SYMBOLS

A	area, cross section; without index: missile body cross section = reference area for aerodynamic coefficient
$b/_{lat}$	lateral acceleration
B_{cl}	cowl lip bluntness
c, $\bar{c}$	velocity, average velocity
C_{D_0}	zero lift drag coefficient
C_F	ramjet thrust coefficient
D	diameter
H	duct hight
m	mass
$\dot{m}$	massflow
M	Mach number
p	pressure
t	time
x	longitudinal dimension
ΔX_{EK}	length of internal contraction zone (Fig. 1)
ΔX_{ZK}	centerbody translation for closure of intake entrance (Fig. 1)
y	radial dimension
α	angle of incidence
ε	nozzle expansion area ratio
η_{Ke}	kinetic energy efficiency
θ_c	centerbody cone angle (Fig. 1)
θ_{div}	duct divergence angle downstream of throat (Fig. 1)
θ_{HLi}	internal cowl lip angle of intake (Fig. 1)

Subscripts

∞	condition at free stream (Fig. 1)
1	condition at intake exit (Fig. 1)
4	condition at nozzle throat
5	condition at nozzle exit
cr	critical intake operation
E	condition at intake entrance (Fig. 1)
K	condition at intake throat (Fig. 1)
L	nominal intake capture area (Fig. 1)
sol	shock on lip condition
st	starting of intake supersonic internal compression
t	total condition

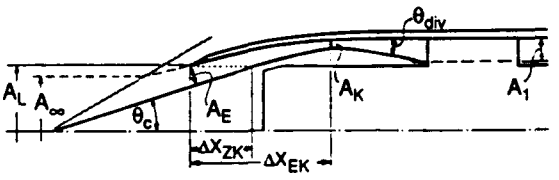

Fig. 1 Geometrical parameters of closeable mixed compression front intakes

1. Introduction

Rampropulsion provides favourable performance characteristics, penetration capability and growth potential for future supersonic tactical missiles [1].
Therefore boron loaded ducted rockets have been tested extensively since 1970 at MBB and Bayern Chemie [2] for missiles operating from Mach 2 at SL up to more than Mach 3 at

altitude.
The influence of higher (moderate hypersonic) flight Mach numbers on design and performance of ramjets and ducted rockets was investigated since 1983 under funding of the German MOD [3, 4, 5].
Within this program, the closeable mixed compression front intake concept (Fig. 2) was born in 1985 at MBB [3] and led to the first DLR - test models Hy 1 (with) and Hy 1A (without internal bleed; $M_{st} = 4.3$, $M_{sol} = 4.5$) in 1987 [4, 6].

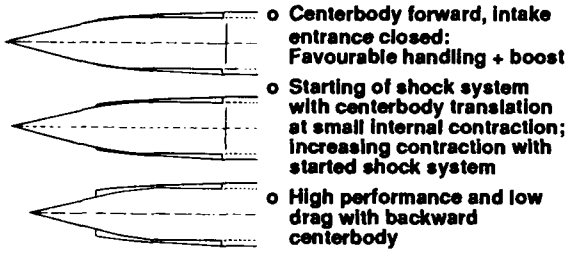

Fig. 2 Features of closeable front intakes

Based on the corresponding experimental experience [6, 7], the Hy 6 - intake family, having wider operation limits ($M_{st} = 3.5$, $M_{sol} = 5.57$), different internal contraction, different throat divergence and lip bluntness has been designed at MBB [8].
Using a common boost cruise nozzle and a boron loaded ducted rocket with subsonic self-throttling gasgenerator outflow, a Mach 5 anti-radiation missile (Fig. 3) with superior performance characteristics (in comparison to a rocket powered configuration) has been designed [4].

o C/C structures	30 kg	PERFORMANCE:
o Payload	21 kg	+ 30 km at SL
o Cruise propellant	23 kg	+ $\bar{c}$ = 1500 m/s
o Boost propellant	53 kg	+ blat = 50 g
		+ Mmax = 5.1
LAUNCH MASS	127 kg	
FINENESS RATIO	14 : 1	

Fig. 3 220 mm Ø anti-radiation missile with integrated ducted rocket propulsion [4]

In 1991 an additional series of tests with Hy 6M-intakes were performed at the DLR-Cologne [11].
This paper will present details of the experimental experience gained with

+ the aforementioned mixed compression closeable Hy 6M-intakes
+ and two different Mach 4.8 (on principle) external compression intakes RH3A (with cylindrical internal cowl) and RH3C (with large cowl angle) [13].

The consequences of total pressure recovery, massflow characteristic and external drag (of these different intakes) on missile performance will be discussed at the end of the paper.

2. Experimental experience with closeable mixed compression Hy 6M-intakes

Fig. 4 summarizes design data of selected Hy X-intake configurations tested at the DLR-Cologne.

Designation	Design	M_{sol} [-]	θ_{HLi} [°]	$\frac{A_E}{A_L}$	$\frac{\Delta X_{EK}}{D_L}$	$\frac{A_K}{A_E}$	$\frac{\Delta X_{ZK}}{D_L}$
Hy 1	DLR-87	4.5	7.3	.52	1.76	.26	.85
Hy 1A	DLR-88	4.5	7.3	.52	1.76	.30	.85
Hy 1Dump	DLR-88	4.5	7.3	.52	1.66	.30	.85
Hy 6M-1.Y.Z	MBB-89	5.57	6.0	.43	.87	.38	.59
Hy 6M-2.Y.Z	MBB-89	5.57	6.0	.43	.75	.40	.59
Hy 6M-3.Y.Z	MBB-89	5.57	6.0	.43	.66	.41	.59
Hy 7M	DLR-89	5.57	9.3	.44	.98	.32	.55

Fig. 4 Design data of closeable Hy X - front intakes

All the intakes mentioned in Fig. 4 have 14° centerbody-halfcone angles.
Only the Hy 1-model (and in a few tests the Hy 1A- and Hy 7-models) were equipped with internal centerbody bleed.
The Hy 1Dump-model exhibited a dump type area expansion with an area ratio of two.
All the Hy 6M-intakes have identical internal cowl-, but different centerbody contours resulting in three values of internal contraction and three values of throat divergence angle θ_{div} (1°, 2°, 4°, designated by the label Y).
Seven cowl lips with different bluntness B_{el} (0.065, 0.17, 0.20, 0.25, 0.30, 0.405, 0.90 mm, designated by the label Z) have been used during tests of the Hy 6M-models.

The Hy 7M-intake was an alternative DLR-design with a steeper cowl lip and nearly continuous compression (following the cowl shock) at Mach 5 freestream condition.

Fig .5 gives an overwiew of the Hy 6M-intake test objectives:

- **Intake characteristics at Mach numbers 3.5, 3.6, 4.0, 4.5 and different angles of incidence**
- **Influence of M ∞ and α on the critical values of total pressure recovery and massflow**
- **Evaluation of minimum starting- and unstarting Mach numbers**
- **Critical starting values of total pressure recovery and massflow**

Fig. 5 Hy 6M-intake test objectives

During the first successful test campaign [10] most of the tests were run at Mach 4.5 freestream conditions.
With regard to the limited blow down tunnel running time and the initially unknown critical intake total pressure recovery a coarse step by step throttle closure had to be used. This resulted in critical total pressure recovery data with a margin of uncertainty in the order of 8%.

During the following tests [11], smaller closure steps of the throttle gave more accurate data especially in the important transition Mach number regime (3.5 - 3.6).
Fig. 6 shows the corresponding critical kinetic energy efficiencies based on measured total pressure recoveries and perfect gas flow transformation.

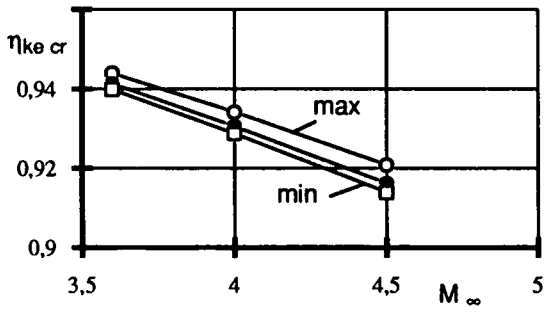

Fig. 6 Influence of Mach number on critical kinetic energy efficiency

The 94% critical kinetic energy efficiency at a transition Mach number of 3.6 corresponds to more than 60% of total pressure recovery.
While the critical kinetic energy efficiency increases from 91.6% at Mach 4.5 up to 94.1% at Mach 3.6, the corresponding capture massflow ratio drops gradually from 0.83 to 0.70 due to the 14° cone shock external flow deflection.

The moderate influence of incidence on the Hy 6M-intake performance is illustrated by Fig. 7.

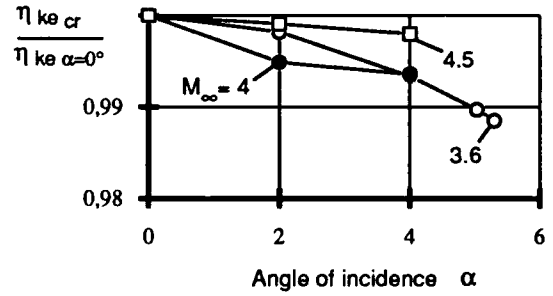

Fig. 7 Influence of incidence on critical performance of the Hy 6M-1.2.2-intake model

While the Hy 6M-1.2.2-intake model could be operated (at Mach 3.6) up to 5.3° of incidence, the Hy 6M-3.2.2-model (with slightly smaller internal compression and performance) exhibited stable operation even up to 7.2° of incidence.

Based on the experimental data, gained from tests with the intakes, listed in Fig. 4, the principal influence of internal area contraction on minimum starting Mach number $M_{\infty st}$ and the corresponding Mach 4.5 critical kinetic energy efficiency was assessed:
A moderate internal area contraction results in a wide operating margin with a low minimum starting Mach number, but degrades the corresponding critical intake efficiency at higher freestream Mach numbers.

Fig. 8 shows, that the Mach 4.5 critical kinetic energy efficiency of closeable Hy-X-type mixed compression intakes could be improved from ≈ 91% up to ≈ 93%, when an increase of the minimum starting Mach number from Mach 3.5 to Mach 4.5 could be tolerated.

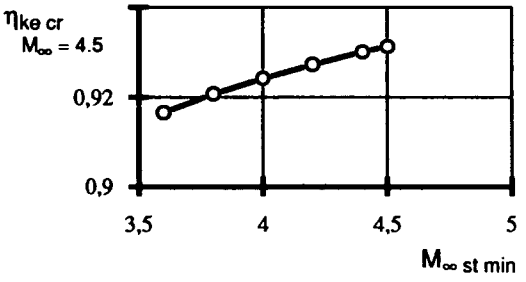

Fig. 8 Growth of Mach 4.5 critical kinetic energy efficiency of Hy X-type intakes with increasing minimum starting Mach number

Starting phenomena with Hy X-type closeable mixed compression intakes:
The original Hy 6m- and Hy 7m- intake models as designed by the DLR-Cologne and MBB could not be started even at Mach 4.5 freestream conditions [8, 9, 10, 11].
Small modifications of the centerbody contours

+ eliminated the formation of intermediate throats during centerbody translation of the Hy 7m-intake model and allowed starting of the renamed Hy 7M-intake down to Mach 4 freestream conditions,
+ reduced the initial increase of internal area contraction during centerbody retraction of the Hy 6m-intake model by nearly 50% and allowed starting of the renamed Hy6M-intakes down to Mach 3.5 freestream conditions.

Fig. 9 summarizes key aspects for starting of Hy X-type intakes, which must be considered in relation to the "contour design principles"discussed previously [4, Fig. 15]:

A **No multiple throat formation during centerbody retraction**

B **Limitation of internal contraction during initial centerbody retraction**

C **Sufficient initial internal contraction for required starting pressure recovery (excessive heat release due to high starting ER and / or booster silvers)**

D **Limitation in cowl lip bluntness**

Fig. 9 Aspects, governing the starting phenomena of Hy X -type intakes

In contradiction to requirement B a sufficient initial contraction (at small degree of entrance area opening) is required to get a satisfactory level of the starting critical total pressure recovery.
In spite of the small initial air massflow during intake entrance opening, an excessive heat release due to a high start-

ing fuel massflow (equivalence ratio ER) and / or booster residuals can prevent the intake from starting, if the critical total pressure recovery is to poor in comparison to the corresponding massflow, so that the fixed ramjet nozzle cannot swallow the combustion gases.
As illustrated by Fig. 10 the Hy 6M-intake exhibits a promising starting critical total pressure recovery characteristic:

More than 50% of the final total pressure could be demonstrated at 24% of the full air massflow.

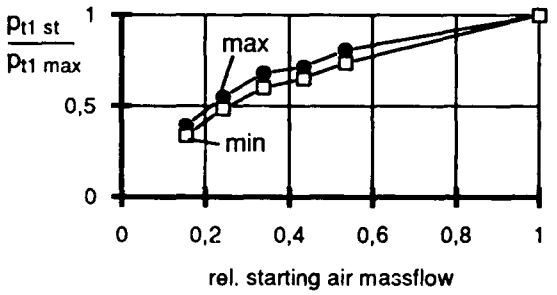

Fig. 10 Influence of starting air massflow (centerbody retraction) on critical total pressure recovery of the Hy 6M-intake model

The internal supersonic compression could be started below 26% of the final ceterbody retraction corresponding to an entrance area duct height well below 2.3 mm.
The high performance starting process, illustrated by Fig. 10, could however only be realized using relatively sharp intake cowl lips:
While a bluntness of 0.17 mm (D_L = 104 mm) allowed starting of the Hy 6M-1.2-intake models without problems, a cowl lip bluntness of 0.2 mm or more prevented intake starting under all conditions tested.

Additional remarks on Hy X-type intake behaviour:

- The internal supersonic total pressure losses of these mixed compression intakes are predominated by friction effects, while the oblique shock losses are very small.
- Installation of centerbody-boundary layer bleed upstream of the throat of an intake, that could be started without any bleed, resulted in a reduction of massflow, effective internal contraction and critical total pressure recovery.
- A sudden dump in the throat region of a Hy X-type intake means, that the terminal pseudo-shock [17] is extended into the dump area during critical intake operation. Therefore unacceptable supersonic Carnot-losses will degrade the intake performance to a great extent.

3. Comparison of different circular intakes

Within an independent MOD funded research programm an other family of different axisymmetric intakes, but with mainly external supersonic compression has been designed and tested at the DLR-Cologne [13].
Fig. 11 shows the contours of the so called RH3A- and RH3C-intake in comparison to the Hy 6M-intake and summarizes corresponding key parameters.

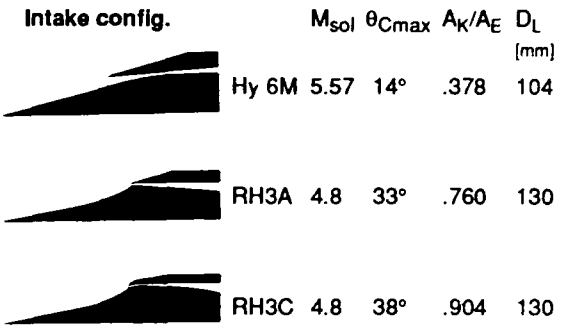

Fig. 11 Contours and data of different circular intakes

While the Hy 6M-intake with 14° conical centerbody deflection has an internal cowl lip angle of 6°, the RH3A-intake shows a 33° maximum semi isentropic centerbody deflection in conjunction with a cylindrical internal cowl contour and a noticeable amount of internal area contraction.
The RH3C-intake exhibits an even larger centerbody deflection angle but only a small internal area contraction due to the tremendous 30° internal cowl lip angle.
All these intakes were tested at Reynolds numbers in the order of 8.3-million (Hy 6M-intakes) or 10.4-million (RH3-intakes) based on cowl lip diameter and freestream conditions.

Due to maximum external compression and minimum internal friction losses, the RH3C-intake shows superior compression efficiencies (Fig. 12).

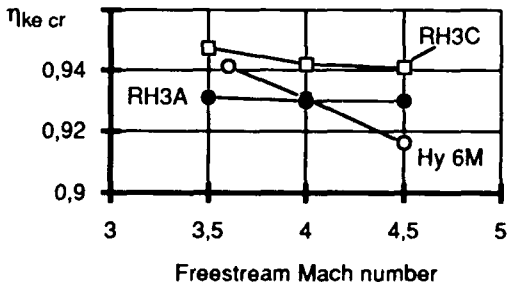

Fig. 12 Critical kinetic energy efficiency of different circular intakes

With regard to the Hy 6M-intake performance characteristic, it must be mentioned, that this intake has a moderate internal contraction designed for starting at Mach numbers around 3.5, far away from Mach 5.57 shock on lip operation.
A reduction of the operation range, defined by minimum starting- and shock on lip Mach number would result in a remarkable performance improvement.
The efficiency of the RH3A-intake is superior to Hy 6M-1.2 only at freestream Mach numbers above 4.1.
It is interesting, that this superiority vanishes with increasing angle of incidence. Fig. 13 illustrates, that the decrease of critical kinetic energy efficiency (or total pressure recovery) is much more pronounced for the external compression

intakes.

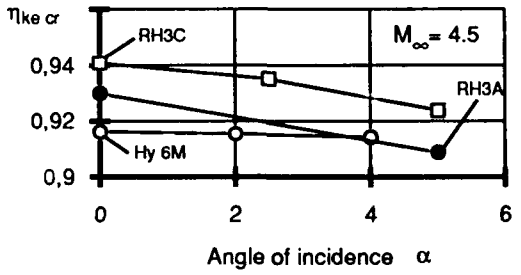

Fig. 13 Influence of incidence on critical kinetic energy efficiency

Moreover the decrease of capture massflow ratio with incidence is larger in the case of the RH3-intakes.
This observed influence of incidence on performance of external and mixed compression intakes is in contrast with the classical literature, where a stronger incidence sensitivity on performance is generally quoted to the mixed compression intakes.

Pre-entry drag, cowl drag and front intake-missile total drag:
While the pre-entry drag of the Hy X-type intakes could be calculated exactly using a method of characteristics code [14], a comparable calculation was not available in the case of the external compression intakes:

- o The RH3A-intake shows cowl shock detachment at a freestream Mach number of approximately 4.5 due to excessive internal flow turning.
- o Below a freestream Mach number of roughly 4 no regular isentropic flow compression seems to be possible along the 38° spike deflection of the RH3C-intake.

A crude assessment of the pre-entry drag data resulted in a much more pronounced increase of pre-entry drag for both external compression intakes below shock on lip Mach numbers (in comparison to the Hy 6M-intakes).
A final more reasonable recalculation of pre-entry drag data [14] came too late for the (intake governed) performance calculations presented in this paper, but would have led to even slightly higher drag levels for both external compression intakes.

Based on the internal cowl contours of the tested windtunnel models, the external cowl contours were designed with regard to the different Mach 4.5 internal critical pressure levels assuming a C/C-structure following the baseline missile configuration of Fig. 3.
Fig. 14 shows the resulting intake cowl contours:

- o All intakes have an identical cowl lip bluntness corresponding to 0.2 mm (D_L = 163 mm).
- o The lip divergence angle is 17° for both the Hy 6M- and the RH3A-intake missile.
- o To avoid cowl lip shock detachment below shock on lip Mach numbers and / or at incidence an external RH3C-cowl lip angle of 35° had been selected during design of the windtunnel model [13]. The corresponding 5° lip divergence could be realized with a steel made cold flow windtunnel model but may be impracticable with a C/C-high temperature resistant structure. Nevertheless an external cowl lip angle of 35° was presumed for the drag evaluation.

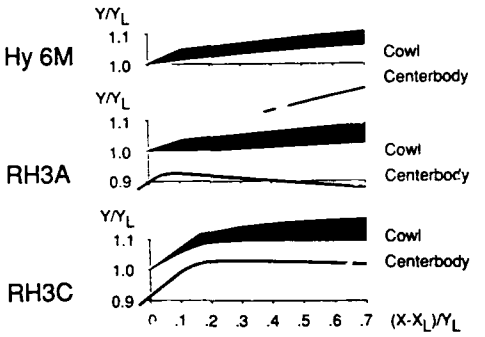

Fig. 14 Comparison of intake cowl contours

In spite of the unrealistic small cowl lip divergence angle of 5°, the RH3C-intake exhibits by far the highest external cowl drag (assessed by a shock expansion theory).

Front intake missile total drag:

The front intake missile drag depicted in Fig. 15, represents the sum of the aforementioned pre-entry drag, cowl wave drag (A_L/A = .55) and a fuselage friction and tail drag as calculated for the original missile configuration (Fig. 3):

The drag characteristic of the Hy 6M-intake missile shows a continuous slope beyond Mach 5 due to the high design shock on lip Mach number of 5.57.

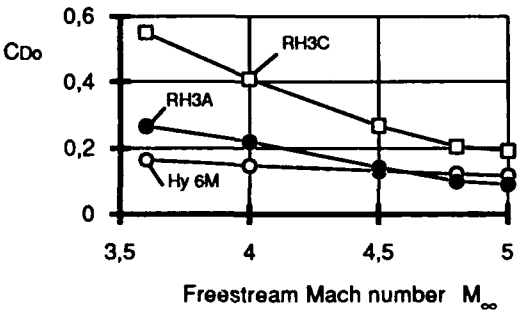

Fig. 15 Zero lift drag coefficients of different front intake missiles

At Mach 4.8 (shock on lip operation) the RH3A-intake missile exhibits the lowest drag due to the fact having the smallest cowl angles. Below shock on lip however, the pre-entry drag of the external compression intake increases rapidly, so that already at Mach 4.5 the RH3A-intake missile drag exceeds the corresponding Hy 6M-intake missile drag level.

Despite its unrealizable small cowl lip divergence angle, the RH3C-intake missile shows an unacceptable high drag level resulting from both pre-entry drag and cowl wave drag.

Engine performance calculations for comparison of different intakes:

The RH3C-intake offers a nearly 2.5% improvement in kinetic energy efficiency at Mach 4.5 in comparison to the Hy 6M -intake.

Therefore the question arises:

Up to which extent the specific impulse of a ducted rocket or a ramjet will be improved by the higher intake efficiency?

Based on NASA Lewis Code [16] generated nozzle data [15], the performance values of boron fuelled ducted rockets were calculated assuming transition to frozen flow downstream of the nozzle throat at 120% of the throat area while the total nozzle area expansion ratios are in the order of 10.

An exit momentum loss coefficient of 97.5% has been assumed for all these example calculations.

Influence of critical kinetic energy efficiency on Mach 4.5 ducted rocket performance

Operating at a maximum combustor total pressure corresponding to 90% of the critical intake exit total pressure, the pressure ratio for a Hy 6M-intake ducted rocket designed for Mach 4.5 cruise would reach 93.7.

The extremly high RH3C-intake critical kinetic energy efficiency of 94.1% (without any bleed) would permit an impressive increase in the cruise flight nozzle pressure ratio up to 122.4, but on the other side only 10% to 15% of thrust improvement are obtained, depending on the fuel to air ratio, specified.

On the other hand the RH3C-intake missile exhibits more than twice the drag of the baseline Hy 6M-intake missile, as illustrated by Fig. 15 and Fig. 16.

INTAKE	Hy 6M	RH3A	RH3C
$p_{t1\ cr}$	100 %	116 %	131 %
$C_F = C_{Do}$	100 %	109 %	204 %
ε	11.2	12.9	13.3
i_{sp}	100 %	108 %	133 %
$\dot{m}_{cp}$	100 %	101 %	153 %

Fig. 16 Influence of total pressure recovery and thrust coefficient on specific impulse and fuel consumption

While the baseline Hy 6M-intake missile can cruise (at Mach 4.5) at a very low equivalence ratio (low drag) and a correspondingly poor specific impulse level, the doubled thrust demand of the RH3C-intake missile requires a 50% higher equivalence ratio.

As listed in Fig. 16, the higher thrust demand improves the specific impulse in addition to the pressure related increase by a total of 31 %.

Nevertheless the RH3C-intake missile would require a 53% higher fuel consumption in comparison to the Hy 6M-baseline configuration.

The RH3A-intake permits an improvement of the specific impuse, which compensates the higher drag level at Mach 4.5 cruise flight. Due to its lowest configuration drag above Mach 4.6 (see Fig. 15), this intake would yield minimum cruise flight fuel consumption at higher Mach numbers.

Suitability of different front intakes for medium range air to ground missile propulsion:

The final judgement on intake qualities will be based on appropriate missile design and performance studies.

Under the presumption, that a detacheable (or consumeable) intake entrance area cover cap with only 16° half cone angle can be realized, the RH3A-intake missile drag during boost will rise by merely 15% in comparison to the Hy 6M-baseline configuration.

The higher operating pressures will require heavier chamber structures and just compensate the weight reduction due to the much simpler intake structure including no sliding centerbody shell.

Both missiles (with Hy 6M- and RH3A-intake) will be boosted up to a Mach 3.6 transition.

As illustrated by Fig. 17, the Hy 6M-baseline configuration shows a much higher initial acceleration due to the much lower pre-entry- and total missile drag.

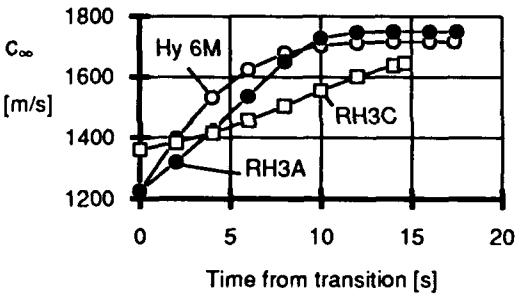

Fig. 17 Flight velocity versus time for air to ground missiles with different front intakes

A ducted rocket gasgenerator burn rate pressure exponent of 0.5 is required for the Hy 6M-baseline missile, to realize the baseline mission without variable geometry.

The higher initial fuel consumption due to the lower critical total pressure recovery of the RH3A-intake missile will vanish, when this missile exceeds Mach 4.5, where it operates at both favourable drag and intake total pressure recovery.

Due to its large increase in capture air massflow with flight Mach number (up to Mach 4.8 shock on lip operation) a pressure exponent of only 0.25 is required for the RH3A-missile to perform the comparable 30 km mission at sea level.

The RH3C-intake missile must be boosted up to about Mach 4 due to its excessive external drag at lower Mach numbers. Even if neglecting

- the higher boost-propellant demand due to both increased drag level (cowl drag) and transition Mach number
- heavier chamber structures due to increased design operating pressures,

the prohibitive cruise flight drag would reduce the missile range by more than 20%.
Fig. 18 illustrates after all, that a high critical total pressure recovery at high flight Mach numbers can not be utilized with fixed nozzle rampropulsion engines.

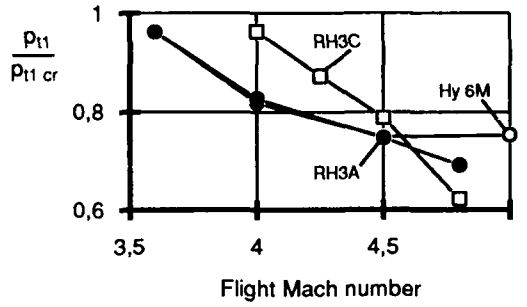

Fig. 18 Influence of flight Mach number on supercritical margin for fixed geometry ducted rockets with different front intakes

Even the Hy 6M-intake exhibiting a remarkable decrease in critical total pressure recovery with growing flight Mach number will operate at increasing supercritical margins with rising velocity.
Therefore tactical missile intakes must show high values of critical total pressure recovery in the transition Mach number regime only.

4. Conclusions

Fig. 19 summarizes the selection criteria of the three different circular missile intakes under consideration.

Intake configuration	Hy 6M	RH3A	RH3C
Critical total pressure recovery at transition	+	o	+
Sensitivity to incidence	+	-	-
Air massflow characteristic	-	+	+
External drag	+	o	- -
Practicable operation range	+	o	-
RANKING	1	2	3

Fig. 19 Front intake selection criteria

The RH3C-intake looks most unfavourable due to its prohibitive pre-entry drag and cowl drag. Furthermore the 5°-limitation of cowl lip divergence may be impracticable for a hypersonic flight structure.

The RH3A-intake requires no moveable structures for starting but an additional gadget for closure of intake entrance area during boost.
Except for incidence sensitivity, the overall performance of the RH3A-intake missile is comparable to the baseline Hy 6M-configuration. Integration of the seeker within the semi-isentropic centerbody spike may be an additional problem.
Therefore the original selection of the closeable mixed compression Hy 6M-1.2.2-intake for the propulsion system of future medium range anti-radiation missiles seems to be justified. By the way, the high shock on lip Mach number of 5.57 will prevent cowl lip cone-shock interactions with corresponding excessive thermal loads [18] within the Mach number- and incidence- envelope of the missile.

REFERENCES

[1] Crispin, B.
Ramjet and ramrocket propulsion systems for missiles; Introduction and overview. AGARD-LS-136, 1984

[2] Besser, H.-L.
Solid propellant ramrockets. AGARD-LS-136, 1984

[3] Weinreich, H.-L.
Antriebskriterien für Hochgeschwindigkeitsflugkörper (Hyperschall), Teil 2. MBB UA-1018/86, 31. 10. 1986

[4] Weinreich, H.-L.
Highly integrated ducted rocket propulsion modules for future hypersonic tactical missiles.
AGARD-CP-479, paper 30, Madrid, June 1990

[5] Weinreich, H.-L.
Untersuchungen zu Antriebskonzepten für Hochgeschwindigkeitsflugkörper (Hyperschall), Teil 3.
MBB UK-0153-91, 31. 3. 1991

[6] Krohn, E.-O.; Triesch, K.
Hochgeschwindigkeitseinlauf mit hoher Innenverdichtung. DFVLR IB-39113-88-C-16, 22. 8. 1988

[7] Krohn, E.-O.
Ergänzende Messungen an den Einläufen Hy 1 und Hy 1A. Persönliche DFVLR- Mitteilungen, 1988/89

[8] Weinreich, H.-L.
Auslegung, Leistungsabschätzung und Entwurf rotationssymmetrischer Fronteinläufe für Hochgeschwindigkeitsflugkörper. MBB UK TN-KY25-3/89, Nov. 1989

[9] Triesch, K.; Krohn, E.-O.
Hochgeschwindigkeits-Einläufe mit hoher Innenverdichtung (erste Ergebnisse mit den Modellen Hy 6 und Hy 7). DLR IB-39113-90-C-02, 20. 1. 1990

[10] Triesch, K.; Krohn, E.-O.
Hochgeschwindigkeits-Einläufe mit hoher Innenverdichtung (Modelle Hy 6 und Hy 7 mit geänderter Geometrie). DLR IB-39113-90-C-07, 10. 5. 1990

[11] Krohn, E.-O.
Ergänzende Nachmessungen am Hochgeschwindigkeitseinlauf Hy 6M im TMK (Versuchsserie 91-3).
DLR-Köln, WT-WK-KP, Pers. Mitteilung, 7. 10. 1991

[12] Weinreich, H.-L.
Entwurf modifizierter rotationssymmetrischer Fronteinläufe; Auswertung und vergleichende Bewertung der Hy 6M- sowie Hy 7M-Versuchsergebnisse.
MBB UK TN-KY25-90-09, 31. 3. 1991

[13] Krohn, E.-O.; Triesch, K.
Hochgeschwindigkeitseinläufe vom Typ RH; Teilbericht: Versuche im TMK.
DFVLR IB-39113-89-C-22, 20. 11. 1989

[14] Triesch, K.
Calculation of C_{Dpre}-data for Hy 6M, RH3A and RH3C -intake geometries below M_{bol}.
DLR-Cologne, Private commun., Jan. 1990 - Feb. 1992

[15] Besser, H.-L.
Calculation of characteristic chamber and nozzle parameters for a generic boron loaded ducted rocket propellant based on a modified NASA Lewis code [16].
MBB UK KT302, Private communication, Feb. 1992

[16] Gordon, S.; McBride, B. J.
Computer program for calculation of complex chemical equilibrium compositions, rocket performance, incident and reflected shocks, and Chapman-Jouguet detonations.
NASA SP-273, NASA Lewis Research Center, 1971

[17] Jungclaus, G.
Auslegungskriterien für Überschalleinläufe mit Pseudo-Shocks.
MBB UK TN-KY-9/89, 25. 7. 1989

[18] Edney, B. E.
Anomalous heat transfer and pressure distributions on blunt bodies at hypersonic speeds in the presence of an impinging shock.
FFA Rep. 115, Aeronaut. Res. Inst. of Sweden, 1968

Discussion

Question from M. RAMETTE, DASSAULT, France

What aerodynamics results did you obtain in the Mach 4,5 to Mach 5,6 domain for the Hy 6 M inlet ?

Author's reply

We did not test the Hy-type intakes above a Mach number of 4,5 because the wind tunnel did not allow the simulation of higher Mach number. In addition, we feel that the intake performance data at higher Mach number will be of minor importance because critical intake operation cannot be achieved with fixed geometry ramjet systems as illustrated by figure 18. Wether the intake may operate at 20 % or 30 % supercritical margin is not interesting.

MULTIPLE-INLET CONFIGURATION FOR MISSILES WITH SKID-TO-TURN CONTROL MODE

by
W.-D. Pohl
Messerschmitt-Bölkow-Blohm GmbH
Postfach 80 11 69, 8000 München 80
and
E.- O. Krohn
Deutsche Forschungsanstalt für Luft- und Raumfahrt
Postfach 90 60 58, 5000 Köln 90

SUMMARY

For missiles with cartesian control mode a symmetrical configuration with four inlets is most common. The operation of a multiple inlt system is significantly influenced by the interaction of the coupled inlets. Inherent problems are discussed by means of a simplified model and windtunnel test results.

First a configuration with four axisymmetrical inlets is presented. Different inlet geometries and the influence of an external boundary layer bleed are investigated in order to obtain an enlarged stable operation regime. Windtunnel tests of individual inlets and of four coupled inlets showed the effects of inlet matching and the resulting overall performance.

Furthermore a configuration with four rectangular inlets is discussed. Problems and advantages of the conventional and the inverted integration mode are illustrated using wind tunnel test results. It is shown that the use of a pre compression ramp is especially beneficial to the inlet matching of four inverted inlets.

List of Symbols

A	area
c*	characteristic velocity
c_D	drag coefficient
d	diameter
h	boundary layer diverter height
l	length
l/d	finess ratio
M	Mach number
$\dot{m}$	massflow
p	pressure
q	dynamic pressure
Re	Reynolds number
v	velocity
x_s	slot width of the boundary layer bleed
α	angle of attack
δ	boundary layer thickness
φ	roll angle
θ	miscellaneous inlet geometry angles

Indices

0	free stream condition
1	capture area (inlet lip)
2	single inlet exit
3	common chamber after mixing
4	nozzle throat
t	total condition
Bl	boundary layer bleed
c	cone
r	ramp

1. INTRODUCTION

With regard to the demanded flight-trajectory, for many missiles a cartesian control mode is required. Mostly this control mode is applied to a missile configuration with 4 control surfaces and 4 wings in x-position. The fixed roll angle at maneuvers simplifies the automatic control, since pitch and yaw planes are decoupled. Compared with a bank-to-turn control mode the skid-to-turn control mode causes a higher maneuvering agility, which may be important during the final approach of the missile. Previous system investigations for anti-ship-missiles have shown, that the skid-to-turn control mode is also superior in order to maintain constant altitude at sea-skimming flight,. Furthermore seeker problems are reduced.

Concerning the air intakes of airbreathing engines, the cartesian control mode is less favourable. Depending on the orientation of the lateral acceleration, the plane of incidence may vary. With respect to an undistorted flow there is no preferred position to install a single aft-intake. In most cases a configuration with a nose inlet is not applicable because the "field of view" of the seeker would be affected. Moreover nose or front inlets do not allow a modular system design. The sensitivity to incidence of a single aft mounted inlets depends strongly on the incidence plane. Therefore in the case of a cartesian control mode of the missile a 4-intake configuration is frequently used. Besides the advantage of a symmetrical missile aerodynamics there are other arguments for a 4-inlet configuration concerning the combustion chamber of a ramjet:

- In a modern design of ramjet powered missiles the boost motor is integrated in the ramjet combustion chamber.

This design does not allow the application of mechanical flameholder devices in the combustion chamber. Therefore the configuration of the entering air is used to generate recirculation zones in the dome section in order to stabilize the flame. A system with four inlets leads to a better uniformity of flow and temperature compared to a system with one or two intake ducts.

- For the operation of the rudders this type of missile needs four actuators. If the control surfaces are in-line with the inlets, the actuators can be mounted in the extended inlet-fairings, without producing additional drag.

Therefore it is evident, that the most common configuration of recent ramjet-powered missiles represents a design with 4-inlets combined with one chamber.

2. INTERACTION PROBLEMS OF MULTIPLE INLET CONFIGURATIONS

A system of multiple inlets connected with a common chamber induces an interaction of the inlets which can cause unstable flow in one or more inlets up to reverse flow. Depending on the inlet characteristics this can even happen at zero or small angle of attack.
To understand this interaction, it is useful to apply a simplified assumption.
Fig. 1 shows 2 inlets connected with one chamber. In principle this may also be representative for 4 inlets, if we assume, that the characteristics of two inlet pairs are exactly equal (e. g. inlets in X-position).
The dashed lines indicate walls of air-ducts, which take care that the air enters the chamber with parallel flow. In the entrance plane the static pressure is considered constant.

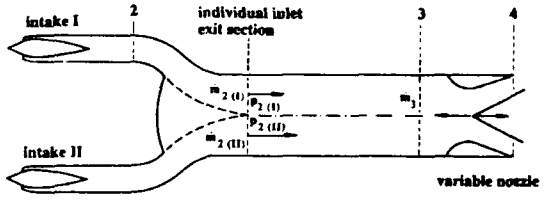

Fig. 1 Multiple inlet flow model with simplified assumptions

Measurements have shown, that this assumption is approximately valid down to zero massflow in one inlet. Even without the duct for parallel flow (dashed line) the single inlet operation changes not too much.

Fig. 2 shows a typical inlet characteristic (pressure recovery versus air massflow ratio) of two inlets, one having a lower performance, which may be caused by an angle of attack. Both curves show a supercritical range, a small stable subcritical range, a drop caused by unstable operation and a pressure increase at reverse flow.

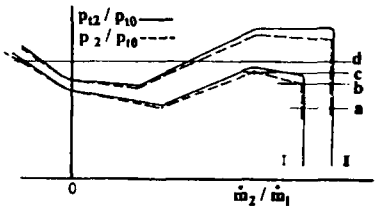

Fig. 2 Individual inlet characteristics (total - and static pressure ratio).

To measure the operation at reverse flow, we have conducted tests, in which we have throttled the mass flow down to zero and then have led additional air at the rear into the inlet, in order to cause reverse flow.

At the air duct entrance section the static pressure for each inlet can be determined (Fig. 2, dashed line). According to the assumption of constant static pressure at the entrance section, the operation points of the single inlets can be found out by following a line of constant pressure. At low pressure ratios (line a) both inlets operate supercritically.
The total massflow is

$$\dot{m}_3 = \dot{m}_{2(I)} + \dot{m}_{2(II)}$$

To determine the total pressure ratio, the mixing losses of the different flows have to be considered.
If the critical pressure ratio of inlet I is exceeded (line b), the inlet I operates subcritically near to the stability limit (line c). By a further increase of the pressure a solution is only possible, if inlet I operates at reverse flow (line d). In this example the operation point of inlet I jumps from the last stable point to reverse flow.

To find out the characteristics of the total system, besides the pressure condition the flow condition of the choked nozzle has to be fulfilled:

$$\dot{m}_3 = p_{t3} \cdot A_4/c^*$$

For constant nozzle areas this gives straight lines. The inclination of these lines increases for decreasing nozzle areas (Fig. 3 b dashed lines).
In a ramjet combustor these lines are equivalent to different fuel mass flows.

To demonstrate more clearly the various modes of inlet matching, we assume idealized individual inlet characteristics of the four inlets, shown in Fig. 3 a. These characteristics are typical for a 4- inlet configuration in x-orientation at angle of attack. Different from the common presentation of inlet characteristics the static pressure at the entrance section of the individual inlet is used. Diagram Fig. 3 b shows the corresponding characteristics of the total system. Starting at point A, all inlets operate supercritically. If the maximum pressure ratio of the worst performing inlet is exceeded (B), the next possible solution is point (C), where inlet I operates at reverse flow. Further throttling increases the pressure ratio up to the critical point of inlet II at point (D). At point (E)

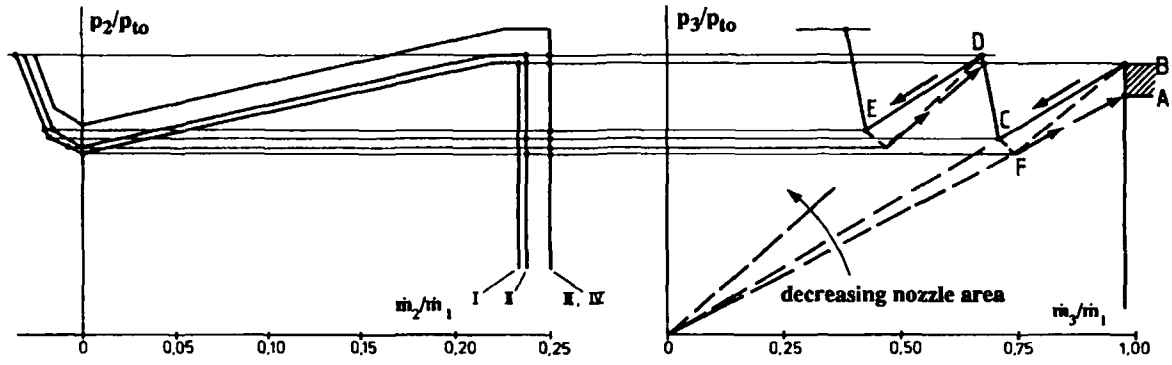

a) individual inlet characteristics

b) total inlet characteristic

Fig. 3 Typical individual characteristics of a 4-inlet system at angle of attack and resultant total characteristic

two inlets (I and II) operate at reverse flow.

Upon opening the nozzle the system follows a different operation scheme. Following back the individual characteristics the pressure reaches its minimum. In the total characteristics this corresponds to operation point (F), where one inlet operates near zero massflow, while the others operate at supercritical conditions. If we follow the line for constant nozzle area we arrive at point (A). This means, that there are two solutions, one with reverse flow of one inlet, one with 4 inlets in supercritical operation. This operational mode can only be changed when the pressure decreases below point (A).

This means, if we have nozzle areas between point (A) and (B) or equivalent conditions in the ramjet combustion chamber, the following can happen:

The engine operates between point (A) and (B) in the supercritical range. Upon a short distortion, caused by an exceeded angle of incidence, one inlet reaches reverse flow. The reverse flow remains after this disturbance at normal incidence. Only when the operation point falls below point (A) the reverse flow will stop. Therefore it is important for a ramjet with multiple inlets to find out whether any operational conditions may fall into this regime of hyteresis.

The diagram Fig. 4 shows test results of a configuration with 4 half axisymmetrical inlets at Mo = 2.5.

To induce an operation with reverse flow, the boundary layer bleed sections of the inlets were closed, so that the stable range of the single inlet became very small. The mass flow in each duct was determined by venturi nozzles. Massflow measurements at certain operation points indicated, that one inlet after the other ran into reverse flow.

Fig. 5 shows test results with a measured hysteresis. The test results belong to a test arrangement of four axisymmetrical inlets, installed for semi-free-jet tests with a ramjet at Mo = 2.1. At the beginning of the tests the boundary-layer bleed was blocked incidently, with the result, that the desired pressure recovery was not reached and two inlets ran into reverse flow. Only when the nozzle area was nearly at its maximum, all inlets returned to normal flow

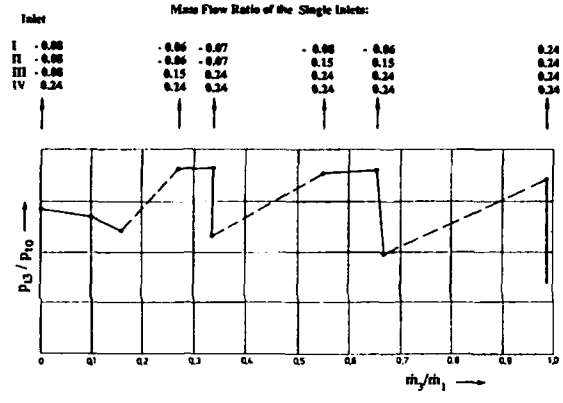

Fig. 4 Characteristic of a 4-inlet configuration with a small stable range of the individual inlet. (negative values indicate reverse flow)

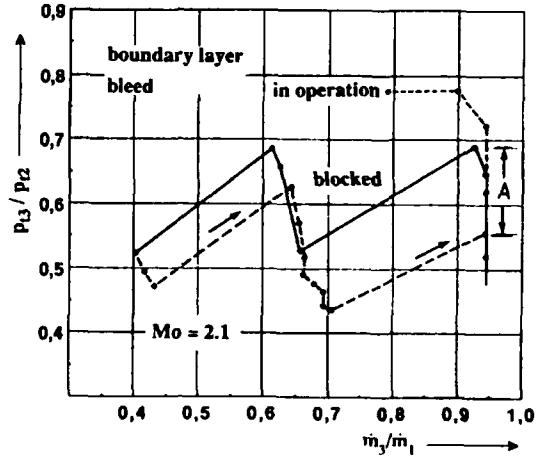

Fig. 5 Characteristics of a 4-inlet configuration measured at semi-freejet tests. (A = range in which reverse flow may occur)

With boundary layer bleed in operation, the strong pressure drop was suppressed and up to the measured subcritical point reverse flow did not happen (Fig. 5 dashed line).

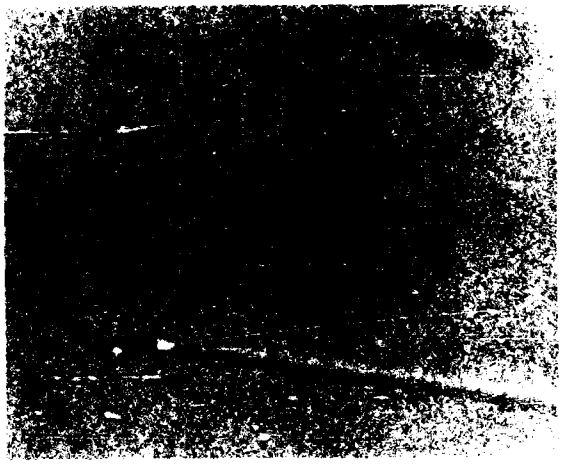

Fig. 6 Ram rocket free flight test EFA
The flash at the inlet indicates reverse flow

Reverse flow is not only a phenomenon of wind tunnel tests, as the photo (Fig. 6) shows, which was taken during free-flight testing of the ram rocket test missile EFA. Its four half axisymmetrical inlets were designed to have wide stable subcritical range up to 8°angle of incidence. By incorrect separation from the tandem booster, the missile got a lateral push inducing angles of incidence of approximately 30° at the beginning of the cruise phase. Caused by the pressure recovery drop reverse flow occurred in one or two inlets as to be seen by the flash coming out of the inlet for some milliseconds. Due to the stable inlet characteristics normal flow was restored at smaller incidence.

A method to avoid the sudden transition to reverse flow is to provide a high velocity in the section where the single ducts enter the common chamber. This reduces the static pressure level at critical operation and an increasing slope of the subcritical branch of the chracteristic can be obtained (Fig. 8).

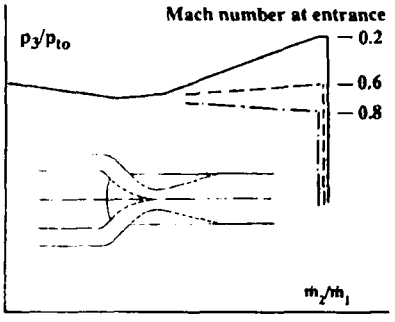

Fig. 7 Influence of increased entrance Mach numbers on the static pressure inlet characteristics

We have run windtunnel tests with a 4-inlet system applying different Mach numbers in the mixing region. The test results, Thus the worst performing can meet the critical pressure of the other inlets at subcritical operation forcing them into subcritical operation, too.

Fig. 8, show, that with increasing mixing Mach number the saw-tooth shape of the curves is smoothed. The individual inlet mass-flow was not determined, but there have been indications that no reverse flow occurred at M = 0,8 and all inlets operated at similar subcritical conditions. The disadvantage of the lower critical pressure recovery can be reduced by an efficient diffuser after the entrance section. However, in several cases of ramjet application this waste of volume can not be accepted.

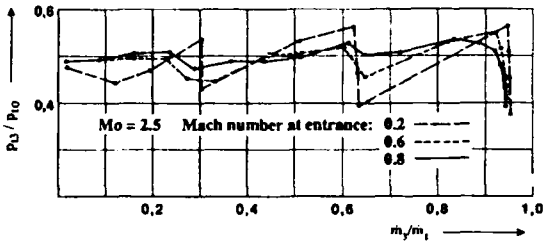

Fig. 8 Influence of increased Mach numbers at the exit of the air ducts

The previous considerations have shown, that depending on the decrease of the subcritical pressure recovery and the difference of the individual inlet pressure levels the following can happen:

- the stable operating regime of the multiple inlet system is reduced compared to the conditions of the single inlet;
- in the subcritical regime reverse flow can occur as sudden phenomenon;
- even the supercritical branch can be affected by a range of hysteresis. If the engine uses this part of the inlet characteristic, reverse flow once established remains, even when the responsible disturbance has disappeared.

According to our experience all methods to damp these phenomena, as for example to avoid pressure drop in the subcritical branch, lead to lower total pressure recovery. Compared with the advantages of a higher supercritical margin this gain of stability is rather doubtful.
Consequently, during design and development of the single air intake we try

- to reduce the sensitivity against angle of incidence.
- to avoid pressure drop at the beginning of the subcritical branch, for example caused by Dailey-instability;

Concerning the inlet integration it has to be considered, that the intake at the position with the highest sensitivity to incidence limits the maximum pressure recovery, and that a high pressure recovery of the other inlets has no positive influence.

3. INVESTIGATED CONFIGURATIONS

3.1 Four Side Mounted Axisymmetrical Intakes

In Germany the predevelopment of a solid propellant ramrocket for an anti-ship missile led to investigations of a configuration with four axisymmetrical cone inlets.

To meet the requirement of high lateral "g" load maneuvers without loss of speed a high pressure recovery at incidence was necessary.

The angle of incidence had to be limited to about 6° to ensure that the increasing drag can be compensated by engine thrust. The requirement of a long range at high cruise velocity induced a high propulsion mass. In order to save propulsion mass it was necessary to use inlets with a very low structural weight. Therefore axisymmetrical cone-inlets were chosen instead of ramp inlets.

The design of the single inlet was influenced by the experience with multiple inlet systems. Therefore the need for a certain stable subcritical range of the individual intake and a low sensitivity to incidence have been important design criteria.

The windtunnel tests started with measurements of a nearly full-scale isolated inlet model. The tests were carried out approximately with the original flight Re-number.

Fig. 9a shows the geometry of the basic wind tunnel model. The inlet design featured a halfcone angle of 25° and an internal contraction of 5 %. In the first step, a boundary layer

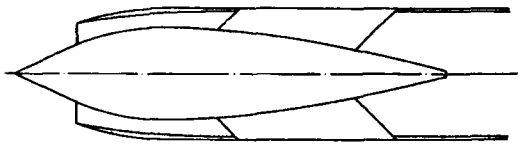

a) Single cone inlet, $\theta_c = 25°$

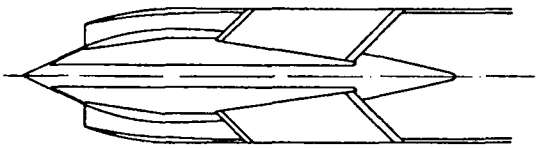

b) Single cone inlet with boundary layer bleed at the cone surface ($\theta_c = 25°$)

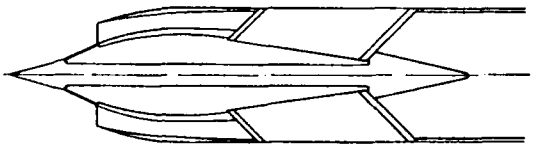

c) Double cone inlet with boundary layer bleed at the cone surface ($\theta_c = 15, 25°$)

Fig. 9 Geometry of the investigated axisymmetrical inlets

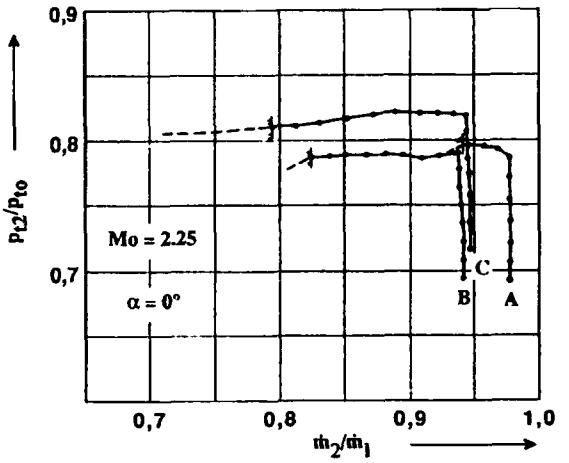

Fig. 10 Investigated axisymmetrical inlets, at zero incidence
A: single cone;
B: single cone with boundary layer bleed;
C: double cone with boundary layer bleed

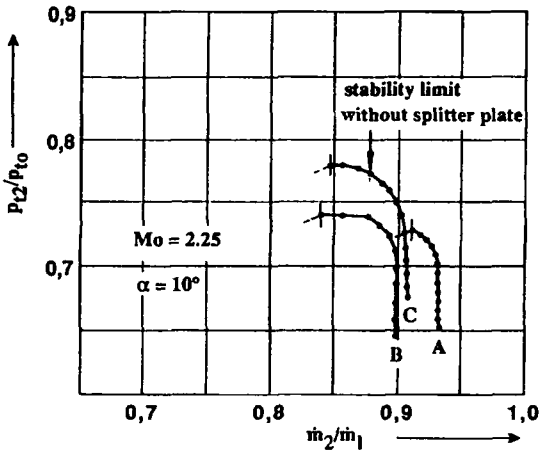

Fig. 11 Investigated axisymmetrical inlets at incdence
A: single cone;
B: single cone with boundary layer bleed;
C: double cone with boundary layer bleed

bleed was not provided. The demonstrated test results were measured at a Mach number slightly lower than the nominal shock on lip Mach number of 2.3.

According to a missile incidence angle of $\alpha = 6°$the inlet incidence sensitivity during the isolated inlet tests was investigated up to $\alpha = 10°$ because of a higher local angle occurring in the integrated configuration. The measured pressure recovery at $\alpha = 0°$ (Fig. 10) was found to be high and acceptable even at incidence (Fig. 11). However, the stable range was relatively small. Therefore as a next step a boundary layer bleed was installed.

To avoid a pressure decrease caused by Dailey Instability [8] a perforated bleed area was provided on the external cone surface (Fig. 9b) [4], [5]. The bleed air was led through the centerbody and channels in two struts. A rather high bleed

The measured inlet-characteristics (Fig. 10, 11) exhibited no gain in pressure recovery, but the stable range was increased. Theoretical considerations [6] and Schlierenphotos showed, that the shear layer enters the inlet at the stability limit. This is caused by the intersection of the oblique and normal shock at subcritical operation.
Inlet instability induced by this slip-line is called Ferri-Instability [9]. With respect to this problem a double cone inlet was designed (Fig. 9c). Here the intention was to keep the slip-line of the first oblique shock outside the captured flow over a wide range of the subcritical regime. Only the weaker slip-line of the second oblique shock was allowed to enter the cowl.
The Schlierenphotos Fig. 12 show the shock pattern at supercritical operation, at subcritical operation with a relatively forward positioned shock and at an incidence angle of 10°. At subcritical operation the two slip-lines can be identified clearly.
The pressure recovery was increased (Fig. 10) by the double cone and a higher internal compression. The inlet was stable down to a massflow ratio of 0.78. At lower ratios a high frequency buzz was initiated with growing amplitude but without strong decrease in pressure ratio. At incidence of $\alpha = 10°$ (Fig. 11) an additional gain in pressure recovery and stability could be obtained by a splitter plate, which separated the windward and leeward flow within the bleed duct (Fig. 9 c). Because of a smaller bleed area at the double cone inlet the loss of mass flow by boundary layer bleed is reduced, but is still too high concerning the resulting drag. Therefore the influence of different perforated surfaces and reduced bleed rate was investigated.

Fig. 13 shows the measured maximum pressure recovery for different types of perforation and bleed rates. The installation of the boundary layer bleed leads to an improvement of pressure recovery. The tendency of decreasing pressure recovery

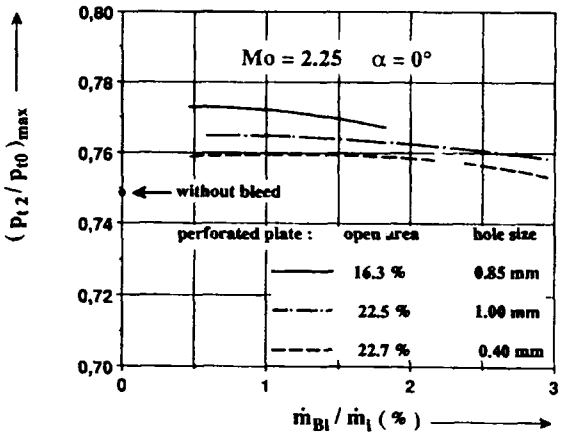

Fig. 13 Influence of different bleed surfaces and the bleed rate on the maximum pressure recovery

at higher bleed rate can be explained by the severe distortion of the cone flow caused by the bleed flow, resulting in a slightly higher flow Mach number. It is surprising, that the plate with the smaller holes shows inferior results, though the percentage of the open area is equal. Perhaps the different production methods - punched plate or perforation by electronic beams - may have an influence. Fig. 14 shows, that with a reduced bleed rate the increase in pressure recovery is combined with a decrease of the stable range at angle of attack.

Another effect which has to be considered is the drag, induced by the boundary layer bleed. Especially the suction through a perforated plate, leads to a relatively high loss of total pressure in the bleed flow. The measured pressure loss for different perforated plates is shown in Fig. 16. At the maximum bleed rates the flow in the holes is choked.

$\alpha = 0°$
supercritical operation

$\alpha = 0°$
subcritical operation

$\alpha = 10°$
critical operation

Fig. 12 Schlierenphotos of the double-cone inlet, Mo = 2.25

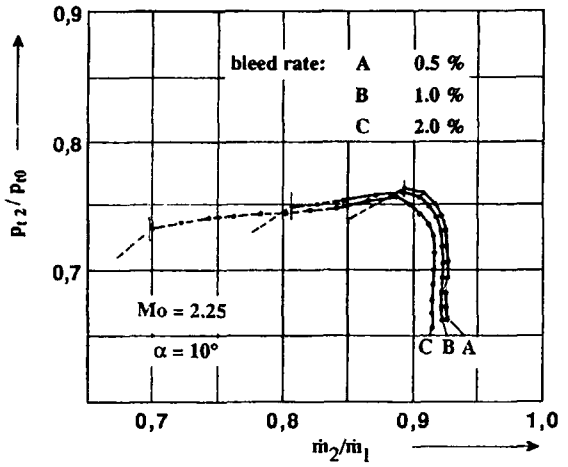

Fig. 14 Double-cone inlet, influence of the bleed rate on the stable subcritical range

The drag produced by a boundary layer bleed is primarily caused by the impulse loss in the bleed flow. With some simplified assumptions the induced drag can be estimated as a function of total pressure loss in the bleed flow [10]. The corresponding bleed drag coefficients for different bleed flow exit angles can be taken from Fig. 16. Measured values are 20 - 25 % higher [11] compared to these calculated curves.This deviation may be explained by the tolerances of the measuring devices. We believe that drag coefficients of $c_{DBl} = 1.2 - 1.5$ are realistic.

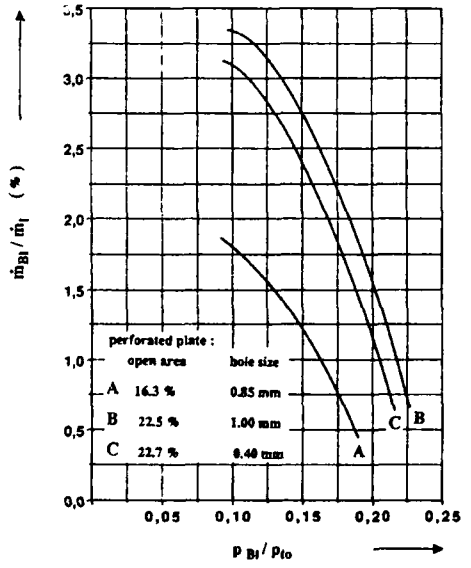

Fig. 15 Measured pressure loss in the bleed chamber for different perforated plates

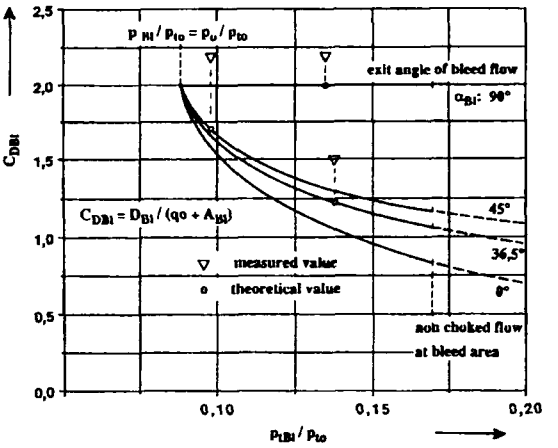

Fig. 16 Bleed drag coefficients for different bleed flow exit angles upon the bleed pressure losses [11].

The optimal bleed rate has to be selected with respect to pressure recovery, stability limits and induced drag.
Integrated windtunnel tests are usually run with scaled models. In our case, the tests were conducted in the 60 x 60 cm trisonic windtunnel of the DLR in Cologne. Here, a scale of 1 : 3.5 was possible allowing an inlet diameter of about 30 mm.

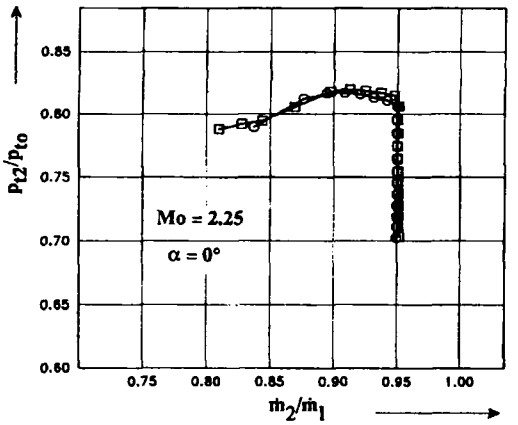

Fig. 17 Test results of two identical double-cone inlets (small scale, 30 mm diameter)

To obtain four equally performing individual inlets including boundary layer bleed device a very precise method of manufacturing was necessary. Tolerances of 1/10 mm in the inlet geometriy caused significant differences of the inlet characteristics. After some corrections we obtained a good equality of the four inlets. Fig. 17 shows test results with two of those inlets. Nevertheless the pressure recovery differs only little. The maximum pressure recovery compares well to the full scale test results.

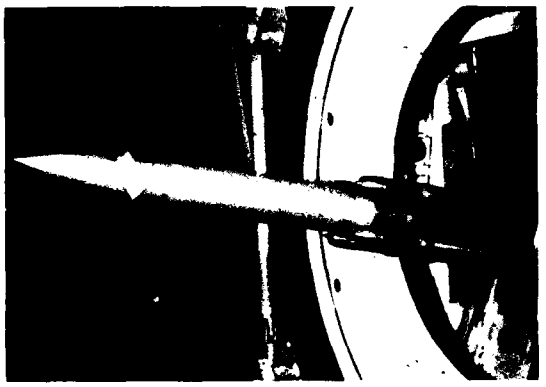

Fig. 18 Windtunnel model with four double-cone inlets

In the 4-inlet windtunnel model the inlets are mounted at a station of l/d = 7.3. To reduce pressure losses the air mass flow is led into the common chamber at a small entrance angle and avoiding sudden expansion. The windtunnel model with four double-cone inlets is shown by the photo Fig. 18. The bleed area on the cone and the slots of the bleed exit can be recognized.

As a first step a single mounted inlet was tested in different roll positions. The test results for a roll angle of $\varphi = 45°$ corresponding to a x-position are plotted in Fig. 19. Compared with the isolated inlets (Fig. 17) the pressure recovery drop at $\alpha = 0°$ can be explained by losses induced by the missile nose shock and internal flow. The small stable range is

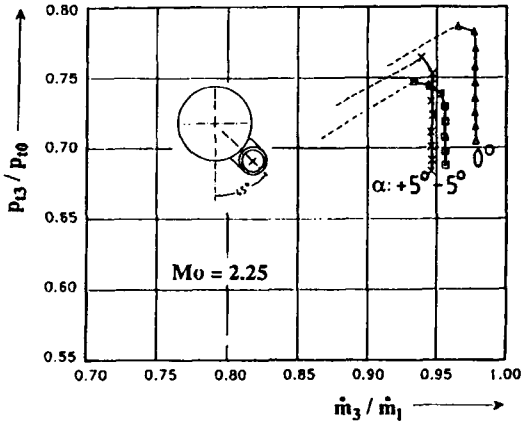

Fig. 19 Test results with one integrated inlet (double-cone inlet, l/d = 7.3, h/δ = 1.1)

caused by a reduced bleed rate. In this case the height of the boundary layer diverter was h/δ = 1.2. The investigated ratios varied from h/δ = 0.9 to 1.3. The ratio should be h/δ > 1.0 in order to ensure an acceptably stable operation under unfavourable conditions.

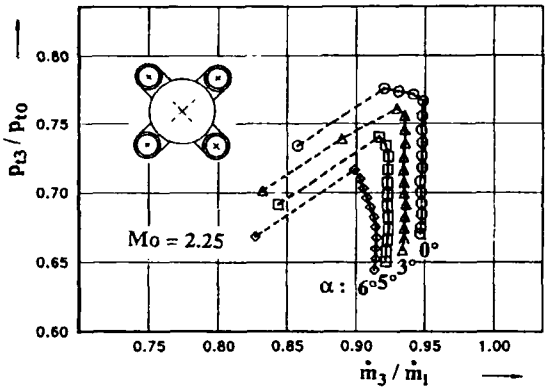

Fig. 20 Test results with four integrated inlets (double-cone inlets, x-position, l/d = 7.3, h/δ = 1.1)

Fig. 20 shows the test results with four inlets in x-position. Caused by a higher bleed rate the airflow ratio is reduced while the inlet stability is increased at $\alpha = 0°$.

At $\alpha = 5°$ there is no stable subcritical operation. A comparison with the results of Fig. 19 at $\alpha = +5°$ and $\alpha = -5°$ shows, that the inlet position with the lowest pressure recovery limits the overall pressure recovery.

Reasons for the low pressure recovery at $\alpha = 6°$ are the growing boundary layer thickness and the separation of vortices on the lee ward side of the forebody.

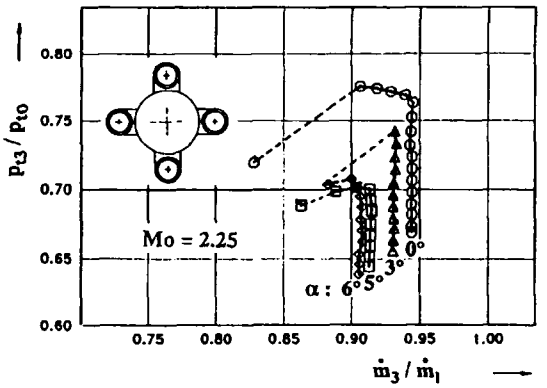

Fig. 21 Test results with four integrated inlets (double-cone inlets, +-position, l/d = 7.3, h/δ = 1.1)

Fig. 21 presents the sensitivity to angle of attack of inlets installed in +-position. At small incidence the decrease of pressure ratio is stronger than for the case of x-position, whereas at $\alpha = 6°$ the pressure ratio has a tendency to rise.

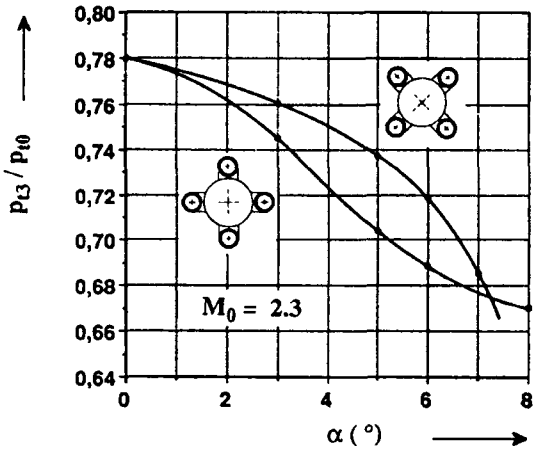

Fig. 22 Incidence sensitivity of a 4 double-cone inlet configuration in x-position and +-position

The different incidence sensitivities in x- and +-position are shown in Fig. 22. Other tests applied have demonstrated, that at higher incidence angles (α = 8° - 10°) the +-position is superior to the x-position, but in both cases the low level of pressure recovery does not allow an engine operation with sufficient thrust for maneuvering. Therefore in the interesting range of smaller incidence angles, the x-position is preferable.

3.2 Four Side-Mounted Ramp Inlets

A study of a small, low-cost anti-ship missile, powered by a solid propellant ramrocket led to investigations of a configuration with four side-mounted ramp-intakes.
The missile had a wingless design to allow lower mass, lower drag and facilitated handling. Therefore an increased angle of attack at maneuvers with high lateral acceleration had to be assumed.
With respect to this requirements the ramp type inlet system offers two advantages:

- The rectangular fairings of the ramp inlets produce an acceptable aerodynamic lift at incidence, thus partly compensating the lack of wings.
- According to the experience of ONERA [7] the inverted integration of ramp inlets reduces the sensitivity to incidence up to 8° or 10°.

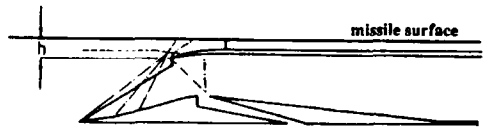

Fig. 23 Installation of inverted ramp inlets

Inverted integration means that the compression ramp of the inlet is mounted opposite to the missile body (Fig. 23).

This position often leads to interference problems between inlet and missile surface:

- In the region where the oblique shocks from the ramp or the cowl-lip meet the missile wall, the pressure gradient can thicken or detach the wall boundary layer.
- The strong pressure rise of the expelled normal shock often induces a boundary layer separation.
- The compression between inlet cowl and missile wall can produce a choked flow with a normal shock.

The design of the invidivual inlet took care of these problems.
Corresponding to the flight regime of the missile, the inlet had a shock on lip Mach number of Mo = 2.15. The external compression was generated by three ramps with a maximum deflection angle of θ_T = 18° (Fig. 24). The three oblique shocks were focussed on the lip at Mo = 2.15. Considering the interference problem between inlet and missile, the lip angles of the cowl should be dimensioned as small as possible. But the requirement of a low swallowing Mach number of Mo = 1,9 limited the option of a small lip angle. Consequently a relatively high internal lip angle of θ_L = 13°had to be accepted.

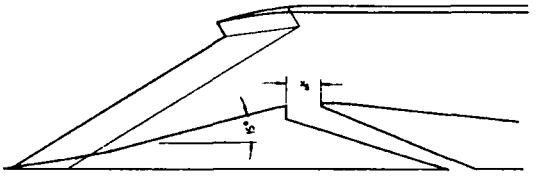

Fig. 24 Contour of the modified 3-ramp inlet (shock on lip Mach number 2.15, internal compression 5 %)

A boundary layer bleed was installed to improve the pressure recovery and to keep the normal shock inside the inlet for a certain part of the subcritical regime. In several wind tunnel tests the bleed rate was optimized by variation of the slot width (Fig. 25). The bleed rates (0,8 - 1,5 %) were evaluated by comparing the massflow ratios of tests with and without boundary layer bleed (x_s = 0.) The gain of pressure recovery by the bleed is also illustrated by Fig. 25.

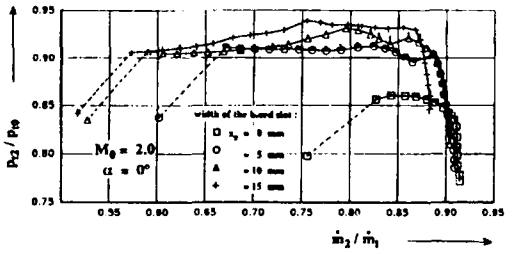

Fig. 25 Isolated tests of ramp inlet, influence of the bleed rate on inlet performance

The isolated tests were conducted with an inlet model having a capture area of 50 x 50 mm. For the integrated tests the scale was reduced to an inlet size of 30 x 30 mm. Fig. 26 shows the windtunnel model with one integrated intake. The airducts of the other three inlets are closed. The tests with this one inlet model in different roll positions and at different incidence angles up to 8° gave a good illustration of the problems and disclosed the potential performance of the multiple inlet configuration.

Fig. 26 Windtunnel model with one installed inlet

In accordance with the missile design the inlet was mounted at a station of l/d = 6.5 downstream the nose. The boundary layer thickness had been calculated as δ = 6.6 mm. The diverter height h, defined as the distance between inlet lip and body surface (Fig. 23) was varied from h/δ = 1 to 2.

Based on the inlet height the Reynolds number of the tests was Re = 2 10^6.

The first tests, conducted at α = 0°, revealed unexpected results. Compared to isolated tests, the measured inlet characteristics (Fig. 27) showed a reduced massflow ratio. It could be recognized from Schlierenphotos, Fig. 28 (inlet in supercritical operation: (a) isolated test, (b) integrated test), that in the integrated case the reduction is due to a normal shock spillage,which is generated by the interaction with the missile wall.

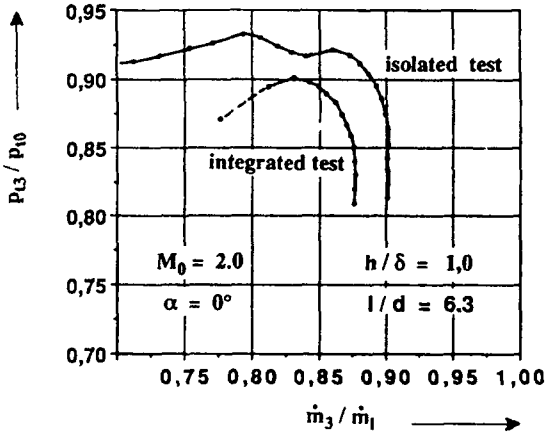

Fig. 27 Inverted ramp inlet, comparison of isolated and integrated tests

An increase of the diverter height moved the shock towards the lip and shock swallowing occurred at h/δ = 2.0. At these tests the massflow ratio slightly increased, whereas the pressure recovery (at α = 0°) was not influenced.
To investigate this problem a lot of windtunnel tests were carried out .
Measurements, where the missile wall was simulated by a short tube, have shown, that the boundary layer thickness is a less important parameter. Therefore we have done a great portion of the investigations with this simulated missile surface. During these tests we modified the external and internal contours of the inlet:

- the external cowl lip angle was reduced;
- the maximum ramp angle as well as the lip angle were reduced;
- the internal contraction was reduced, in order to increase the minimum Mach number at the inner surface of the cowl;
- the sharpness of the leading edges of lip and sidewalls was increased;

a) isolated test

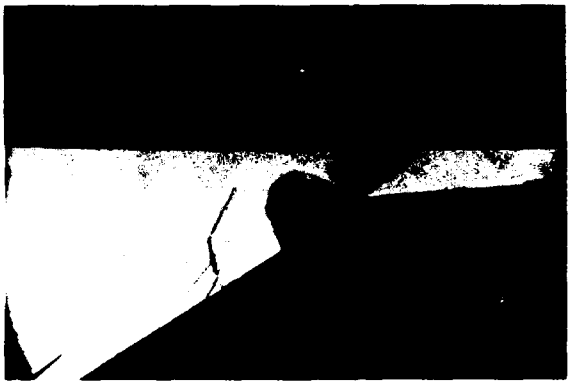

b) installed inlet, h/δ = 1.1

Fig. 28 Schlierenphotos of ramp inlets, comparison of shock pattern of isolated and integrated test (Mo = 2.0)

With these modifications the disappearance of the normal

shock was shifted to smaller diverter heights.
The greatest influence was measured with a smaller ramp and lip angle. With a modified inlet, with a maximum ramp angle of $\theta_r = 12°$ and a lip angle of $\theta_L = 9°$ the interference effect did not occur down to a diverter height of $h/\delta = 1.1$. However, this modification caused a loss of 5 % inlet performance. Therefore as a compromise we have chosen the inlet contour with a maximum ramp angle of $\theta_r = 15°$.

The reduction of interference effects by these modifications is evident from Fig. 29. The two Schlierenphotos show the different position of the normal shock measured with the original and the modified inlet geometry, both having a diverter height of $h/\delta = 1.2$.
A comparison of the intake performances is given in Fig. 30. The reduction of the interference effects results in an increased massflow ratio.

The design of the wind tunnel model allowed various positions of the inlet ramp. Thus it was possible to investigate the incidence sensitivity in conventional (ramp on side of body) and inverted position.

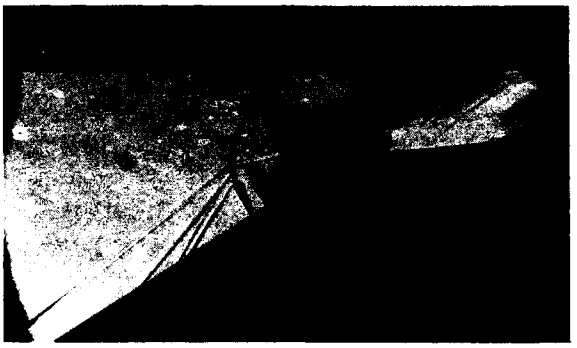

a) original geometry

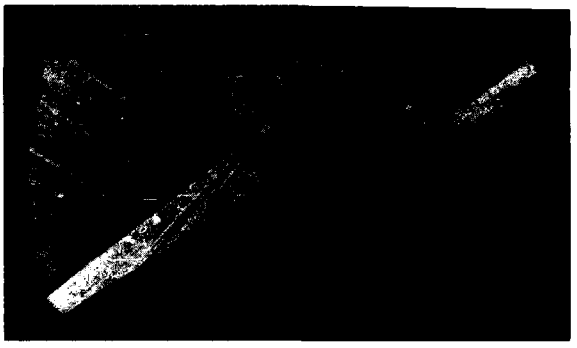

b) modified geometry

Fig. 29 Schlierenphotos of ramp inlets, effect of the modified inlet contours (Mo = 2.0, h/δ = 1.2)

Fig. 31 shows the effects at $\alpha = 8°$. In the conventional position the inlet on the windward side ($\alpha = +8°$) takes advantage of the precompression of the forebody and of the fact that the crossflow component increases the effective ramp angle.
The leeward inlet operates in an expanded flow (increased Mach number). The cross flow component reduces the effective ramp angle. Therefore the performance of the windward

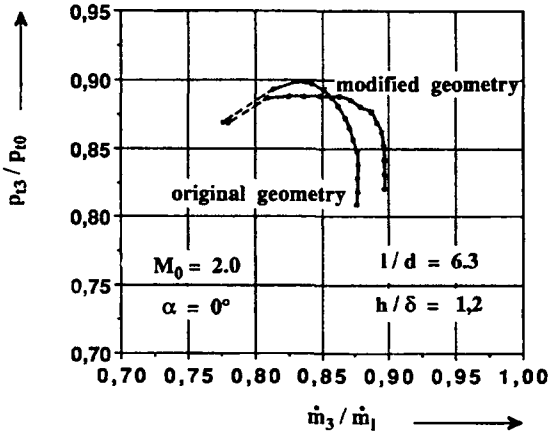

Fig. 30 Inverted ramp inlet, influence of the modified geometry at integrated tests

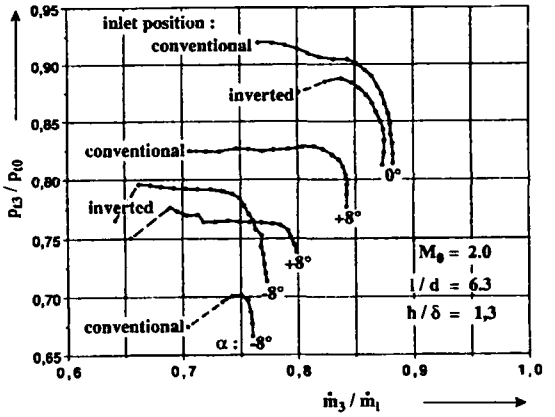

Fig. 31 Inverted ramp inlet, tests with inlet in conventional and inverted position

and leeward inlet differs strongly.
In the inverted position the effect of the local cross flow on the ramps is vice versa. Therefore in both positions the two effects compensate each other to a certain degree. This results in a smaller difference of performance between the two inlet positions. According to the rule of multiple inlet configuration, that the overall pressure recovery is equal to the lowest pressure recovery of the single inlets, the performance in the inverted position at $\alpha = 8°$ is nearly 10 % higher than for the conventional installation.

In order to reduce the inlet/wall interaction we have also investigated a precompression ramp, as known from investigations of ONERA [7] at Mo = 6.
We found out, that positive effects are sensitive to the distance (a) between precompression ramp and inlet lip and even to the ramp base angle (v) (Fig. 32) .

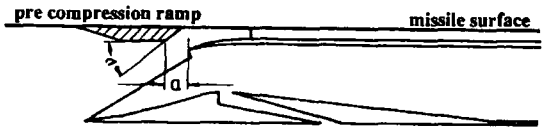

Fig. 32 Geometry of the pre compression ramp

The effects of the ramp at different incidence angles are shown in Fig. 33.
At $\alpha = 0°$ the reduced inlet/wall interference results in a higher pressure recovery at subcritical operation and an increase of stable range. At $\alpha = 8°$ the pressure ratio of the leeward inlet is slightly reduced. On the other hand the low pressure recovery of the windward inlet is significantly improved. The massflow ratio is increased, too. For a 4-inlet configuration this means an improvement in performance of 8 - 10 %.

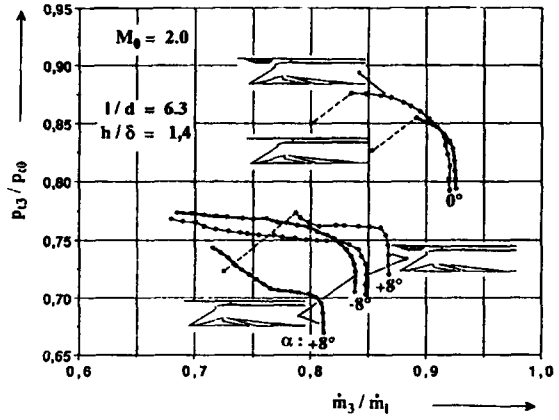

Fig. 33 Inverted ramp inlets, tests with and without pre compression ramp

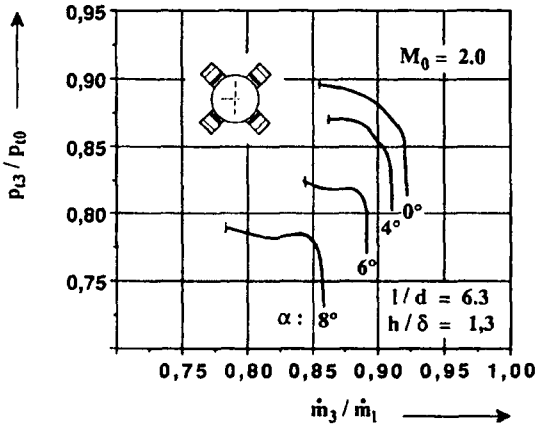

Fig. 34 Overall inlet characteristics calculated from the individual inlet tests

Unfortunately final tests with the 4-inlet system could not be performed due to limited funding. However, using the measured characteristics of the individual inlet in representative positions the performance of the multiple inlet system could be determined with acceptable accuracy.

In Fig. 34 the calculated total inlet characteristics of four inlets in x-position at Mo = 2.0 are presented. The high pressure recovery at $\alpha = 8°$ demonstrates the suitability of this inlet configuration for a cartesian controlled missile performing high "g" lateral maneuvers.

4. CONCLUSIONS

Many flight trajectories require a cartesian control mode for the missile. A configuration with four aft-intakes is most appropriate if the missile uses airbreathing propulsion. A system of multiple intakes having a common chamber induces an interaction of the inlets. The following effects have to be taken into account:

- the individual inlet with the lowest pressure recovery limits the overall performance;
- exceeding the limited angle of attack or fuel mass flow can suddenly cause reverse flow which may remain after the disturbance has disappeared.

To reduce this risks, it is necessary to avoid steep degression of the pressure recovery in the subcritical range or to provide sufficient supercritical margin.

For a missile with wings needing only moderate incidence for high "g" lateral maneuvers, a configuration with four axisymmetrical side inlets offers a high performance combined with low structural mass.
For missile configurations which require higher angles of attack, a configuration with four inverted ramp inlets may be the better solution. With this type of intake installation sufficient performance can be obtained up to angles of incidence of more than 8°.

REFERENCES

[1] C. S. Jell;
Air Intake Aerodynamics, AGARD-FDP-VKI Course on Missile Aerodynamics (1987).

[2] W.-D. Pohl;
Untersuchungen zum Betriebsverhalten von mehreren Lufteinläufen, die in eine Brennkammer münden.
MBB TN-RT31-16/76 (1976).

[3] E.-O. Krohn; K. Triesch;
Multiple Intakes for Ramrockets. AGARD CP 307 (1982).

[4] G. Jungclaus;
Analyse von Ferri- und Dailey -Instabilitäten bei Überschalleinläufen. MBB TN-AY75 17/88 (1988)

[5] G. Jungclaus; W.-D. Pohl
Neue experimentelle Ergebnisse zur Entstehung und Struktur von Ferri- und Dailey -Instabilitäten (Brummen) bei rotationssymmetrischen Überschalleinläufen. MBB TN-KY25-1/89 (1989).

[6] E.-O. Krohn;
Inlet Buzz in Ramjets and its Suppression.
Paper 8th ISABE (1987)

[7] G. Laruelle;
Missile Intakes. VKI Lecture Series on Intake Aerodynamics (1988).

[8] C. L. Dailey;
Supersonic Diffusor Instability. Journal of the Aeronautical Sciences, Vol. 22, No. 11 (1955).

[9] A. Ferri; L. M. Nucci;
The Origin of Aerodynamic Instability of Supersonic Inlets at Subcritical Conditions. NACA RM L 50 K 30 (1951).

[10] W.-D. Pohl;
Experimentelle Untersuchung zur Bestimmung des durch Grenzschichtabsaugung verursachten Widerstandes bei Überschalleinläufen. MBB TN-AE15-2/87 (1987).

[11] W.-D. Pohl;
Untersuchungen an invertierten Einläufen (I + II).
MBB TN-AY75-12/88, TN-KY25-12/90 (1990).

Aerodynamic Engine/Airframe Integration for High Performance Aircraft and Missiles

Review of the 69th Symposium of the Fluid Dynamics Panel
7. - 10. October 1991, Fort Worth, TX, US

P.W.Sacher*), W.Schmidt**)
Messerschmitt-Bölkow-Blohm GmbH
Aircraft Division
P.O.Box 801160
D-8000 Munich 60

ABSTRACT

This paper is a FDP contribution to the 79th symposium on "Airbreathing Propulsion for Missiles and Projectiles" being held from May 11 - 15, 1992 in St. Médard-en-Jalles, Bordeaux, France. It presents an overview of the main findings of the last FDP meeting during October 7 - 15, 1991 in Fort Worth, TX, US on the subject of the title of this review paper.

The meeting was structured in six sessions, **one of them having been organized and chaired in form of an invited session by PEP contributions.** Each session will be reviewed separately in this paper and conclusions (in some cases recommendations for future AGARD activities) are made based on the major outcome of the sessions including contributions and comments from the auditorium after the presentations or from the closing Round-Table-Discussion at the end of the meeting.

It has been clearly demonstrated, that the subject of the symposium is an highly interdisciplinary effort, which overlaps the terms of reference of both AGARD Panels, FDP and PEP to a large extend. This is specifically true for major components of the propulsion system like the air intake and the nozzle. Both experimental and computational techniques for analysis and design used during engine/airframe integration for all kinds of flight vehicles have been reported.

INTRODUCTION

This is the second FDP meeting focussed on the subject of aerodynamic engine/airframe integration. The preceding one was organized together with the AGARD Propulsion and Energetics Panel in May 1981. Due to the overall positive response to the first Symposium, realizing the tremendous progress in the related technical area and due to the raising need for more and more integrated design of civil and military aircraft and missiles in recent applications, this second symposium after 10 years seemed to be timely.

The aerodynamic engine/airframe integration of aircraft and missiles involves complex flows, highly influenced by viscous effects and, in most cases by aerodynamic interactions between the airframe and the propulsion system. This engineering task is considered to be a "Key-Problem" during the design phase of new flight vehicles of any kind. The continuing demand for highest efficiency in civil transport aircraft and the increase in performance and maneuverability for both missile and fighter aircraft development has led to an extensive increase of experimental and specifically CFD-related design efforts.

It is the aim of the symposium to review the state of the art in aerodynamic engine/airframe integration techniques reached at present time and to report on the progress which has been achieved during engineering project work in the past years. Because of the fact that engine/airframe integration has become a highly interdisciplinary challenge, both experimentalists and theoreticians have been invited to

*) Project Manager, Advanced Design Dept.
**) Director, Air Vehicle Engineering

contribute to the success of the meeting.

This conference was technically associated with several other activities within the AGARD community. So the AGARD FDP has organized in 1987-1990 WG13 on "Air Intakes for High Speed Vehicles", (AGARD-AR-270) and in 1985-1988 PEP WG18 on "Test Cases for Computation of Internal Flows in Aero Engine Components", (AGARD-AR-275). More recently PEP has arranged a symposium in May 1991 on "CFD Techniques in Propulsion Applications", (AGARD CP 510). It was decided to include at least the technical evaluations of this AGARD activities in the programme of this symposium. So PEP was invited to organize an "Invited Session" on "Engine Related Integration Problems", (Session II). The Programme Committee gratefully acknowledged the efforts of PEP and specifically the support given by **Prof. Leonhard Fottner, University of Neubiberg, GE**, who organized and chaired this session.

Statistics :
33 Papers (including three invited papers and four papers in an invited session) have been presented. Contributions to the meeting came from Belgium (1), France (7), Germany (10), Italy (2), The Netherlands (2), United Kingdom (9) and USA (9).

This symposium was structured into six sessions :

(I) Engine Integration for Civil Transport (10 papers)
(II) Engine Related Integration Problems (4 papers)
(III) Experimental Techniques used in Aerodynamic Engine/Airframe Integration (6 papers)
(IV) Aerodynamic Inlet/Airframe Integration (5 papers)
(V) Aerodynamic Nozzle/Airframe Integration (5 papers)
(VI) Aerodynamic Engine/Airframe Integration for Hypersonic Speed vehicles (3 papers)

Each session will be reviewed separately in this paper and conclusions (in some cases recommendations for future AGARD activities) are made based on the major outcome of the sessions including contributions and comments from the auditorium after the presentations or from the closing Round-Table-Discussion at the end of the meeting.

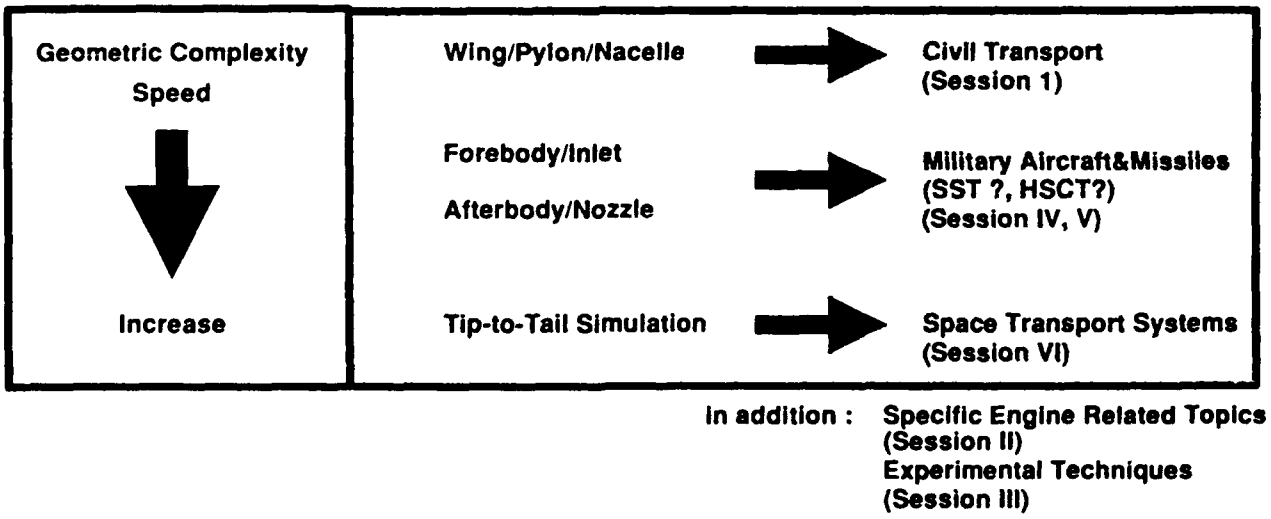

Fig. 1 Logic of the programme of the symposium on aerodynamic engine/airframe integration

As outlined in Fig. 1, there is some logic in the structure of the programme given by more and more complex applications.

The contributions specifically mentioned in this review will be referenced by the paper number, as to be found in the conference proceedings (AGARD CP 498).

SESSION I : ENGINE/INTEGRATION FOR CIVIL AIRCRAFT

The main objectives of this session can be summarized as follows :

(1) Survey of experimental test techniques for engine/nacelle/wing integration, [1]
(2) Survey of numerical prediction methods for engine/nacelle/wing interference effects, [3], [4], [5], [6], [7], [8]
(3) Integration effects of installed thrust reverser, [9], [10]

This has been a quite well balanced session. Both experimental investigations and theoretical work has been reported. The invited introductory paper, given by A.E.Harris [1], was an extremely detailed description of all major aerodynamic interference effects due to propulsion systems integration for civil and military aircraft at all speeds (see **Fig. 2** and **3** for a summary). The use of CFD for engine/airframe integration was reported in several papers and for different classes of flow models. In **Fig. 4** results obtained by van Beek/Piers/Oskam [6] demonstrate the usefulness of linearized potential flow codes ("Panel Methods") and in **Fig. 5** engine installation effects on the wing planform are shown by Godard/Jaquotte/Gisquet [4] predicted by a solution of the full potential flow equations.
As highest level of 3D CFD, solutions of the Euler equations, were demonstrated by Rossow/Ronzheimer, GE [5], see **Fig. 6**, Gippet/Fratello/Lecordix from France [3] and Naik/Chen/Su/Kao from US [7]. Two papers, [9] and [10], were dealing with the important aspects for civil transport aircraft of thrust reversing in flight and in ground effect.

In conclusion the session may be characterized as follows :

(1) Civil transport aircraft are dominated by **economic requirements.** Airframe/engine integration is important for
- second segment climb
- cruise
- thrust reverser interference

(2) In Europe well established testing techniques exist using **TPS for Turbo-Fan and Turbo-Prop simulation** in WT's, (TPS is facility equipment).
US industry prefers powered nacelles using pressurized air

(3) **CFD applications still rather limited** for cruise conditions
- No N.S. solutions
- Euler analysis [3], 85], [7]
- Still work using Panel [6] and full potential [4] methods

(4) CFD limited not only due to computing cost - to a large degree due to **mantime cost** (e.g. for grid generation)

(5) Many engineering efforts restricted to **simply adding pylon/nacelle/engine** to clean wing design

(6) **Wing design procedures** taking account the effects of propulsion systems installation are required

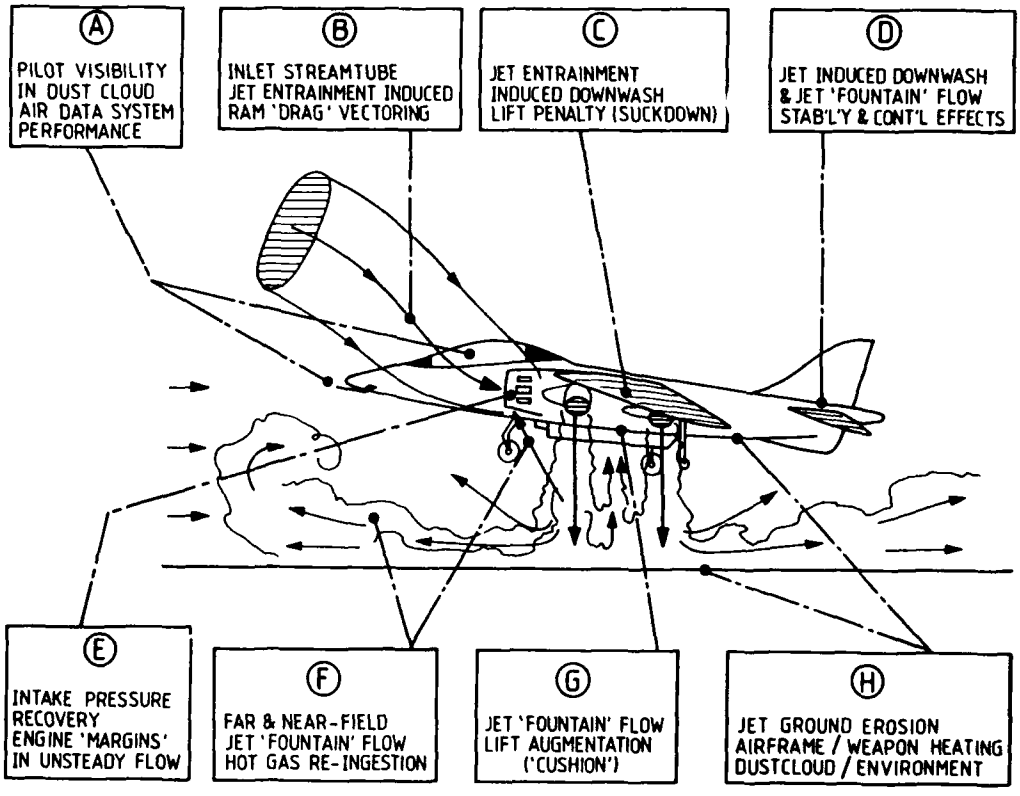

Fig. 2 **VTOL Engine/Airframe Interactions**

A.E.Harris : "Test Techniques for Engine/Airframe Integration", [1]

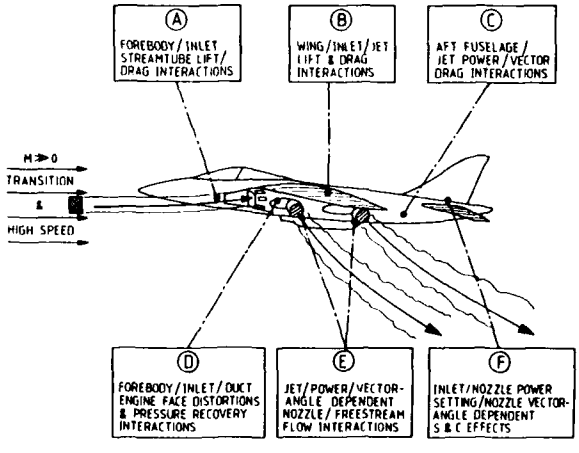

Aerodynamic Engine/Airframe Interferences for Military aircraft

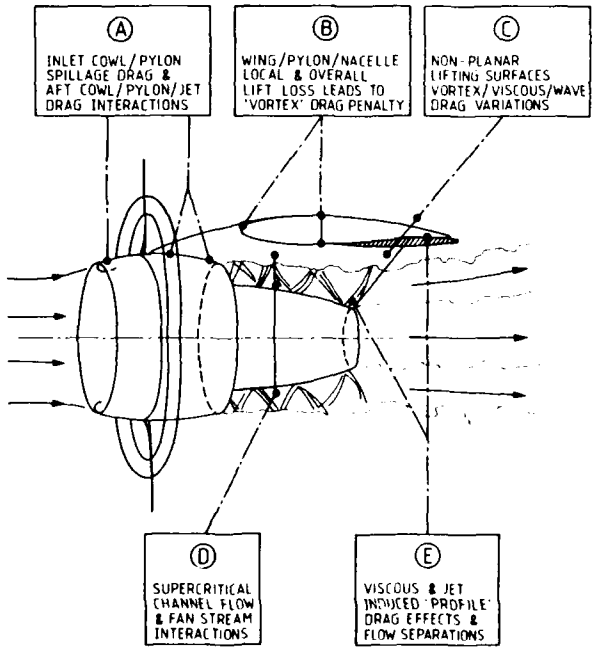

High Speed Integration Problems for a VHBPR Turbofan

Fig. 3 **Military and civil A/C engine/airframe interactions**

A.E.Harris : "Test Techniques for Engine/Airframe Integration", [1]

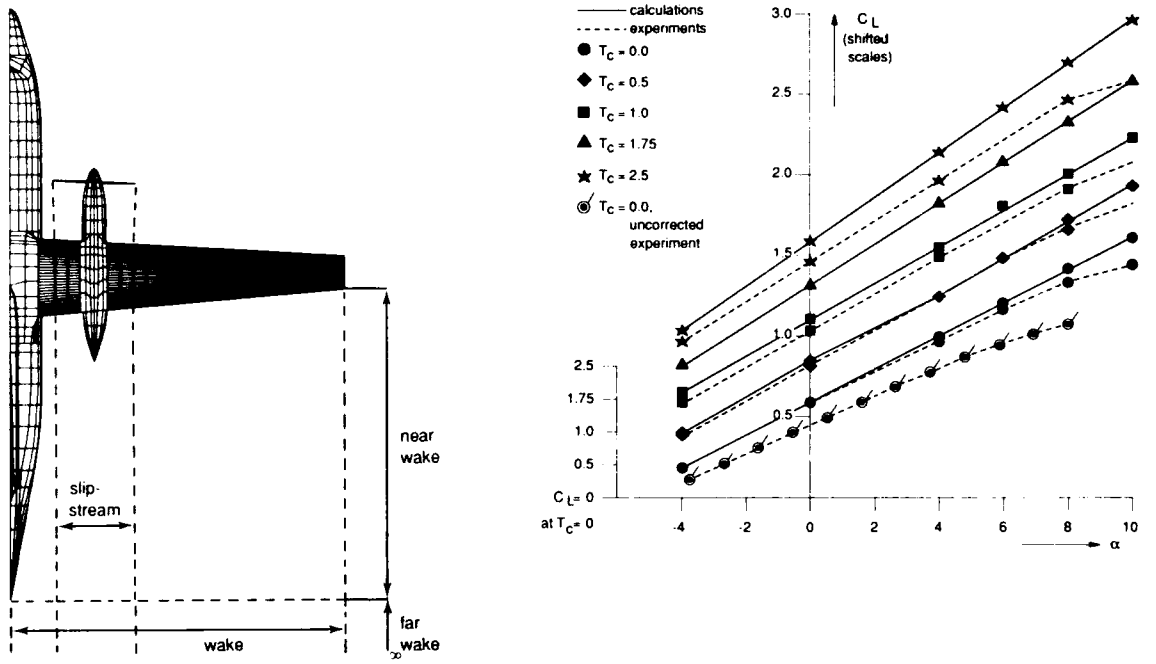

Fig. 4 **Use of potential flow codes (Panel Methods) for the prediction of propeller/wing interference effects**

C.M. van Beek, W.J.Piers, B.Oskam : "Aerodynamic Analysis of Slip-stream/Wing/Nacelle Interference for Preliminary Design of Aircraft Configurations", [6]

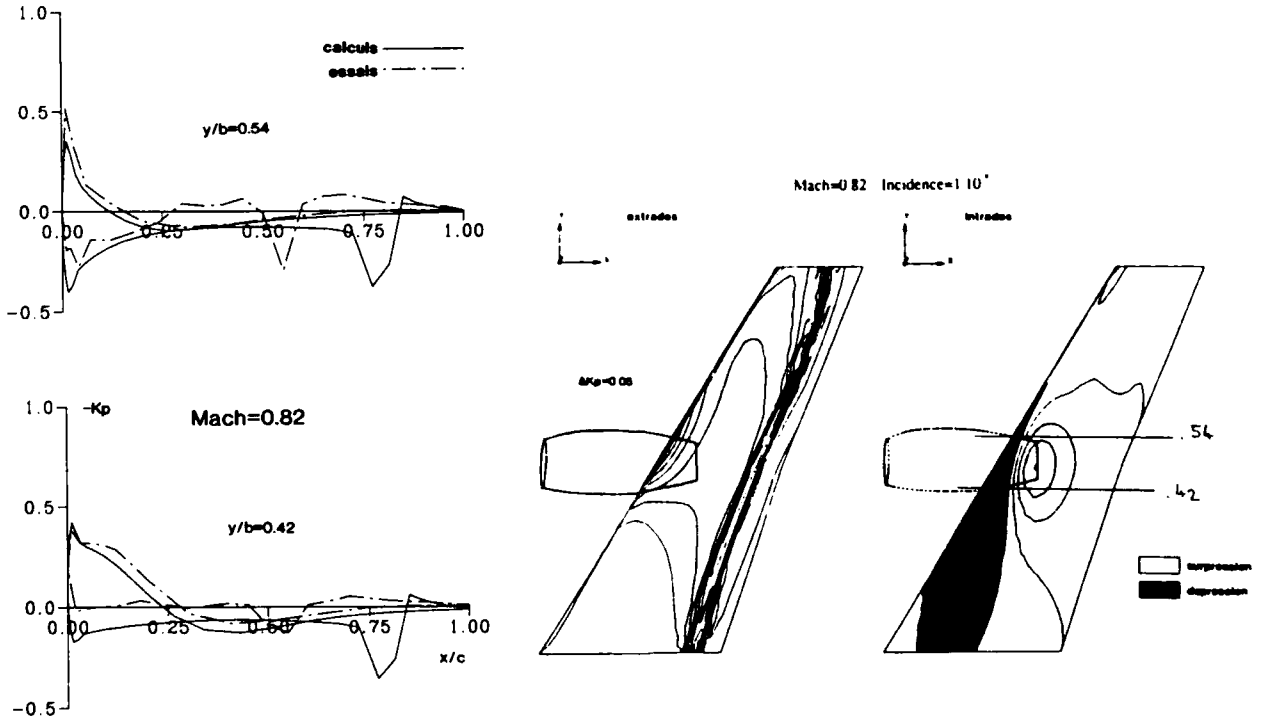

Fig. 5 **Prediction of engine installation effects using full potential flow solvers**

J.L.Godard, O.P.Jaquotte, D.Gisquet : "Detailed Analysis of Wing/Nacelle Interaction for Civil Transport Aircraft", [4]

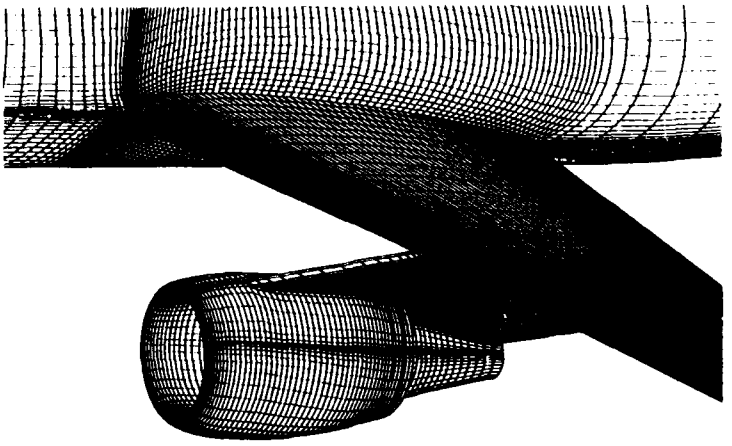

CFM-56 engine

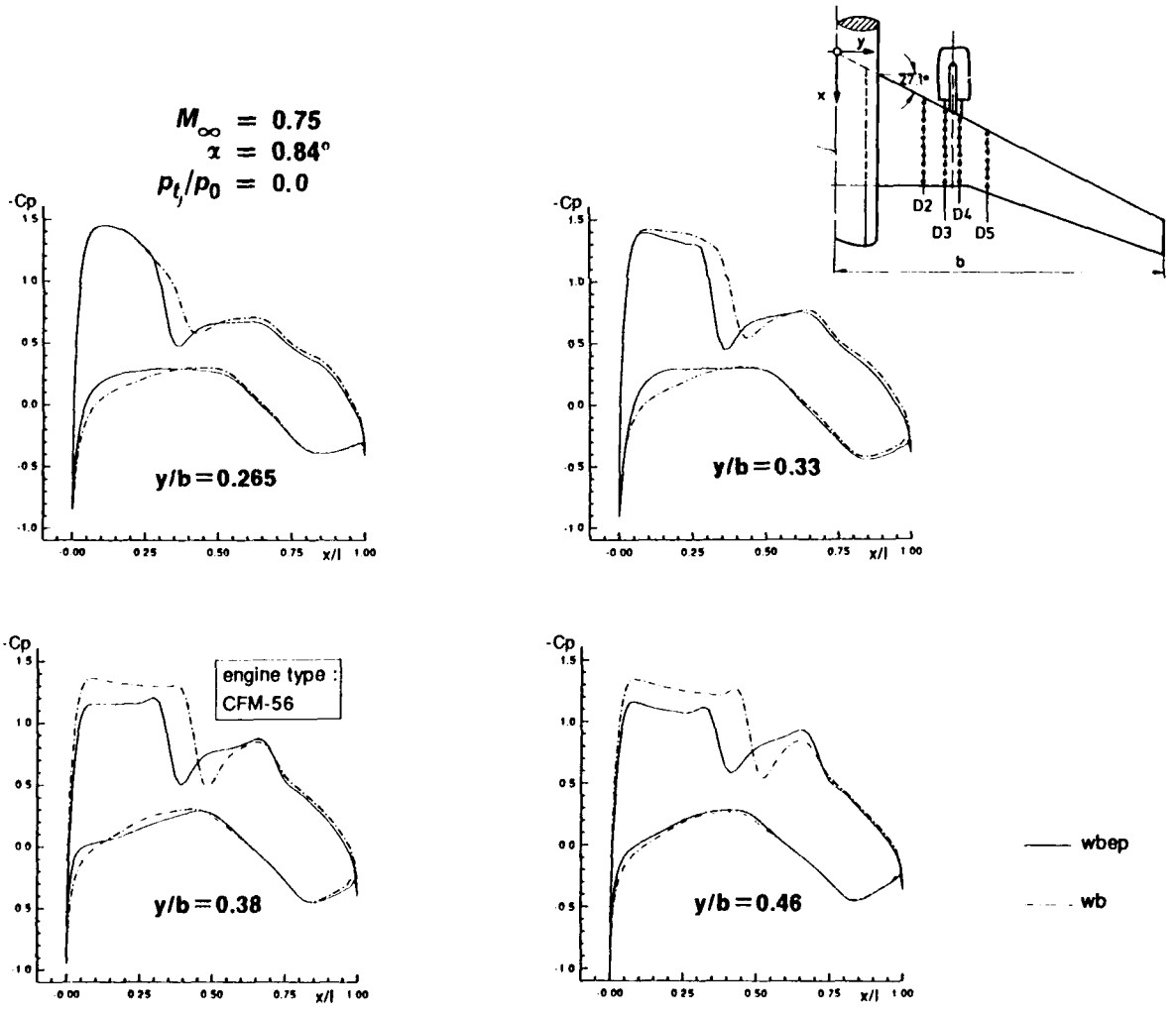

Fig. 6 **Mesh grid for wing(nacelle installation and pressure distribution for WB and WBEP configuration**

C.C.Rossow, A.Ronzheimer : "Investigation of Interference Phenomena of Modern Wing-Mounted High Bypass Ratio Engines by the solution of Euler-Equations", [5]

SESSION II : ENGINE-RELATED INTEGRATION PROBLEMS (INVITED PEP-SESSION)

The Session was chaired by L. Fottner from the PEP and all contributions came from this panel. The objectives of the session can be summarized as follows :

(1) Survey on PEP WG 18, "Test Cases for Internal Flows in Turbomachines", [11]

(2) Survey on PEP symposium "CFD Techniques for Propulsion Applications", [12]

(3) Intake - engine compatibility, [13], [14]

The WG18 has compiled an extensive experimental database on various test cases as L.Fottner [11] showed. The impression remains that a follow-on activity is needed and the question comes up whether the experimental data being available are sufficient for code validation or not.

The review from Ch.Hirsch [12] reports on the outcome of the PEP symposium Spring 1991 in San Antonio, US, on the subject of "CFD Techniques in Propulsion Applications". This Panel is very well informed on this event, so there is no need to go into details of this excellent presentation.

The remaining two papers dealt with the important effects of intake/engine compatibility. In **Fig. 7** the test apparatus and test instrumentation arrangement for the assessment of the flow field at the engine entry cross section is shown by Meyer/Pazur/Fottner [13]. Swirl distortion is generated by a "Vortex-Generating" Delta Wing planform.

Steady and unsteady distortion of total pressures obtained in ground and flight testing were compared by Joubert/Eyraud in [14] and typical results are shown in **Fig. 8.**

Conclusions for session II :

(1) Pep WG18 compiled an extensive experimental data base but **follow-on activities are needed**

(2) **Experiment needs new quality** to satisfy requirements for accuracy and details to be datum solutions for validation of CFD
therefore:
CFD validation extremely difficult since nothing to validate against in real 3-D flow (only calibration?)

(3) Air **intake distortions** require extensive experimental efforts. So far very limited CFD work (if not none),
therefore:
Communication airframe/engine manufacturer mandatory

(4) Session indicates many **common areas of interest in PEP and FDP activities**
therefore:
coordination, communication and more joined efforts strongly recommended

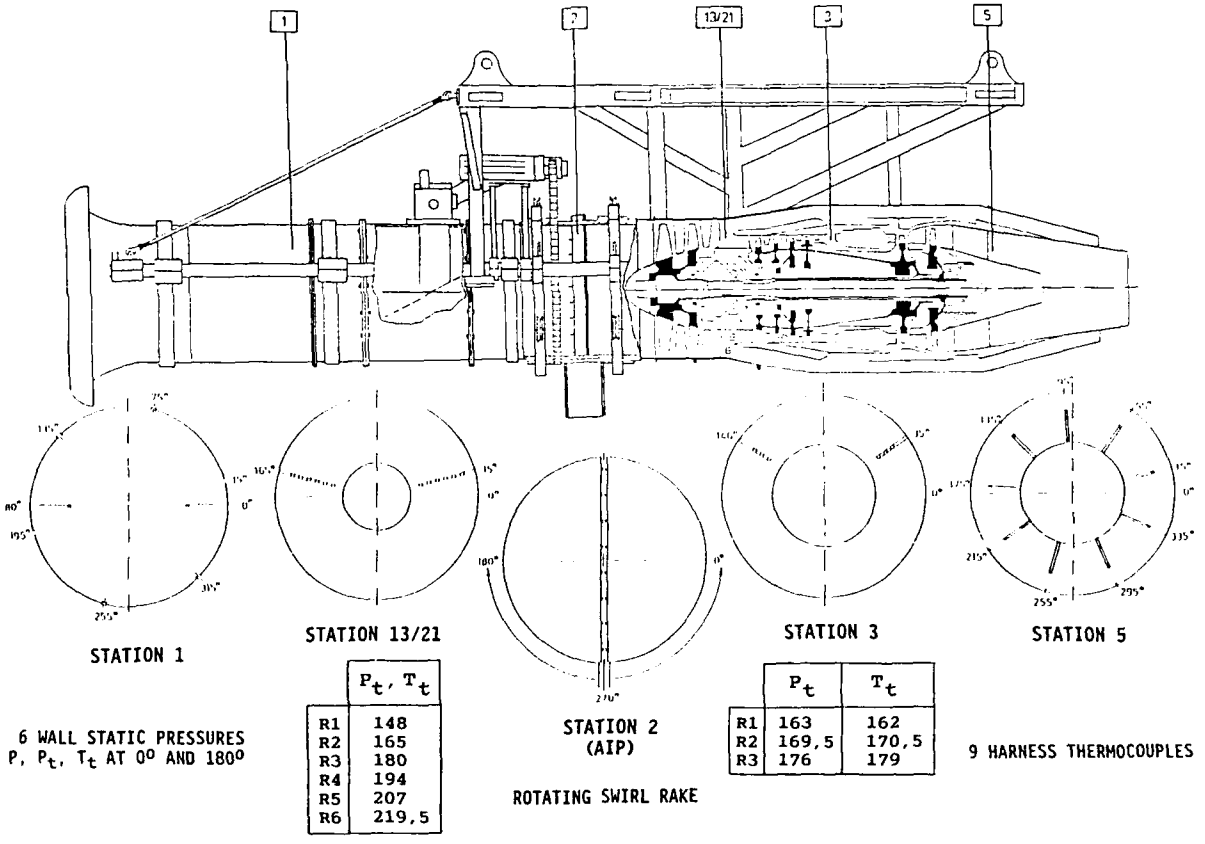

	P_t, T_t
R1	148
R2	165
R3	180
R4	194
R5	207
R6	219,5

	P_t	T_t
R1	163	162
R2	169,5	170,5
R3	176	179

Fig. 7 **Test apparatus and test engine instrumentation arrangement for flow field assessment**

W.Meyer, W.Pazur, L.Fottner : "The Influence of Swirl Distortion on the Steady State Performance of a Low Bypass, Twin-Spool Engine", [13]

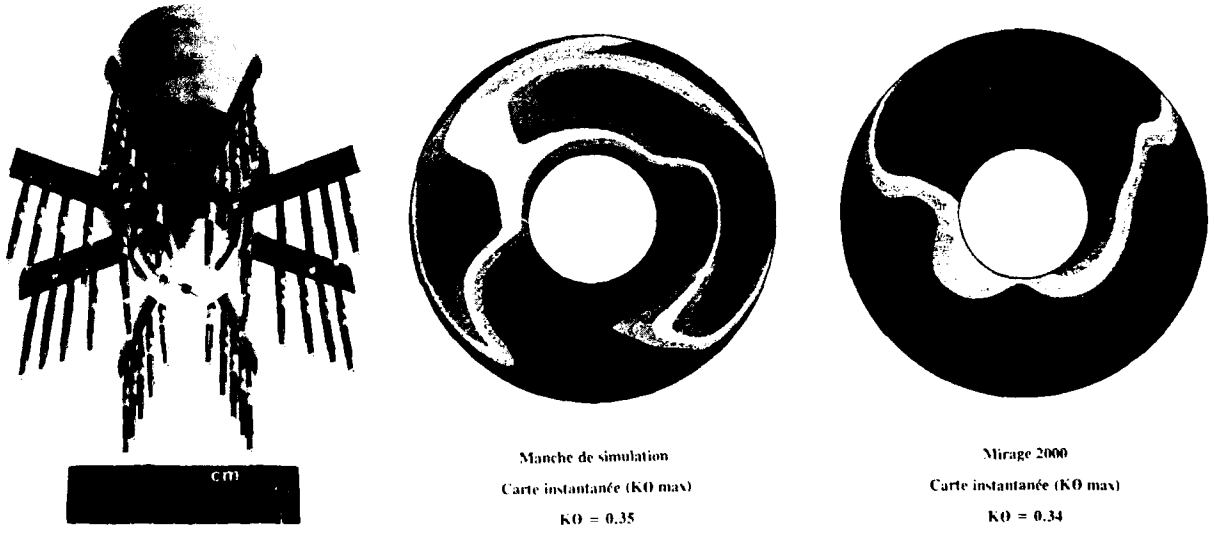

Fig. 8 **Test equipment and unsteady distortion of total pressure obtained in flight and on ground**

M.M Joubert, M.Eyraud : "In-Flight Analysis of Intake-Engine compatibility", [14]

SESSION III : EXPERIMENTAL TECHNIQUES USED IN AERODYNAMICS ENGINE/AIRFRAME INTEGRATION

Again the main objectives of the session will be described first :

(1) Engine simulators for wind tunnel research of engine integration effects, [15]

(2) Intake flow field data acquisition systems used for investigation of intake/airframe interaction, [16], [17], [18]

(3) Test technique used for investigation of jets in the ground effect region, [19], [20]

Wind tunnel, see Harris/Wilds/Smith/Mundell/Davidson [15], **Fig. 9**, water tunnels, see Magio [18], **Fig. 10**, and ground-, see Hoheisl/Bütefisch/Lehmann/Henke/Roscher/Seelhorst [20], **Fig. 11** and flight testing war reported extensively. Each of this engineering techniques is heavily in use during investigations of engine/airframe installation effects and during the configuration optimization process during design of an new aircraft. TPS Technique begins also to be used for military fighter aircraft design. In addition complex data reduction and data acquisition system on a mobile basis are now available and laser doppler anemometrie starts to be used for full scale flow analysis allowing for validation of experimental tools like TPS in addition to CFD tools. There is a remarkable increased effort on the airframe manufacturer side to understand complex flow physics due to engine integration effects and the question arises whether there is also the same kind of parallel effort on the engine manufacturers side.

Conclusions for session III :

(1) Wind tunnel, water tunnel, ground and flight test used for investigations to **understand interference effects** due to engine/airframe integration

(2) **TPS is standard in Europe**, tools owned by test facilities therefore reasonable ROI because being used in many programmes

(3) **TPS starts to move in military A/C development**, problem with hot gas (afterburner) simulation

(4) **LDA techniques** start to be used for full scale flow analysis (209) allowing for validation of TPS and CFD work

(5) Extensive **data reduction and data acquisition** systems on a mobile basis available
Question:
What can the engine manufacturer do with large amount of flow details obtained?

(6) Increased effort on airframe side to **understand complex flowfields** due to engine integration

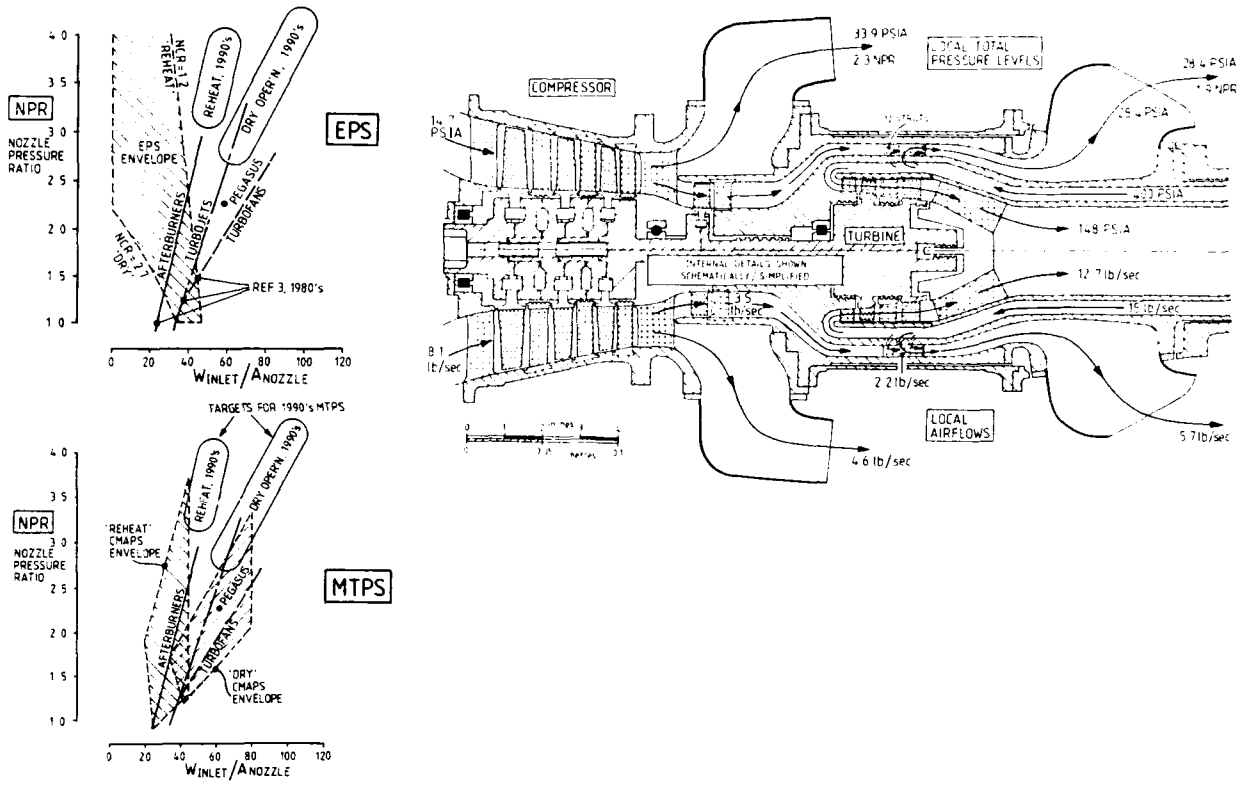

Fig. 9 **Engine simulators and full scale cycle characteristics and (Pegasus) engine simulator layout**

A.E.Harris, G.L.Wilds, V.J.Smith, A.R.G.Mundell, D.P.Davidson : "Aerodynamic Engine/Airframe Integration for High Performance Aircraft and Missiles", [15]

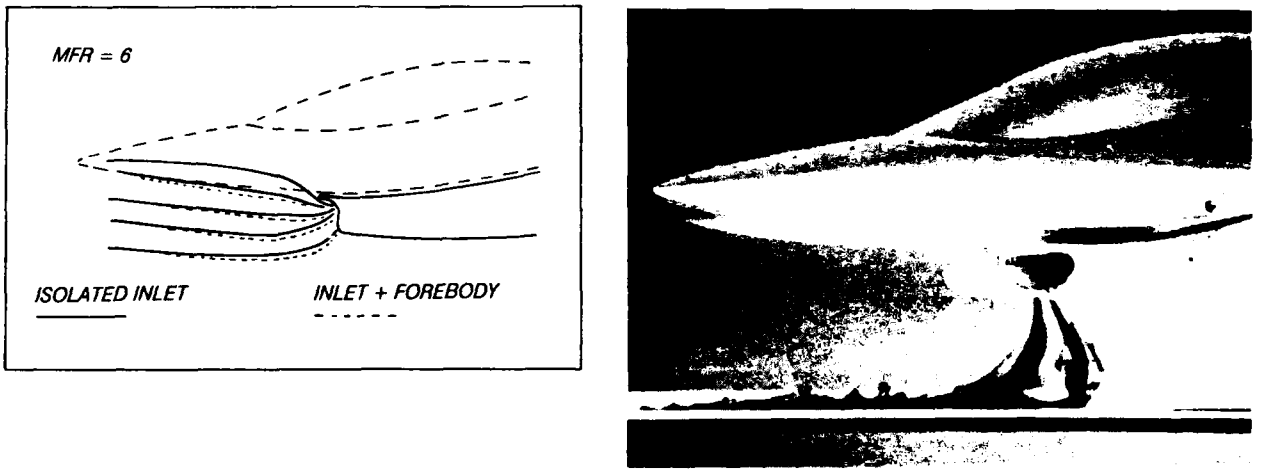

Fig. 10 **Streamtube displacement due to aircraft forebody and vortex formation due to ground effect**

R.Magio : "Water-Tunnel Studies of Inlet/Airframe Interference Phenomena", [18]

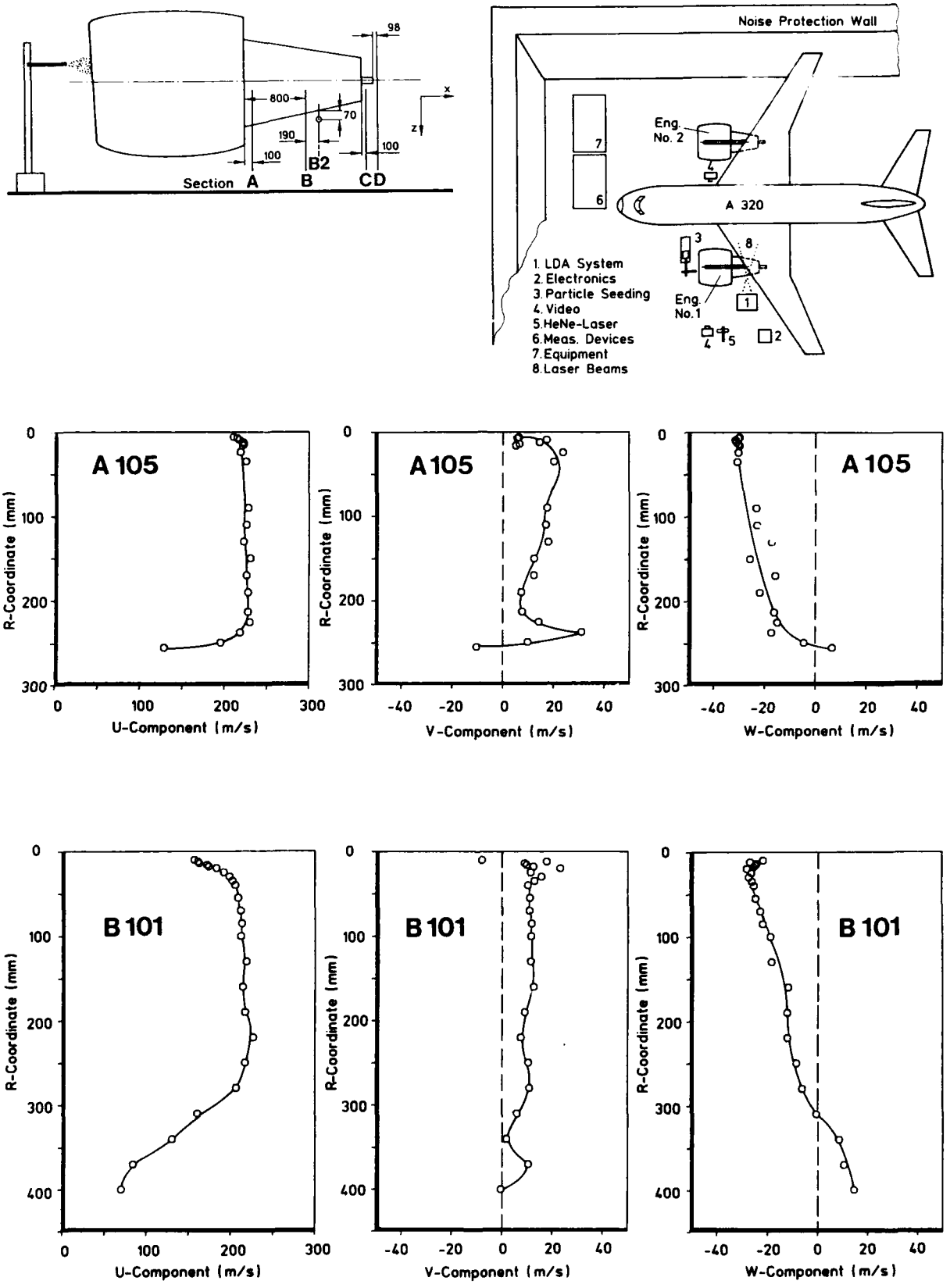

Fig. 11 **Fullscale test engine for flow field analysis in ground effect and typical data obtained by LDV**

H.Hoheisel, K.A. Bütefisch, B.Lehmann, R.Henke, H.J.Roscher, U.Seelhorst: "The Jet Behaviour of an Actual High Bypass Engine as Determined by LDA Measurements in Ground Tests", [20]

SESSION IV : AERODYNAMICS INLET/AIRFRAME INTEGRATION

Five papers were presented in this session. They focussed on the following subjects :

(1) Techniques used for aerodynamic inlet/airframe integration, [21]

(2) CFD applications to inlet airframe integration, [24], [25] and the survey on FDP WG13 activities: "Aerodynamics of High Speed Air Intakes", [22]

(3) Experimental investigations of pitot type air intakes in several European WT's, [23]

An introductory invited paper was given by L. Goldsmith [21] on the techniques used for aerodynamic inlet/airframe integration. A huge variety of geometrical arrangements of intakes exists in different aircraft and missile designs. There was no tendency to find an optimum of the inlet position, because this is dependent on mission profile and geometric shape. The individual result may be an answer to high angle-of-attack or speed requirements and it is completely different for aircraft and missiles. What was missing is a general philosophy on how to find the optimum position of the inlet in each different application. Garnero/Lacau have addressed this question in [24] as **Fig. 12** shows.

The results of the FDP WG13 have been quite impressive, see Bissinger/Benson/Bradley, [22]. The compilation of test cases and contributions for CFD application is shown in **Fig. 13**. A huge amount of data has been produced but the main conclusion from this exercise is, that for code validation "specific designed experiments" are needed. But CFD results show also differences for the same class of equations having been solved. The mesh refinement plays obviously a most important role for the quality of any solution.

Another observation is the need for highly experienced, trained-on-the-job engineers, because these CFD codes are really not any more black boxes which may be used by anyone.

Also experimental investigations on intakes of the same geometry in different wind tunnels show differences as Mackrodt/Goldsmith/McGregor/Leynaert/Garcon/Brill report in [23]. This is another remarkable international effort which has been performed in true cooperation. **Fig. 14** shows one of the comparisons of data obtained in three different windtunnels as an representative example.

In summary the following **conclusions might be drawn** from the session on inlet/airframe integration problems :

(1) **Huge variety of geometrical arrangements** of intakes for different A/C and missile designs [21], [24]

(2). **Optimum of intake position** dependent on mission profile, vehicle design, AOA- and speed range

(3). **Outcome of WG13**, [22] :
- impressive collection of data
- CFD needs specifically designed experiments
- CFD results differ even for the same class of physical model
- Grid resolution plays an important role
- need for highly experienced (trained-on-the-job) engineers
- Results from internal flow test cases even more confusing than for external flow

(4) Experimental (Pitot-Type) inlet test case, [23], shows significant deviations for DC60 in three different WT's and comparison with CFD is missing.

(5) Remarkable effort dedicated to HSCT (2<M<5), CFD-Tools have been applied to 3D external and internal flow simulation (AGV, AST, Missiles ...), [24]

(6) FDP WG13-Report considered as "State-of-the-ART" notebook for designers and guide for CFD and testing techniques

(7) As already stated new quality of experiments is needed for validation of EFD and CFD

(8) More approaches needed to set up a design concept philosophy for engine/airframe integration [24] using data base, CFD and EFD

(9) CFD community should not only share success but also bad luck (to get "lessons learned")

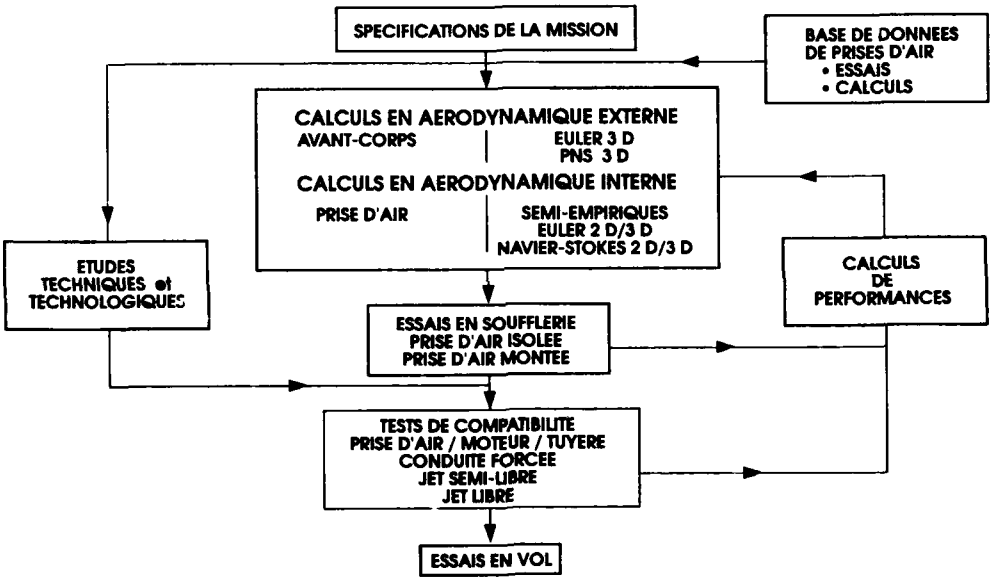

METHODOLOGIE DE DEVELOPPEMENT D'UNE PRISE D'AIR SUPERSONIQUE INTEGREE

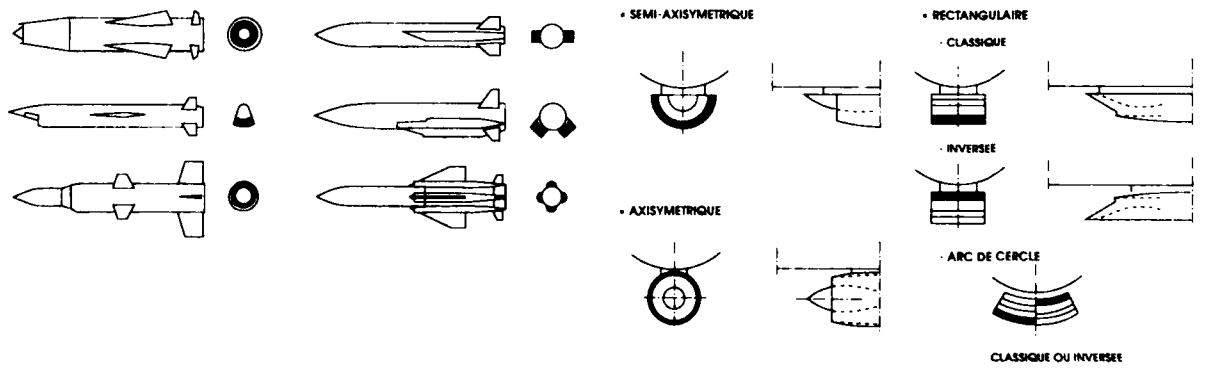

Fig. 12 **Methodology for the development of integrated supersonic intakes**
P.Garnero, G.Lacau : "Numerical Simulations for Aerodynamic Investigations of Supersonic Inlets", [24]

TEST CASE	FLOW TYPE	NUMBER OF CALCULATIONS
1	Transonic Normal Shock/Turbulent Boundary Layer Interactions	2
2	Glancing Shock/Boundary Layer Interaction	5
3	Subsonic/Transonic Circular Intake	3
4	Subsonic/Transonic Semi-circular Intake	1
5	Supersonic Circular Pitot Intake	2
6	2D Hypersonic Intake	10
7	Axisym. Mixed Compression Intake	2
8	Intake/Airframe Integration	2

CODE	USER	TYPE	TEST CASE
PARC3D	SVERDRUP-AEDC SVERDRUP-CLEVE.	NS	1 2 6 8 2 7
HAWK3D	GENERAL DYNAMICS	NS	2
FALCON	GENERAL DYNAMICS	NS	6
PEPSI-S	NASA-LEWIS	PNS	2 6 7
NS2D	ONERA AEROSPATIALE	NS	2 6
FLU3M	AEROSPATIALE	EU	6 8
	ARA	EU EUBL	3 4 5
ENSFL2D	DORNIER	NS	5
IKARUS	DORNIER	NS	3 6
RANSAC	BAE	NS	3
NSFLEX	MBB	NS	1 6

Fig. 13 **Test cases for CFD calculations and codes used in CFD assessment**

N.C.Bissinger, T.J.Benson, R.G.Bradley : "Aerodynamics of high speed air intakes, assessment of CFD results", [22]

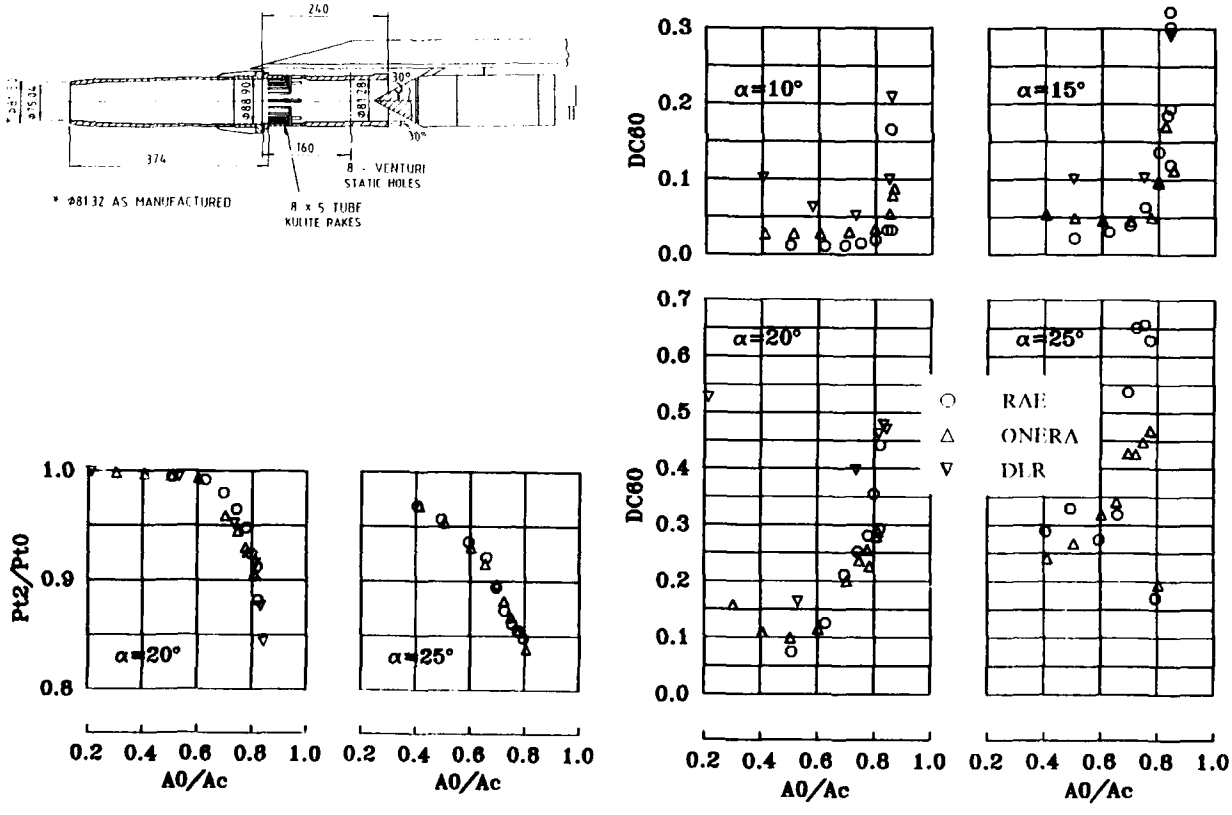

Fig. 14 **Pitot-inlet in RAE, ONERA and DLR windtunnels, comparison of pressure recovery and DC60**

P.-A.Mackrodt, E.L.Goldsmith, I.McGregor, J.Leynaert, F.Garcon, J.Brill : "Comparative Performance Tests of a Pitot-Inlet in Several European Windtunnels at Subsonic and Supersonic Speed", [23]

SESSION V : AERODYNAMIC NOZZLE/AIRFRAME INTEGRATION

The main emphasis was given to the following objectives :

1. Survey on progress made since WG08 (1984) with respect to experimental and numerical techniques, [26]

2. Calibration of 2D full N.S. solutions for complex highly integrated propulsive exhaust systems, [27], [28]

3. Propulsion integration results of the STOL and Maneuver Technology Demonstrator Programme (S/MTD), [30]

The survey on exhaust system design requirements given by Bowers/Laughrey in [26] is characterized in **Fig. 15**. The increasing requirements on the overall performance of nozzle designs lead to the conclusion that "Exhaust Nozzles Aren't Round Anymore" ! More and more of advanced technology has to be implemented in modern military aircraft designs. This has let to technology demonstrator vehicles like Laughrey/Moorhouse describe in [30], see also **Fig. 16**. Typical representative data from N.S. CFD simulations in comparison with experimental results are shown in **Fig. 17 and 18** reported by Reed/Muyshondt, [28].

The **major findings of this session** can be summarized as follows :

1. **No major break-through since WG08 (1986)** in experimental techniques
   Interesting Question :
   "Will the "State-of-the-Art" of tomorrow be as good as today? (D. Bowers)

2. Major findings from **CFD applications** :
   - only the highest level (full Navier-Stokes) promising to simulate the complex viscous flow regime
   - again strong requirements for test cases "designed" for CFD validation
   - Progress in 2D NS Solvers but turbulence modelling still unsatisfactory
   - Geometric restrictions due to lack of 3D N.S. codes
   - strong requirement for "User-Friendlyness" of CFD codes
   - "Magic Triangle" :

Experiment
Test Cases

Engineering Application
Requirements for user environment
"Friendliness"

Code Development
Code Validation

AGARD WG17 starts in 1992 !

1950	1985	1990
Engine Control Valve	Engine Control Valve Thrust Efficiency Minimize Drag	Engine Control Valve Thrust Efficiency Minimize Drag Thrust Reversing Thrust Vectoring Pitch Thrust Vectoring Yaw Thrust Vectoring Roll Signature Reduction Acoustics

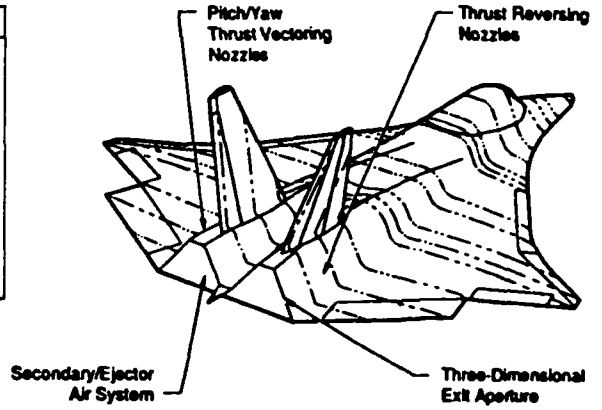

Fig. 15 **Evolution of exhaust system design requirements and "...Exhaust Nozzles Aren't Always Round Anymore"**

D.L.Bowers, J.A.Laughrey : "Survey on Techniques used in Aerodynamic Nozzle/Airframe Integration", [26]

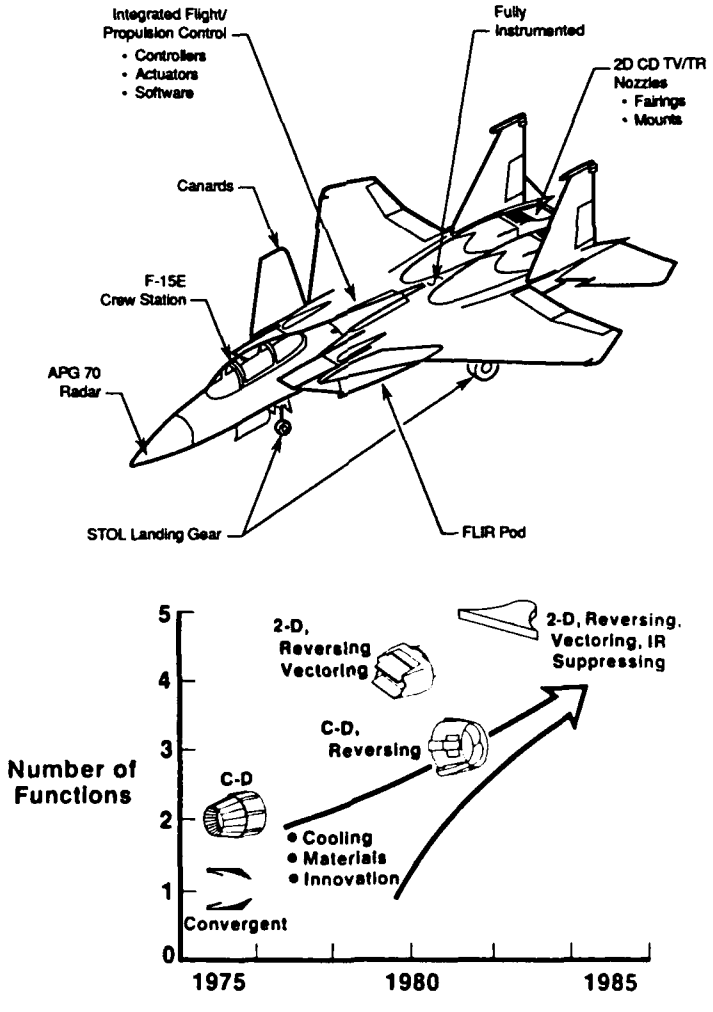

Fig. 16 **Technology implemented in the STOL and technology demonstrator vehicle**

J.A.Laughrey, D.J.Moorhouse : "Propulsion Integration Results of the STOL and Maneuver Technology Demonstrator (S/TMTD)", [30]

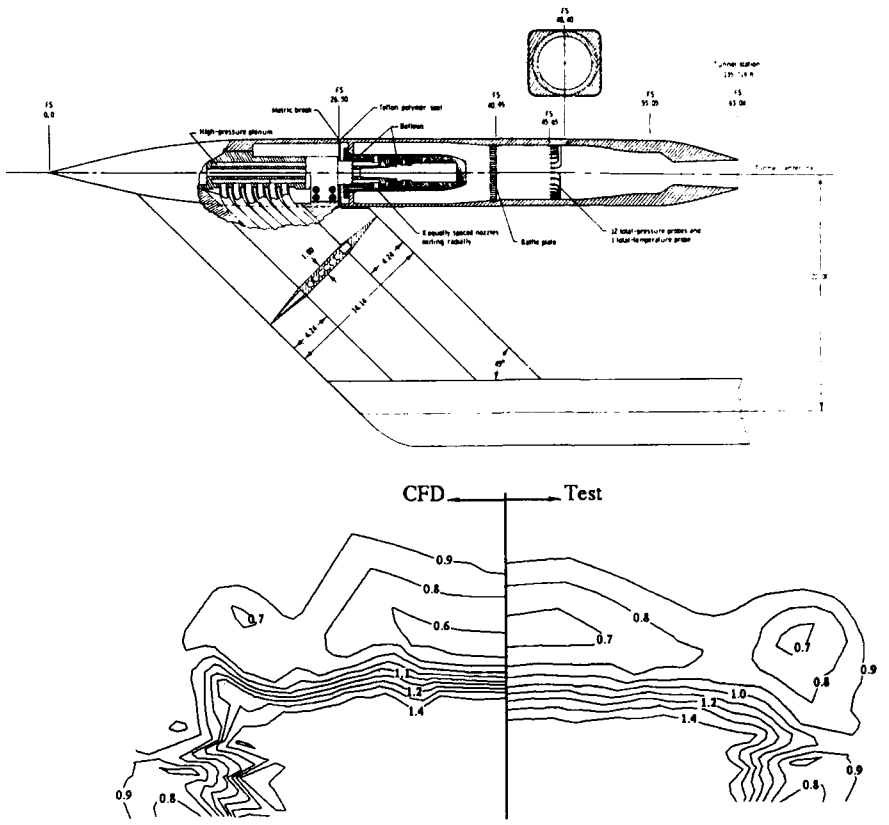

Fig. 17 **Afterbody model test rig and comparison of experimental and computed total pressure contours**

C.I.Reed, A.Muyshondt : "CFD Calibration for Three-Dimensional Nozzle/Afterbody Configurations", [28]

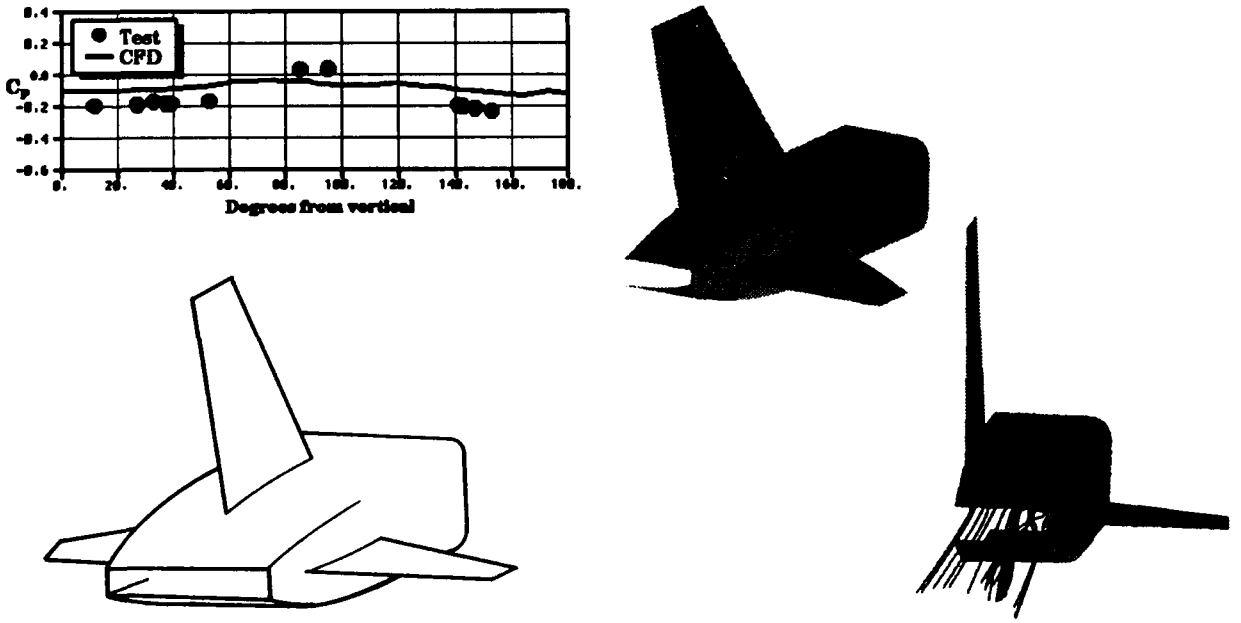

Fig. 18 **Pressure distribution and particle traces at a high aspect ratio conformal nozzle design**

C.I.Reed, A.Muyshondt : "CFD Calibration for Three-Dimensional Nozzle/Afterbody Configurations", [28]

SESSION VI : AERODYNAMIC ENGINE/AIRFRAME INTEGRATION FOR HYPERSONIC SPEED VEHICLES

The last session was quite short. Only three papers have been submitted, but it concentrates on the highest degree of engine/airframe integration.

Objectives :

(1) Force accounting systems for hypersonic propulsion system integration

(2) Integration of turbo - ramjet engines for hypersonic aircraft

(3) Variable-capture-area intakes for hypersonic vehicles

The integration of the airbreathing propulsion system for hypersonic flight vehicles is not yet engineering routine today and therefore it can be explained that the highest identification with the national programmes has to be accepted. This leads to the conclusion that most of the data but even more the procedures used during systems design are "Company Confidential". But nevertheless the contributions given to this session have been impressive. So O.Herrmann reviews the problems of the integration of turbo-ramjet engines for hypersonic aircraft intensively in [32] and **Fig. 19** gives some impression of the complexity of the engineering task. Again CFD is extensively used and typical representative results obtained by 2D Euler solutions for the nozzle aftbody integration are shown in **Fig. 20**. The force accounting system for hypersonic flight vehicles was addressed by K.Numbers in [21], see **Fig. 21.** nearly each airframe and engine manufacturer has introduced his own version of creating the "engine/airframe-interface". A specific problem for vehicles flying with airbreathing propulsion over an extended Mach number range is treated by Falempin/Duveau in [33]. Three concepts for variable capture area intakes to compromise diverging requirements for massflow and drag at low and high speed are presented according to **Fig. 22.**

Conclusions from session IV :

(1) Only three papers submitted but highly qualified and impressive presentations given

(2) Highest degree of engine/airframe integration needed - not yet "Routine Engineering Procedure" therefore:

(3) Highest identification with programme/project status
- NASP
- HOTEL
- SÄNGER — Results classified !
- STAR-H

(4) Subject for future AGARD activities (e.g. FDP WG18)

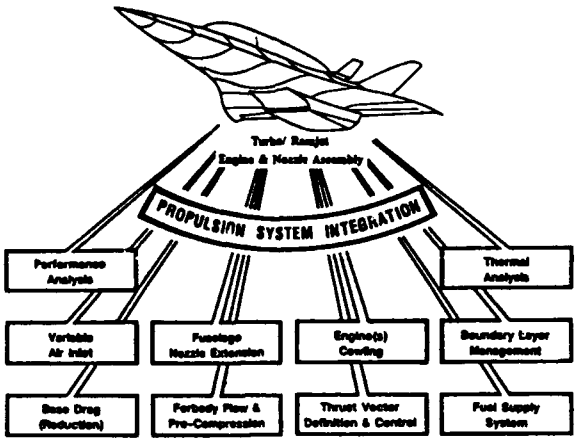

Fig. 19 **Tasks for airbreathing-propulsion-systems integration for hypersonic launchers**

O.Herrmann : "Integration of Turbo-Ramjet Engines for Hypersonic Aircraft", [32]

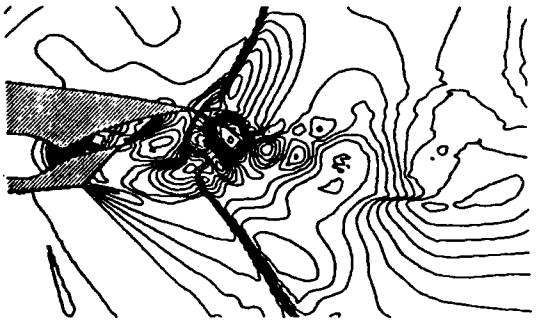

MTU-Configuration, Pressures at Ma_∞=1.2

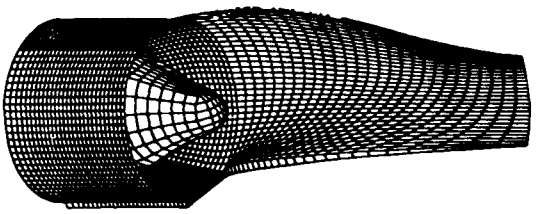

Plug-Configuration, 3-D Grid Lines

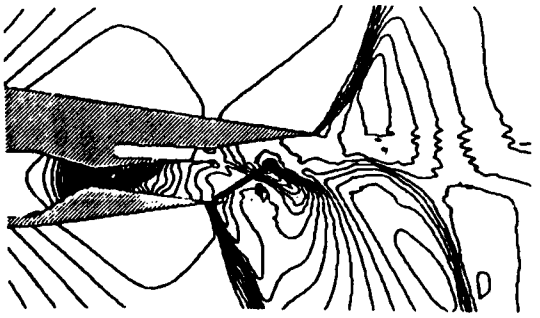

Alternate Configuration, Pressures at Ma_∞=1.2

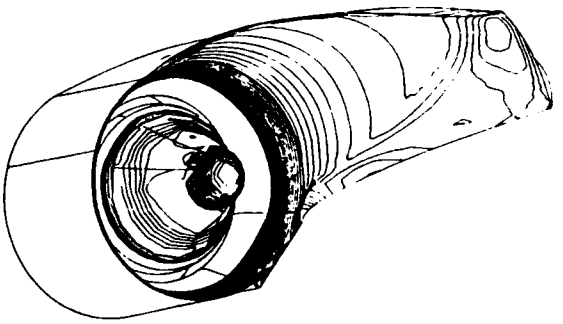

Plug-Configuration, Pressures at Ma_∞=5.6

Fig. 20 **SERN-nozzle/afterboy integration for hypersonic launchers using CFD**

O.Herrmann : "Integration of Turbo-Ramjet Engines for Hypersonic Aircraft", [32]

Propulsion Definition	Description	Pro	Con
	• All Surfaces Wetted by Propulsion Flow	• Prop Analysis Starts in Uniform Flow • Minimum Corrections at Off-Reference Conditions • Prop Includes Aft Thrust Surface	• Aero Excludes Major Lifting Surfaces • Interface is a Function of M, α, Π
	• Wetted Surfaces Aft of First Compression Ramp	• Aero Includes Forebody Lifting Surface • Minimum Corrections at Off-Reference Conditions • Prop Includes Aft Thrust Surface	• Aero Excludes Nozzle Lift & Trim • Prop Analysis Starts in Complex Flow • Interface is a Function of M, α, Π
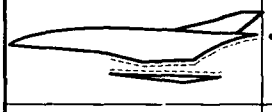	• Wetted Surfaces Aft of Inlet Cowl Lip	• Aero Includes Forebody & Inlet Lifting Surfaces • Boundary is Well Defined • Prop Includes Aft Thrust Surface	• Aero Excludes Nozzle Lift & Trim • Prop Analysis Starts in Complex Flow • Aero May Include Ramp Variable Geometry
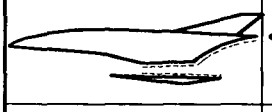	• Wetted Surfaces Aft of Engine Face	• Aero Includes Forebody & Inlet Lifting Surfaces • Boundary is Well Defined • Prop Includes Aft Thrust Surface	• Aero Excludes Nozzle Lift & Trim • Prop Analysis Starts in Complex Flow • Extensive Corrections at Off-Reference Conditions
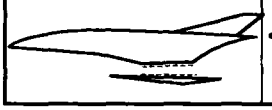	• Wetted Surfaces Between Engine Face and Nozzle Throat	• Aero Includes Major Lifting Surfaces • Boundary is Well Definced	• Aero Excludes Nozzle Lift & Trim • Prop Analysis Starts in Complex Flow • Extensive Corrections at Off-Reference Conditions

Fig. 21 Survey on database available for aero-propulsion interface

K.Numbers : "Hypersonic Propulsion System Force Accounting", [31]

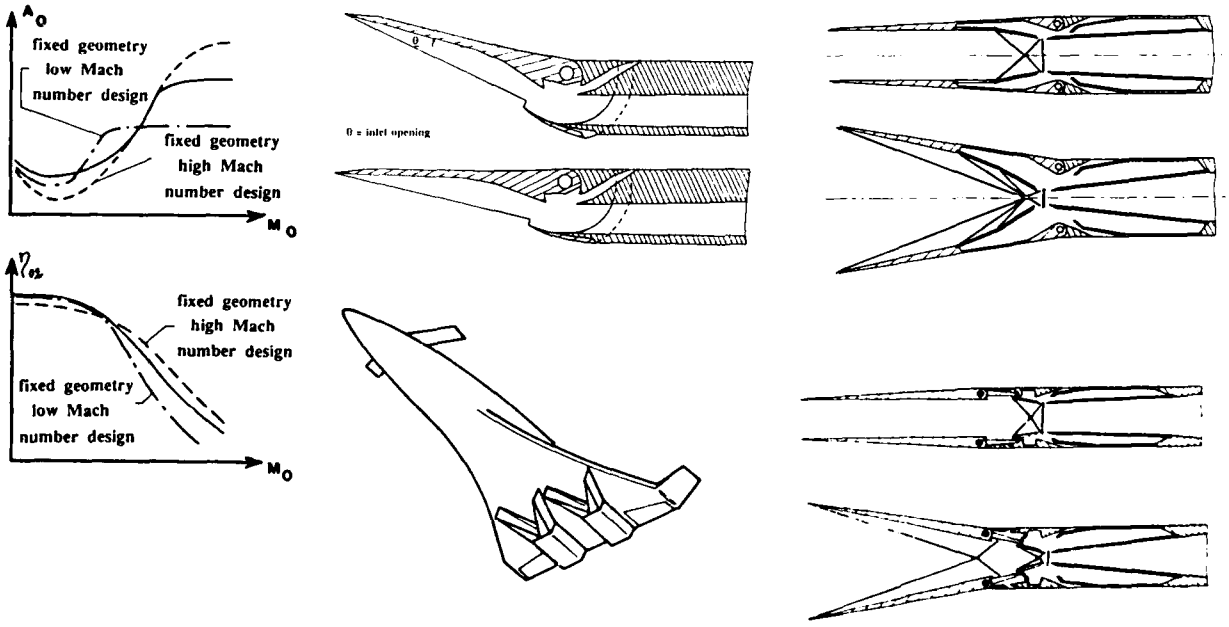

Fig. 22 Three concepts for variable capture area intakes to compromise transonic/hypersonic performance requirements

F.Falempin, Ph.Duveau : "Variable capture area inlets - Applications to Launchers", [33]

CONCLUSIONS

Some general observations may be as follows :

(1) Objectives of the meeting (according to the call for papers) have been reached to a large degree

(2) Successful attempt to "integrate people" working in different engineering areas
- experimentalists/theoreticians
- civil/military/space transport applications
- external/internal flow specialists
- FDP/PEP AGARD community

(3) Active and stimulating discussions have taken place
- all papers being available in written form at the meeting
- excellent professional presentations
- perfect organization, optimal local arrangements and outstanding hospitality

The technical evaluation of the outcome of the meeting comes to the following conclusions :

(1) Propulsive flowfields involve more and more complex geometry and complex physics

(2) Successful engine/airframe integration relies to a large degree on extensive WT-testing using engine simulation tools (TPS)

(3) Optimization of civil and military configurations need complementary support from CFD

(4) Need for viscous flow representation in CFD, but still limitations for practical ("engineering") work exist

(5) CFD even more important (and complex) for internal flow

(6) Future trend to even higher integrated designs therefore requirements for "Tip-to-Tail" numerical simulation

A more extensive Technical Evaluation Report has been written by W.Schmidt (AGARD AR-308), all papers of the symposium including the closing RTD are published in AGARD CP-498 .

Development and Qualification of the US Cruise Missile Propulsion System

William H. Reardon
Anthony J. Cifone
Naval Air Warfare Center Aircraft Division, Trenton
250 Princton Blvd., Trenton, N.J. 08628-0176, U.S.A.

Summary

This paper provides a description of the very successful Cruise Missile gas turbine propulsion program managed by the United States Department of Defense. The paper contains a summary of the procurement process, the technical and programmatic milestones, issues and challenges, and lessons learned. In the past fifteen years, testing at the Naval Air Propulsion Center has included over 800 cruise engine development and component substantiation efforts spanning the engine specification qualification requirements. This paper provides a detailed account of environmental test techniques used to qualify the F107 family of gas turbine engines which propel the US Cruise Missile. In addition, a missile freestream flight test simulation for the TOMAHAWK Cruise Missile is discussed along with current and future program efforts.

Historical Background

Cruise missile ancestry can be traced back to World War II and the German V-1 buzz bomb. It was that missile's success that drove US development of the submarine launched REGULUS I and II, and the Air Force's MATADOR, SNARK, MACE and HOUND DOG missiles in the early 1950's . Cruise missile development interest dropped off sharply in the mid 1950's, when the development of long range ballistic missiles showed performance characteristics more suitable to the strategic policies being formed for the "era of deterrence". In addition, the loss of Gary Powers and his U-2 reconnaissance aircraft showed that high flying vehicles could no longer penetrate the current Soviet defensive systems with a high probability of success. It was not until the Egyptians used a soviet built Styx cruise missile to sink the Israeli destroyer Elath in the 1967 war that the United States interest was rekindled. As a hedge against the Soviet military build up, the development of the Air Force Subsonic Cruise Armed Decoy (SCAD) and the Navy HARPOON missiles began. [1]

The Navy established the Cruise Missiles Project (CMP) under management of Naval Air Systems Command (NAVAIR) on 19 December 1972. The Naval Ordnance Systems Command (NAVORD) and the Naval Ship Systems Command (NAVSEA) assisted in its management. NAVAIR and NAVORD published a joint charter on 16 April 1973 which established the CMP as a designated Program Manager Air (PMA) under direction of COMNAVAIR.

The Navy and the Air Force were directed in January 1977 by the Deputy Secretary of Defense to enter into joint development of the air, sea and ground launched cruise missiles under a single Joint Cruise Missiles Project (JCMP). The creation of this organization was to ensure that the cost savings inherent in common components and subsystems development, testing, resources sharing and quantity buy were realized. In July 1977, production of the B-1 bomber was put on hold and increased emphasis was placed on development of the cruise missile.

On 30 September 1977, the Director of Defense Research and Engineering (DDR&E) formed the Joint Cruise Missiles Program Office (JCMPO). DDR&E assigned the JCMPO the highest National priority and directed that the Navy and the Air Force JCMPO was responsible for developing the Air Launched Cruise Missile (ALCM) through its Defense Systems Acquisition Review Council (DSARC) III production decision. After DSARC III, the plan was to assign the ALCM and Ground Launched Cruise Missile (GLCM) program management responsibilities to the Air Force and the Sea Launched Cruise Missile (SLCM) to the Navy.

In 1978, the defense department sponsored a competitive ALCM fly off between Boeing and General Dynamics Convair Division (GD/C). A strengthening of the JCMP was also directed with program managers and the director co-located in Washington, DC.

In March 1980, the Boeing AGM-86B was selected to be the Air Force strategic air launched cruise missile. Although the ALCM was transferred to the Aeronautical Systems Division (ASD) at Wright Patterson Air Force Base (AFB), Ohio in June 1980, the common subsystems including the engine and guidance system remained the responsibility of the JCMP. Also, the JCMP maintained the development responsibility for the GLCM and all the TOMAHAWK SLCM variants (for which GD/C was the principal contractor), as well as the TOMAHAWK Medium Range Air to Surface Missile (MRASM).

In August 1982, the ALCM and GLCM programs transitioned from the development to the production phase, with the SLCM close behind, moving from development into qualification testing.

Because of the importance of cruise missiles, the JCMP entered into some unique contractual arrangements. For example, the joint project dual sourced the engine and

airframe as well as critical guidance components. This dual sourcing allowed for competition throughout the production phase, attaining lower costs. The joint project also adapted some innovative strategies to meet reliability requirements. These strategies included Contractor warranties on the engine and guidance sets delivered to the Government. The acquisition strategy was innovative and unique in the application of design-to-cost, warranty, dual sourcing, licensing and rights to data techniques and requirements. By virtue of common designs, joint testing, off the shelf hardware and this unique acquisition strategy, the overall development schedule was met, and in some cases exceeded, at reduced cost. [2]

The Navy awarded dual source competitive contracts in December 1984 for 270 All UP Round (AUR) missiles. Under terms of the agreement, GD/C and McDonnell Douglas Missile Systems Corporation (MDMSC) provided each other with the necessary data and technical knowledge to allow them to compete annually for output of all TOMAHAWK variants. GD/C was the expert on airframe design and MDMSC on the guidance set.

After the program moved to full rate production in August 1986, GLCM unique hardware was turned over to ASD, Wright Patterson AFB, in October. Also in October, under the Air Force and Navy Cruise Missile Transition Management Plan of June 1985, the JCMPO reverted to Program Director Air for Cruise Missiles (PDA14) as a Navy program under the NAVAIR Command.

Program Firsts

Date	Event
5 June 1976	First fully guided flight of a TOMAHAWK
2 Feb 1978	First launch of land attack and anti-ship SLCM from submarine (USS Barb)
13 Mar 1980	First flight of TOMAHAWK from ground based Armored Box Launcher
19 Mar 1980	First surface ship launch of TOMAHAWK conducted from an ABL from a DD-963 class destroyer.
April 1984	Completed surface ship TSAM and TLAM OPEVAL's.
July 1984	Conducted an extremely successful test of a TLAM/C with a live warhead. This was the first end-to-end demo of horizontal mode of attack with a live warhead. The missile impacted a concrete structure located on San Clemente Island dramatically depicting TOMAHAWK's accuracy and the destructive power of the warhead.
31 May 1985	First vertical launch of TOMAHAWK from surface ship (USS Norton Sound)
Initial Fleet Introduction	Aboard the battleship USS New Jersey in March 1983. (TSAM & TLAM/C) Aboard submarines in November 1983 (TSAM).
Initial Operational Capabilities	GLCM United Kingdom in December 1983 Italy in March 1984 Belgium in March 1985 Germany in March 1986 SLCM Sub anti-ship in November 1983 Surface ship anti-ship in June 1984 Sub & Surface Ship land attack in June 1984

TOMAHAWK Commonality and Variants

TOMAHAWK Cruise Missiles share a common aft end that contains the propulsion and flight control assemblies and fuel cells. The forward half of the BGM-109 contains the guidance set , payload section and extra fuel cells. Three different guidance sets are utilized in the TOMAHAWK missiles. The anti-ship weapon (BGM-109B) utilizes a modified HARPOON unit; the nuclear land attack weapon (BGM-109A) has an inertial unit with terrain contour matching (TERCOM) updating, and the conventional land attack weapon (BGM-109C,D) uses TERCOM plus digital scene matching area correlation (DSMAC). All TOMAHAWK variants are provided environmental protection with either a canister (surface ship launch) or capsule (submarine launch).

	DESIGNATION	GUIDANCE	WARHEAD
ANTI-SHIP	BGM-109B	MODIFIED HARPOON	WDU-25/B
LAND ATTACK	BGM-109A/G	TERCOM	W-80/84
	BGM-109C	TERCOM & DSMAC	WDU-25/B
	BGM-109D		BLU-97/B

TOMAHAWK Family
Figure 1

TOMAHAWK Cruise Missiles in Desert Storm

Only TOMAHAWKs and F-117s were sent to destroy heavily defended Bagdad targets. Although ALCMs were also used during the first day of the conflict, they delivered conventional munitions against sites in northern Iraq. TOMAHAWK targets included power plants, command and control centers and air defense systems. Over 100 TOMAHAWKs were expended in the first 24 hours of the confrontation, nearly 200 in the first 48 hours. Eighteen TOMAHAWK platforms expended 294 missiles from 477 available missiles in the theater.

Surface Ship = 252 TLAM-C, 28 TLAM-D
Submarine = 14 TLAM-C

Of the 294 attempted launches, 8 experienced pre-launch anomalies which prevented firing, and only 7 were lost due to boost failure, none of which is attributable to the engine. This equates to a launch rate of 97% and a cruise rate for successful launches of 98%. [3] It is estimated that 85% of the 279 missiles that attained cruise hit their targets.

Engine History

In the early 1970's the AIR FORCE cruise missile program emphasized the development of a Subsonic Cruise Armed Decoy (SCAD) for use in degrading enemy defenses that might be used against the B-52. In July 1972 contracts were awarded to Williams Research Corporation (WRC) and Teledyne Corporation, Continental Aircraft Engine Division (TCAE) for an eight month competitive turbofan engine development program, with WRC declared the winner in April 1973. Similarly, in 1971 TCAE had won a competitive contract to develop a light weight low cost expendable turbojet engine (J402) for HARPOON, the precursor to the Navy cruise missile project.

During the early 1970's the Navy was becoming interested in both tactical and

strategic cruise missiles in response to growing Soviet surface fleet and cruise missile threat. The SLCM TOMAHAWK Cruise Missile required a 1200 NM range, the ability to fit into a 21 inch diameter cylindrical torpedo tube and provide an accuracy at that distance commensurate with the payload yield. In addition, lower life cycle costs were emphasized. A major player in minimizing production and operational costs is maximizing missiles on target, requiring high system reliability and high probability of surviving enemy defenses. In response to the requirements for minimum life cycle costs and development time each missile contractor was encouraged to make maximum use of existing technology and proven hardware. With two small engine developments already underway, the TCAE turbojet and the WRC turbofan, the advantages of off the shelf hardware and commonality dictated against separate development of a unique TOMAHAWK sustainer engine. The B-52 launched SCAD turbofan engine candidates were integrated into the competing airframe contractors design for the competition phase.

The major technology breakthrough in the SCAD program was the small turbofan engine being developed by WRC. This engine showed great promise in reducing SFC, while significantly reducing the missiles infra-red signature. In the interest of commonality, it was decided to evaluate the Williams engine for use in the Navy cruise missiles. These decisions began to tie together several cruise missile programs. There was a sharing of guidance and engine components from both the HARPOON and the Air Force ALCM.

In mid 1973, development of the SCAD missile was canceled. However, the AIR FORCE continued to work on technology areas critical to early development of a cruise missile, including further development of the WI engine.

In December 1973, due to similarity between the Air Force and Navy missiles, Deputy Secretary of Defense William Clements directed that the Air Force be responsible for developing an engine suitable for use in both missiles, while the Navy develop the land attack guidance system for both. Following the December 1973 authorization to develop a long range strategic ALCM, the Air Force rapidly converted the SCAD design to the new objective. WRC had already been selected to supply the engine, and continued as contractors for the ALCM. Although the Air Force had chosen the WRC engine for the ALCM, in January 1974 the Navy encouraged them to include a second candidate, the TCAE engine, to allow for a competitive fly off of two different engine/airframe pairings for the SLCM. The Navy wanted to reduce production risk and identify the best engine by the end of the validation phase. In April 1974, WRC was paired with GD/C and TCAE with Vought Systems Division of Ling Temco Vought Aerospace Corporation (LTV), in a competition for the Navy SLCM flight vehicle. The competition was structured so that either engine contractor could be selected.

In the intervening two year period from the issuance of the competitive development contracts for SLCM to GD/C and LTV, both contractors had designed, developed, and fabricated candidate cruise missiles which were subjected to a variety of tests, including observables, active wind tunnel flight, shock resistance, and B-52 compatibility. On March 5, 1976 the Navy issued a stop work order to LTV, before the completion of the competitive airframe demonstration phase of development, because of a potential $5 million cost over run. [4] The Navy selected GD/C as the winning contractor on March 17, 1976. In May 1976, WRC, a small privately owned firm, that at the time had no experience with the production rates that would be required by the cruise missiles project, was named as the developer of the SLCM turbofan engine in addition to already being the ALCM engine developer.

The Demonstrator Flight Rating Tests (DFRT) for the WRC F107 engine were completed in May 1976, and On 5 June 1976, the first TOMAHAWK flight test missile was successfully launched from a Navy A-6A aircraft over White Sands Missile Range, New Mexico. The engine was unique, establishing a new niche for military turbine engines, a 600 pound thrust class, 136 pound engine 12 inches in diameter and 37 inches long.

F107 TOMAHAWK Engine Acquisition Program Background

Williams International, a privately owned company is the designer, developer, and prime manufacturer of the F107 engine. In 1978, Teledyne CAE was selected as the F107 Licensee and in 1982 TCAE delivered its first production F107 engine as a subcontractor to Williams International (WI) (WRC became WI in 1981). TCAE continued to perform as a subcontractor to WI in accordance with JCMP/WI MOA of August 1978 throughout the production of the F107-WR-400 engine which ended in 1989.

The cruise missile engine, competitively purchased under a dual source program, was evaluated each year to determine if dual sourcing remained in the best interest of the US Government. As an example, in 1988 (following eight years of production), WI's unit price dropped eleven percent from that of 1987, mainly due to competition from TCAE. TCAE became even more competitive in 1988, continuing to show a positive trend through the completion of F107-WR-400 production in 1989. [5] In 1990, a new version of the F107 engine went into production for the TOMAHAWK program. The new 402 series engine, developed by WI, was second sourced to TCAE. TCAE payed all costs for technology transfer and their qualification. The Navy competed the 1990 buy, and with a total of 370 engines proposed, TCAE received approximately 40 percent. In 1991, a program decision was made to go to single source based on competitive bids. There was no additional cost to the Government since TCAE funded both the technology transfer and their qualification. In return for these commitments, the Government signed a Memorandum of Understanding (MOU) with TCAE guaranteeing them an opportunity to compete through 1990. Over the years, TOMAHAWK's dual source competitions have provided better affordability and the establishment

of cooperative teamwork leading to better problem solutions and a higher quality product.

Engine Design

The F107 engines are direct descendants of the WR19 series of turbofan engines conceived by WRC in the 1963-64 timeframe. The entire core of the WR19 was derived directly from the WR2 series of turbojet engines developed by Williams in the 1950's. The first use of the WR19 engine series was as the powerplant for the flying platform now known as the X-Jet or WASP. This engine made its initial run in August, 1967. It was also used in the Bell Aerospace Company's Jet Belt which first flew in September 1968.

Since the cruise missile engine is strongly constrained by the missile package (inlet airflow and location, exhaust nozzle geometry, diameter and length limitations), a trade off between optimization of specific thrust and specific fuel consumption was necessary. The result was the selection of a moderate bypass ratio cycle (0.9) with fan pressure ratios of 2.0 - 2.5. [6] The standard problems encountered with small turbine engine design are that once the specific thrust has been narrowed, major improvement in SFC is limited due to physical size constraints, mainly in the aft compressor stages, limiting core engine performance growth. In addition to the physical size limitations, the boundary layer becomes a greater proportion of blade height resulting in greater losses.

The F107 turbofan engine was originally produced in two versions, the F107-WR-101 to power the Air Force ALCM and the F107-WR-400 for the Navy TOMAHAWK. Both engines had identical gas paths with differences in the location of accessories and types of fuel and lubricant used.

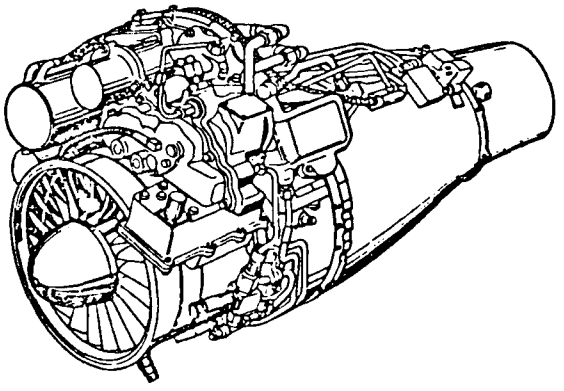

F107-WR-400 Engine
Figure 2

The engine was originally designed to have a useful life of ten years. This life consists of periods of fleet deployment including up to 25 hours of engine operation. The engine is returned to the depot from the field after 36 months for recertification primarily due to the concern of the storage life of the number one grease packed bearing.

Over the years, weight growth of the missile resulting from several upgrades required greater engine performance. A derivative of the F107-WR-400, the F107-WR-402 engine provides improved performance, enhanced missile inlet/engine compatibility and increased storage life as compared to the F107-WR-400. These advantages were obtained by replacing the low pressure (LP) compressor section of the F107-WR-400 with higher efficiency LP compressors. The modification also included an oil lubricated number one bearing which removed the limitations that the grease packed bearing imposed on engine storage life. The engine operational storage life is then extended from three to six years (minimum).

These modifications were also scheduled to be incorporated into F107-WR-400 engines as they returned from the fleet for recertification, because the retrofit is fairly simple and straightforward. Subsequently, program objectives continued to be met at relatively low recurring and non-recurring costs.

The F107-WR-402 combines the design features of two successful qualified engines: the F107-WR-400 with a demonstrated operating reliability of .994 and over 19,000 test hours, and the F112-WR-100 which was developed for the Air Force Advanced Cruise Missile (ACM) with over 3,500 developmental test hours. [7]

- **17.5 TO 19 PERCENT INCREASED THRUST AT LOW ALTITUDE, MACH 0.7, HOT DAY**
- **1.5 TO 2.5 PERCENT BETTER TSFC AT SEA LEVEL, MACH 0.7, STANDARD DAY**
- **IMPROVED ENGINE/INLET COMPATIBILITY**
- **INCREASED STORAGE LIFE**
- **EASILY RETROFITTABLE**
- **LIFE CYCLE COST SAVINGS**

F107-402 Program Objectives
Figure 3

The F107-WR-402 turbofan engine is a non-augmented, twin spool, axial flow, turbofan engine with a single, fixed geometry convergent jet nozzle. It is in the 700 pound thrust class and has a nominal inlet airflow of 14.6 lb/sec, an overall compressor pressure ratio of 16.5 and a bypass ratio of 0.81 at Sea Level, Static, Standard Day conditions at its maximum continuous rating.

To meet the goals of improved performance and extended storage life, the engine utilizes components developed and qualified on other programs. Thrust uprating of the engine is achieved by replacing the existing LP compressor section with improved components developed under the F112-WR-100 program. The Intermediate Pressure (IP) compressor section is the F112-WR-100 "high rise" design. The "high rise" IP compressor achieves significantly higher pressure ratio than the existing F107-WR-400 stages. Therefore, the engine achieves increased thrust without increased shaft speeds or

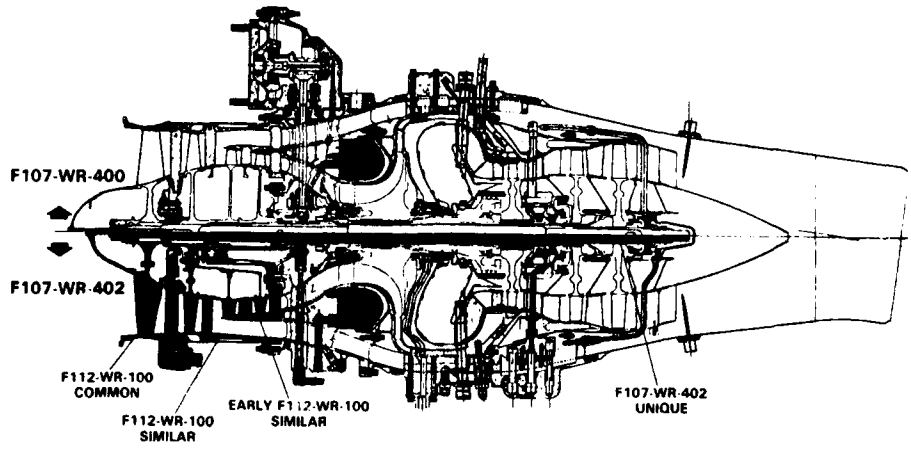

F107-400/-402 Comparison
Figure 4

temperature. These changes to the LP compressor section improve the thrust by 17-20 percent at Mach 0.7, low altitude, Hot Day conditions. The compressor has 30 percent higher temperature rise and operates at the same efficiency. The higher pressure ratio IP increases the engine overall compressor pressure ratio at a given HP spool speed. Since the HP turbine and therefore the turbine flow parameter (WTAP) remains unchanged, increased turbine pressure and temperature result in increased airflow through the turbine. This reduces engine bypass ratio resulting in higher energy core flow which provides significant increase in thrust at a fixed HP spool speed. The increased pressure ratio of the IP has opposing impacts on SFC. The increased overall PR benefits SFC, while the reduced bypass ratio makes it worse. The end result is improved SFC (in the range of two to four percent).

Incorporating the oil-lubricated number one bearing improves the storage reliability and extends the storage life of the engine. Because the grease in the F107-WR-400 bearing is highly hydroscopic, the bearing has been considered a major factor in limiting extended storage life of the engine. Oil lubricated bearings retain sufficient oil film and are relatively unaffected by humid conditions for extended periods of time.

With the F107-WR-402 engine installed, missile inlet/engine airflow compatibility is also improved. Testing has verified the stability model predictions of more surge margin at corrected airflows above approximately 14.0 lbm/sec, which is an area of concern for the F107-WR-400 installed in TOMAHAWK .

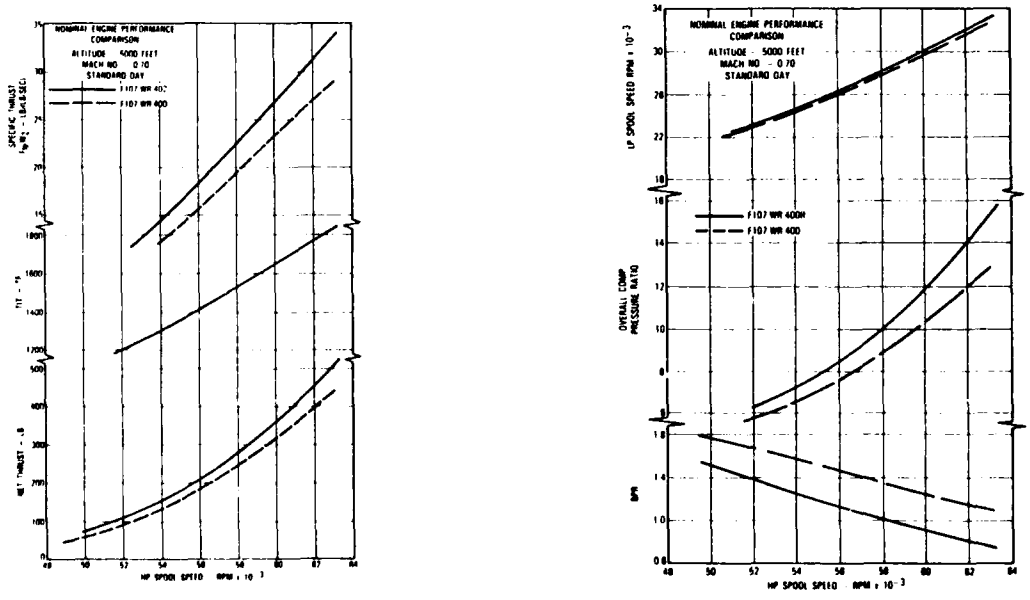

F107-400/-402 Performance Comparison
Figure 5

o	1ST WR19 ENGINE RUN	1967
o	1ST CRUISE PROTOTYPE RUN	6/1970
o	1ST SCAD DEMO RUN	10/1972
o	1ST ALCM F107 RUN	9/1974
o	PFRT COMPLETE	12/1975
o	1ST ALCM FLIGHT	4/1976
o	START FSED	3/1977
o	QUAL TEST COMPLETE	3/1980
o	DSARC III	3/1980
o	FOT&E COMMENCED	3/1980
o	1ST PRODUCTION DELIVERY	3/1981
o	LICENSEE PRODUCTION BEGIN	10/1982
o	INITIAL ALCM OPERATIONAL	12/1982
o	GLCM DT&E COMPLETE	7/1983
o	TOMAHAWK GO AHEAD	9/1983
o	ALCM DELIVERIES COMPLETE	3/1986
o	402 DEMO TESTED	4/1986
o	402 PROGRAM GO AHEAD	6/1987
o	GLCM PROGRAM COMPLETE	1987
o	402 SUBSTANTIATION COMPLETE	10/1989
o	1ST 402 DELIVERY	10/1990

F107 Program History
Figure 6

Naval Air Propulsion Center Role
The Naval Air Propulsion Center (NAPC) was first tasked to support the SLCM engine development in August 1975. Commencing in February 1976, testing began on the demonstration flight rating test DFRT phase, during which time a number of potential problems were revealed through altitude/Mach number (Alt/Mn) testing. After the DSARC decision to create the JCMP in February 1977, full scale development was underway and NAPC was now tasked with development testing on SLCM and ALCM engines. That tasking expanded to include areas of qualification, warranty, alternate source substantiation, development and review of specifications and engineering changes, reliability and maintainability, and integration of engine and missile fuel system program management.

Engine Specification
The F107 Prime Item Development Specification 24235WR9501 encompassing both Air Force and Navy engine models, was developed from the Military General Specifications with the incorporation of an extensive tailoring package. Because the engine was designed and developed for expendable, unmanned application, the design criteria and evaluation/qualification test requirements were substantially modified for cost effective demonstration and achievement of specific goals.

Some of the major design requirement deviations from Navy General Specification MIL-E-005007 are in the areas of environmental conditions for storage, humidity and corrosion resistance. A number of tests represented specialized requirements, and were not taken directly from the guidelines of the General Specification:

- o Pre Launch Shock & Shock Test
- o Stability Margin Demonstration
- o Engine Cartridge Starting Test
- o Storage Reliability Demonstration
- o Altitude Mission Simulation

Qualification Test
NAPC conducted early program testing to support DFRT, aero performance determination and system integration phases of TOMAHAWK and GLCM qualification encompassing over 135 test hours and 15 engines. In support of FSED and QT, between 1976 and 1979, over 300 hours of testing were performed at NAPC on over 40 different engines. These engines were subjected to Specification requirements including altitude and functional performance, corrosion and icing environments, ice, water and sand ingestion, starting and relight envelope evaluation, endurance and altitude mission simulation, inlet compatibility and effects of misalignment, surge margin evaluation, smoke and emissions, heat rejection and oil cooling, oil interruption, oil consumption, vibration surveys and distortion.

As the program shifted from the development to production phase in August 1982, NAPC had run over 220 Cruise Missile engines under altitude environmental conditions, totaling over 1500 hours of experience with the engine design.

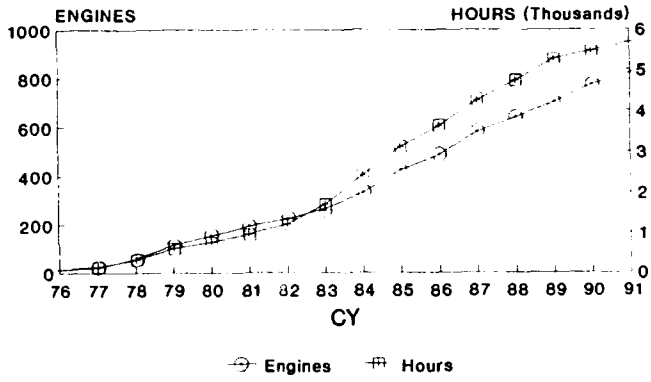

Naval Air Propulsion Center
History of Cruise Missile Engine Test
1976 - 1991
Figure 7

The F107 engine has been a model of success as demonstrated in Operation Desert Storm, but the road to reliability has not been a smooth one. Altitude and environmental development and substantiation testing at NAPC included over 30 anomalous engine tests out of 42 tested. Problems encountered included those related to the mechanical system - lubricating oil, oil consumption and bearing failures - cold starting incapability, fuel distribution - fuel slinger failures, burner cover failures - fuel control mis-scheduling and slew rate anomalies, and a number of turbine blade/disk failures. Many of these discrepancies were directly related to the extreme environment seen by engine internal compartments during Alt/Mn operation.

During alternate source substantiation testing of a Nichols lube and scavenge pump and second source substantiation of TCAE, both for the F107-402 design, anomalies related to oil consumption and system design deficiencies were only detectable under simulated environments of low altitude/high Mach/ Hot Day conditions.

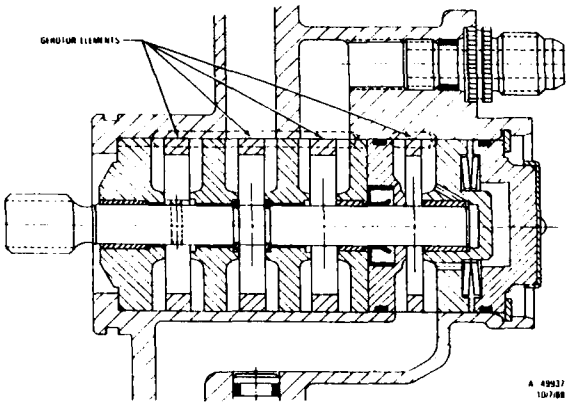

Nichols Lube and Scavenge Pump
Figure 8

Nichols Lube Pump: During attempted second source lube pump substantiation of Nichols Division of Parker Hannifin for the F107-WR-402 in 1988, oil consumption measured on the Sea Level, Static (SLS) acceptance test stand was 0.009 gallons per hour (GPH) which was typical for a F107-WR-400 pump. The Nichols pump was similar to the existing pump in both materials and design. When the pump was tested in the flight environment at NAPC, it failed. Failure investigation revealed no dimensional or metallurgical discrepancies, but the failure was duplicated at the vendors facility. At the time of the start, the engine interstage assembly, oil reservoir and oil inlet tube were dry. The outlet line was full of oil including the oil cooler. Under cold soak conditions, with oil at -5F, the pump seized due to insufficient gerotor side clearance (0.0006 inches). The dry inlet and full outlet condition was more severe than previous evaluation tests performed by the vendor. After increasing the gerotor side clearance to 0.0010 inches, bench priming tests were re-evaluated at -20F and +160F with minimum and maximum tolerance pumps (0.0009 - 0.0016 inches gerotor side clearance) and were successful. The pump substantiation testing was then repeated at NAPC with cold soak/starts at -5F and hot endurance tests on the engine to determine if the increased clearances affected oil consumption. The engine successfully completed cold starts and a seven-hour cold endurance run. The ensuing seven-hour hot endurance run was terminated at four hours due to loss of oil pressure and elevated number 4 & 5 scavenge oil temperatures. At this point, the Nichols lube pump substantiation was halted.

TCAE Second Source Substantiation: In a similar test scenario, during TCAE second source substantiation for the F107-WR-402 engine in 1989, initial Hot Day mission simulation testing of the engine exceeded oil consumption limits of 0.023 GPH by 30 percent. Disassembly and evaluation of hardware revealed coking on LP and HP shafts, an oversized carbon seal ring ID on the number 5 carbon seal and excessive contamination and degradation of the oil. After pressure testing the oil system for leak sources and a complete inspection of mechanical system hardware, O-rings, seals and bearings were replaced and the engine was rebuilt for additional testing. An acceptance test oil consumption run was successfully performed at SLS conditions by TCAE, and the engine was returned to NAPC for further evaluation at flight conditions. Once again, oil consumption was excessive during one-hour oil consumption runs and Hot Day mission simulation testing at 0.7 Mach, 160F inlet temperature. The engine was once again returned to TCAE for disassembly inspection, which revealed no additional coking/carbon on the LP or HP shafts, no damage to O-rings, conical seals or any other hardware. The second stage turbine nozzle assembly which was originally thought to be the culprit was very clean, including carbon seal ID's and seal runner OD's within print tolerances. The number one bearing shaft sleeve was found to be undersized and had been mismachined at the bearing oil dam and oil separator areas of the sleeve. The mismachined number one bearing shaft sleeve was allowing oil to leak into the oil system vent downstream of the air/oil separator, causing excessive oil consumption. The original coking and deterioration of seals in the first build was believed to have been a secondary effect. With the problem source determined, new parts were cut and drawings changed. The engine, with new seals and bearings, was then successfully run at Hot Day mission conditions. The engine design was deemed acceptable, allowing TCAE to complete substantiation and win a fair percentage of the Fiscal 1990 production.

F107-402 Number One Bearing Sleeve
Figure 9

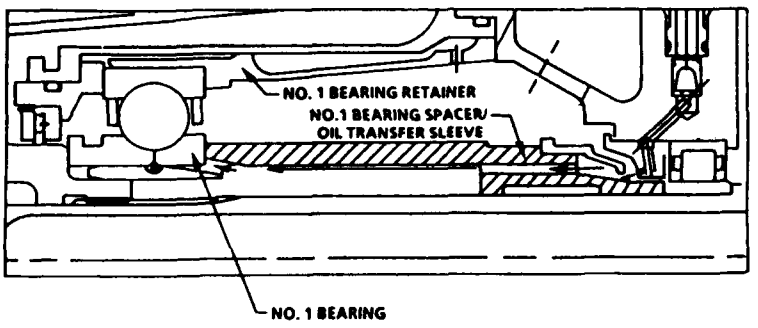

Production Verification (Warranty) Testing
Because this engine is essentially exposed to a storage environment as opposed to an operational one, a warranty program was put in place to confirm product quality assurance and monitor achievement of reliability goals. The program sampled production, storage and flight engines under the Product Assurance Test (PAST), Effectiveness Verification and Improvement Program (EVIP) and Operational Test Launch (OTL) programs. The PAST represented the "as bought" or zero (0) age engine, the EVIP represented the fleeted engine after one deployment cycle and the OTL was a random sampling of engines between the ages of 0 - 36 months. The PAST and EVIP were performed at NAPC as mission simulation tests while the OTLs were AUR flight demonstrations. WI coordinated the data bases from all three programs and predicted operational reliability for the engine system for up to the three year warranty period. With the conversion to the F107-WR-402 in Fiscal Year 1990, the F107-WR-400 Warranty program came to an end. The final tally of tests and results from each test program are documented below.

F107 PROGRAM STATISTICS

4878 ENGINES DELIVERED THROUGH 31 DECEMBER 1992

1926 ALCM (-101,-102)
2614 TOMAHAWK (-400)
338 TOMAHAWK (-402)

WARRANTY PROGRAM STATISTICS (0-36 MONTH AGE ENGINES)

104	**PAST TESTS :**	**101 SUCCESSFUL**
		2 UNSUCCESSFUL
		1 NO TEST
292	**OTL TESTS :**	**271 SUCCESSFUL**
		2 UNSUCCESSFUL
		19 NO TEST
76	**EVIP TESTS :**	**73 SUCCESSFUL**
		1 UNSUCCESSFUL
		2 NO TEST

The overall operational reliability of the system under the 36 month constraint exceeded the specification goal of 98.1 percent. With the coming of the F107-WR-402, the missile storage period extends to 60 months, and the engine extends to a maintenance interval of 84 months. This engine is also undergoing production assurance and flight testing and will eventually be exposed to aged testing.

The engine has been very successful in fulfilling requirements, and the design has certainly proven effective. The PAST/EVIP has been essential in finding and resolving problems encountered in the operational environment which cannot be duplicated on the Acceptance stand at SLS conditions. The following data summary provides the differences in compressor exit conditions and gas generator parameters for the Altitude/Mn to SLS comparison.

SLS to Alt/Mn Comparison

Gas Generator Speed (RPM)/Fuel Flow (LBM/HR)

ALT/MN	STD DAY	HOT DAY	COLD DAY
0/0	**62796/411**	62834/347	59523/490
0/.78	62948/484	**62950**/395	58379/**551**
5K/.9	62924/455	62838/370	62144/550

Net Thrust (LBF)/Gross Thrust (LBF)

ALT/MN	STD DAY	HOT DAY	COLD DAY
0/0	**608/608**	509/509	**763**/763
0/.78	458/931	346/785	605/**1119**
5K/.9	416/921	316/785	537/1080

Compressor Discharge Temperature (R)/Pressure (PSIA)

ALT/MN	STD DAY	HOT DAY	COLD DAY
0/0	**1253/203**	1277/174	1094/253
0/.78	1290/245	**1315**/204	1090/**293**
5K/.9	1290/230	**1315**/192	1234/277

Compressor Bleed Temperature (R)/Pressure (PSIA)

ALT/MN	STD DAY	HOT DAY	COLD DAY
0/0	**772/48**	797/42	654/57
0/.78	810/60	837/53	667/**69**
5K/.9	810/57	**838**/49	762/66

Worst Case Altitude/Mach Effects

N2 = +0.2% Wf = +34% FG = +84%
T3 = +5% PJ = +44%
TBLD = +9% PBLD = +44%

These differences do not represent large changes in parameters; however, the following summary of problems encountered with the qualified engine design through warranty testing indicates that the Acceptance Test Procedure (ATP) did not always provide a measure of durability and that the stresses imposed by the flight environment provide the information critical to maintaining propulsion system reliability at goal levels.

F107-WR-400/-101 Warranty Program
Red O-Ring deficiency: During 1987 warranty testing of two EVIP engines, fuel control scheduling and feedback anomalies were experienced which resulted in instability and eventually termination of the mission tests. Both of these anomalies were traced to the fuel control unit (FCU) and fuel contamination of electrical components inside the control. One was the Globe motor, which translates electronic metering valve position request to mechanical position; the other was the feedback potentiometer, which transmits actuator position to the control for comparison. The fuel contamination was due to leaking flourocarbon (red) O-ring seals at the fuel

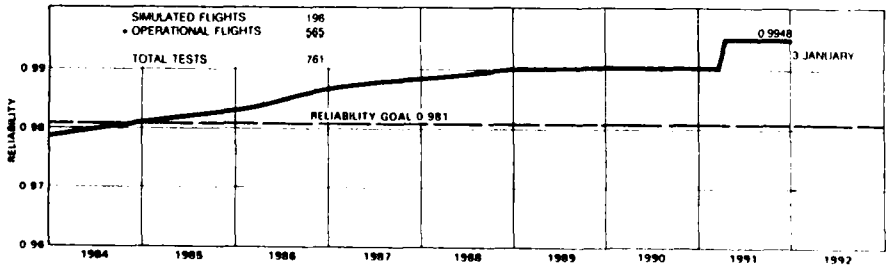

* INCLUDES 279 PERSIAN GULF SUCCESSES WITH ZERO ENGINE FAILURES

F107 Cruise Missile Engine Demonstrated Operating Reliability Figure 10

and electronic seal locations of the FCU body. In 1984, the CMP had approved an ECP to replace the red O-rings with flourosilicon (blue) ones due to a reported 64 occurrences of fuel leakage on ALCM engines, 25 attributable to O-ring seals at various locations in the FCU and fuel system. The flourosilicon provides greater resistance to compression set and lower susceptibility to deterioration from contact with the T-H Dimer propellant. Since these changes were incorporated as engines returned to depot after deployment, the EVIP engines tested at NAPC had not been recertified and provided solid proof of the problems which would have been encountered had the ECP not been incorporated in the engine design.

Hot Gas Start Tubes: During the cartridge start attempt of four different EVIP engines at flight conditions of 1500 ft, 0.5 Mach, flames were observed at the engine service island near the HGST mounting flange. The fuel source was determined to be combustible products introduced during the manufacture of the HGST insulation. No cartridge gas leaks were found in the tubes, and starts were completed successfully and within specification limits. The combustibles were determined to be a kerosene based lubricant used during the insulation quilting process by the manufacturer, Johns Manville. The problem occurred on four of 76 EVIP tests during warranty testing and led to process changes, i.e., eliminating the combustible lubricant and baking of new tubes to eliminate residual combustibles. A retro-fit was not introduced, because the problem had not been seen on a limited sample of OTL recoveries. The problem has since resurfaced in greater frequency in older engines which have the kerosene lubrication.

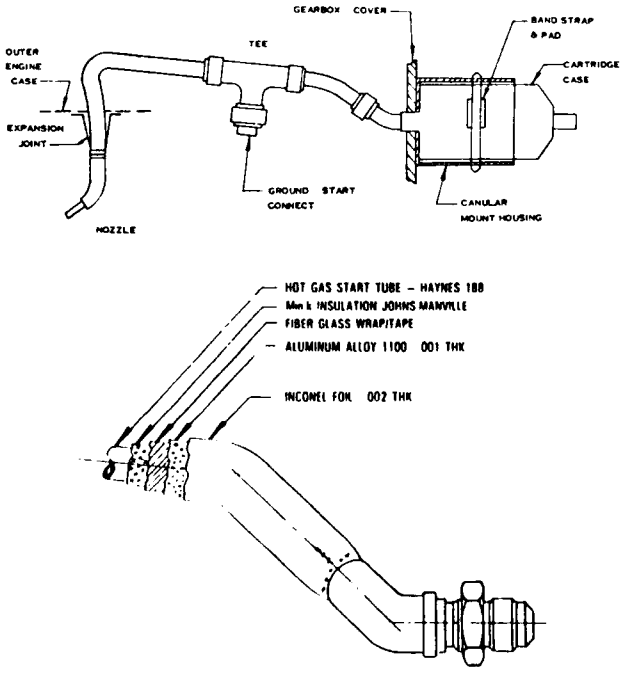

F107 Starter Cartridge/Hot Gas Start Assy
Figure 11

Fuel Shut Off Valve: The history of RJ-4 T-H Dimer fuel and its propensity to form "gum" or "varnish" on fuel system components is well documented. RJ-4 is extremely susceptible to gum formation through hydroperoxidation when its anti-oxidant additive is depleted. The fuel reacts with the environment under conditions of light, humidity and heat, forming a product associated with oxidation/hydrolysis of T-H Dimer, a sticky brown resinous material that has been referred to as "varnish".[8] To prevent degradation of the fuel, it must be stored in relatively full, closed, darkened containers. RJ-4 will produce large quantities of hydroperoxides and eventually will auto-oxidize (and hydrolyze) to form viscid gums. The combination of oxygen and water result in decomposition of the fuel because the oxygen forms peroxides in the presence of the fuel and the fuel decomposes into gum by hydrolysis. These degradation products can cause metal to corrode, Buna N rubber to liquefy and moving parts to bind and seize. Varnish forms from the evaporation of the volatile constituents in degraded T-H Dimer, especially when affected surfaces are only wetted with the oxidized fuel. In the presence of humid air, vapors of degraded T-H Dimer produce varnish on adjacent and nearby surfaces that have not been wetted with fuel. The viscid gum coating internal parts can cause hysteresis, binding and non-operation of close tolerance moving parts. For Buna N O-Rings and seals, attack of the rubber results in drastic loss of the hardness, severe swelling, and a great weight increase. Continuous contact causes depolymerization (liquification).[9] Two EVIP engines failed to start following cold soak in September and August 1987. Gum formation at the fuel shutoff valve (FSOV) of both engines was in the form of peroxides, a by-product of fuel which has reacted to light, air and heat, and plasticizers introduced into the fuel when in contact with rubber components. Both engines failed to start under simulated missile launch conditions below 40F with the problems isolated to the FSOV. The internal plunger and guide sleeve were coated with the sticky substance. The valve, designed to open at a cracking pressure of 70 - 100 psi, would stick under pressures as high as 600-700 psi (FCU discharge limit) because the clearance between the guide sleeve and the plunger (0.002") provided sufficient surface area for shear forces to develop when exposed to the extremely viscous material under cold conditions.

History of Talos, TOMAHAWK and testing performed by the Naval Weapons Station, Seal Beach indicated that the fuel can be stored for long periods in bladders or tanks by precluding exposure to humid air; however, additional failures were reported in the missile fuel system at the depots, including the fuel shut off valve and the guidance set cooling pump. The contamination was initially observed as part of a detailed investigation of EVIP test failures. Further investigation of the ALCM fuel system (JP-10/PF-1) verified no contamination and provided the first step in the change to JP-10 as TOMAHAWK missile fuel. The gumming problem was eventually traced to a batch of Ashland Oil Company manufactured fuel from the 1984 time frame.

Ashland began delivery of RJ-4 fuel to WI in February 1983 on approximately quarterly deliveries until December 1985. It appeared that there was not enough anti-oxidant in some batches of fuel. With the bad lots of fuel identified, short and long term fixes to the problem were defined as follows:

Short Term: Depot engine FSOV's were recalled. Engine FSOV recertification at the vendor was implemented which included change out of O-rings, improved surface finish on valve face and removal of existing varnish.

Long Term: Engine final acceptance was to be performed on JP-10 fuel to be implemented via ECP.

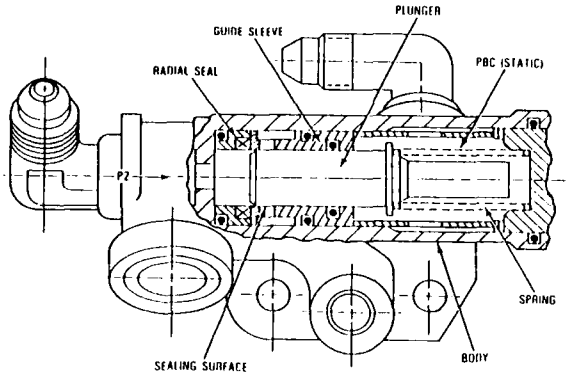

F107 Fuel Shut Off Valve
Figure 12

F112-WR-100 Warranty Program

The Air Force F112-WR-100 Warranty test program which began with production in 1987, was a natural extension of the F107 warranty program although the engine designs differ substantially. Once again, PAST is being performed at NAPC as will EVIP beginning in 1992. The following is a current program summary:

PAST Tests performed = 36
31 Successful
3 Unsuccessful
2 No Tests
EVIP Tests = Scheduled to begin in 1992

As with the F107 Warranty program, there have been unsuccessful tests, which again point to the crucial nature of altitude/Mach number simulation.

Second Turbine Nozzle Braze Failure: At approximately 30 minutes into a PAST run in April 1991, a slight step change increase in EGT of approximately 10F was observed. During the remainder of the run, N1 speed decayed from 35,000 rpm to 33,500 rpm (at constant N2 of 64,100 rpm), and thrust decayed to less than the minimum specification requirement of 95 percent at maximum PLV. Analysis of the data clearly indicated that the N2 (HP spool) was performing adequately. The N1 (LP spool) however, did not respond correctly, and since it is aerodynamically coupled to the HP rotor, an LP turbine efficiency change was the prime suspect. Engine disassembly inspection revealed a hole in the second turbine nozzle assembly. This diaphragm is an annular channel section made from 0.008 inch Hastelloy X and is a non-structural part whose purpose is to prevent leakage of engine core flow gas into the bypass duct. Although non-structural, this part is subjected to flexing which results from the differential thermal expansion between the second turbine nozzle (core flow) and its aft mounting flange (bypass flow). The rupture of this diaphragm permitted the discharge from the second turbine nozzle to escape into the bypass duct. This leakage was the cause of the drop in LP spool speed and the resultant performance degradation. WI materials and processes group isolated the cause of the second nozzle diaphragm failure to extensive braze attack at the inner braze joint. The dye penetrant inspection of the second nozzle inner diaphragm braze joint was inadvertently omitted from a planning revision in late 1990. A total of 72 nozzles had not received the inspection and were subsequently recalled for investigation. Failure duplication testing revealed very conclusively that use of a low temperature braze alloy (in this case AMI 780) fully duplicated the 100 percent braze attack seen in the engine nozzle and the suspect lot. Also, use of the low temperature alloy caused 100 percent braze attack when used for re-braze of properly brazed joints. The primary cause of the second nozzle failure was the use of the wrong braze alloy during re-braze. A secondary cause of failure was omission of the dye penetrant inspection which had been performed earlier in 1990 and would have rejected the discrepant hardware.[10] Corrective actions were implemented in both the braze application area and the planning for production.

Flight Program Testing

Engine/Missile Inlet Compatibility Tests: In support of the TOMAHAWK flight test program, NAPC has been involved in the extensive evaluation of missile inlet and engine compatibility.

Most recently, compatibility tests were performed in the Freestream flight environment at NAPC in early 1991. As background, during the 1983 Operational Test Launch (OTL) of a GD/C TOMAHAWK, the F107-WR-400 engine experienced excessive and violent surge. Flight telemetry indicated that, under the cold inlet conditions flown, the engine inlet corrected airflow exceeded the missile inlet flow limit, choking the inlet and resulting in surge. Under such conditions, the engine surges with increasing frequency as the throttle is advanced in attempts to maintain flight Mach number. An adaptive throttle management (ATM) algorithm was developed by GD/C to limit the throttle of the engine during low altitude, high Mach, Cold Day flight conditions. The ATM prevents the engine from obtaining high speeds which relate to high inlet airflows resulting in the onset of repeated, destructive surge. From these tests the ATM was designed to limit inlet corrected airflow to 14.1 lbm/sec for the F107-WR-400 and 13.9 lbm/sec for the F107-WR-402 engine, somewhat limiting

DATE LOCATION TEST
1985 Elmendorf AFB A-6E Captive Carry
Confirm inlet choking results in engine surge seen during 1983 test flight.
1985 NAPC, Trenton Inlet Compatibility
Provide information on engine durability after sustained surging.
1985 AEDC, Tullahoma Freestream
Determine engine surge characteristics based on altitude, Mach, temperature, angle of sideslip and attack, and inlet variations.
1987 NAPC, Trenton Inlet Compatibility
Determine effects of stub duct misalignment on engine surge characteristics.
1988 NAPC, Trenton Inlet Compatibility
Compare surge characteristics of the -400 engine to the -402 engine and conduct additional stub duct misalignment tests.
1989 AEDC, Tullahoma Freestream
Determine the effects of engine, inlet, stub duct and angle of sideslip on engine surge characteristics.
1989 Elmendorf AFB A-6E Captive Carry
Demonstrate the effectiveness of the ATM algorithm for the -402 engine and obtain surge data for both the -400 and -402 engines at conditions unattainable in the test cell.
1991 NAPC, Trenton Freestream
Evaluate the characteristics of a new production inlet with -400 and -402 engines.

TOMAHAWK Freestream Test History
Figure 13

takeoff and terrain following performance under cold inlet conditions. These ATM limits were analytically determined and empirically verified sufficient to prevent the engine from reaching a surge frequency of 0.3 hertz (one surge event every 3 seconds). Through mission risk analysis, this had been determined to be the threshold surge limit for mission success.

In support of the ongoing efforts to improve TOMAHAWK performance and mission capability, the freestream test was performed at NAPC in January 1991 to evaluate the surge characteristics of the F107 engine design with various missile inlets. The goal was to reduce surge variability by reducing hardware variability. WI F107-WR-400 and -402 engines were tested in a full scale model of the BGM-109 TOMAHAWK Cruise Missile in the altitude test chamber, as shown below.

The installation was designed to allow testing at angles of side slip of 0 and +2 degrees (nose left aft looking forward) and was at a fixed angle of attack of 0 degrees. Facility conditioned air was supplied to a 44 inch diameter duct which contained the missile model. A bypass was installed at the top of the duct exit to remove the boundary layer which formed above the missile body section centerline. The TOMAHAWK aft body section, which houses the missile inlet and stub duct (which bleeds inlet air for generator cooling and inlet temperature measurement) was suspended from a TF34-GE-400 engine test stand. The F107 engine was installed inside the TOMAHAWK tailcone section and mounted to the rear of the aft body, with a stub duct seal mating to the engine face. High response on-line acquisition of critical parameters, including engine rotor speeds, power lever and CDP were recorded. The sampling rate on CDP, which represented the main indicator of surge, was 3000 samples/second. In addition, exhaust viewing systems permitted visual confirmation of surge (ie, fire balls at the tail pipe due to the accumulation of fuel in the combustor during flow reversal) provided graphic documentation. Engine airflow was calculated from an

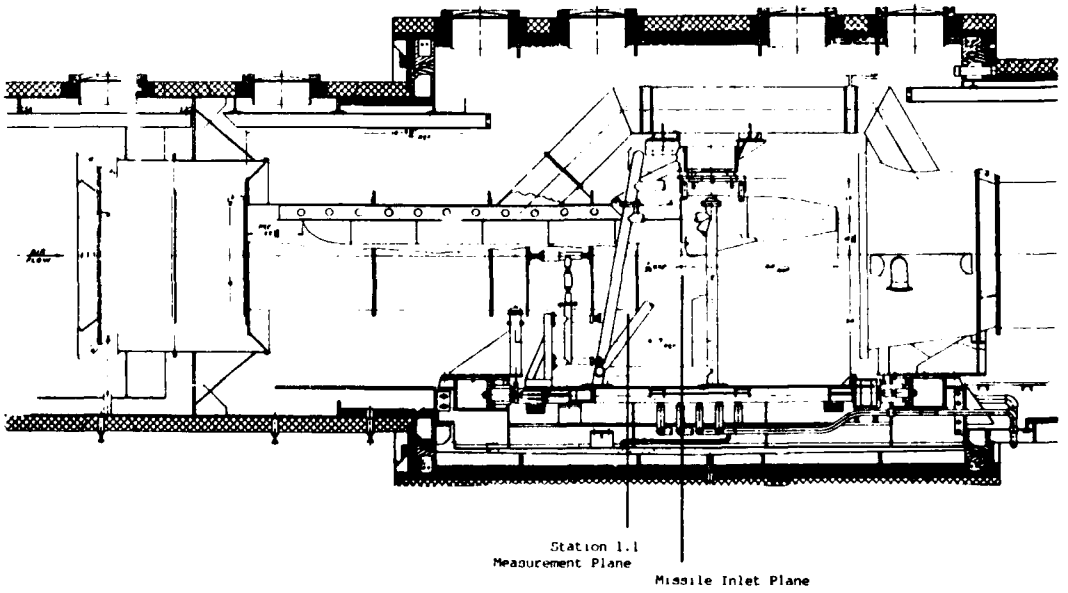

NAPC TOMAHAWK Freestream Installation
Figure 14

area weighted pitot-static pressure measuring station, located at the engine inlet plane, during calibrations in a direct connect installation, prior to the Freestream Test, as shown below.

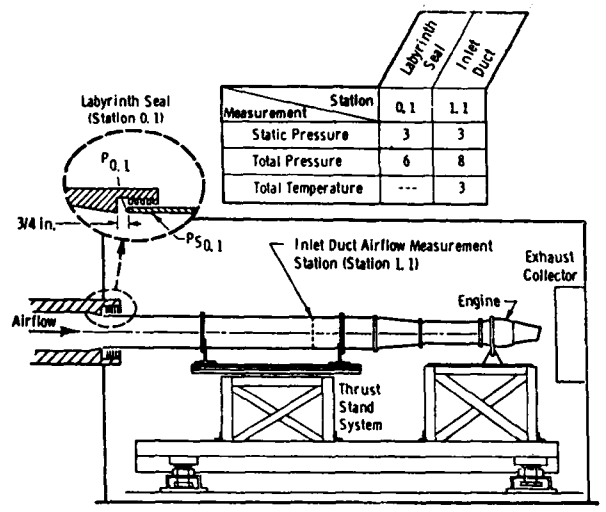

NAPC Direct Connect Installation
Figure 15

Inputting a correlation of measured N1 to airflow into the data reduction program allowed prediction of airflow in the freestream installation, based on acquired N1. Flow field fidelity tests were conducted with the supply duct and missile body heavily instrumented with total and static pressures, boundary layer pressures, cone probe static pressure (for side slip angle measurement) and temperatures. The test provided good correlation with tests previously performed with the same hardware. The F107-WR-400 and -402 engines had similar surge characteristics, indicating that the initial ATM limit for the -402 had been conservative and should be increased by 1.5 percent, which will enhance missile performance. Future testing will investigate the variability (if any) of inlet profiles and their effects on engine surge characteristics in production lots of machined inlets.

Current Efforts

Quality Evaluation Program: Established in 1988, the TOMAHAWK Quality Evaluation Program (QEP) was put in place to address the aging fleet of missiles. With the existing maintenance interval of 36 months, funding is inadequate to recertify all the missiles through the depot. The QEP focused on extending the maintenance interval through inspection,test and evaluation of aged missile components. NAPC was tasked with the QEP of the engine and airframe generator-regulator. Funding constraints precluded sufficient testing to attain the required confidence levels for the engine reliability goals. Assuming a level of risk, the program was divided into two test scenarios, disassembly inspection and functional test. Using the F107 warranty test program as a data base, engines tested after extended fleet storage periods are factored into an overall system reliability model, to predict long term effects on parameters such as performance and oil consumption. Data received from disassembly inspection are used to predict aging trends on hardware and potential failure modes during functional test. Combining these data bases produces a model of the engine which provides a reasonable level of confidence for life extension. As the engine and generator undergo this program at NAPC, the other energetic components of the missile such as pyrotechnic devices, the warhead and batteries also undergo QEP. Reliability estimates from all activities are then combined at the AUR level to determine optimum missile shelf life.

Specification Performance Verification Test: As with the F107-WR-400, the F107-WR-402 engine production quality must be assessed in the test cell and through flight test. A program established in 1989 for verification of initial production and documentation of

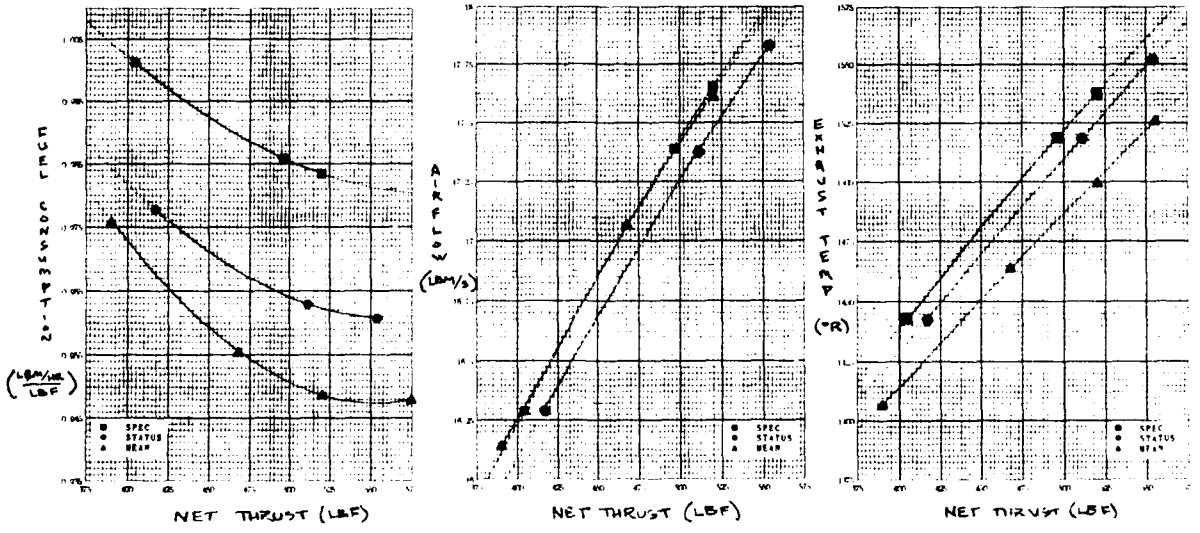

Sample: NAPC SPVT Phase I Test Results
Figure 16

actual production lapse characteristics is the Specification Performance Verification Test Program (SPVT). Sixty of the first 190 F107-WR-402 engines produced (30 percent) were evaluated via altitude/Mach testing to verify performance lapse and system durability. In this unique program the altitude testing became part of the engine acceptance, providing excellent correlation of SLS to altitude/Mach rating performance while precluding expensive engine refurbishment prior to installation in the missile. This represents the first time that a large production engine data base has been used to document the "status" or nominal performance of the production engine, which in some cases varied greatly from the analytical model. In addition, deficiencies in the acceptance test procedures surfaced which led to modifications to procedures and limits.

Conclusion

The high reliability of the TOMAHAWK Propulsion system demonstrated in the Desert Storm conflict can be traced directly to the research, development , test and evaluation efforts performed by the Cruise Missile Engine community. Throughout development, qualification, substantiation and warranty demonstration test programs, the Naval Air Propulsion Center has amassed a vast data base for F107 engine family which has been crucial in confirming and constantly improving the engine design and performance. As the defense environment shifts from one of deterrence to one of economy and frugality, the emphasis dictated to those who develop and execute the methods to maintain system reliability are redirected to life extension and maintenance optimization concepts. NAWC AD TRN (formerly NAPC) continues to lead the propulsion community in these efforts for TOMAHAWK, HARPOON and all other lethal/non-lethal UAV propulsion systems.

References

1 Cruise Missiles, A Deterrent With A New Dimension
Walter M. Locke, RADM, USN, Director JCMP; AUVS symposium L.A. and Salt Lake Chapters; 11 May 1981

2,4 The Joint Cruise Missiles Project: An Acquisition History
E.H. Conrow, G.K. Smith, A.A. Barbour; Rand, Santa Monica, Ca.; August 1982

3 SLCM Presentation for the 2nd Annual SEP Technical Conference
J. Fagan, AUR-SEIA, General Dynamics, Convair Division; September 1991

5 TOMAHAWK Cruise Missile Engine Program Facts
W. Balderson, Cruise Missiles Project; 8 August 1988

6 Propulsion Concepts for Advanced Cruise Missiles
J.E. Lueke, R.L. Spencer, K.S. Bauman, Captain, USAF
Aero Propulsion Laboratory
Air Force Wright Aeronautical Laboratories, Wright Patterson Air Force Base, Ohio; Not Dated

7 F107-WR-400R Improvement Program Proposal 8407C, Book 1 - Technical
Williams International; April 1986

8 Summary Report on RJ-4 Storability and Compatibility
J.L. Bicknell, Bendix Aerospace Systems Division,
Mishawaka, Ind. MAL Report No. 3082; 22 December 1977

9 Minutes of Fuel System Anomalies Meeting - 6 Jan 1988
W. Birchell, AUR-SEIA Program Integration, General Dynamics, Convair Division AUR-SEIA 3771; 21 January 1988

10 F112-WR-100 Engine E.544 Failure Investigation Report
W. Fant, Williams International; 15 October 1991

Discussion

Question from M. RAVIER, MATRA

You have presented in the future trends at system level one action about signature reduction. I guess it is in infrared. Do you foresee other domain of signature reduction ?

Author's reply

Efforts in this area are strongly preliminary. Certainly the "State of the art" in reduction of signatures will be considered in future upgrades of the missile, for example inlet design and control intakes.

Question from Ph. CAZIN, ONERA

To increase the missile's penetration, what will you try for the future ?

Increase the speed or reduce the optical signature ?

Author's reply

TOMAHAWK will remain a subsonic system. Improvements in signature, if they occur, will probably be optical.

Question from Maj. CLARK, Ottawa

Is it true that 8 hours of acceptance run represents 32 % of the life time of 25 hours of the engine ?

Author's reply

It is true. The engine acceptance procedure allows up to 8 hours of operation prior to acceptance. Additional cycles will increase this number. However, although the design life is 25 hours, the majority of the engine hardware has a maximum run limit of approxomately 100 hours. Although no complete engine will work more than 25 hours, the hardware will be redistributed until the component life has been exhausted.

Question from J.P. PAUL, Microturbo, France

In the light of the recent desert storm operation what are the items you consider have to be improved in the field of maintenance of the engine of the TOMAHAWK ?

Author's reply

As demonstrated in operation desert storm, the maintenance aspects of the TOMAHAWK engine are very good. The upgraded engine has incorporated what one believes to be the items needed to extend maintenance interval from approximatively 5 hours to 10 hours.

Question from M. RODGERS

All engines passed ATP but 30 % failed mission rating performance. What was the reasons of these failures ?

Author's reply

30 % failed specification altitude performance requirements. The TOMAHAWK inlet is limited at certain flight conditions. The altitude thrust problem were corrected by softening the acceptance thrust trim band up 1,5 %.

TURBOREACTEUR SIMPLE ET PERFORMANT A COMPRESSOR AXIAL QUADRI-ETAGE ET TURBINE AXIALE POUR LA PROPULSION DE MISSILES SUBSONIQUES

Jean-Paul LOPEZ
Ingenieur de Marque
Turboréacteur TRI 60-30
MICROTURBO

Charles MISCHEL
Chef du Service Calculs
Aérothermodynamiques
MICROTURBO

RESUME

Dans la lignée de ses turboréacteurs pour propulsion de missiles et engins cibles, application dans laquelle elle connaît un grand succès, la Société MICROTURBO développe un turboréacteur simple et performant à compresseur axial quadri-étage et turbine axiale destiné à la motorisation de l'APACHE.

Ce nouveau turboréacteur simple flux simple corps, de la classe des 550 daN de poussée à un Mach de vol de 0,8 au niveau sol, affiche une consommation spécifique voisine de 1 kg/daN.h dans la zone des 300 à 400 daN, et de 1,10 pour 550 daN au point fixe, dans un diamètre de 343 mm imposé par l'intégration.

La présentation porte sur les travaux thermodynamiques et la conception mécanique.

Les quatre compresseurs axiaux ont été définis à partir de l'expérience acquise par MICROTURBO sur les compresseurs tri et quadri-étages de la famille TRI 60 et grâce à l'utilisation intensive du code 3D-EULER de l'ONERA. Chacun des étages a été fabriqué, puis essayé au banc RACE du CEPr dans un temps relativement court. Il en fut de même pour le compresseur complet. Les performances ont été atteintes voire dépassées.

La turbine prédimensionnée à l'aide d'une méthode traditionnelle a aussi été optimisée à l'aide du code 3D EULER.

Les exigences données à la conception mécanique sont durée de vie limitée, maintenance minimum, respect des performances et coût de production peu élevé. Très tôt dans le programme, la "fabricabilité" au moindre coût a été prise en compte. Les discussions de procédés entre bureau d'études et méthodes, s'appuyant sur les informations communiquées par les fournisseurs, ont déterminé les différentes solutions de production. Le classement s'est alors fait en tenant compte du coût de production, des risques et de l'intégration dans le moteur et l'engin. Il en résulte l'utilisation large de la fonderie pour rotor, redresseurs et carters.

Les systèmes ont aussi été réduits au minimum possible par le démarrage en autorotation, l'entraînement quasi direct de la pompe et de l'alternateur et la suppression d'une lubrification par huile.

OVERVIEW

The design and development of turbojet engines for missile and target drone propulsion is a field in which MICROTURBO enjoy considerable success, and one of these engines has been selected and is in current development for the APACHE standoff missile. This new single-flow, single-spool turbojet produces 550 daN at Mach 0.8 ; giving an SFC figure of 1.10 kg/daN/h at 550 daN and SL Static which drops to the region of 1 kg/daN/h at 300-400 daN, all this within a 343 mm diameter.

This preview outlines the tasks carried out to obtain the optimum thermodynamic definition and mechanical design of the engine.

Extensive experience in the design of three and four stage compressors of this type has been gained by MICROTURBO on their TRI 60 engine family. This experience was used as a basis for the conceptual design of the subject compressor with concurrent intensive used of the 3D EULER code developed by ONERA, France. The turbine, pre-dimensioned using conventional design methods, was also optimized by means of the EULER code. In a relatively short time, each compressor stage was manufactured then tested separately in the RACE test cell at the CEPr facilities in France, this being closely followed by complete compressor testing, during which performance expectations were met and even exceeded.

Major mechanical design requisites for this life-limited engine were minimum maintenance, guaranteed performance and low-cost production. A feasibility study on production cost effectivity, involving close liaison between the design office and methods department, was initiated in the early stages of the program. Using data provided by external suppliers, various solutions were investigated, the final selection taking into account production cost and risk factors relative to engine and/or missile integration. The result of this investigation is the wide use of castings for rotors, stators and casings.

Maximum simplicity has been achieved for engine systems by designing in features such as windmill start capability, a virtually direct drive transmission to the fuel pump and the alternator and finally, the elimination of the oil lube system.

SOMMAIRE

NOTATIONS

Cs	Consommation spécifique (kg/daN.h)
F	Poussée (daN)
ΔH	Variation d'enthalpie (J/kg)
K_p	Marge au pompage (%)
MVx	Nombre de Mach débitant moyen (-)
MWe	Nombre de Mach relatif en tête (-)
P/P	Rapport de pression / taux de détente (-)
Q	Débit d'air ou de gaz (kg/s)
Q*	Débit réduit ($Q\sqrt{T}/P$ ou $Q\sqrt{\frac{T}{288}} \cdot \frac{101,3}{P}$)
Sx	Section débitante ou annulaire (m^2)
T	Température totale (K)
Ue	Vitesse périphérique (m/s)
$\eta$is	Rendement isentropique
ν	Rapport de moyeu
ϕe	Diamètre extérieur

INDICES

- 1 entrée du 1er étage
- 3 sortie du 1er étage
- 9 sortie du 4ème étage

1 - INTRODUCTION

Depuis près de 20 ans, MICROTURBO a acquis une très grande expérience dans le domaine des turboréacteurs consommables à poussée spécifique élevée, pour engins cibles et missiles, facilement adaptables à de nombreuses conditions d'environnement et d'utilisation (compatibilité d'entrée d'air, carburants turboréacteur tous types).

Ces turboréacteurs sont équipés d'un compresseur axial, à trois ou à quatre étages, d'une chambre de combustion directe et d'une turbine axiale d'un diamètre maximum de 330 mm.

Pour la gamme des turboréacteurs à trois étages axiaux (TRI 60-1 à TRI 60-5), la poussée s'étage de 350 daN à 440 daN, la consommation spécifique de 1,20 à 1,30 kg/daN.h, le débit d'air de 5,8 kg/s à 6,70 kg/s, le rapport de pression de 3,7 à 4,1 et la température d'entrée turbine de 930°C à 1050°C au point fixe.

Pour le turboréacteur à quatre étages axiaux TRI 60-20 ces grandeurs deviennent respectivement 500 daN ; 1,16 kg/daN.h ; 8,35 kg/s ; 5,0 ; 935°C au point fixe.

Forte de cette expérience, MICROTURBO a entrepris il y a 3 ans le développement d'un turboréacteur performant TRI 60-30, à compresseur quadri-étage axial et turbine axiale, suite logique du turboréacteur ci-dessus et destiné à la propulsion du missile APACHE de MATRA dont il satisfait les exigences. Les performances visées pour ce réacteur sont de 532 daN de poussée ; 1,09 kg/daN.h de consommation spécifique ; 8,1 kg/s de débit d'air ; 5,74 de rapport de pression ; 975°C de température d'entrée turbine au point fixe et dans un diamètre légèrement augmenté à 343 mm.

La présentation porte sur les travaux aérothermodynamiques et la conception mécanique qui ont conduit à la fabrication et les travaux de développement et de mise au point des premiers exemplaires du TRI 60-30.

2 - ETUDE, FABRICATION ET ESSAIS DU COMPRESSEUR DU TRI 60-30

2.1. EXPERIENCE ANTERIEURE

Dans le passé, la société MICROTURBO a réalisé, grâce à un contrat DRME, l'étude et la mise au point d'un compresseur axial transsonique de petites dimensions à trois étages pour réacteurs consommables. La roue et le redresseur d'un étage étaient conçus à l'aide d'un calcul d'équilibre radial amont et aval, puis coupe par coupe la pale était élaborée à l'aide d'un squelette circulaire et d'un habillage issu d'un catalogue (NACA ou NGTE). La recherche d'une augmentation de la poussée spécifique (dans le même diamètre) a conduit à la mise en place d'un quatrième étage en amont des trois autres. Cette opération nous obligea à utiliser une méthode de calculs plus performante en vue de l'élaboration des profils de la roue et du redresseur. Il fut définie la roue du 1er étage dès 1986 avec le code de calculs des écoulements 3D EULER CADET de l'ONERA. Les performances atteintes furent très intéressantes puisqu'à la vitesse périphérique de la roue de 405 m/s les valeurs suivantes ont été mesurées :

- débit spécifique $Q_1/Sx_1 = 197$ kg/s m^2
- rapport de pression de l'étage $P_3/P_1 = 1,62$
- rendement isentropique de l'étage $\eta is_{1-3} = 82$ %

Dès 1988 MICROTURBO adhère au Club du Calculateur Aéronautique en vue de l'utilisation intensive de ce code sur ordinateur CRAY localisé à Chatillon pour développer ses compresseurs et turbines, essentiellement axiaux.

2.. ETUDE DU COMPRESSEUR AXIAL QUADRI-ETAGE DU TRI 60-30

A la lumière de cette première expérience, la société décide d'étudier les quatre étages axiaux de ce compresseur en se servant du code 3D EULER CADET. La coupe du réacteur apparaît sur la figure No. 1.

2.2.1. POINT DE CALCUL DES QUATRES ETAGES

Les calculs de cycle ainsi que la prise en compte de l'expérience acquise ont conduit au point de calcul du compresseur complet et de chaque étage. Dans le tableau No. 1 figurent leurs grandeurs caractéristiques.

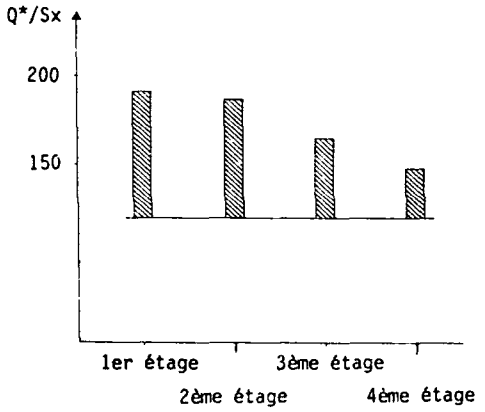

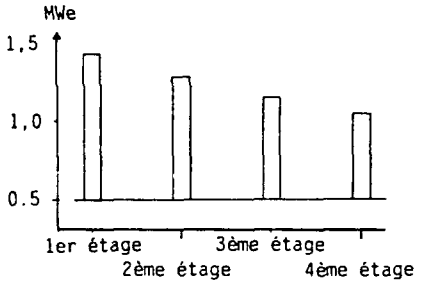

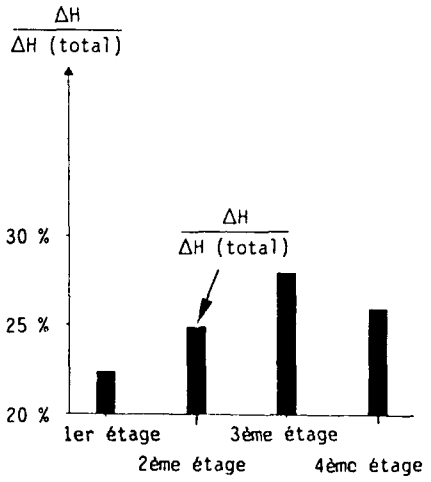

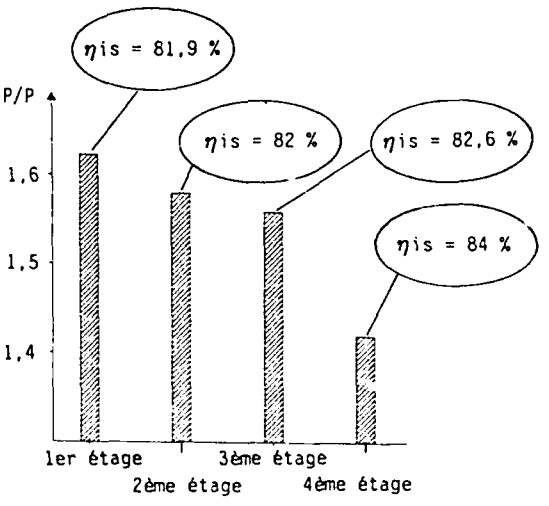

Tableau No. 1 : Point de calcul de chaque étage au point fixe, à la vitesse nominale périphérique moyenne de 410 m/s (N = 28500 tr/mn) et pour un débit d'air de 8,20 kg/s.

L'association de ces quatre étages permet de prévoir un rapport de pression de 5,67 avec un rendement isentropique de 79,2 %.

La répartition des charges par étage correspond à notre expérience ; un premier étage relativement peu chargé compte tenu du nombre de Mach relatif élevé et en prévision d'éventuels problèmes de proximité de décollement tournant ou de pompage au cours du démarrage, une progression jusqu'au troisième qui assure les 28 % de l'augmentation d'enthalpie de l'ensemble et un dernier étage moins chargé en raison de l'importante diffusion à réaliser dans le dernier redresseur avant l'entrée dans la chambre de combustion.

2.2.2. OPTIMISATION DE LA GEOMETRIE DES PROFILS DE LA ROUE ET DU REDRESSEUR DE CHAQUE ETAGE

La définition de chacun des 4 étages de ce compresseur à l'aide du code de calcul 3D-EULER de l'ONERA a constitué une première pour MICROTURBO. L'optimisation a été faite dans l'ordre suivant : 1er étage en raison du nombre de Mach relatif élevé dans la roue, 4ème étage en raison de l'importante déviation à réaliser dans le redresseur, 3ème étage en raison de sa charge importante et finalement 2ème étage. L'optimisation de chacun des étages a été effectuée de la manière suivante :

- première définition de la géométrie de la roue à la suite d'un calcul d'équilibre radial simplifié,

- réalisation du maillage de la géométrie des pales de la roue,

- utilisation intensive du code 3D EULER CADET conduisant à des changements successifs du profil et du nombre de pales de la roue à l'aide d'un certain nombre de critères dont les principaux sont les suivants :

  . optimisation de la [illegible] afin d'aspirer le débit d'air voulu,
  . optimisation de la sortie des profils et du nombre de pales afin de réaliser le rapport de pression désiré avec le meilleur rendement possible,
  . optimisation de l'extrados et de l'intrados afin d'éviter les survitesses et donc les risques de choc trop intenses et les décollements,
  . éviter les déviations trop élevées à réaliser dans le redresseur.

- cette optimisation est réalisée grâce à l'utilisation conjointes des résultats du code 3D EULER et du logiciel de CAO 3D STRIM 100 T utilisé par MICROTURBO. Ce logiciel permet de réaliser facilement l'adaptation des profils.

La définition de la géométrie des aubes des redresseurs a été acquise en utilisant la méthode issue du NACA. Seul pour le 1er étage un calcul 3D EULER roue et redresseur a été effectué.

La veine du compresseur axial quadri-étage du TRI 60-30 apparaît sur la figure No. 2, avec le nombre de pales et d'aubes, leur forme et les dimensions.

Pour illustrer ce travail de définition des profils des pales des roues apparaissent :

. sur la figure No. 3, une modification effectuée sur le profil de la roue du 4ème étage en cours d'optimisation,
. sur la figure No. 4, sa répercussion sur l'évolution, sur l'extrados et l'intrados des pales de la roue du 4ème étage du rapport P/Pi, pression statique locale sur la pression génératrice amont,
. sur la planche No. 5, l'évolution des iso-Mach pour les coupes de tête de la version définitive de la roue de 4ème étage.

2.2.3. FABRICATION DES ROUES ET REDRESSEURS, ET DES MODULES D'ESSAIS

Afin d'acquérir rapidement les performances de chacun des étages ainsi que celles du compresseur complet MICROTURBO a étudié 5 modules d'essais destinés à l'expérimentation au banc RACE du CEPr.

La fabrication des roues et des redresseurs des quatre étages, ainsi que leur contrôle ont été effectués à un rythme soutenu après une optimisation de l'usinage sur un centre à commande numérique 4-axes afin de respecter au mieux les exigences de l'aérodynamique (tolérance relativement serrée, respect strict des bords d'attaque et de fuite, état de surface...) et aussi celles de la résistance des matériaux et des vibrations.

L'usinage pour les essais au banc des aubes des redresseurs ont posé quelques problèmes en raison de leur nombre relativement élevé conditionné par une recherche de raccourcissement du compresseur par rapport au précédent compresseur quadri-étage de MICROTURBO.

Une photographie du bi-étage mobile de tête (RM1 + RM2) apparait sur la figure No. 6, et du redresseur du 1er étage (RD1) sur la figure No. 7. Ce dernier a été élaborée par fonderie pour le moteur.

La figure No. 8 présente la configuration schématique du compresseur, la figure No. 9 celle du module d'essais du 1er étage et la figure No. 10 celle du compresseur complet.

2.2.4. ESSAIS DES QUATRE ETAGES ET DU COMPRESSEUR COMPLET, ET RESULTATS

Les résultats de ces essais furent acquis au CEPr dans un temps relativement court puisque l'essai du 1er étage fut effectué le 29 mai 1989 et celui du compresseur complet livra ses résultats le 28 novembre 1989. Le 4ème étage a subi deux essais pour tester deux types de diffusion en aval du dernier redresseur à l'entrée de la chambre de combustion : diffusion à bi-canaux et diffusion à éclatement de jet.

2.2.4.1. Essais des étages

Les résultats de chacun des étages furent proches des prévisions comme le montre le Tableau 2 ci-dessous.

Désignation	1er étage		2ème étage		3ème étage		4ème étage	
	Objectif	Résultats d'essais	Objectif	Résultats d'essais	Objectif	Résultats d'essais	Objectif	Résultats d'essais
N*	28500	28500	26225	26000	24250	24500	22500	22500
Q*	8,2	8,244	5,494	5,445	3,763	3,783	2,602	2,602
P/P	1,622	1,614	1,579	1,583	1,559	1,554	1,419	1,500
$\eta$is	81,9 %	80,3 %	82 %	84,9 %	82,6 %	82,6 %	84 %	83,2 %
Kp	> 10 %	20 %	> 10 %	20,4 %	> 10 %	18 %	> 10 %	12 %

Tableau No. 2 : Comparaison entre l'objectif et les résultats des essais au CEPr de chacun des quatre étages du compresseur du TRI 60-30.

Les performances (rapport de pression et rendement isentropique) sont annoncées avec la pression totale en aval du redresseur recalculée à l'aide des mesures de la pression statique de parois extérieures et intérieures, de la mesure de la température totale, du débit d'air en amont du compresseur et de l'équation de continuité en supposant que toute la section géométrique est occupée. Seul pour le 4ème étage les performances sont obtenues à l'aide de la moyenne de 20 pressions totales en raison de la présence de la diffusion aval qui simule l'entrée dans la chambre de combustion. D'ailleurs, à la suite des deux essais du 4ème étage, a été sélectionnée la diffusion par éclatement du jet, environ 2 % de la pression est perdue dans cet éclatement.

Est à noter la marge au pompage importante essentiellement pour le 1er étage.

Sur les figures No. 11 et 12 apparaissent le diagramme compresseur et le rendement du 1er étage.

2.2.4.2. Essais du compresseur complet

Les résultats de ces essais confirment notre attente à la suite des bons résultats des essais de chacun des étages. Le Tableau No. 3 ci-dessous le montre.

DESIGNATION	OBJECTIF	RESULTATS DE L'ESSAI	POINTS D'ESSAIS DE RENDEMENT MAXIMAL	
N*	28500	28000	28000	28500
Q*	8,2	8,24	8,234	8,382
P/P	5,666	5,670	6,06	6,118
$\eta$is	79,2 %	81,2 %	82,1 %	80,7 %
Kp	> 10 %	21 %	12,9 %	13,4 %

Tableau No. 3 : Comparaison entre l'objectif et les résultats des essais au CEPr du compresseur complet du TRI 60-30.

Les performances complètes sont illustrées par les figures No. 13 à 16.

Les performances (rapport de pression et rendement) ont été mesurées à l'aide de 20 pressions totales situées en sortie de la diffusion en aval du 4ème redresseur.

Parallèlement aux essais de performances classiques a été mis en évidence à l'aide de capteurs Kulite la présence d'un décollement tournant entre 13000 et 19000 tr/mn étendu sur toute la plage de débit à ces vitesses. Le niveau d'instabilité est néanmoins relativement faible (40 mb au maximum) et la chute de rendement occasionnée par ce phénomène limitée (de l'ordre de 2 à 3 points)

L'iso-vitesse N* = 20000 tr/mn s'est vu réduite à une verticale d'abscisse quasiment égale au débit de pompage du compresseur 1er étage essayé isolement.

Ces deux points pourraient d'ailleurs occasionner quelques problèmes lors d'essais en autorotation, le turboréacteur n'étant pas pourvu de géométrie variable.

3 - ETUDE ET FABRICATION DE LA TURBINE

3.1. POINT DE CALCUL

Le point de calcul de la turbine a été choisi comme suit :

Vitesse réduite	$N/\sqrt{T}$ (tr/mn $\sqrt{K}$)	878
Débit de gaz réduit	$Q\sqrt{T}/P$ (kg/s $\sqrt{K}$/kPa)	0,5022
Taux de détente	P/P (-)	2,73
Rendement isentropique visé	$\eta$is (%)	85,9 %
Chute d'enthalpie spécifique	$\Delta H/T$ (J/kg K)	219
Diamètre de la veine extérieur de la roue	Øe (mm)	310

3.2. OPTIMISATION DE LA GEOMETRIE DES PROFILS DU DISTRIBUTEUR ET DE LA ROUE DE TURBINE

Un calcul d'équilibre radial avec simulation des pertes dans les deux composants a permis, grâce à l'utilisation de profils d'aubes et de pales classiquement utilisés à MICROTURBO, d'accéder à une géométrie que nous avons par la suite optimisée et validée à l'aide du code 3D EULER et du logiciel de CAO 3D STRIM 100 T. Cette méthode d'optimisation de profils fut utilisée pour la première fois dans notre société.

Sur la figure No. 17, apparaît le schéma de la veine de la turbine axiale du TRI 60-30.

Pour illustrer ce travail d'optimisation des profils des aubes du distributeur et des pales de la roue apparaissent :

- sur la figure No. 18, l'évolution sur l'extrados et l'intrados des aubes du distributeur en pied et des pales de la roue en tête de la veine du rapport P/Pi, pression statique locale sur la pression génératrice amont,

- sur la figure No. 19, l'évolution des iso-Mach pour les coupes de pied du distributeur et le tête de la roue de turbine.

3.3. FABRICATION DU DISTRIBUTEUR ET DE LA ROUE DE TURBINE

Après calculs de résistance de matériaux dans les pales et le disque de turbine et analyse vibratoire des pales, la roue de turbine a été fabriquée par fonderie avec un très bon respect des profils et notamment des épaisseurs. Ainsi au bord de fuite de la roue une épaisseur de 0,8 mm a été obtenue.

Cette turbine n'a pas été essayée sur un banc d'essais, mais a été intégrée dans le turboréacteur.

4 - CONCEPTION MECANIQUE

4.1. LES CONTRAINTES A LA CONCEPTION

Les applications définies ci-dessus au paragraphe 1 présentent des caractéristiques spécifiques quant à la conception du produit :

- durée opérationnelle courte mais longue durée de stockage,
- minimum de maintenance en stockage et minimum d'opération de mise en condition opérationnelle,
- haute fiabilité,
- forte capacité d'accélération depuis la mise à feu jusqu'à la puissance de croisière,
- une durée de vie opérationnelle définie en fait par le développement plutôt que par la mission. En effet la faible durée de vie imposerait qu'un grand nombre de moteurs soit affecté aux essais de mise au point et qualification. Pour des raisons évidentes de coût, on définira le produit avec une durée de vie telle qu'un nombre minimal de moteurs soit utilisé en développement (par exemple huit moteurs seulement pour les essais motoriste),
- coût d'acquisition le plus faible possible, pour illustrer l'importance relative du coût total d'un programme, nous citerons les chiffres relevés dans une étude du constructeur Williams concernant le turboréacteur F107-WR-101.

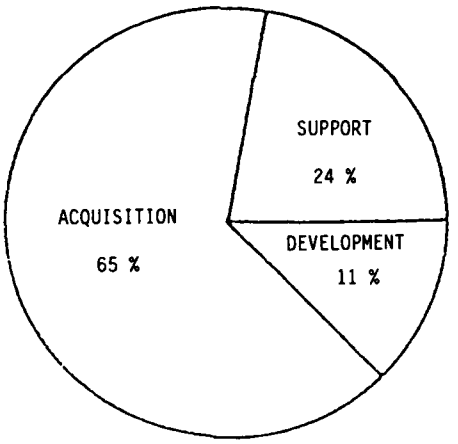

Références

1. J. Weitzner, "Cruise Missile Engine Program Life Cycle Cost Estimate for the F107 Turbofan Engines", DAL-800D-1 contract N00019-80-3003, January 1981.

Historiquement, deux voies ont été suivies :

- utiliser un moteur dérivé de turboréacteurs ou turbines existants,
- développer un moteur simple spécifiquement conçu pour le besoin.

Cette seconde voie est celle choisie par MICROTURBO depuis 1972, date des premières études de turboréacteur à faible coût et courte durée de vie adaptée à la propulsion de missiles, drones et cibles.

Actuellement, cette ligne de produit comprend 6 types de réacteurs avec plus de 1700 unités produites intégrées dans plus de 30 programmes différents.

4.2. ETUDE COMPRESSEUR

Au cours de la phase initiale d'étude mécanique et de détermination des performances, le compresseur a été prévu à 4 étages axiaux. On a préféré aussi cette solution "tout axial" à cause du plus faible maître-couple donné par ce type de configuration pour une poussée donnée et pour la flexibilité possible de fabrication : fonderie, usinage à partir de matricé, disques monobloc ou à pales rapportées.

Une étude conduite par le service estimation de MICROTURBO a conclu en faveur de la solution usinage à partir de galets matricés.

COMPARAISON DES METHODES D'OBTENTION DU BI-ETAGE 3 + 4 COMPRESSEUR

	OUTILLAGE (KF)	MATIERE (F)	MAIN D'OEUVRE (h)	COUT (%)
FONDERIE	790	10 230	21,5	100 %
USINAGE	32	1 400	34,1	75

Un jeu uniforme en tête des pales, réalisé en utilisant des rotors à veine externe cylindrique constant est maintenu quel que soit le mouvement axial du rotor. Ce procédé assouplit les tolérances sur le diamètre extérieur des rotors et sur l'empilage axial au cours du montage. On peut alors s'attendre à une baisse du coût de revient par rapport à un moteur à veine convergente.

La veine d'air comporte des redresseurs avec respectivement 56, 68, 80 et 66 pales.

Le canal interaube est ainsi trop étroit pour qu'une solution de fabrication par usinage reste compétitive. L'usinage des aubes est aussi plus complexe que pour un rotor puisqu'il devrait se faire par l'intérieur du disque. C'est pourquoi une solution fonderie en Inconel 718 a été choisi. Ce matériau est utilisé ici pour des raisons de coulabilité et non à cause de contraintes thermiques.

L'ensemble rotor est du type tambour, assemblage mis en oeuvre sur les moteurs de forte puissance : M88, Adour, Larzac.
Toutes choses égales par ailleurs, ce type d'assemblage est plus léger qu'une structure classique du type "disques empilés". Le quatrième étage du compresseur 4ème étage (type disque) du TRI 60-20 a une masse de 4150 grammes contre 3300 grammes pour l'équivalent sur le TRI 60-30 (type tambour).

Le rotor est couplé à la turbine par l'intermédiaire d'un arbre fixé sur le disque 4ème étage d'un côté et par curvic coupling du côté turbine (voir page 13).

Cet arbre arrière de liaison est monobloc pour supprimer soudure et traitements thermiques.

4.3. CORPS CENTRAL RD4 ET CHAMBRE

4.3.1. Corps central

Le corps central RD4 est la pièce structurale principale du moteur. C'est elle qui permet la liaison moteur/cellule et reçoit les efforts.
La conception définitive retient une solution mixte : fonderie + mécano-soudure.

La mécano-soudure est choisie pour l'arrière du corps car elle autorise une réduction de l'épaisseur de peau.

La fonderie donne un redresseur 4ème étage intégral qui assure la bonne tenue aux efforts. Une telle fonderie est complexe. C'est pourquoi les moteurs de pré-qualification auront une structure combinant usinage et mécano-soudure.

Le redresseur 4 est obtenu par usinage de deux couronnes qui sont ensuite assemblées par brasage (voir ci-après).

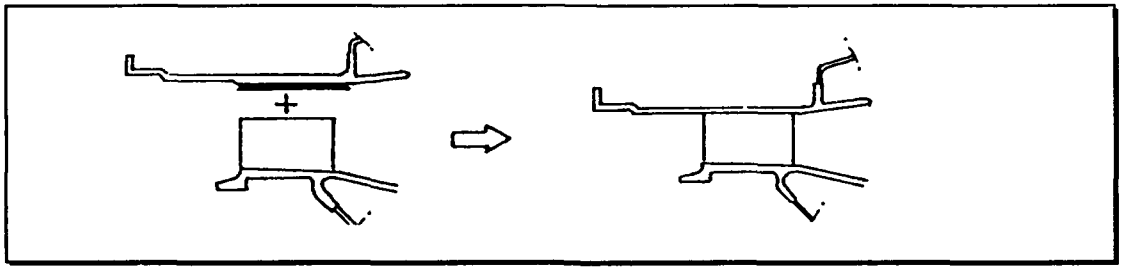

Le corps central RD4 supporte 3 points de suspension situés à 3, 9 et 12 heures. Les suspensions à 3 et 9 heures sont rotulées. Le plan des suspensions est quasiment situé au droit du centre de gravité du moteur.

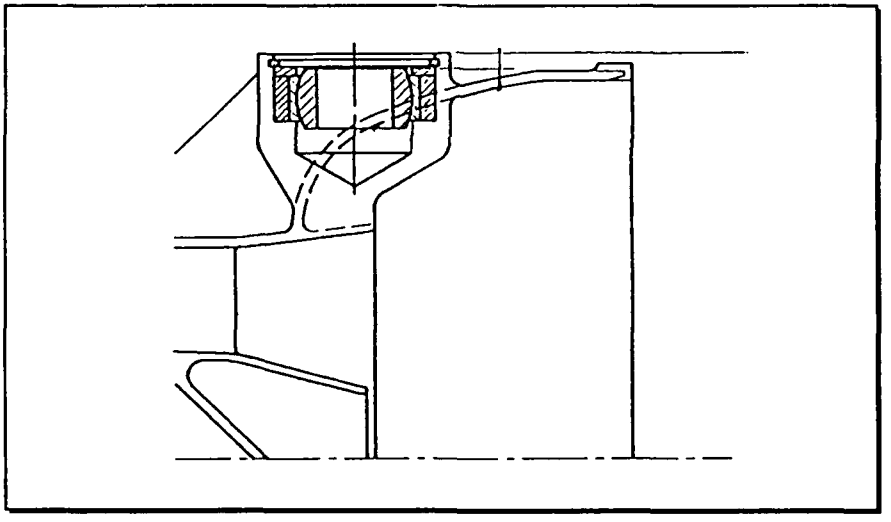

4.3.2. CHAMBRE DE COMBUSTION

Le moteur de missile a une durée de vie courte (quelques heures au maximum), on peut alors se contenter d'un refroidissement peu important des parties chaudes du tube à flamme.
La chambre TRI 60-30 est une extrapolation de la chambre TRI 60-20.

PARAMETRES	TRI 60-20	TRI 60-30
Charge aérodynamique	-	-17 %
Volume du tube à flamme	8,45 l	8,40l
Perte de charge	-	-3 points

Elle est constituée de deux viroles et d'un fond de chambre arrondi. Les trous de refroidissement sont à "bord lisse". Les orifices de combustion et de dilution voient la tôle repoussée vers l'intérieur ("bords tombés") pour diminuer les pertes de charge et augmenter la pénétration du jet dans la chambre par un meilleur guidage.

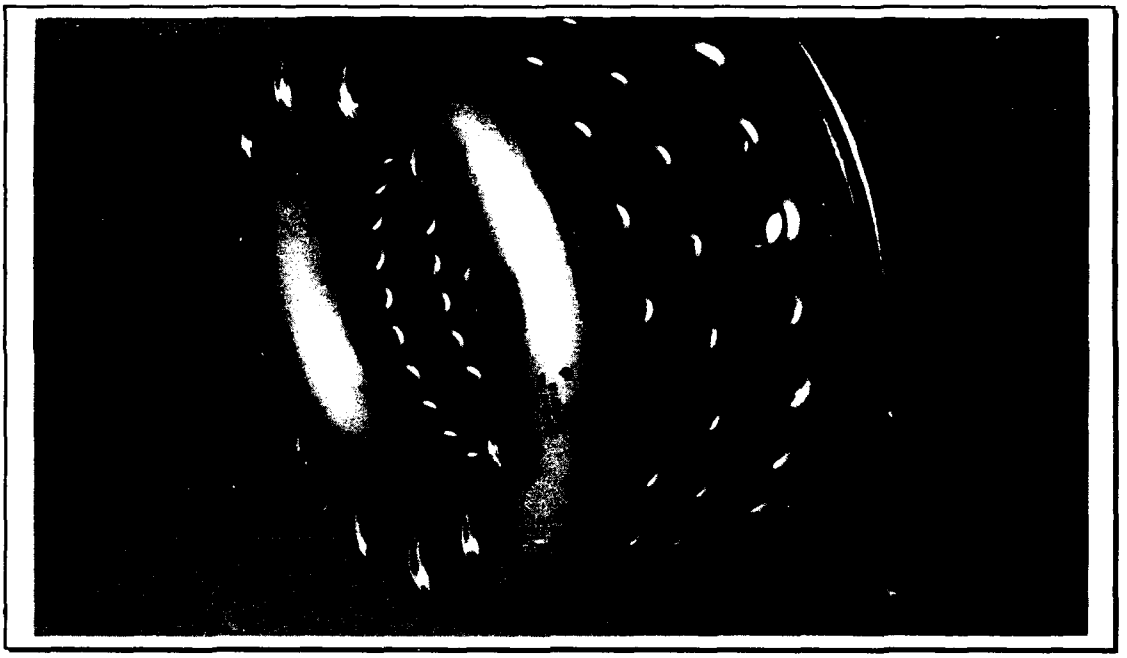

4.4. TURBINE

L'ensemble est à un seul étage de type axial. La partie mobile est constituée par l'arbre creux arrière et la roue de turbine.

Ces éléments mobiles sont assemblés par "curvic coupling" et tirant + boulon qui permet un démontage/remontage sans nécessité de rééquilibrage dynamique.

La partie fixe est formée par le distributeur lui aussi en Inconel 713 LC à aubes pleines (fonderie). Ce distributeur est fixé sur la bride arrière du corps RD4.

La roue de turbine est réalisée en alliage Inconel 713 LC et est monobloc (fonderie).
Cette technique est acceptable pour des moteurs à faible durée de vie (quelques heures voire quelques dizaine d'heures) (voir page 13).

Cette roue fait appel à la même technologie que la roue de turbine de la version TRI 60-20 qui a été calculée pour une vitesse d'éclatement de 46 680 tr/mn et qui a démontré en essais au CEAT une vitesse de 48 120 tr/mn.

4.5. TUYERE

Le système d'échappement des gaz est constitué par une tuyère simple conique de conception identique à celle de la famille TRI 60.

C'est un ensemble chaudronnée réalisé en Z10CNT18 matériau classique pour cette fonction fixé sur la bride arrière du corps central RD4. Son moyeu interne est creux et est supporté par 5 bras.

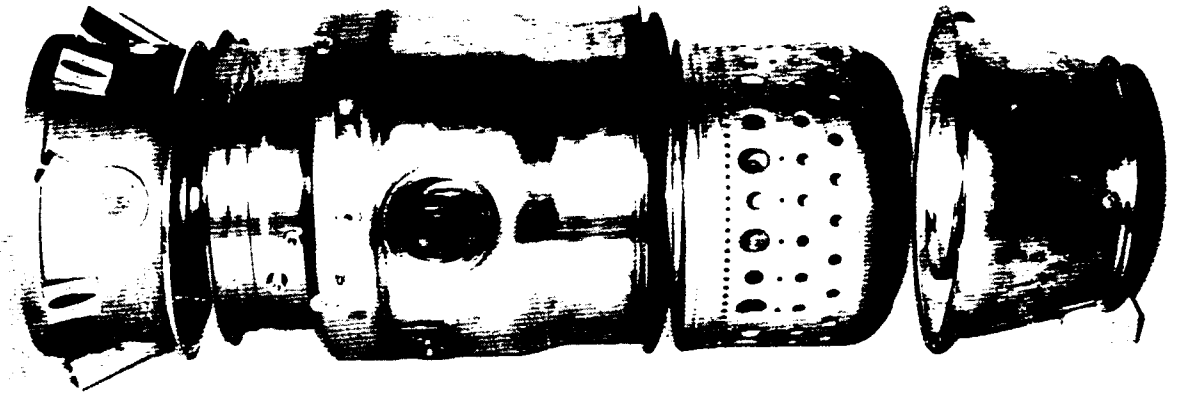

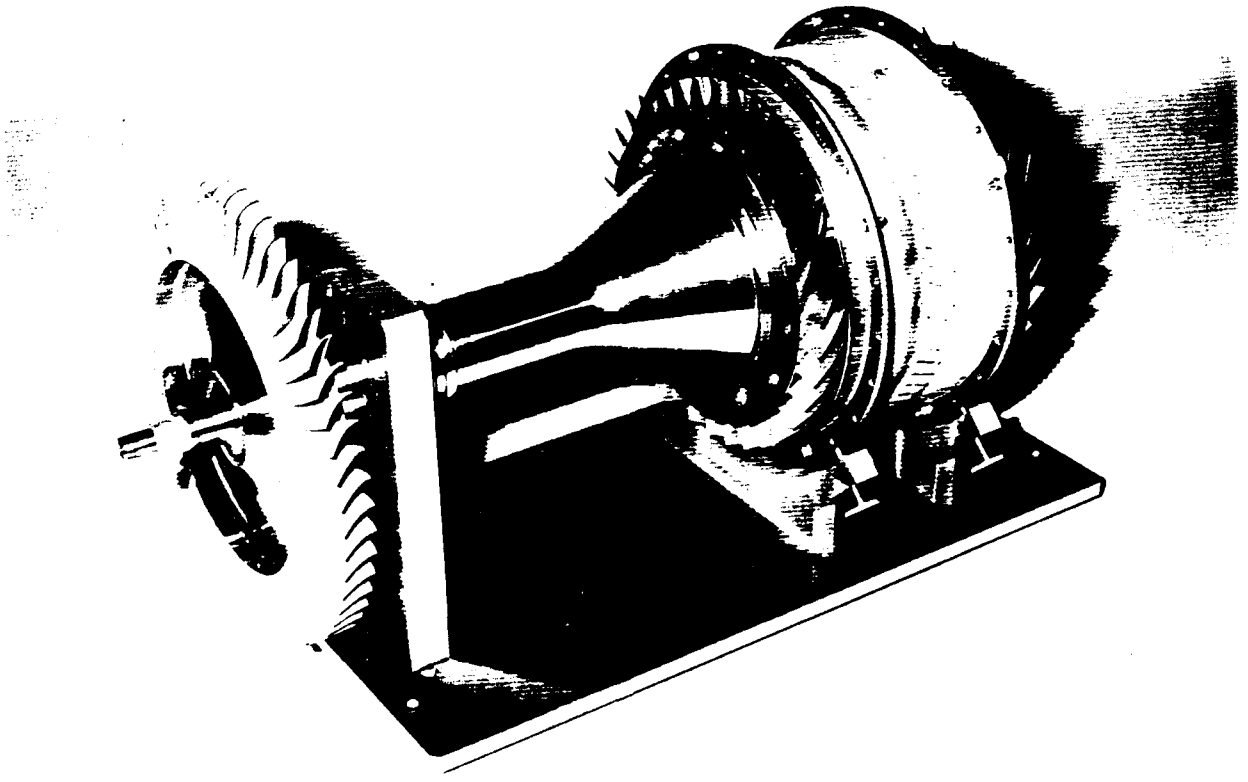

COMPOSANTS DU TRI 60-30

5 - ESSAIS DE TURBOREACTEUR TRI 60-30 AU POINT FIXE

Après un certain nombre de mises au point, surtout dans le domaine mécanique (voir paragraphe 6), les essais du turboréacteur TRI 60-30, équipé du compresseur axial quadri-étage et de la turbine axiale, performants décrits, ont permis de satisfaire les objectifs.

Les performances Cs = f(F) (consommation spécifique fonction de la poussée) au point fixe apparaissent sur la figure No. 20. La poussée de 550 daN est réalisée avec une consommation spécifique de 1,10 kg/daN.h, un débit d'air de 8,11 kg/s un rapport de pression de 6,52 et une température devant turbine de 1040°C.

Lors des premiers essais de compatibilité et performances au point fixe avec l'entrée d'air du missile équipée de ses lèvres de vol, le démarrage du turboréacteur a pu être effectué avec une géométrie fixe. Ce qui est de très bonne augure pour l'avenir et notamment pour les essais de démarrage en autorotation.

Le développement de turboréacteurs TRI 60-30 va se poursuivre par :

- des essais de démarrage au froid au banc A07 du CEPr,
- des essais de démarrage en autorotation au banc R1 du CEPr,
- des essais de performances en vol simulé au banc R1 du CEPr.

6 - LES PREMIERS RESULTATS MECANIQUES

Au cours des premiers essais, des criques en pied de pales de la roue premier étage du compresseur sont apparues au bout d'un quinzaine de démarrage au banc (voir schéma ci-après).

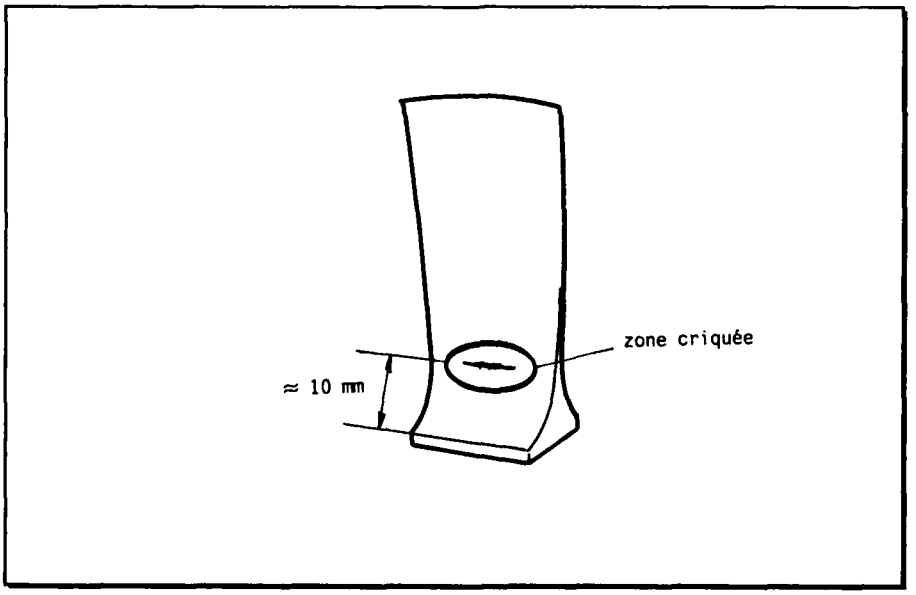

Notre moteur est spécifié pour démarrer en autorotation et ne dispose pas de système de démarrage intégré. La société MICROTURBO ne dispose pas d'installation dite "veine forcée" capable de simuler les conditions d'opération et de démarrer le moteur selon les conditions d'emploi. Aussi, ayant toujours à l'esprit le moindre coût, le moteur est démarré au point fixe à l'aide de 4 buses débitant de l'air comprimé sur les pales de la roue du premier étage du compresseur.

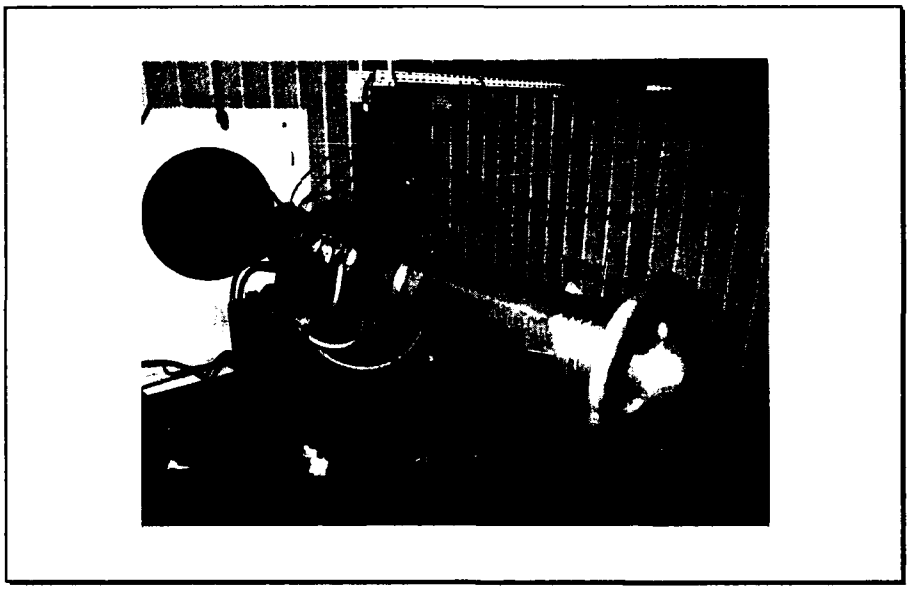

Une analyse par jauge de contrainte a mis en évidence une série de résonance entre premier mode de flexion de la pale et les ordres 6, 8, 10 jusqu'à 22 avec des amplitudes croissantes pouvant atteindre 64 hb crête.

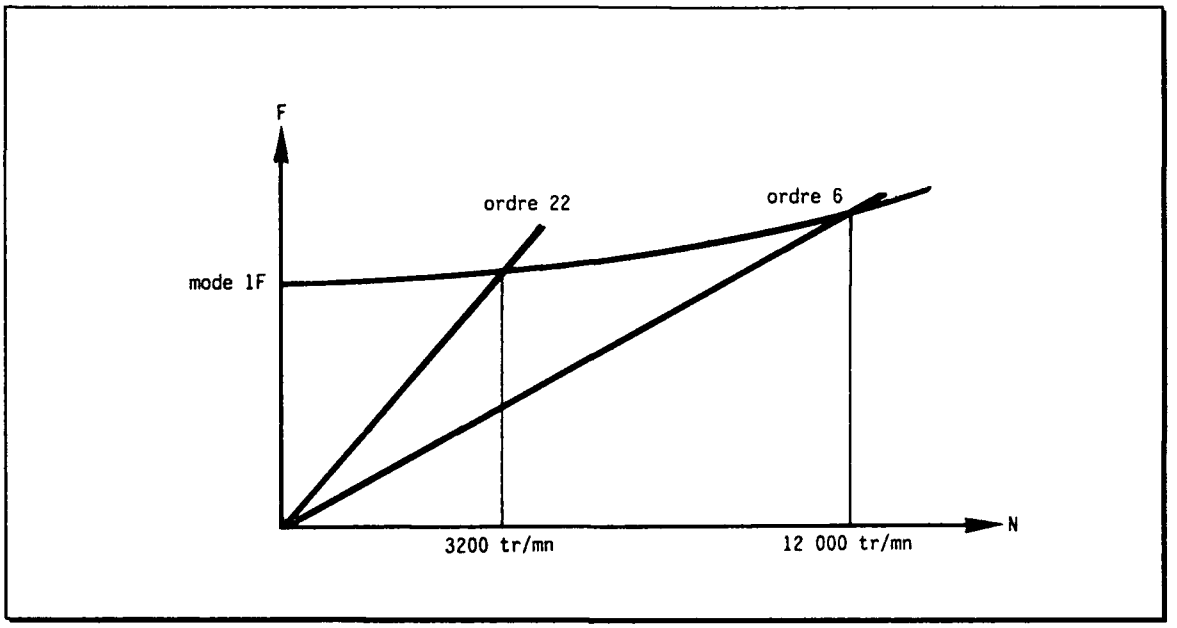

La solution apportée et qui s'est révélée satisfaisante a été d'implanter une série de 17 injecteurs de démarrage à la place des quatre buses initiales.

Cette solution est certes plus compliquée du point de vue fabrication mais la mise en oeuvre au banc reste facile. De plus, cette solution peut être réalisée par fonderie, procédé initialement choisi pour le carter d'entrée d'air moteur.

Après résolution des maladies de jeunesse du type ci-dessus et qui sont attendues sur tout programme de développement, le turboréacteur a montré un comportement satisfaisant pour la mission de courte durée qui lui est demandée.

COUPE DU REACTEUR TRI60-30

Figure 1

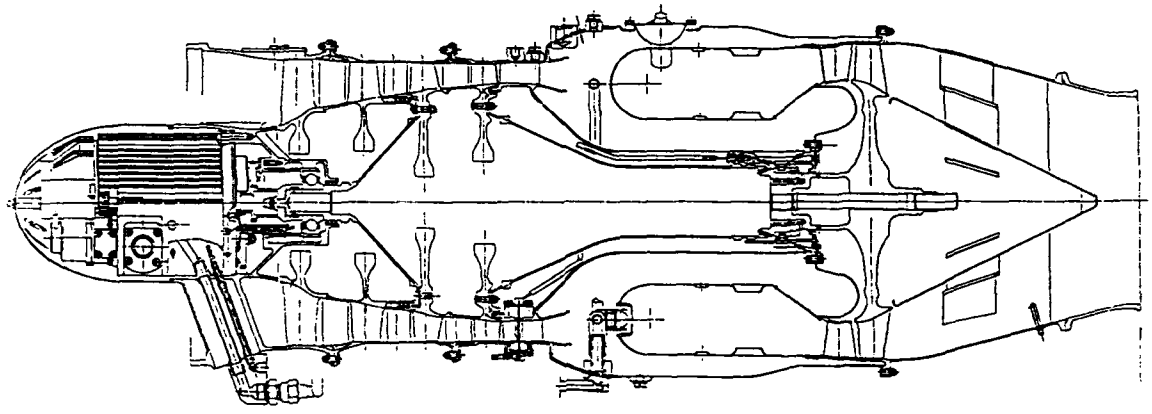

VEINE DU COMPRESSEUR AXIAL
QUADRI ETAGE DU TRI60-30

Figure 2

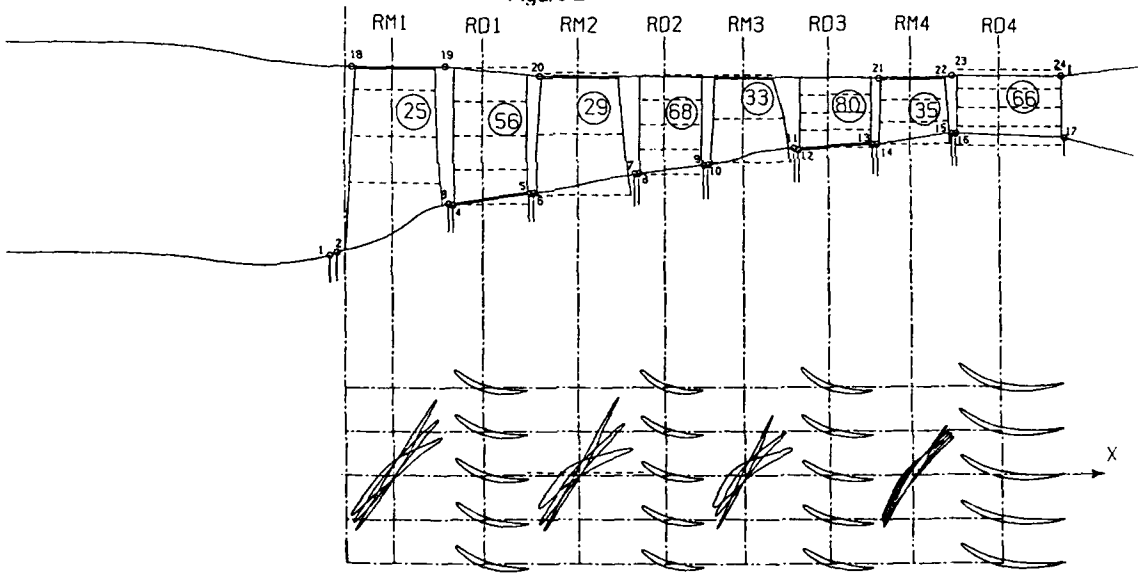

MODIFICATION EFFECTUEE SUR LE PROFIL DES PALES
DE LA ROUE DU 4ème ETAGE EN COURS D'OPTIMISATION

Figure 3

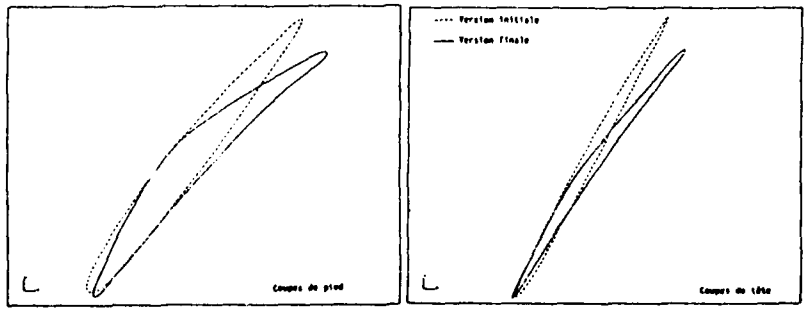

EVOLUTION DU RAPPORT Pst/Pi SUR L'EXTRADOS ET L'INTRADOS DES PALES DE LA ROUE DU 4ème ETAGE EN COURS D'OPTIMISATION

Figure 4

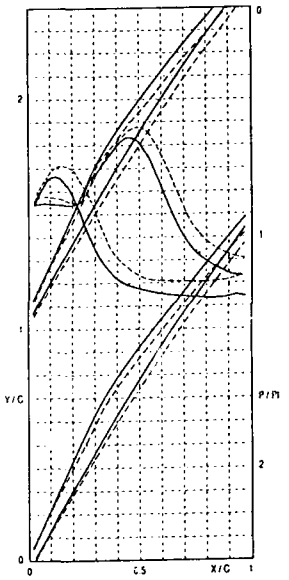

PHOTOGRAPHIE DU BI-ETAGE MOBILE DE TETE (RM1 + RM2)

Figure 6

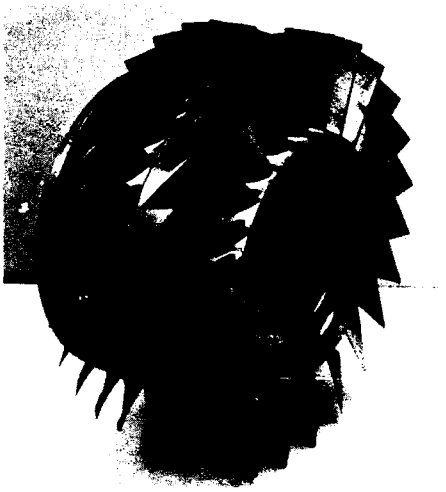

EVOLUTION DES ISO-MACH POUR LA COUPE DE TETE DE LA VERSION DEFINITIVE DE LA ROUE DU 4ème ETAGE

Figure 5

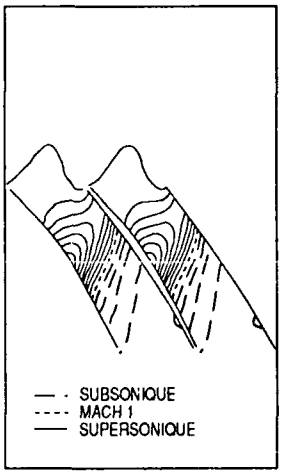

PHOTOGRAPHIE DU REDRESSEUR DU 1er ETAGE RD1

Figure 7

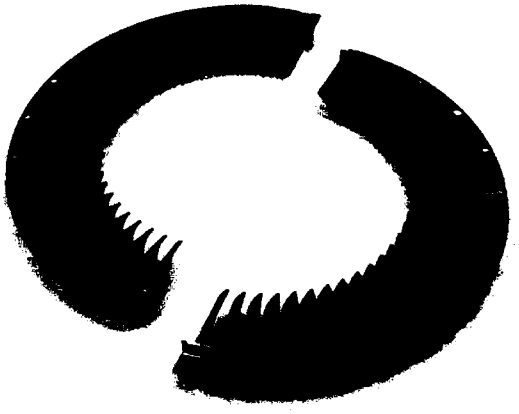

CONFIGURATION SCHEMATIQUE
DU COMPRESSEUR

Figure 8

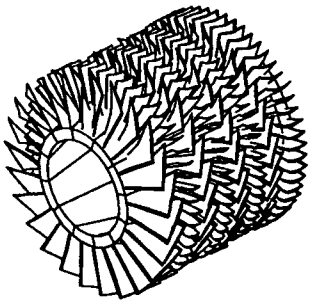

MODULE D'ESSAI DU 1er ETAGE

Figure 9

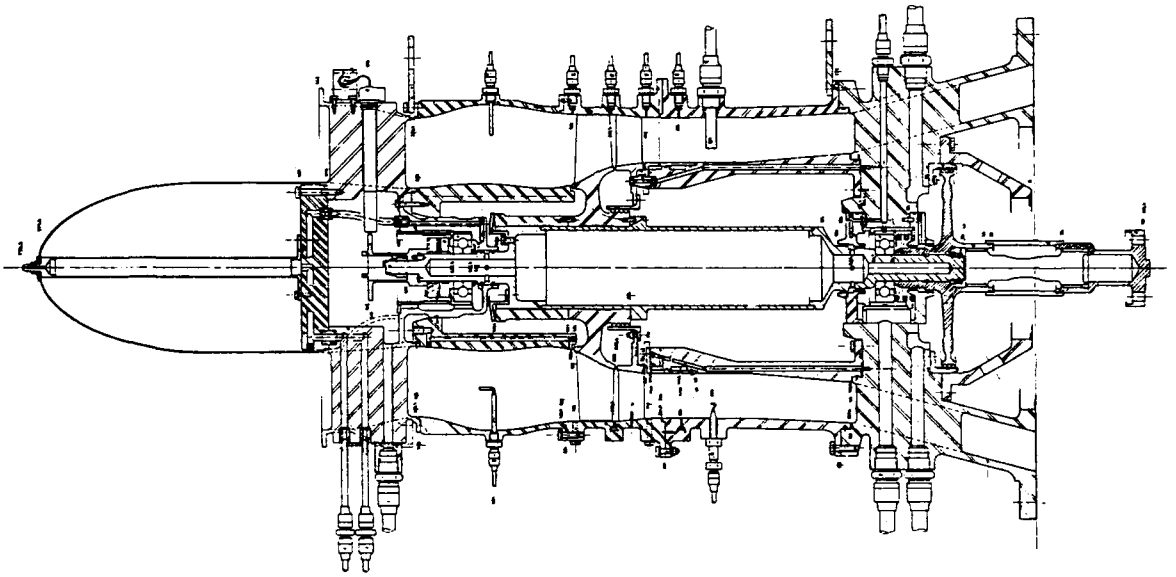

MODULE D'ESSAI DU
COMPRESSEUR COMPLET

Figure 10

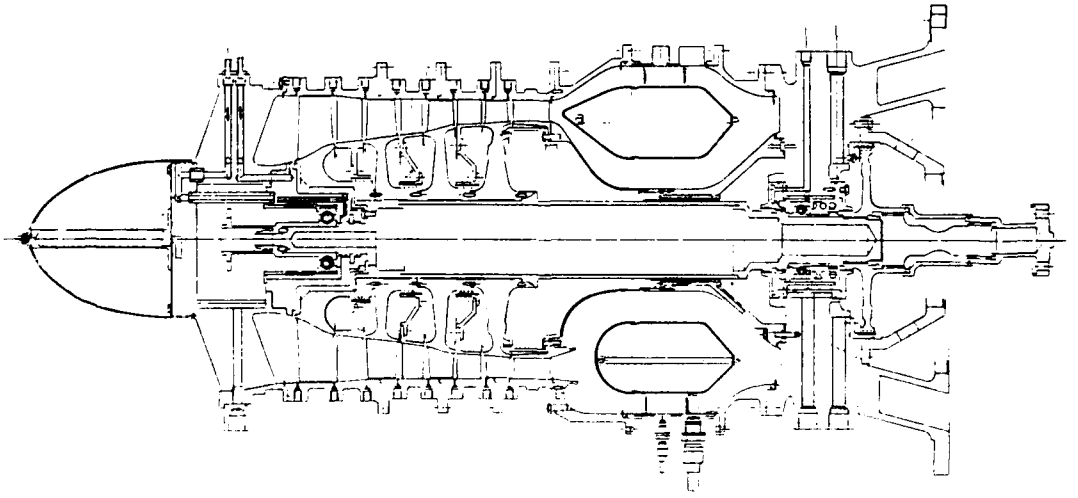

DIAGRAMME COMPRESSEUR DU 1er ETAGE

Figure 11

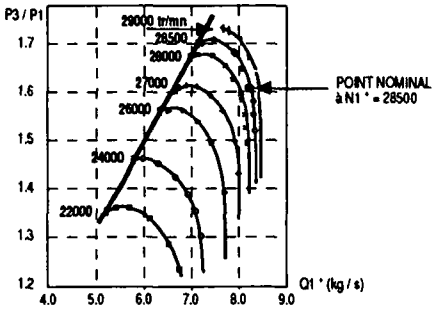

RENDEMENT DU COMPRESSEUR DU 1er ETAGE

Figure 12

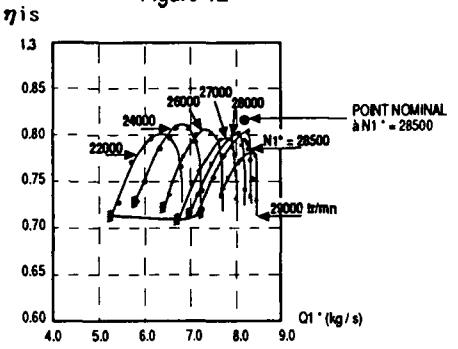

DIAGRAMME DU COMPRESSEUR COMPLET DU TRI60-30 (VITESSES ELEVEES)

Figure 13

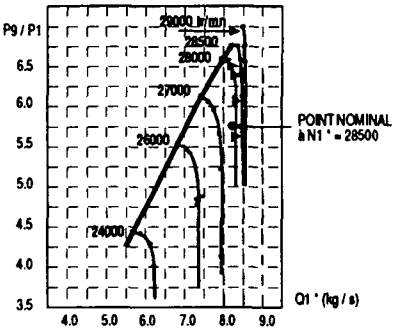

RENDEMENT DU COMPRESSEUR COMPLET DU TRI60-30 (VITESSES ELEVEES)

Figure 14

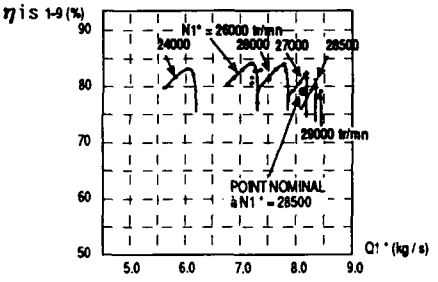

DIAGRAMME DU COMPRESSEUR COMPLET DU TRI60-30 (VITESSES FAIBLES)

Figure 15

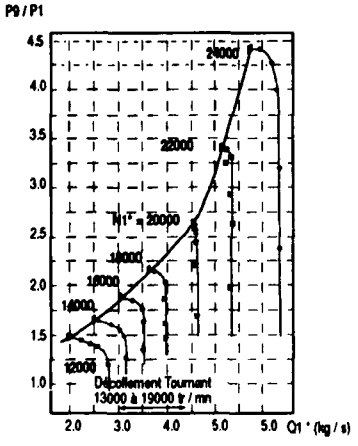

RENDEMENT DU COMPRESSEUR COMPLET DU TRI60-30 (VITESSES FAIBLES)

Figure 16

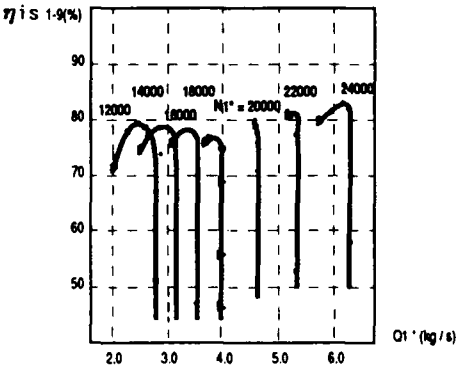

VEINE DE LA TURBINE AXIALE DU TRI60-30

Figure 17

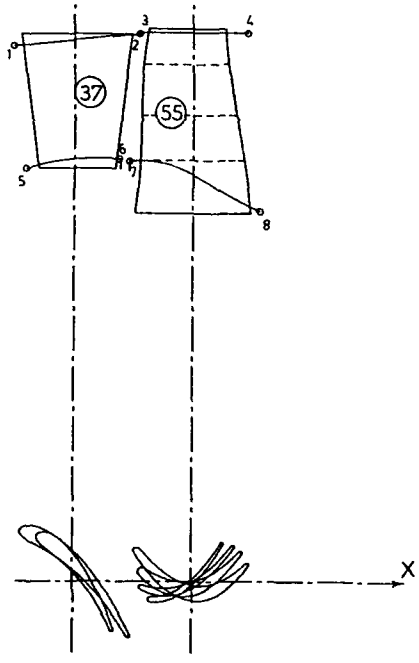

EVOLUTION DU RAPPORT Pst/Pi SUR L'EXTRADOS ET L'INTRADOS DES AUBES DISTRIBUTEUR EN PIED ET DES PALES DE LA ROUE DE TURBINE EN TETE DE LA VEINE

Figure 18

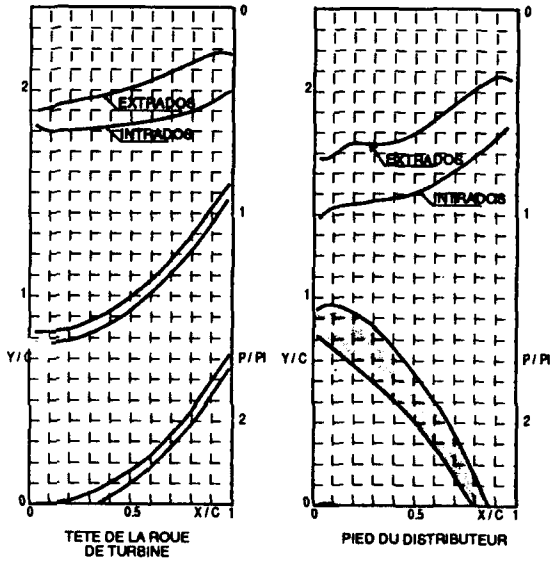

EVOLUTION DES ISO-MACH POUR LES COUPES DE PIED DU DISTRIBUTEUR ET DE LA TETE DE LA ROUE DE TURBINE

Figure 19

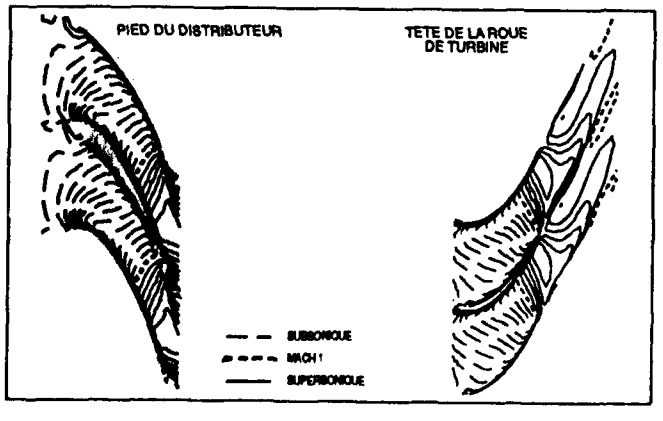

PERFORMANCES Cs= f(F) AU POINT FIXE DU TRI60-30

Figure 20

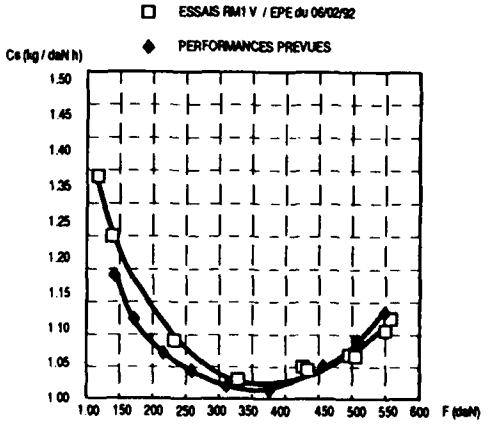

SMALLER EXPENDABLE TURBOJETS

C. Rodgers, (et al.)
Chief, Aerothermo Conceptual Design
Sundstrand Turbomach
4400 Ruffin Road
San Diego, CA 92123

ABSTRACT

One current focus of propulsion research is to increase gas turbine power density through improved aerothermodynamic component technologies and lower density, higher temperature materials. The objective of increased power density is to decrease engine size for a given output power. For example, increasing power density 100%, which is being projected by the 21st century, would be accompanied by a 40% reduction in engine size and 40% increase engine speed.

The trend towards reduced engine size tasks the ability of the turbojet designer to maintain the high levels of component efficiencies needed and to achieve the projected power density goals. Furthermore, parallel technology improvements projected in propulsion vehicle, system and electronics technologies, further anticipate engine size reduction.

Smaller smarter airbreathing propelled tactical missiles are being proposed and developed. They will function for various operational duties currently performed by larger, limited range missiles or manned surveillance and interdiction aircraft. The extreme compactness of these advanced missiles requires relatively high power density small turbojets.

Several design configuration options are possible for these turbojets including centrifugal and axial turbomachinery compressor and turbines, straight annular and reverse flow annular combustors, and fuel injectors etc. The attributes of candidate configurations are discussed with respect to maximum thrust per frontal area and low manufacturing cost.

NOMENCLATURE

A	Area		
Atm	Atmosphere		
BTU	British Thermal Unit	Greek	
C	Velocity	β	Blade angle
CFS	Volume Flow	σ	Blade Solidity
D	Diameter	ω	Angular Velocity
F	Thrust or Fahrenheit	ϕ	Velocity Ratio
FOD	Foreign Object Damage	η	Efficiency
g	Gravitational Constant	Subscripts	
H_{ad}	Adiabatic Head		
H_{RR}	Heat Release Rate	C	Compressor
K	Constants	B	Combustor
LHV	Lower Heating Value	e	Exit
M	Mach Number	t	Turbine
N	Rotational Speed		
Ns	Specific Speed		
q	Compressor Work Factor		
RPSC	Relative Propulsion System Cost		
R_c	Compressor Pressure Ratio		
SFC	Specific Fuel Consumption		
SLS	Sea Level Static		
TIT	Turbine Inlet Temperature		
U_2	Tip Speed		
Vo	Turbine Spouting Velocity		
V	Volume		
W	Airflow		

1.0 INTRODUCTION

One current focus of propulsion research and development is increasing gas turbine power density through improved aerothermodynamic component technologies and lower density, higher temperature materials. Increased power density reduces engine size for a given output power. For example, increasing power density 100%, which is being projected by the 21st century, would be accompanied by a 40% reduction in size and 40% increase in engine speed.

The trend towards diminished size tasks the ability of the turbojet designer to maintain the high levels of component efficiencies needed, and, to achieve the projected power density goals. Furthermore, parallel technology improvements are projected in propulsion vehicle, system and electronics technologies, which will further reduce engine size.

Small expendable turbojets in the 50–150 lbf (23–68 kgf) are being considered to propel miniature drone aircraft acting as airborne decoys. These decoys are designed to suppress enemy defenses and maintain air superiority in the battlefield of the future.

Several design configuration options are possible for such turbojets including, for example, centrifugal and axial turbomachinery compressor and turbines, straight annular and reverse flow annular combustors, fuel injectors, etc. Some specific examples of these configurations are discussed in Ref. 1 through 7. The attributes and characteristics of each design choice are discussed as constrained primarily by the objectives of maximum thrust per frontal area and low manufacturing cost.

Candidate small expendable turbojet engine design configurations in the 50–150 lbf thrust range are presented with projections of their aerothermodynamic performances. The dependency of total system relative cost with size and various performance parameters is also discussed. The objective is to identify important design variables, which could lead to cost savings in high quantity production.

2.0 SMALL TURBOJET DESIGNS

Major contraints for the design of small low cost expendable turbojets for missile applications are:

- Minimum number of components
- Low frontal area
- Low mission wet weight
- High start reliability

Cost often mandates a simple turbomachinery configuration with a minimum number of components and simple external impingement cooling of the hot-end module.

Although "simplifying design through component reduction" can be construed as an overstatement of probable gas turbine reliability, the establishment of a design goal to reduce components and parts is a big step forward in attaining the ultimate reliability goal. Component reduction is also an obvious technique to minimize cost and tolerance stackup restraints. Consequently, the compressor and turbine rotors are often single-piece castings similar to those of the mass-produced turbocharger rotors.

Some typical small turbojet design flowpath configurations are shown in Figure 1. They tend to use single-stage components, with the exception of multistage axial compressors cast as a single monolithic rotor assembly. All, with exception of the overhung rotor configuration, feature a hot-end bearing which is cooled with either air or throwaway fuel/oil.

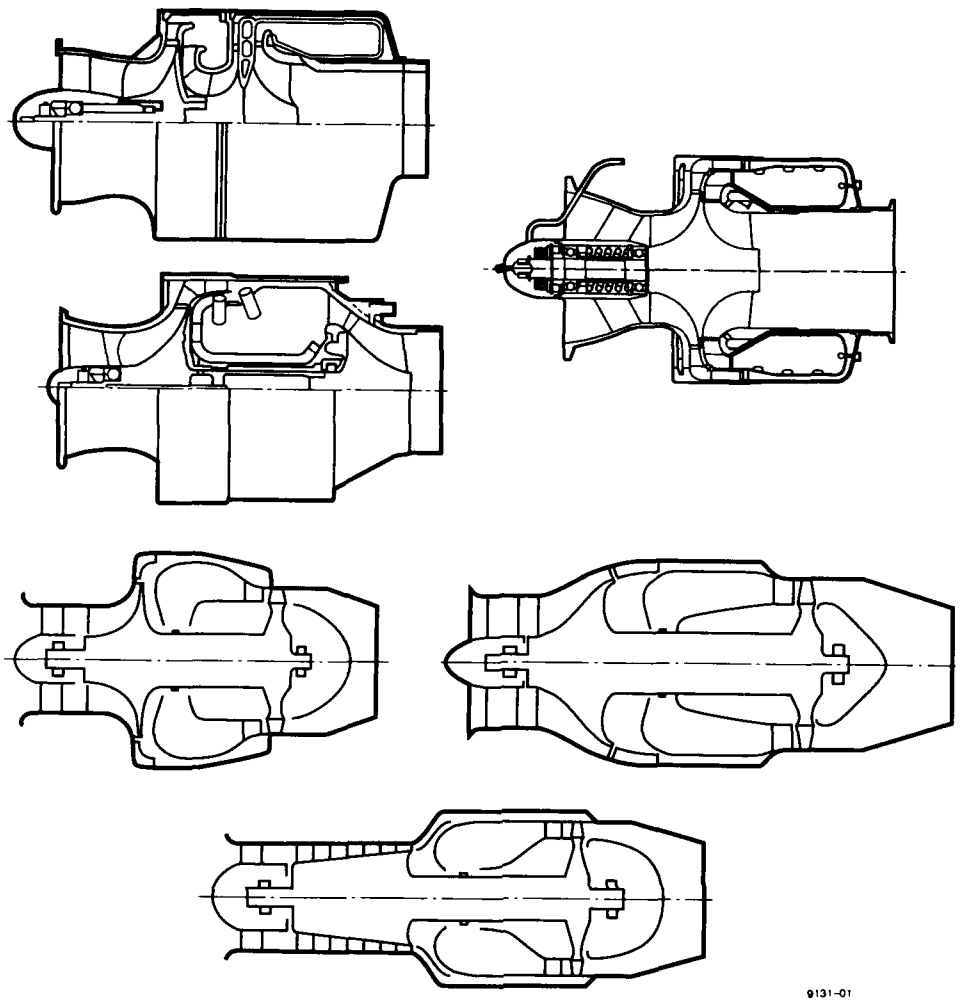

Figure 1. Small Turbojet Flowpaths

The choice of flowpath is influenced to a large degree by the design agency's technology and experience with specific small gas turbine turbomachinery components and combustion system fuel injection.

Small turbojets for missile applications are being developed in the 4.0–6.5 inch (100–260 mm) diameter range. Even smaller ones of 2.5 in (63 mm) are being examined for model aircraft applications.

The lower limit in size is dictated by the feasibility of stable combustor operation, and high speed bearing life in the 150 to 200 krpm speed range with relatively high axial thrust load conditions.

The typical performance characteristics of small turbojets are shown in Figure 2, where specific fuel consumption (SFC) and specific thrust (F/Wa) are plotted, and normalized to a reference cycle condition with a pressure ratio of 5.0 and turbine inlet temperature (T.I.T.) to ambient temperature ratio of 4.5. In the range of interest near maximum specific thrust, it is observed that pressure ratio has only a small effect on thrust output, but a stronger effect on fuel economy.

In contrast, T.I.T. ratio has a significant effect on specific thrust depending upon the turbine material temperature and life constraints.

Some of the design considerations in selecting cycle parameters, flowpath configurations, and characteristics of the various engine components are discussed in more detail as follows:

3.0 COMPRESSOR TYPES

Three types of compressors used in small expendable turbojets are:

- Single-Stage Centrifugal
- Single-Stage Mixed
- Multi-Stage Axial

The various advantages and disadvantages of each of these three types are listed in Table 1 below.

All are sensitive to blade tip clearance losses which are best minimized by the use of abradable shrouds. The centrifugal is the least sensitive and is capable of wide surge margins with high inlet distortion tolerance. The specific capabilities of each type are discussed in detail in the following sections:

3.1 Centrifugal Compressors

The simplicity and reduced cost features of the single-stage compressor are ideal assets for small gas turbine auxiliary power units(APUs); small, expendable turbojets; and small turboprop,

TABLE 1. COMPRESSOR TYPE COMPARISON

Type	Advantage	Disadvantage
Single-Stage Centrifugal	Lowest Cost.Minimum Number of Components High Distortion Tolerance Good FOD characteristics	Increased Frontal Area High Rotational Speed
Single-State Mixed	Lower Frontal Area Low Component Number Reduced Distortion Tolerance (Good FOD characteristics)	Increased chord with higher hub stress. Higher Rotational Speed
Multi-stage Axial	Lowest Frontal Area Lower Rotational Speed	Higher Cost Max Component Number Limited Distortion Tolerance Poor FOD Characteristics Clearance Sensitivity

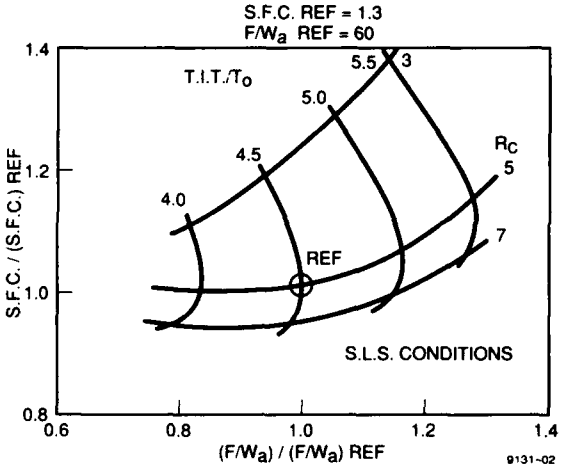

Figure 2. Small Turbojet Cycle Performance

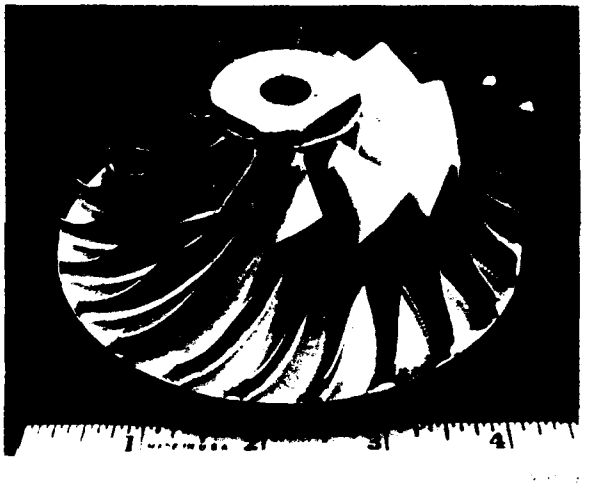

Figure 3. Small High Specific Speed Centrifugal Compressor

turboshaft engines. The most prevalent applications are in engines up to approximately 500-hp output. Larger power engines in the 500-3000 hp range feature two-stage centrifugal compressors, or combined axial centrifugal compressors, in single or two-spool arrangements. Small expendable turbojet gas turbine cycle optimization studies, using single-stage centrifugal compressors and single-stage radial inflow turbines, were presented in Reference 5. These studies indicate that the weight and cost contraints of small intermittent duty APUs and short duration expendable turbojets usually mandate the selection of specific speed (Ns) close to unity with the a configuration shown in Figure 3.

The attainable total-to-static efficiency levels of single-stage centrifugal and mixed compressors with ambient sea level (air) suction conditions largely dependent upon five parameters:

- Inlet Specific Speed Ns
- Impeller Tip Diameter D_2
- Inducer Tip Relative Mach Number M_{ls}
- Exit Mach Number M_e
- Blade Tip Clearances

The two common forms for specific speed based on inlet stagnation conditions used in the gas turbine industry are:

$$N_s \text{ Dimensional Specific Speed} = \frac{N\sqrt{CFS}}{(gHad)^{3/4}} \quad (1)$$

$$N_s \text{ Non-Dimensional Specific Speed} = \frac{\omega\sqrt{CFS}}{(gHad)^{3/4}} \quad (2)$$

The non-dimensional form will be used in this paper to avoid conversion factors.

The importance of the specific speed efficiency relationship, and the design parameters selection that enables optimum performance on a peak efficiency locus, are paramount technology for successful competitive designs.

Even with this information, good design, manufacturing, and test development practices are still necessary to achieve peak efficiency levels. Therefore, choosing specific speed "a-priori" is not an unconditional guarantee of maximum performance.

Figure 4 shows attainable total-static efficiencies for small 4.0-inch (100 mm) tip diameter impeller centrifugal compressors for expendable turbojet applications, with diffuser exit Mach number of 0.35. These are computed from the correlation procedure of Ref. 8.

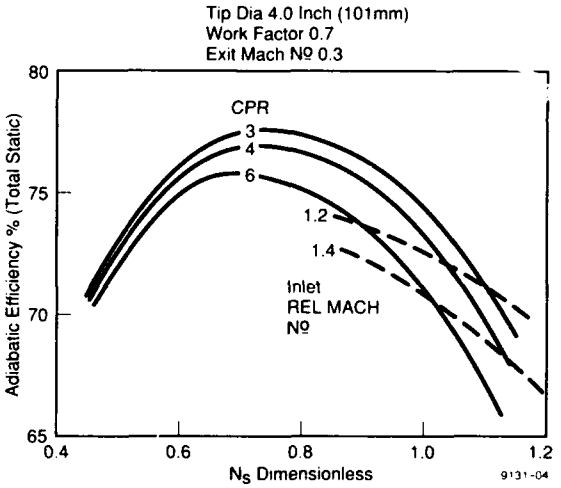

Figure 4. Small Centrifugal Compressor Efficiencies

The need to increase thrust/frontal area with specific speeds of unity and high exit Mach numbers produces total to static efficiencies as low as 70%, accompanied by inducer tip relative Mach numbers at the 1.4 level.

3.2 Mixed Flow Compressors

Frontal area of the centrifugal stage can be further reduced by diminishing the radial extent of the diffuser with consequent efficiency decrements (Ref. 9), or by selecting a diagonal exducer discharging into an axial diffuser (stator). This classifies the mixed flow compressor, which is an intermediate between the centrifugal and axial flow stages of the type shown in Figure 5. Ref. 10 describes the design and test of an advanced high specific speed compressor with a two-stage starter. Ref. 11 discusses the use of high specific speed centrifugal and mixed flow compressors for turbochargers. Mixed flow impellers are normally characterized by lower impeller to inducer tip diameter ratios (< 1.3). They will normally produce less work for a given diffusion factor and blade solidity than the centrifugal impeller. This is indicated by the trends shown in Figure 6. In order to produce the same work, either the tip speed (and Mach number) must be increased and/or the tip sweepback reduced both, ending to compromise flow range.

The relative specific speed characteristics of the single-stage contrifugal and mixed compressors are discussed in Ref. 12.

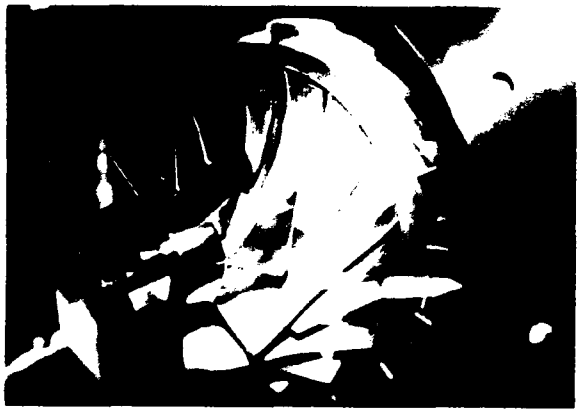

Figure 5. Small Mixed Flow Compressor

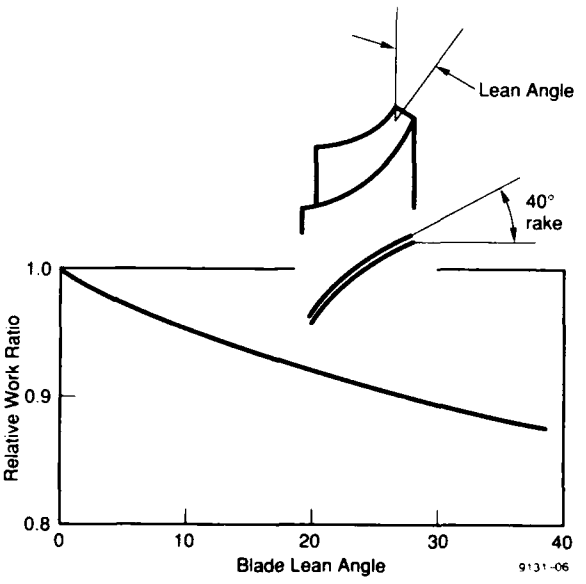

Figure 6. Compressor Work Factor Reduction Flowpath Leon

3.3 Axial Flow Compressors

State-of-the-art performance for small two-stage and multi-stage axial compressors are summarized in Table 2. Figure 7 shows a small six-stage axial compressor tested by NASA with a first-stage rotor tip diameter of 3.7 inch (94 mm). An overall total-to-total isentropic efficiency of 76% was acheived with machined rotors and stators.

TABLE 2 SMALL AXIAL COMPRESSOR DATA

Stage Ref	Pressure Ratio	Corrected Flow pps	* Efficiency tt	Tip Diameter Inches	Speed krpm	Ns Number
Smith 3.3.1	2.72	4.02	77.0 (75.0 Cast)	6.0	33.0	4
Davis 3.3.2	3.1	4.9	80	5.6	59.6	2
Tysl 3.3.3	2.8	1.55	76	37	49.1	6
Wiggins 3.3.4	6.2	5.3	84	6.0	39.6	8
Tyler 3.3.5	3.3	7.3	84	7.0	50.4	2
Chapman 3.3.6	3.7 .	3.5	77	-	-	6

References

3.3.1 - R. Smith "A Jet Fuel Starter for Lowest System Life Cycle Cost AGARD CP-352, Pg 11-1.

3.3.2 - J.V. Davis, "Design and Development of Small Highly Landed Two Stage Transonic Axial Compressor", SAE 720712, 1972.

3.3.3 - E.R. Tysl, L.J. Heideberg, C.Weigel, "Overall Performance in Argon of a 3.7 in Six Stage Axial Flow Compressor." NASA TX-2194, 1971.

3.3.4 - J.C. Wiggins, G.L. Waltz, "Some Experiences in Scaling the NASA Eight Stage Transonic Axial Flow Compressor", SAE 720711, 1972.

3.3.5 - T.M. Tyler, J.P. Sullivan, "Design and Test of a Small High Speed Axial Compressor". AIAA90-1911, 1990.

3.3.6 - W.I. Chapman, "Conceptual Design Study of an Improved Gas Turbine Powertrain". NASA CR-159852, 1980.

Comparative performance testing of a small four-stage axial compressor with both machined and cast aluminum rotors and stators was conducted during the development of a Jet Fuel Starter by Teledyne Corporation (Ref. 3.3.1). Peak isentropic compressor efficiency was reduced from 77.0 to 75.0% with installation of the cast stages together with a 5.7% reduction in flow. As a general rule, the efficiencies of axial and centrifugal compressors are quoted on total-total and total-static values respectively. The difference may account for up to 2% points difference in efficiency depending upon the reference Mach number at the exit measurement plane, and subsequent downstream diffusion losses.

Precision casting techniques now enable the manufacture of lower cost, small multi-stage axial flow compressor rotors in monolithic form. Likewise, the outer casing and stators can be precision cast in (split) monolithic form. Although significant manufacturing cost savings occur from this technique, both rotor and stator clearances are critical in such small sizes, and necessitate subsequent deposition of abradable coatings on both rotor and stator assemblies.

Attributes of the multi-stage axial compressor for small turbojet designs are lower rotational speed for a given flow and pressure ratio, and outer diameter discharge permitting maximum utilization of combustor volume within a given diameter.

4.0 COMBUSTORS

Aerodynamic design of turbomachinery for small expendable turbojets is guided by the classic scaling relationships for effects of Reynolds number, surface finish, and clearance gaps. Scaling techniques for the design of small combustors are less defined, due to the effects of:

- Dome height reduction increasing the effects of wall quenching.
- Surface area/volume increase.
- Necessity to minimize the number of injectors.
- Limitation on fuel injector orifice sizing.
- Concentricity limitations between inner and outer liner.
- Increased effect of leakage gaps on pattern factor.

As a consequence, there is reluctance to directly apply scaling techniques in the design of small turbojet combustors, and alternative design configurations are being researched to satisfy the demands of reduced cost and volume.

Current small turbojet combustors are configured in either the axial annular, or reverse flow annular configuration (Figure 8). Many small gas turbines use the single can scroll combustor configuration, but scroll asymmetry is not suitable for turbojets launched from cylindrical container installations. Engine size reduction and resultant "squashing" of the combustor increase the combustor heat release rate as defined by:

$$HRR = \frac{FuelFlow x LHV}{Volume \; x \; R_c} \qquad (3)$$

It can be shown that specific thrust per unit volume (F/V) is proportional to:

$$\frac{F}{V} \; a \; \left[\left(\frac{K_{CT}}{F/W} \right) + \left(\frac{K_B \; . \; SFC}{HRR.R_c} \right) \right] \qquad (4)$$

where K_{CT} = Compressor and Turbine Geometry Constants

where K_B = Combustor Geometry Constant

The specific thrust per unit airflow and SFC trends of Figure 2 can now be translated into specific thrust per unit volume trends

depicted in Figure 9 with HRR as a parameter using a baseline HRR of 5.0 MBTU/hr ft3 atm and pressure ratio of 4.0. Increasing the HRR from 5.0 to 30.0 would permit a 50% increase in thrust per unit volume. · Fuel injection, atomization, and evaporation is probably the single most important criteria in the design and successful development of small high heat release rate combustors, particularly during starting. Fuel flow rates at ignition may be very low, making atomization difficult without high energy ignition sources.

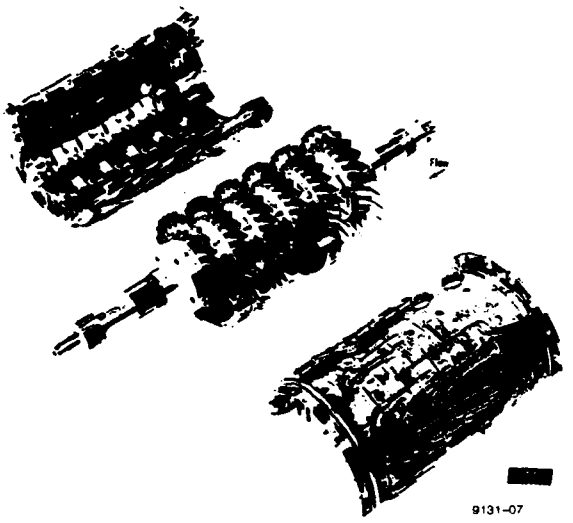

Figure 7. Small Multistage Axial Compressor

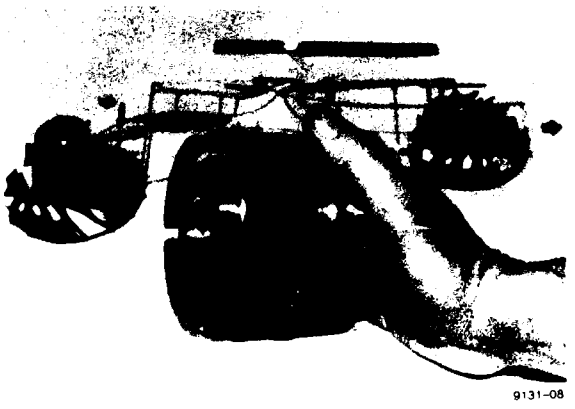

Figure 8. Small Reverse Flow Annual Combustor

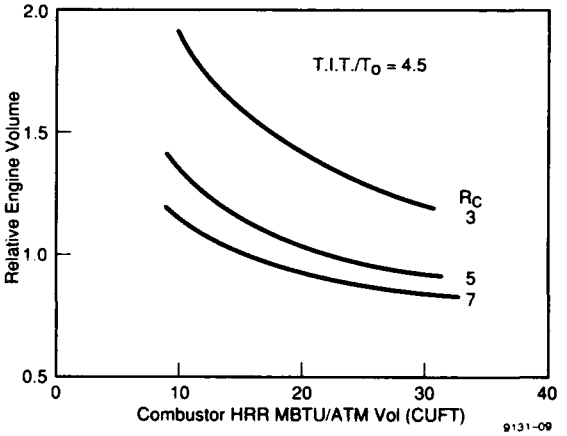

Figure 9. Effect of Combustor HRR on Volume

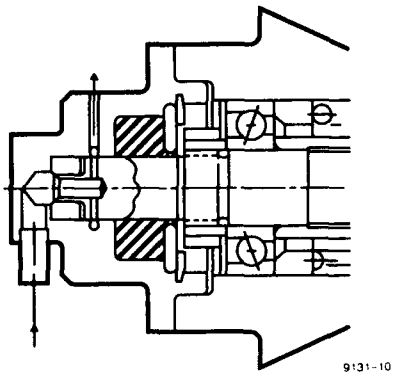

Figure 10a. Nose Mounted Slinger Pump Ref.

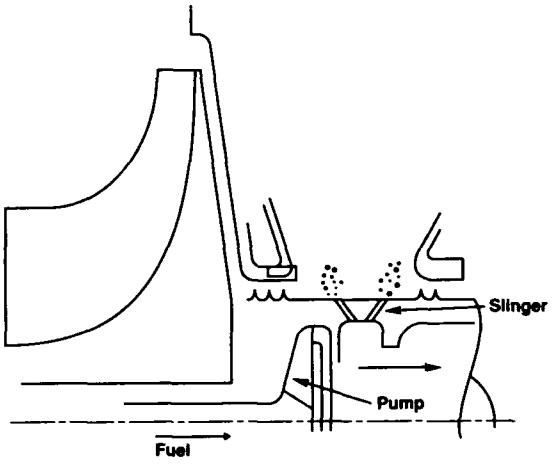

Figure 10b. Combustor Liquid Ring Pump Ref.

Fuel injection with a rotating slinger pump is a popular choice and may be directly sprayed from the shaft mounted slinger into the combustor, as shown in Figure 10a, or supplied from the slinger pump via a manifold into the combustor as Figure 10b.

5.0 TURBINE TYPES

Three types of small single stage turbines used in small expendable turbojets are:

- Radial Inflow
- Axial Flow
- Mixed Flow

The various advantages and disadvantages of each three types are listed in Table 3 below:

TABLE 3 TURBINE TYPE COMPARISON

TYPE	ADVANTAGE	DISADVANTAGE
Radial	• High Pressure Ratio Capability • Reduced Clearance Sensitivity • Lowest Cost • Higher Temperature Capability	• High Inertia • Low FOD Tolerance
Axial	• Low Cost • Low Inertia • Better FOD	• Limited Pressure Ratio • High Clearance Sensitivity
Mixed Flow	• Intermediate between axial and radial	

The specific features and capabilities of each type is discussed in more detail in the following sections:

5.1 RADIAL INFLOW TURBINES.

Inward flow radial and mixed flow turbines have established prominence in the field of small turbomachinery because of their simplicity, cost, relatively high performance, and simple installation.

Two notable major applications of these turbines are in small turbocharger and "radial type" gas turbines. These major applications are typically in the 0.10 to 5.0 kg/sec flow range.

The aerodynamic excellence of both radial inflow and axial turbines is determined by two major performance parameters:

- Velocity ratio = Ut/Vo, Ratio of tip speed to theoretical spouting velocity, and
- Exit flow coefficient = ϕ = Ce/Ut, ratio of exit axial velocity to tip speed.

The velocity ratio is a direct measure of the blade loading. The exit flow coefficient for a radial turbine is an indirect measure of the specific speed, since for zero exit swirl and incompressible flow, it can be shown that:

$$\text{Dimensionless specific speed } Ns \sim \phi 1/2 \left(\frac{U_t}{Vo}\right)^{1.5} \frac{2.98}{Dt} D_e^2 \qquad (5)$$

State-of-the-art levels for the total-to-static efficiency of uncooled radial inflow turbines are shown in Figure 12 (this information is derived from references). The data indicate that peak efficiencies are obtained with velocity ratios close to 0.7 with exit flow coefficients of 0.2 to 0.3. The efficiency trends were derived from the performance examination and correlation of thirty different single-stage radial inflow turbines, complying with the size range and nominal clearances. Similar design charts have been produced for axial turbines showing comparable trends. For a particular turbine design, the level of efficiency is dependent upon specific criteria, such as:

- Solidity of Nozzle and Rotor
- Effects of Diameter Ratio
- Tip Clearance Losses
- Vane and Blade Trailing Edge Thickness
- Entry Flow Conditions
- Mach and Reynolds Numbers

The efficiency levels shown in Figure 11 are for nominal shroud axial clearance/blade height ratios of 6%.

In general, small radial turbines are less sensitive than small axial turbines to clearance effects. Note, however, that most turbine rotor discs are deeply scalloped to reduce thermal stress and inertia. Flow leakage between the rotor blade tip and stationary shrouds are incurred on both hub and shroud boundaries, and it is necessary to minimize both endgaps.

Radial turbines are commonly used in small gas turbine APU's mounted back-to-back with a centrifugal compressor in combination with a reverse flow annular combustor. As mentioned previously, diameter constraints of small turbojets with such flowpath configurations generally result in relatively small combustor heights and increased combustor loadings.

Monolithic ceramic radial inflow turbine rotors are now in mass production for automotive applications. They offer distinct advantages for small expendable turbojets, such as higher temperature capability and lower weight.

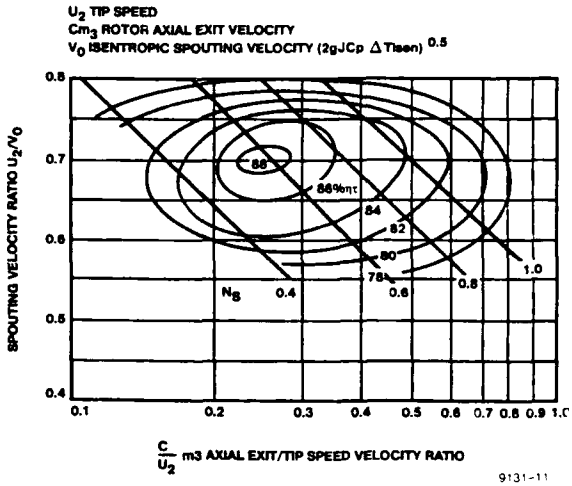

Figure 11. Attainable Efficiency Levels of Radial Turbines

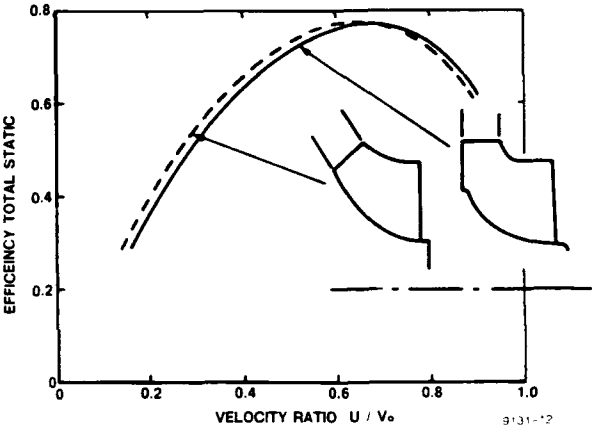

Figure 12. Comparison of Radial and Mixed Flow Turbines

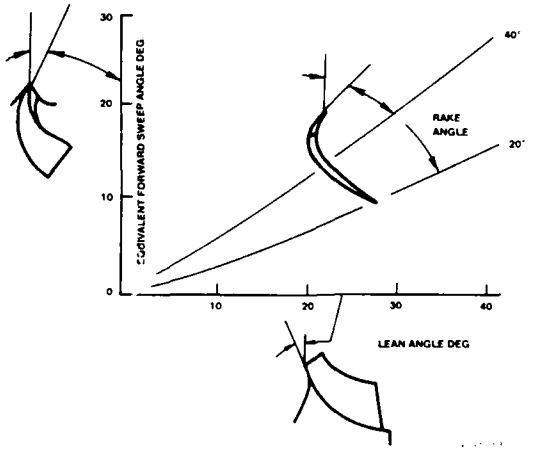

Figure 13. Mixed Flow Path Blade Angles

5.2 Mixed Flow Turbines

Mixed flow turbines are now being used in some high specific speed turbochargers and turbojet applications because of reduced radial height extent (diameter) of the stator and their capability of operating at slightly higher blade loadings.

A performance comparison of radial and mixed flow rotors from Reference 1 is shown in Figure 13, where some slight beneficial displacement of the efficiency velocity ratio characteristics was achieved toward lower velocity ratios. Detailed design and test of an 8.5-inch diameter mixed flow turbine rotor is also presented in

Reference 14. The effects of blade lean and rake on blade inlet angle are depicted in Figure 13 and reveal that, for example, the equivalent of 20 deg. forward sweep can be obtained with a combined lean and rake of 30 to 40 deg., respectively, while still retaining desirable radial blade elements. This could improve turbine efficiency by up to 1.5% points at a velocity ratio of 0.60 compared to the straight radial blading.

The "equivalent" forward sweep due to a combination of rake and lean in a mixed flow turbine inlet blade angle can be approximated by the following relationship:

$$\text{Equivalent blade angle} \quad B = \tan^{-1}(\sin\lambda \tan\Theta) \qquad (6)$$

λ = Blade Lean angle

Θ = Blade rake angle

A second aerodynamic advantage of the mixed flow path arises from the reduced streamline curvature in the meridional plane. From the mechanical design viewpoint, the mixed flow rotor benefits from the reduction of relative total temperature with decreasing radius (as in the radial inflow rotor), while individual radial filaments are shorter (lower local AN^2). However, the need to support the cantilevered blade tips reduces the scope for disc stress reduction by deep scalloping. Higher disc stresses result, in addition to higher blade stresses as a result of increased blade mass, using rake.

The potential efficiency improvements of the mixed flow turbine are not achieved without flowpath and mechanical implications. The flow path axial length is increased, additional nozzle turning may be required, and the disc mass may be heavier than a single-stage axial or radial rotor. This could result in possible shaft dynamics and/or bearing considerations due to greater mass overhang as well as tri-hub burst speed margin. These factors require careful consideration and integration into the design process. The mixed flow rotor is most attractive as an alternative to a two-stage axial turbine configuration.

5.3 AXIAL TURBINES

The small single-stage axial turbine is particularly suitable for low cost expendable turbojets in that overall pressure ratios selected are normally no higher than 5.0, resulting in near optimum turbine pressure ratios in the 2.0–2.5 range. Current state-of-the-art performances for small axial turbines are listed in Table 4. Small axial turbines are very sensitive to blade tip clearance effects, and thus the ratio of tip clearance to blade height. With minimum feasible tip clearances, the efficiency becomes largely influenced by blade height. Figure 11 illustrates the effect of blade height on relative efficiency of small axial turbines.

6.0 BEARING DESIGN CONSIDERATIONS

The use of single-stage, high specific speed compressors leads to shaft speeds on the order of 100,000 rpm for 100 lbf (45 kg) thrust unit, with antifriction and bearing sizes in the 10 to 12 mm range. Such bearings are quite sensitive to internal clearances and tolerances, as influenced by operating temperature and axial thrust loads, in particular hot-end rear bearing locations. Adequate cooling either from compressor discharge air or throwaway oil/fuel is paramount in preventing a runaway thermal condition, even for a few minutes of operation. Three alternate design options to this hot end bearing difficulty are:

- Front end air inlet housing bearing capsule location, with an overhung rotor assembly.
- Use of multistage compressor with lower rotational speed for a given pressure ratio.
- Use of air bearings, or advanced material ceramic hybrid ceramic, or diamond coated bearings.

Ceramic turbine rotors, besides enabling operation at higher TIT's, offer the advantage of reduced bearing loads due to reduced mass and inertia. Rotor axial thrusts may be on the same order as the net propulsion thrust dependent upon mechanical design and provision for thrust balance cavities. Large axial rotor thrusts may require relatively large thrust faces for the air bearing option.

7.0 ENGINE STARTING CHARACTERISTICS

It is difficult to estimate with any reasonable accuracy the starting characteristics of small gas turbines because of the synergistic nature of the problem. Engine starting characteristics are influenced (among other intangibles) by:

- Temperature and altitude
- Initial engine design selection
- Transient engine and combustor performances
- Engine fuel, control scheduling
- Mechanical features and associated viscous drag
- Acceleration rate
- Starter selection and torque characteristics

Small gas turbines are particularly sensitive to tip clearance effects, since clearance gap to blade height ratios tend to be greater than those of larger gas turbines. In most instances, the minimum engine operating clearances are established by transient engine tests to determine limiting rub clearance gaps. Some tuning can be accomplished by matching thermal responses of the rotors and stationary shrouds and by appropriate material selection. Computation of engine transient performance using steady-state component performance characteristics does entail small errors due to the effect of transient clearance effects on both component efficiency and pressure flow characteristics.

The previous effects are relatively small when compared with the transient behavior of the combustor. Transient combustor efficiencies as low as 20 percent have been experienced for small short reverse flow annular combustors on cold starts following ignition and light-off.

Most important in increasing engine acceleration assisting torque are early ignition and good fuel atomization. These affect the transition from engine resisting to positive acceleration torque characteristic. A major constraint for reliable early ignition under a wide range of operating conditions is in the design of the fuel injection (atomization) system.

The use of pyrotechnic igniters and high pressure air impingement start methods for small expendable turbojets is discussed in Ref.

TABLE 4. SMALL AXIAL TURBINE DATA

REF		5.31	5.3.2	5.33
Pressure Ratio		1.8	1.94	1.5
Inlet Temp	°R	2460	2380	2160
Inlet Flow	pps	0.81	1.32	0.12
Efficiency	%	80	82.5	75
			78.3 as cast	(Volute)
Blade Height	in	0.5	0.44	0.40
	mm	12.6	11.2	10.2
Tip Dia	in	4.4	4.4	1.79
	mm	112	112	45.5
Speed krpm		83.2	58.5	110
Velocity Ratio		0.73	0.50	0.5

Ref. 5.31 Papendreas, E., "SCAT: A Small Low Cost Turbojet for Missile & RPV's," AIAA 88 3249, 1988.

Ref. 5.3.2 Roelke, R.J., Haas, J.E., "Cold Air Performance of Compressor - Drive Turbine of D.O.E. Upgraded Automobile Gas Turbine," NASA Tech Memo 82818, 1982.

Ref. 5.3.3 Rankke, O.J., "Axial Flow Automotive Turbocharger," ASME 85-GT-123.

14. Pyrotechnic igniters are capable of providing a strong ignition source with high impingement torques, but are relatively costly. They also create a sensitive munitions issue. The use of high pressure air impingement is favored for developmental testing.

8.0 COST SENSITIVITY STUDY

Cost sensitivity studies for a complete tactical missile propulsion system were described in Reference 7. The intent was to identify critical design parameters which are major cost drivers.

A computerized performance analysis, weight and cost program was generated upon the aerothermodynamic design philosophy previously discussed, together with the additional cost increments for the overall system, including the control system, start system, fuel and fuel tanks.

The impact of various design parameters upon overall system cost is discussed as follows.

8.1 Compressor Specific Speed

Missile and engine size are minimized by providing high thrust/frontal area. This combined with a common cost constraint to use single-stage compressor requires the use of high flow, high specific speed compressors. This is illustrated in Figure 14 where relative propulsion system cost (RPSC) trends are plotted as a function of compressor dimensionless specific speed and pressure ratio. This assumes a maximum cycle temperature of 2460°R (1367°K). Specific speeds greater than unity produce no further reduction in RPSC and introduce the complication of higher rotor stresses. The optimum pressure ratio and specific speed combination is near 5.0 and unity, respectively.

8.2 Turbine Inlet Temperature (TIT)

The impact of turbine inlet temperature upon RPSC is shown on Figure 15 for mission durations at full thrust for 1, 3, and 5 minutes. Since higher TIT's lead to higher specific fuel consumptions, RPSC optimizes out in the 2060–2460°R (1145–1367°K) TIT range, for a given thrust level. The delta RPSC per minute of duration is surprisingly small at 2.5%. Extended duration is more related to missile thrust/weight limitations.

8.3 Compressor And Turbine Efficiencies

The desire to minimize component costs often results in performance compromises such as the effects of surface finish, clearances and blade thickness. The effect of both compressor and turbine component efficiencies on RPSC is shown in Figure 16, where 1% change in either compressor or turbine efficiency is worth 1% in RPSC. This may seem innocuous but in large quantity production, 1% improvement in efficiency could reflect a cost savings of close to one million dollars for a given thrust.

In reality the compounding effect of reduced compressor efficiency on pressure ratio and airflow for a given TIT would actually result in a slightly higher penalty for compressor efficiency than indicated in Figure 6.

8.4 Effect Of Engine Size

Correlations of component efficiencies with normalized inlet flow parameters as shown in Figure 17, are useful in assessing the effects of size in cycle performance. Typical results of such correlations are shown in Figure 18 for small turbojet configurations developed at the author's affiliation, where thrust, specific fuel consumption and rotational speed are plotted versus external diameter.

Since cost of the fuel control and accessories tends to remain constant in the relevant thrust class, it is anticipated that RPSC/lb of thrust will increase with diminishing size. This is indeed the trend shown in Figure 19 where the cost/lbf becomes asymptotic below the 50 lbf (13 g) level. This would imply that small turbojet propulsion may not become cost effective at lower thrusts, without cost reduction to the fuel control system via:

- Design simplification or innovation.
- Relaxation of the environmental operating envelope.
- Relaxed sensitivity to hostile threats.

This conclusion warrants an in-depth study of control system design and specifications for small expendable turbojets focusing on the objectives identified here.

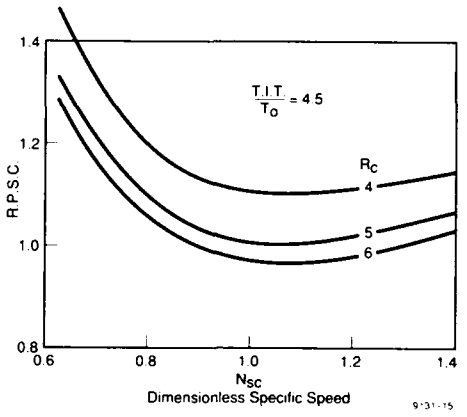

Figure 14. RPSC vs. Specific Speed

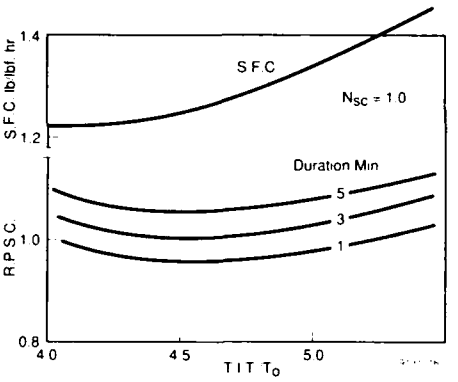

Figure 15. Effect of T.I.T. on Relative Cost

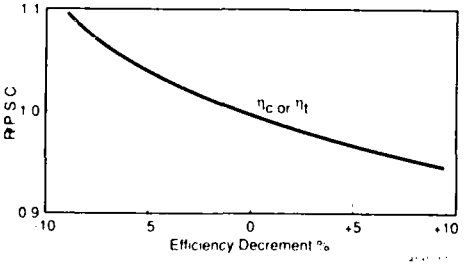

Figure 16. Effect of Component Efficiencies

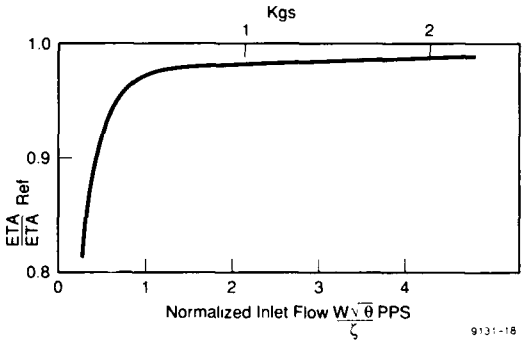

Figure 17. Size Effects on Small Turbomachinery

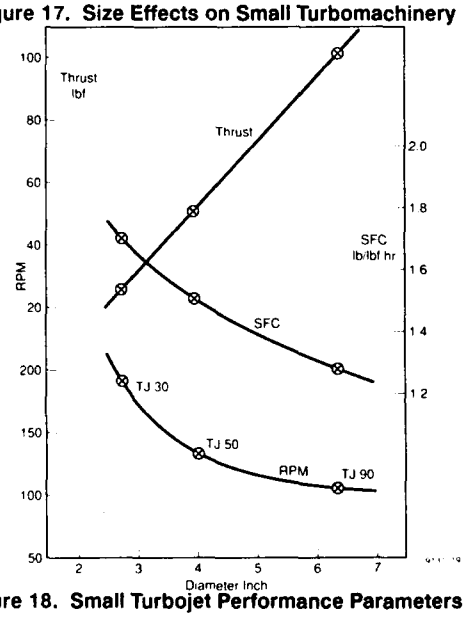

Figure 18. Small Turbojet Performance Parameters

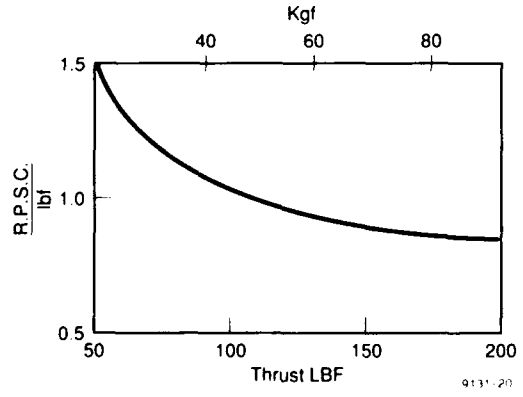

Figure 19. Effect of Engine Size on Relative Cost

9.0 CONCLUSIONS

Smaller, smarter, airbreathing propelled tactical missiles are being proposed and developed for various operational duties currently performed by larger limited range missiles, or manned surveillance and interdiction aircraft. The extreme compactness of these advanced missiles requires equally compact high power density small turbojets.

Various candidate small turbojet design configurations were presented with a collage of possible component types, especially with single-stage compressor and turbine components to minimize manufacturing cost.

Limiting the feasibility of very small, almost miniature expendable turbojets was the suitability of very small, high speed bearings to provide even, short life under conditions as of high thrust and hot end temperature environments. Size reduction (if scalar) brings weight reduction through the classic "square/cube" relationship. Engine and airframe control functions tend to remain constant with size. Relative propulsion system cost/lbf is therefore shown to substantially increase at thrust levels below 50 lbf (23kg), based upon current cost breakouts.

It is suggested that the most profitable development avenues for attaining improved cost effectiveness for small expendable turbojets with thrusts less than 100 lbf are those focusing upon:

- Control system and engine design simplification and innovation
- Integration of the engine and missile control system
- Aerothermodynamic performance improvement of high specific speed single stage compressors and turbines
- Compact high intensity, low cost annular combustors
- Use of low cost ceramic materials to increase TIT's specific thrust and reduce rotor inertias.

Very small turbojets may not become cost effective without cost reduction and simplification of the fuel control system, plus relaxation of stringent military standards currently on larger thrust extended operation turbojets.

Potential control system cost reductions are feasible by off-loading engine instrumentation and computational requirements to the missile or ground-based guidance systems.

10.0 REFERENCES

1. Jones, A., Weber, H., Fort, E., "Gemjet - A Small Low Cost Expendable Turbojet" AIAA-87-2140, 1987
2. Papendreas, E., "SCAT-A Small Low Cost Turbojet for Missiles and RDV's". AIAA 88-324g, 1988
3. Chevis, R.W., Grant, I.J., "A Family of Small Low Cost Gas Turbines for Unmanned Vehicle Systems", R.A.E.S. Journal June/July 1983.
4. Mandle, R.J., "Twenty Year Evolution of the WR2/WR24 Series of Small Turbojet Engines", SAE 770998, 1977
5. Rodgers, C., "A Jet Fuel Starter and Expendable Turbojet" ASME 86-GT-1.1986
6. Lilley, J.S., "The Demonstration and Evaluation of Low Cost Engines for the FOG-M", JANNAF Propulsion Meeting, December 1987.
7. Rodgers, C., "Propulsion System Cost Considerations for Small Expendable Turbojets". JANNAF Propulsion Meeting, December 1987.
8. Rodgers, C., "The Efficiencies of Single Stage Centrifugal Compressors for Aircraft Applications". ASME 91-6T-77. 1991
9. Elliot, K., Exley, T., "Correlation of Radial-to-Axial Vaneless turns for Centrifugal Compressors". AIAA90-1917. 1990.
10. Dooley, P.E., Dodge, J.L., "Mixed Flow Compressor Program". AFWAL-TR-80-2047. 1980
11. Saito, M., et al. "Development of High Specific Speed Centrifugal Compressor for Turbochargers". GTSJ.83Tokyo.IGTC-71

12. Balje, O.E., "Turbomachines". Wiley & Sons. 1981

13. Rodgers, C., "Review of Mixed Flow and Radial Turbine Options". AIAA.90-2414. 1990

14. U. Okapuu, "Design and Aerodynamic Performance of a Small Mixed Flow Gas Generator Turbine". AGARD-CP-421. May 1987.

15. Rouse, G., "Impingement Starting of Small Expendable Turbojets". JANNAF Propulsion Meeting, October 1990.

11.0 ACKNOWLEDGMENT

The author wishes to thank Nancy Roussakis and Diana Prince in the preparation of the manuscript and Sundstrand Power Systems for publication permission.

PREDICTION DES PERFORMANCES EN COMBUSTION DE STATO-REACTEURS ET STATO-FUSEES PAR EXPERIMENTATIONS ISOTHERMES ET MODELISATIONS

P. HEBRARD
G. LAVERGNE
A. TORGUE
F. BISMES
G. HEID
CERT-ONERA/DERMES, B.P. 4025 - 31055 TOULOUSE CEDEX
FRANCE

SOMMAIRE

On présente dans cette publication une approche semi-empirique visant à étudier les caractéristiques de l'aérodynamique interne de foyers et à prédire les performances de différentes chambres de combustion de stato-réacteurs et stato-fusées en fonction de leurs caractéristiques géométriques et de leur point de fonctionnement. La démarche proposée, qui s'est révélée tout à fait opérationnelle pour de nombreux cas traités, est fondée sur l'utilisation conjointe d'expérimentations effectuées en conditions simulées isothermes, et d'une modélisation 1D utilisant le concept de réacteurs élémentaires. Les expériences sont menées sur bancs hydrauliques ou sur installations aérodynamiques à partir de maquettes à échelle réduite du foyer à étudier. Des techniques classiques de visualisation permettent alors d'accéder à une première description qualitative de l'écoulement. Celles-ci sont complétées par un certain nombre de mesures issues d'un traitement d'images effectué sur les visualisations précédentes ; ces informations quantitatives : distribution de débit et de temps de séjour, concentration, ... sont alors traduites sous forme de données d'entrée pour le code de calcul. Ce calcul, effectué dans un deuxième temps, peut utiliser une cinétique chimique plus ou moins complexe pour décrire la combustion et permet ainsi de prédire, avec un bon degré de précision, les performances globales du foyer (limites de statibilité, rendement de combustion en fonction des caractéristiques de fonctionnement,...). L'intérêt d'une telle démarche au stade d'un avant-projet a été démontré pour un nombre important de foyers en comparant les résultats obtenus en combustion avec ceux issus du calcul.

NOMENCLATURE

B	blocage
C	concentration
d	diamètre de goutte
D_H	diamètre hydraulique des manches
f	fonction de distribution de temps de séjour
F	fonction de répartition de temps de séjour
J	rapport de quantité de mouvement
q, Q	débits
t	temps
T	température
U	vitesse
V	volume
W	vitesse de combustion

SYMBOLES GRECS

α	angle des manches
μ	viscosité
σ	tension superficielle
ρ	densité
τ	temps de séjour moyen
τ_V	temps d'évaporation
φ	richesse

INDICES

A	air
D	dôme
K	carburant
L	latéral
R	recirculé ou réel
S	simulation

INITIALES

RPM	réacteur parfaitement mélangé
RP	réacteur piston

1. INTRODUCTION

Dans le fonctionnement d'un foyer, les performances en combustion sont fonction de la présence simultanée d'un ensemble de processus physiques complexes qui interagissent (1) : aérodynamique 3D turbulente et fortement instationnaire, combustion turbulente, transfert de chaleur, cinétique chimique complexe, éventuellement présence simultanée de plusieurs phases... De ce fait, devant le manque de connaissance encore important sur ces divers mécanismes physiques et leur interaction, la conception des foyers est encore très largement fondée sur l'utilisation de résultats empiriques associés à un ensemble d'expérimentations en combustion du foyer étudié afin de prévoir les caractéristiques globales de fonctionnement de celui-ci. On constate cependant qu'il est souvent difficile de lier les évolution des ces caractéristiques, constatées lors de telle modification de la géométrie ou de l'injection, à une modification de l'aérodynamique interne du foyer.

Ces dernières années, grâce au développement rapide des calculateurs et à l'amélioration des procédures de résolution numérique, on a vu se développer plusieurs programmes de calcul visant à décrire et, dans une certaine mesure, prédire, l'aérodynamique interne de foyers (2). Cependant, même si les progrès dans ce domaine sont très rapides, il faut constater que souvent ces outils constituent avant tout une aide à la compréhension plus qu'un instrument prédictif sur le fonctionnement du foyer. Ceci est en particulier le cas dès que l'on essaye de dépasser la simple évaluation des tendances pour rechercher des prévisions chiffrées. En plus des difficultés associées à la complexité des mécanismes en présence cités plus haut, une telle situation s'explique aussi du fait du manque de méthodes de diagnostic permettant de vérifier, in situ, la validité des modèles physiques utilisés ainsi que la faible connaissance sur certaines des données relatives aux conditions aux limites à introduire dans un code 3D (par exemple transfert convectif pariétal (3), phase liquide (1)). Enfin, il convient de noter que cette démarche visant à calculer localement et de façon détaillée l'écoulement interne se révèle finalement trop précise (quant à la discrétisation spatiale) si

l'on s'interesse avant tout aux conséquences globales de cette aérodynamique interne à savoir : rendement de combustion et limite de stabilité. Une telle situation est bien caractéristique du foyer de stato si on la compare aux foyers aéronautiques pour lesquels, par exemple, la donnée précise d'une carte de vitesses et de températures en sortie constitue une information précieuse.

Cette remarque contribue à priviligier un second type de modélisation, plus simplifié quant à la description géométrique de l'écoulement, mais autorisant de ce fait l'emploi de mécanismes physiques plus détaillés (par exemple, au niveau de la cinétique chimique). Cette seconde approche, de type 0D ou 1D, utilise le concept de réacteurs élémentaires : "parfaitement mélangé" et "piston" et est issue des travaux effectués en génie chimique (4). Employée depuis de nombreuses années dans les études de foyers, cette seconde approche est intéressante si les caractéristiques des réacteurs élémentaires (nature, volume, débit, interconnexion, ...) ne sont pas données a priori, comme ce fut pendant longtemps le cas, mais si celles-ci sont effectivement représentatives du foyer étudié. Pour ce faire, la technique consiste à utiliser des "traceurs" injectés et analysés de façon adéquate afin de pouvoir, par une identification appropriée, associer à l'écoulement étudié, une description simplifiée sous forme d'un assemblage de réacteurs élémentaires. Une telle démarche, pratiquée depuis plusieurs années au DERMES, peut s'effectuer de deux façons différentes :

- au moyen de traceurs physiques injectés dans des maquettes étudiées en conditions simulées. C'est l'objet de la présente étude.
- avec des traceurs numériques injectés dans un calcul détaillé de l'écoulement dans le foyer étudié afin d'extraire de celui-ci une description simplifiée en terme d'assemblage de réacteurs élémentaires (5).

Dans l'approche utilisée au CERT-DERMES, les expériences sont menées en conditions simulées sur des maquettes transparentes expérimentées en eau ou en air. Des méthodes classiques de visualisation associées à différents moyens de traitement d'images permettent de procéder à diverses mesures (concentration, temps de séjour, débit, ...) relatives au traceur. Ces mesures permettent, par identification, de décrire l'écoulement en termes d'assemblage de réacteurs élémentaires pour lesquels les caractéristiques, au lieu d'être fixées a priori, sont directement issues de ces expériences. De telles expériences sont menées afin de préciser les caractéristiques de l'air alimentant le foyer ainsi que du combustible, que celui-ci soit injecté sous forme gazeuse ou liquide.

L'objet de la présente contribution est donc de montrer, après une description des techniques expérimentales et de modélisation utilisées, comment une telle approche peut, malgré sa relative simplicité, se révéler particulièrement efficace quant à la prévision des performances globales d'un foyer en cours d'étude. De nombreuses comparaisons avec les essais au banc effectués par la Direction de l'Energétique de l'ONERA sur des maquettes en combustion ont permis, en effet, de valider cette méthode sur un nombre significatif de géométries et de concepts de foyer. Par ailleurs, la banque de données constituée par ces études nous autorise aussi à améliorer la compréhension des phénomènes intervenant dans le fonctionnement de ces différents "réacteurs élémentaires". En particulier, il devient possible de traduire en termes de modifications des caractéristiques de ces réacteurs (volume, débit, ...) les changements apportés à la géométrie du foyer ainsi qu'aux conditions d'injection. Une telle information constitue un guide particulièrement précieux, non seulement pour améliorer la compréhension d'essais en combustion, souvent limitée par la difficulté de mesures internes en conditions métrologiques délicates, mais aussi pour guider le concepteur vers des choix permettant une optimisation des performances. On présente enfin quelques comparaisons montrant que, pour certaines configurations, la démarche proposée peut aussi constituer un outil efficace permettant de prédire, si ce n'est en comprendre tous les mécanismes, certains phénomènes d'instabilités de combustion.

2. METHODES EXPERIMENTALES - DESCRIPTION DE LA PHASE GAZEUSE

Les expérimentations relatives à la phase gazeuse sont effectuées en conditions isothermes sur une maquette représentant, à échelle réduite, la géométrie réelle du foyer à étudier. Compte tenu de la plus grande facilité à effectuer des visualisations en écoulement hydraulique plutôt qu'en essais aérodynamiques, les maquettes sont étudiées en simulation hydrodynamique. En général, on s'arrange pour que les conditions d'essais simulées respectent sensiblement le nombre de Reynolds relatif aux conditions d'entrée (8) :

$$Re = \frac{\rho_A U_A D_H}{\mu_A} \qquad (1)$$

La veine d'essai, régulée en débit jusqu'à une valeur de 20 l/s, peut recevoir différents types de maquettes de foyers. Comme le montre la figure 1, celles-ci, réalisées en altuglass pour assurer une transparence suffisante, sont montées dans un réservoir parallélépipèdique rempli d'eau afin de limiter les distorsions optiques dues aux variations d'indices des milieux traversés.

2.1. Visualisations qualitatives

Premier stade dans l'étude d'un nouveau foyer, celles-ci permettent déjà de fournir une première description de l'écoulement interne au foyer. Pour ce faire, on utilise des techniques classiques de traceurs : bulles d'air (obtenues par adjonction de teepol dans le circuit), bulles d'hydrogène (générées par électrolyse) ou fluorescéine injectée ponctuellement ou dans certaines zones caractéristiques (recirculation par exemple). L'éclairage est réalisée au moyen d'une tranche lumineuse ou d'un plan laser permettant de délimiter les zones caractéristiques à étudier.

Quelques exemples de telles visualisations sont présentés aux figures 2 et 3. On peut distinguer, en particulier, la zone de recirculation principale située en fond de chambre et due à l'impact des jets issus des manches (figure 2).

Effectuée pour chaque nouvelle maquette étudiée, cette première étape permet, tout d'abord, de repérer les principales zones de l'écoulement en précisant, en particulier, les régions à forte recirculation permettant d'initier et d'entretenir la combustion. On distingue, en général, les régions suivantes :
- En fond de chambre (dôme), la zone de recirculation principale, due à l'impact du (ou des) jet(s) issu(s) de la (ou des) manche(s) et permettant à une fraction de l'air frais de participer à la combustion.

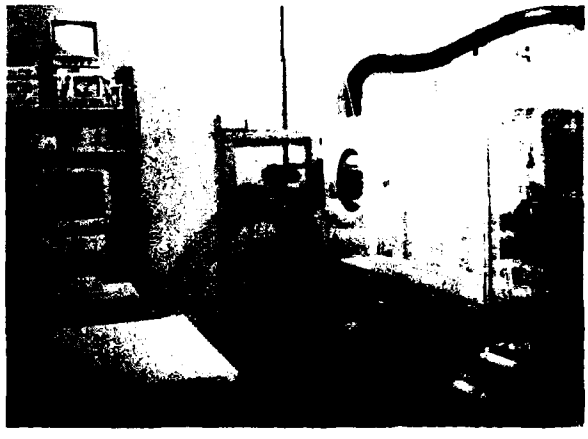

Figure 1 : Vue générale du banc hydraulique

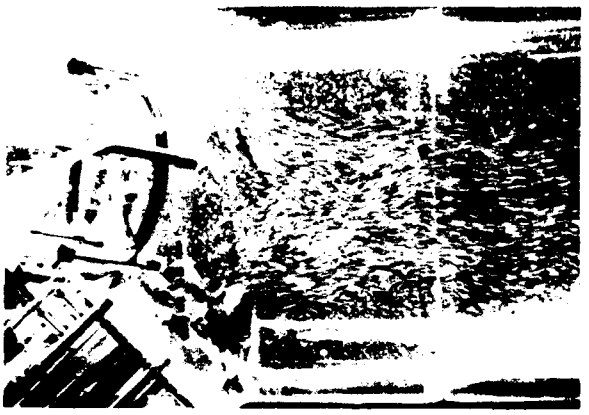

Figure 2 : Exemple de visualisation - 4 entrées semi-latérales

Figure 3 : Exemple de visualisation - 4 entrées latérales avec accroche-flamme

- En prolongement de la (des) manche(s) une zone de jet dans laquelle la combustion, initiée dans les recirculations adjacentes, peut se propager.
- Entre cette zone de jet et les parois du foyer, une (ou plusieurs) zone(s) de recirculation latérale(s) recevant ainsi sous forme d'air frais une autre partie du débit issu du (des) jet(s).

Bien qu'elle change en fonction de la géométrie du foyer (1, 2 ou 4 manches, symétriques ou non) et des caractéristiques des plans de sortie des manches ainsi que du mode d'injection, cette description en terme de "dôme", "latéral" et "jet" se retrouve dans la quasi totalité des foyers étudiés.

Toujours sur un plan qualitatif, cette première analyse permet aussi de distinguer certaines configurations pour lesquelles l'écoulement est particulièrement instable (battement de jets par exemple) et risque de constituer une des causes d'instabilités de combustion.

Le dernier élément, enfin, associé à ces premières visualisations, se situe dans le fait que celles-ci constituent un guide précieux pour choisir les emplacements où injecter et mesurer le traceur utilisé pour déterminer les caractéristiques quantitatives (débit, nature, volume, interconnexion) associées aux différents réacteurs élémentaires utilisés par la suite dans la modélisation.

2.2. Traitement quantitatif des visualisations - Découpage en réacteurs élémentaires

La méthode utilisée consiste à mesurer en continu la concentration d'un traceur injecté de façon contrôlée dans l'écoulement ; un choix judicieux des conditions d'injection et de mesures permet ensuite, par identification, d'effectuer des mesures de débit, temps de séjour et volumes de réacteurs élémentaires.

. Mesure de concentration

Effectuée de façon non intrusive, la mesure de concentration de fluorescéine est fondée sur la mesure locale du niveau de gris de l'image observée à 90° du plan lumineux délimitant la zone observée. Cette méthode, décrite en (9), utilise une caméra CCD, associée à un micro-ordinateur permettant de mesurer en continu, au sein d'une surface de mesure, de position et taille réglables, le niveau de gris moyen de l'image. Celui-ci est relié, après un étalonnage préalable effectué dans les mêmes conditions d'environnement lumineux, à la concentration spatiale moyenne à l'intérieur de la zone étudiée.

. Mesure de débit

La mesure du débit traversant les zones principales de l'écoulement est effectuée par la technique classique de "dilution". Le principe (7) consiste à injecter en continu un débit contrôlé et connu q de traceur dans le volume étudié. La mesure de la concentration moyenne C de ce traceur au sein du même volume, au moyen de la méthode décrite ci-dessus, permet d'accéder au débit Q traversant ce volume. En effet :

$$Q = q / C \qquad (2)$$

Cette méthode, pratiquée pour le réacteur "Dôme" en fond de chambre, permet par exemple d'évaluer la fraction :

$$Q_{RD} / Q_A \qquad (3)$$

du débit d'air principal Q_A, venant recirculer dans le dôme et pouvant participer à la combustion.

La même méthode, utilisée en injectant successivement la fluorescéine dans les différents volumes "Dump", "Latéral", "Jet" et en mesurant les concentrations résultantes dans ces mêmes réacteurs permet une première estimation des différents débits transitant entre ces divers volumes, au moyen d'une simple écriture de bilan.

. Mesure de temps de séjour

La mesure de temps de séjour (fonction de distribution f(t), fonction de répartition F(t) ou valeur moyenne τ) utilise une injection de traceur sous forme de Dirac ou d'échelon. Dans ce cas, on montre aisément (4) que la concentration instationnaire est proportionnelle à f(t) ou F(t).

Une telle mesure, utilisant alors une injection de debit contrôlée au moyen d'une (ou deux très légèrement décalées dans le temps) électrovanne(s) permet d'accéder, dans chacun des réacteurs élémentaires précités, à la distribution ou répartition de temps de séjour. Cette information, essentielle pour connaître la capacité du réacteur élémentaire correspondant à initier une combustion stable, est aussi précieuse en complément de la valeur du débit Q traversant celui-ci pour connaître son volume. On montre aisément, en effet, que, pour un réacteur élémentaire isolé, le temps de séjour moyen τ défini par :

$$\tau = \int_0^\infty f(t)\, dt \qquad (4)$$

a la valeur suivante :

$$\tau = V / Q \qquad (5)$$

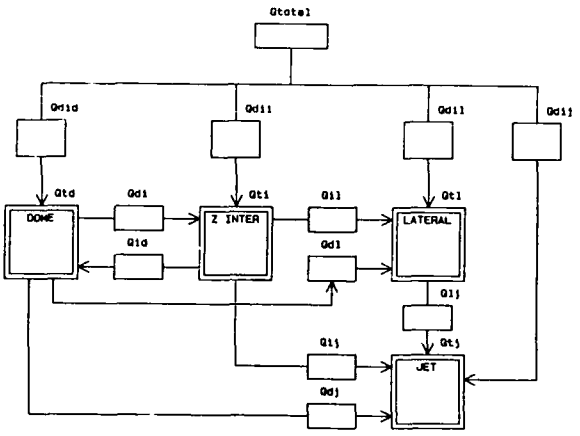

Figure 4 : Exemple de découpage en réacteurs élémentaires

Découpage en réacteurs élémentaires
L'utilisation conjointe des mesures de débit et de temps de séjour associée à des techniques simples d'identification (7) permet donc, pour chaque nouveau foyer étudié, de représenter l'écoulement interne sous une forme simplifiée au moyen d'un assemblage de réacteurs élémentaires dont les caractéristiques sur un plan qualitatif et quantitatif ne sont pas fixées a priori mais résultent d'une analyse effectuée selon la démarche présentée ci-dessus.

Un exemple d'un tel découplage, correspondant à une géométrie de foyer à entrées est présenté à la figure 4. On y retrouve les trois réacteurs élémentaires : "Dôme", "Latéral", "Jet", les deux premiers étant assimilés à des réacteurs parfaitement mélangés (RPM) le troisième à un réacteur piston (RP) avec diffusion (7). Le découpage et les répartitions de débit sont issus des mesures avec traceur.

2.3. Caractéristiques principales de l'écoulement - Paramètres significatifs

La démarche précédente, effectuée et validée sur un nombre très important de foyers réels mais aussi de géométries simplifiées, nous a conduit à obtenir un ensemble de corrélations donnant l'évolution de certains pourcentages de débit en fonction des données géométriques du foyer et des conditions de fonctionnement (11).

Deux exemples de telles corrélations sont présentés aux figures 5 et 6 où l'on voit les influences respectives du blocage B (rapport de la surface projetée des jets à la section droite du foyer) et de l'angle α de pénétration des jets dans le foyer sur les taux de débits Q_{RD}/Q_A et Q_{RL}/Q_A respectivement recirculés dans les réacteurs "Dôme" et "Latéral".

Une telle information, ainsi que d'autres semblables, constitue une donnée précieuse non seulement pour aider à interpréter l'effet d'une modification géométrique (qui peut se traduire en termes de blocage, angle de jet, débit en fond de chambre, ...) sur les résultats en combustion, mais aussi pour guider le choix vers telle ou telle solution en vue de modifier les caractéristiques globales de fonctionnement pour qu'elles répondent à un cahier des charges donné.

3. METHODES EXPERIMENTALES - ETUDE DE L'INJECTION

Afin de compléter les données du découpage en réacteurs élémentaires par celles relatives à l'injection. Des mesures supplémentaires doivent être effectuées.
Deux cas sont à considérer selon que le carburant est sous forme gazeuse ou liquide :

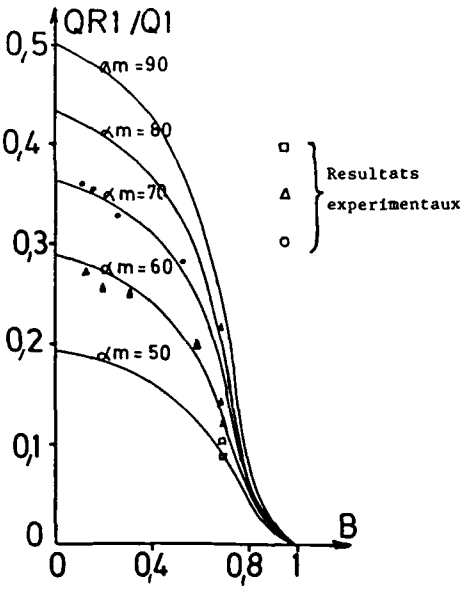

Figure 5 : Pourcentage de débit d'air recirculé dans le dôme - Influence du blocage et de l'angle du jet

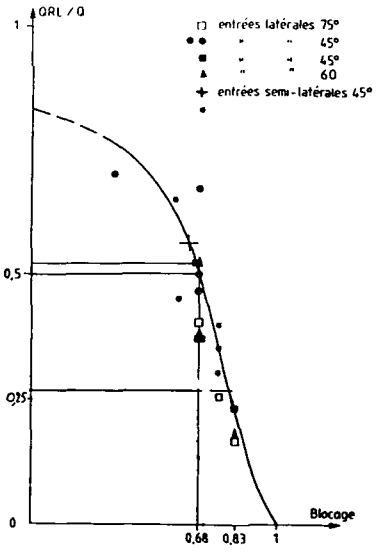

Figure 6 : Pourcentage de débit d'air recirculé dans le réacteur latéral - Influence du blocage et de l'angle du jet.

. Dans le premier cas, des méthodes semblables de mesure de concentration et de débit sont utilisées, la maquette étant toujours étudiée sur banc hydraulique.
. Dans le second cas, les méthodes précédentes sont extrapolées à l'analyse de la phase liquide et complétées par d'autres spécifiques du biphasique, la maquette de foyer étant étudiée, cette fois-ci, sur un banc aérodynamique.

3.1. Combustible gazeux

Le carburant est alors simulé par de l'eau, les conditions d'injection (vitesse, débit) étant choisies de façon à ce que les effets de pénétration et de mélange entre carburant et air soient simulés au mieux. La similitude utilisée s'appuie sur la conservation du rapport entre les quantités de mouvement respectives du carburant et de l'air.

$$J = \frac{\rho K\, U_K 2}{\rho A\, U_A 2} \qquad (6)$$

Le traceur fluorescéine simulant le carburant étant alors injecté dans l'écoulement , des mesures de concentration moyenne effectuées de façon semblable aux précédentes permettent donc de connaître, en fonction des conditions d'injection simulées (richesse, géométrie, ...) les valeurs de richesse dans chacun des réacteurs élémentaires.

Il est évident que cette analyse ne s'applique que pour le carburant arrivant "directement" dans le réacteur étudié et non pas après transit dans un ou plusieurs autres réacteurs.

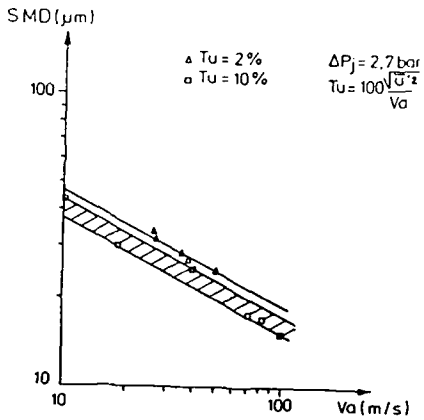

a) Influence de la vitesse et du taux de turbulence de l'air

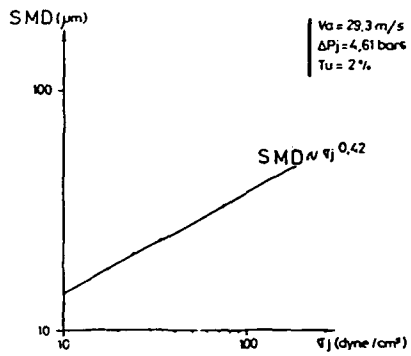

b) Influence de la tension superficielle

Figure 7 : Exemple de distribution de taille de gouttes en aval d'un injecteur

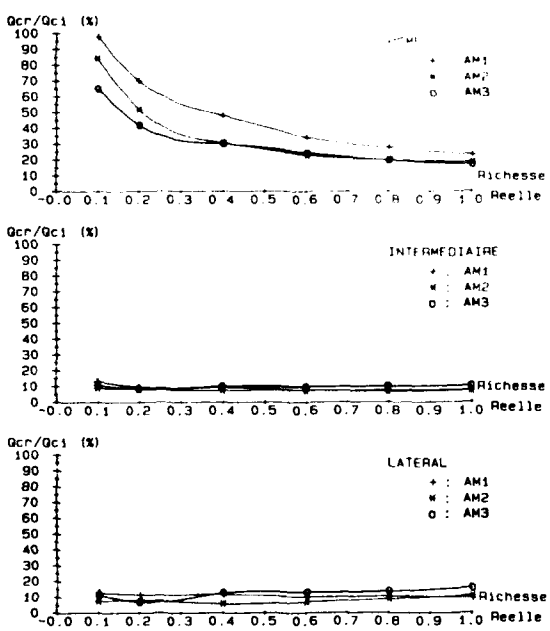

a) Influence de la position radiale de la rampe d'injecteurs.

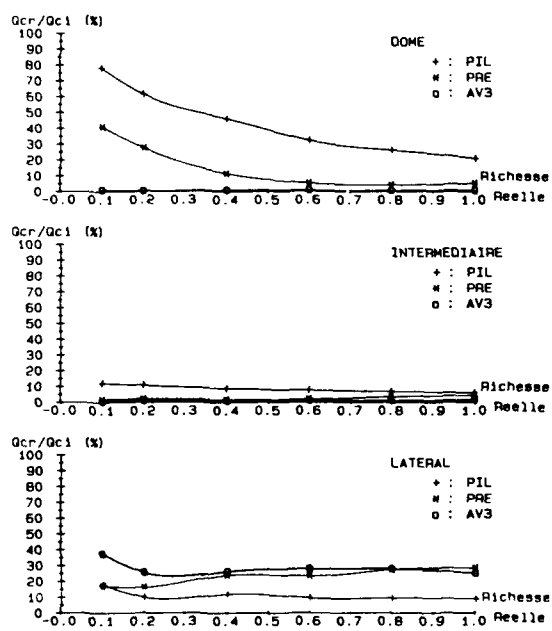

b) Influence de la position axiale de la rampe d'injecteurs.

Figure 8 : Pourcentage de débit carburant recirculé dans les différents réacteurs - une entrée latérale

3.2. Combustible liquide

Dans ce cas, seule une simulation effectuée en conditions biphasiques est suffisamment réaliste pour fournir des données pouvant être ensuite utilisées dans la modélisation. De nombreuses études effectuées sur différents types d'injecteurs utilisés pour les foyers de stato-réacteurs (13) et figure 7 nous ont conduit à connaître, sous forme de corrélations, l'influence des caractéristiques physiques du fluide injecté (viscosité μ_K, tension superficielle σ_K) de la géométrie de l'injecteur et des conditions de fonctionnement sur les caractéristiques géométriques (expansion du panache par exemple) et granulométrique du jet. Ainsi, pour la simulation en biphasique, on choisira en fonction du cas étudié des caractéristiques physiques du liquide et des conditions de fonctionnement simulées privilégiant plutôt l'aspect granulométrie ou expansion de jet (13). Pour la valeur de richesse utilisée en simulation, soit φ_S, celle-ci correspond à la richesse réelle φ_R en fonction de la relation suivante :

$$\varphi_S = \varphi_R \left(\frac{P_{AR}}{P_{AS}} \times \frac{T_{AS}}{T_{AR}} \right)^{1/2} \qquad (7)$$

P_A et T_A étant respectivement les valeurs de pression et température de l'air en conditions réelles (R) ou simulée (S).

Comme pour le carburant gazeux, les mêmes méthodes de mesure de concentration, appliquées, cette fois, à un traceur liquide, permettent d'accéder aux résultats suivants (14) :
. richesse locale dans chaque réacteur en fonction de la richesse globale injectée et des conditions d'injection (nombre, position et orientation des injecteurs, ...).
. transfert de débit entre réacteurs.

Comme dans le cas précédent, on remarquera que ces résultats ne sont applicables que tant que les réacteurs élémentaires traversés ne sont pas en situation de combustion. Dans le cas contraire, où une partie du carburant arrive dans un réacteur élémentaire en combustion, on considère que ce carburant est totalement vaporisé ; le complément éventuel d'imbrûlés se comportant alors comme la phase gazeuse.

Quelques exemples de mesures relatives au carburant liquide sont présentés à la figure 8 On y remarquera en particulier la grande sensibilité des valeurs aux conditions d'injection : (richesse, position et orientation des injecteurs). Ces résultats, qui ont une influence directe sur l'évaluation des performances du foyer, montrent l'absolue nécessité de représenter au mieux le comportement de la phase liquide si l'on veut en déduire une évaluation des performances avec un caractère prédictif suffisant. Cette remarque s'applique aussi bien aux simulations expérimentales telles que celles décrites ici qu'à la prise en compte de la phase liquide dans une modélisation détaillée de foyer.

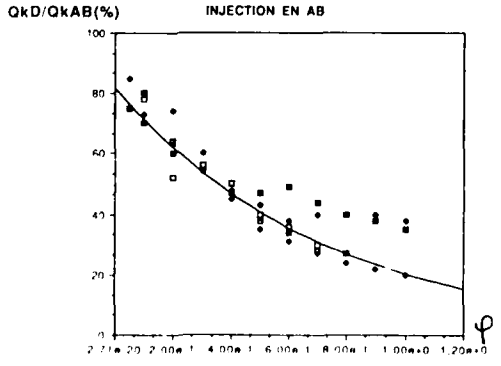

Figure 9 : Pourcentage de débit carburant recirculé dans le dôme - Synthèse des résultats pour différentes géométries avec une injection côté intérieur du coude.

3.3. Conclusions sur l'injection

Malgré le nombre important de configurations d'injection étudiées au CERT-DERMES, il semble difficile d'effectuer, comme pour la phase gazeuse, des corrélations permettant de donner des pourcentages de débit carburant en fonction de paramètres significatifs. Ceci est dû principalement à l'extrême sensibilité des résultats aux conditions d'essai simulées et à l'influence des détails de la géométrie du foyer. On peut cependant noter les quelques remarques suivantes :
- Si le combustible est introduit dans le foyer sous forme gazeuse, par exemple par le fond avant, il peut, par effet d'entraînement, modifier les répartitions de débit de la phase gazeuse. Ceci est particulièrement vrai pour la fraction de débit d'air Q_{RD}/Q_A alimentant le dôme et pour laquelle les corrélations doivent tenir compte de la présence éventuelle de ce débit en fond de chambre.

Malgré les remarques ci-dessus sur la difficulté de faire des corrélations, on peut cependant essayer de dégager certaines tendances. Un exemple, présenté à la figure 9, montre l'influence de la richesse en carburant liquide, injecté (valeur simulée) du côté rayon intérieur du coude d'une manche, sur le taux de carburant alimentant le réacteur "dôme". Ce résultat, qui représente une compilation sur six configurations différentes, montre bien, malgré la dispersion, l'effet très sensible de la richesse injectée sur l'alimentation du dôme.

Enfin, pour conclure sur la phase liquide, il convient d'ajouter que l'influence de la granulométrie du jet peut être aussi prise en compte dans le calcul, en comparant le temps de séjour moyen τ dans le réacteur étudié au temps d'évaporation τ_{ev}, fonction directe du diamètre moyen des gouttes.

$$\tau_{ev} = \frac{d^2}{\lambda_{ev}} \qquad (8)$$

d : diamètre moyen de Sauter

λ_{ev} : constante d'évaporation

Dans ce cas, on considère que seule la fraction évaporée participe à la combustion.

4. MODELISATION

Afin d'effectuer la modélisation de la combustion au moyen du découpage en réacteurs élémentaires issus des expériences décrites ci-dessus, on utilise un modèle de calcul permettant de résoudre les équations de bilan (masse, énergie) et celles relatives à la cinétique chimique. Selon le cas, ces dernières peuvent se résumer à une seule réaction globale entre fuel et oxygène (16) :

$$F + \nu O_2 \rightarrow P \qquad (9)$$

On prendra en compte une cinétique chimique plus détaillée comme, par exemple, décrit dans le tableau ci-dessous :

Réactions	--->	k	α	ε
$C_{10}H_{20} + 5O_2$ ---> $10\,CO + 10\,H_2$		8.10^{11}	0	7 500
$CO + OH$ ---> $CO_2 + H$		$1,5\,10^{11}$	0	500
$O + H_2O$ ---> $2OH$		$1,76\,10^{13}$	0,02	8 370
$H + H + M$ ---> $H_2 + M$		10^{12}	-1	0
$O + O + M$ ---> $O_2 + M$		$2\,10^{9}$	-0,4	0
$OH + H + M$ ---> $H_2O + M$		$1,5\,10^{11}$	0,5	0
$H + O_2$ ---> $OH + O$		$2\,10^{14}$	0	8 330
$O + H_2$ ---> $OH + H$		$6\,10^{13}$	0	5 000
$H + H_2O$ ---> $OH + H_2$		$5,5\,10^{13}$	0,01	9 890
$OH + M$ ---> $O + H + M$		$6,96\,10^{13}$	0,21	50 650
$N_2 + O$ ---> $NO + N$		$0,8\,10^{13}$	0	37 500
$N + O_2$ ---> $NO + O$		$2,67\,10^{10}$	0,92	3 521
$N + OH$ ---> $NO + H$		$2,8\,10^{13}$	0	0

TABLEAU

Dans tous les cas, la vitesse de réaction fait intervenir une loi d'Arrhenius (1).
Cet ensemble d'équations non linéaires est alors résolu au moyen d'une méthode de Raphson-Newton

5. EXEMPLES DE RESULTATS

Compte tenu du nombre très important de configurations testées, seuls quelques exemples caractéristiques de performances globales de foyers calculées au moyen de cette approche sont présentes. Ces résultats calculés sont comparés avec les mesures effectuées en combustion, sur ces mêmes foyers ; mesures réalisées en général à la direction de l'Energétique de l'ONERA avec qui ces études sont menées en collaboration suivie.

Comme on peut le voir, ces comparaisons démontrent parfaitement le bien fondé de cette approche qui, malgré la simplicité de la démarche et des hypothèses utilisées, permet de mieux comprendre et prédire avec une fiabilité intéressante les évolutions de performances des foyers étudiés.

5.1. Limite de stabilité - Domaine de fonctionnement

En général, la comparaison entre limites d'extinction calculée et mesurée est bonne, voire très bonne, pour la limite pauvre. Un tel exemple caractéristique est montré à la figure 10 correspondant au cas d'un foyer à quatre entrées par le fond avant. La comparaison calcul-expérience montre l'influence du rapport de débit carburant injecté côté extérieur du coude (CD) à celui côté intérieur (AB) est particulièrement bonne.

Cette bonne concordance entre les valeurs calculées et mesurées de la limite pauvre, qui, dans ce cas comme dans la plupart des configurations traitées, correspond à celle du dôme, montre que les valeurs des débits d'air (Q_{RD}) et carburant (q_{KD}), bien qu'évaluées en conditions isothermes, sont correctes.

Toujours pour cet exemple présenté à la figure 10, on remarquera que, même si la tendance est correctement représentée, l'évaluation de la limite riche du foyer (qui, dans ce cas, est celle du réacteur latéral) est moins précise. En plus de l'aspect strictement lié à la définition de cette limite riche, cet écart peut aussi être dû à un effet de la combustion et du transfert de chaleur résultant sur les caractéristiques du réacteur latéral (en particulier sur le débit recirculé Q_{RL}) ainsi qu'à l'effet sur l'évaporation des gouttes.

Toujours sur ce même exemple, on notera aussi que le fonctionnement de chaque réacteur élémentaire "Dôme" et "Latéral" est très nettement visible. En particulier, pour les faibles valeurs de CD/AB (≤ 35/65), il existe une zone sans combustion pour des richesses voisines de 0,4 qui correspondent à des valeurs de φ supérieures à la limite riche du dôme et inférieures à la limite pauvre du latéral (ces deux limites étant, par ailleurs, prédites avec une très bonne précision comme en témoigne la figure 10). Il est évident que pour ce dernier cas, inattendu, la méthode proposée constitue aussi un outil d'analyse et de compréhension particulièrement précieux des essais en combustion.

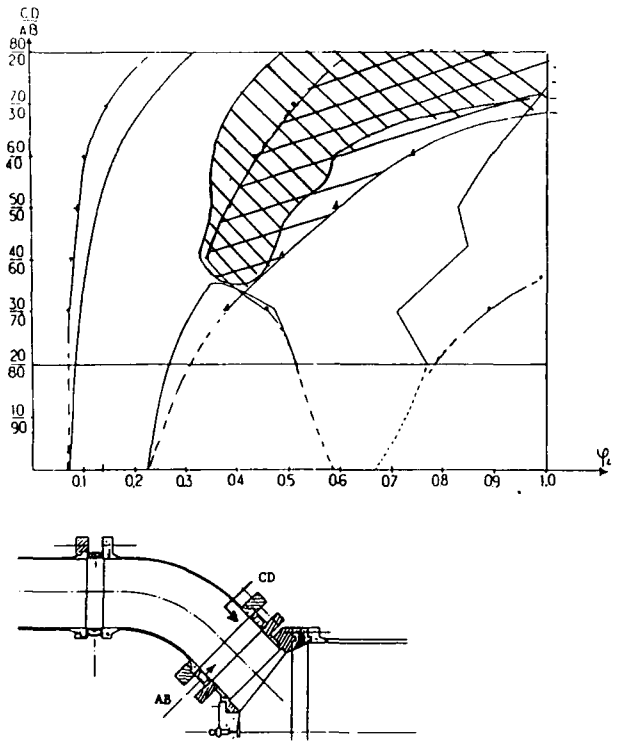

Limites d'extinction
+ dôme - pauvre
Δ dôme - riche
o latéral - pauvre
. latéral - riche
- pauvre et riche
expérimentales

Instabilités de combustion
/// résultats de calcul
\\\ résultats expérimentaux.

Figure 10 : Influence des conditions d'injection sur les limites d'extinction et les instabilités de combustion - 4 entrées latérales.

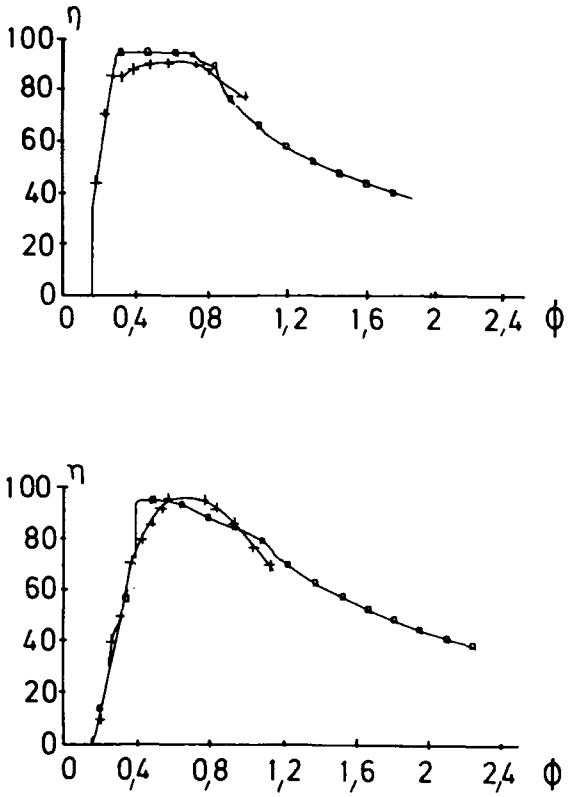

□ calcul
+ expérience
a) avec chambre pilote
b) sans chambre pilote

Figure 11 : Influence de la richesse sur le rendement et les limites de stabilité - 2 entrées latérales.

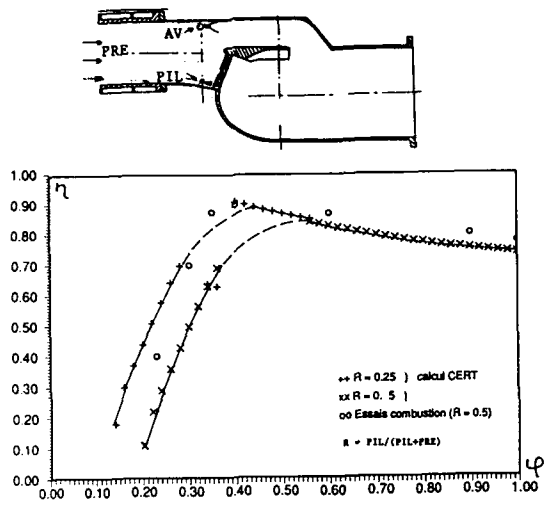

Figure 12 : Influence de la richesse et du mode d'injection sur le rendement de combustion - 1 entrée latérale.

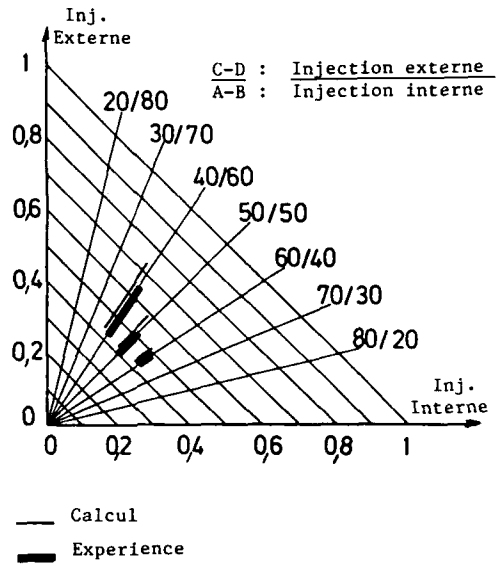

Figure 13 : Domaine d'instabilités de combustion - 4 entrées latérales - Influence des conditions d'injection.

D'autres exemples de comparaison sur les plages de fonctionnement sont aussi présentés à la figure 11. Cet ensemble de comparaisons nous permet donc de disposer d'un véritable outil d'aide à la conception et à l'optimisation des foyers en cours d'étude. En effet, en partant des résultats calculés (et si possible validés par des essais en combustion) sur une géométrie de base de foyer, il devient possible de guider les choix des modifications à effectuer sur la géométrie du foyer (blocage ou angle des jets, ...) ainsi que sur les paramètres d'injection pour faire évoluer une plage de stabilité vers des valeurs correspondant, par exemple, à un cahier des charges. Il est clair que l'étude paramétrique à effectuer alors s'appuie largement sur les corrélations dont certains exemples ont été présentés en 2.3 et 3.3.

5.2. Rendement de combustion

Quelques exemples de comparaisons entre valeurs calculées et mesurées sont présentés aux figures 11 et 12 qui correspondent à plusieurs cas de foyers à une ou deux entrées.

Dans ces exemples aussi, les comparaisons sont bonnes tant pour les tendances que pour les niveaux et l'influence de certaines modifications géométriques y sont bien représentées.
Il faut cependant noter que, même si cette tendance est en général bonne, la comparaison entre les niveaux de rendement conduit parfois à une sous évaluation pour le calcul. Ce résultat, plus fréquent lorsque le foyer comporte des petites zones de recirculation (Dôme et Latéral) et des jets très marqués, est en partie dû à la non prise en compte, dans cette modélisation modulaire, de la combustion pouvant exister dans les zones de jet (et initiée dans le Dôme ou réacteur latéral).

5.3. Instabilité de combustion

Il n'est pas question, dans cet article et avec cette méthode, d'aborder dans le détail l'étude des instabilités de combustion, phénomène particulièrement complexe qui a déjà fait l'objet de très nombreuses publications et auquel le CERT-DERMES s'est aussi intéressé (19). Notre seul but ici est de montrer comment une analyse aussi simple que celle que nous préconisons peut constituer, elle aussi, un élément permettant de prévoir, dans un certain nombre de cas, l'apparition d'instabilités de combustion.

Cette analyse repose sur l'examen de la figure 10. On y constate en effet que la zone pour laquelle des instabilités de combustion sont mises en évidence expérimentalement correspond sensiblement au domaine calculé pour lequel les réacteurs dôme et latéral fonctionnent simultanément (φ supérieure à la limite pauvre du latéral et inférieure à la limite riche du dôme). Une des explications de ce phénomène peut être un mécanisme de couplage entre ces deux réacteurs, l'état de fonctionnement du dôme ayant un effet direct sur l'évaporation des gouttes passant en son voisinage et donc sur le réacteur latéral lui-même.

Cette correspondance, notée ici, s'est trouvée très souvent confirmée comme en témoigne, par exemple, la figure 13.

Remarques : Les quelques exemples de résultats présentés ci-dessus et les diverses interprétations qui en découlent sont fondés sur certaines hypothèses sur le fonctionnement des différents réacteurs élémentaires ou sur la présence de combustion dans telle ou telle zone de l'écoulement. Il est sûr qu'une vérification directe serait intéressante mais, jusqu'à présent, les moyens de diagnostic en combustion la rendent délicate. On peut cependant s'appuyer sur les constatations suivantes permettant, en partie, de valider certaines hypothèses.
. Les limites d'extinction d'un réacteur élémentaire donné sont directement fonction des valeurs de la richesse locale, elle-même, directement conditionnée par les valeurs de débits air et carburant alimentant le réacteur élémentaire. Ainsi, toute mauvaise évaluation de ces débits se traduirait directement en erreur correspondante sur l'estimation des limites d'extinction.
. Lors des essais en combustion effectués à la direction de l'Energétique de l'ONERA, en plus des mesures globales, des analyses thermographiques par caméra IR permettant, au moins sur un plan qualitatif, de préciser les zones de combustion. La correspondance entre la localisation de celles-ci et leur état (avec ou sans combustion) et les résultats de nos modélisations est, en général tout à fait probante.

6. CONCLUSIONS ET PERSPECTIVES

Une approche semi-empirique, associant des expérimentations effectuées en simulation isotherme et une méthode simple de calcul, a été mise en oeuvre afin d'étudier les performances globales de plusieurs modèles dc foyers de stato-réacteurs et stato-fusées.. La validation de cette démarche par les expérimentations en combustion conduit à des comparaisons particulièrement intéressantes entre les valeurs calculées et mesurées des performances globales. L'emploi de cette méthode pour un nombre important de géométries de foyers, modes et conditions d'injection, conditions d'essais, permet de disposer d'un outil particulièrement utile au niveau des avant-projets. Il s'agit, en effet, d'une méthode permettant, non seulement de mieux interpréter les résultats d'essais en combustion mais aussi de calculer, avec une bonne fiabilité, l'évolution des performances en combustion.

Pour atteindre ce degré de prédictivité, la méthode utilise les résultats d'expériences qui doivent être suffisamment représentatives de la réalité. C'est en particulier le cas pour les statos à combustible liquide pour lesquels la simulation expérimentale doit être la plus réaliste possible afin d'en déduire des prévisions correctes pour les performances globales.

Enfin, dans certains cas, la méthode permet ainsi de donner des informations relatives aux instabilités de combustion.

Tout en améliorant les techniques de mesures et en conditions de simulation, la méthode est actuellement complétée par une approche voisine dans laquelle les données nécessaires au découpage en réacteurs élémentaires ne sont plus issues de résultats d'expériences mais résultent de l'analyse de "traceurs numériques" injectés dans un calcul local d'écoulement de foyer (5). Une telle méthode, à condition que les modèles physiques introduits dans ces codes soient représentatifs de la réalité, permet d'étendre la démarche actuelle, tout d'abord en limitant le nombre d'expériences physiques à réaliser et ensuite en prenant mieux en compte l'influence de la combustion et du transfert de chacun sur l'aérodynamique interne.

REMERCIEMENTS

Ce travail s'appuie sur les résultats d'un ensemble d'études financées par la DME, l'AEROSPATIALE ainsi que les directions scientifiques de l'Energétique et des études de synthèse à l'ONERA que les auteurs tiennent à remercier pour leur soutien.

REFERENCES

1 Lefevbre A., "Gas turbine combustor design problems", Mac Graw Hill, 1990

2 Amsdem A. & al, "Computer program for two and three dimensional flows with chemical reactions and fuel sprays". Los Alamos National Laboratory Report LA 10245 - MS, 1985

3 Desaulty M. "Turbine engine combustor design at SNECMA" 10th ISOABE (Nottingham), 1991

4 Levenspiel O., "Chemical reaction engineering" John Willey and Sons, 1972

5 Hebrard P.& al, "Numerical simulation of two phase flow in combustion chambers" International IGTI congress (Orlando), 1991

6 Swithenbank, "Closing the gap between finite difference and stirred reactor combustor modelling procedures", 20th symposium on combustion. The combustion Institute,1984

7 Frager G. & al, "Etude aérodynamique de la combustion dans les foyers de turbomachines : approches expérimentales et théoriques". AGARD Conference proceedings n° 353 (Cesme), 1983

8 Ben-Arosh R., "Similarity and scale effects in solid fuel ramjet combustors", 9th ISOABE (Athens) 1989.

9 Toulouse G. & al, "Quantitative flow visualization with video methods and microcomputer", 3rd International Symposium of visualization, (Ann Arbor), 1983.

10 Lavergne G. & al, "Experiments and computation study of liquid droplets impinging on air afterburner" ISOABE Conference (Nottingham), 1991.

11 Hébrard P., Internal Report, not published.

12 Mercadier Y. & al, "Reflectography applied to optical particle sizing : theoretical and experimental approaches", 2nd International Congress on optical particle sizing, (Tempe), 1990.

13 Hébrard P. & al, "Etude par simulation des phénomènes de pulvérisation, de ruissellement et de vaporisation liés à l'injection de carburant" AGARD Conference proceedings, n° 422 (Chania), 1987.

14 Hébrard P.& al, "Experimental investigation of two phase flow in the near field of an airblast atomizer". 5th ICLASS conference (Gaithersburg), 1991.

15 Murty A. & al, "*Introduction to combustion phenomena*", Gordon and breach science publishers, 1975.

16 Mir A., "Ecoulements réactifs ou de convection naturelle, différentes approches théoriques", thesis of doctorat es sciences, Toulouse, 1983.

17 Edelman R. & al, "A quasi global chemical Kinetic model for the finite rate combustion of hydrocarbon fuel with application to turbulent burning and mixing in hypersonic engines and nozzle", AIAA paper 69-86, 1969.

18 Cathonet M., & al "Experimental study and numerical modelling of high temperature oxydation of propane and n-butane", 18th symposium on combustion, 1981.

19 Pauzin S. & al "Experimental study of the acoustic coherent structure coupling on a simplified geometry installation". 10th Australian fluid mechanics conference (Melbourne), 1989.

REPORT DOCUMENTATION PAGE

1. Recipient's Reference	2. Originator's Reference	3. Further Reference	4. Security Classification of Document
	AGARD-CP-526	ISBN 92-835-0685-5	UNCLASSIFIED

5. Originator Advisory Group for Aerospace Research and Development
North Atlantic Treaty Organization
7 Rue Ancelle, 92200 Neuilly sur Seine, France

6. Title AIRBREATHING PROPULSION FOR MISSILES AND PROJECTILES

7. Presented at the Propulsion and Energetics Panel 79th Symposium held in Villepreux, Nr Bordeaux, France, 11th—15th May 1992.

8. Author(s)/Editor(s)	9. Date
Various	September 1992
10. Author's/Editor's Address	**11. Pages**
Various	226

12. Distribution Statement This document is distributed in accordance with AGARD policies and regulations, which are outlined on the back covers of all AGARD publications.

13. Keywords/Descriptors

Air intakes for ramjets
Airbreathing propulsion
Combustion
Ducted rockets
Fuels for ramjets
Hydrocarbon fuels
Hypersonic propulsion
Materials for ramjets
Missiles
Projectiles
Propergols
Ram rockets
Ramjets
Thermal projection
Turbojets
Turborockets

14. Abstract

The Conference Proceedings contains 15 unclassified papers and a Keynote Address presented at the Propulsion and Energetics Panel 79th Symposium on "Airbreathing Propulsion for Missiles and Projectiles" which was held 11th—15th May 1992 in Villepreux, near Bordeaux, France.

The Symposium was arranged in the following sessions:

Ramjets and Ramrockets: Survey papers (2 unclassified papers); Ramjets and Ram Rockets: Propulsion Systems (2); Ramjets and Ram Rockets: Combustion, Fuels, Materials (3); Projectile Airbreathing Propulsion (1); Aerodynamics and Engine Integration (3); Turbojets and Turborockets (3), and Common Techniques (1).

The Technical Evaluation Report is included at the beginning of the Proceedings. Questions and answers of the discussions follow some of the papers. Nineteen additional classified papers will be published in a classified volume.

Being faced with more advanced detection and interception systems, there is a need for the development of missiles with increased penetration capabilities and propulsion systems for flight at low altitude and high speed with long range and diversified trajectories. For these requirements air-breathing engines are highly economic and flexible. The Symposium was intended to be a forum for discussing advances made in this field since the conduct of a similar Symposium in the autumn of 1981. The Technical Evaluation Report lists the conclusions of each of the sessions and points out that a very good scientific understanding was achieved not only for turbojets but also for ramjets.

AGARD Conference Proceedings 526
Advisory Group for Aerospace Research and Development, NATO
AIRBREATHING PROPULSION FOR MISSILES AND PROJECTILES
Published September 1992
226 pages

The Conference Proceedings contains 15 unclassified papers and a Keynote Address presented at the Propulsion and Energetics Panel 79th Symposium on "Airbreathing Propulsion for Missiles and Projectiles" which was held 11th–15th May 1992 in Villepreux, near Bordeaux, France.

The Symposium was arranged in the following sessions:

Ramjets and Ramrockets: Survey papers (2 unclassified papers); Ramjets and Ram Rockets: Propulsion Systems (2); Ramjets and Ram Rockets: Combustion, Fuels, Materials (3); Projectile Airbreathing Propulsion (1); Aerodynamics

P.T.O.

AGARD-CP-526

Air intakes for ramjets
Airbreathing propulsion
Combustion
Ducted rockets
Fuels for ramjets
Hydrocarbon fuels
Hypersonic propulsion
Materials for ramjets
Missiles
Projectiles
Propergols
Ram rockets
Ramjets
Thermal projection
Turbojets
Turborockets

AGARD Conference Proceedings 526
Advisory Group for Aerospace Research and Development, NATO
AIRBREATHING PROPULSION FOR MISSILES AND PROJECTILES
Published September 1992
226 pages

The Conference Proceedings contains 15 unclassified papers and a Keynote Address presented at the Propulsion and Energetics Panel 79th Symposium on "Airbreathing Propulsion for Missiles and Projectiles" which was held 11th–15th May 1992 in Villepreux, near Bordeaux, France.

The Symposium was arranged in the following sessions:

Ramjets and Ramrockets: Survey papers (2 unclassified papers); Ramjets and Ram Rockets: Propulsion Systems (2); Ramjets and Ram Rockets: Combustion, Fuels, Materials (3); Projectile Airbreathing Propulsion (1); Aerodynamics

P.T.O.

AGARD-CP-526

Air intakes for ramjets
Airbreathing propulsion
Combustion
Ducted rockets
Fuels for ramjets
Hydrocarbon fuels
Hypersonic propulsion
Materials for ramjets
Missiles
Projectiles
Propergols
Ram rockets
Ramjets
Thermal projection
Turbojets
Turborockets

AGARD Conference Proceedings 526
Advisory Group for Aerospace Research and Development, NATO
AIRBREATHING PROPULSION FOR MISSILES AND PROJECTILES
Published September 1992
226 pages

The Conference Proceedings contains 15 unclassified papers and a Keynote Address presented at the Propulsion and Energetics Panel 79th Symposium on "Airbreathing Propulsion for Missiles and Projectiles" which was held 11th–15th May 1992 in Villepreux, near Bordeaux, France.

The Symposium was arranged in the following sessions:

Ramjets and Ramrockets: Survey papers (2 unclassified papers); Ramjets and Ram Rockets: Propulsion Systems (2); Ramjets and Ram Rockets: Combustion, Fuels, Materials (3); Projectile Airbreathing Propulsion (1); Aerodynamics

P.T.O.

AGARD-CP-526

Air intakes for ramjets
Airbreathing propulsion
Combustion
Ducted rockets
Fuels for ramjets
Hydrocarbon fuels
Hypersonic propulsion
Materials for ramjets
Missiles
Projectiles
Propergols
Ram rockets
Ramjets
Thermal projection
Turbojets
Turborockets

AGARD Conference Proceedings 526
Advisory Group for Aerospace Research and Development, NATO
AIRBREATHING PROPULSION FOR MISSILES AND PROJECTILES
Published September 1992
226 pages

The Conference Proceedings contains 15 unclassified papers and a Keynote Address presented at the Propulsion and Energetics Panel 79th Symposium on "Airbreathing Propulsion for Missiles and Projectiles" which was held 11th–15th May 1992 in Villepreux, near Bordeaux, France.

The Symposium was arranged in the following sessions:

Ramjets and Ramrockets: Survey papers (2 unclassified papers); Ramjets and Ram Rockets: Propulsion Systems (2); Ramjets and Ram Rockets: Combustion, Fuels, Materials (3); Projectile Airbreathing Propulsion (1); Aerodynamics

P.T.O.

AGARD-CP-526

Air intakes for ramjets
Airbreathing propulsion
Combustion
Ducted rockets
Fuels for ramjets
Hydrocarbon fuels
Hypersonic propulsion
Materials for ramjets
Missiles
Projectiles
Propergols
Ram rockets
Ramjets
Thermal projection
Turbojets
Turborockets

and Engine Integration (3); Turbojets and Turborockets (3); and Common Techniques (1).

The Technical Evaluation Report is included at the beginning of the Proceedings. Questions and answers of the discussions follow some of the papers. Nineteen additional classified papers will be published in a classified volume.

Being faced with more advanced detection and interception systems, there is a need for the development of missiles with increased penetration capabilities and propulsion systems for flight at low altitude and high speed with long range and diversified trajectories. For these requirements air-breathing engines are highly economic and flexible. The Symposium was intended to be a forum for discussing advances made in this field since the conduct of a similar Symposium in the autumn of 1981. The Technical Evaluation Report lists the conclusions of each of the sessions and points out that a very good scientific understanding was achieved not only for turbojets but also for ramjets.

ISBN 92-835-0685-5

and Engine Integration (3); Turbojets and Turborockets (3); and Common Techniques (1).

The Technical Evaluation Report is included at the beginning of the Proceedings. Questions and answers of the discussions follow some of the papers. Nineteen additional classified papers will be published in a classified volume.

Being faced with more advanced detection and interception systems, there is a need for the development of missiles with increased penetration capabilities and propulsion systems for flight at low altitude and high speed with long range and diversified trajectories. For these requirements air-breathing engines are highly economic and flexible. The Symposium was intended to be a forum for discussing advances made in this field since the conduct of a similar Symposium in the autumn of 1981. The Technical Evaluation Report lists the conclusions of each of the sessions and points out that a very good scientific understanding was achieved not only for turbojets but also for ramjets.

ISBN 92-835-0685-5

and Engine Integration (3); Turbojets and Turborockets (3); and Common Techniques (1).

The Technical Evaluation Report is included at the beginning of the Proceedings. Questions and answers of the discussions follow some of the papers. Nineteen additional classified papers will be published in a classified volume.

Being faced with more advanced detection and interception systems, there is a need for the development of missiles with increased penetration capabilities and propulsion systems for flight at low altitude and high speed with long range and diversified trajectories. For these requirements air-breathing engines are highly economic and flexible. The Symposium was intended to be a forum for discussing advances made in this field since the conduct of a similar Symposium in the autumn of 1981. The Technical Evaluation Report lists the conclusions of each of the sessions and points out that a very good scientific understanding was achieved not only for turbojets but also for ramjets.

ISBN 92-835-0685-5

AGARD

NATO OTAN

7 RUE ANCELLE · 92200 NEUILLY-SUR-SEINE

FRANCE

Telephone (1)47.38.57.00 · Telex 610 176
Telecopie (1)47.38.57.99

DIFFUSION DES PUBLICATIONS
AGARD NON CLASSIFIEES

L'AGARD ne détient pas de stocks de ses publications, dans un but de distribution générale à l'adresse ci-dessus. La diffusion initiale des publications de l'AGARD est effectuée auprès des pays membres de cette organisation par l'intermédiaire des Centres Nationaux de Distribution suivants. A l'exception des Etats-Unis, ces centres disposent parfois d'exemplaires additionnels; dans les cas contraire, on peut se procurer ces exemplaires sous forme de microfiches ou de microcopies auprès des Agences de Vente dont la liste suite.

CENTRES DE DIFFUSION NATIONAUX

ALLEMAGNE
Fachinformationszentrum,
Karlsruhe
D-7514 Eggenstein-Leopoldshafen 2

BELGIQUE
Coordonnateur AGARD-VSL
Etat-Major de la Force Aérienne
Quartier Reine Elisabeth
Rue d'Evere, 1140 Bruxelles

CANADA
Directeur du Service des Renseignements Scientifiques
Ministère de la Défense Nationale
Ottawa, Ontario K1A 0K2

DANEMARK
Danish Defence Research Board
Ved Idraetsparken 4
2100 Copenhagen Ø

ESPAGNE
INTA (AGARD Publications)
Pintor Rosales 34
28008 Madrid

ETATS-UNIS
National Aeronautics and Space Administration
Langley Research Center
M/S 180
Hampton, Virginia 23665

FRANCE
O.N.E.R.A. (Direction)
29, Avenue de la Division Leclerc
92322 Châtillon Cedex

GRECE
Hellenic Air Force
Air War College
Scientific and Technical Library
Dekelia Air Force Base
Dekelia, Athens TGA 1010

ISLANDE
Director of Aviation
c/o Flugrad
Reykjavik

ITALIE
Aeronautica Militare
Ufficio del Delegato Nazionale all'AGARD
Aeroporto Pratica di Mare
00040 Pomezia (Roma)

LUXEMBOURG
Voir Belgique

NORVEGE
Norwegian Defence Research Establishment
Attn: Biblioteket
P.O. Box 25
N-2007 Kjeller

PAYS-BAS
Netherlands Delegation to AGARD
National Aerospace Laboratory NLR
Kluyverweg 1
2629 HS Delft

PORTUGAL
Portuguese National Coordinator to AGARD
Gabinete de Estudos e Programas
CLAFA
Base de Alfragide
Alfragide
2700 Amadora

ROYAUME UNI
Defence Research Information Centre
Kentigern House
65 Brown Street
Glasgow G2 8EX

TURQUIE
Milli Savunma Başkanlığı (MSB)
ARGE Daire Başkanlığı (ARGE)
Ankara

LE CENTRE NATIONAL DE DISTRIBUTION DES ETATS-UNIS (NASA) NE DETIENT PAS DE STOCKS DES PUBLICATIONS AGARD ET LES DEMANDES D'EXEMPLAIRES DOIVENT ETRE ADRESSEES DIRECTEMENT AU SERVICE NATIONAL TECHNIQUE DE L'INFORMATION (NTIS) DONT L'ADRESSE SUIT.

AGENCES DE VENTE

National Technical Information Service
(NTIS)
5285 Port Royal Road
Springfield, Virginia 22161
Etats-Unis

ESA/Information Retrieval Service
European Space Agency
10, rue Mario Nikis
75015 Paris
France

The British Library
Document Supply Division
Boston Spa, Wetherby
West Yorkshire LS23 7BQ
Royaume Uni

Les demandes de microfiches ou de photocopies de documents AGARD (y compris les demandes faites auprès du NTIS) doivent comporter la dénomination AGARD, ainsi que le numéro de série de l'AGARD (par exemple AGARD-AG-315). Des informations analogues, telles que le titre et la date de publication sont souhaitables. Veuiller noter qu'il y a lieu de spécifier AGARD-R-nnn et AGARD-AR-nnn lors de la commande de rapports AGARD et des rapports consultatifs AGARD respectivement. Des références bibliographiques complètes ainsi que des resumés des publications AGARD figurent dans les journaux suivants:

Scientifique and Technical Aerospace Reports (STAR)
publié par la NASA Scientific and Technical
Information Division
NASA Headquarters (NTT)
Washington D.C. 20546
Etats-Unis

Government Reports Announcements and Index (GRA&I)
publié par le National Technical Information Service
Springfield
Virginia 22161
Etats-Unis

(accessible également en mode interactif dans la base de données bibliographiques en ligne du NTIS, et sur CD-ROM)

Imprimé par Specialised Printing Services Limited
40 Chigwell Lane, Loughton, Essex IG10 3TZ

AGARD

NATO OTAN

7 RUE ANCELLE · 92200 NEUILLY-SUR-SEINE

FRANCE

Telephone (1)47.38.57.00 · Telex 610 176
Telefax (1)47.38.57.99

DISTRIBUTION OF UNCLASSIFIED AGARD PUBLICATIONS

AGARD does NOT hold stocks of AGARD publications at the above address for general distribution. Initial distribution of AGARD publications is made to AGARD Member Nations through the following National Distribution Centres. Further copies are sometimes available from these Centres (except in the United States), but if not may be purchased in Microfiche or Photocopy form from the Sales Agencies listed below.

NATIONAL DISTRIBUTION CENTRES

BELGIUM
Coordonnateur AGARD — VSL
Etat-Major de la Force Aérienne
Quartier Reine Elisabeth
Rue d'Evere, 1140 Bruxelles

CANADA
Director Scientific Information Services
Dept of National Defence
Ottawa, Ontario K1A 0K2

DENMARK
Danish Defence Research Board
Ved Idraetsparken 4
2100 Copenhagen Ø

FRANCE
O.N.E.R.A. (Direction)
29 Avenue de la Division Leclerc
92322 Châtillon Cedex

GERMANY
Fachinformationszentrum
Karlsruhe
D-7514 Eggenstein-Leopoldshafen 2

GREECE
Hellenic Air Force
Air War College
Scientific and Technical Library
Dekelia Air Force Base
Dekelia, Athens TGA 1010

ICELAND
Director of Aviation
c/o Flugrad
Reykjavik

ITALY
Aeronautica Militare
Ufficio del Delegato Nazionale all'AGARD
Aeroporto Pratica di Mare
00040 Pomezia (Roma)

LUXEMBOURG
See Belgium

NETHERLANDS
Netherlands Delegation to AGARD
National Aerospace Laboratory, NLR
Kluyverweg 1
2629 HS Delft

NORWAY
Norwegian Defence Research Establishment
Attn: Biblioteket
P.O. Box 25
N-2007 Kjeller

PORTUGAL
Portuguese National Coordinator to AGARD
Gabinete de Estudos e Programas
CLAFA
Base de Alfragide
Alfragide
2700 Amadora

SPAIN
INTA (AGARD Publications)
Pintor Rosales 34
28008 Madrid

TURKEY
Milli Savunma Başkanlığı (MSB)
ARGE Daire Başkanlığı (ARGE)
Ankara

UNITED KINGDOM
Defence Research Information Centre
Kentigern House
65 Brown Street
Glasgow G2 8EX

UNITED STATES
National Aeronautics and Space Administration (NASA)
Langley Research Center
M/S 180
Hampton, Virginia 23665

THE UNITED STATES NATIONAL DISTRIBUTION CENTRE (NASA) DOES NOT HOLD STOCKS OF AGARD PUBLICATIONS, AND APPLICATIONS FOR COPIES SHOULD BE MADE DIRECT TO THE NATIONAL TECHNICAL INFORMATION SERVICE (NTIS) AT THE ADDRESS BELOW.

SALES AGENCIES

National Technical
Information Service (NTIS)
5285 Port Royal Road
Springfield, Virginia 22161
United States

ESA/Information Retrieval Service
European Space Agency
10, rue Mario Nikis
75015 Paris
France

The British Library
Document Supply Centre
Boston Spa, Wetherby
West Yorkshire LS23 7BQ
United Kingdom

Requests for microfiches or photocopies of AGARD documents (including requests to NTIS) should include the word 'AGARD' and the AGARD serial number (for example AGARD-AG-315). Collateral information such as title and publication date is desirable. Note that AGARD Reports and Advisory Reports should be specified as AGARD-R-nnn and AGARD-AR-nnn, respectively. Full bibliographical *references and abstracts of AGARD publications are given in the following journals:*

Scientific and Technical Aerospace Reports (STAR)
published by NASA Scientific and Technical
Information Division
NASA Headquarters (NTT)
Washington D.C. 20546
United States

Government Reports Announcements and Index (GRA&I)
published by the National Technical Information Service
Springfield
Virginia 22161
United States

(also available online in the NTIS Bibliographic Database or on CD-ROM)

Printed by Specialised Printing Services Limited
40 Chigwell Lane, Loughton, Essex IG10 3TZ

ISBN 92-835-0685-5